GDAŃSK UNIVERSITY OF TECHNOLOGY

GDAŃSK UNIVERSITY OF TECHNOLOGY
FACULTY OF OCEAN ENGINEERING AND SHIP TECHNOLOGY

Polish Maritime Research

Special Issue S1 (97) 2018
Vol. 25

Coastal, Offshore and Ocean Engineering

ADDRESS OF PUBLISHER & EDITOR'S OFFICE:

GDAŃSK UNIVERSITY OF TECHNOLOGY

Faculty of Ocean Engineering & Ship Technology
G. Narutowicza 11/12
80-233 Gdańsk, POLAND

tel.: +48 58 347 13 66
fax: +48 58 341 13 66

EDITORIAL STAFF:

Jacek Rudnicki
| Editor in Chief
Rafał Szłapczyński
| Associate Editor
Jerzy Świrydczuk
| Associate Editor
Przemysław Wierzchowski
| Associate Editor
Aleksander Kniat
| Editor for international relations

Price:
single issue: 25 zł

Prices for abroad
single ussue:
- in Europe EURO 15
- overseas USD 20

WEB:
pg.edu.pl/pmr

e-mail : pmr@post.pl

ISSN 1233-2585

CONTENS

5 **Natalia Wawrzyniak, Andrzej Stateczny**
AUTOMATIC WATERCRAFT RECOGNITION AND IDENTIFICATION ON WATER AREAS COVERED BY VIDEO MONITORING AS EXTENSION FOR SEA AND RIVER TRAFFIC SUPERVISION SYSTEMS

14 **Rafał Szłapczyński, Tacjana Niksa-Rynkiewicz**
A FRAMEWORK OF A SHIP DOMAIN-BASED NEAR-MISS DETECTION METHOD USING MAMDANI NEURO-FUZZY CLASSIFICATION

22 **Marcin Drzewiecki**
THE PROPAGATION OF THE WAVES IN THE CTO S.A. TOWING TANK

29 **Duje Veic, Wojciech Sulisz**
IMPACT PRESSURE DISTRIBUTION ON A MONOPILE STRUCTURE EXCITED BY IRREGULAR BREAKING WAVE

36 **Henryk Olszewski, M.Hossein Ghaemi**
NEW CONCEPT OF NUMERICAL SHIP MOTION MODELLING FOR TOTAL SHIP OPERABILITY ANALYSIS BY INTEGRATING SHIP AND ENVIRONMENT UNDER ONE OVERALL SYSTEM

42 **Olga Kazimierska**
SIMULATION OF LIFE RAFT MOTIONS ON IRREGULAR WAVE - AN ANALYSIS OF SITUATIONS LEADING TO RAFT CAPSIZING

51 **Aleksander Kniat, Paweł Dymarski**
VERTICAL MOTIONS DAMPING MODEL TEST OF A LIFEBOAT LOWERED ONTO A FLAT SEA SURFACE

56 **Lech Kobyliński**
NEW GENERATION STABILITY NORMS –HOW TO APPROACH THE TASK

63 **Artur Karczewski, Janusz Kozak**
COMPARISON OF SELECTED PARAMETRIC METHODS FOR PREDICTION OF INLAND WATERWAYS SHIP HULL RESISTANCE IN TOWING TANK TEST

68 **Jan Kulczyk**
METHODS OF DETERMINATION OF FRICTIONAL RESISTANCE FOR PREDICTION OF TOTAL RESISTANCE OF INLAND WATERWAY VESSELS

74 **Maciej Reichel**
LONGITUDINAL MOTION DUE TO ACTION OF TUNNEL THRUSTERS

ADDRESS OF PUBLISHER & EDITOR'S OFFICE:

GDAŃSK UNIVERSITY OF TECHNOLOGY

Faculty of Ocean Engineering & Ship Technology
G. Narutowicza 11/12
80-233 Gdańsk, POLAND

tel.: +48 58 347 13 66
fax: +48 58 341 13 66

80 **Tomasz Tabaczek, Maciej Zawiślak**
HULL RESISTANCE OF AN INLAND WATERWAY VESSEL IN MODEL SCALE AND IN FULL SCALE

85 **Mojtaba Barjasteh, Hamid Zeraatgar**
NUMERICAL SIMULATION OF CUSHIONING PROBLEM FOR BLUNT BODIES USING BOUNDARY ELEMENT METHOD

94 **Seyyed Mohammad Reza Tabatabaei, Hamid Zeraatgar**
PARAMETRIC COMPARISON OF RECTANGULAR AND CIRCULAR PONTOONS PERFORMANCE AS FLOATING BREAKWATER NUMERICALLY

104 **Dominika Witos-Okrasińska, Grażyna Grelowska, Eugeniusz Kozaczka**
INFLUENCE OF NATURAL CONDITIONS ON THE IMAGING OF THE BOTTOM OF THE GDAŃSK BAY BY MEANS OF THE SIDE SCAN SONAR

111 **Grażyna Grelowska, Eugeniusz Kozaczka, Dominika Witos-Okrasińska, Wojciech Szymczak**
THE IMAGING OF GDANSK BAY SEABED BY USING SIDE SONAR

119 **Mariusz Deja, Michał Dobrzyński, Paweł Flaszyński, Jacek Haras, Dawid Zieliński**
APPLICATION OF RAPID PROTOTYPING TECHNOLOGY IN THE MANUFACTURING OF TURBINE BLADE WITH SMALL DIAMETER HOLES

124 **Michał Taraska, Remigiusz Iwańkowicz, Tomasz Urbański, Tadeusz Graczyk**
REVIEW OF ASSEMBLY SEQUENCE PLANNING METHODS IN TERMS OF THEIR APPLICABILITY IN SHIPBUILDING PROCESSES

134 **Tomasz Urbański, Tadeusz Graczyk, Michał Taraska, Remigiusz Iwańkowicz**
ASSESSMENT OF TECHNOLOGICAL USEFULNESS OF PANEL PRODUCTION LINE IN SHIPBUILDING PROCESS

145 **Czesław Dymarski, Tomasz Pająk**
LABORATORY TEST RIG FOR EXAMINING AGGREGATE MINING FROM SEABED USING THE AIRLIFT METHOD

151 **Łukasz Pyrzowski**
TESTING CONTRACTION AND THERMAL EXPANSION COEFFICIENT OF CONSTRUCTION AND MOULDING POLYMER COMPOSITES

159 **Jakub Szulwic, Paweł Tysiąc**
MOBILE LASER SCANNING CALIBRATION ON A MARINE PLATFORM

166 **Piotr Zima**
MODELING OF THE TWO-DIMENSIONAL FLOW CAUSED BY SEA CONDITIONS AND WIND STRESSES ON THE EXAMPLE OF DEAD VISTULA

172 **Piotr Bzura**
INFLUENCE OF LUBRICATING OIL IMPROVERS ON PERFORMANCE OF CRANKSHAFT SEALS

178 **Paweł Śliwiński**
THE INFLUENCE OF WATER AND MINERAL OIL ON MECHANICAL LOSSES IN THE DISPLACEMENT PUMP FOR OFFSHORE AND MARINE APPLICATIONS

189 **Damian Jakowski, Marek Dzida**
INCREASING POWER SUPPLY SAFETY IN THE ASPECT OF SUPPORTING THE RENEWABLE ENERGY SOURCES BY CONVENTIONAL AND VIRTUAL POWER STORES

198 **Wojciech Olszewski, Marek Dzida**
SELECTED COMBINED POWER SYSTEMS CONSISTED OF SELF-IGNITION ENGINE AND STEAM TURBINE

204 **Natalia Szewczuk-Krypa, Marta Drosińska-Komor, Jerzy Głuch, Łukasz Breńkacz**
COMPARISON ANALYSIS OF SELECTED NUCLEAR POWER PLANTS SUPPLIED WITH HELIUM FROM HIGH-TEMPERATURE GAS-COOLED REACTOR

MOST WIEDZY Downloaded from mostwiedzy.pl

ADDRESS OF PUBLISHER & EDITOR'S OFFICE:

GDAŃSK UNIVERSITY OF TECHNOLOGY

Faculty of Ocean Engineering & Ship Technology
G. Narutowicza 11/12
80-233 Gdańsk, POLAND

tel.: +48 58 347 13 66
fax: +48 58 341 13 66

211 **Zbigniew Korczewski, Konrad Marszałkowski**
ENERGY ANALYSIS OF PROPULSION SHAFT FATIGUE PROCESS IN ROTATING MECHANICAL SYSTEM
PART I TESTING SIGNIFICANCE OF INFLUENCE OF SHAFT MATERIAL FATIGUE EXCITATION PARAMETERS

218 **Natalia Szewczuk-Krypa, Anna Grzymkowska, Jerzy Głuch**
COMPARATIVE ANALYSIS OF THERMODYNAMIC CYCLES OF SELECTED NUCLEAR SHIP POWER PLANTS WITH HIGH-TEMPERATURE HELIUM-COOLED NUCLEAR REACTOR

225 **Andrzej Tomporowski, Izabela Piasecka, Józef Flizikowski, Robert Kasner, Weronika Kruszelnicka, Adam Mroziński, Kazimierz Bieliński**
COMPARISON ANALYSIS OF BLADE LIFE CYCLES OF LAND-BASED AND OFFSHORE WIND POWER PLANTS

234 **Ryszard Zadrąg, Tomasz Kniaziewicz**
RANKING OF TOXIC COMPOUND CONCENTRATIONS AS DIAGNOSTIC PARAMEETRS OF MARINE INTERNAL COMBUSTION ENGINE

243 **Roman Liberacki**
INDICES FOR ASSESSING POTENTIAL ENVIRONMENTAL HAZARD FROM FUTURE SHIP SCRAPPING PROCESS, DETERMINABLE IN SHIP DESIGN STAGE

MOST WIEDZY Downloaded from mostwiedzy.pl

Editorial

POLISH MARITIME RESEARCH is a scientific journal of worldwide circulation. The journal appears as a quarterly four times a year. The first issue of it was published in September 1994. Its main aim is to present original, innovative scientific ideas and Research & Development achievements in the field of **:**

Engineering, Computing & Technology, Mechanical Engineering,

which could find applications in the broad domain of maritime economy. Hence there are published papers which concern methods of the designing, manufacturing and operating processes of such technical objects and devices as : ships, port equipment, ocean engineering units, underwater vehicles and equipment as well as harbour facilities, with accounting for marine environment protection.
The Editors of POLISH MARITIME RESEARCH make also efforts to present problems dealing with education of engineers and scientific and teaching personnel. As a rule, the basic papers are supplemented by information on conferences , important scientific events as well as cooperation in carrying out international scientific research projects.

Scientific Board

Chairman : Prof. JERZY GIRTLER - Gdańsk University of Technology, Poland
Vice-chairman : Prof. MIROSŁAW L. WYSZYŃSKI - University of Birmingham, United Kingdom

Dr POUL ANDERSEN
Technical University of Denmark
Denmark

Dr MEHMET ATLAR
University of Newcastle United Kingdom

Prof. GÖRAN BARK
Chalmers University of Technology
Sweden

Prof. SERGEY BARSUKOV
Army Institute of Odessa Ukraine

Prof. MUSTAFA BAYHAN
Süleyman Demirel University
Turkey

Prof. VINCENZO CRUPI
University of Messina, Italy

Prof. MAREK DZIDA
Gdańsk University of Technology
Poland

Prof. ODD M. FALTINSEN
Norwegian University of Science and Technology
Norway

Prof. PATRICK V. FARRELL
University of Wisconsin Madison, WI
USA

Prof. HASSAN GHASSEMI
Amirkabir University of Technology
Iran

Prof. STANISŁAW GUCMA
Maritime University of Szczecin
Poland

Prof. ANTONI ISKRA
Poznań University of Technology
Poland

Prof. JAN KICIŃSKI
Institute of Fluid-Flow Machinery of PASci
Poland

Prof. ZBIGNIEW KORCZEWSKI
Gdańsk University of Technology
Poland

Prof. JANUSZ KOZAK
Gdańsk University of Technology
Poland

Prof. JAN KULCZYK
Wrocław University of Technology
Poland

Prof. NICOS LADOMMATOS
University College London United Kingdom

Prof. JÓZEF LISOWSKI
Gdynia Maritime University Poland

Prof. JERZY MATUSIAK
Helsinki University of Technology
Finland

Prof. JERZY MERKISZ
Poznań University of Technology
Poland

Prof. EUGEN NEGRUS
University of Bucharest Romania

Prof. YASUHIKO OHTA
Nagoya Institute of Technology
Japan

Dr YOSHIO SATO
National Traffic Safety and Environment Laboratory
Japan

Prof. KLAUS SCHIER
University of Applied Sciences
Germany

Prof. FREDERICK STERN
University of Iowa, IA, USA

Prof. ILCEV DIMOV STOJCE
Durban University of Technology
South Africa

Prof. JÓZEF SZALA
Bydgoszcz University of Technology and Agriculture
Poland

Prof. WITALIJ SZCZAGIN
State Technical University of Kaliningrad, Russia

Prof. BORIS TIKHOMIROV
State Marine University of St. Petersburg, Russia

Prof. DRACOS VASSALOS
University of Glasgow and Strathclyde United Kingdom

MOST WIEDZY Downloaded from mostwiedzy.pl

POLISH MARITIME RESEARCH Special Issue 2018 S1 (97) 2018 Vol. 25; pp. 5-13
10.2478/pomr-2018-0016

AUTOMATIC WATERCRAFT RECOGNITION AND IDENTIFICATION ON WATER AREAS COVERED BY VIDEO MONITORING AS EXTENSION FOR SEA AND RIVER TRAFFIC SUPERVISION SYSTEMS

Natalia Wawrzyniak
Marine Technology Ltd., Poland
Andrzej Stateczny
Polish Naval Academy, Gdynia, Poland

ABSTRACT

The article presents the watercraft recognition and identification system as an extension for the presently used visual water area monitoring systems, such as VTS (Vessel Traffic Service) or RIS (River Information Service). The watercraft identification systems (AIS - Automatic Identification Systems) which are presently used in both sea and inland navigation require purchase and installation of relatively expensive transceivers on ships, the presence of which is not formally required as equipment of unconventional watercrafts, such as yachts, motor boats, and other pleasure crafts. These watercrafts may pose navigation or even terrorist threat, can be the object of interest of the customs, or simply cause traffic problems on restricted water areas. The article proposes extending the traffic supervision system by a module which will identify unconventional crafts based on video monitoring. Recognition and identification will be possible through the use of image identification and processing methods based on artificial intelligence algorithms, among other tools. The system will be implemented as independent service making use of the potential of SOA (Service Oriented Architecture) and XML/SOAP (Extensible Markup Language/Simple Object Access Protocol) technology.

Keywords: ship identification, unconventional crafts, video monitoring, SOA systems

INTRODUCTION

Ship traffic monitoring is a key issue for safety of navigation on restricted water areas. It becomes even more important in sea ports situated deep at the river mouth, such as ports of Hamburg or Szczecin for instance, in which sea/river navigation is well developed. On sea waters, the systems which are responsible for traffic supervision and management are so-called VTSs (Vessel Traffic Services) [1], while on inland waters, the navigation assistance system is the RIS (River Information Service) [2]. Although functional assumptions of these two systems are slightly different, their common aim is to deliver widely understood traffic information. On the areas covered by these systems, various technologies are used for this purpose, including AIS (Automatic Identification System) [3], radars, and video monitoring cameras. Among other activities, the monitoring centres of these systems share the nautical information with watercraft users, store the information about ships, and/or observe the watercraft traffic. Throughout the day, or even round-the-clock, the systems are operated by human operators, but there is a tendency to automate system operation using the XML/SOAP (Extensible Markup Language/Simple Object Access Protocol) technology [4] and SOA (Service Oriented Architecture) [4] for independent operation of individual service centres and transmission of the information stored by one system to other systems and end users, such as customs, police, port operators, ship owners, etc.

MOST WIEDZY Downloaded from mostwiedzy.pl

Nowadays there is no automated system nor method to identify small crafts navigating on water areas supervised by VTS/RIS systems. The only way to identify these objects is their visual observation and recognition based on craft side marks. The RIS or VTS information systems are equipped with video monitoring subsystems, which collect the information from cameras mainly mounted on river bridges and in ports, thus providing good opportunities for ship observation from different directions and distances. Here, monitoring is mainly used by the operator to observe current situation on the water area, or to make an assessment of archival situations in cases of events requiring a more detailed analysis. The information on ships and/or events is not processed in any way, nor passed to other receivers in the system. Moreover, there is no unambiguous marking system for small crafts, including standardisation of their side marks which would possibly facilitate remote craft identification.

To make identification of such a small craft possible, it should be firstly recognised in the video image and then compared with the existing database of similar crafts. The river information systems have databases of ships, and these data can be interchanged between systems. Automatic ship recognition implies the possibility of its identification in the European Hull Data Base.

However, a problem is what to do with the information on the recognised object when it is not in the database. One of possible solutions is its assignment to one of already defined categories based on the database of patterns. Developing such an automatic classification procedure would allow the system to take further action based on the category to which it has been assigned.

The article proposes the automatic watercraft identification system which provides opportunities for automatic video data-based traffic monitoring, thus eliminating the work presently done by VTS/RIS operators.

BACKGROUND

DEVELOPMENT PLANS FOR INLAND WATERWAYS IN POLAND

The assumptions adopted by the Council of Ministers on the development plan of inland waterways in Poland in years 2016-2020, with perspective to year 2030, say that until 2030, the river Odra, on its whole length, and the river Vistula, from Warsaw to Gdansk, will become international shipping lanes on which the River Information System (RIS) will be implemented. To create stable conditions for functioning and development of inland navigation in Poland, actions are planned to improve the condition of the river transport, which is very poor now. That is why the Ministry of Maritime Economy and Inland Navigation had recommended signing the European Agreement on Main Inland Waterways of International Importance (AGN), which was ratified this year.

Due to the planned considerable river traffic intensification, extending the length of navigable waterways to the entire river Odra and the river Vistula between Warsaw and the Baltic sea will require installation of monitoring systems on the modernised river segments.

The modernisation programme for inland waterways in Poland includes implementation of the harmonised river information system (RIS) on all waterways of international importance, i.e. of class IV and higher. The main observation sensors within the area of RIS activity are video cameras. For instance, in the second stage of RIS development in the lower and border part of the river Odra, 16 new cameras are to be installed along the river fragment from Ognica to the A2 highway bridge at Świecko.

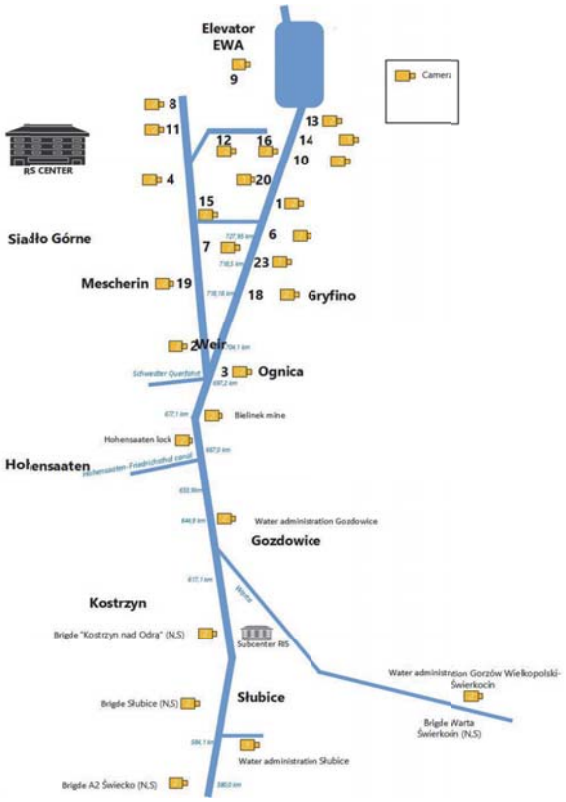

Fig.1. Schema of existing and planned cameras on Odra RIS area. [own elaboration based on 5]

Indeed, the observation of such a vast area of inland waterways cannot be done by human operators working in RIS Centres, therefore introducing assistance systems which will substitute their work is an absolute imperative. Introducing the RIS systems on the entire length of the river Odra and long fragments of the river Vistula is even more challenging [6].

ANALYSIS OF EXISTING WATERCRAFT MONITORING/ IDENTIFICATION SYSTEMS

The main and commonly used ship identification system is AIS. It makes use of the information on ship position and additional data introduced by the navigator, provided that the ship is equipped with a proper transmitter. The information

MOST WIEDZY Downloaded from mostwiedzy.pl

on all ships situated within the monitored area is collected by the network of base stations and passed to all other crafts and monitoring centres equipped with AIS receivers. There is also an inland version of the AIS system (Inland AIS), which is consistent with the basic system and used on rivers and other inland water areas [7]. The SOLAS Convention [8] worked out by IMO (International Maritime Organization) says that AIS transmitters are to be installed on:

- all ships with gross tonnage of 300 and more, engaged in international navigation,
- all ships with gross tonnage of 500 and more, not engaged in international navigation,
- all passenger ships, irrespective of size.

All other watercrafts which navigate on water areas, including non-commercial and recreation crafts, yachts, and other small crafts, cannot be unmistakably identified by the system, which means that they are not seen by it, or seen as unidentified objects. That is why, among other reasons, a system of cameras is added to the AIS and radar systems. In older solutions, these were the CCTV (Closed Circuit TeleVision) systems making use of industrial cameras [9] and a closed dedicated network for signal transmission to the central unit, where the images recorded by the cameras were observed on-line. However, with the development of digital technologies and popularisation of broadband Internet, the more and more frequent solutions are those based on networks and IP cameras [10], from which the digital image is transmitted to the system via internet.

A different function is played by professional commercial monitoring systems, especially in port areas. These systems are based on military systems and are mainly implemented in strategic or extremely sensitive areas, such as ports, offshore military bases, or offshore electric power plants [11]. They are dedicated hardware-software solutions of systems making use of different remote observation technologies, such as radars, surface and underwater cameras, sonars, and motion detectors. They deliver the information on moving crafts and help to detect and track their motion, or even counteract in emergency situations. A huge number of information sources requires their fusion into one integral piece of information concerning the motion of one individual object [12]. However, professional systems store sufficiently large amounts of data about crafts (especially military watercrafts) to make their identification possible [13]. Such a possibility does not exist in information systems, although they have their own databases on ships navigating in their areas and can interchange the data with other systems of the same type.

IMAGE PROCESSING FOR WATERCRAFT RECOGNITION

Recognising objects from streams of video images is a widely used methodology in different fields. Dynamic development of computer techniques affects the range of use of traditional image processing methods, which are still intensively developed, as well as artificial intelligence methods in video signal analyses performed using most recent technological solutions and a variety of digital devices. A good example here are commonly used smartphones which can recognise faces in the recorded photos, and more advanced extended reality systems making use of such tools as interactive glasses and helmets which can superimpose the on-line generated 3D graphics onto real images.

Each time, the object recognition problem starts with formulating a goal: what object is to be recognised in the given scene. Then, the process comprises two main stages: (1) processing, segmentation, extraction and description of features, and (2) final recognition and identification/interpretation. To extract and describe features, the system filters the analysed object using an edge filter and then analyses the created geometric shapes, circles for instance, with the aid of the EDCircles algorithm working online [12] or making use of properties of isosceles triangles [13]. Another approach to feature extraction is analysing image colours and texture. A good example here is skin cancer diagnosis described in [14]. The approach making use of these two relations is frequently applied for recognising distinguished objects [15]. Sometimes, for better object recognition, all three elements are taken into account: shape, colour, and texture [16-17]. There is also a possibility to use methods which base on certain pieces of information a priori introduced to the system and not coming directly from the image analysis. These data may refer to the object alone or the entire scene, the data transmission method, the optical system, or the used processing method. This approach replicates human way of image data analysis, which bases on earlier experience gained by the person interpreting the observed scene [18]. At each stage of the object recognition process, a method or algorithm is to be selected or developed which will lead to the final effect. On utmost importance is selecting a classifier from a relatively long list of available options. Depending on problem complexity, such methods can be used here as: decision trees, naive Bayes classifiers, kNN, neural networks, and machine learning.

Due to high availability of Computer Vision (CV) in free libraries, attention should be paid to the Viola–Jones algorithm [19]. Indeed, the first implementation of the algorithm took place as early as in 2001 when it was used for face image detection, but its assumptions and principles have been developed and used until now. This is particularly true for the use of the Haar-like feature for street traffic monitoring, to identify vehicles and their registration plates [20-21]. An example of applicability of image recognition systems can be the Polish registration plate identification system GV-LPR, produced by GeoVision.

The problem of watercraft recognition and identification in images recorded by the monitoring system is solved in the existing, individually dedicated and comprehensive, military systems created to protect most sensitive strategic objects, such as nuclear power plants, military bases, weapon test centres, etc., from the sea. Advanced research work in this field is mainly performed by commercial companies, such as General Dynamics, for instance. These systems make use of local features and geometric relations between them, which do not depend on changes in the remaining content

MOST WIEDZY Downloaded from mostwiedzy.pl

of the image, nor in its illumination, sharpness, scale, and orientation [22]. The most recent achievement in detecting small crafts has been made by ViNotion, a company which delivers comprehensive monitoring systems for different transportation fields.

When analysing images for watercraft detection purposes, it is worth pointing out that nowadays, it is common practice to use satellite images [23-24]. Unfortunately, they do not provide opportunities for precise identification of small watercrafts, and the time resolution of satellite systems limits the access to most recent data.

POTENTIAL OF SEA AND RIVER TRAFFIC SUPERVISION SYSTEMS

Both sea and inland traffic supervision systems provide their various users with, first of all, the access to nautical information. On the area of their activity, the systems frequently make use of video monitoring as the source of complementary information to that obtained from the AIS system and/or the radar sensor system, or even as the basic source of information on ship traffic. These systems are more or less open and their architecture can vary. Nevertheless, there are technologies and standards which make it possible to use the information collected and processed by them. Depending on the monitored region, these systems deliver services strictly related with the performed tasks. Aspects of sensor planning in RIS systems are discussed in [25-26]. To provide opportunities for system extension by incorporating a subsystem of automatic identification of unconventional watercrafts based on the image information collected from the monitoring, it is essential to know system architecture, applied technologies, and formats of data transfer between individual modules A key element here is the access to the module which collects and/or stores the data about watercraft motion on the monitored area, as these data will make the basis for final watercraft comparison and identification.

SERVICES AND SYSTEM ARCHITECTURE ASSUMPTIONS

On the restricted sea areas and, more rarely, on inland areas monitored by VTS systems, three types of services are provided: (1) Navigational Assistance Service (NAS) which provides ships with instructions and navigational assistance, (2) Traffic Organisation Service (TOS) which is responsible for operational traffic management and ship route planning to avoid dangerous traffic situations, etc., and (3) Information Service (INS) which provides the users with relevant information on request, or when a certain event has occurred, or at a pre-determined time (or after certain period of time). The data are transmitted in the IVEF format developed by IALA [27], which in the standardised form (XML scheme) makes it possible to share the data between different VTS receivers, and to transmit them to other e-Navigation systems, or even completely external systems which need the information on ship traffic.

The operating scheme of IVEF service is given in Fig. 2.

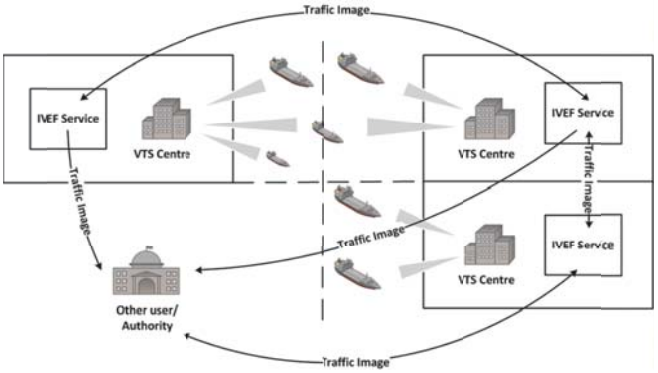

Fig. 2. Operating scheme of IVEF service [own elaboration based on 27]

This service refers to the Vessel Traffic Image Data, which contain statistical data about watercrafts, their positions and voyages. These data come both from the AIS system and the Global Integrated Shipping Information Systems (GISIS), while the dynamic data come from fusion of AIS and radar data. Aspects of AIS and radar data fusion are discussed in [28]. In this case the camera system is neglected. Data exchange with IVEF is done using the TCP/IP protocol for data transfer and TLS/SSL for encoding. It is based on client-server architecture, which means that it is not predefined, but negotiated between sides after the connection is established [29].

On inland areas covered by RIS, ship traffic supervision and monitoring of navigational situations takes a slightly different course. This results from the fact that the main method to reach the same goal as VTS (safety and performance of navigation) is, first of all, delivering the largest possible amount of information to the navigating objects connected with the system. Navigational aspects of inland watercraft traffic are discussed in [30].

The burden of proper use of the received data is borne by their users. With this approach, greater emphasis is placed on information distribution, and not on navigational traffic management, which is reflected in system architecture. The system provides 8 main services related with, among other actions, delivering information on traffic, waterways and transportation, and calamity abatement assistance. The data belonging to 5 different categories can be passed both between individual users within the RIS operation area, and between other interested users in Poland and Europe that use XML/SOAP technology and benefits of SOA architecture, being the basis for the RIS system architecture.

The system architecture for RIS data exchange is shown in Fig. 3 [31].

MOST WIEDZY Downloaded from mostwiedzy.pl

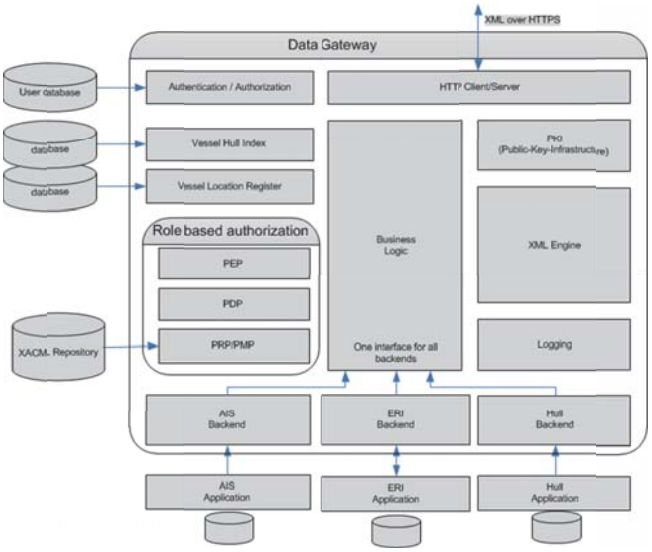

Fig. 3. Architecture of National and International Data Exchange module for RIS systems [31].

The system can be complemented with other services, which will deliver the information to system users indirectly (by improvement or extension of the existing information resource), or directly as an additional service. Therefore, the information on monitoring- based watercraft identifications can either supplement the existing traffic data obtained from other systems, Inland AIS for instance, or be an independent assistance service for monitoring centres, by presenting the information on the identified watercraft together with the camera image. An interesting approach to the problem of information presentation is described in [32].

MAIN ASPECTS OF EXTENDING VTS/RIS SERVICES BY AUTOMATIC IMAGE DATA ANALYSIS

The VTS system delivers information services, but first of all it ensures supervision and provides active navigational assistance to the watercrafts navigating on the monitored area. In this case, system extension should take into account implementation of the recognition module which will have access to the video data stream from the monitoring system and to the GISIS database. This module will pass the obtained information mainly to its operators in VTS coastal stations. Passing the verified/confirmed information to the module responsible for preparing static information about ships, which can be further exported to other internal VTS modules in the IVEF structure and to external systems, is a secondary concern.

In turn, for the RIS system with service-oriented architecture, its extension can have a form of separate service which can be used by other system components. The information can be structured and disseminated in the entire system in a fully automatic way. In this case, it is essential to ensure direct connection with the monitoring system to obtain the source data, and with the hull database connected with the RIS European Hull Data Base for final watercraft identification.

These two different approaches do not make it impossible to create an extension which would be sufficiently flexible to meet conditions of both the VTS and RIS system. This service should:

- have access to the watercraft database in the given system,
- ensure communication with a given video monitoring system to perform current image analysis,
- have an interface to other services and systems, to which it would pass the information on the identified watercrafts.

The data exchange concept in the RIS system is much wider than in the VTS system. However, a tendency is observed in recent years to develop the IVEF format, which is related with development of the entire e-Navigation concept. Among other things, this is indicated by creation of IVEF SDK, intended to facilitate implementation of IVEF model in different systems and services making use of ship traffic information. This mean at least partial opening of the VTS system for data delivery to other receivers than only the own VTS centres.

Taking into account properties of these two systems, it is possible to develop an extension which would satisfy both solutions.

SERVICE ARCHITECTURE OF THE EXTENSION MAKING USE OF SOAP/ XML TECHNOLOGY

By assumption, the watercraft recognition and identification system is designed as a separate module representing the service which can be united with the existing navigation supervision system, only in minimal way limiting further work related with implementation of the extension to a given VTS or RIS centre. This solution is possible due to service-oriented architecture of the extension. Its individual components are considered as separate units which share their interfaces and communicate with each other as black boxes. All messages are parsed and controlled by implemented schemes, and in this form they are passed between individual services. Here, use is made of XML technology with XSD schemes to control the transmitted information, due to the SOAP protocol over the HTTM/SMTP protocol for the transmission alone.

FUNCTIONAL CONCEPT

Simplified architecture is shown in Fig. 4.

When the existing ship database exchanges the information with other systems (for instance between different RIS systems in the European network of inland waterways), the system will ensure an opportunity to identify watercrafts stored in the network of databases. However, when after recognising the watercraft, its further identification is not possible, the system will enable its classification based on the own base of patterns.

MOST WIEDZY Downloaded from mostwiedzy.pl

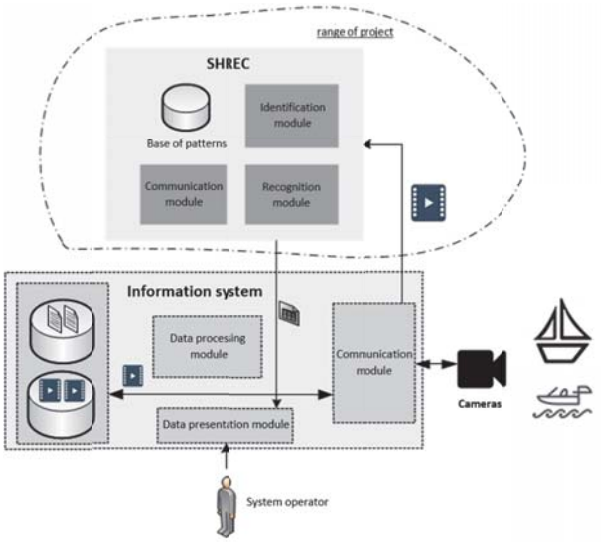

Fig.4 Simplified architecture scheme of traffic supervision system extension [own elaboration].

As already mentioned, the extension has modular structure. The communication module is responsible for transmitting the images from the supervision system monitoring database and the data on watercrafts required for ship identification. Additionally, it transmits the recognition and/or identification results back to the system for information presentation or further processing by systems connected with the RIS or VTS system. The recognising module makes use of the pattern database extracted from test images of watercrafts, worked out and introduced for system operation purpose. The identification module, in turn, utilizes the results of operation of the recognition module, and after comparing with the information on ships stored in the databases, passes the results to the communication module.

To sum up, the proposed extension is an independent system which can be integrated with an arbitrary sea or river information system which:

a. uses or stores data from video monitoring installed in its jurisdiction area,
b. has the database on watercrafts navigating on its area.

RECOGNISING AND IDENTIFYING

The created recognition method was mainly based on: (1) the analysis of current regulations, norms and standards used in European solutions concerning conventional and unconventional watercraft identification, (2) the analysis of current regulations on vessel marks on sea and inland waters, and (3) the analysis of the existing algorithms of image recognition from the video stream, from the point of view of their use for ship identification. A number of inland watercrafts, selected as examples of different ways of identification number and name marking, are shown in Fig. 5.

Pusher tug	
RZGW craft	
Inland pleasure boat	
Push train	
Hydrographic boat	

MOST WIEDZY Downloaded from mostwiedzy.pl

Yacht	

Fig.5.Examples of unconventional watercrafts [own elaboration]

The recognition method can be based on a set of local properties of individual watercrafts or, for instance, on recognising craft side marks. A frequent problem here is that the regulations concerning craft marking are not precise, which makes fast craft identification extremely difficult. A test database should be created which will help to determine situational and technical requirements, and to select patterns for craft classification purposes. A preliminary approach assumes two possibilities: recognising the object and its further identification based on the existing external ship database (for instance, Hull Database in the RIS system), or classifying the object when its unmistakable identification is not possible. A number of variants of the method will be developed, with further comparison analysis of the results of the performed tests. The method will take into account achievements in machine vision and artificial intelligence methods, in particular the use of artificial neural networks [33] for recognising patterns, and other video image processing methods, for instance those used in short-range photogrammetry [34].

SUMMARY

A basic novelty being the direct result of the project is the possibility to identify unconventional watercrafts on the areas monitored by RIS or VTS systems, which has not been carried out so far by any existing navigation monitoring system. At present, the installation of neither the AIS system, which is currently used for ship identification, nor the Inland AIS system is required on small non-commercial watercrafts. The identification will be independent of craft equipment, which means that no additional devices will have to be bought nor operated by the craft's owner. Moreover, the system will ensure automaticity of the entire process, which means that the camera image does not need to be tracked by human operator. The system will be an independent service, able to integrate with an arbitrary nautical information system equipped with video monitoring and database on ships which can navigate on the monitored area. The system will make use of XML/SOAP technology and other most recent solutions for systems with Service Oriented Architecture (SOA), which are expected to be implemented in European RIS navigation system networks. In cases when unmistakable watercraft identification from its marking or side superscription is impossible, or there is no information about it in the ship database, the system will perform watercraft recognition based on classification principles and the possessed base of patterns. The entire system will be based on an innovative method of watercraft recognition from the video data stream, which will make use of most recent achievements in the fields of machine vision and artificial intelligence (in particular artificial neural networks and rough set algebra-based inference). The effect of action of the described system will be the appearance of automatic and structured information in RIS/VTS about the recognised/identified watercraft, which can be passed through the defined interfaces to other connected external systems (for instance, services responsible for taking steps on water areas, customs, ports, police, etc.).

Activities towards the modernisation of the rivers Odra and Vistula within the framework of the development programme for inland waterways in Poland have been already started on both rivers. Once the modernisation is completed, the implementation of RIS services, including video monitoring, will begin.

ACKNOWLEDGMENTS

This scientific research work was supported by National Center for Research and Development (NCBiR) of Poland (grant No. LIDER/17/0098/L-8/16/NCBR/2017).

BIBLIOGRAPHY

1. IALA Recommendation V – 128 on Operational and Technical Performance Requirements for. VTS Equipment Ed. 2.0, 2005.
2. PIANC RIS Guidelines and Recommendations for River Information Systems, 2011
3. Zajac, P.: Evaluation of Automatic Identification Systems According to ISO 50001: 2011, Progress in Automation, Robotics and Measuring Techniques: Control and Automation, Book Series: Advances in Intelligent Systems and Computing vol. 350, pp: 345-355, 2015.
4. Kubik, T.: GIS – Network solutions (in Polish), PWN, 2009
5. Stateczny, A.: Full Implementation of the River Information Services of Border and Lower Section of the Oder in Poland. Proceedings of Baltic Geodesy Congress, Gdansk, Poland, 2016.
6. Wlodarczyk-Sielicka M., Wawrzyniak N.: Problem of Bathymetric Big Data Interpolation for Inland Mobile Navigation System. In: Damaševičius R., Mikašytė V. (eds) Information and Software Technologies. ICIST 2017. Communications in Computer and Information Science,

MOST WIEDZY Downloaded from mostwiedzy.pl

vol 756, pp 611-621. Springer, Cham,

7. Kazimierski, W., Stateczny, A.: Radar and Automatic Identification System track fusion in an Electronic Chart Display and Information System. Journal of Navigation, volume: 68, issue: 6, pp: 1141-1154, 2015.

8. International Maritime Organisation, SOLAS International Convention for the Safety of Life at Sea, 1974.

9. Jines, SP., Dwyer, DM., Lewis, MB.: The utility of multiple synthesized views in the recognition of unfamiliar faces, Quarterly Journal of Experimental Psychology, vol. 70, issue 5, pp 906-918, 2017.

10. Choi, K., Jeong, Y., Gil, J.: Design and implementation of P2P home monitoring system architecture with IP cameras for a vacuum robot in ubiquitous environments, International Journal of Sensors Network, vol.20, pp 166-176, 2016.

11. Yuksel, G, Yalituna, B., Tartar, O., Yoruk, O.: Ship recognition and classification using silhouettes extracted from optical images, In Proceedings of Signal Processing and Communication Application Conference (SIU), IEEE 2016.

12. Akinlar, C., Topal,: EDCircles: A real-time circle detector with a false detection control, Pattern Recognit., vol. 46, no. 3, pp. 725–740, 2013.

13. Zhang, H., Wiklund, K., Andersson, M.: A fast and robust circle detection method using isosceles triangles sampling, Pattern Recognition, vol. 54, pp. 218–228, 2015.

14. Barata, C., Ruela, M., Francisco, M., Mendonca, T. & Marques, J. S.: Two systems for the detection of melanomas in dermoscopy images using texture and color features, IEEE Syst. Journal., vol. 8, no. 3, pp. 965–979, 2014.

15. Hu, P., Wang, W., Zhang, C. & Lu, K.: Detecting Salient Objects via Color and Texture Compactness Hypotheses, IEEE Trans. Image Process., vol. 25, no. 10, pp. 4653–4664, 2016.

16. Chaudhary, P., Sharma, S.: A Color, Texture and Shape Based Hybrid Approach for Clothing Retrieval Techniques, IJMCA, vol. 6, no. 4, pp. 382–387, 2016.

17. Kadir, A., Nugroho, L., Susanto, A. & Santosa, P.: Leaf Classification Using Shape, Color, and Texture Features, Int. J. Comput. Trends Technol., pp. 225–230, 2011.

18. Wawrzyniak, N., Stateczny, A.: MSIS Image Positioning in Port Areas with the Aid of Comparative Navigation Methods. Polish Maritime Research, vol. 24, Issue. 1, pp. 32-41, 2017.

19. Viola, P., Jones M.: Rapid object detection using a boosted cascade of simple features, Computer Vision Pattern Recognition, vol. 1, p. I--511-I-518, 2001.

20. Wen, X., Shao, L., Fang, W. & Xue, Y.: Efficient feature selection and classification for vehicle detection, IEEE Trans. Circuits Syst. Video Technol., vol. 25, no. 3, pp. 508–517, 2015.

21. Wen, X., Shao, L., Xue, Y., & Fang, W.: A rapid learning algorithm for vehicle classification, Inf. Sci. (Ny)., vol. 295, pp. 395–406, 2015.

22. Feineigle, P.A., Morris, D.D., Snyder, F.D.: Ship Recognition Using Optical Imagery for Harbor Surveillance, Proceedings of Association for Unmanned Vehicle Systems International (AUVSI), Washington DC, 2007.

23. Tang, J., Deng, C., Huang, G., & Zhao, B.: Compressed-Domain Ship Detection on Spaceborne Optical Image Using Deep Neural Network and Extreme Learning Machine, IEEE Trans. Geosci. Remote Sens., vol. 53, no. 3, pp. 1174–1185, 2015.

24. Zou, Z., Shi, Z.: Ship detection in spaceborne optical image with SVD networks, vol. 54, no. 10, pp. 5832–5845, 2016.

25. Stateczny, A.: Sensors in River Information Services of the Odra River in Poland: Current State and Planned Extension. Proceedings of Baltic Geodesy Congress, Gdansk, Poland, 2017.

26. Stateczny, A., Lubczonek, J., Kantak T.: Radar Sensors Planning for the Purpose of Extension of River Information Services in Poland. Proceedings of 16th International Radar Symposium (IRS), International Radar Symposium Proceedings, H. Rohling (Ed.), Dresden, Germany, 2015.

27. IALA Recommendation V-145 on the Inter-VTS Exchange Format (IVEF) Service, Edition 1.0, 2011.

28. Kazimierski, W., Stateczny, A.: Fusion of Data from AIS and Tracking Radar for the Needs of ECDIS. Signal Processing Symposium, Jachranka, 2013.

29. Kazimierski, W., Wawrzyniak, N.: Exchange of navigational information between VTS and RIS for inland shipping user needs, in Mikulski J.(ed.) Telematics in the Transport Environment, Book Series: CCIS vol.471, pp. 294-303, 2014.

30. Galor, W.: Sea-river shipping in Polish inland water, Scientific Journal of Maritime University of Szczecin, vol. 50 (122), pp. 84–90, 2017.

31. IRIS 2 Europe, Implementation of River Information Services in Europe, Technical concept for RIS data exchange (part of R2D2), SuAc 3.4, 2010.

MOST WIEDZY Downloaded from mostwiedzy.pl

32. Kazimierski, W., Zaniewicz, G., Olkowska, I.: Integrated presentation of navigational data in a mobile navigation system for inland waters with the use of HUD, Scientific Journal of Maritime University of Szczecin, vol. 49 (121), pp. 84–92, 2017.

33. Wlodarczyk-Sielicka, M.: Importance of neighbourhood parameters during clustering of bathymetric data using neural network. G. Dregvaite and R. Damasevicius (Eds.): ICIST 2016, Communications in Computer and Information Science 639: Information and Software Technologies, pp 441-452, 2016,

34. Kedzierski, M., Wierzbicki, D.: Methodology of improvement of radiometric quality of images acquired from low altitudes, Measurement, Vol. 92, pp. 70-78, 2016.

CONTACT WITH THE AUTHORS

Natalia Wawrzyniak
e-mail: n.wawrzyniak@marinetechnology.pl

Marine Technologu Ltd.
Cyfrowa 6, B.3.04a
71-441 Szczecin
Poland

Andrzej Stateczny
e-mail: andstate@pg.gda.pl

Gdansk University of Technology
Faculty of Civil and Environmental Engineering,
Narutowicza 11/12
80-233 Gdansk
Poland

MOST WIEDZY Downloaded from mostwiedzy.pl

POLISH MARITIME RESEARCH Special Issue 2018 S1 (97) 2018 Vol. 25; pp. 14-21
10.2478/pomr-2018-0017

A FRAMEWORK OF A SHIP DOMAIN-BASED NEAR-MISS DETECTION METHOD USING MAMDANI NEURO-FUZZY CLASSIFICATION

Rafał Szłapczyński
Tacjana Niksa-Rynkiewicz
Gdańsk University of Technology, Poland

ABSTRACT

Safety analysis of navigation over a given area may cover application of various risk measures for ship collisions. One of them is percentage of the so called near- miss situations (potential collision situations). In this article a method of automatic detection of such situations based on the data from Automatic Identification System (AIS), is proposed. The method utilizes input parameters such as: collision risk measure based on ship's domain concept, relative speed between ships as well as their course difference. For classification of ships encounters, there is used a neuro-fuzzy network which estimates a degree of collision hazard on the basis of a set of rules. The worked out method makes it possibile to apply an arbitrary ship's domain as well as to learn the classifier on the basis of opinions of experts interpreting the data from the AIS.

Keywords: near-miss, collision risk, ship domain, fuzzy classification

MOST WIEDZY Downloaded from mostwiedzy.pl

INTRODUCTION

Real number of collisions between ships (especially the collisions in the true sense of this word, i.e. a crash) is so low in many sea regions that safety analysis of navigation over a given water area or fairway [5] requires introducing additional measures. One of them is a percentage of ships passing in so close distance that it may be considered dangerous – the so called near-miss situtation. Such situations are usually detected on the basis of the data from the Automatic Identification System for ships . Many works dealing with the methods for detection of such situations, differring mainly in choosing a set of input parameters as well as a way of subsequent processing the data, have been made so far. A common element of most of them is the application of the so called ship's domain [6, 7, 19], i.e. an area surrounding a given ship, which should not be violated by other ships.

In this article there is proposed a novel method for detecting near-miss situations on the basis of the data from the AIS. The method in question makes use of three input parameters. The crucial parameter is a collision risk measure based on ship's domain concept. The supplementing parameters are: relative speed between ships as well as difference in their courses. For classification of ships encounters a neuro-fuzzy network which estimates a degree of collision hazard by using a set of fuzzy rules, was here applied. The proposed method is characteristic of a high flexibility as it makes it possible to employ an arbitrary ship's domain as well as to learn the classifier on the basis of opinions of experts interpreting the data from the AIS. The possible modifications of the method cover also either a change or expansion of the set of input parameters. In such situation it would be necessary only to overwrite the existing rules by new ones without introducing any change into the main structure of the system.

In the subsequent sections of this paper there are presented existing methods for detection near-miss situations as well as the proposed methods: choice of its input parameters, structure of the neuro-fuzzy classifier as well as the conducted analysis of the method's performance.

EXISTING METHODS FOR DETECTING THE SO CALLED NAVIGATIONAL CONFLICTS AND NEAR-MISS SITUATIONS

Investigations on detection of near-miss situations are carried out for various sea water areas. In the publication [22] its authors made use of data from the AIS intended for the analyzing of ship traffic in coastal waters of Southeast Texas, Sabine–Neches Waterway (SNWW), important for oil transportation. It is assummed that collision risk is tightly associated with number of the so called conflicts and this number has been tested by examining violations of circular or eliptical ship's domains as well as relative speeds between ships. Similar investigations were performed for the North Sea and recorded in [21]. The navigational conflict was there defined as a potential future violation of ship's domain within a given time horizon. And, the near-miss situation was defined as a real violation of ship's domain to a degree greater than 50%. For detecting both the conflicts and near-miss situations an eliptical domain was used without applying any additional parameters. The investigations presented in [7] were also based on the data taken from the AIS, concerning encounters of ships sailing over the North Sea. The ship's domain was there determined empirically: experiments confirmed its eliptical form for main types of ships encounter situations, especially for overtaking as well as head-on encounters. Next, the obtained ship's domains were used for determining near-miss situations while, apart from ship's domain violations , the classical parameters such as the Distance at the Closest Point of Approach (DCPA) as well as of the Time to the Closest Point of Approach (TCPA) were additionally taken into account . A more advanced method for detecting near-miss situations was presented in [24]. The criterion for ship's domain violation was there supplemented with a series of other decision variables , a. o.: the Minimum Distance to Collision (MDTC), DCPA, TCPA, distance to ship's domain, relative speed between ships as well as the Bow Crossing Range (BCR). The worked out method served then for analyzing near-miss situations over the northern part of the Baltic Sea.

All the above specified methods are characteristic of a relatively inflexible approach as far as choice of input parameters, formulation of criteria or decision rules as well as a form of results is concerned.

In opinion of these authors it is justified to develop a more flexible and versatile method. Application of a risk measure based on ship's domain makes it possible to account for specificity of a local ships traffic by means of a domain prepared for a given sea area. And, the basing of the system on a neuro-fuzzy classifier allows to feed back both a detailed information on collision danger and a degree of certainty or uncertainty of such assessment. Therefore, both the above mentioned elements constitute the basis for the proposed novel method.

CHOICE OF INPUT PARAMETERS FOR THE PROPOSED NOVEL METHOD

These authors decided to choose three , crucial in ther opinion , parameters – decision variables - describing a degree of collision danger. The first variable is the Degree of Domain Violation (DDV). The DDV is a number from the interval <0,1>,where 0 stands for lack of domain violation, and 1 – coincidence of mass centres of both ships.

The parameter allows to use an arbitrary model of ship's domain (especially unsymmetrical ones) as well as an arbitrary parametrization of such model.

As a result , it can replace a few earlier applied parameters such as: DCPA, BCR and bearing.

The second selected variable is the relative velocity between two ships V_r – most of the authors is in agreement as to its influence on degree of collision danger [22, 24]. The third selected variable is the difference between directions of motion of two ships, α, calculated by means of the relations (1):

$$\varphi = |\varphi_1 - \varphi_2| ,$$

$$\gamma = 360^{\circ} - \varphi, \qquad (1)$$

$$\alpha = min\big(min(\varphi,\gamma), 180^{\circ} - min(\varphi,\gamma)\big)$$

where:
φ_1, φ_2– courses of two ships,
φ – difference in courses of two ships,
γ – complementary angle for φ up to 360°,
$min(\varphi,\gamma)$ – the smaller value out of .

Consequently, the variable α takes values from the interval <0°,90°>:
- 0° – for parallel courses (identical or opposite ones),
- 90° – for mutually perpendicular courses,
- intermediate values – for other combinations of courses.

It was assumed, that at constant relative speed between ships collision probability is lowest for parallel courses (overtaking and head-on encounters), whereas it is greatest for perpendicular courses (crossing encounters) because mutual situation of ships is more difficult to predict as well as it is necessary to make a greater maneouvre to avoid collision. Values of all the three selected variables can be determined for every ships encounter by automatic processing the data available from the AIS: lengths of ships and their instantaneous positions and courses. For simulation purposes the data available from the portal www.marinetraffic.com, were utilized in this work.

GENERAL STRUCTURE OF THE SYSTEM

The neuro-fuzzy systems constitute a synthesis of concepts of neural networks and fuzzy systems [2,14,15]. A characteristic feature of such classifiers is an incorporation

MOST WIEDZY Downloaded from mostwiedzy.pl

of experts knowledge directly into their structures. Among the family of neuro-fuzzy systems the three groups can be distiguished: Mamdani systems, logic systems and Takagi-Sugeno ones. For classification tasks , Mamdani systems are usually applied. Their effectiveness was confirmed many times [1,13,14,23]. Into the system is introduced the knowledge which is defined as initial, basic or expert one. It is represented by means of fuzzy rules which make it possible to interpret it appropriately at any instance, which is not possible in case of application of systems based only on neural networks [13].

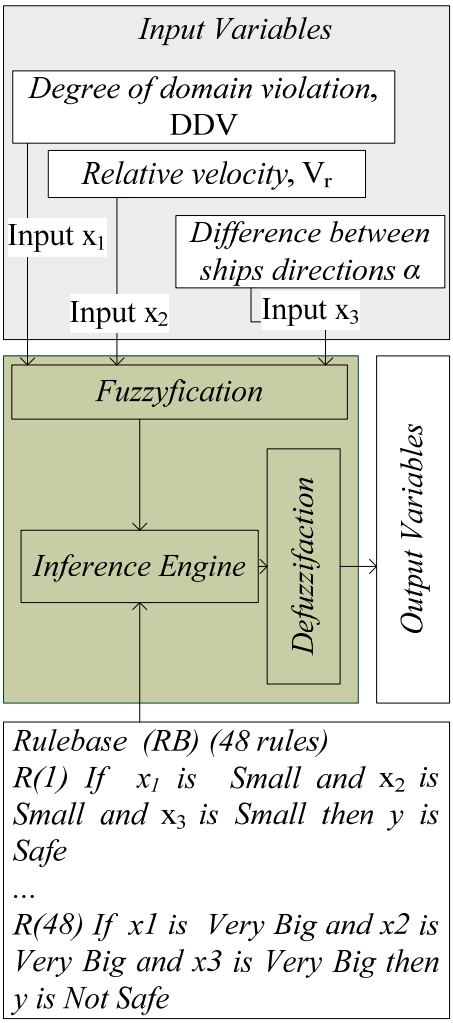

Fig. 1. Architecture of the system for classification based on Mamdani model

Hence, in this work it is proposed to develop a neuro-fuzzy system, to base its architecture on Mamdani model, as wel as to make use of an input data space and a set of fuzzy rules determined in advance. Additionally, the application of such solution allows to extend the system in the future and use it for interpretation and classification of the knowledge dynamically gained from the AIS. The general schematic diagram of the system is shown in Fig. 1.

The distinguished fragment of the classifier (Fig. 1) is built of the following elements: "Fuzzyfication", "Inference Engine"and "Defuzzyfication". The "Fuzzyfication" is responsible for fuzzifying process and allows to present input data in the domain of fuzzy sets. The values appropriately activate the rules which have been declared in advance and placed into the block „Rulebase (RB)". The set of the RB rules is usually called the base of rules or linguistic model [3,23]. A degree of activation of the rules affects final classification result achieved as a result of defuzzyfication process carried out in the block "Defuzzyfication".

In the worked out system there is assumed that it contains N fuzzy rules where a number of the particular rule $R^{(r)}$ is identified by the variable r so that $r = 1,\ldots,N$.

Inputs to the system are numbered beginning from 1 up to n, while subsequent input variables of the linguistic model are denoted as follows: $x_1, x_2,\ldots,x_n$.

The space of input variables is denoted in the form of X_i, $i = 1,..,n$, and the space of output variables – Y_j, where $j = 1,\ldots,m$. Fuzzy sets are defined in the domain of real numbers and denoted respecting the inputs and outputs according to the relation (2):

$$A_i^r \subseteq X_i \subset R\,,\; B_j^r \subseteq Y_i \subset R \tag{2}$$

Form of fuzzy rules is determined in compliance with the formula given in [2], i.e.:

$$R^{(r)}: If\ x_1\ is\ A_1^r\ and\ \ldots\ and\ x_n\ is\ A_n^r$$
$$then\ y_1 is\ B_1^r\ \ and\ \ldots\ and\ y_m\ is\ B_m^r$$

ARCHITECTURE OF THE WORKED OUT SYSTEM

In this paper, an emphasis is put on utilization of the basic knowledge in its unchanged form. Initially, the defined rules were implemented directly together with some fuzzy sets. The basic knowledge comprises 48 fuzzy rules defined in the space of three input variables: *DDV*, V_r, α, which are attributed to the signals x_1, x_2, x_3, respectively. The system has one output only; hence: n = 3, N = 48, m = 1.

For purposes of better matching up the system to experts knowledge the fuzzy sets were described not only by means of Gauss function. The membership functions (MFs) may have a sigmoidal or triangular, f_{tri} or trapezoidal, f_{trap}, form as well as f_s and f_z, i.e. spline-based functions also called Zadeh's S-function [4]

$$f_{tri}(x,a,b,c) = \begin{cases} 0\ dla\ x \le a \\ \frac{x-a}{b-a}\ dla\ a < x \le b \\ \frac{c-x}{c-b}\ dla\ b < x \le c \\ 0\ dla\ x > c \end{cases} \tag{3}$$

MOST WIEDZY Downloaded from mostwiedzy.pl

$$f_{trap}(x,a,b,c,d) = \begin{cases} 0\ dla\ x \le a \\ \frac{x-a}{b-a}\ dla\ a < x \le b \\ 1\ dla\ b < x \le c \\ \frac{d-x}{d-c}\ dla\ c < x \le d \\ 0\ dla\ x > c \end{cases} \quad (4)$$

The parameters a, b, c, d (Param. MFs) characterize particular fuzzy sets according to the relations (3,4). Their applied values are given in Tab.1 through Tab. 4.

Tab. 1. Collection of characteristic values of the fuzzy sets A_1 described in the space of the variable x_1 (DDV)

Linguistic variable	Name	MFs	Param. MFs
Zero	Z	f_{tri}	[0 0 0]
Small	S	f_{trap}	[0 0 0.1 0.3]
Medium	MID	f_{tri}	[0.2 0.3 0.4]
Big	BIG	f_{tri}	[0.3 0.4 0.5]
Very Big	VB	f_{trap}	[0.4 0.6 1 1]

Tab. 2. Collection of characteristic values of the fuzzy sets A_2 described in the space of the variable $x_2(V_r)$

Linguistic variable	Name	MFs	Param. MFs
Small	S	f_{trap}	[0 0 5 10]
Medium	MID	f_{tri}	[5 10 20]
Big	BIG	f_{tri}	[10 20 30]
Very Big	VB	f_{trap}	[20 30 60 60]

Tab. 3. Collection of characteristic values of the fuzzy sets A_3 described in the space of the variable $x_3(\alpha)$

Linguistic variable	Name	MFs	Param. MFs
Small	S	f_{trap}	[0 0 15 30]
Medium	MID	f_{tri}	[15 30 45]
Big	BIG	f_{tri}	[30 50 70]
Very Big	VB	f_{trap}	[50 70 90 90]

Tab. 4. Collection of characteristic values of the fuzzy sets B described in the space of the output signal y

Linguistic variable	Name	MFs	Param. MFs
Very Safe	VS	f_{tri}	[0 0 0]
Safe	MID	f_z	[0 0.8]
Not Safe	BIG	f_s	[0.2 1]
Dangerous	D	f_s	[1 1]

The produced fuzzy sets are presented in Fig. 2 through Fig. 5.

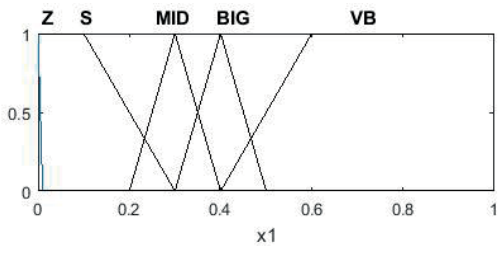

Fig. 2. Diagram of the fuzzy sets A_1 described in the space of the variable x_1 (DDV)

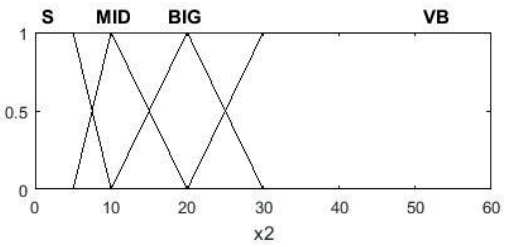

Fig. 3. Diagram of the fuzzy sets A_2 described in the space of the variable x_2 (V_r)

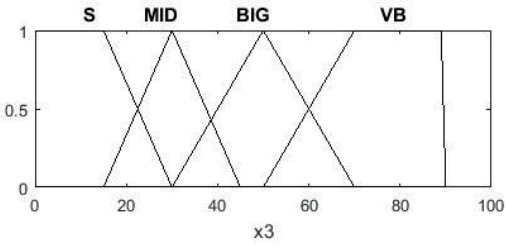

Fig. 4. Diagram of the fuzzy sets A_3 described in the space of the variable x_3 (α)

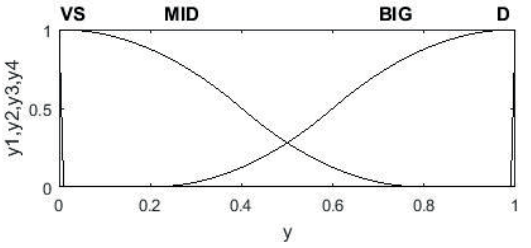

Fig. 5. Diagram of the fuzzy sets B described in the space of the output signal y

The general network structure of the proposed system is presented in Fig. 6.

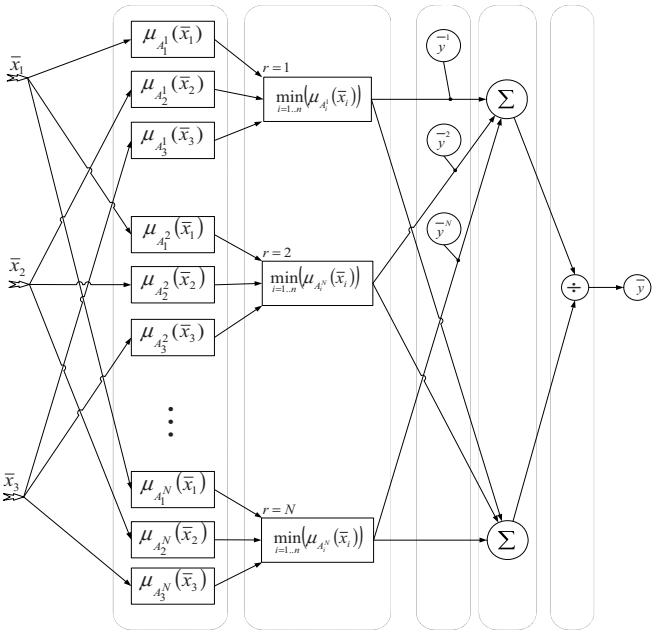

Fig. 6. Model of the general network structure of the neuro-fuzzy system using Mamdani inference method.

MOST WIEDZY Downloaded from mostwiedzy.pl

Signals introduced to inputs of the system are read from the space of fuzzy sets.

A value obtained this way is expressed in the form of the membership degree $\mu_{A_i^r}(\bar{x}_i)$. Basing the system's architecture on the classical neuro-fuzzy model of Mamdani [2, 6, 8, 15], one is able to use the minimum inference rule (5):

$$\mu_{R^r}\left(\mu_{A_i^r}(\bar{x}_i)\right) = \min_{i=1..n} \mu_{A_i^r}(\bar{x}_i) \tag{5}$$

In such case the output signal of the system is expressed by the relation (6). This operation is executed by the block "Deffuzzyfication" (Fig. 1).

$$\bar{y} = \frac{\sum_{r=1}^{N} \bar{y}^r \min_{i=1..n} \mu_{A_i^r}(\bar{x}_i)}{\sum_{r=1}^{N} \min_{i=1..n} \mu_{A_i^r}(\bar{x}_i)} \tag{6}$$

The designed system generates a response on whether a given situation has been more or less safe. A degree of the assesment is dependent on a value obtained from the output1 – the closer this value to 1 the more dangerous the situation.

SIMULATION TESTS AND EXAMPLE RESULTS OF OPERATION OF THE SYSTEM

The proposed system serves as a classifier. It was initiated together with experts knowledge as well as tested with the use of real data. The observed results are presented below.

INITIALIZATION OF THE SYSTEM

The worked out neuro-fuzzy system makes use of the set of 48 basic rules. They determine the space which may be presented on diagrams which illustrate dependence of output signal on particular input signals (Fig. 7 through Fig. 9).

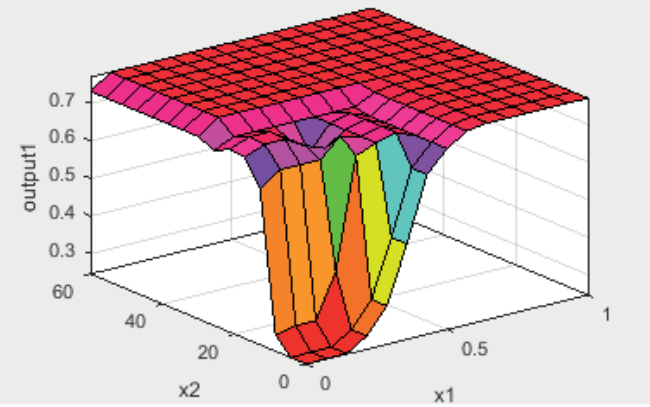

Fig. 7. Diagram of relation between values of the input variables x_1 (DDV), x_2 (V_r) and values of the output signal y from the system

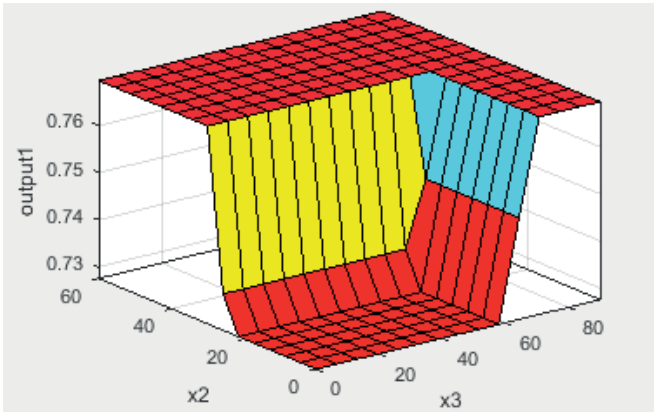

Fig. 8. Diagram of relation between values of the input variables x_2 (V_r), x_3 (α) and values of the output signal y from the system

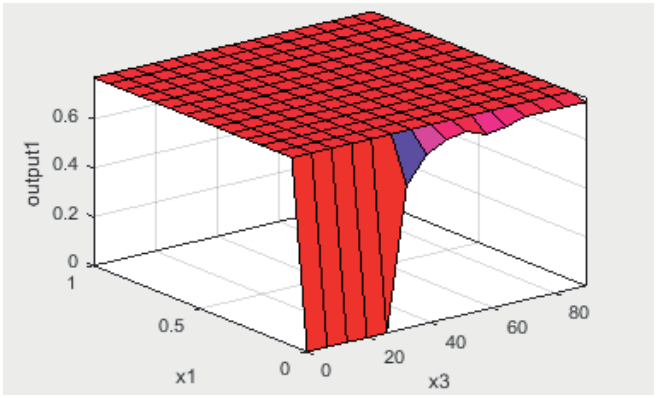

Fig. 9 Diagram of relation between values of the input variables x_1 (DDV), x_3 (α) and values of the output signal y from the system

The signal 'output1' takes values from the interval <0, 1>, while values more close to 1 indicate a greater probability of collision.

INPUT DATA

For simulation purposes there was selected a decentralized ellipse whose half-axis lengths as well as longitudinal and transverse shift of the ship relative to centre of the ellipse depend on the ship length *L* (Fig. 10). This shape is based on the today domains determined experimentally [6, 20].

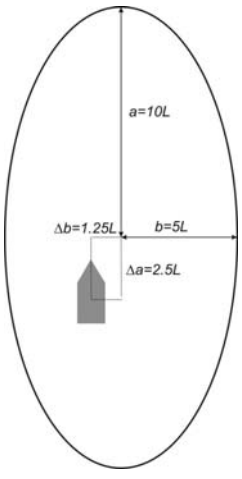

Fig. 10. Decentralized elliptical domain of the ship (L – ship's length)

MOST WIEDZY Downloaded from mostwiedzy.pl

And, as far as the data dealing with ships' encounters are taken into account, the use was made of the data available from the portal www.marinetraffic.com, because no direct access to the data from the AIS has been possible.

A part of the data was generated during direct observation of motions of ships sailing over the Baltic Sea, carried out with the use of the above mentioned portal, (Fig. 11). Selection of the ships under observation was aided by filters available in this portal.

Fig. 11. Screen dump of an example observation taken in the coastal area of Gdynia port on 2017-11-21, 14:50

EXAMPLE RESULTS OF OPERATION OF THE METHOD

In neuro-fuzzy systems, there are analyzed values obtained after defuzzyfication.

They have sharp quantities from the interval <0,1>. The proposed system performs a simple classification. A safe situation is indicated by values <0.5, while a hazardous sitution – by values ≥0.5.

The example results are given in Tab. 5 which covers values of the evaluation made by the system for selected sets of input data.

Tab. 5. Collection of example values introduced into inputs to the system together with output information and final evaluation of the situation

Nr.	DDV	Vr	α	Output co	Verdict
1	0,1	12	10	0,39	Safe
2	0,1	12	32	0,44	Safe
3	0,1	12	52	0,49	Safe
4	0,1	12	72	0,53	Near-miss
5	0,1	22	10	0,47	Safe
6	0,1	22	32	0,52	Near-miss
7	0,1	22	52	0,56	Near-miss
8	0,1	22	72	0,61	Near-miss
9	0,1	32	10	0,54	Near-miss
10	0,1	32	32	0,59	Near-miss
11	0,1	32	52	0,64	Near-miss
12	0,1	32	72	0,68	Near-miss
13	0,25	5	10	0,41	Safe
14	0,25	5	32	0,46	Safe
15	0,25	5	52	0,51	Near-miss
16	0,25	5	72	0,55	Near-miss
17	0,25	12	10	0,47	Safe
18	0,25	12	32	0,51	Near-miss
19	0,25	12	52	0,56	Near-miss
20	0,25	12	72	0,60	Near-miss
21	0,25	22	10	0,54	Near-miss
22	0,25	22	32	0,59	Near-miss
23	0,25	22	52	0,63	Near-miss
24	0,25	22	72	0,68	Near-miss
25	0,25	32	10	0,62	Near-miss
26	0,25	32	32	0,66	Near-miss
27	0,25	32	52	0,71	Near-miss
28	0,25	32	72	0,75	Near-miss
29	0,32	5	10	0,44	Safe
30	0,32	5	32	0,48	Safe
31	0,32	5	52	0,53	Near-miss
32	0,32	5	72	0,57	Near-miss
33	0,32	12	10	0,49	Safe
34	0,32	12	32	0,54	Near-miss
35	0,32	12	52	0,58	Near-miss
36	0,32	12	72	0,63	Near-miss
37	0,42	5	10	0,46	Safe
38	0,42	5	32	0,51	Near-miss
39	0,42	5	52	0,56	Near-miss
40	0,42	5	72	0,60	Near-miss

While analyzing the results presented in Tab. 5 one may observe an impact of all the three variables on final evaluation of the situation of two ships encounter. In compliance with the initial assumptions, the greatest impact has the variable *DDV* which expresses a degree of violation of the domain, the next are: the relative speed and difference in courses. Worth stressing, that even a significant violation of the domain (value of 0.42 in the row No. 37) does not determine verdict on the situation to be near-miss if only it is accompanied with a low relative speed (5 kn), and the courses are close to parallel (10 deg difference). On the other hand, even a rather small violation of the domain (value of 0.1) leads to classification of the situation to be dangerous at the simultaneous large relative speed (32 kn in the rows No. 9 through12) or at the courses close to perpendicular (72 deg in the row No. 4). The obtained results correctly reflect the assumed set of estimation criteria. However it's worth stressing that the set is subjective and both the choice of domain dimensions and theshold values for fuzzy rules should be adjusted to a specifity of ship traffic on a given water area and respective expectations of navigators.

MOST WIEDZY Downloaded from mostwiedzy.pl

SUMMARY AND DEVELOPMENT PROSPECTS

In this article there was proposed a novel method for detection of near-miss situations, (i.e such where a collision has not yet happened, but a degree of risk has been much higher than average). The method makes use of three input parameters: a collision risk measure based on the ship's domain, DDV, relative speed as well as difference in courses of both ships. The parameters are then transformed by means of a neuro-fuzzy classifier which feeds back output information – a collision risk degree for a given encounter of ships.

The proposed system applies initial rules whose set can be updated or extended.

The planned future extension of the system will contain verification of the rules by a team of experts, learning the system as well as its extension with procedures for taking up and processing a large amount of real data from the AIS.

The method for detection of collision hazardous situations, which is implemented in the system, may be also used in the systems for determining anticollision maneouvres [8, 9, 10, 16], navigator's decision supporting systems [12, 17, 19] or in the systems for ship's route planning and monitoring [18]. These authors conduct preliminary research on the above mentioned issues.

BIBLIOGRAPHY

1. Chai, Y., L. Jia, Z. Zhang: Mamdani Model based Adaptive Neural Fuzzy Inference System and its Application.
2. Cpałka, K.: Design of Interpretable Fuzzy Systems, Springer, 2017.
3. Cpałka, K., L. Rutkowski: On Designing of Flexible Neuro-Fuzzy Systems for Classification.
4. Driankov, D., H. Hellendoorn, M. Reinfrank: An Introduction to Fuzzy Control, Springer Berlin Heidelberg, 1996.
5. Goerlandt, F., J. Montewka: Maritime transportation risk analysis: Review and analysis in light of some foundational issues, Reliab. Eng. Syst. Saf. 138 (2015), pp. 115–134.
6. Hansen, M.G., T.K. Jensen, F. Ennemark: Empirical Ship Domain based on AIS Data, (2013), pp. 931–940.
7. van Iperen, E.: Classifying ship encounters to monitor traffic safety on the North Sea from AIS data, TransNav - Int. J. Mar. Navig. Saf. Sea Transp. 9 (2015), pp. 53–60.
8. Lazarowska, A.: Multi-criteria ACO-based Algorithm for Ship's Trajectory Planning, TransNav, Int. J. Mar. Navig. Saf. Sea Transp. 11 (2017), pp. 31–36.
9. Lisowski, J.: Game control methods in avoidance of ships collisions, Polish Marit. Res. 19 (2012), pp. 3–10.
10. Lisowski, J., A. Lazarowska: The radar data transmission to computer support system of ship safety, Solid State Phenom. 196 (2013), pp. 95–101.
11. Nowicki, R.K.: Fuzzy decision systems in issues of limited knowledge (in Polish), Akademia Oficyna Wydawnicza EXIT, 2009.
12. Pietrzykowski, Z., P. Wo, P. Borkowski: Decision Support in Collision Situations at Sea, (2017), pp. 447–464.
13. Rutkowska, D.: Neuro-Fuzzy Architectures and Hybrid Learning, Physica-Verlag HD, Heidelberg, 2002.
14. Rutkowska, D., R. Nowicki: Implication-Based Neuro-Fuzzy Architectures, Int. J. Appl. Math. Comput. Sci. 10 (2000), pp. 675–701.
15. Rutkowski, L., K. Cpalka: Flexible neuro-fuzzy systems, IEEE Trans. Neural Networks. 14 (2003), pp. 554–574.
16. Szlapczynski, R.: A new method of planning collision avoidance manoeuvres for multi-target encounter situations, J. Navig. 61 (2008).
17. Szlapczynski, R., J. Szlapczynska: Customized crossover in evolutionary sets of safe ship trajectories, Int. J. Appl. Math. Comput. Sci. 22 (2012).
18. Szłapczynska, J.: Multi-objective Weather Routing with Customised Criteria and Constraints, J. Navig. 68 (2015), pp. 338–354.
19. Szłapczyński, R., R. Smierzchalski: Supporting navigator's decisions by visualizing ship collision risk, Polish Marit. Res. 16 (2009).
20. Wang, Y., H. Chin: An Empirically-Calibrated Ship Domain as a Safety Criterion for Navigation in Confined Waters, (2015).
21. Van Westrenen, F., J. Ellerbroek: The Effect of Traffic Complexity on the Development of Near Misses on the North Sea, IEEE Trans. Syst. Man, Cybern. Syst. 47 (2017), pp. 432–440.
22. Wu, X., A.L. Mehta, V.A. Zaloom, B.N. Craig: Analysis of waterway transportation in Southeast Texas waterway based on AIS data, Ocean Eng. 121 (2016), pp. 196–209.
23. Zadeh, L.A.: The Concept of a Linguistic Variable and its Application to Approximate Reasoning-I, (1975), pp. 199–249.

MOST WIEDZY Downloaded from mostwiedzy.pl

24. Zhang, W., F. Goerlandt, P. Kujala, Y. Wang: An advanced method for detecting possible near miss ship collisions from AIS data, Ocean Eng. 124 (2016), pp. 141–156.

25. A historical review of evolutionary learning methods for Mamdani-type fuzzy rule-based systems: Designing interpretable genetic fuzzy systems, Int. J. Approx. Reason. 52 (2011) pp. 894–913.

CONTACT WITH THE AUTHORS

Rafał Szłapczyński
e-mail: rafal@pg.edu.pl

Tacjana Niksa-Rynkiewicz
e-mail: tacniksa@pg.edu.pl

Gdansk University of Technology
Faculty of Ocean Engineering and Ship Technology
11/12 Narutowicza St.
80 - 233 Gdańsk
Poland

MOST WIEDZY Downloaded from mostwiedzy.pl

POLISH MARITIME RESEARCH Special Issue 2018 S1 (97) 2018 Vol. 25; pp. 22-28
10.2478/pomr-2018-0018

THE PROPAGATION OF THE WAVES IN THE CTO S.A. TOWING TANK

Marcin Drzewiecki
CTO S.A. Ship Design and Research Centre, Poland
Gdańsk University of Technology, Poland

ABSTRACT

The paper presents the results of research focused on the wave propagation in the CTO S.A. deepwater towing tank. In the scope of paper, the wavemaker transfer function was determined for regular waves, based on the Biésel Transfer Function and further for irregular waves, based on Hasselman model of nonlinear energy transfer. The phenomena: wave damping, wave breakdown and wave reflection, were measured, analyzed and mathematically modeled. Developed mathematical models allow to calculate the impact of mentioned phenomena on the wave propagation and furthermore to calculate the wave characteristics along the whole measurement area in the CTO S.A. deepwater towing tank, based on wavemaker flap motion control.

Keywords: waves, propagation, nonlinear transfer function, towing tank

INTRODUCTION

During the hydromechanical tests with a model of the object in a sea wave, such as the tests carried out in the CTO S.A. deepwater towing tank (Fig. 1), it is crucial to obtain the spectrum of the generated wave consistent with the modeled sea wave in a reduced scale. The wave should be properly modeled along whole measurement area. The transfer function of the wavemaker and moreover the damping, breakdown and reflection phenomena, have impact on modeling the marine environment conditions.

The knowledge of the above factors is important for realization of the model tests. In the scope of this paper, mentioned factors have been analyzed. The analysis was carried out on the basis of measurements made in CTO S.A.

Fig. 1. The seakeeping tests in the CTO S.A. deepwater towing tank.

MOST WIEDZY Downloaded from mostwiedzy.pl

TOWING TANK

The CTO S.A. deepwater towing tank is a research object with 270 m length, 12 m width and 6 m depth, as shown in Fig. 2. Investigations carried out in the towing tank consist in testing the properties of objects floating freely (vessels), anchored (oil rigs) or permanently fixed to the bottom (offshore wind turbines). The tests are conducted for models of objects in a reduced scale. The models are tested in the uniform flow (simulated by motion of the carriage at constant speed) or subjected to the impact of the waves for modeling the impact of the marine environment.

WAVEMAKER

The waves corresponding to ocean waves in a reduced scale are generated by the rigid flap wavemaker with single articulation above channel bed (and below water level). The flap is an actuator with 4.15 m height and 12.00 m width, articulated 2.30 m above channel bed, as it shown in Fig. 2.

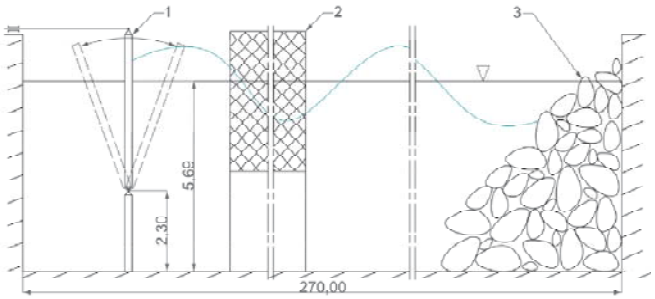

Fig. 2. Longitudinal profile of deepwater towing tank with the wavemaker (1), waveguides (2) and artificial beach (3) (dimensions are given in meters).

SURVEY OF RELATED WORKS

In 1951, F. Biésel and F. Suquet published formulas known as Biésel Transfer Functions *BTF*. The *BTF* allow to calculate the wave height in a towing tank for several types of wavemakers, also for wavemaker with rigid flap and single articulation above channel bed, like in CTO S.A. [1].

The research carried out in 1972, in the Laboratório Nacional de Engenharia Civil (Lisbon, Portugal) has shown that *BTF* is proper for regular waves. However, for irregular waves, the measured transfer function is inconsistent with theoretical *BTF*. [2] One possible reason indicated by the authors was the lack of linearity and energy losses.

In 1985, S. Hasselmann and K. Hasselmann described a mechanism of the formation of the JONSWAP spectrum and proposed a model of the nonlinear energy transfer in wind waves [3]. The model has two parameters proposed by the authors. Proper parameterization of the model allows to calculate an energy stream transferred from higher frequency bands to lower frequency bands of the wind wave spectrum.

Van Vledder in 2012 discussed the ambiguity of selection of values of the C and λ parameters [4].

In 2014 group of people from Kyushu University (Japan), carried out simulations and study for the method mentioned and for a few others methods of wave model implementation [5].

The control system of the wavemaker in the CTO S.A. deepwater towing tank was modernized in 2015 – an analog control system was replaced by a new digital control system [6]. In 2017 research was conducted on optimization of the digital control system [7].

Research described in this paper is intended to develop mentioned works to enable the prediction of wave characteristics in CTO S.A. deepwater towing tank.

OBJECTIVES AND SCOPE OF THE WORK

The objectives of research were to determine the way of wave propagation and to develop the method of prediction of the wave characteristics in the CTO S.A. deepwater towing tank. For this purpose, transfer function for the wavemaker and further the impact of the damping, breakdown and reflection were investigated. The scope of research included the measurements of the waves along whole measurement area and analysis of registered signals.

SOLUTION

MEASUREMENTS

The measurements were made along whole measurement area of the towing tank, between 1st end on the beach side and 2nd end on the wavemaker side. The 1st end is in 205 m distance from the wavemaker. The 2nd end is in 60 m distance from the wavemaker. The measurements were made during generation of the waves: regular and irregular. The regular wave is a harmonic wave. The irregular wave is a synthesis of harmonic waves corresponding to the determined spectrum. Parameters of the generated and measured waves are shown in Tab. 1.

The waves were measured by the resistance probe of the water level (Fig. 3), manufactured by CTO S.A. The resistance probe was mounted to the towing carriage in the towing tank axis, i.e. on the actual track of the models tested in waves. During wave generation, the displacement of the wavemaker flap was measured by linear displacement sensor WDS-1000-P60-SR-U manufactured by MicroEpsilon.

MOST WIEDZY Downloaded from mostwiedzy.pl

Table 1. Parameters of the generated and measured waves

No.	Type of the wave	Height of the wave HW [cm]	Frequency of the wave f [Hz]
1	regular	2.5	0.8
2	regular	2.5	0.9
3	regular	2.5	1.0
4	regular	2.5	1.1
5	regular	2.5	1.2
6	regular	5.0	0.3
7	regular	5.0	0.4
8	regular	5.0	0.5
9	regular	5.0	0.6
10	regular	5.0	0.7
11	regular	5.0	0.8
12	regular	5.0	0.9
13	regular	5.0	1.0
14	regular	5.0	1.1
15	regular	5.0	1.2
16	regular	10.0	0.3
17	regular	10.0	0.4
18	regular	10.0	0.5
19	regular	10.0	0.6
20	regular	10.0	0.7
21	regular	10.0	0.8
22	regular	10.0	0.9
23	regular	10.0	1.0
24	regular	10.0	1.1
25	regular	10.0	1.2
26	irregular	$H_{1/3}^{(*}$=9.5	$f_{01}^{(**}$=0.75
27	irregular	$H_{1/3}^{(*}$=12.9	$f_{01}^{(**}$=0.78
28	irregular	$H_{1/3}^{(*}$=14.1	$f_{01}^{(**}$=0.69

(* significant height of the irregular wave

(** average frequency of the irregular wave (corresponding to average period of the irregular wave *T01*)

Fig. 3. Resistance probe of the water level manufactured by CTO S.A.

TRANSFER FUNCTION

For rigid flap wavemaker with single articulation above channel bed, the wave height *HW* is dependent on flap displacement *a*, wave frequency *f,* water depth *h* and articulation height above channel bed *h0* [1]. The formulas representing this dependence are given as (1) and (2). The Biésel Transfer Function *BTF* is understood as the relation (3). The *BTF* for mentioned type wavemaker was experimentally checked for two types of waves – regular and irregular, in the scope consistent with Tab. 1. For this purpose, two signals were measured: the wave *HW* – measured at the 2nd end of the measurement area using resistance probe and the flap displacement *a* – measured using the displacement sensor.

$$HW = \frac{2 \cdot a}{k \cdot (h - h0)} \cdot \left[\frac{\sinh(kh) \cdot \left((h - h0) \cdot k \cdot \sinh(kh) - \cosh(kh) + \cosh(kh0) \right)}{\sinh(kh) \cdot \cosh(kh) + kh} \right] \tag{1}$$

$$k = \frac{2\pi \cdot f^2}{1.56} \tag{2}$$

$$BTF = \frac{HW}{a} \tag{3}$$

Regular waves

The BTF for regular waves in the CTO S.A. deepwater towing tank with the rigid flap wavemaker was checked. The theoretical BTF was corrected as it shown in (4). Implementation of the correction factor *Cr*=0.8 was necessary to obtain the agreement of the calculations with the results of measurements. As shown in Fig. 4, the results of the measurements are consistent with the calculated *BTFcorr* with satisfactory accuracy.

$$BTFcorr = Cr \cdot BTF \tag{4}$$

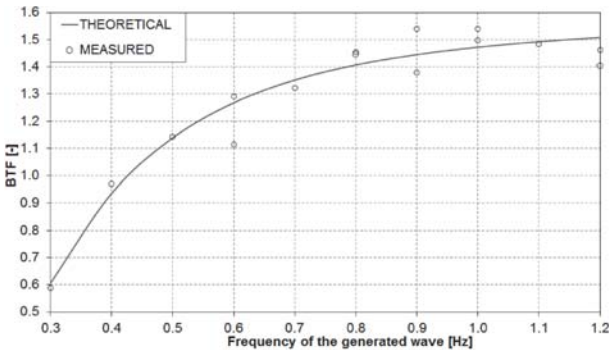

Fig. 4. The transfer function for the regular waves in CTO S.A. deepwater towing tank

Irregular waves

The transfer function for irregular waves *TF* was obtained, based on the FFT analysis of the signal *HW* and signal *a*. The signals were measured for irregular waves no. 26-28 (Tab. 1). As it shown in Fig. 5, the measured *TF* is consistent with the calculated *BTFcorr* in scope from 0.3 Hz to 0.6 Hz. For frequencies higher than 0.6-0.7 Hz, *TF* is significantly increasing and further rapidly falling below *BTFcorr* characteristic.

The rapidly falling characteristics below the theoretical transfer function has been also observed in other hydrodynamics laboratory [2]. It is mentioned there that this phenomenon may be due to lack of linearity and probably

MOST WIEDZY Downloaded from mostwiedzy.pl

caused by energy losses as effect of the variations of velocity and acceleration in irregular waves.

Other works devoted to gravity waves, like [3] and further [4] and [5], describes and proves that in the wind waves there are nonlinear interactions that cause the nonlinear energy transfer. It occurs in this way that the energy stream *Snl* is transferred from higher frequency bands to lower frequency bands of the wind wave spectrum. A similar phenomenon can occur in irregular waves generated in the towing tank. It can be seen in Fig. 5.

These papers ([3], [4], [5]) describe the physics of the phenomenon and the methods of calculation *Snl* for wind waves spectra.

The mathematical model of nonlinear energy transfer proposed in [3] is described by formula (5), where: δSnl relates to the frequency f, δSnl^{+} relates to the frequency (6) and δSnl^{-} relates to the frequency (7). Furthermore, *C* is the strength of the nonlinear interaction parameter [3] and λ is the Hasselmann's shape parameter [8].

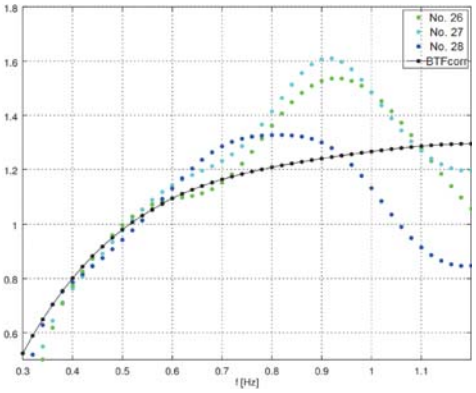

Fig. 5. The transfer functions for the irregular waves no. 26-28

$$Snl = \sum_{f=0,1Hz}^{f=1,5Hz} \begin{bmatrix} \delta Snl \\ \delta Snl^{+} \\ \delta Snl^{-} \end{bmatrix} = \begin{bmatrix} -2 \\ 1+\lambda \\ 1-\lambda \end{bmatrix} \times C \cdot g^{-4} \cdot f^{11} \cdot \left[F^2 \cdot \left(\frac{F_{+}}{(1+\lambda)^4} + \frac{F_{-}}{(1-\lambda)^4} \right) - 2 \cdot \frac{F \cdot F_{+} \cdot F_{-}}{\left(1-\lambda^2\right)^4} \right] \quad (5)$$

$$f^{+} = f \cdot (1+\lambda) \quad (6)$$

$$f^{-} = f \cdot (1-\lambda) \quad (7)$$

Values of mentioned parameters were proposed as λ=0.25 and *C*=3×106. The values have been chosen empirically as optimal. Another proposition was given as λ=0.15 and *C*=3.75×105 [4].

The ambiguity of selecting the parameters may indicate necessity of individual optimization for given towing tank or even for given spectrum.

Following this path, the λ and *C* were chosen individually for each spectrum of the waves no. 26-28 (Tab.1), using binary search algorithm to obtain the best compatibility of the nonlinear transfer function *NTF* (8) with the measured *TF*. Chosen parameters are listed in Tab. 2. The results are shown in Fig. 6-8. The *tnl* (9) is the time of nonlinear transfer of *Snl* at the distance *xnl*=60 m between wavemaker flap and resistance probe.

As can be seen in Fig. 6-8 the results of the calculated *NTF* are consistent with the measured *TF* with satisfactory accuracy in the frequency scope up to 1.0 Hz.

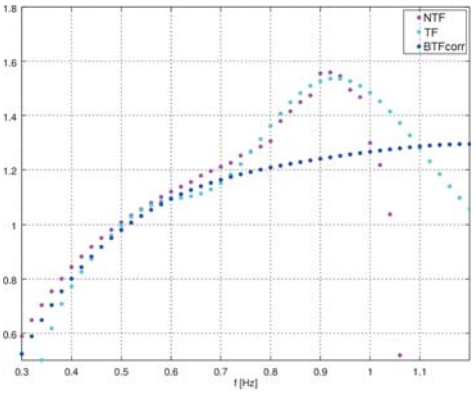

Fig. 6. The NTF for the irregular wave no. 26.

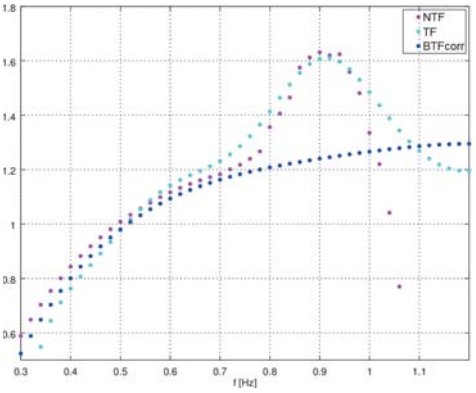

Fig. 7. The NTF for the irregular wave no. 27.

$$NTF(f) = \frac{BTFcorr(f) \cdot a(f) + Snl(f) \cdot tnl(f)}{a} \quad (8)$$

$$tnl(f) = \frac{xnl \cdot f}{1.56} \quad (9)$$

MOST WIEDZY Downloaded from mostwiedzy.pl

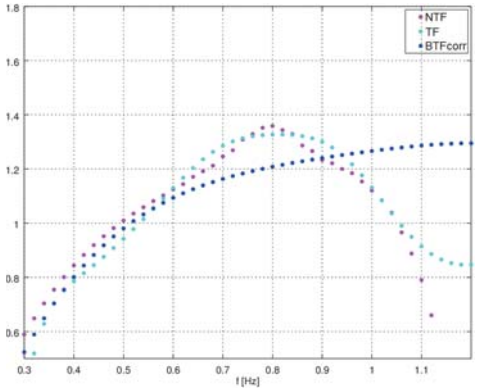

Fig. 8. The NTF for the irregular wave no. 28.

Table 2. Parameters of the nonlinear energy transfer model, chosen for the irregular waves.

No.	Strength parameter C	Shape parameter λ
26	1.4×107	0.20
27	2.4×106	0.22
28	1.5×105	0.33

WAVE DAMPING

The wave damping was investigated on the axis of the towing tank along the whole measurement area. For this purpose, the *HW* for waves no. 6-15 (Tab. 1) was measured at the 2nd end (*HW2nd* in Tab. 3) and then at the 1st end (*HW1st* in Tab. 3). The measurements were made while the towing carriage was stationary.

Relative damping factor *DF*, understood as (10) allows to calculate the *DF* as function *DF(x)*, where *x*=145 m is the distance traveled by generated wave from 2nd end to 1st end. Dependence of *DF* on f, shown in Fig. 9, was linearly approximated (11). Finally, the resulting height of the wave under damping conditions as function $HW_{DF}(HW2^{nd}, f, x)$ can be calculated as (12).

$$DF = \frac{HW2^{nd} - HW1^{st}}{HW2^{nd} \cdot x} \tag{10}$$

$$DF(f) = 0.0079 \cdot f - 0.0029 \tag{11}$$

$$HW_{DF}(HW2^{nd}, f, x) = HW2^{nd} \cdot \left[1 - \left(0.0079 \cdot f - 0.0029\right)\right] \tag{12}$$

Table 3. Relative damping factors for regular waves, based on wave height on the both ends of the measurement area.

Frequency f [Hz]	Wave height at the 2nd end HW2nd [cm]	Wave height at the 1st end HW1st [cm]	Relative damping factor DF [m^{-1}]
0.4	4.88	4.72	0.0002
0.5	4.30	4.02	0.0005
0.7	6.18	4.60	0.0017
0.9	5.62	2.72	0.0035
1.0	5.04	0.78	0.0057
1.1	4.82	0.20	0.0065
1.2	3.68	0.12	0.0065

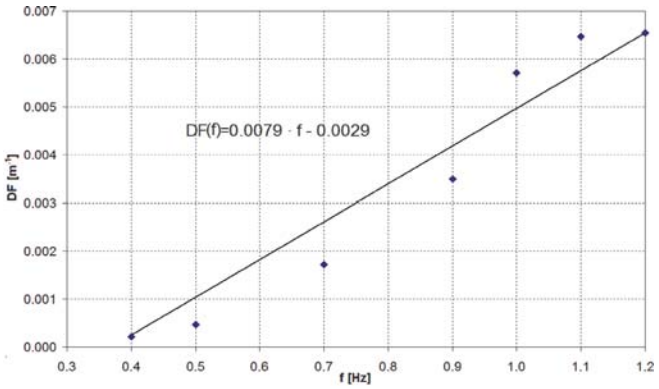

Fig. 9. The damping factor DF as a function of regular wave frequency f.

WAVE BREAKDOWN

The wave breakdown was investigated on the axis of the towing tank between 1st end and 2nd end of the measurement area. The goal of investigation was to determine the content of the power spectral density of harmonic wave at main frequency in the generated waves along whole measurement area. By the main frequency, we mean the frequency generated by the wavemaker. The *HW* was measured on five sections between 1st end and 2nd end during generation of the regular waves listed in Tab. 1. Each section had length *dx*=29 m. Based on the spectrum in frequency domain, obtained from measured *HW* using FFT, the percentage content of the power spectral density of harmonic wave at main frequency – $P_{\%}$ in the spectrum was calculated according to (13). The $HW_M(f)$ means power spectral density of the main frequency band. The $HW_{0.0\text{-}1.5Hz}(f)$ means power spectral density of the frequency bands up to 1.5 Hz. Characteristics of $P_{\%}$ as function of *x* are shown in Fig. 10. As shown, there are a three groups of regular waves due to the dynamics of $\mathbf{P}_{\%}$ changes:

- group A: the waves with frequencies from 0.3 Hz to 0.9 Hz – approximated CP1A as (14),
- group B: the waves with frequencies from 1.0 Hz to 1.1 Hz – approximated CP1B as (15),
- group C: the waves with frequencies from 1.1 Hz to 1.2 Hz – approximated CP1C as (16).

As shown in Fig. 10, the $P_{\%}$ for waves from the A group is relatively constant. For waves from B group, the $P_{\%}$

MOST WIEDZY Downloaded from mostwiedzy.pl

decreases according to S-characteristic and in midway of the measuring area falls below 50%. For waves from C group, the P% decreases according to J-characteristic and in midway of the measuring area falls to about 20%.

$$P_{\%} = \frac{HW_M(f)}{HW_{0.0-1.5\,Hz}(f)} \cdot 100\% \quad (13)$$

$$CP1A = 0.0095 \cdot x + 81.629 \quad (14)$$

$$CP1B = -5 \cdot 10^{-5} \cdot x^3 + 0.0104 \cdot x^2 - 0.1872 \cdot x + 21.424 \quad (15)$$

$$CP1C = -5 \cdot 10^{-5} \cdot x^3 - 0.0059 \cdot x^2 + 0.2065 \cdot x + 15.153 \quad (16)$$

WAVE REFLECTION

The wave reflection was investigated on the axis of the towing tank between 1st end and 2nd end of the measurement area. The goal of investigation was to determine the reflections arising from the wave reflections from the artificial beach (Fig. 1.) For this purpose, two signals were measured: *HW* and velocity of the driving towing carriage *V*. The towing carriage was driven from the beach to the wavemaker.

The Doppler effect for measured waves, when towing carriage was driven, allows to extract the mean height of the generated waves *HWg* and the mean height of the reflected waves *HWr* from the wave spectrum in frequency domain. The frequency bands were appropriately shifted depending on measured *V*.

The mean reflection coefficient R, understood as (17), calculated for measured *HWg* and HWr, is listed in Tab. 4. The numbers in the first column of Tab. 4 are consistent with Tab. 1.

Characteristic of *R* as function of f is shown in Fig. 11. As shown, R ranges from below 10% up to 25%, depending on the *f*. This dependency was approximated as (18).

Table 4. Reflection coefficient based on generated and reflected waves.

No.	Height of the generated wave *HWg* [cm]	Height of the reflected wave *HWr* [cm]	Reflection coefficient *R* [-]
1	3.88	0.94	0.24
2	3.56	0.54	0.15
3	2.72	0.58	0.21
4	2.34	0.52	0.22
5	1.7	0.32	0.19
8	4.44	0.4	0.09
9	4.7	0.74	0.16
10	4.44	0.68	0.15
11	4.76	1.18	0.25
12	4.36	0.66	0.15
13	3.16	0.64	0.20
14	2.12	0.54	0.25
18	8.82	0.66	0.07
19	9.4	1.32	0.14
20	9.26	0.88	0.09
21	7.64	1.08	0.14
22	4.02	0.92	0.23

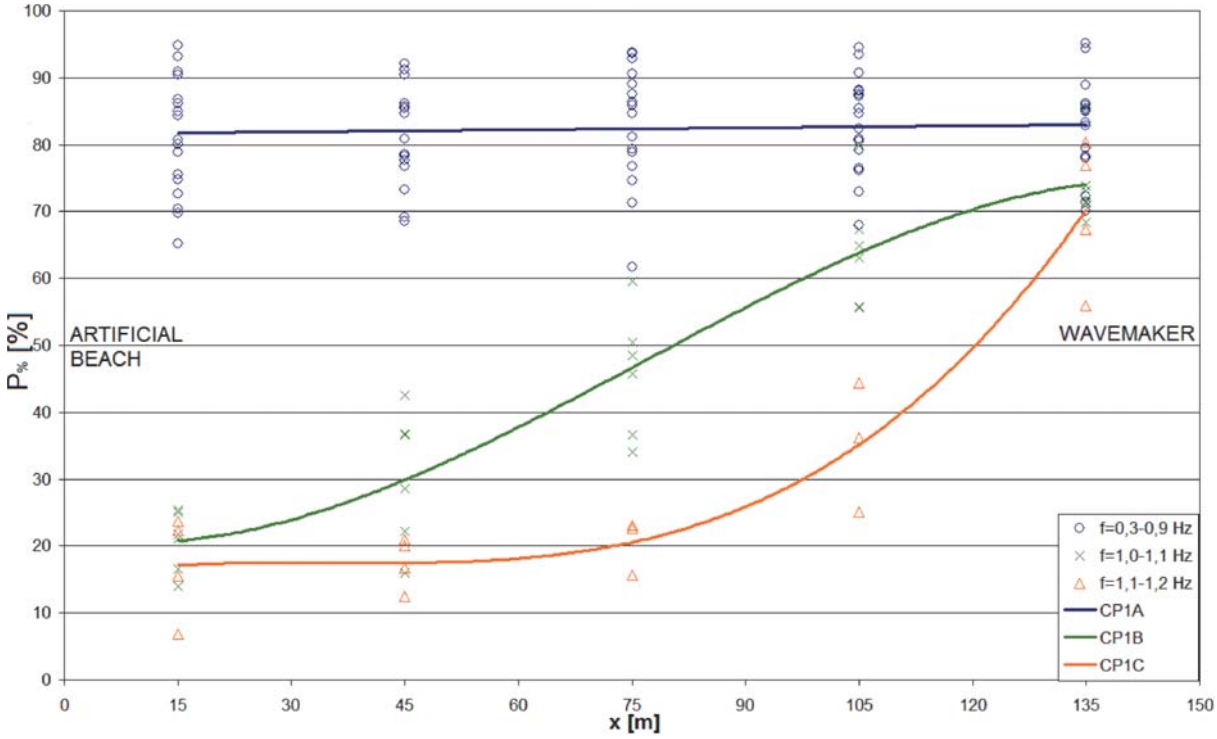

Fig. 10. The content of the main frequency P% as function of distance x.

MOST WIEDZY Downloaded from mostwiedzy.pl

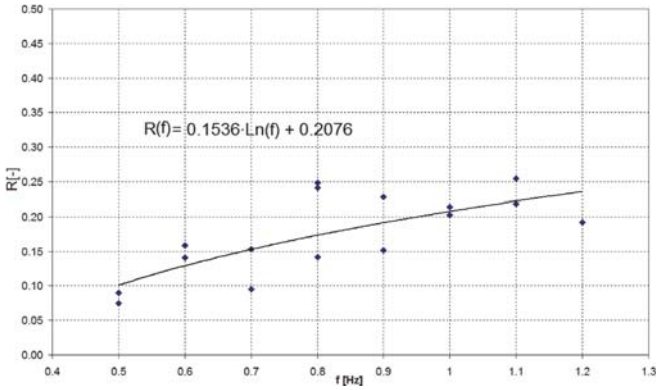

Fig. 11. The reflection coefficient for regular waves R as function of frequency f.

$$R = \frac{HWr}{HWg} \tag{17}$$

$$R(f) = 0.1536 \cdot \ln(f) + 0.2076 \tag{18}$$

CONCLUSIONS

In the range of waves listed in Tab. 1, it is valid to use *BTF* for prediction of *HW* of regular waves in CTO S.A. towing tank. Moreover, it is possible to use *BTF* and properly parameterized *Snl* model for prediction *HW* of irregular waves.

The wave damping phenomenon is dependent on the *f*. As *f* increases, *DF* will increases. It is possible to predict *HW* on given *x* and for given *f* basing on the $HW2^{nd}$.

The wave breakdown phenomenon is dependent on the *f*. $P_{\%}$ is constant along the whole measurement area for *f* up to 0.9 Hz. From *f* equal to 1.0 Hz the phenomenon is noticeable and for *f* above 1.1 Hz the phenomenon is significant and waves are rapidly collapsing.

The wave reflection phenomenon arising from reflections from the artificial beach is dependent on *f*. As *f* increases from 0.5 Hz to 1.2 Hz, *R* increases from about 10% to 25%.

Using the developed models of the phenomena: wave damping, wave breakdown, wave reflection, nonlinear energy transfer and the transfer function, it will possible to predict how the wave will propagate along the measurement area in the CTO S.A. towing tank, basing on wavemaker flap motion control.

Finally, hitherto the wavemaker control system will be developed in CTO S.A. to the adaptive wave control system.

REFERENCES

1. F. Biésel and F. Suquet, "Les appareiIs générateurs de houle en laboratoire", La Houille Blanche, no. 2, pp. 161-163, 1951.

2. C. Campos, F. Silveira and M. Mendes, "WAVES INDUCED BY NON-PERMANENT PADDLE MOVEMENTS", Coastal Engineering Proceedings, vol. 13, pp. 707-722, 1972.

3. S. Hasselmann, K. Hasselmann, J. Allender and T. Barnett, "Computations and Parametrizations of the Nonlinear Energy Transfer in a Gravity-Wave Spectrum. Part II: Parametrizations of the Nonlinear Energy Transfer for Application in Wave Models", JOURNAL OF PHYSICAL OCEANOGRAPHY, vol. 15, 1985.

4. G. van Vledder, "Efficient algorithms for non-linear four-wave interactions", ECMWF Workshop on Ocean Waves, 25-27 June 2012.

5. N. Hashimoto, F. Suciaty, M. Yamashiro, M. Yokota and M. Kodama, "Numerical study on frequency downshift of gravity wave spectra in deep and intermediate water depths due to nonlinear energy transfer", Coastal Engineering, pp. 1-13, 2014.

6. M. Drzewiecki, „Digital Control System of the Wavemaker in the Towing Tank", AUTOMATYKA, ELEKTRYKA, ZAKŁÓCENIA, vol. 7, no. 4, pp. 138-146, 2016.

7. M. Drzewiecki, „Modelling, Simulation and Optimization of the Wavemaker in a Towing Tank", Springer, XIX Polish Control Conference post-conference materials, 2017.

8. The SWAMP group, "Ocean Wave Modeling", Springer Science+Business Media, p. 225, 1985.

ACKNOWLEDGEMENT

The research was financed by the Ministry of Science and Higher Education of the Republic of Poland, earmarked for the statutory activity of CTO S.A. Ship Design and Research Centre.

CONTACT WITH THE AUTHOR

Marcin Drzewiecki
e-mail: marcin.drzewiecki@pg.edu.pl

Gdańsk University of Technology
11/12 Narutowicza St.
80 - 233 Gdańsk
Poland

MOST WIEDZY Downloaded from mostwiedzy.pl

POLISH MARITIME RESEARCH Special Issue 2018 S1 (97) 2018 Vol. 25; pp. 29-35
10.2478/pomr-2018-0019

IMPACT PRESSURE DISTRIBUTION ON A MONOPILE STRUCTURE EXCITED BY IRREGULAR BREAKING WAVE

Duje Veic
Wojciech Sulisz
Institute of Hydro-Engineering, Polish Academy of Sciences, Poland

ABSTRACT

The problem of impact pressure distribution on a monopole structure excited by irregular breaking waves is investigated. The analysis is performed by applying a numerical model that combines potential flow model with a Navier-Stokes/VOF solution. The temporal pressure distribution is analysed for two breaking wave cases characterized by the significant difference in the steepness of the wave front. The peak impact pressures are observed in the region below the overturning wave jet where the pressure increases rapidly resulting in a peak value of the slamming coefficient equal to Cs=2π. The vertical load distribution provided by the derived model is more realistic than a rectangular shape distribution applied in engineering practice. This is because the vertical load distribution strongly depends on breaking wave shape and it is difficult to uniquely approximate such a load distribution by a rectangle.

Keywords: impact pressure distribution, monopile structure, breaking wave slamming process

INTRODUCTION

The monopile structure is a typical offshore wind tower foundation, which provides the most cost efficient solution for water depths from 15 to 45m. In these relatively shallow waters, storms can induce large breaking wave impact loading, which needs to be assessed during the design stage. The hydrodynamics of the breaking wave interaction with a monopile foundation is a complex 3-D phenomenon, influenced by the non-linear wave kinematics. This complex phenomenon is usually simplified by 2-D theoretical approaches e.g. Wienke (2001). However, in order to increase the knowledge on breaking wave impact, a study on the 3-D pressure distribution during the wave impact is essential.

Laboratory analyses are very challenging and often provide results with significant scatter, e.g. studies of Zhou et al. (1991) and Chan et al. (1995). Furthermore, the spatial resolution of pressure measurements is too low for complete understanding of the breaking wave impact phenomenon. In fact, the highest resolution of pressure measurement available in the literature, is every $\alpha=10^{o}$ around the span of the cylinder (Hildebrandt & Schlurmann 2011), which is not sufficient to determine vertical impact load characteristics.

In order to obtain insight into the breaking wave slamming process, a numerical model that combines potential flow model with a Navier-Stokes VOF solution is applied. The application of the numerical models enables us to evaluate impact pressures on the structure with high spatial and

MOST WIEDZY Downloaded from mostwiedzy.pl

temporal resolution. The numerical models that could be found in literature are mainly focused on the analysis of the impact force considering different stages of the breaking wave impact, e.g. Xiao and Huang (2014), Kamath et al. (2015), and Bihs et al. (2015). However, the pressure distribution during the wave impact is rarely discussed in numerical analysis. In recent study of Ghadirian et al. (2016), discussion on the impact pressure distribution was mainly related to the validation of the numerical model. More detailed discussion on the impact pressure distribution during the wave impact provide Hildebrandt & Schlurmann (2012). Both aforementioned studies on impact pressure distributions are based on analysis of one breaking wave case. Dependency between the impact pressure distribution and the shape of the breaking wave profile, according to the author's knowledge, has not been discussed so far.

This paper presents numerical analysis on temporal impact pressure distribution on a monopile structure for two breaking wave cases characterized by different shape of wave profiles. The computed impact loads on a monopile structure are presented by applying a vertical slamming coefficient distribution C_s (z). Considering a procedure applied in engineering practice, the area under the C_s (z) distribution is approximated by a rectangular-shape defined by the slamming coefficient ($C_{sr.}$) along the impact area (A). This study addresses importance of the breaking wave shape in the determination of C_{sr} and A parameters. Results from this study are compared with an approximate solution suggested by Wienke (2001).

TYPICAL DESIGN PROCEDURE

This section briefly describes the procedure for calculation of hydrodynamic loads related to the breaking wave impact on monopile structures. Typical industry standard is based on the embedded stream function wave approach, where the highest wave from irregular wave train is selected and modelled by a stream function wave theory. For a small ratio between the diameter of the monopile and the wavelength, the hydrodynamic load is usually estimated according to the well-known equation presented by Morison et al. (1950). However, in the case of breaking waves, the structure is additionally excited by the impact load, which is out of the scope of Morison's equation. For the estimation of hydrodynamic load excited by the breaking wave on a cylinder, the Morison's equation is extended with additional impact force component

$$F_{wave_breaking} = \underbrace{F_d + F_m}_{Morison} + \underbrace{F_i}_{impact} \quad (1)$$

According to the design standard of IEC (2009), the impact force is calculated from the approximate solution proposed by Wienke (2001). For calculation of the impact force F_i (t), Wienke (2001) suggested the rectangular distribution of the 2-D line forces f_i (t) along the area of the impact, as it is illustrated in Fig. 1a. The impact force F_i (t) is approximated by

$$F_i(t) = f_i(t) A_{vrtical} = f_i(t) \lambda \eta_b \quad (2)$$

where λ is the curling factor, which indicates the vertical area of the impact, or how much of the wave crest η_b is contributing to the impact force, and $f_i(t)$ is 2-D line-force (Fig. 1). The formula for the 2-D line-force $f_i(t)$ is

$$f_i(t) = C_s(t) \rho R c_b^2 \quad (3)$$

where C_s (t) is the slamming coefficient, R is the radius of the cylinder, and c_b is the wave phase speed. Theoretical value of the slamming coefficient is presented in Fig. 1b. In this study, the slamming coefficient, which refers to the rectangular line force distribution, is described by C_{sr}. The curling factor is usually estimated semi-empirically as $F_{imax,measured/fimax}$. For the case of the plunging wave breakers, Wienke & Oumeraci (2005) and Goda et al. (1966) suggested that λ=0.4-0.6.

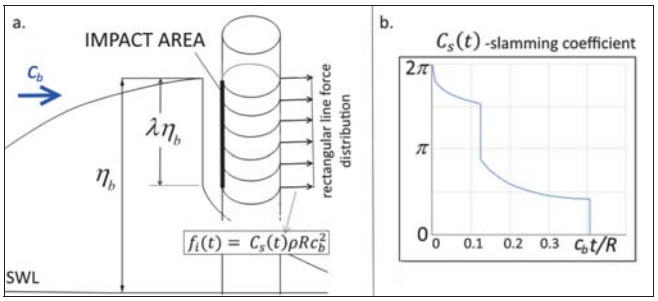

Fig. 1 Schematic view related to Wienke et al. (2001) formulation

THE SELECTED CASE STUDY

The wave loads are estimated on the bases of the storm occurring once per 50 years. Wave conditions are idealized by assuming JONSWAP energy spectrum. Parameters of the spectrum are H_s=10m, T_p=13s and γ_J=3.3. The duration of the sea storm is 3-hours.

The simulation of irregular wave propagation is conducted by applying the numerical toolbox OceanWave3D (OCW3D) developed by Engsig-Karup, et al. (2009). OCW3D is fully non-linear potential flow model which solves propagation of regular and irregular waves. OCW3D provides accurate and reliable results Paulsen (2013), Ghadirian et al. (2016 & 2017). This numerical model, however, is not suitable for solving near-breaking and breaking wave cases. In the case of breaking wave, the numerical stability is ensured by implementing an additional function which artificially reduces the energy of waves whose vertical water particle acceleration exceeds a certain limit (Paulsen 2013)

$$\frac{dw}{dt} < \gamma g \text{ with } \gamma \in [0.4:1] \quad (4)$$

In this study, the OCW3D solver is used to identify the highest wave during the 3-hour storm which would break and eventually induce the significant impact loading on a

MOST WIEDZY Downloaded from mostwiedzy.pl

structure. Numerical simulations are conducted in a 2-D domain of length 3000 m and depth d=30 m. In order to identify the occurrence of a extreme wave which have breaking wave characteristics, the simulations are conducted for two values of the breaking wave filter γ=0.9 and γ=0.4 (Fig. 2). This provides time window for the application of the Navier-Stokes VOF model.

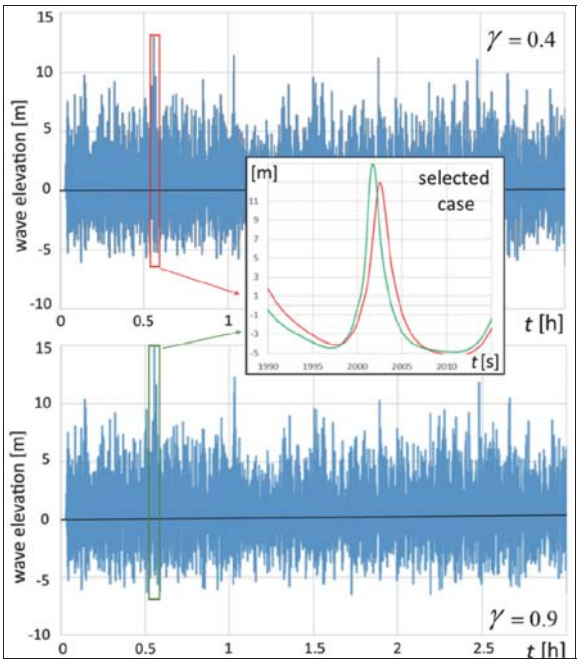

Fig. 2 Irregular wave train simulated by the numerical model

NUMERICAL MODEL

A numerical model is based on the decomposition strategy proposed by Paulsen et al. (2014), where the outer region is solved within the framework of potential flow solver OceanWave3D and inner region within the framework of the open-source computational fluid dynamics toolbox OpenFoam®.

The incompressible Navier-Stokes VOF set of equations are discretized using a finite volume approximation on generally unstructured grids. The solutions in relaxation zones are relaxed towards a solution from the potential flow model (Fig. 3). The slip condition are applied on the whole structure surface. This is because in the wave breaking zone the shear forces on a monopile structure and the pressure forces due to viscous effect are negligible, while below the wave breaking zone inertia forces dominate due to small Keulegan-Carpenter number (KC<13). Slip boundary conditions are also applied along the seabed. The time step is controlled by adaptive time stepping procedure based on Courant-Friedrichs-Lewy criterion. For all the computations, the maximum Courant number is kept below 0.2. Governing equations are solved within 2nd order discretisation scheme.

To achieve numerical convergence a very fine computational grid refinement near boundary region of the monopile structure is necessary (dx ≈0.5%D), Veic (2018). The numerical domain used for analyses in this study is constructed with nearly 4.5 million of computational cells (Fig. 3, level 4). The presented numerical model is successfully validated considering the laboratory measurements of total impact force, pressures at the front line of the monopile, and wave elevation, Veic (2018).

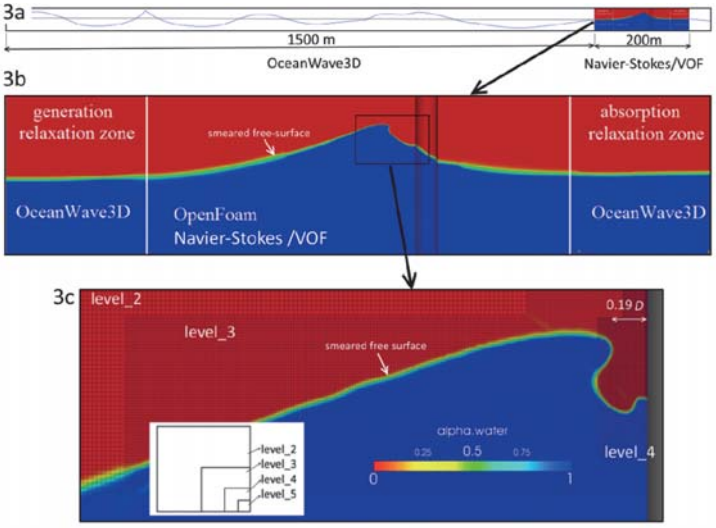

Fig. 3 Sketch of the decomposed numerical domain, water-air interface and unstructured computational grid refinement; level 5 corresponds to dx=dy=dz=0.25%D

RESULTS

The mechanism of the wave impact mainly depends on the shape of the wave front and the wave celerity at breaking (Chella, 2016). The wave profile near the location of breaking is asymmetric and characterized by the steep wave front. Breaking waves with the steeper front interacts with the structure in a larger area of the impact and the curling factor is larger.

In the scope of this paper two breaking wave cases are analysed, which are characterized by significant difference in the shape of the wave profile. The case 1 refers to irregular wave breaks over a flat seabed (Fig. 2). The case 2 refers to the identical irregular wave train as in the case 1, however propagating over the slopped seabed. For this case wave breaks at the water depth of 15m. Breaking wave profiles are presented in Fig. 4 and corresponding wave parameters are defined in Table 1.

Tab. 1 The asymmetric parameters of the breaking wave profile

	H	ηb	ε	δ	bed-type	depth
	[m]	[m]	[/]	[/]	[/]	[m]
1	15.9	12.8	0.55	0.28	flat	30
2	15.7	9.9	2.43	0.18	slope (1:10)	15

MOST WIEDZY Downloaded from mostwiedzy.pl

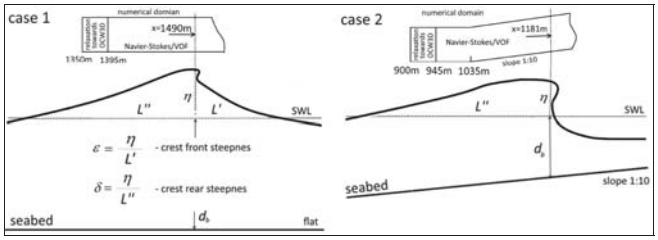

Fig. 4. The breaking wave shapes with corresponding wave asymmetric parameters

In the studies of Wienke et al. (2001) and Chan et al. (1995), the maximum impact force is identified for the stage when wave breaks slightly before the structure. In such scenario, the breaker tongue hits the cylinder just below the wave crest level. This stage of the breaking wave impact is analysed in this study. The length of the overturning wave jet before impact on the structure is l_1=0.13R and l_2=0.26R for the case 1 and the case 2, respectively (Fig. 5).

Velocity distribution in the overturning wave crest for the aforementioned braking wave stage is shown in Fig. 5. When the water particle velocity exceeds the wave celerity, the wave crest propagates forward in the form of an overturning jet. In this study, the breaking wave celerity is identified as the horizontal particle velocity at the toe of the overturning jet (Fig. 5). Approaching the shallow water, the wave height and the particle velocity at the wave crest increase while the wave length and wave celerity decrease. Therefore, the breaking wave celerity for the case 1 is higher than for the case 2. The breaking wave celerity for the case 1 is c_{b1}≈17.4 m/s while for the case 2 is c_{b2}≈16.77 m/s.

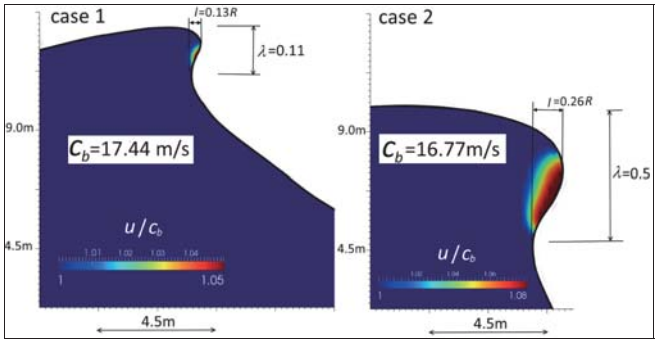

Fig. 5 Wave kinematics for the overturning wave crest, approximation of the overturning wave crest length (l) and the vertical impact area (λ)

The hydrodynamic forces are computed for the monopile with the uniform diameter of 7.2m (Fig. 6). The results show that the magnitude of impact force is higher than the magnitude of non-impact force in both analysed cases. In the case 1 wave kinematics is well approximated by the stream function wave theory, so the Morison's equation provides good approximation for the non-impact part of the force. In the case 2 wave elevation is very asymmetric and beyond the scope of the stream function wave theory. The results show that the crest height in the case 1 is 25% higher than in the case 2, while the impact area on the structure is much higher in the second case. The curling factor is estimated from the toe of the overturning jet to the wave crest height (Fig. 5). The curling factor for the case 1 is λ_1=0.14 while for the case 2 is λ_2=0.5. The impact force is identified from the moment when dynamic pressure on the structure in the impact area exceeds p=0.5ρc_b^2. The analysis shows that the magnitude of the computed impact force for the case 2 is 30% higher than for the case 1 (Fig. 6).

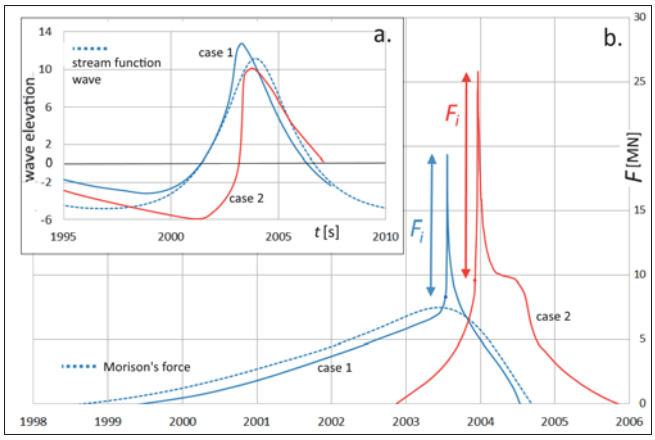

Fig. 6 Wave elevation (a) and hydrodynamic load on the monopile structure (b)

The maximum impact force is normalized by assuming the rectangular impact load distribution along the impact area (Fig. 1), $C_{sr}=F_{imax}/\rho\eta_b\lambda R c_b^2$. The corresponding slamming coefficient for the case 1 is C_{sr1}=1.8π while for the case 2 is C_{sr2}=π. The theoretical slamming coefficient proposed by Wienke (2001) is C_{sr}=2π. Figure Fig. 7 shows comparison between computed impact forces and the results of an approximate solution of Wienke (2001). In addition to the differences in the magnitude of impact force, the temporal characteristic of the impact force are also different in both approaches. The rise phase of the impact force, defined by the rise time (t_{Fi}), is out of the scope of Wienke solution. In the case 1 the peak of computed impact force is comparable to the Wienke approximation, however, the decay of the computed impact signal part is several times faster than in Wienke approximation. The effects of presented differences on the structure response is a matter for discussion for structural analysis, which is out of the scope of this paper.

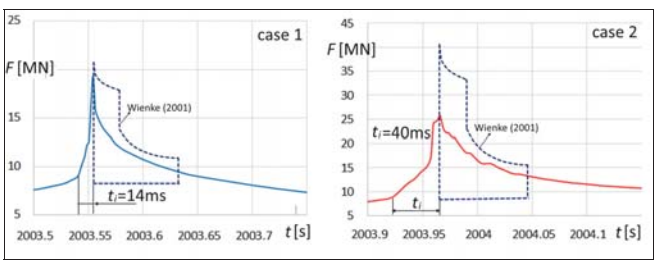

Fig. 7 Comparison between the computed impact force and analytically calculated according Wienke (2001)

MOST WIEDZY Downloaded from mostwiedzy.pl

In order to better understand the mechanism of the wave impact on the structure, a temporal impact pressure distribution on the structure is investigated. The impact pressure distribution for different moments of wave impact is presented in snapshots of Fig. 8. The pressure is normalized by ρc_b^2. The presented snapshots t_{a1} and t_{a2} refers to the initial stage of wave impact. The initial stage of impact for the case 1 is the result of the interaction between the breaking wave tongue and the wave run up on the structure. The observed peak pressure is in the range of $2\rho c_b^2$. The initial stage of the impact for the case 2 is the result of the interaction between the breaking wave tongue and the structure. The observed peak pressure is in the range of $5\rho c_b^2$.

The presented snapshots t_{b1} and t_{b2} corresponds to the time between the initial stage of the impact and the time of the peak impact force. The snapshot t_{b1} shows beginning of the interaction between the breaking wave tongue and the structure. The observed peak pressure is in the range of $5\rho c_b^2$, the same as for the snapshot t_{a2}. The snapshot t_{b2} shows the interaction of the breaking wave tongue with the structure at the higher azimuth angles. Because of the higher angle of attack between the propagating overturning wave crest and the structure, impact pressures around the span of the structure are lower, and are in the range of $3\rho c_b^2$. At the equivalent moment, the impact pressures at the front line of the structure are in a decay phase, and are in the range of ρc_b^2.

The presented plots t_{c1} and t_{c2}, as well as the plots t_{d1} and t_{d2}, corresponds to the time around the peak of the impact force. Higher impact pressures are observed for t_c, while for t_d a higher impact area is observed which results in similar magnitude of the impact force. The maximum impact pressures on the structure are observed in the region below the overturning wave jet, where overturning wave jet meets the wave run-up. At the selected moments t_{c1} and t_{c2}, the peak impact pressures are in the range of $20\rho c_b^2$ and $14\rho c_b^2$, respectively, which are of the same order of magnitude as observed in laboratory study of Zhou et al. (1991) and Chan et al. (1995). When the breaking wave tongue hits the structure, the impact energy dissipates. Majority of the impact energy is transformed into the kinetic energy of water jets, which are generated in all directions. The speed of water jets is several time faster than the speed of the wave propagation. When high speed

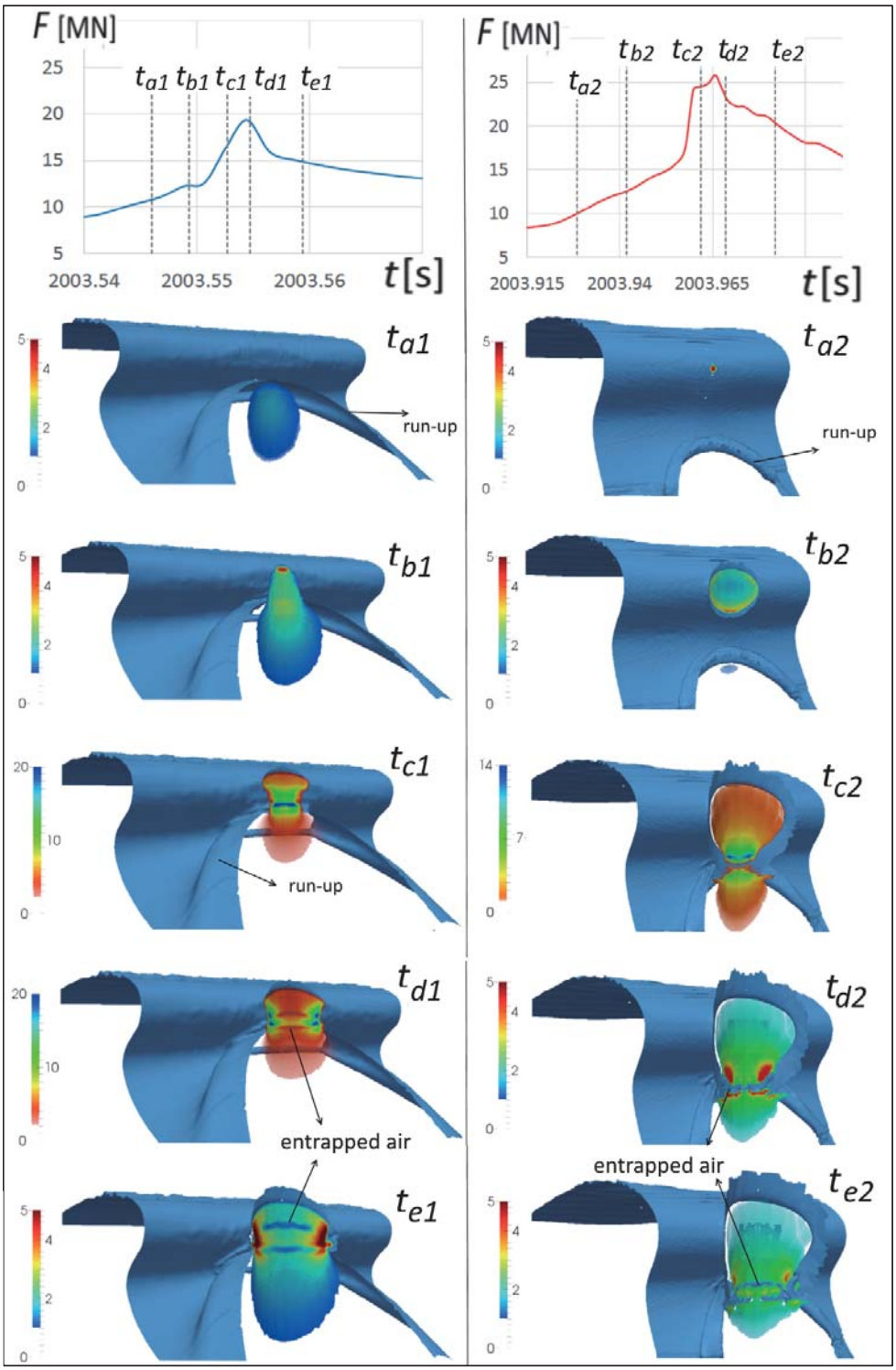

Fig. 8 Temporal dynamic pressure distribution during the selected moments of the wave impact

MOST WIEDZY Downloaded from mostwiedzy.pl

water jets interacts with the wave run-up on the structure the impact energy dissipation is significantly reduced due to the fact that generation of water-jets is limited. This is the region of the highest impact pressure.

The distribution of the load is determined by integrating the pressure around the strips of the monopile structure. The vertical distribution of the load and the corresponding slamming coefficient can be obtained by dividing the monopile structure into small strips (dz=90mm), integrating pressure over the each strip, subtracting the non-impact part of the force, and normalizing calculated strip forces by $\rho R c_b^2 dz$. The vertical distribution of the slamming coefficient is presented in Fig. 9. The peak slamming coefficients are detected in the zone of the highest pressure area, as it was presented in Fig. 8. The peak slamming coefficient is $C_s=2\pi$ for both analysed cases. Away from the peak region, slamming coefficient decays rapidly. The area of the impact load on the structure is significantly higher than the impact area which is usually defined by the curling factor.

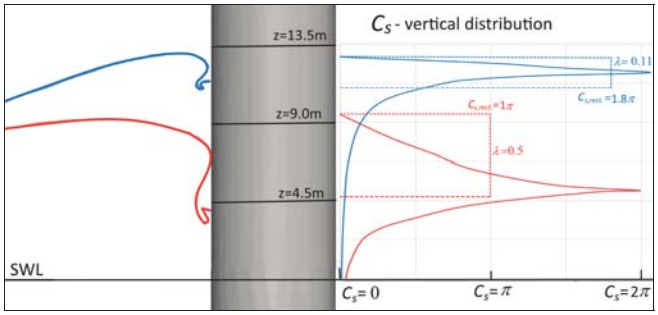

Fig. 9 The slamming coefficient and corresponding area of rectangular distribution defined by C_{sr} and λ

The engineering practice approximates the area under the vertical slamming coefficient by a rectangle (Fig. 9). The problem is that C_{sr} and λ values are not uniquely defined in the literature. This is illustrated in Fig. 9 which shows that by assuming geometrically defined parameter λ (Fig. 5), C_{sr} is a function of the wave shape. This leads to non unique and confusing results.

Additional analyses indicate that C_s-vertical distribution for breaking waves characterized by the parameter of the crest front steepness (ε) in the range of 0.55 (case 1) to 2.43 (case 2), fits into the boundaries between two curves presented in Fig. 10. Therefore, the focus of the future work is to identify the unique C_s(t)-vertical characteristics, which would present the best approximation for analysed ε-range. The derived model enable us to determine such a distribution for engineering applications which confirm preliminary results. However, more studies are required to derive more precise results.

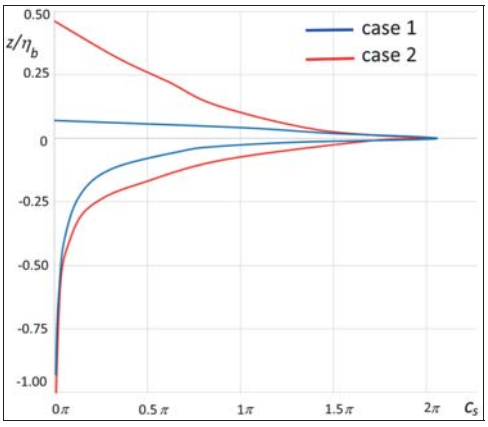

Fig. 10 The vertical slamming coefficient for the normalized vertical position (zero ordinate corresponds to the vertical location of the highest impact pressures)

CONCLUSIONS

The problem of the impact of irregular breaking waves on a monopole structure is investigated. The numerical model, which provides high spatial and temporal pressure distribution on the monopile structure arising from wave impact, is derived. The temporal pressure distribution is analysed for two breaking wave cases characterized by significant differences in the steepness of the wave front. The analysis focuses on the stage of wave impact for which the overturning wave jet hits the structure just below the wave crest level.

The results show a similar mechanism of the breaking wave impact on a structure in both impact cases. The peak impact pressures is detected in the region below the overturning jet, where the overturning wave jet meets the wave run-up on a structure. The impact pressures in this region are more than 4 times higher in comparisons with the pressures at the beginning of the wave impact when the tongue of the overturning jet hits the structure.

The analysis shows that the value of the peak slamming coefficient is approximately equal to $C_s=2\pi$. Away from the peak region, slamming coefficient decays rapidly. The area of the impact load on the structure is significantly higher than the impact area defined by the curling factor.

A rectangular distribution of loads applied in engineering practice to approximate the maximum impact force results in the non-unique outcome. This is because the parameters, which defined the rectangular distribution, depend on breaking wave shape which changes from case to case and it is difficult to define them unequally beforehand.

ACKNOWLEDGMENT

A part of this work was carried out in the framework of MareWint project under research area FP7-PEOPLE-2012-ITN Marie-Curie Action: "+Initial Training Networks" conducted in CTO, Gdansk, Poland.

MOST WIEDZY Downloaded from mostwiedzy.pl

REFERENCES

1. Bihs, H., Kamath, A., Alagan Chella, M., & Arntsen, Ø. A. (2016). Breaking-Wave Interaction with Tandem Cylinders under Different Impact Scenarios. Journal of Waterway, Port, Coastal, and Ocean Engineering, 04016005.

2. Chan, E. S., Cheong, H. F., & Tan, B. C. (1995). Laboratory study of plunging wave impacts on vertical cylinders. Coastal Engineering, 25(1), 87-107.

3. Chella M.A. (2016). Breaking Wave Characteristic and Breaking Wave Forces on Slender Cylinders, Ph.D. at NTNU

4. Engsig-Karup, A. P., Bingham, H. B., & Lindberg, O. (2009). An efficient flexible-order model for 3D nonlinear water waves. Journal of computational physics, 228(6), 2100-2118.

5. Ghadirian, A., Bredmose, H., & Dixen, M. (2016, September). Breaking phase focused wave group loads on offshore wind turbine monopiles. In Journal of Physics: Conference Series (Vol. 753, No. 9, p. 092004). IOP Publishing.

6. Goda, Y., S. Haranaka, and M. Kitahata (1966). Study of impulsive breaking wave forces on piles. Report Port and Harbour Technical Research Institute 6.5, 1-30

7. Hildebrandt, A., & Schlurmann, T. (2012). Breaking Wave Kinematics, local Pressures and Forces on a Tripod Support Structure. In Proceedings of the Coastal Engineering Conference, No. 33

8. IEC (2009), International Electrotechnical Commission, IEC 61400-3, Wind Turbines, Part 3.

9. Kamath, A., Chella, M. A., Bihs, H., & Arntsen, Ø. A. (2015). Breaking Wave Interaction with a Vertical Cylinder and the Effect of Breaker Location. CFD based Investigation of Wave-Structure Interaction and Hydrodynamics of an Oscillating Water Column Device, 171.

10. Morison, J. R., Johnson, J. W., & Schaaf, S. A. (1950). The force exerted by surface waves on piles. Journal of Petroleum Technology, 2(05), 149-154.

11. Paulsen (2013), Efficient computations of wave loads on offshore structures, PhD thesis, DTU –Department of Mechanical Engineering

12. Paulsen, B. T., Bredmose, H., & Bingham, H. B. (2014). An efficient domain decomposition strategy for wave loads on surface piercing circular cylinders. Coastal Engineering, 86, 57-76.

13. Veic D (2018), Effect of the Breaking Wave shape on the Temporal and Spatial Pressure Distribution around a Monopile Support Structure, Ph.D.

14. Wienke, J. (2001). Druckschlagbelastung auf schlanke zylindrische Bauwerke durch brechende Wellen. Technical University of Braunschweig, Germany.10

15. Wienke, J., & Oumeraci, H. (2005). Breaking wave impact force on a vertical and inclined slender pile—theoretical and large-scale model investigations. Coastal Engineering, 52(5), 435-462.

16. Xiao, H., & Huang, W. (2014). Three-dimensional numerical modeling of solitary wave breaking and force on a cylinder pile in a coastal surf zone. Journal of Engineering Mechanics, 141(8), A4014001.

17. Zhou, D., Chan, E. S., & Melville, W. K. (1991). Wave impact pressures on vertical cylinders. Applied Ocean Research, 13(5), 220-234.

CONTACT WITH THE AUTHOR

Duje Veic
e-mail: dujeveic@ibwpan.gda.pl

Wojciech Sulisz
e-mail: sulisz@ibwpan.gda.pl

Institute of Hydro-Engineering
Polish Academy of Sciences
7 Kościerska St.
80 - 328 Gdańsk
Poland

MOST WIEDZY Downloaded from mostwiedzy.pl

POLISH MARITIME RESEARCH Special Issue 2018 S1 (97) 2018 Vol. 25; pp. 36-41
10.2478/pomr-2018-0020

NEW CONCEPT OF NUMERICAL SHIP MOTION MODELLING FOR TOTAL SHIP OPERABILITY ANALYSIS BY INTEGRATING SHIP AND ENVIRONMENT UNDER ONE OVERALL SYSTEM

Henryk Olszewski
The State University of Applied Sciences (PWSZ), Elbląg, Poland
H. Ghaemi
Gdańsk University of Technology, Poland

ABSTRACT

The paper presents a new concept of overall ship motion modelling for application to total ship operability. The delivered model is a multi-phase and includes both submerged part of ship's hull and the surrounding water as a unique body. The Discrete Finite Element Method is applied. The model is successfully examined and illustrated for a selected AHTS

Keywords: ship motion modelling, ship operability, total system

INTRODUCTION

The present analytical and numerical models of ship motions have been made so far based on a unique concept of dividing ship and environment into individual parts, modelling each of them separately and then analysing the ship motion under external forces and moments induced by wind, waves, currents or other steady or floating objects near to the ship by including hydrodynamic forces and moments generated due to ship velocity and acceleration [1-7].

In this paper, it is considered that there is only one total system which includes both the environment and ship, i.e. there is one multi-phase body with different rigid and elastic parts and its motion is modelled as a single body. The concept is simple but differs in philosophy of modelling in comparison to the present models. The model is numerical one worked out on the basis of the discrete finite elements method. The meshing is dynamic, changed at each step of simulation after linearization and varies from the dynamic meshing of today available software since the latter considers motion of boundary of the hull as a separate body. By combining the hull and environment under one total system it is possible to determine the added masses directly and identify interactions between solid and elastic elements of the system with no additional boundary conditions imposed upon the system. In practice, it means increasing the number of elements of the generated mesh and need of powerful computing facilities, but it generalizes and simplifies the model.

MOST WIEDZY Downloaded from mostwiedzy.pl

The paper illustrates a part of results of a project related to the total ship operability. The presented model and results will be used for total ship operability analysis in further steps of the project.

Ships are examples of complex mechanical systems which perform specific tasks under coupled static and dynamic loads in the form of forces and moments generated by the ship motion or enforced externally. To assess the ship total operability it is necessary to generate a total model which includes all ship's subsystems, connected elements and her environment. Today, it is a usual practice to divide such a complex floating system into subsystems and then analyse each of them individually to assess the operability of the ship and its components [14]. An example of overall ship model is presented in Fig. 1.

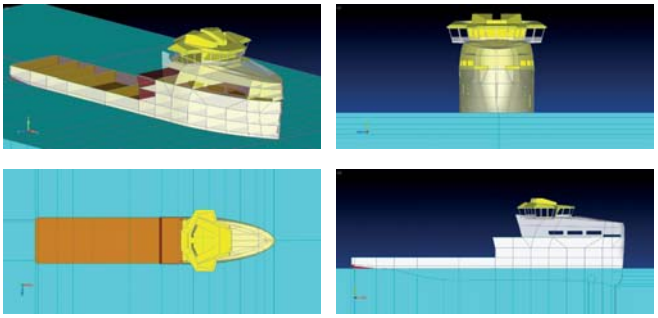

Fig. 1. Overall model of a ship at sea

The main subsystems of a ship motion model include ship's hull and its components, deck and auxiliary equipment, cargo, propulsion plant, control and navigation equipment, as well as model of waves, currents, wind and all other related environmental impacts. These subsystems may also include other complex mechanical, hydraulic, pneumatic, electrical or thermal complex elements which interact with the ship's environment. To analyse ship motion it is then necessary to work out a mathematical model which include all the subsystems and their elements. The first step of the modelling is therefore preparing a common mathematical model of ship hull and its environment. We focus now on such model in a numerical sense.

There are different methods of numerical modelling of the considered system. Solid Finite Elements Method (SFEM) [9], Deformation Finite Elements Method (DFEM) [10], Hybrid Finite Elements Method (HFEM) (a combination of SFEM and DFEM), Boundary Elements Method (BEM) and Discrete Finite Elements Method (DEM) are some examples which can be found in the literature. In practice, due to the complex dynamics of the ship's operability the interaction of individual subsystems is defined by the impact factors or coefficients [13,14]. Mutual interaction of partial subsystems can be initiated due to their different natural frequencies or those excited by enforced external inputs. Therefore, impact factors or coefficients should indicate the dependencies between the motion parameters of partial subsystems or forces which cause the motion. Generally, the impact factors depend on the motion of the subsystems.

For description of partial subsystems both linear and non-linear models are used. In case of mutual interaction of partial subsystems described by linear models, impact factors are functions of forced vibration frequencies. The frequencies coincide with forcing frequencies. The impact factors depend then on natural vibration frequencies and damping. The subsystems described by non-linear models are analyzed in time domain. Mutual interaction of the subsystems can be determined by means of impulse functions. However, to use the impact factors for description of mutual interaction of non-linear models, linearization of the models is required [14].

Development of numerical methods as well as computational capacity of computers made it possible to work out a method for total modelling the ship together with its surrounding sea environment without necessity of dividing the model into partial subsystems. Fig. 2 presents the geometrical model of water mass, in which an outline of ship underwater part can be observed.

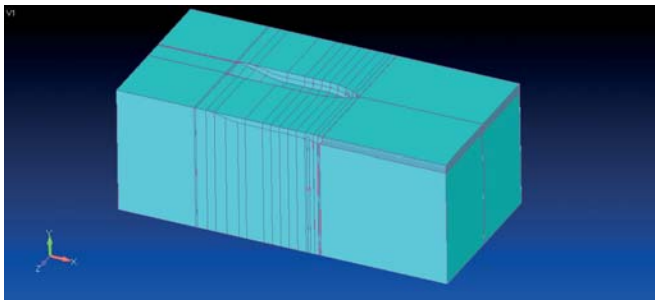

Fig. 2. Geometrical model of water mass – a part of total ship model

MODELLING

GEOMETRY

In case of the total modelling of ship operability a floating unit model may be defined at maintaining a required accuracy of mapping the ship's structure, as a result it is possible to analyze mutual interaction of between elements of hull structure, shipboard equipment and the environment. Fig. 3 shows a hull geometrical modelwith of a AHTS ship in this case.

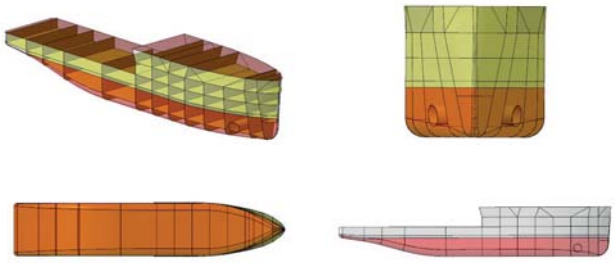

Fig. 3. Ship hull geometrical model

MOST WIEDZY Downloaded from mostwiedzy.pl

The geometrical model of superstructure of the analyzed AHTS ship is shown in Fig. 4. The geometrical models assumed in this work constitute simplified physical systems representing real construction in the range of exactly determined mutual interactions. The simplifications were so assumed as to obtain deformations of ship and its equipment which differ from real ones in the range of a permissible error.

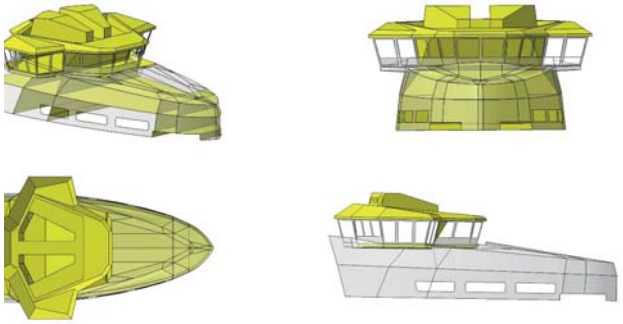

Fig. 4. Geometrical model of ship's superstructure

The ship together with its surrounding sea environment was subjected to digitization at maintaining full continuity of finite elements' mesh Fig. 5 and 6.

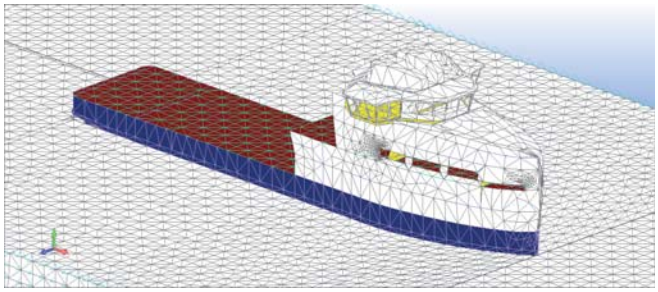

Fig. 5. Finite elements 'mesh of total ship model

MASS DISCRETE MODEL

For digitization of water mass the tetragonal elements (3D tetrahedron ones) were used. The tetragonal elements are simplexes in 3D Euclidean space, owing to this they make it possible to digitize arbitrarily complex geometrical spatial models, Fig. 6. To digitization of the complex geometrical model of the ship the triangular plate elements – simplexes in 2D Euclidean space were applied, Fig. 7.

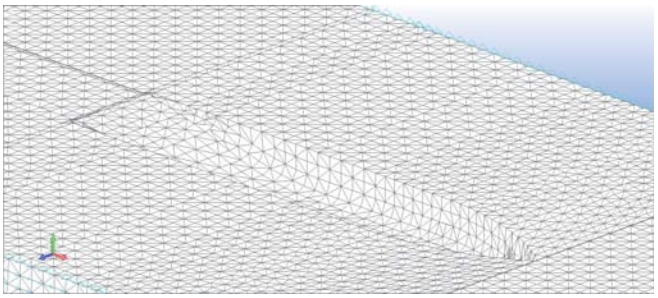

Fig. 6. Mesh of tetragonal finite elements of water with ship's hull "imprinted "in it.

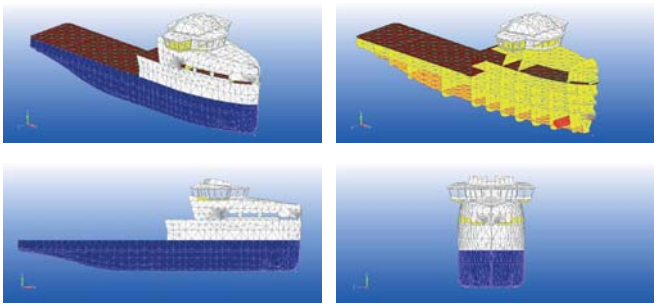

Fig. 7. Discrete model of the ship

In total modelling attention should be paid especially to making correct assumption of boundary conditions, sea environment parameters as well as parameters of ship machines and equipment.

In total modelling water waving and additional water mass result from analyzes but not assumptions as it is the case of classical modelling methods, Fig. 8.

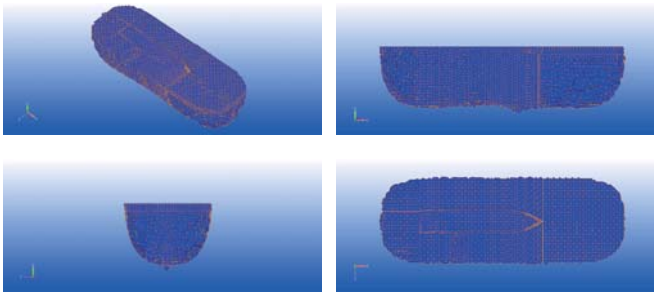

Fig. 8. Mesh of tetragonal finite elements of additional water mass

ADDED MASS

Digitization of water mass around floating unit made it possible to carry out 3D numerical calculations of water waving and analyzes of additional water mass in case when ship moves parallel to boundary of the analyzed area, Fig. 9. In the total model water mass is in direct contact with shell elements of underwater part of ship's hull therefore it is not necessary to assess assumed hydrodynamic quantities by means of e.g. the 3D Rankine SWAN (Ship Wave ANalysis)

MOST WIEDZY Downloaded from mostwiedzy.pl

method worked out by the Laboratory for Ship and Platforms Flows, MIT, [11, 12].

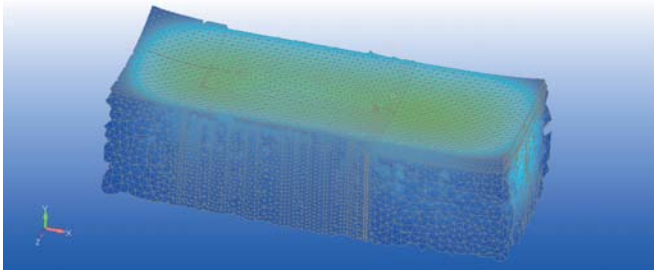

Fig. 9. Deformed mesh of finite elements of water mass around moving ship

Fig. 10 presents subsequent cross-sections of finite elements' mesh of additional water mass. Ship's movement excites displacements of fluid mass, greater in close neighbourhood of ship's hull. As the distance from the hull is growing the displacements of water are smaller and smaller, while the drop of the displacements is non- linear. It depends on distribution of physical properties of water mass as well as form of ship's hull – hence a geometrical non-linearity occurs.

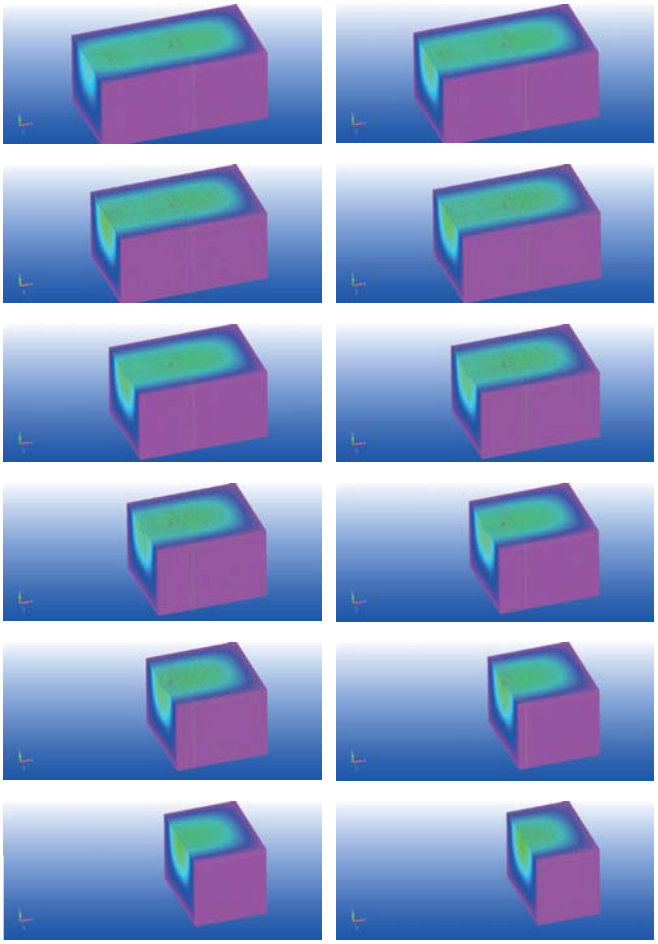

Fig. 10a. Cross-sections of additional water mass (1st part)

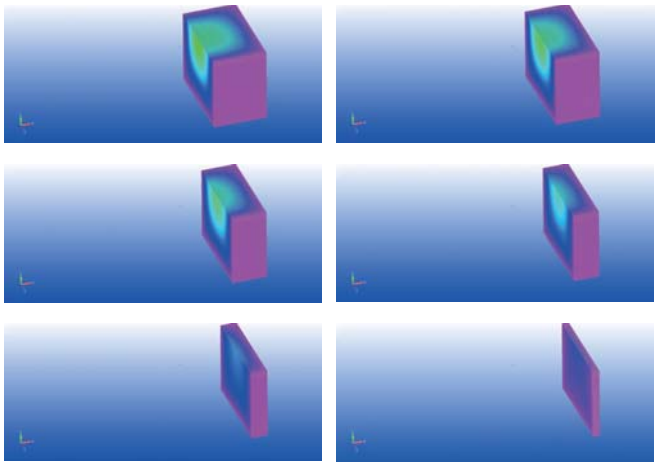

Fig. 10b. Cross-sections of additional water mass (2nd part)

DYNAMIC MESHING ADAPTATION

For modelling and discretising of the vessel body, mainly the plate elements are used , see Fig. 7. An adaptive method for generating finite elements' mesh has been applied in order to make it denser in those regions, where sudden changes in ship hull form occur. In this way the finite elements' mesh is adjusted not only for the geometry of the model but also to generate the expected deformations (as the mesh was made denser in places where the largest deformations were expected). During discretisation of geometrical model special attention has been paid to proportions of dimensions of spatial elements; and as a result their height is comparable to their breadth and length, like in the case of plate elements, where their breadth is comparable to their length.

MODEL ACCURACY

On the one hand - and calculation duration time -on the other hand- are associated with the density of finite elements' mesh [10]. The required density of finite elements' mesh of the total model depends on many factors among which the following are crucial : shape of finite elements and digitized geometrical objects, expected increase of deformations, type of loads, boundary conditions, type of applied finite elements and their shape functions , and the required accuracy. In modelling and discretising of different objects, one should pay special attention to making the mesh denser in regions where sudden change in deformations is expected. The decreasing of dimensions of finite elements and increasing their number is called *h*-adaptive method used to increase calculation accuracy. Strain, displacement and stress energy allows to estimate accuracy of the performed calculations. Accuracy of calculations conducted by means of total modelling may be also determined by the error assessment method based on adopted standards [8]. Strain state inside a deformable finite element is determined on the basis of displacements of nodes which define the element (i.e. nodal quantities of the finite element), constituting

MOST WIEDZY Downloaded from mostwiedzy.pl

arguments of shape function. In the *h*-adaptive method the order of polynomial of finite element's shape function is not changeable. Such elements are called *h*-elements. Total model of floating unit's operability comprises: ship's model together with shipboard equipment , additional water mass model as well as air mass model (not considered in this paper). For modelling and discretising of the models different types of finite elements were used. Analysis of calculation results were based on nodal quantities of finite elements' mesh. In future analyzes the increasing of calculation accuracy is planned by rising order of shape function polynomials at maintaining shape of the mesh and dimensions of used finite elements. Such method is called *p*-adaptive one , and the elements used in it - *p*-elements.

The problem of assuming correct density of the mesh in total model was not the only which appeared during digitization of the geometrical model. Mesh discontinuity occurred in connections between finite elements of different types : shell elements with solid ones, triangular elements with quadrangular ones. The above mentioned transitions of finite elements' meshes were forced by geometry of modelled ship structure or necessity of joining solid elements digitizing water mass with plate and shell elements modelling underwater part of ship's hull. On account of the complex form of ship , its decks, bulkheads and equipment it was necessary to introduce intermediate stripes of finite elements to assure mesh continuity . The intermediate stripes of elements should not be applied to model regions to be analyzed in detail as well as to such parts of the mesh in which sudden changes in stresses and deformations are expected. The intermediate stripes of triangular elements (triangular shell elements and tetragonal ones) were also used for modelling transitions from regions of rough mesh of finite elements to regions of dense mesh.

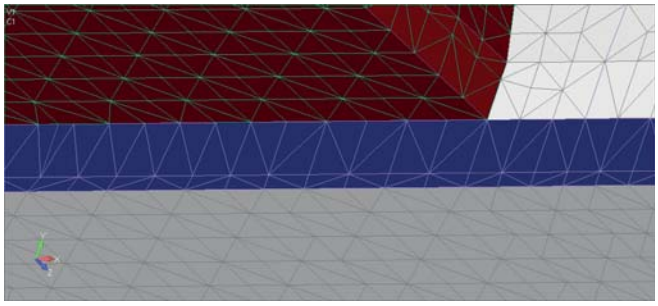

Fig. 11. Connection between plate elements of ship hull and tetragonal elements of water mass

In the course of modelling of underwater part of ship's hull a problem of making connection between plate elements of the hull and tetragonal spatial elements of water mass, appeared. The problem was associated with incompatible description of nodal quantities of the finite elements in question. The spatial elements have stiffness defined only for translational degrees of freedom while the plate elements – also for rotational degrees of freedom. The incompatibility of stiffness matrix of tetragonal elements and that of plate elements may lead to occurrence of solution singularity. There are many methods of joining together incompatible finite elements : it is possible to block surplus degrees of freedom or add intermediate elements to a discrete model : i.e. *R*-elements which transform rotations of a given node into displacements of neighbouring node.

CONCLUSION

The paper presents a new concept of overall ship motion modelling for application to total ship operability. The model is multi-phase one and includes both submerged part of ship's hull and the surrounding water as a unique body. The considered body includes both rigid and elastic elements with different parameters. It is assumed that the whole body moves with different speeds of its different elements. The DFEM is applied to make the numerical model of body motion. This modelling concept was successfully examined and illustrated for a selected AHTS. The main issues and challenges in making such model are discussed and the possible solutions are presented. In the next step of investigations the concept will be used to build multi-phase model of ship motion including air, additionally. Then natural frequency vibrations and forced motion will be analysed to pave the way for total operability analysis.

REFERENCES

1. Fossen, T. I.: *Guidance and Control of Ocean Vehicles*, John Wiley, 1994.
2. Fossen, T.I.: *Marine Control Systems*. Marine Cybernetics, 2002.
3. Perez, T.: *Ship Motion Control*. Springer Verlag, 2005.
4. Jensen, A. G.: *Fluid dynamic derivatives: marine and wind engineering approaches*. Journal of Wind Eng. and Industrial Aerodynamics 69(71),, 1997, pp. 777–793
5. Lewis, E.V.: *Principles of Naval Architecture Vol. III: Motions in Waves and Controllability*, 3rd ed. Society of Naval Architecture and Marine Engineers, New York, 1998.
6. Price, W. C. and R. E. D. Bishop : *Probabilistic theory of ship dynamics*. Chapman and Hall, London, 1974.
7. Son, K.H. and K. Nomoto : *On the coupled motion of steering and rolling of a high-speed container ship*. Naval Architecture and Ocean Engineering, 1982.
8. Gawronski W.K.: *Advanced Structural Dynamics and Active Control of Structures*. Springer-Verlag New York Inc., 2004.

MOST WIEDZY Downloaded from mostwiedzy.pl

9. Kruszewski J., Gawroński W., Wittbrodt E., Najbar F., Grabowski S.: *Method of stiff finite elements* (in Polish), Arkady, Warsaw 1975.

10. Larson M.G., Bengzon F.: *The Finite Element Method: Theory, Implementation, and Practice*. Springer-Verlag New York Inc., 2010.

11. Newman J.N.: *Marine Hydrodynamics*. The MIT Press, 1977.

12. Sclavounos P.D., Purvin S., Tahla U., Kim S.: *Simulation based resistance and seakeeping performance of high-speed monohull and multihull vessels equipped with motion control lifting appendages.* In Keynote Lecture, FAST 2003 Conference, Ischia Italy, 2003.

13. Walczyk Z., Kahsin M., Olszewski H.: *Dynamic analysis of high power turbo set*. 14th Internationale Tagung Forschung – Praxis - Didaktik im modernen Maschinenbau. Stralsund, 5.-8.5.2004. Stralsund: Fachhochsch. Stralsund (Univ. Appl. Sci.) Fachbereich Masch. 2004.

14. Walczyk Z., Olszewski H.: *Dynamic properties of a structure supporting turbine set rotors* (in Polish). Materials of 6th School of modal analysis. Cracow, 11-12 December 2001, Ed. T.Uhl.: Department of Robotics and Machine Dynamics, AGH, Cracow 2001

CONTACT WITH THE AUTHORS

Henryk Olszewski
e-mail: h.olszewski1@wp.pl

The State University of Applied Sciences in Elbląg
1 Wojska Polskiego St.
82-300 Elbląg
Poland

M. Hossein Ghaemi
e-mail: ghaemi@pg.edu.pl

Gdańsk University of Technology
11/12 Narutowicza St.
80 - 233 Gdańsk
Poland

MOST WIEDZY Downloaded from mostwiedzy.pl

POLISH MARITIME RESEARCH Special Issue 2018 S1 (97) 2018 Vol. 25; pp. 42-50
10.2478/pomr-2018-0021

SIMULATION OF LIFE RAFT MOTIONS ON IRREGULAR WAVE - AN ANALYSIS OF SITUATIONS LEADING TO RAFT CAPSIZING

Olga Kazimierska
Gdańsk University of Technology, Poland

ABSTRACT

Successful rescue action at sea is based on a. o. a correct choice of rescue means and their reliability. Operational characteristics of life-saving appliances determine their performance in a given water area. Therefore they affect duration time of rescue action and decide this way on survival time of shipwrecked persons. This paper presents impact of characteristics of circular inflatable life rafts on their dynamics in a given sea environment. Particular issues dealing with raft motion were analyzed and their solutions were then presented in the form of computer programs built into MATLAB environment. The programs operate on the open choice basis– the user is requested to introduce data of a raft to be investigated. The program clearly informs which units should be used for the data. The obtained results allow to limit survivours searching area and simultaneously form the basis for working out a model of searched object drift motion. In this work the use was made of the results obtained from the KBN research project No. 4T12C03827 in which an attempt was made to analyzing capsize probability of a raft at given sea states. The raft investigated in the project is also used as a reference raft in the computer programs developed in this work.

Keywords: life rafts, inflatable rafts, circular rafts , drift anchors, simulations of motions on irregular wave, raft dynamics, wave spectrum

INTRODUCTION

Maritime navigation has been always connected with a risk. In spite of scientific and technological developments , tragic accidents at sea which require to undertake search and rescue operations , still happen.

Success of a sea rescue operation depends not only on knowledge of hydro-meteorological conditions , proper choice and effectiveness of rescue means but first of all on used life saving appliances and - most importantly - their reliability.

In spite of a high resistance against loads and environmental factors of contemporary life rafts it happens that they capsize in extreme weather conditions. As a rule such situation ends with loss of all life raft crew. Though life raft construction is continuously under improvement, conducting research on their effectiveness in real conditions leads not only to a high cost but also constitutes a hazard for research team. This work is aimed at development of a software intended for the analyzing of situations which may lead to the capsizing of raft , i.e. investigations on its longitudinal and oscillating motions. The calculations would allow to verify and compare reactions against sea environment action of circular inflatable rafts of various dimensions .

Life rafts used on open water areas rarely float in still water , usually they are exposed to wave and wind action. Though during life rafts design there are taken into account also other environmental factors such as ice and icing, minimum and maximum temperature of air and water , the factors do not have such impact on raft motion as the factor which decides

MOST WIEDZY Downloaded from mostwiedzy.pl

on its dislocation (translation) , namely wind-generated waves [1-4]. In this work attention was focussed on storm waving , called also irregular. For simulation of wave surface profile , Neumann spectrum was used. In the next chapter results obtained from the KBN research project No. 4T12C03827 [5] are referred to in order to be used for the software developed in this work , and subsequent chapters present own results of this author's work.

RESEARCH PROJECT AND REFERENCE LIFE RAFT

Results of this work were reached on the basis of measurements carried out in Ship Design and Research Centre (CTO) , Gdańsk, and Aviation Institute, Warsaw , where three life rafts for 6, 10 and 20 persons, respectively , were tested. The tests were conducted in the frame of the KBN research project No. 4T12C03827 [5].

All the computer programs presented in subsequent chapters operate by making comparisons between selected quantities and results of the above mentioned research project obtained for the 10-person life raft. There were utilized also results of raft resistance measured during towing tests with and without drift anchor in CTO towing tank and results of the tests of aerodynamic forces and moments performed in IL wind tunnel. Below, in Tab. 1 and 2 there are presented the selected results of the referred to research project , which were subsequently implemented in the computer programs.

Tab. 1. Resistance of the raft with and without drift anchor (V_{tr} - wind speed) [5]

Resistance of the raft without drift anchor	
Percentage of crew persons	Regression equation of raft resistance
100%	$Rt_{100\%} = 7{,}38776\text{-}30{,}4399 \cdot V_{tr} + 258{,}83 \cdot V_{tr}^2$
50%	$Rt_{50\%} = 3{,}02773 + 7{,}71107 \cdot V_{tr} + 237{,}813 \cdot V_{tr}^2$
10%	$Rt_{10\%} = 6{,}3795\text{-}35{,}6088 \cdot V_{tr} + 268{,}987 \cdot V_{tr}^2$
Drift anchor resistance	$Rd = 0{,}485404\text{-}63{,}3809 \cdot V_{tr} + 385{,}023 \cdot V_{tr}^2$

Tab. 2. Measurement results for aerodynamic forces and rolling moment (V_w - wind speed) [5]

Aerodynamic forces	
X0	$= 0{,}266556 + 1{,}66005 \cdot V_W + 0{,}795924 \cdot V_W^2$
Y0	$= 0{,}943574 - 3{,}21311 \cdot V_W + 0{,}0154846 \cdot V_W^2$
Z0	$= 7{,}37481 - 16{,}047 \cdot V_W + 1{,}57432 \cdot V_W^2$
Rolling moment	
MX0	$= - 0{,}893263 - 1{,}69975 \cdot V_W + 0{,}191677 \cdot V_W^2$

Tab. 3 shows dimensions of the 10-person life raft used as the reference raft in the worked -out computer programs.

Tab. 3. Dimensions of the 10-person life raft used as the reference raft [5]

Raft mass	m_T	85 kg
Raft total height	H_{TOT}	1,24 m
Raft diameter	D	2,9 m
Raft depth	H	0,58 m
Raft draught	T	0,144 m
Raft displacement	Δ	935 kg
Height of gravity centre over reference plane of the raft	ZG	0,313 m
Height of buoyancy centre	ZF	0,072 m
Block coefficient	C_B	~1,0

The movable raft-fixed coordinate frame OXYZ is so orientated that OX –axis is pointed towards raft motion under action of waves and wind and dragged by drift anchor; OY –axis - towards conventional left side of the raft , and OZ – axis – upwards [5]. The line connecting the drift anchor with the raft is placed in the OXZ plane on the odd side of OX - axis. The coordinate frame origin O is placed in the mid-point of the raft's bottom. The motionless coordinate frame $O_0X_0Y_0Z_0$ is located on the still water level . In the initial instance of raft motion the movable coordinate frame OXYZ coincides with the frame $O_0X_0Y_0Z_0$.

The experiment on raft model motions performed in CTO towing tank as well as respective observations in real conditions show that the raft in waves makes the following motions [1, 2, 5, 6]:

- vertical motion (heaving) following wave profile;
- oscillation motion (pitching) around OY- axis perpendicular to direction of wave propagation , following wave slope angle.

The raft with drift anchor moving in waves is placed in OXZ plane and makes very small yawing motions around OZ- axis.

The above presented observations allowed to make the following assumptions simplifying mathematical model to a time-dependent simulation of raft motion in irregular waves, namely:

- wind pressure force and Froude-Krilov buoyancy forces are the main forces exciting raft motion;
- in view of the very small draught (not exceeding 0,4 m at the raft side under heel), influence of wave pressure distribution on the forces exciting raft motion was not taken into account;
- the raft undergoes motions mainly in OXZ plane;
- wind and waves have the same directions;
- average wind force does not cause any heel of the raft;
- there is no correlation between heaving and pitching around OY- axis;
- the heaving is excited by irregular wave , wind and drift anchor;

MOST WIEDZY Downloaded from mostwiedzy.pl

- added water mass inertia moment is constant during heaving.

Heeling moments generated by drift anchor , wind pressure and resistance forces incline the raft by the angle θ, assumed positive for "bow" immersion [5]. Within the frames of the research project there was determined the righting moment arm of the 10-person raft , described by 5th order polynomial in respect to the pitching angle θ [°] (Tab. 4.). The curves were determined for the least favourable arrangement variant for different numbers of persons in the raft.

Tab. 4. Righting moment arm [5]

GZn	Righting arm
GZ10	= -0,0160587 + 0,0794899·θ-0,0032757·θ² + 0,0000625384·θ³ - 6,05361E-7·θ⁴ + 2,29939E-9·θ⁵
GZ5	= -0,637218 + 0,101485·θ-0,00487179·θ² + 0,000110211·θ³- 0,00000118823·θ⁴ + 4,85768E-9·θ⁵
GZ1	= -0,421806 + 0,11902·θ-0,00666039· θ²+ 0,000162703·θ^3-0,00000183171·θ⁴ + 7,68054E-9·θ⁵

In the computer programs there was taken into account a standard drift anchor recommended for floating units of up to 4,5 m in length (Fig. 1.). Its dimensions and masses are given in Tab. 5 [7]. For analyzing operation of the programs the use was made of LALIZAS firm catalogue which contains technical characteristics of LALIZAS OCEANO circular inflatable rafts produced in accordance with the latest recommendations of SOLAS convention (Tab. 6.)[8].

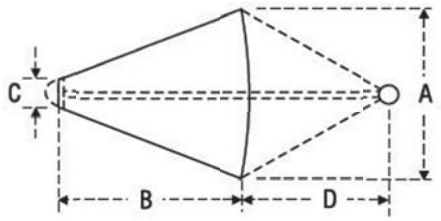

Fig. 1. Schematic diagram of the drift anchor [7]

Tab. 5. Dimensions and mass of the drift anchor used in the computer programs [7]

ØA	0,50 m
B	0,55 m
C	0,08 m
D	0,64 m
Mass:	0,26 kg
Volume:	2552 cm3

Tab. 6. Technical characteristics of LALIZAS circular inflatable rafts (M_T- raft mass, H_{TOT}- raft total height, H_N- raft tent height, D- diameter) [7]

A PACK version (for ships engaged in international shipping)				
Net capacity	6	8	10	12
MT [kg]	68	77	92	101
H_{tot} [m]	1,2	1,4	1,42	1,64
H_N [m]	0,742	0,875	0,88	1,014
H [m]	0,458	0,525	0,54	0,626
D_1 [m]	2,0	2,48	3,106	3,04
D_2 [m]	2,828	2,864	2,692	3,28
D average [m]	2,414	2,672	2,899	3,16
Net capacity	16	20	25	
M_T [kg]	129	150	173	
H_{tot} [m]	1,65	1,663	1,75	
H_N [m]	0,975	1,004	1,034	
H [m]	6,75	0,659	0,716	
D_1 [m]	3,622	3,622	4,25	
D_2 [m]	3,965	3,971	4,48	
D average [m]	3,7935	3,7965	4,365	

SIMULATION OF RAFT MOTIONS ON IRREGULAR WAVE

Wind generated waving may be considered as a superposition of many simple regular wave harmonic components every of which has its own amplitude, length, frequency , period and propagation direction [1-4, 9]. This concept allows to predict irregular phenomena on the basis of regular wave theory. As results, time stationary and uniform in space waving may be represented as a sum of elementary regular harmonic waves. For many practical issues a model of two-dimensional irregular waving based on the assumption that entire waving energy comes from one direction only, is satisfactory. In such case the 2D irregular wave propagating in the direction which coincides with X - axis may be approximated as a sum of of elementary harmonic waves and described in the form of Fourier series (1):

$$\eta(x,t) \approx \sum_{n=1}^{N} A(n) \cdot \cos[k(n) \cdot x - \omega(n) \cdot t + \varepsilon(n)] \quad (1)$$

where:

ε - phase shift of *n-th* harmonic wave [rad]; *A(n)*- amplitude [m]; *k(n)*- wave number [1/m]; *ω(n)*- circular frequency [rad/s].

Distribution of waving energy into particular harmonic components depends on squares of the harmonic amplitudes *A(n)* and may be represented by a function dependent on frequency of *n-th* harmonic wave . Below , the harmonic wave amplitude is presented in the form of a wave spectrum (6):

$$S_\eta\big(\omega(n)\big) \cdot \Delta\omega = \sum_{\omega(n)}^{\omega(n)+\Delta\omega} \frac{1}{2} \cdot A^2(\omega) \quad (2)$$

MOST WIEDZY Downloaded from mostwiedzy.pl

If there is assumed that the frequency increment $\Delta\omega$ approaches zero the frequency histogram will approach spectrum density function and Eq. (2) will take the form (3):

$$S_\eta(\omega) \cdot d\omega = \frac{1}{2} A^2(\omega) \tag{3}$$

Many of the worked out approximation function for wave energy spectrum usually concern the fully developed storm waving [1, 2, 4]. They assume the wave energy spectrum dependent on : the average wind speed V_W, the significant wave height H_s, and the characteristic wave period T_1. For angular motions calculation and accompanying phenomena there is recommended to use a wave energy spectrum density function obtained on the basis of measurements performed over water areas on which the raft in question will be used. To this work, Neumann spectrum , a direct function of wind speed , was applied (4):

$$S_{\eta N} = 1{,}525 \cdot \pi \cdot \omega^{-6} \cdot e^{-2 \cdot \left(\frac{9{,}807}{V \cdot \omega}\right)^2} \tag{4}$$

where : V stands for a set of wind speed values, and ω - a set of frequency values being random numbers.

In this work for simulating a wave profile two computer programs were prepared: Program No. 1 which contains the probability density functions (4) and constitutes an input function to the crucial program No.2 from which a function describing wave profile (based on the input data from Tab. 7) and its diagram are obtained. The program calculates also all wave heights as well as significant wave height.

Tab. 7. Input data to Program No. 2

Variable	Value	Description
V	25 m	Wind speed assumed constant
ω_0	0°	Initial value of wave frequency
ω_N	2°	Final value of wave frequency
N	50	Total number of frequency bands
t	1 s	Time instance
η_0	0	Iniial value of wave profile function
X	<0;300>; step = 0,1 m	Step in wave profile calculation

CALCULATION OF HORIZONTAL DRIFTING SPEED OF THE RAFT GENERATED BY WAVE AND WIND

Eq. (5) describes horizontal motion of the raft (along *OX* -axis) [1, 2, 5]:

$$m_{CD} \cdot \ddot{x} = -R_{dX} + R_W \tag{5}$$

It contains only the horizontal components: R_{dX} – resistance (drag) forces from drift anchor and immersed part of the raft, and R_W – wind pressure force , because during one wave cycle values of the averaged buoyancy forces components and mass forces resulting from raft sliding along wave slope are equal to zero. Assuming that accelerations in this motion are rather small compared with vertical one in heaving and angular in pitching , we are able to write the equation (6):

$$\frac{1}{2} \cdot \rho_w \cdot \dot{x}^2 \cdot (C_{Ddh} \cdot S_d + C_{DRh}(T) \cdot S_{R1}) =$$

$$= C_{DRa}(V_W) \cdot \frac{1}{2} \cdot \rho_a \cdot V_W^2 \cdot S_{R2}(z_W) \tag{6}$$

where:

ρ_w – water density [kg/m³];

ρ_a – air density [kg/m³];

dx/dt – instantaneous drifting speed, always positive even in case of very low speed of wind and wave;

C_{Ddh} – resistance coefficient of draft anchor against water;

$C_{DRh}(T)$ - resistance coefficient of immersed part of raft against water, depending on period – position on wave;

$C_{DRa}(V_W)$ - resistance coefficient of above-water part of raft against air, depending on wind speed in a given sea state;

S_d – cross-section area of drift anchor [m2];

S_{R1} – cross-section area of immersed part of raft [m2];

$S_{R2}(z_W)$ - cross-section area of above-water part of raft [m2], a function dependent on z_W –wave surface rise either above or below still water level (zero level).

To describe raft motion with the use of wave spectrum there is possible to take into account mass forces acting on the raft.. The equation which describes horizontal motion of the raft (along *OX*-axis) takes then the following form (7):

$$m_{CD} \cdot \ddot{x} = -R_{dX} + R_W + R_x \tag{7}$$

Its additional term R_x expresses just mass forces (8).

$$R_x = m_c \cdot g \cdot \sin(\alpha) \cdot \cos(\alpha) \tag{8}$$

The wave slope $tg(\alpha)$ can be expressed as a derivative of wave profile in respect of the translation x (9):

$$\tan(\alpha) = \frac{d\eta(x,t)}{dx} \tag{9}$$

From the partial derivative of the wave profile function $\eta(x,t)$ it is possible to get wave steepness (10):

$$\frac{d\eta(x,t)}{dx} = \frac{H_x}{\lambda} \cong \frac{H_s}{\bar{\lambda}} = \frac{H_s}{1{,}25^2 \cdot T_1^2} \tag{10}$$

which is the ratio of the wave height H_x in the point x to wave length λ, approximately equal to the ratio of the

MOST WIEDZY Downloaded from mostwiedzy.pl

significant wave height H_s to the respective average wave length , and where T_1 stands for the characteristic wave period. Knowing Eq. (10) one can obtain the formula for α (11):

$$\alpha = arc\tan\left(\frac{H_s}{1{,}25^2 \cdot T_1^2}\right) \tag{11}$$

The remaining forces in Eq. (7) are described by the Eq. (12) and (13):

$$R_{dX} = -\frac{1}{2} \cdot \rho_w \cdot \dot{x}^2 \cdot C_{Ddh} \cdot S_d \tag{12}$$

$$R_W = \frac{1}{2} \cdot \rho_a \cdot (V_W - \dot{x})^2 \cdot C_{DRa}(V_W) \cdot S_{R2}(z_W) \tag{13}$$

It should be added that m_c – stands for mass of raft together with people in it, and the mass m_{CD} (14) is additionally enlarged by the drift anchor mass m_d:

$$m_{CD} = m_c + m_d \tag{14}$$

Program No. 3 calculates resistance forces during towing the raft with or without drift anchor (friction forces generated by water flowing around the raft) for raft crew percentage of 100, 50, 10%, as well as resistance of drift anchor itself , on the basis of a raft diameter set by the program's user. Input data to the program are given in Tab. 9. Based on geometrical similarity a new speed range for the investigated raft is established. In the calculations the regression equations from the CTO tests are used (Tab. 3.) Finally , we obtain diagrams of the forces resulting from the selected speed range V_{TT}.

Tab. 8. Input data to the program No. 3

Variable	value range	Comments
D_{Tod}	(see Tab. 3.)	Data concerns reference raft
V_{tr}	<0,5;1>; step = 0,01 m/s	Raft speed
$RT_{od100\%}$, $R_{Tod50\%}$, $R_{Tod10\%}$	(seeTab. 1.)	Resistance without drift anchor
R_{dTod}	(see Tab. 1.)	Drift anchor resistance

Program No. 4 calculates wind pressure force. It makes use of the relation $X0(V_W)$ which describes aerodynamic force acting on the raft along *OX* –axis direction, the formula comes from the tests in IL laboratory (Tab. 4.). The analysis is made for the raft with the maximum number of persons . It was assumed that the tested raft is placed on wave crest . This simplification was chosen in view of the quantity $S_{R2}(z_W)$ which appears in Eq. (13) describing forces acting onto the raft.

Tab. 9 contains the input data dealing with the reference raft and additional values necessary for the calculations.

Tab. 9. Input data to the program No. 4

Variable	Value range	Comments
m_{Tod}, D_{tod}, H_{Tod}	(see Tab. 3.)	Data concerns reference raft
$X0_{Tod}$	(see Tab. 2.)	Aerodynamic force
ρ_w	1025 kg/m3	Water density
m_{os}	80 kg	Assumed mean mass per person
N	50	Value partition number
V_w	<1; 34>; step = 0,5 m/s	Wind speed

After introducing , by the user , the data which describe a chosen raft the results' matrix $X0_{TT}(V_W)$ is produced and the diagram is formed showing the aerodynamic force in function of wind speed acting onto the reference raft as well as that investigated by the user.

In the program No. 5 there was used the working space of the preceding program (No. 4) - both the input data to it and its results – in order to determine a relation between raft drifting speed and wind speed.

After reading the data out of the file as well as the working space (Tab. 10) and making the respective calculations, the diagram illustrating the relation Vu(VW) was depicted.

Tab. 10. Input data to the program No. 5

Variable	Value range	Comments
D_d ($D_d/2=R_d$)	0,5 m	Drift anchor diameter (radius)
C_{DRh}	1,0	Water resistance coefficient of immersed part of the raft [10]
C_{Ddh}	1,5	Coefficient of drift anchor resistance to water [11]
T_{TT}, D_{TT}, $X0_{TT}$,	(Results of the program No. 4)	Data concerning the tested raft
ρ_w	1025 kg/m^3	Water density
V_W	<1; 34>;step = 0,5 m/s	Wind speed

In the program No. 6 there are verified - for the raft investigated in the program No. 4 - the relations of : relative speed versus time - *u(t)*, dislocation (translation) versus time - *x(t)*, as well as the attractor *u(x)*, by using the significant wave height from the program No. 2 , as well as values derived from the program No. 4. The use is made of a function which describes raft motion (along *OX* – axis) with taking into account mass forces affecting the raft.

MOST WIEDZY Downloaded from mostwiedzy.pl

The saved data concerning the drift anchor and those required for the subsequent calculations are contained in Tab. 11. After reading the significant wave height H_s obtained from Neumann wave spectrum, the user must put in its characteristic period T_1. Finally, the diagrams of the relations : *u(t), x(t), u(x)* are depicted.

Tab. 11. Input data to the program No. 6

Variable	Value range	Comments
D_d ($D_d/2=R_d$)	0,5 m	Drift anchor diameter, (radius)
C_{Ddh}	1,5	Drift anchor resistance coefficient [11]
m_d	0,26 kg	Drift anchor mass
$X0_{Tod}$, $X0_{TT}$, S_{R2TT}, M_{cTT}	(see Tab. 3. and results of the program No.4)	Data concerning the tested raft
H_s	(Result of the program No. 2)	Significant wave height
ρ_w	1025 kg/m^3	Water density
ρ_a	1,2 kg/m^3	Air density
V_W	25 m/s	Wind speed
T	<0; 100>; step = 1,0 s	Solving time range
Y=[X0; Y0]	[0;1], [m; m/s]	Vector of initial values

CALCULATION OF RAFT PITCHING MOTION ON IRREGULAR WAVE

The above described environmental forces acting onto the raft generate moments exciting its oscillations around *OY*-axis by the angle θ. Under their action the raft takes such inclination angle at which the inclination moment is in balance with the righting moment [12-15]. The larger the righting moment the greater the raft capability of keeping a given equilibrium position as well as recovering this position if the raft is led off the equilibrium. A quantity used for raft stability determination and assessment is the righting moment arm *GZ*.

To obtain the righting arm *GZ* (Tab. 6.), the relation (15) can be applied :

$$\frac{GZ}{GM} = \sin\theta \tag{15}$$

where GM stands for the metacentric height.

The program No. 7 calculates the righting arm GZ for a selected raft in three different variants of crew occupancy percentage: 100, 50 i 10% for the least favourable variant of crew arrangement within the raft. At first, the input data to the program are read - Tab. 12. Into the program there are already written three polynomials of the gravity centre height *GZ* for the reference raft : *GZ10, GZ5, GZ1* (Tab. 4.) – corresponding to the above mentioned crew percentage. For the assumed angle range there are formed matrices of resulting *GZn* values for the reference raft. Next, the user puts in the data for a raft to be considered and in a few steps the function which calculates the height GZ_{TT} of the raft in the form of 5th order polynomial, is achieved.

Tab. 12. Input data to the progam No. 7

Variable	Value range	Comments
m_{Tod}, D_{Tod}, H_{Tod}	(see Tab. 3.)	Data concerning the reference raft
GZ100%, GZ50%, GZ10%	(see Tab. 4.)	Righting arm of the reference raft
ρ_w	1025 kg/m^3	Water density
m_{os}	80 kg	Assumed average mass per person
θ	<0;90°>; step = 1°	Pitching angle

All the calculations are carried out for different crew percentage occupancy - 100, 50 and 10%. After completing the calculations, from the achieved results the program forms a diagram.

RESULTS

Below is presented the diagram which shows the wave profile generated by the program No.2 (Fig. 2) for the input data of Tab. 7.

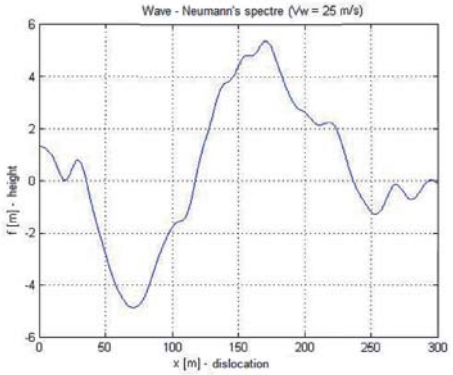

Fig. 2. The wave profile generated by the program No.2

Six values of wave height were achieved from the program (Tab. 13). The user is required to give height indices to calculate its mean value. As the significant height should be the mean calculated from 1/3 of the highest waves , two highest waves were selected to calculate it. As a result , the mean height H_s = 5,4034 m was obtained and then saved in the working space.

It should be stressed that the program does not calculate immediately a mean value because the generated wave is a random function – in case if the generated wave had only – for instance - three heights over sea level it would be not justified to select only one of them to be significant.

MOST WIEDZY Downloaded from mostwiedzy.pl

Tab. 13. Wave heights resulting from the program No. 2

H [m]					
0,7772	9,6740	0,5846	0,1020	1,1329	0,7420

In the program No. 3 , the diameters of the rafts accommodating 6, 8, 12, 16, 20 and 25 persons, respectively , were used for calculating resistance forces during towing the raft. An example diagram is presented below (Fig. 3.).

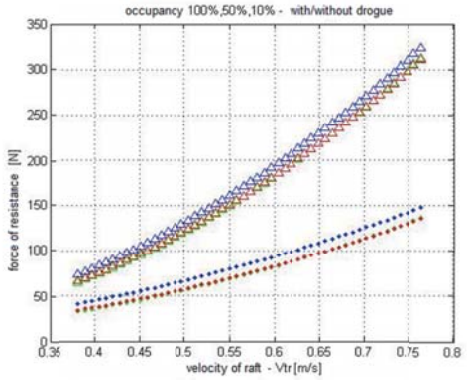

Fig. 3. Resistance forces during towing the 20-person raft with and without drift anchor , respectively ; (green colour stands for 100% crew occupancy, blue - 50%, red - 10%. Dots stand for resistance of the raft without drift anchor , triangles – for resistance of the raft with drift anchor.)

As the rift size is greater and greater , its speed and - consequently – the resistance force acting onto the rafts during towing decreases and only the range of diagrams is changed, that is especially visible when the results for 6-person raft and 20-person raft are compared to each other. On the both diagrams, at the speed of 0,7 m/s , the resistance force acting onto the raft without drift anchor amounts to abt. 130÷120 N (for the range of 100÷10% crew occupancy), and for the raft with drift anchor – to abt. 270÷250 N. The true is that the diagram showing relations between 6- person raft resistance force and its speed poses an extension of the respective diagram for 20-person raft. It's interesting, that the results for the raft with 100% crew occupancy coincide with those for that with 10% crew occupancy.

In the program No. 4 which calculates wind pressure force, the diameters of the rafts for 6, 8, 12, 16, 20 and 25 persons were used as previously. Below is presented the example diagram showing the obtained aerodynamic forces in function of wind speed values (Fig. 4.).

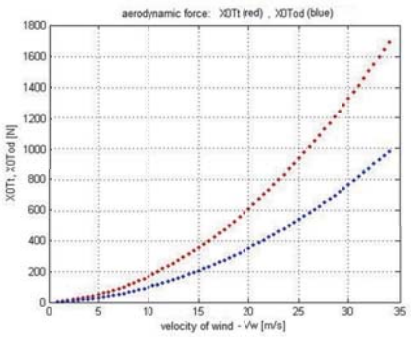

Fig. 4. Aerodynamic force acting onto 20-person raft compared with 10-person reference raft

Comparing subsequent diagrams to each other one can observe that along with growing size of the raft the wind pressure force acting onto the raft at a given wind speed increases. However, the results for 16 - and 20-person rafts do not differ significantly to each other – this probably results from the quantities describing the 20-person raft . This question may be solved by the next program where relations between raft drifting speed and wind speed can be mutually compared. For the calculations in the program No. 5 the use was made of the raft data introduced already into the program No. 4. The example diagram is presented below (Fig. 5.)

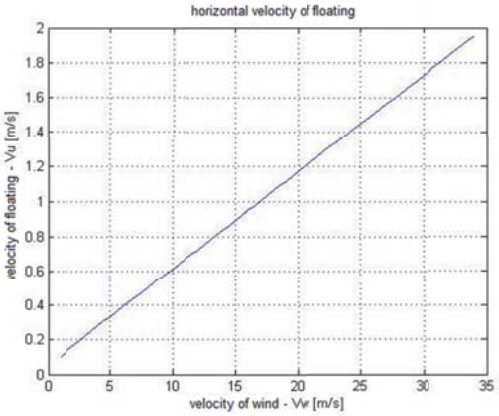

Fig. 5. Raft drifting speed in function of wind speed - relation for 20-person raft

As may be observed on the drawings which show relations for the rafts of 6, 8, 12, 16 - person capacity, along with increasing capacity of the considerd raft the linear function $V_u(V_W)$ becomes more and more " steep". The effect vanishes on the diagram for 20-person raft . The inclination angle of this function is clearly smaller than that for the preceding,16-person raft. It results from the dimensions of the raft. If we examine more thoroughly the catalogue data (Tab. 6.) it may be observed that inasmuch as diameter, tent height and mass of particular rafts increase along with their capacity, such correlation disappears just in case of the depth (pontoon height) of 20-person raft. Its depth as well as its total height is smaller than that of the preceding raft because , though the total cross-section area of 20-person raft is greater, the emerged part of this raft has smaller area than that of 16-person raft – and just on this area wind force acts. And, for this reason the inclination angle of the function $V_u(V_w)$ is smaller.

For the calculations in the program No. 6 there were used the raft data already introduced into the program No. 4. In the program in question the use was made of the significant wave height achieved on the basis of the wave spectrum from the program No. 2 ,namely : H_s = 5,3729 m. The user had to put in its respective period T_1 = 8 s (characteristic for the North Sea [15]). One of the drawings illustrating results of the calculations is shown below (Fig. 6.):

MOST WIEDZY Downloaded from mostwiedzy.pl

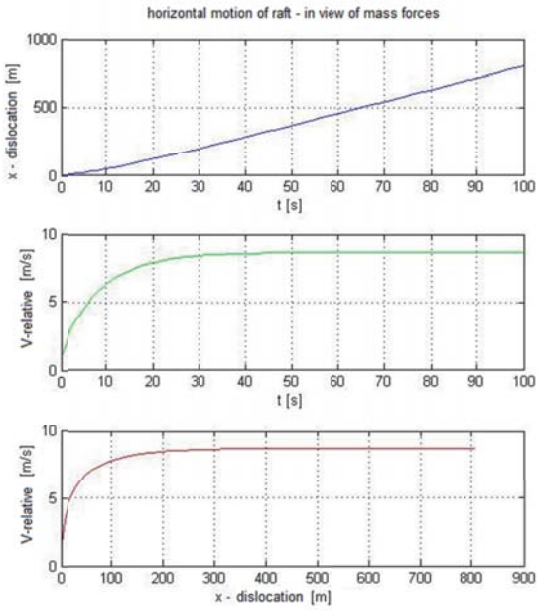

Fig. 6. Horizontal dislocation of the raft (relative speed , dislocation, attractor) reached with taking into account mass forces acting onto the raft – relations for 20-person raft

Examining the diagrams one may observe three unambiguous correlations resulting from size and mass of the rafts – the greater raft capacity the greater the inclination angle of the function of raft dislocation versus time, and the function of raft relative speed versus time as well as the attractor reach stable course at greater values. It should be stressed that in case of the dislocation- time function we have not to do really with an inclination" angle" of a linear function but rather an exponential function , while the diagrams concerning relative speed approach a definite value because the analysis was made for only one, constant value of wind speed.

For the calculations in the program No.7 there were used the same rafts as in the preceding programs, i.e. the rafts for 6, 8,12,16, 20 and 25-person, respectively. The achieved results are presented in the form of diagrams ; the examplary one is shown in Fig. 7, where green colour stands for 100% crew occupancy, cyjanide - 50%, magenta - 10%.

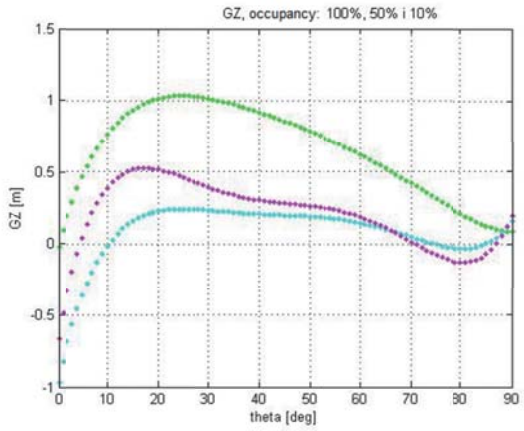

Fig. 7. The righting arm GZ in function of the heel angle theta for 20-person raft with 100, 50,10% crew occupancy

On the following diagrams as the rafts capacity increases the functions describing their righting arms are shifted towards greater and greater values. Additionally, the distances between particular functions at their points at GZ-axis for different percentage of crew occupancy, increase. The only exception from this relation is observed on the diagram for 20-person raft where the functions in question are located in the range of lower values , compared with that for the preceding raft of smaller capacity; the distances between the points of the functions at GZ –axis are also smaller. The limit angle of righting arms curve is not constant for all the rafts – for the rafts with 10 and 50% crew percentage it amounts to abt. 70°, and for 100% - to abt. 90°.

SUMMARY

The programs presented make it possible to show – in the form of diagrams – an influence of raft characteristics on raft performance in a critical situation as well as to compare to each other responses of various circular rafts against given environmental factors. In particular situations leading to raft capsizing its longitudinal and oscillation motions were examined. The investigations were conducted for given weather conditions in which at first wind speed and then - based on the generated wave spectrum - the significant wave height and characteristic wave period was determined. However , enough to modify somewhat the code to get similar analytical tool for selected hydrometeorological parameters – hence the programs may serve as a useful tool for inflatable raft designers , because they allow to select such raft dimensions as to assure the best effectiveness / highest reliability level for the raft in dangerous weather conditions possible to met in a given water area.

Effectiveness of a rescue action depends on action time of a search & rescue system as well as survival time of survivours. And, duration time of such action depends on an extent of area to be searched. Knowing operational characteristics of life saving appliances one is able to restrict search area and – consequently - to shorten duration time of a search & rescue action.

Determining search area one must take into acount not only wind drift generated along wind direction but also occurrence of wind drift components deflected right or left from the wind direction [6]. The deflections are caused a. o. by raft tent supporting bows [17], that results in a nonlinearity of aerodynamic coefficients. Knowledge of the following information: drift anchor usage (its application results in stabilization of wind drift direction as well as reduction in wind drift speed), size and form of the raft as well as its tent (change in their technical parameters affects drift parameters), raft occupancy (number of survivours also affects drift parameters) can significantly reduce fuzziness of a search area. The programs prepared within the frames of this work make it possible to use the above specified information for analyzing raft motion (prediction of its path); owing to this they may serve as an introduction to development of a

MOST WIEDZY Downloaded from mostwiedzy.pl

drift model of to- be- searched object and contribution in shortening time to rescue of survivours.

BIBLIOGRAPHY

1. Cepowski T.: Numerical modelling of seakeeping qualities of selected types of ships in preliminary desige stage (in Polish). WNAM, Szczecin 2011.
2. Sobczyk K.: Stochastic differential equations (in Polish). WNT, Warszawa 1996.
3. Massel S.: Hydrodynamic problems of offshore buildings (in Polish). PWN, Warszawa 1981.
4. Sobczyk K.: Stochastic waves (in Polish). PAN, Warszawa-Poznań 1982.
5. Bielański J.: The probability analysis of the life raft capsizing on the rough sea, 16'th International Conference on Hydrodynamics in Ship Design, 3'rd International Symposium on Ship Manoeuvring, 7-10 September 2005, Gdańsk - Ostróda, Poland, pp. 219-227.
6. Burciu Z.: Life raft reliability in sea transport (in Polish). Oficyna Wydawnicza Politechniki Warszawskiej, Warszawa 2011.
7. http://www.smart.gda.pl, (access date : 21.01.2016r.)
8. Krajewska, P.: Analysis and assessment of requirements for building and usage of life saving appliances in sea transport (in Polish). Logistyka 3/2014
9. Sawicki J. Free surface liquid flows (in Polish). PWN, Warszawa 1998.
10. White, F.: Fluid Mechanics (in English). 3rd edition, McGraw-Hill, Inc., International Edition 1994, p. 419.
11. Gryboś R.: A book of problems on technical mechanics of fluids (in Polish). PWN, Warszawa 2011.
12. Jeżowiecka-Kabsch K., Szewczyk K.: Fluid mechanics (in Polish). Oficyna Wydawnicza Politechniki Wrocławskiej, Wrocław 2001.
13. Pacześniak J.: Design of sea-going mercantile ship (in Polish). I,II,II vol., a course book. Gdansk University of Technology, Gdańsk 1984.
14. Szozda Z.: Stability of sea-going ship (in Polish). Akademia Morska w Szczecinie, Szczecin 2002.
15. Więckiewicz W.: Essentials of floatability and stability of merchant ships (in Polish) . Wydawnictwo Akademi Morskiej w Gdyni, Gdynia 2006.
16. Dudziak J.: Theory of ships (in Polish). Wydawnictwo Morskie, Gdańsk 1988.
17. Morawski, M.: Inflatable rafts in sea rescue (in Polish). WMG, Gdynia 1961.

CONTACT WITH THE AUTHOR

Olga Kazimierska
e-mail: olga.kazimierska@pg.gda.pl

Department of Hydromechanics and Hydroacoustics
Faculty of Ocean Engineering and Ship Technology
Gdańsk University of Technology
11/12 Narutowicza St.
80 - 233 Gdańsk
Poland

MOST WIEDZY Downloaded from mostwiedzy.pl

POLISH MARITIME RESEARCH Special Issue 2018 S1 (97) 2018 Vol. 25; pp. 51-55
10.2478/pomr-2018-0022

VERTICAL MOTIONS DAMPING MODEL TEST OF A LIFEBOAT LOWERED ONTO A FLAT SEA SURFACE

Aleksander Kniat
Paweł Dymarski
Gdańsk University of Technology, Poland

ABSTRACT

The article presents the experiment's results of the lifeboat model lowered with an initial speed and then released to fall onto a flat water surface. The purpose of the research is to determine the trajectory of the vertical boat motion and describe it with a mathematical model. This is closely related to determining the damping factor since the vertical motion is damped and the lifeboat gets balanced and stops moving after some time. The procedure of selecting parameters in the mathematical model to adjust to the results of the experiment was described in details. The summary describes the imperfections of the presented damping model and their probable causes.

Keywords: damping, dynamics, differential equations, lowering a lifeboat, numerical simulations

MOST WIEDZY Downloaded from mostwiedzy.pl

INTRODUCTION

The subject of the study of the lifeboat motion during the lowering in the performance of evacuation action from the ship is important for the safety of the evacuees. A comprehensive description of this process is included in publications [4] and [5]. Safety problems are a constant challenge for companies operating in the field of maritime economy as well as the scientific community. Emerging new requirements and solutions are reflected in the SOLAS Convention (part III) and applied in the regulations of classification societies.

Due to the more and more perfect computational tools in the field of fluid dynamics (CFD), continuous progress is observed in the motion simulation of different types of vessels. Publication [7] presents a three-dimensional dynamic model of the vessel's behavior in the time domain.

The problem of damping the motions of a floating vessel is widely known and described. In [2] this issue is presented from the point of view of harmonic wave propagation. Publications [1] and [11] present the details of determining the damping coefficient for rolling motion. In [10], the relationships between different damping coefficients for symmetrical ship hulls are described.

The aim of this research is to describe the physical phenomena as accurately as possible so that they can be simulated with an appropriate mathematical model. However, for now, only classical Newton's mechanics is applied without the use of CFD methods. It is assumed that the mathematical model will then be used to analyze the proposed new technical solutions or changes in procedures using computer simulations, which is cheaper and easier to perform than experiments. Of course, this does not mean that experiments and trials will be abandoned completely, but their number might be limited and thus the design process can be improved.

THE RESULTS OF THE EXPERIMENT

The experiment included recording the vertical motions of a lifeboat being lowered with initial speed and then released on a flat water surface. According to the classification societies' guidelines [8] the safe speed at which the lifeboat can fall into water is considered to be about 0.6m/s.

The model of a lifeboat used for experiments at the test basin of the Faculty of Ocean Engineering and Ship Technology at Gdańsk University of Technology was borrowed from the Ship Hydromechanics Center of the Ship Design and Research Center in Gdańsk. The model was made in 1:20 scale. Its physical parameters are: length: 440mm, width: 200mm, draft: 80mm, weight: 5.2kg.

The model must be freely dropped from a height of 18mm to achieve a speed of 0.6m/s at the time of contact with water. For this purpose, a special handle was prepared, on which the boat model was suspended at a specific height. The handle has been equipped with a release mechanism that allows the boat to fall freely into water.

The model motion during the experiment was recorded using the QualiSys measurement system. It is an optical registration system, which uses cameras that track special markers attached to the model. The system consists of five cameras. Four of them are used only for spatial registration of marker motions, and the fifth allows for recording of the whole image for illustrative purposes. During registration with a sampling rate of 60 Hz, marker motions are recorded at all six degrees of freedom - three displacement components and three rotation angles. In the case of this test, a cross with four markers, shown in Figure 1, was attached to the deck of the lifeboat model. Its mass was included in the calculations.

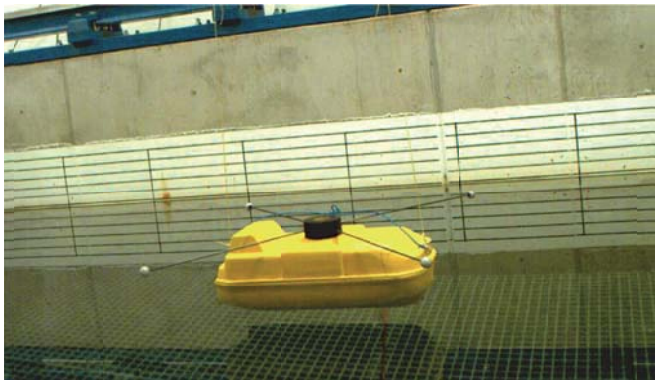

Fig. 1. The lifeboat model suspended on lines with visible QualiSys markers.

The numerical data obtained during the experiment was analyzed. It was confirmed that the speed at the time of contact with water was approx. 0.6 m/s. The changes of z coordinate of the lifeboat position during the experiment are shown on the graph in Figure 2.

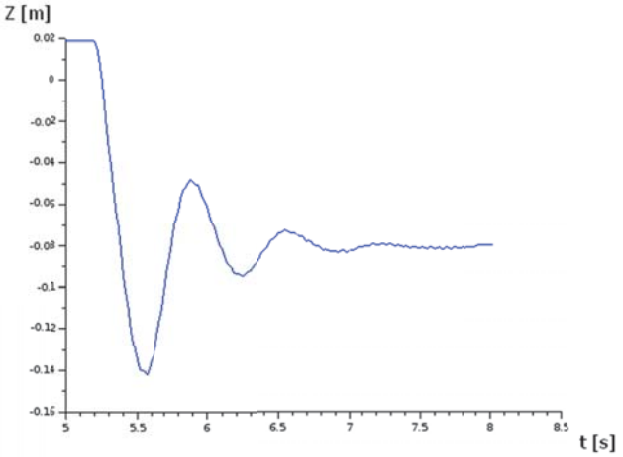

Fig. 2. The z coordinate value of the lifeboat position recorded during the experiment.

The experiment proves the damping of the lifeboat's vertical motions. Both from the observations during the experiment and from the graph it follows that after releasing the lifeboat from the holder it performs two full oscillations: two sequences of successive descents and ascents. Further boat motions are almost unmeasurable.

DAMPED MOTION MODEL

The basic mathematical model of the damped motion presented in [6] is described by formula (1)

$$m \cdot \ddot{x} = -k \cdot x - b \cdot \dot{x} \tag{1}$$

where

- m - object mass [kg]
- x - x coordinate of position in [m]
- k - coefficient of elasticity in [N/m]
- b - damping factor in [N·s/m]

In this formula, the damping is represented by the force linearly dependent on velocity and directed opposite to it - component $b \cdot \dot{x}$ on the right side of the equation (1). The b coefficient present in this component is called the damping factor.

Formula (1) is a second order differential equation and has an analytic solution in the form of a function (2).

$$x(t) = A \cdot e^{-\frac{b}{2m} \cdot t} \cdot \sin\left(t \cdot \sqrt{\frac{k}{m} - \frac{b^2}{4m^2}} + \varphi\right) \tag{2}$$

The time of the oscillation decay depends on the value of the factor b. Fig. 3 shows how the value of the b factor influences the attenuation of the oscillations. The larger the b, the faster the oscillations decay. At a sufficiently large value of b, damping becomes critical and oscillations do not occur at all.

MOST WIEDZY Downloaded from mostwiedzy.pl

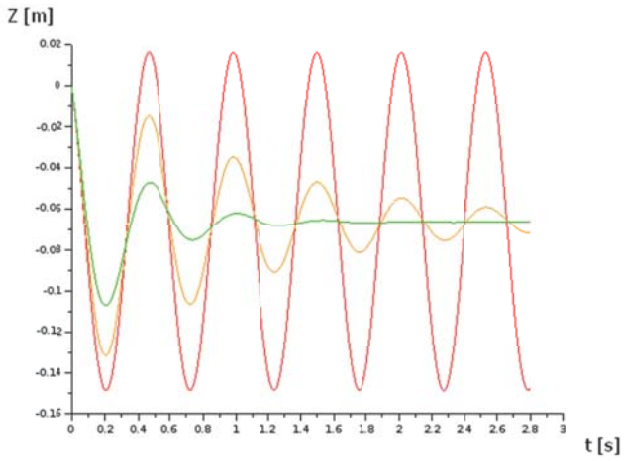

Fig. 3. The graphs of damped motion depending on the damping factor b value (red: b=0, orange: b=10 , green: b=30).

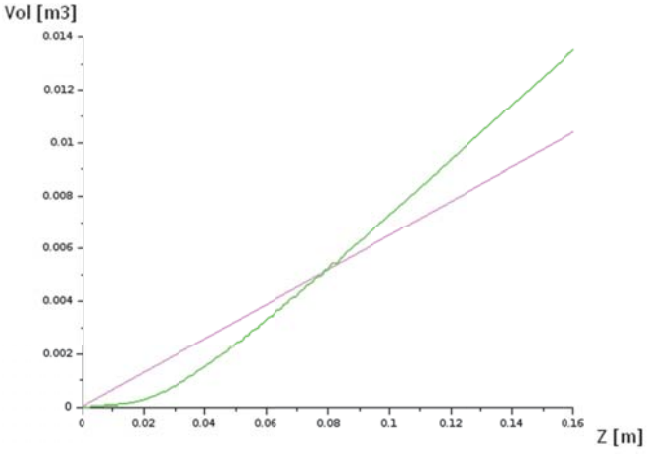

Fig. 4. The graph of the function Vol(z), which defines the water volume displaced by the lifeboat model depending on the draft (green) against the diagram of water displaced by a cylinder with a cross-section such as the average waterline of the model (violet).

In the case of a lifeboat, the equation of vertical motion is given by the formula (3)

$$m \cdot \ddot{z} = -m \cdot g - \rho_w \cdot Vol(z) \cdot g - b \cdot \dot{z} \quad (3)$$

where

m - lifeboat mass in [kg]

z - coordinate of the boat position or negative draft in [m]

g - gravity constant in [m/s^2]

ρ_w - water density in [kg/m^3]

$Vol(z)$ - function, describing the volume of water displaced by the boat depending on the draft in [m^3]

b - damping factor [kg/s]

It is also a second order differential equation. The second component to the right of the equation (3) contains the function *Vol(z)*, which gives the volume of water displaced by the boat. This function is not an algebraic function but returns linearly interpolated tabular values. Fig. 4 shows the graphical form of this function for the model of the lifeboat being tested.

Since one of the components of the right side of equation (3) is not an algebraic function, the equation can be solved only with numerical methods.

SETTING PARAMETERS OF DAMPING MODEL

In equation (3), the *Vol(z)* function is known. It is determined for the model of the lifeboat being tested. All other parameters except the damping factor b are also known. Because equation (3) does not have an analytical solution, the coefficient b cannot be calculated from such a solution.

The solution and selection of the value of the b factor must therefore be pursued with the use of numerical methods. To resolve a differential equation, the initial conditions must be specified. In this case, the initial position of the boat (z coordinate) and the speed (derivative $\dot{z}$) at this position are known. It is assumed that the boat touching the water with the keel is in position $z = 0$, and falling descends towards the negative z values. According to assumptions in pt. 1, in the initial position $z = 0$ the speed of the boat should be $\dot{z}$ m/s.

To solve the numerical differential equation, the Adams method was used, using the SciLab [9] calculation software. The Adams method, as a method of solving ordinary differential equations, additionally requires the conversion of the 2nd order equation into the system of two first order equations.

In Fig. 5. the red color presents the solution of equation (3) for m = 5.2kg, g = 9.81m/s^2, ρ_w = 1000kg/m^3 and b=0.0kg/s in the time interval $t\epsilon\langle 0.0, 2.8\rangle$. The results measured during the experiment are shown in blue.

MOST WIEDZY Downloaded from mostwiedzy.pl

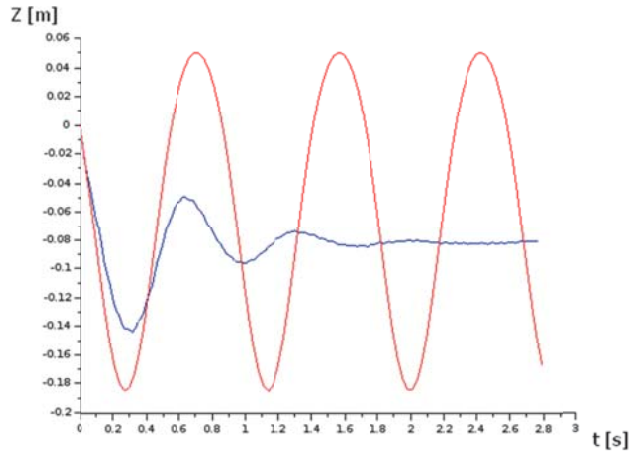

Fig. 5. The numerical solution of equation (3) for m = 5.2kg , g=9.81 m/s² , ρ$_w$= 1000 kg/m3 and b = 0kg/s (red) against the results from the experiment (blue).

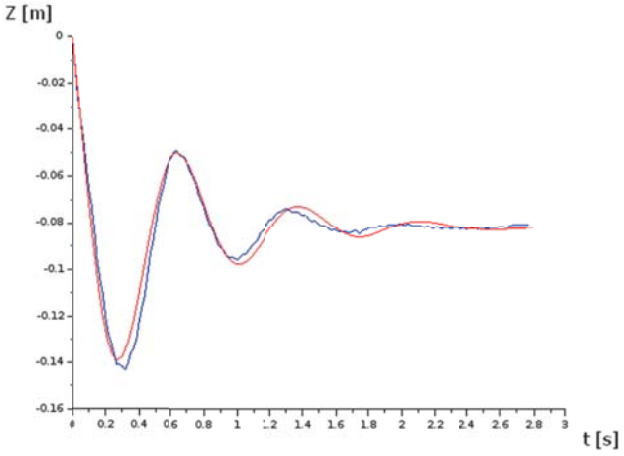

Fig. 6. The numerical solution of equation (4) for m = 5.2kg , m$_a$= 7.5kg , g = 9.81m/s² , ρ$_w$=1000 kg/m³ and b = 44.0kg/s (red) against the results from the experiment (blue).

Because factor b = 0.0kg/s was assumed, the lifeboat's motions in the numerical simulation were not damped. The graph also shows that the period of oscillations recorded during the experiment does not match with those resulting from the calculation. To obtain the correct period in the calculations, the concept of added mass should be introduced and formula (3) should be modified accordingly. The new form of this formula is shown as (4).

$$(m + m_a) \cdot \ddot{z} = -m \cdot g - \rho_w \cdot Vol(z) \cdot g - b \cdot \dot{z} \quad \textbf{(4)}$$

where

m_a - added mass in [kg]

The added mass is the mass that is conventionally considered as a mass of water that moves along with the hull of the boat. It represents additional inertia during the motions of the boat so it is taken into account only in the inertial part on the left side of the equation (4).

Equation (4) has two unknown parameters: the damping factor b and the added mass m_a. Increasing the added mass m_a increases the period, and increasing the damping factor b decreases the amplitude of subsequent oscillations.

Next, the values of m_a and b were increased until the graph of the calculation results matched with the graph recorded during the experiment. This happened for m_a = 7.5 and b = 44.0. The result is shown in Figure 6.

The standard deviation between the simulation results and the measured data from the experiment for parameters m_a = 7.5 and b = 44.0 assumed in the model is 0.004m. This means that 68% of recorded samples do not differ from simulations by more than 0.004m, and 95% of samples do not differ by more than 0.008m.

SUMMARY

The presented method of numerical calculations and determining the damping factor confirmed the correctness of the assumed damping model for describing the examined physical phenomenon.

It should be noted that the mathematical model described above has been proved for specific initial conditions during the experiment and corresponding to the typical situations occurring when lowering a lifeboat. Detailed analysis of the graph in Figure 6, however, shows that the differences between the simulation and the experiment increase with time. Since the speed drops significantly over time, the damping factor may not be constant, but it may be slightly dependent on speed. However, confirmation of such a dependence requires further research.

The damping factor determined for a given shape of the lifeboat hull with a value of b = 44.0 allows to consider the presented damping model as a good approximation of the examined physical phenomenon, because the standard deviation is small and amounts to only 0.004m, which is 2.8% of the depth of the first largest dive.

The appropriate damping model allows to perform precise simulations of the motions of this particular lifeboat in the future and the calculated values of acceleration, velocity and position can be used for further analysis without bearing the costs of tests in reality.

MOST WIEDZY Downloaded from mostwiedzy.pl

BIBLIOGRAPHY

1. Chakrabarti S., EMPIRICAL CALCULATION OF ROLL DAMPING FOR SHIPS AND BARGES, Ocean Engineering, Volume 28, Issue 7, pp. 915-932, 2001.

2. Chen J.P., Zhu D.X, NUMERICAL SIMULATIONS OF WAVE-INDUCED SHIP MOTIONS IN TIME DOMAIN BY A RANKINE PANEL METHOD, Journal of Hydrodynamics, Ser. B, Volume 22, Issue 3, pp. 373-380, 2010.

3. Dudziak J., TEORIA OKRĘTU. Wydawnictwo Morskie, Gdańsk 1988.

4. Dymarski P. Dymarski Cz., COMPUTATIONAL MODEL FOR SIMULATION OF LIFEBOAT MOTIONS DURING ITS LAUNCHING FROM SHIP IN ROUGH SEAS, Polish Maritime Research Vol. 19 No. 3(75), 2012.

5. Dymarski C., Dymarski P., Kniat A., SEARCHING FOR CRITICAL CONDITIONS DURING LIFEBOAT LAUNCHING – SIMULATIONS, Polish Maritime Research, Vol. 24 Special Issue 2017 S1 (93), 53-58, DOI: 10.1515/pomr-2017-0021, 2017.

6. Hibbeler R.C., Engeineering Mechanics: Dynamics, Pearson Prentice-Hall, 2016.

7. Kring D., TIME DOMAIN SHIP MOTIONS BY A THREE-DIMENSIONAL RANKINE PANEL METHOD, PhD thesis, MIT, 1994.

8. POZAKLASYFIKACYJNE PRZEPISY WYPOSAŻENIA STATKÓW MORSKICH, Polski Rejestr Statków, Gdańsk 1990.

9. SciLab, https://www.scilab.org.

10. Timman R. Newman J., THE COUPLED DAMPING COEFFICIENTS OF A SYMMETRIC SHIP, Journal of Ship Research, Vol. 5, No. 4, 1962.

11. Wassermann S., Feder D.F., Abdel-Maksoud M., ESTIMATION OF SHIP ROLL DAMPING - A COMPARISON OF THE DECAY AND THE HARMONIC EXCITED ROLL MOTION TECHNIQUE FOR A POST PANAMAX CONTAINER SHIP, Ocean Engineering, Volume 120, pp. 371-382, 2016.

CONTACT WITH THE AUTHORS

Aleksander Kniat
e-mai: olek@pg.edu.pl

Paweł Dymarski
e-mail: pawdymar@pg.edu.pl

Gdańsk University of Technology
11/12 Narutowicza St.
80 - 233 Gdańsk
Poland

MOST WIEDZY Downloaded from mostwiedzy.pl

POLISH MARITIME RESEARCH Special Issue 2018 S1 (97) 2018 Vol. 25; pp. 56-62
10.2478/pomr-2018-0023

NEW GENERATION STABILITY NORMS –HOW TO APPROACH THE TASK

Lech Kobyliński
Polish Academy of Sciences
Foundation for Safety of Navigation and Environment Protection, Poland

ABSTRACT

International stability norms included in the Code of Intact Stability 2008 adopted by IMO on 4 December 2008 constitutes the latest set of international requirements on intact stability of ships. However the requirements included in the Code, part of them compulsory (Included in the Part A of the Code), other only recommended (included in the Part B of the Code) are considered as not totally sufficient to assure safety of ships. Because of that, IMO decided that there would be the necessity to develop so called new generation stability criteria covering certain identified hazards, such as parametric resonance, loss of stability in the wave crest broaching, dead ship condition and excessive accelerations when rolling .Those criteria, or rather stability norms, are under development since 2008.The present approach, the work on which is well advanced, is however, not fully satisfactory and several important problems were discovered. This approach may need to be reconsidered or supplemented. The author in the paper presented discusses the weak points of the current approach and proposes possible different approach in order to make future ships safer from the stability point of view.

Keywords: ship stability, stability standards, risk assessment

CURRENT INTERNATIONAL STABILITY REQUIREMENTS AND THEIR DEVELOPMENT

The current stability standards are included in the International Code on Intact Stability 2008, adopted by the expanded Marine Safety Committee of the International Maritime Organisation (IMO) on 4 December 2008 [1]

The short history of the Code is as follows. The first internationally accepted stability criteria were statistical criteria developed by the STAB Sub-committee of IMCO (IMO) in the years 1962-67 and adopted as recommended in 1968 by IMCO Assembly resolutions A.167(AS.IV) and A.168(ES.IV). Those standards were developed by delegations of Poland and Federal Republic of Germany. They were based on statistical data.

During the period 1978-82 STAB Sub-committee developed so called "Weather Criterion" for passenger and cargo vessels, adopted ultimately in 1985 by IMO Assembly Resolution A.562(14) and later on, for fishing vessels in 1991 by Resolution A.685(17). Weather criterion was based on the approach adopted in national requirements of the USSR several years earlier. This approach consisted of consideration of action of severe wind and waves in dead ship condition. There were also adopted in the meantime several other resolutions related to various aspects of stability, amongst them resolutions related to stability of vessels of different

MOST WIEDZY Downloaded from mostwiedzy.pl

types. All requirements included in these resolutions were recommended only, none of them was considered compulsory.

The standards developed were criticised from the very beginning after they were adopted. During the discussions at STAB Sub-Committee and also in other places it was stressed that in development of those standards several assumptions were made making them non-rigorous. However the practical application of the above stability standards revealed, that for the great majority of ships they worked well and the number of stability accidents was greatly reduced. Still, however, several delegations to IMO insisted on further development of more rigorous stability standards in order to increase safety of ships at sea. Several proposals were advanced in this context, none, however, gained wider support. Obviously the problem is to complex.

In order to make some progress IMO decided to make one comprehensive document that would include all resolutions and requirements already developed and split between several different documents. The idea of development of Intact Stability Code was advanced and finally, after lengthy discussion, the Code was developed. It was also agreed that this code should be based on system approach [2]. Finally Intact Stability Code was adopted in 1993 by IMO Assembly by resolution A.749(18). The Code was subsequently amended in 2002. Since then, however, discussion started again on the possibilities to improve level of safety against capsizing and to revise the criteria. It was agreed by the IMO that the most important motion would be to make stability criteria compulsory. This was achieved by drafting new edition of the Code, that was adopted ultimately in 2008. Both editions of the Code included stability criteria virtually unchanged from the original criteria recommended by the above mentioned resolutions.

The 2008 edition of the Code consists of three parts: Part A, Part B and Explanatory Notes.

Part A of the Code was made compulsory by proper reference in the SOLAS Convention. It includes basic criteria: statistical criteria and weather criterion for both passenger and cargo ships and fishing vessels. Only minor improvements from the previous editions were included.

Part B of the Code includes provisions for specific types of ships and other provisions that are recommended only. That makes possible to amend this part of the Code more often as deemed necessary and to include criteria and provisions that may be not sufficiently validated during a trial period.

SECOND GENERATION STABILITY CRITERIA

Having prepared the 2008 edition of the Intact Stability Code, the SLF Sub-Committee was, however, not satisfied with the stability criteria in force. The point was raised by some delegations, that several situations dangerous from the point of view of stability are not covered by the criteria. According to some delegations the following situations or stability failure modes should be considered:

- Parametric resonance in following and head seas
- Loss of stability in the wave crest
- Broaching to and surfing
- Dead ship condition, and
- Excessive accelerations when rolling

Actually the proposal was not new. Those situations were considered by the Sub-committee during late seventies and early eighties of the last century. At that time Polish delegation to IMO proposed to consider those situations [3], apart from the last one, but after brief discussion the Subcommittee decided that it was unable to work out usable recommendations in that respect. Several years later the Sub-committee agreed to consider those situations under the agenda item "Second generation stability criteria".

Tab. 1. Three levels vulnerability approach within second generation stability criteria

	LEVEL 1	LEVEL 2	DIRECT STABILITY ASSESSMENT	OPERATIONAL GUIDANCE
stability failure mode	simple and conservative criteria based on geometry of hull and speed	less conservative criteria, based on simplified physics and involving simplified computations	numerical simulation of physical phenomena based on computer codes developed	based on experience

Work on second generation stability criteria started in 2008 [4]. After rather lengthy discussion of the matter during several sessions, the Subcommittee agreed that with regard of those situations safety assessment based on the three-levels vulnerability check have to be applied. The idea of this approach is that during the design stage of the ship, vulnerability to those stability failures at three levels have to be checked [5]. as shown in the table 1. Fig.1 shows schematically process of checking vulnerability to all four stability failure modes.

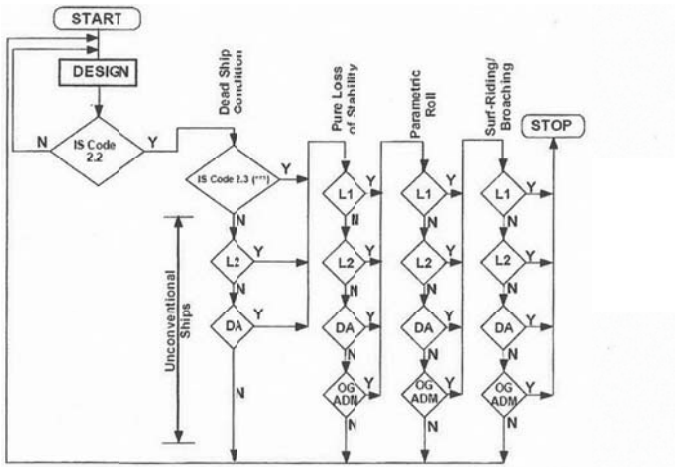

Fig.1. Schematic presentation of the process of checking vulnerability to four stability failure modes (from [6])

MOST WIEDZY Downloaded from mostwiedzy.pl

The SLF Subcommittee assumed that three to four years may be sufficient to complete the criteria, however, when the work started the Subcommittee realized that this is not an easy task. After eight years of discussion and extensive work on the criteria, the present situation is as follows: draft of the level 1 and 2 criteria has been finalized, however is still under discussion because of several minor improvements needed and inconsistencies removed. Draft criteria of the level 3 are far from completion and first draft of explanatory notes is available for further discussion by the SDC Subcommittee [7].

Under pressure of higher bodies of IMO the SDC Sub-committee agreed that finalized second generation stability criteria (SGSC), should be presented for acceptance by the MSC by 2019 at the latest. This means, that actually they must be completed at the next session of the SDC Sub-committee. This seems to be unrealistic [8].

APPLICATION OF THE SECOND GENERATION STABILITY CRITERIA TO SAMPLE SHIPS

Preliminary criteria of the level one and two for all five stability failure modes as drafted in 2013 were verified by several countries against a rather large number of sample ships of different types and the results obtained were submitted to IMO Sub-committee. However, only criteria of level one and two were used for verification as only those were available. Criteria of level three are not yet finalized.

Results of the verification revealed two main problems with application of SGSC. Problem one appears to be inconsistency in application of level 1 and level 2 criteria for almost all stability modes. Inconsistencies occur when standards of vulnerability criteria level one is satisfied without satisfying level two. This is the serious problem discussed by the delegation of the United States, [9] where proposal were made to further consider the criteria and to make attempt to discover causes of these inconsistencies in order to improve standards accordingly.

According to the opinion of the author, this inconsistency could be expected. The method of checking any phenomenon in stages, using subsequently more accurate tools, is logical and well known. But the results would be consistent only if the same tools, but more accurate, were used in subsequent stages. If different tools were used. inconsistencies will occur inevitably. In case of proposed SGSC different tools were used in level one and two

The second problem is more serious. The working group noted the concern of Norway. It was shown that when applying the five vulnerability criteria, about 40 out of 57 ships tested do not meet the level 1 and 2 criteria, hence need to apply either operational restrictions or undertake the expensive and time consuming process of level 3 calculations, that are not yet available. Norway pointed out, that these results are not backed by experience on operating existing ships, nor by any accidents statistics [8]

Tompuri et al from NAPA [10] pointed out correctly that the hull form is the most critical parameter governing two of the five stability scenarios, namely parametric resonance and loss of stability on wave crest. Changing the hull form by adopting more fuller form of the water plane in order to satisfy the standards is unrealistic, because it will affect negatively ship resistance and therefore fuel consumption. Eco-efficiency is the most important parameter governing ship design. It is very unlikely that these kind of very rare stability failure events would be used as determining design factor, instead of eco-efficiency.

PRESCRIPTIVE VERSUS RISK-BASED CRITERIA. GOAL ORIENTED APPROACH

Traditional regulations were of prescriptive nature. They are formulated in the way where ship dimensions or other characteristic (e.g. metacentric height) must be greater (or smaller) than certain prescribed quantity. Prescriptive regulations could be developed on the basis of experience, statistics, analytical methods, computer simulation, model tests and full-scale trials. Deterministic or probabilistic calculations may be employed when developing the criteria, although, as a rule, deterministic approach is used in most cases.

The main shortcoming of prescriptive regulations is that they are bounding designers and they do not allow introduction of novel design solutions. They are based on experience gained with existing objects and they are not suitable for novel types. Usually they were amended after serious casualties happened. The risk involved with the application of prescriptive regulations is not known.

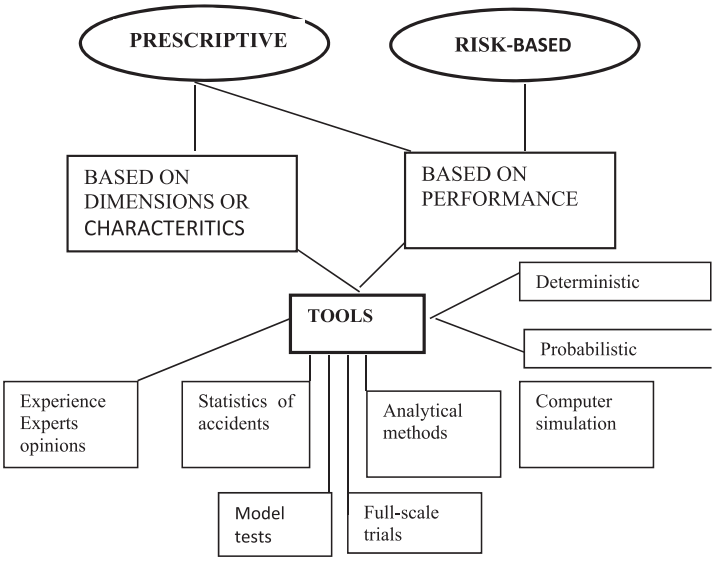

Fig.2. Comparison of risk based and prescriptive standards

At the opposite of the prescriptive regulations, there is risk-based approach. In the risk-based approach, the regulations specify objectives to be reached, which are safe performance of an object. Risk-based approach could be described as a goal-oriented performance based approach utilizing, as a rule,

MOST WIEDZY Downloaded from mostwiedzy.pl

probabilistic calculations. However, it is possible to imagine risk-based approach utilizing deterministic calculations as well. The same tools could be used as when developing prescriptive regulations.

The schematic representation of comparison of these two approaches is shown in fig. 2. The advantages of risk-based approach are obvious. They give free hand for the designer to develop new solutions, they actually allow taking optimal decisions from the point of view of economy and safety and the risk to the public and to the environment is assessed and accepted. Risk-based approach includes risk control options either related to design or operation including human factor. Risk based approach is used in situations of high uncertainity.

All existing stability regulations are of the prescriptive nature. At present, however, the need to apply risk-based approach is recognized. The Marine Safety Committee of IMO recommended this approach as Formal Safety Assessment (FSA) [11]. Risk-based approach is widely used in many fields of technology, also in maritime industry [12]. It was used also in the new IMO regulations on damage stability and survivability of ships

The risk-based concept of assuring safety is supplemented by goal-based approach to safety requirements. Goal based approach does not specify the means of achieving safety but sets goals that allow different or alternative ways of achieving safety [13]. Goal-based approach is for some time considered at IMO and appraised by some authors as a best solution to assure safety in very complex situations [14], It was introduced in some areas, albeit not in the systematic manner. Marine Safety Committee of IMO recommended in 2004 at MSCC 78 s work on goal-based standards in relation to ship construction adopting five-tier systems shown in the table 2.

Tab.2. Five-tier system for goal-based requirements

Tier I:	Goals
Tier II:	Functional requirements
Tier III:	Verification criteria of compliance
Tier IV	Technical procedures and guidelines, classification rules and industry standards
Tier V	Codes of practice and safety and quality systems for shipbuilding, ship operation, maintenance, training etc.

The advantage of goal-oriented approach is that in order to achieve goal which is to make shipping safer, various means have to be used, not only prescriptive regulations. All means that may contribute to safety have to be used as is specified in the table 2. This approach includes risk analysis, which is one of the most important method to achieve compliance.

CRITICAL OBSERVATIONS REGARDING SECOND GENERATION STABILITY CRITERIA

The adopted methodology of second generation criteria leads to purely prescriptive design standards. Analysis of causes of casualties reveals without doubt that in almost all cases the casualty scenario is very complex and several factors contribute to the end result. Casualties where one single cause may be identified are extremely rare. Usually, apart from design faults, also operational factors, including human factor, play important part. In particular, according to general opinion of ship operators, human factor is responsible for about 90 per cent of all casualties. In order to improve safety and reduce the number of casualties related to stability focus should be concentrated on human factor.

As mentioned the five modes of stability deficiency chosen for consideration are actually selected quite a long time ago, but the SLF Sub-committee decided to abandon the subject and instead include wording, that is still present in the latest edition of the IS Code in the part A (paragraph 1.2) and in Part B (paragraph 5.1). In particular the last one is drawing attention to human factor:

"Compliance with the stability criteria does not ensure immunity against capsizing, regardless of circumstances, or absolve the master from his or her responsibilities. Masters should therefore exercise prudence and good seamanship having regard to the season of the year, weather forecasts and navigational zone and should take appropriate action as to speed and course warranted by the prevailing circumstances."

This is very important statement. Human performance may be affected by several factors, e.g. by education, training, physical and psychical attributes of people at the control, etc. This is separate subject that will not be discussed here. Hazards considered in the present second generation criteria are important. However, with the current approach to drafting standards, no attempt was made to evaluate risk of the considered stability failures on the basis of statistics, expert opinions, analysis of casualties or using other means.

Moreover, physically five modes of stability failure considered are widely different, and they should be considered separately, perhaps using different methods. Trying to consider all of them using the same schematic procedure seems to be wrong, because different physical phenomena require appropriate, perhaps different, methods of analysing and control.

This could be the crucial point. For example casualties resulting from parametric resonance in head or following seas appears to be extremely rare events. Parametric resonance may happen quite often when the wave encounter period is twice the natural period of roll (which is a function of GM). This phenomenon may be easily avoided if period of encounter is slightly changed by changing speed or heading or both of the ship. Moreover hazardous situation may occur only when resulting rolling amplitudes increase and are finally larger than certain accepted value. Therefore if amplitudes resulting

MOST WIEDZY Downloaded from mostwiedzy.pl

from parametric resonance are small, there is no danger. In an unpublished paper Wawrzyński and Krata [15] correctly proved, that because of the form of GZ curve, metacentric height at larger angles of inclination quickly changes and parametric resonance disappears.

Extremely large effort to investigate parametric resonance was devoted during recent years and a great number of important papers were published on this subject (e.g. [16, 17]). Also a large number of documents containing studies of the effect of parametric resonance on stability were submitted to IMO. Actually, the main reason of taking parametric resonance into consideration was one casualty of large container ship [18] where due to parametric resonance in head waves serious damage to the container staples leading to loss of several containers and some damage to the ship hull happened.

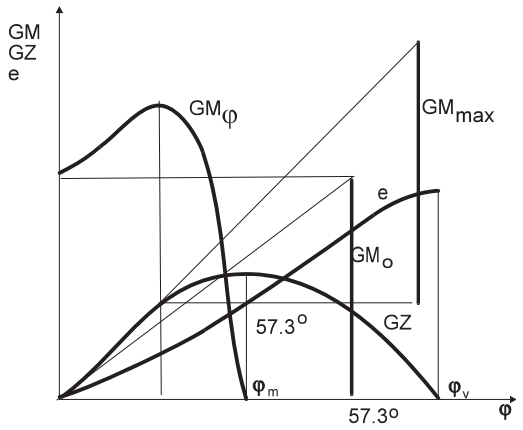

Fig.3. Relation between GM_0 and GM_φ

However, careful analysis of about three hundreds casualty reports [19] reveals that cases where the casualty may be attributed solely to parametric resonance could not be found and if parametric roll happened, usually was associated with other hazards.

It appears that this approach is charged by some disadvantages and even some countries expressed now the view that the criteria proposed until now are too complicated and in particular at level three they require application of the rather sophisticated computer programmes that are not commercially available [10].

SOME THOUGHTS ON FUTURE APPROACH TO STABILITY

The present approach to SGSC does not include hazards evaluation. However hazard identification and evaluation of its probability, as already pointed out, constitutes first step in safety assessment. Various means may be used to identify hazards to stability and to evaluate their probability. Important hazards are caused by forces of the sea.

Ship sailing in rough seas is subjected to external forces created by waves, wind, and current. In the paper presented to STAB conference [20] the author identified numerous hazards to the ship due to action of sea forces apart from changes of GZ curve on wave crest and broaching. All of them should be taken into account. Some of them may happen more often than parametric resonance but somehow they are not included into consideration (see Table 3).

Tab. 3. Some simple capsizing scenarios in waves

Scenario	
1	Pure loss of stability in wave crest
2	Parametric resonance, following or head seas
3	Quartering seas
4	Bow submergence, "green seas"
5	Rolling in beam sea, resonance, parametric resonance
6	Beam seas, "three sisters" waves
7	Beam seas, wind gust, icing, loose goods
8	Freak waves
9	Lurching, non-linear singularities
10	Breaking waves
11	Water on deck, pseudostatic heel
12	Broaching to

It must be noted, that motions of the ship in sea waves is strongly nonlinear process as well as also irregular wind created waves are strongly non-linear. Because of that it must be expected that certain singularities must appear. So called lurching, i.e. sudden very large heel in comparatively calm sea, that sometimes is reported by ship masters, may be result of this phenomenon that usually is attributed to parametric resonance, where in fact it is caused by singularity of the process. This may be very rare event, but an example of this is shown in fig. 4, where record of wave height shows a single wave of the height 25 metres, that is 2,5 higher than significant wave height approximately equal to about 10 metres.

Another hazard considered, loss of stability in wave crest, happens more often, however both effects, parametric resonance and loss off stability in wave crest may be easily avoided with proper handling of the ship and not putting the ship in situation when those phenomena may occur (e.g respecting recommendation MSC.1/Circ.1228). The same reasoning is applicable to surf riding and broaching, hazards in fact dangerous for rather fast small ships.

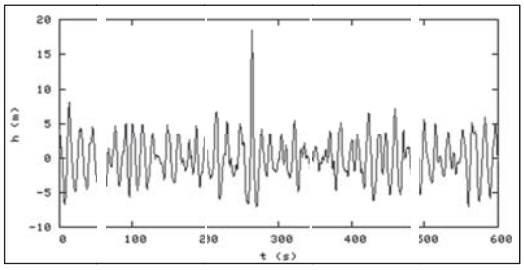

Fig.4. Record of the waves with singularity shown..[21]

MOST WIEDZY Downloaded from mostwiedzy.pl

With broaching criterion the obvious difficulty, as pointed out by Tompuri et al [10], is that the calculation require the calm water resistance as a function of velocity and detailed data on the propulsion. Those data are generally not available in preliminary design and certain approximations must be used. Moreover, stability does not affect the results.

Different situation exists regarding hazard defined as dead ship condition. The present weather criterion, as it appears in the IS Code, in fact covers the situation of the dead ship condition. In general opinion weather criterion is working well for the majority of ships, However some unconventional ships, e.g. ships with large windage area and large B/L ratio, as for example large cruise vessels and similar, often have difficulty to meet this criterion. On the other hand experience shows that large passenger ships are reasonably safe.

IMO SLF Subcommittee already took care of this effect developing guidelines for alternative assessment of the weather criterion adopted by resolution MSC.1/Circ.1200. In the view of the author, problem of dead ship condition, that is virtually problem of the weather criterion, could be considered as solved, at least for the time being.

Barnett [22] pointed out, that the safety system or organisation should be considered as a series of barriers against potential failure. Similar concept was proposed by Gower-Jones and van der Graaf as "Tripod method", also including concept of barriers.[23]. These barriers may take different forms including hardware, software, human action etc. Presence of those barriers will prevent casualty Sometimes only the last barrier will hold (a near miss). This idea was tested by Szozda [24] on the example of casualty of ferry boat "Jan Heweliusz", where several barriers were discovered, all of them could hold, but in fact they did not, and the ship capsized.

Improvement of the design characteristics of the ship or even eliminating all possible causes where faulty design is the main cause of casualty may affect only small percentage of casualties. Concentrating main effort on design characteristics of ships is therefore not the most important task.

IMO current work on second generation stability criteria consisting of taking into account some stability failure scenarios identified as important, will certainly increase the level of safety from the stability point of view. However, analysis of stability casualties reveals that chosen stability failure modes are not the most frequent ones. Although current approach to second generation stability criteria includes consideration of some important hazards it does not take into account hazards probability.

It seems, that if the probability of hazard is lower than certain assumed value, such hazard may not be considered further. How to assess hazard probability is another matter. Obviously probability of hazard depend to some extent on ship design, but more on ship operation and human factor. Parametric resonance may be easily avoided by following by the master operational guidance. Within the second generation stability criteria operational guidances are included in the scheme. They may be. developed on the basis of existing resolution MSC.1/Circ.1228. Operational guidelines are proposed however as alternative to direct stability assessment as shown in the table 1.

CONCLUSIONS

IMO current work on second generation stability criteria is almost completed, however its application to sample ships revealed certain inconsistencies and deficiencies of the approach creating some concern of interested parties. Finalisation of the criteria and developing corresponding stadards in short time seems to be unrealistic.

In general opinion existing criteria as in the IS Code 2008 are working well for conventional ships. Experience of application of the existing intact stability requirements reveals that stability failures with ships meeting the criteria are extremely rare.

The main weakness of the approach used in developing the second generation stability criteria is lack of the analysis of the risk involved with the chosen stability failures. Analysis of stability casualties reveals that stability failure modes considered in the second generation stability criteria are not the most frequent ones and some of the are extremely rare. The major benefit of the results of second generation stability criteria is increased knowledge of physical phenomena related to motions of a ship in a seaway.

For non-conventional ships the existing requirement of the IS Code 2008 may be inadequate and alternative ways of assuring safety should be used. Applying alternative means is allowed under the provisions of SOLAS Convention. Alternative means may include risk assessment and goal oriented approach.

In the opinion of the author it is now time to apply different, more universal procedures to stability criteria. These are already considered widely, recommended by IMO higher bodies and already used in drafting safety precautions.

REFERENCES

1. IMO, International Code for Intact Stability, 2008
2. Kobyliński L., Kastner S.: Stability and Safety of Ships. Vol. 1, ELSEVIER 2003
3. IMO: Intact stability. General philosophy for ships of all types. Submitted by Poland, doc STAB XXII/6, 1978
4. IMO: Report to the Maritime Safety Committee. Sub-committee on stability, and load lines and on fishing vessel safety, Doc. SLF 51/17, 2008
5. Peters W., Belenky V., Bassler C., Spyrou K., Umeda N., Bulian G., Altmayer B. (2011). The Society of Naval Architects and Marine Engineers. Annual Meeting Paper.
6. IMO: Second generation stability criteria. Submitted by

MOST WIEDZY Downloaded from mostwiedzy.pl

Poland, doc. SLF 54/ 14, Annex1, 2012

7. IMO, Report of the working group, doc SDC 1/5/6, 2013

8. IMO 2017. Finalization of second generation intact stability criteria. Report of the corresponding working group (Part 1), doc. SDC 4/WP.4

9. IMO 2017. Concerns relating to the finalization of the second generation intact stability criteria. Submitted by the United States, doc. SDC 4/5/7

10. Tompuri M., Ruponen, F., Forsa M., Lindroth D, 2016: Application of the second generation intact stability criteria in initial ship design. SNAME Annual Meeting

11. IMO: Interim guidelines for the application of Formal Safety Assessment (FSA) to the IMO rule-making process, doc. MSC/Circ.829; MEPC/Circ.335, 1997.

12. Safedor. Risk-Based Approaches in the Maritime Industry. , Second International Workshop Glasgow, May 2008

13. Hoppe H.: Goal based standards – a new approach to the international regulation of ship construction. IMO News, Issue 1., 2006

14. Papanicolau A. D.: Goalds-Goal based damage stability of passenger ships. SNAME Annual Meeting, 2012

15. Wawrzyński W., Krata P.: Proposal of revision of the practical approach towards IMO Circ. 1228 and the Intact Ship Stability Code application with regard to the naturel period of roll calculation. Unpublished paper presented to Polish IMO Committee, 2017

16. Peters W., Belenky V., Bassler C., Spyrou K., Umeda N., Bulian G., Altmayer B. (2011). The Society of Naval Architects and Marine Engineers. Annual Meeting Paper.

17. Belenky V. L., Weems K.M., Paulling J.R.: Probabilistic analysis of roll parametric resonance in head seas. 8th Stab Conference, Madrid, 2003

18. France, W.N., Levadou, M., Treakle, T W., Paulling, J.R., Michel, R.K., Moore, C.,: An investigation of head sea parametric rolling and its influence on container lashing systems. SNAME Annual meeting, 2001

19. Kobyliński L.: Zestawienie statków uległych awariom LOSA. Unpublished report. Foundation for Safety of Navigation, 2006

20. Kobylinski L.: Capsizing scenarios and hazards identification. 9th International STAB Conference, Madrid. 2003

21. Dysthe K.B., Krogstad H.E., Socquet-Juglard H., Trulsen K.: Freak waves, rogue waves, extreme waves and ocean wave climate. www.math.uio.no, 2007

22. Barnett M., L.: Searching for root causes of maritime casualties. WMU Journal of Maritime Affairs, Vol.4, No. 2, 2005

23. Gower-Jones A.D., van der Graaf G.C.: Experience with Tripod BETA incidents analysis. Society of Petroleum Engineers International Conference, Caracas, 1998

24. Szozda Z.: Application of the TRIPOD method for human factor analysis on the example of m/f Jan Heweliusz capsizing. 10th International STAB Conference, St Petersburg, 2009

CONTACT WITH THE AUTHOR

Lech Kobyliński
e-mail: lechk@portilawa.com

Polish Academy of Sciences
The Committee on Transport of the Polish Academy of Sciences
Palace of Culture and Science, Plac Defilad 1
00-901 Warsaw
Poland

MOST WIEDZY Downloaded from mostwiedzy.pl

POLISH MARITIME RESEARCH Special Issue 2018 S1 (97) 2018 Vol. 25; pp. 63-67
10.2478/pomr-2018-0024

COMPARISON OF SELECTED PARAMETRIC METHODS FOR PREDICTION OF INLAND WATERWAYS SHIP HULL RESISTANCE IN TOWING TANK TEST

Artur Karczewski
Janusz Kozak
Gdańsk University of Technology, Poland

ABSTRACT

In the paper selected approximate methods for calculation of inland waterways ship resistance and their verification by towing tests, compared on the example of a small urban ferry, are presented. The test results are made for both the bare hull and the hull with appendages (skeg, azimuthal propeller). Significant differences between results of the theoretical methods and experimental ones, especially in the case of the model with skegs and propulsion, are pointed out. The purposefulness of using several parametric methods and the use of average results at the preliminary design stage were also discussed.

Keywords: ship resistance, inland waterways

MOST WIEDZY Downloaded from mostwiedzy.pl

INTRODUCTION

The ship design is a difficult, multi-stage process. Its typical structure is illustrated by Evans spiral [1] [2]. This is like a multi-flavoured pizza, where each triangle is only one part of a whole project, but composed of other parts as well. According to Michalski [2], the first step of such project is a parametric design phase. It identifies ship's parameters which determine the qualities of the whole project. One of the important actions in this design stage is proper prediction of the hull resistance. This usually is based on approximate calculation methods. Then the results are verified based on experiments in the towing tank. The parametric formulas are often useful only for a given ship type and hull arrangement, and for a set of its main parameters. The results of such calculations should be considered approximate. However the obtained data are used for defining the initial characteristics of the ship's propulsion system. They also serve as a starting point for experimental test. Forecasts based on experimental model studies are more accurate. They can be used to verify the design and determine a direction of possible modifications. The aim of these studies was verification of known parametric methods for resistance estimation, which could be used in the first design phase , as well as the defining of appropriate formulas which are easily adopted for PC without a high computing power. It is very important , especially for small ships , that such methods are not expensive. In this case the total price of project cannot be too high because building cost of a small ship is relatively low.

PROJECT

The project in question is the ship "Motława II" which should replace the existing ferry 'Motława' being in service since 1987. The new ship should be capable of meeting growing expectations of the passengers and crews and following today EU regulations. Design work on the 'Motława II' project

started in March 2015 in the form of a collaboration between the National Maritime Museum (NMM) and the Gdansk University of Technology (PG).

The main requirements for the design were as follows:

- type of ship: a passenger urban ferry to be operated on the route between the Main City of Gdańsk and the Ołowianka Island, as the NMM has its buildings on both banks of the river;
- main parameters: hull length - 12,0m, beam - 5,0m, number of passengers: 36 persons, crew: 3 persons;
- structural material: steel;
- equal forward and backward manoeuvring properties.

As a result of the design process containing the elements of optimization [3] the shape of the hull was developed. For this hull the resistance analysis was performed by using parametric methods and model tests.

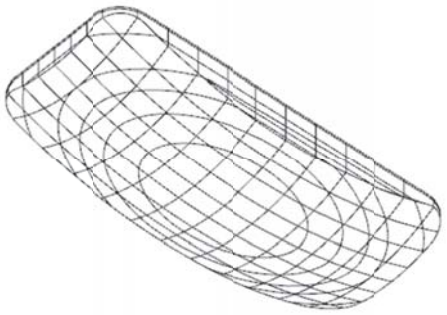

Fig. 1 Bare hull

The optimization showed that the best hull shape lies between a simple cuboid (highest stability) and a part of spheroid (lowest resistance). The new bottom shape was a part of spheroid suitable for changing its longitudinal and transverse curvatures [3].

Because the first study in the towing tank showed that the bare hull model was rather not able to keep a stable course and good manoeuvrability, the correction of hull shape was necessary. This problem was solved by installing skegs. In this case an estimate of resistance for the hull with appendages like skegs and azimuth thruster has been made.

Fig. 2 The final version of 1:10 scale model with skegs and azimuth thruster.

Based on the made assumptions, the classification design project of the ship " Motława II" was developed.

Fig. 3 The ship in operation since 1987

Fig. 4 Visualization of the new ferry

SELECTED APPROXIMATE METHODS

To perform the first estimation of hull resistance the methods presented in the literature [4] [5] have been used. Uncomplicated structure of the formulas is easy to implement to calculation spreadsheet. The methods in question are based on a limited set of hull parameters. They are expressed by nonstructural models elaborated by approximating the set of results of many towing tests.

WRÓBLEWSKA – SIROTINA METHOD

The total resistance of ship, $R_{T(W\text{-}S)}$ [kN], acc. Wróblewska – Sirotina method (W-S), is calculated by using the following equation:

$$R_{T(W-S)} = 0.1295 \cdot \left(48 \left(\frac{v}{\sqrt{g\sqrt[3]{\nabla}}} \right)^2 - 29 \left(\frac{v}{\sqrt{g\sqrt[3]{\nabla}}} \right) + 5,9 \right) \frac{B^2 \cdot T \cdot \delta^2}{\left(\frac{B}{T}\right)^{0.2}} \quad (1)$$

where:

v – ship speed [m/s];
V – volumetric displacement [m^3];
δ – ship hull block coefficient [-];

MOST WIEDZY Downloaded from mostwiedzy.pl

B – ship breadth [m];
T – ship draught [m];
g – 9,81 [m/s^2].

ZWANKOW METHOD

The total resistance of ship, $R_{T(Z)}$ [kN], acc. Zwankow method (Z) , is calculated by using the following equation:

$$R_{T(Z)} = 9,81 \cdot 10^{-3}\left(0.17 \cdot \Omega \cdot v^{1.825} + \delta \cdot A_M \frac{17.7\delta^{2.5}}{\left(\frac{L}{6B}\right)^3 + 2} v^{1.7} + 4\frac{v}{\sqrt{g \cdot L}}\right) \quad (2)$$

where:
Ω – wetted hull area [m^2];
A_M – midship area [m^2];
L- ship length [m].

LENINGRAD DESIGN OFFICE METHOD

The total resistance of ship, $R_{T(LDO)}$ [kN], acc. Leningrad Design Office method (LDO) is calculated by using the following equation:

$$R_{T(LDO)} = 9,81 \cdot 10^{-3}\left(0.17 \cdot \Omega \cdot v^{1.825} + 1.45\left(24 - \frac{L}{B}\right) \cdot \delta^{5/2} \cdot \frac{D \cdot v^4}{L^2}\right) \quad (3)$$

where:
D – ship displacement [t].

TOWING TEST

In the experimental study the laminated 1:10 scale model of the ferry "Motława II " was used. The study was conducted in the towing tank of Faculty of Ocean Engineering and Ship Technology, Gdansk University of Technology, in calm water for two cases , without trim.

The main parameters of the hull model 511 and the real vessel are given in Tab. 1:

Tab. 1 Main parameters of the model and the real ship

PARAMETER	MODEL	SHIP
L – ship length [m]	1.20	12.00
B – ship breadth [m]	0.50	5.00
L_{WL} – ship waterline length [m]	1.047	10.47
T – ship draught [m]	0.093	0.93
V – volumetric displacement [m^3]	0.0231	23.12
Ω – wetted hull area [m^2]	0.5053	50.53

Fig. 5 Side view of the model without appendages

Fig. 6 Front view of the model without appendages

Fig. 7 Side view of the model with appendages

Fig. 8 Front view of the model with appendages

The measured total resistance of the model was recalculated to the scale of the actual ferry by using three-dimensional extrapolation based on the extended Froude method [6]. The total resistance coefficient was assumed to be typically composed of:

- friction resistance coefficient depending on the Reynolds number,
- residual resistance coefficient;
- pressure resistance coefficient taking into account the k shape coefficient, which increases the level of friction resistance of both the ship and the model in relation to corresponding flat plates.

Fig. 9 Model without appendages during the test

MOST WIEDZY Downloaded from mostwiedzy.pl

Fig. 10 Model with appendages during the test

RESULTS

The computational estimation of the hull resistance was determined by means of the three parametric methods : (W-S), (Z), (LDO).

The experimental study included measurement of resistance of the ‘ Motława II “ ferry 1:10 scale model in the speed range from 1.5 to 12.5 km / h. The study was conducted for two cases , without trim:

- Design conditions (A) for the model of bare hull, $R_{T(B)}$,
- Design conditions (B) for the model of hull with appendages, $R_{T(A)}$.

Based on the results of the studies, the forecast for the real ship’s resistance was calculated. Results of both the studies are presented in the graphs.

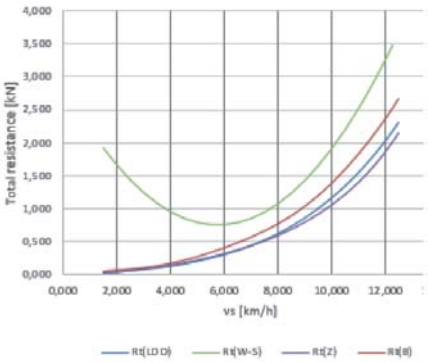

Fig. 11 Total resistance of bare hull

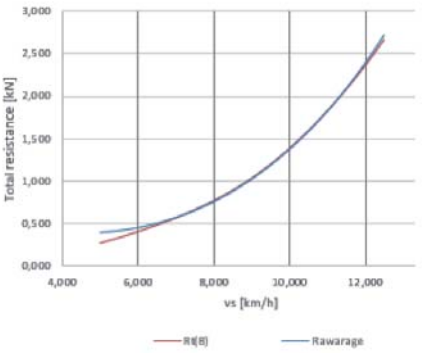

Fig. 12 Comparison of total resistance of bare hull

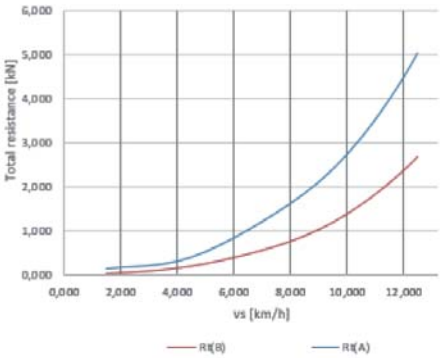

Fig. 13 Comparison of Rt(B) and Rt(A)

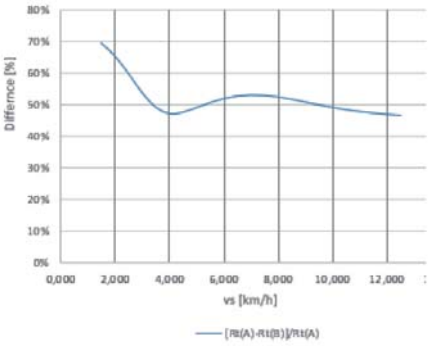

Fig. 14 Increase in the resistance [%]

CONCLUSION

The results of approximate calculations performed by using parametric methods are close to those from the model tests of the hull without appendages. The adding of the skegs and azimuth thruster models resulted in a nearly double resistance and, as a consequence, also an increased demand for power. In the ship speed range between 3,5-:-12,5 [km/h] the increase in total resistance of the hull with appendages compared to that of the bare hull, is ~50%. The significant difference between the results obtained by using parametric methods and the results of model studies for the hull equipped with skegs and thrusters is typical since the approximate parametric methods do not take into account the appendages. Nevertheless, the nearly twofold rise in likely power demand ($R_t \cdot v$) following the mounting of skegs and azimuth thrusters, seems to be overestimated. According to the authors of this design, it results mostly from larger dimensions of the model azimuth thrusters than those resulting from the applied scale. Interesting is the situation in the case of taking the arithmetic mean from the parametric calculations, $\frac{1}{3}\left(R_{T(LDO)} + R_{T(W-S)} + R_{T(Z)}\right)$. It turns out that theoretical and experimental results for design condition are identical. However it should be remembered that the results has been achieved by using the W-S method. The applicability of this method is limited and the designed hull is formally beyond this range.

MOST WIEDZY Downloaded from mostwiedzy.pl

The research shows that it is possible and desirable to use the simplified methods in the initial design phases. They allow very early and without effort and costs to determine the initial parameters of the propulsion system.

ACKNOWLEDGMENTS

The study was performed in the frame of the grant founded by the Provincial Fund for Environmental Protection and Water Management , Gdańsk , with the assistance of the National Maritime Museum in Gdańsk , which is the designated ship-owner of the new- designed ferry.

BIBLIOGRAPHY

1. A. Papanikolaou: Ship Design, Methodologies of Preliminary Design, London, Springer, 2014.
2. J. Michalski: Fundamentals of ship design theory (in Polish), Gdańsk, Wydawnictwo Politechniki Gdańskiej, 2013.
3. A. Karczewski i Ł. Piątek: Reducing the Environmental Impact of the Public Water Transportation Systems by Parametric Design and Optimization of Vessels' Hulls. Study of the Gdańsk's Electric Passenger Ferry (2015-2016), in : Architecture for the Society of Knowledge, Warszawa, 2016.
4. J. Michalski: Methods useful for computer aiding the preliminary design process of inland waterways ships (in Polish), Gdańsk,Wydawnictwo Politechniki Gdańskiej, 2007.
5. A. Zborowski:Ship resistance (in Polish), Gdańsk, Wydawnictwo Uczelniane Politechniki Gdańskiej, 1972.
6. M. Grygorowicz : Resistance tests of the ferry Motława II model in towing tank – results and their analysis (in Polish), Politechnika Gdańska Wydział Oceanotechniki i Okrętownictwa, Gdańsk, 2016.

CONTACT WITH THE AUTHORS

Artur Karczewski
e-mail: artkarcz@pg.gda.pl

Janusz Kozak
e-mail: kozak@pg.gda.pl

Gdańsk University of Technology
11/12 Narutowicza St.
80 - 233 Gdańsk
Poland

MOST WIEDZY Downloaded from mostwiedzy.pl

POLISH MARITIME RESEARCH Special Issue 2018 S1 (97) 2018 Vol. 25; pp. 68-73
10.2478/pomr-2018-0025

METHODS OF DETERMINATION OF FRICTIONAL RESISTANCE FOR PREDICTION OF TOTAL RESISTANCE OF INLAND WATERWAY VESSELS

Jan Kulczyk
Wrocław University of Technology, Poland

ABSTRACT

In the present paper presented are the results of prediction of total resistance of inland waterway vessels based on model test data. In scaling the resistance from model to full scale the extrapolation with two-dimensional frictional resistance formulation (without form factor) was applied, combined with different methods of determination of frictional (viscous) resistance coefficient. There were used the equations that include the effect of water depth, with and without account for pressure gradient. It was shown that limited depth of water substantially affects the frictional resistance. The results of example calculations are compared to resistance prediction made using the ITTC 1957 model-ship correlation line. Example calculations take into account the limited depth of water. Depending on the applied method of determination of frictional resistance coefficient the resultant total resistance of inland waterway vessel is higher or lower than the resistance based on the ITTC 1957 correlation line. The effect of water depth depends on the ratio of water depth to ship draught (h/T), on ship speed, and on the composition of a convoy. The extrapolation of resistance was made without including the form factor. Computations are made based on model test data for an inland waterway cargo vessel, for a kombi-type convoy of an inland waterway cargo vessel and a dumb barge, and for a convoy of two dumb barges without a pushboat.

Keywords: inland waterway vessel, extrapolation of hull resistance, coefficient of frictional resistance

INTRODUCTION

In design of inland waterway vessels the prediction of ship resistance is made based on model tests and using the Froude hypothesis and extrapolation techniques. For determination of frictional resistance the ITTC-1957 model-ship correlation line or the Schoenherr formula are usually applied. In the range of Reynolds numbers that can be encountered in resistance prediction, i.e. $10^5 \leq Re \leq 10^9$, the values of frictional resistance coefficient determined using above formulae differ merely slightly. The difference is about 2% for low Reynolds numbers and less than 1% for $Re \geq 10^8$.

Above methods of determination of frictional resistance are based on the resistance of flat plate and do not account for finite water depth in the case of shallow water. In comparison to deep water the finite depth of shallow water is related to specific phenomena in ship motion:

- significantly higher resistance at the same ship speed,
- change in position of hull in relation to undisturbed surface of water, i.e. trim and sinkage.

The back flow appears and the velocity in flow around the hull is higher than ship speed.

The study of ship motion in shallow water reveal the rapid growth of hull resistance, trim and sinkage when approaching the critical speed. Critical speed is related to the velocity of energy transportation in wave motion. The critical speed in shallow water amounts:

$$V_{kr} = \sqrt{g \cdot h} \quad (1)$$

MOST WIEDZY Downloaded from mostwiedzy.pl

where g is the acceleration due to gravity, and h is the depth of water.

In practice, merchant ships in restricted waters are operated at speeds lower than the critical speed. The hydrodynamically economic speed limit for inland waterway vessels [1] was determined as [3]:

$$V_{gr} = (0{,}5 \div 0{,}65) \cdot V_{kr} \quad (2)$$

The upper value applies to motor cargo vessels and the lower value applies to pushed barge trains composed of two or three rows of dumb barges and a pushboat.

The rapid growth of hull resistance at speeds above the economic speed limit V_{gr} is the effect of increase of wave resistance. The share of viscous resistance in total hull resistance of an inland vessels has not been recognized in details. Based on data from model tests one may assume that at speeds around the economic speed limit the contribution of viscous resistance amounts about 30÷40% of total resistance. This share is higher at speeds below V_{gr}, and is lower at speeds higher than V_{gr}. Because the share is considerable the error in determination of viscous resistance may cause significant error in power prediction for a full scale vessel.

In this paper the results of prediction of total resistance of inland waterway vessels are presented based on model test data and extrapolation procedure. In scaling the resistance from model to full scale the extrapolation with two-dimensional frictional resistance formulation (without form factor) was applied combined with different methods of determination of frictional (viscous) resistance coefficient. There were used the equations that include the effect of water depth, with and without account for pressure gradient. It was shown that limited depth of water substantially affects the frictional resistance. The results of example calculations were compared to resistance predicted using the ITTC-1957 model-ship correlation line. The resultant total resistance of inland waterway vessel is higher or lower than the resistance based on the ITTC-1957 correlation line depending on applied method of determination of frictional resistance coefficient. The ratio of predicted values depends on the proportion between water depth and ship draught (h/T), on ship speed, and on the composition of a convoy of vessels. The extrapolation of resistance was made without account for velocity of back flow and roughness (no roughness allowance). It was assumed that the contribution of above components in any case would be the same, independent from the method of determination of frictional resistance coefficient. Computations were made based on model test data for an inland waterway cargo vessel sailing alone or coupled with a single dumb barge (a kombi-type train) [5], and for a convoy of two dumb barges without a pushboat [2].

FRICTIONAL RESISTANCE IN SHALLOW WATER

The conditions of sailing in shallow water are determined by finite distance between ship bottom and the bed of waterway. Turbulent boundary layer in ship flow is confined. In very simple terms one may assume that the flow is similar to the flow between two parallel flat surfaces where one surface is motionless and the other moves at velocity corresponding to ship speed. Such model of flow does not include the variable gradient of pressure that is the case in actual ship motion in shallow water. One assumes that flow in space between surfaces is a fully developed turbulent flow, and that the distribution of velocity is logarithmic. Accordingly, the following relationship has been derived [4]:

$$\frac{1}{\sqrt{c_F}} = 1{,}768 \cdot \ln\left(\sqrt{c_F} \cdot \mathrm{Re}_h\right) + 1{,}509 \quad (3)$$

where:

c_F -coefficient of frictional resistance,

Re_h -Reynolds number based on distance between surfaces:

$$\mathrm{Re}_h = \frac{V_S \cdot h}{\nu} \quad (4)$$

where:

h -distance between surfaces,

ν -kinematic viscosity of water.

The relationship between the coefficient of frictional resistance c_F and the Reynolds number Re_h is illustrated in Fig.1. It has been approximated using the cubic polynomial:

$$C_F = \text{-}6.541\text{E-}05(\log Re_h)^3 + 1.466\text{E-}03(\log Re_h)^2 - 1.138\text{E-}02 \log Re_h + 3.195\text{E-}02 \quad (5)$$

Zawiślak [6] has completed the formula (3) with the term that accounts for pressure gradient:

$$\frac{1}{\sqrt{c_F}} = 1{,}768 \cdot \ln\left(\sqrt{c_F} \cdot \mathrm{Re}_h\right) + ST + 1{,}326 \cdot f(c_F, \mathrm{Re}_y, y_n) \quad (6)$$

where:

ST = 0.68 for model ship,

ST = 1.509 for full scale ship.

The term $f(c_F, \mathrm{Re}_y, y_n)$ takes into account the averaged pressure gradient between the bottom of vessel and the bed of waterway. The Reynolds number Re_y is based on local distance between the bottom of 'averaged' hull and waterway bed:

$$y_n = h - \frac{Ax(x)}{B} \quad (7)$$

MOST WIEDZY Downloaded from mostwiedzy.pl

where:

Ax(x) -local sectional area of hull,

B -ship beam.

In the case of flat surface the last term in equation (6) equals zero and the equation is identical to eq. (3). Two values of term ST in equation (6) were introduced based on numerical computations of flow between the 'averaged' two-dimensional hull and waterway bed [6]. One may consider it as a partial equivalent of form factor commonly used in extrapolation of ship resistance.

Frictional resistance coefficient c_F calculated according to equation (6), without the effect of pressure gradient ($f(c_F, Re_y, y_n) = 0$), is presented in Fig.1.

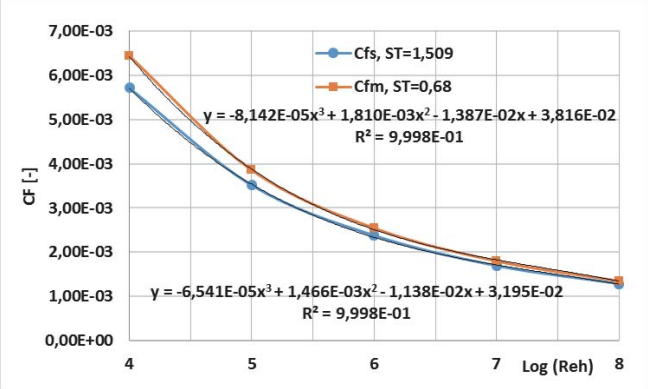

Fig.1. Coefficient of frictional resistance c_F calculated according to equation (6) with $f(c_F, Re_y, y_n) = 0$

The effect of shallow water on resistance prediction was investigated using frictional resistance coefficient calculated according to equation (3), approximated with formula (5). The effects of scale factor and pressure gradient (according to eq. (6)) are presented for one test case of the OBM motor cargo vessel.

RESULTS OF CALCULATIONS AND THE ANALYSIS

The effect of the method of determination of frictional resistance coefficient on resistance prediction was investigated for two vessels that were extensively tested in model scale including the variation of draught and water depth. There are conventional ships operated on inland waterways: the motor cargo vessel (OBM) operated alone or as a kombi-type convoy i.e. coupled with a dumb barge (OBM+BP), and two dumb barges coupled in a single-row convoy without a pushboat (2xT170). Model tests of the motor cargo vessel were carried out in Ship Design and Research Centre in Gdańsk [5]. The convoy of two dumb barges was tested in Development Centre for Ship Technology and Transport Systems (DST) in Duisburg, in the framework of RTD project INBAT [2]. Hull forms of considered vessels are presented in figures 2 and 3. Main particulars are as follows:

OBM
Length between perpendiculars LPP = 67.83 m
Draught T1 = 1.60 m; T2 = 2.36 m
Length at waterline LWL1 = 67.83 m; LWL2 = 69.27 m
Beam B = 8.92 m
Dumb barge (BP)
Length between perpendiculars LPP = 44.12 m
Draught T = 1.60 m
Test conditions
Water depth h = 2.00; 2.25; 2.50; 2.75 m
Model scale 1:16

Dumb barge T170 (INBAT)
Length over all LOA = 48.75 m
Length between perpendiculars LPP = 48.28 m
Design draught T = 1.70 m
Beam B = 9.00 m
Conditions of model tests
Draught T = 0.6; 0.9; 1.4; 1.7 m
Water depth h = 1.2; 2.0; 3.6; 5.0 m
Model scale 1:14

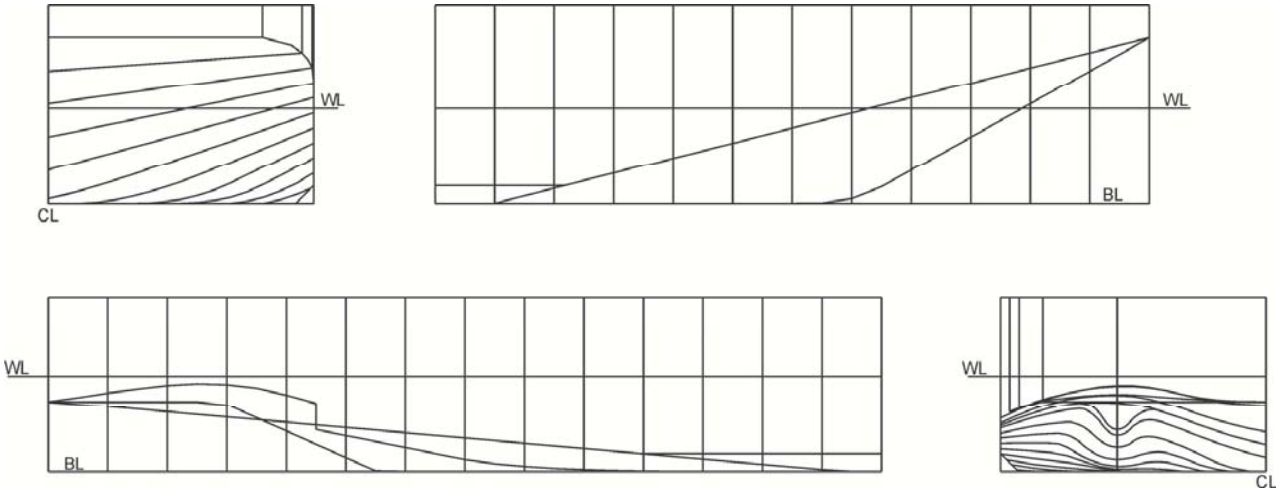

Fig.2. Hull form of motor cargo vessel OBM

MOST WIEDZY Downloaded from mostwiedzy.pl

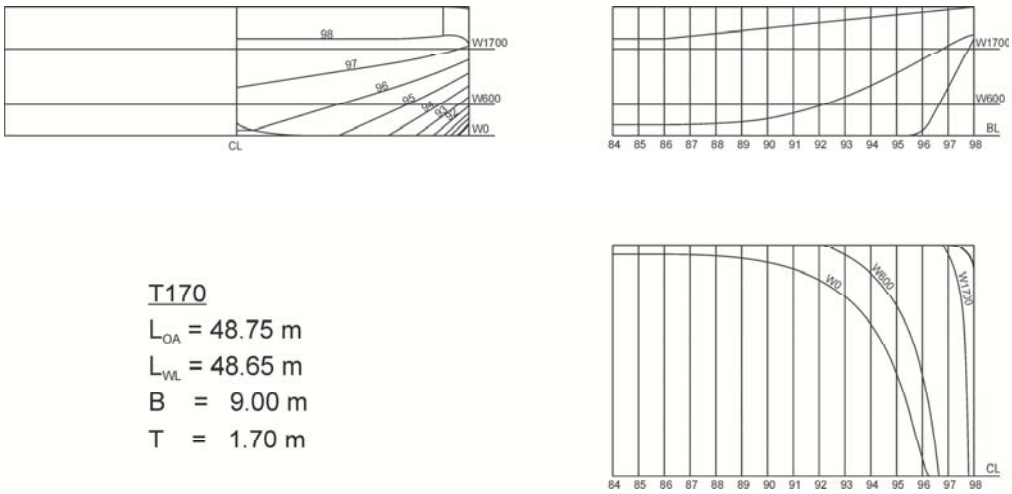

Fig.3. Hull form of dumb barge T170

OBM - THE RESULTS OF CALCULATIONS

The ratio of ship resistance predicted with coefficient of frictional resistance calculated according to eq. (3) (Rths) to ship resistance predicted with coefficient of frictional resistance determined using the ITTC-1957 model-ship correlation line (Rts57) is presented in figures 4, 5 and 6. Resistance predicted with account for restricted depth of water Rths is higher (Fig.4). The differences are within 0.5% to 3% and depend on water depth and ship speed. At lower depths of water these differences are smaller. The increase of ship speed causes that the differences decrease. The trends at ship draught T = 2.36 m are similar (not presented in this paper).

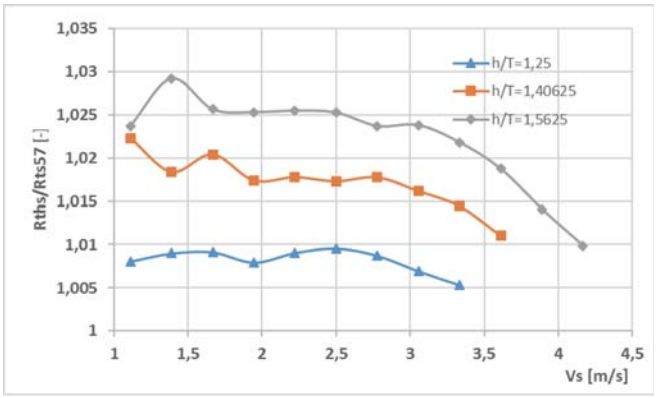

Fig.4. The effect of water depth on resistance prediction, OBM at T = 1.60 m

When the coefficient of frictional resistance is calculated using eq. (3) with term ST adjusted to model ship and full scale ship, as in eq. (6), then the predicted ship resistance is lower than resistance predicted with application of the ITTC-1957 correlation line (Fig.5). The differences amount from 6% to 1%. The effect of depth to draught ratio h/T is not distinct. The effect of ship speed is clear.

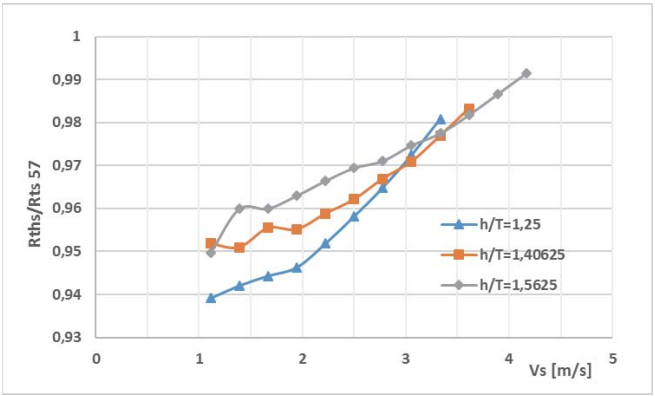

Fig.5. The effect of account for scale factor (last term in eq. (3) adjusted to model ship and full scale ship during extrapolation) on resistance prediction, OBM at T = 1.60 m

The effect of ship length on resistance prediction is shown in Fig.6. In the case of kombi arrangement (OBM+BP) the resistance predicted with account for restricted depth of water is lower. The differences do not exceed 3% and at higher speeds are smaller.

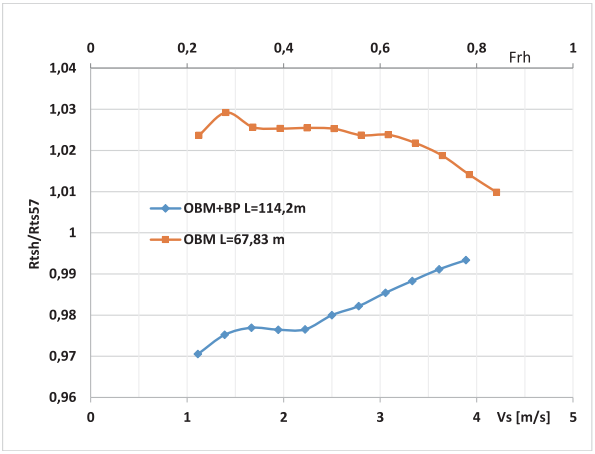

Fig.6. The effect of ship length on resistance prediction, OBM at T = 1.60 m, h = 2.5 m

MOST WIEDZY Downloaded from mostwiedzy.pl

The coefficient of frictional resistance c_F calculated according to eq. (6), i.e. with account for scale factor α and pressure gradient dp/dx, for the motor cargo vessel OBM are presented n fugues 7 and 8. The values calculated with non-zero pressure gradient (dp/dx ≠ 0) were originally published in [6].

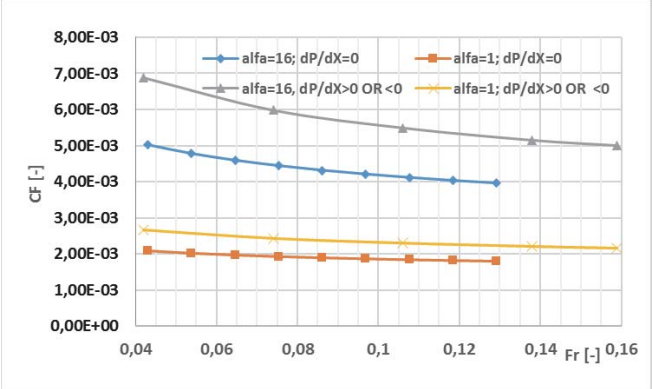

Fig.7. The effect of scale factor α and pressure gradient dp/dx on coefficient of frictional resistance cF calculated according to eq. (6), OBM at T = 1.60 m, h/T = 1.25

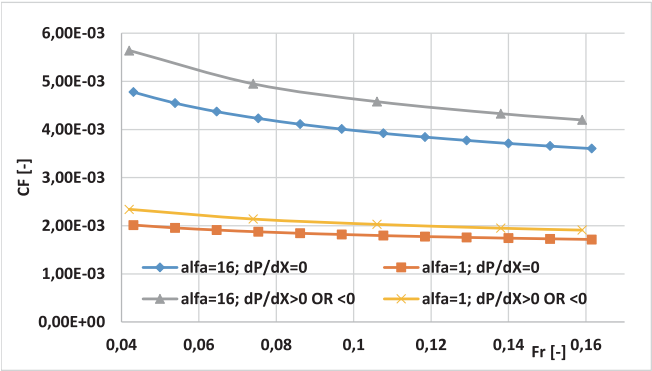

Fig.8. The effect of scale factor α and pressure gradient dp/dx on coefficient of frictional resistance cF calculated according to eq. (6), OBM at T = 1.60 m, h/T = 1.56

The neglect of pressure gradient (dp/dx = 0) makes the difference in frictional resistance coefficient in full scale lower than in model scale. Similar is the effect of increased water depth.

THE CONVOY OF TWO DUMB BARGES T170

Resistance prediction was made for typical convoy of two dumb barges coupled stern to stern in one row. Example results of calculations for the convoy at two settings of ship draught: T = 1.70 m and T = 0.90 m, are presented in figures 9 and 10, respectively. For the different ranges of speed the ratio Rths/Rts57 is drawn versus depth Froude number Fr_h.

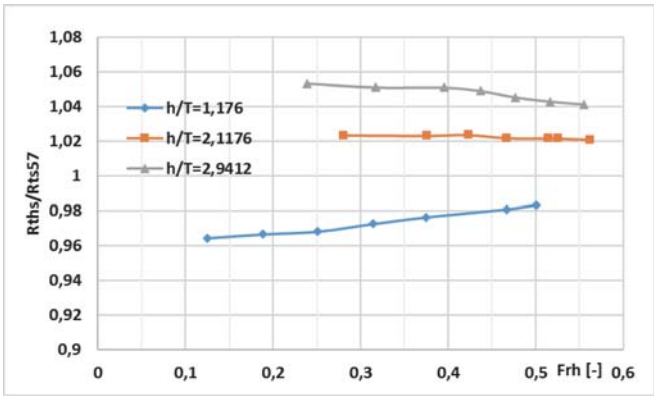

Fig.9. The effect of water depth, 2xT170 at T = 1.70 m

In comparison to OBM the effect of water depth is opposite. For very shallow water ship resistance predicted with application of eq. (3) (Rths) is lower than with ITTC-1957 correlation line, wherein apparent is the effect of ship draught. The differences in ship resistance range from 14% at T = 0.90 m to less than 4% at T = 1.70 m.

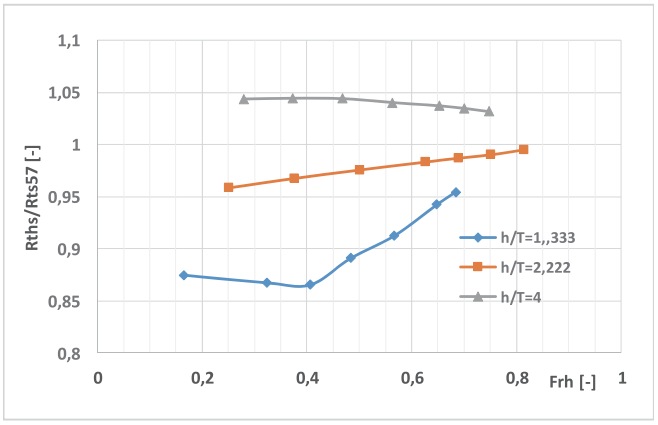

Fig.10. The effect of water depth, 2xT170 at T = 0.90 m

At increased water depth the resistance predicted with eq. (3) becomes higher than resistance predicted with application of ITTC-1957 correlation line. This trend is especially apparent at T = 1.70 m. However, the difference does not exceed 5%.

SUMMARY AND CONCLUSIONS

The ratio of ship resistance predicted using the coefficient of frictional resistance calculated with account for restricted depth of water, to ship resistance predicted using the ITTC-1957 model-ship correlation line (Rths/Rts57) is within 0.95 through 1.05. Considering highly variable conditions of ship operation on inland waterways, the results presented in this paper show that the application of frictional resistance coefficient calculated with account for restricted depth of water has little effect on power prediction. However, the application of frictional resistance coefficient calculated

MOST WIEDZY Downloaded from mostwiedzy.pl

according to equation (3) or (6) enables to determine the influence of important operating parameters as:

- depth of water,
- ship draught,
- composition of convoy.

The neglect of pressure gradient may have a significant effect on resistance prediction based on model tests only at very shallow water.

REFERENCES

1. Hauser H.: Verdrängungsschiffe auf flachem Wasser. Teil II: Anwendung beim Entwurf von Binnenschiffen, Schiffstechnik, Band 33, Heft 1, April 1986

2. Förster W., Guesnet T.: Resistance tests with barge trains, Report, Project INBAT - Innovative Barge Trtains for EffectiveTtransport on Shallow Waters, 5th Framework Programme of EC, Duisburg, 2003

3. Kulczyk J.: Prędkość graniczna w warunkach śródlądowej drogi wodnej, Prace Naukowe Instytutu Geotechniki Politechniki Wrocławskiej Nr 46, Seria: konferencje Nr 19, Śródlądowe drogi wodne i flota, Wydawnictwo Politechniki Wrocławskiej, Wrocław 1985

4. Kulczyk J.: A calculation method of ship frictional resistance on confined waterway, Polish Maritime Research, Vol. 8, No. 4(30), December 2001

5. Sprawozdanie z prób modelowych oporowo-napędowych odrzańskiej barki motorowej, RB-N-M20/B430-13, Ośrodek Hydromechaniki Okrętu, Centrum Techniki Okrętowej, Gdańsk, 1975

6. Zawiślak M.: Wpływ głębokości drogi wodnej na opór lepkościowy statku śródlądowego, Instytut Konstrukcji i Eksploatacji Maszyn Politechniki Wrocławskiej, Wrocław 2004

MOST WIEDZY Downloaded from mostwiedzy.pl

POLISH MARITIME RESEARCH Special Issue 2018 S1 (97) 2018 Vol. 25; pp. 74-79
10.2478/pomr-2018-0026

LONGITUDINAL MOTION DUE TO ACTION OF TUNNEL THRUSTERS

Maciej Reichel
Ship Handling Research and Training Centre
Foundation for Safety of Navigation and Environment Protection, Poland

ABSTRACT

Tunnel thrusters are propulsion and active control devises that provide a side force, or transverse thrust, to support mooring operations or position keeping. They shorten the time of manoeuvring, reduce the cost of towage and since inception, manoeuvrability specifically in ports has become a lot easier. Tunnel thrusters can either be operated manually or with the help of Dynamic Positioning systems which makes it even more efficient.
Theoretically, the transverse force due to tunnel thruster action should generate only lateral and rotational motion. Therefore, it is typical and a common practice during manoeuvring simulations that the longitudinal motion due to the action of tunnel thrusters is neglected. Nevertheless, the experience of masters and pilots shows that some longitudinal motion due to the action of tunnel thrusters appears.
This paper shows some examples of turning manoeuvres carried out with bow thrusters only, i.e. no additional control devices or tug assistance have been used. The manoeuvres have been carried with minimal possible initial longitudinal nor lateral speed. Model tests have been done with the use of large manned models of VLCS, PCTC and LNG carrier, which differ in hull shape, dimensions and shape coefficients.
Results obtained from the tests confirm that the motion caused by bow thruster besides rotational and lateral motion consists additionally of longitudinal motion. Analysis of the combination of motions due to the action of tunnel thrusters have been done and some rationale for this phenomenon has been presented. Additionally a short analysis of position of pivot point during tunnel thruster test has been carried out.

Keywords: VLCS, PCTC, LNG carrier, manned models, free running model tests

INTRODUCTION

Maritime sector is very important when analysing corridors of goods transportation. It is due to its effectiveness, relatively low environmental impact and price competitiveness. Therefore, to explore even more the economy of scale, ships become larger actually every year. On the other hand, port infrastructures do not follow the increase of ship dimensions and issues like safety of port manoeuvres become more and more significant and challenging.

Taking into account increasing ships dimensions, and thus decreasing manoeuvring space, the risk of any damage to vessels or port infrastructure is instantly growing and all possible steps should be taken to minimise this risk. Most important safety improvement aids, e.g. training of seamen, implementation of navigational aids and planning of harbour operations are primarily based on the simulation of ship motion. Therefore, modelling of ship motions during port manoeuvres, i.e. at slow speed in constrained space becomes to be essential. Different necessary aspects are taken into account when improving simulations of motions, e.g. wall effect on the hydrodynamic forces induced by the propellers and thrusters during berthing and unberthing (Abramowicz-Gerigk, 2007) or more precise description of manoeuvring forces at slow speed for azimuth thrusters (Reichel, 2017).

The same attention should be paid to the forces generated by tunnel thrusters, not only during berthing and unberthing, i.e. with very small rotational velocity, but also during other port manoeuvres with larger rotational velocities. In such

MOST WIEDZY Downloaded from mostwiedzy.pl

situations, e.g. manoeuvres in turning basins, additional factors reported by masters and pilots, like increasing longitudinal velocity due to the action of bow thruster should be taken into account. It can be however seen, that this longitudinal motion caused by the action of tunnel thrusters is neglected during simulations and analysis. Brix (1983) and especially Chislett and Björheden (1966) explained in details side force and turning moment generated by lateral thruster with the loss of effectiveness induced by the forward speed of the ship. They did not report however, on the possible occurrence of longitudinal force or velocity caused by the action of tunnel thrusters.

It has to be noted that the described phenomena is not always necessary to be taken into account during port manoeuvres analyses. When simulating crabbing motion, the influence of bow or stern thruster action on the longitudinal motion may be neglected (Quadvlieg and Toxopeus, 1998). In such a case the rotational speed is minimal and the possible longitudinal motion, caused by tunnel thruster action, is compensated by main propulsion system working in "ahead and balancing" propellers mode.

Nevertheless, some researchers have noticed the phenomenon of longitudinal motion due to the action of bow thruster. Artyszuk (2003, 2010) presented some analytical results of forward velocity increase calculations, where a conclusion on the increase of surge velocity with decreasing yaw velocity has been given. The responsibility for such a motion has been put on the centrifugal force in rotational motion. Some attempt to this issue has been also made by Gierusz (2016). The author suggests to introduce a weak surge force proportional to the longitudinal velocity of the ship and to a specific empirical parameter, without however information on increase of the longitudinal velocity from the action of bow thruster at zero surge speed.

This paper makes an attempt to a systematic research on the issue of the influence of tunnel thrusters action on increase of the longitudinal velocity. Three ships have been used to carry out the research - container ship, car carrier and gas carrier. All tests have been done according to the same procedure, i.e. the bow thruster was activated on ships with lowest horizontal velocities possible. The results are shown in terms of rotational and linear horizontal velocities, what allows to perform the quantitative analysis of the described phenomena.

The results obtained during the described experiments and presented in the paper are an introduction to wider research on different aspects on bow thruster actions. Special attention will be paid to the influence of bow thrusters action on the increase of horizontal velocities. Dependence on different initial velocities, especially rotational speed will be taken into account. All the analyses will give valuable feedback to researchers, masters and pilots on the efficiency and performance of tunnel thrusters during port manoeuvres and thus improve navigational safety.

An added value from the presented research is also a short analysis of pivot point position during a turning manoeuver with the use of bow thruster only. Although in the paper only single - bow thruster force is taken into account, the analysis allows, according to the principles of classical mechanics, for further superposition of forces and calculation of actual pivot point during more complicated manoeuvres.

MODEL TESTS

All experiments have been carried out with manned models, that are usually used for training in ship handling at Ship Handling Research and Training Centre at the lake Silm near Iława in Poland. The models are equipped with steering and propulsion devices, whit their geometric, kinematic and dynamic characteristics scaled down from corresponding full scale ships.

The tested models are equipped with GPS system, what with RTK reference station, that covers the lake with the exercise areas, gives nominal accuracy of 10 millimetres. The heading is measured with the use of gyrocompass with 0.1° accuracy. Such a standard of tracking system gives sufficient precision both for position and heading measurements and further for horizontal motion calculations for analyses of the investigated phenomenon.

INVESTIGATED SHIPS

To investigate the described phenomenon three ships equipped with bow thrusters and representing different ship types have been selected for the experiments. Tests have been carried out with the use of manned models build to a scale of 1:24. Principal particulars of tested ships with details of bowthruster are presented in tables below.

Very Large Container Ship

Single-screw, 10 000+ TEU container ship has been chosen for experiments. Principal particulars of this ship are presented in Table 1. The ship is equipped with bowthruster of 3000 kW power and thrust of 38 tons, which in full load condition gives possibility to carry out all port operation without tug assistance up to approx.20 knots.

Table 1. Principal particulars of tested VLCS

	Full scale	Model scale
Length overall (m)	372.00	15.50
Length between perpendiculars (m)	351.84	14.66
Beam (m)	43.00	1.79
Draft (m)	14.50	0.60
Displacement (t)	155 200	10.95
Block coefficient	0.690	0.690
Bowthruster diameter (mm)*	3600	150
Bowthruster power (kW) Bowthruster	3 000	-
thrust (tons)	38	-
Bowthruster thrust (N)	-	27
Position of bow thruster (xBT/LPP)	0.447	0.447

MOST WIEDZY Downloaded from mostwiedzy.pl

Pure Car and Truck Carrier

The car carrier chosen for the tests is a 7000 CEU ship with dimensions presented in Table 2. The ship is single-screw and is equipped with bow and stern thruster. Due to large windage area the ship is equipped with rather strong bowthruster units of 2000 kW power and 30 tons of thrust each.

Table 2. Principal particulars of tested PCTC

	Full scale	Model scale
Length overall (m)	218.85	9.12
Length between perpendiculars (m)	205.00	8.54
Beam (m)	30.50	1.27
Draft (m)	12.09	0.50
Displacement (t)	62 450	4.41
Block coefficient	0.774	0.774
Bowthruster diameter (mm)*	2880	120
Bowthruster power (kW)	2 000	-
Bowthruster thrust (tons)	30	-
Bowthruster thrust (N)		21
Position of bow thruster (xBT/LPP)	0.439	0.439

LNG carrier

Twin azimuth units, 150 000 m3 LNG carrier has been used for the experiments. Table 3 shows the principal particulars of the model. Extremely powerful bowthruster of 9000 kW and a total thrust of 125 tons is used mostly in cooperation with azimuth thrusters, what gives extraordinary manoeuvring abilities at low speeds.

Table 3. Principal particulars of tested LNG carrier

	Full scale	Model scale
Length overall (m)	277.20	11.55
Length between perpendiculars (m)	272.00	11.33
Beam (m)	43.20	1.80
Draft (m)	12.00	0.50
Displacement (t)	113 500	8.01
Block coefficient	0.786	0.786
Bowthruster diameter (mm)*	3600	150
Bowthruster power (kW)	9 000	-
Bowthruster thrust (tons)	125	-
Bowthruster thrust (N)	-	89
Position of bow thruster (xBT/LPP)	0.429	0.429

* - in all cases, bow thruster diameter not from actual ship, but according to available tube diameters in model scale

TEST PROCEDURE

Practically, the purpose of the thruster test is to determine the turning qualities using thruster(s) with the ship dead in the water or running at a given speed. This test is essential to provide the information necessary to comply with IMO Resolution A601(15) (IMO, 1987), which lists information to be available on the bridge in the Pilot Card, Wheelhouse Poster, and Manoeuvring Booklet.

Additional, utilitarian aim of the tests might be obtaining data that can also be useful in future ship and tunnel thruster designs.

Some suggestions and guidelines for the thruster test have been given by Journee, Pinkster (2002) and by SNAME (2015) and can be summarized as follows:

1. With the ship dead in the water at the heading prescribed in the trial agenda and the engine set to "stop engine", start the data acquisition.
2. Order the bow thruster(s) to full thrust.
3. When the thruster(s) operate over 10 minutes or the ship's heading reaches 300, the test is complete.
4. The ship is brought back to a dead in the water condition at the desired heading, in readiness for the subsequent test (reverse bow thruster).

The same procedure could be applied using an initial forward speed designated in the trial agenda (starting point being a stable prescribed speed). Headings for left and right turns should be the same.

With the ship in trial ballast condition, it should be noted that reduced thrust may result unless the thruster is not properly submerged. The thruster should be submerged so that its axis is at a depth of at least 0.8 times the thruster diameter. Bow thruster tests for dry cargo ships in the trial ballast condition are severely influenced by sea and wind and should be conducted only in protected areas or in the open sea when the sea conditions are exceptionally smooth (SNAME, 2015).

In case of presented tests, the experiments have been done in full load condition in windless and waveless conditions.

TEST RESULTS

During the tests, the position of centre of gravity, the heading and the speed over ground and water have been measured. Based on this data, the rate of turn, longitudinal and lateral velocities and pivot point position have been calculated.

Most common in hydrodynamics coordinate system as in Figure 1 has been used during analyses. This denotes an earth-fixed system Ox0y0z0 and a ship-fixed system Mxyz with the origin at midship, where ψ is the ship heading.

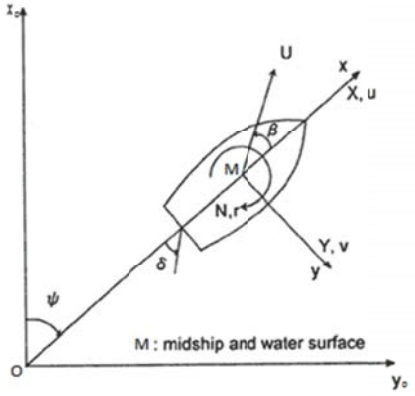

Fig. 1. Coordinate system used during analyses

MOST WIEDZY Downloaded from mostwiedzy.pl

All results presented below are in model scale dimensions. The test for container vessel and LNG carrier have been done for more than 120 seconds, what corresponds to 10min in full scale, while for PCTC for 82 second only (6.7 sec. in full scale). This exception however does not influence the total performance of the ship during the test and gives sufficient information on the overall tendencies.

HEADING AND HEADING RATE

Figures below show changes in heading and heading rate calculated from GPS and gyrocompass. Heading rate, as expected can be divided into two phases. Initial one, when the ship accelerates in turn with increasing rate of turn and the second phase, when the rate of turn is approximately constant and the heading is changing nearly linear.

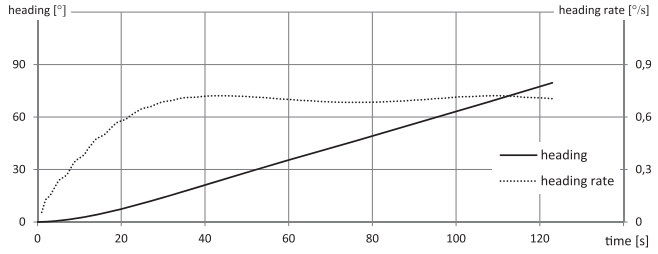

Fig. 2. Container ship heading and heading rate for thruster test with 100% bow thruster power

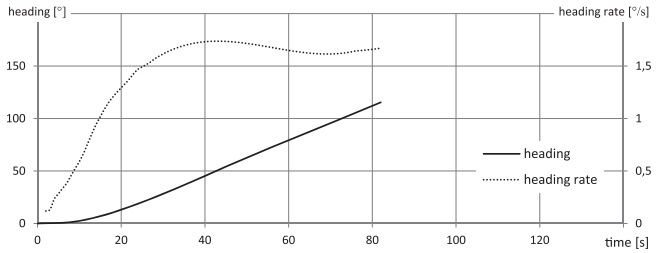

Fig. 3. PCTC heading and heading rate for thruster test with 100% bow thruster power

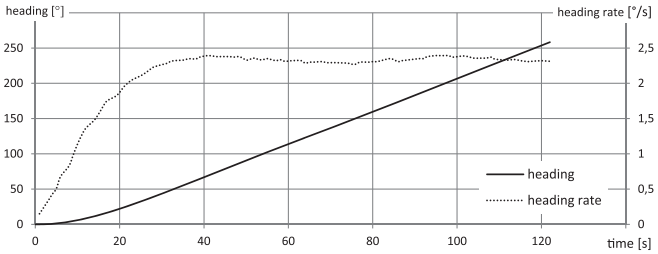

Fig. 4. LNG carrier heading and heading rate for thruster test with 100% bow thruster power

LINEAR VELOCITIES

Figures 5-7 show longitudinal and lateral velocities of centre of gravity calculated from the position received from the GPS. These velocities are presented in ship-fixed coordinate system. Some initial speed, especially in case of lateral velocity, is visible in all presented tests. It does not influence however the total tendencies in changes of the horizontal motions.

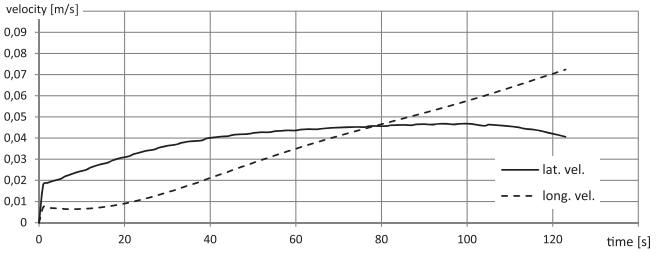

Fig. 5. Container ship lateral and longitudinal velocity for thruster test with 100% bow thruster power

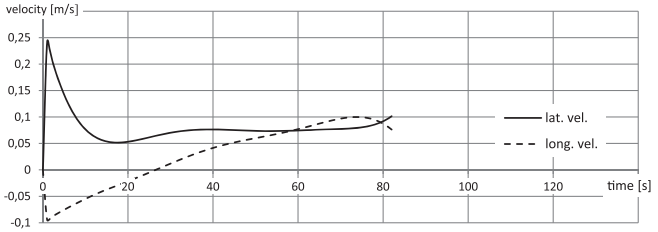

Fig. 6. PCTC lateral and longitudinal velocity for thruster test with 100% bow thruster power

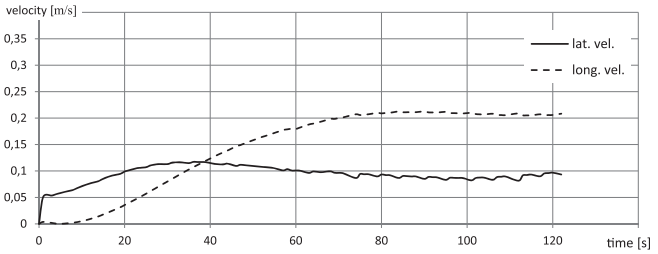

Fig. 7. LNG carrier lateral and longitudinal velocity for thruster test with 100% bow thruster power

PIVOT POINT

Longitudinal position of pivot point has been calculated according to the most common equation $x_{PP} = \frac{\dot{v}}{r}$ In the following figures the longitudinal position has been non-dimensionalised by the length between perpendiculars. It may be seen that the pivot point moves in the initial phase from a point far behind the aft to a point around 20-30% of

MOST WIEDZY Downloaded from mostwiedzy.pl

LPP behind the midship.

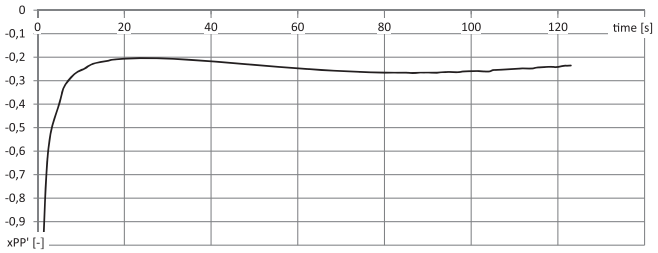

Fig. 8. Dimensionless longitudinal position of pivot point on container ship for thruster test with 100% bow thruster power

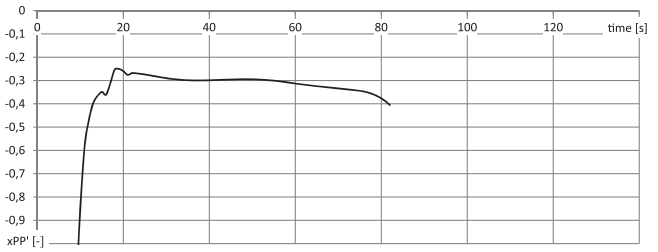

Fig. 9. Dimensionless longitudinal position of pivot point on PCTC for thruster test with 100% bow thruster power

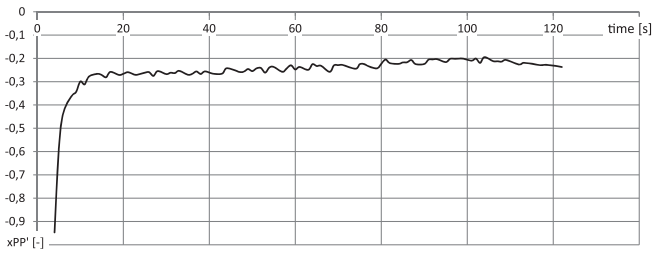

Fig. 10. Dimensionless longitudinal position of pivot point on LNG carrier for thruster test with 100% bow thruster power

DISCUSSION AND CONCLUSIONS

In the paper, initial results from a project on different aspects of bow thruster performance have been presented. Standard bow thruster test on three ships has been carried out to find out the influence of bow thruster action on increase of ship longitudinal velocity.

As can be seen from the analyses, the constant rate of turn is achieved after around 30-40 seconds (2.5 to 3.5 min in full scale) from the bow thruster start for all ships. Afterwards the rotational velocity stabilizes and remains more or less constant.

Also linear velocities have the same tendencies for all tested ships. Except rather large initial velocity for the PCTC, the lateral velocity for other ships increases to some value and remains constant. The same is visible in case of longitudinal velocity. Because of the centrifugal force, the speed increases to a certain value and later due to ship resistance stabilizes.

The best information on the phenomena of the longitudinal velocity increase due to the action of bow thruster gives the test carried out with LNG carrier. Because of very powerful bow thruster the initial phase of acceleration both in rotational and linear velocities is relatively short and thus constant values of those velocities are achieved in a short time.

The pivot point in thruster tests, that have been carried out, moves from very far aft to around 20-30% of the length between perpendiculars behind the midship. The position of pivot point is actually a result of both rotational and longitudinal velocities. Especially the longitudinal motion influences the reduction of distance between the pivot point and the midship.

The information on the actual rotational and linear velocities and on actual pivot point position should be taken into account during planning and execution of manoeuvres and passages in restricted waters, e.g. in harbours or in narrow channel or rivers.

Additional analyses of influence of bow thruster action on longitudinal velocity and position of pivot point will follow.

REFERENCES

1. Abramowicz-Gerigk, T. (2008). Experimental study on the hydrodynamic forces induced by a twin-propeller ferry during berthing. Ocean Engineering, 35(3-4), pp.323-332

2. Artyszuk, J. (2003). Ship sway/yaw motions while turning with bow lateral thruster. 15th International Conference on Hydrodynamics in Ship Design, Safety and Operation HYDRONAV 2003, Gdańsk

3. Artyszuk, J. (2010). Pivot point in ship manoeuvring. Scientific Journals of Maritime University of Szczecin, 20(92), pp.13-24

4. Brix, J. (1993). Manoeuvring technical manual. 1st ed. Hamburg: Seehafen Verlag GmbH, Germany

5. Chislett M.S., Björheden O. (1966). Influence of Ship Speed on the Effectiveness of a Lateral – Thrust Unit. Report no. 8, Hydro- og Aerodynamisk Laboratorium, Kgs. Lyngby, Denmark

6. Gierusz, W. (2016). Simulation model of the LNG carrier with podded propulsion, Part II: Full model and experimental results. Ocean Engineering, 123, pp.28-44

7. IMO (1987). Resolution A.601(15) Provision and display of manoeuvring information on board ships

8. Journee J.M.J., Pinkster J. (2002). Introduction in ship hydromechanics. Delft University of Technology, the Netherlands

MOST WIEDZY Downloaded from mostwiedzy.pl

9. Quadvlieg F.H.H.A. and Toxopeus S.L. (1998). Prediction of crabbing in the early design stage. In: Practical Design of Ships and Mobile Units. Elsevier Science B.V., pp.649-654

10. Reichel, M. (2017). Prediction of manoeuvring abilities of 10000 DWT pod-driven coastal tanker. Ocean Engineering, 136, pp.201-208

11. SNAME (2015). Guide for Sea Trials (Progressive Speed, Maneuvering, and Endurance). SNAME Technical and Research Bulletin 3-47

ACKNOWLEDGEMENTS

Research presented in this paper has been financed from statutory fund of Ship Handling Research and Training Centre, Foundation for Safety of Navigation and Environment Protection.

CONTACT WITH THE AUTHOR

Maciej Reichel
e-mail: maciejr@portilawa.com

Ship Handling Research and Training Centre
14-200 Iława-Kamionka
Poland

MOST WIEDZY Downloaded from mostwiedzy.pl

POLISH MARITIME RESEARCH Special Issue 2018 S1 (97) 2018 Vol. 25; pp. 80-84
10.2478/pomr-2018-0027

HULL RESISTANCE OF AN INLAND WATERWAY VESSEL IN MODEL SCALE AND IN FULL SCALE

Tomasz Tabaczek
Maciej Zawiślak
Wrocław University of Technology, Poland

ABSTRACT

Data from model tests of an inland waterway vessel in shallow water have been used by the authors to prepare the resistance prediction in full scale. The common ITTC-1978 extrapolation procedure was applied using form factor determined according to the Prohaska method and, separately, by fitting the approximation function to resistance data. At the same time a series of CFD computations of ship flow has been carried out in model scale and in full scale, with double-body model as well as including the effect of free surface. The results of computations were used to determine total resistance and form factor. The values of form factor determined using different methods are similar and relatively high in comparison to values being applied to conventional sea going ships. Resistance prediction according to the ITTC-1978 with form factor was compared to prediction without form factor. The relative difference of resistance amounts 28% at ship speed of 10 km/h and 24% at ship speed of 12 km/h.

Keywords: inland waterway vessel, ship resistance, form factor

INTRODUCTION

Prediction of resistance of inland waterway vessels, especially of innovative hull form, is made usually with application of model tests and extrapolation of measured resistance. The International Towing Tank Conference (ITTC) recommends the procedures both for tests [1] and extrapolation [2]. The recommended method of extrapolation is the form factor method with form factor determined according to the concept proposed by Prohaska [3].

When re-analysing model test data for an inland motor cargo vessel designed for operation on the Oder River [4] the authors encountered the relatively high value of form factor. Hull form of that twin-screw vessel is distinctive by bow form with wide-V cross sections, propeller tunnels and stern transom (see Fig.1). The breadth to draught ratio (B/T) of 5.2 is typical for inland waterway vessels operating in shallow inland waterways.

The authors decided to verify, using CFD, the form facto determined according to the Prohaska method. Computations of ship flow have been performed for model ship as well as for full scale vessel, both for double-body model. Form factor has been determined as ratio of total hull resistance to the frictional resistance determined according to the ITTC-1957 model ship correlation line, as suggested in [5].

Because of the high value of form factor the resistance at service speeds predicted using the form factor is lower by about 25% from the resistance

MOST WIEDZY Downloaded from mostwiedzy.pl

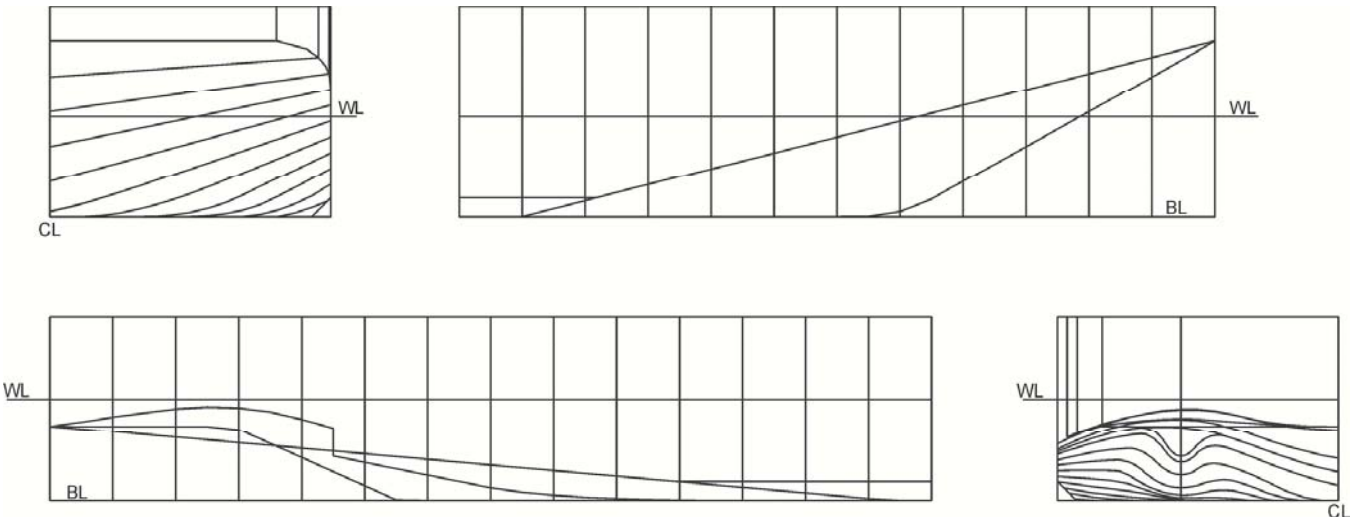

Fig.1. Hull form of the considered inland waterway cargo vessel OBM

predicted according to the original Froude method (k = 0).

INLAND WATERWAY VESSEL OBM

The considered inland motor cargo vessel (referred to as OBM) was originally designed in Inland Navigation Research and Design Centre - Navicentrum in Wrocław, in 1973 year. Main dimensions were fitted to the parameters of the Oder Waterway of that time. The vessel was designed to operate at draught of 1.60 m (optionally at draught of 2.36 m), either alone (L_{OA} = 70 m) or coupled with a single dumb barge (L_{OA} ≈ 116 m). Hull form of OBM is presented in Fig.1, and main particulars are given in Table 1.

Table 1. Main particulars of the inland waterway cargo vessel OBM

Length over all, L_{OA}	70.00 m
Length at waterline, L_{WL}	67.83 m
Breadth, B	8.92 m
Draught, T	1.60 m
Wetted surface area, S	773.1 m^2
Displacement volume, ∇	848.2 m^3

MODEL TESTS

Extensive resistance and propulsion model tests of OBM were carried out in Ship Design and Research Centre in Gdańsk [4]. For the purpose of analysis presented in this paper used were the results of resistance tests in deep water and in shallow water at water depth h = 2.50 m (h/T = 1.56). Tests in shallow water were carried out in auxiliary towing tank (60 m x 7 m) with adjustable depth of water. At the scale of 1:16 water depth was equal 0.156 m.

CFD COMPUTATIONS

CFD computations of ship flow have been performed for the following conditions:

a. in model scale (1:16) for double-body configuration, in order to determine total hull resistance (R_{TM}) without the effect of free surface (no wave resistance) and to determine the form factor in model scale ($1+k = C_{TM}/C_{F0M}$, [5]);
b. in model scale (1:16), including the effect of free surface, in order to validate the applied CFD method;
c. in full (ship) scale for double-body configuration, in order to determine the form factor in full scale.

The resistance in free surface flow in model scale (b) was in satisfactory agreement with the resistance measured in model tests (Fig.2). The authors recognised the applied CFD methodology as reliable to draw conclusions from analysis of results.

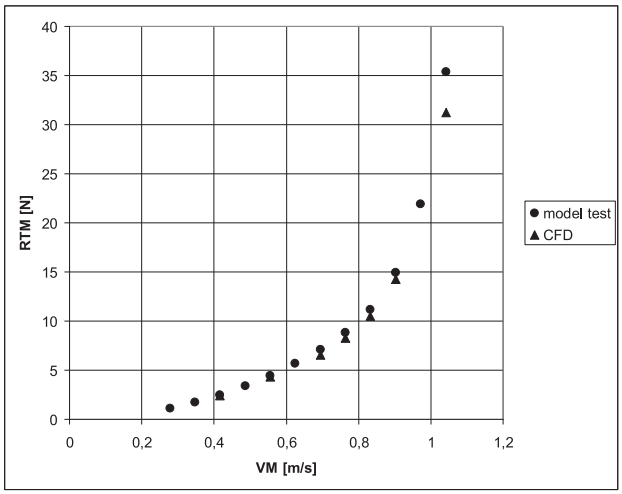

Fig.2. Model ship resistance of OBM in shallow water, h/T = 1.56

MOST WIEDZY Downloaded from mostwiedzy.pl

FORM FACTOR

The value of form factor k for OBM in shallow water has been determined using 3 methods:

- the method proposed by Prohaska [3] and recommended by ITTC [2],
- fitting the approximation function to test data,
- computation of hull resistance with CFD software.

The Prohaska method

Om the assumption that at small speed (0.10 < Fr < 0.20) the coefficient of wave resistance is proportional to Froude number in 4th power and can be represented as $C_W = aFr^4$:

$$C_{TM} = (1+k)\, C_{F0M} + aFr^4$$

and

$$C_{TM}/C_{F0M} = (1+k) + aFr^4/C_{F0M}$$

The ratio C_{TM}/C_{F0M} is a linear function of Fr^4/C_{F0M}. After presenting the data from resistance test in coordinates C_{TM}/C_{F0M} vs. Fr^4/C_{F0M} and fitting them with straight line, the line intercepts the ordinate axis at 1+k [3]. The application of the Prohaska method to determination of form factor of OBM is illustrated in Fig.3.

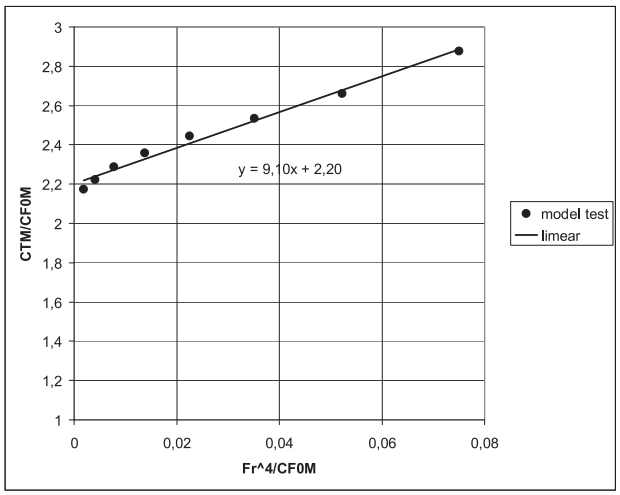

Fig.3. Determination of form factor of OBM at h = 2.50 m according to Prohaska method [3]

Fitting the approximation function

Without the requirement of no flow separation imposed by Prohaska, the relationship between resistance and speed of vessel can be approximated using the following function:

$$C_{TM} = (1+k)C_{F0M} + aFr_h^{\,b}.$$

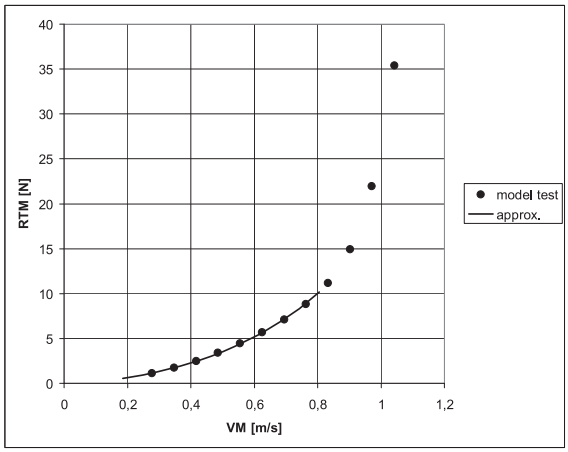

Fig.4. Resistance test data approximated with function $R_{TM} = 0.5\rho V_M^2 S_M [(1+1.134)C_{F0M} + 0.907Fr^{2.847}]$; OBM, h/T =1.56

The authors fitted the above function to resistance test data using the statistics software and least-square method. Only data below Frh = 0.65, i.e. the hydrodynamic ally economic speed limit for small and medium size motor cargo vessels [6], were used for determination of form factor k, coefficient a and exponent b. The fit of approximation is shown in Fig.4.

CFD

Form factor can be computed from the resistance of double-body model computed using CFD:

$$1+k = C_T/C_{F0}$$

where C_T is hull resistance coefficient and C_{F0} is frictional resistance coefficient calculated according to the ITTC-1957 model-ship correlation line [5].

Values of form factor calculated for OBM in model scale and in full scale are given in Tables.2 and 3.

Table 2. Values of form factor for OBM calculated using results of CFD computations in model scale

V_S [km/h]	V_M [m/s]	Fr	C_{TM}	C_{F0M}	1+k
5.00	0.347	0.054	9.18E-03	4.43E-03	2.08
7.00	0.486	0.075	8.78E-03	4.13E-03	2.13
9.00	0.625	0.097	8.49E-03	3.92E-03	2.17

Table 3. Values of form factor for OBM calculated using results of CFD computations in full scale

V_S [km/h]	V_S [m/s]	Fr	C_{TS}	C_{F0S}	1+k
2.00	0.556	0.022	5.30E-03	2.46E-03	2.16
4.00	1.111	0.043	4.95E-03	2.21E-03	2.24
6.00	1.667	0.065	4.76E-03	2.08E-03	2.29
8.00	2.222	0.086	4.65E-03	2.00E-03	2.33
10.00	2.778	0.108	4.57E-03	1.94E-03	2.36

MOST WIEDZY Downloaded from mostwiedzy.pl

COMPARISON OF FORM FACTOR VALUES

Table 4. Values of form factor for inland cargo vessel OBM in shallow water (h/T = 1.56)

Source of data	Method	Range of speed	1+k
model test	by Prohaska	$0.054 < Fr < 0.118$ $0.28 < Fr_h < 0.62$	2.20
model test	fitting the approximation function	$0.054 < Fr < 0.118$ $0.28 < Fr_h < 0.62$	2.13
CFD in model scale	$1+k = C_{TM}/C_{F0M}$	$0.054< Fr < 0.097$ $0.28 < Fr_h < 0.50$	2.08 - 2.17
CFD in full scale	$1+k = C_{TS}/C_{F0S}$	$0.022 < Fr < 0.108$ $0.11 < Fr_h < 0.56$	2.16 - 2.36

RESISTANCE PREDICTION

Ship resistance of OBM in shallow water was predicted according to:

(1) the original Froude method, without form factor

$$C_{TS} = C_{TM} + C_{F0S} - C_{F0M}$$

$$R_{TS} = C_{TS}\, 0.5\rho V^2 S$$

(2) the form factor method, recommended by ITTC [2]:

$$C_{TS} = C_{TM} + (1+k)(C_{F0S} - C_{F0M})$$

$$R_{TS} = C_{TS}\, 0.5\rho V^2 S$$

where:

C_{F0S}, C_{F0M} -coefficient of frictional resistance calculated according to the ITTC-1957 model-ship correlation line:

$$C_{F0} = 0.075 / (\log Re - 2)^2$$

$$Re = VL_{WL} / \nu$$

Predicted ship resistance is shown in Fig.5

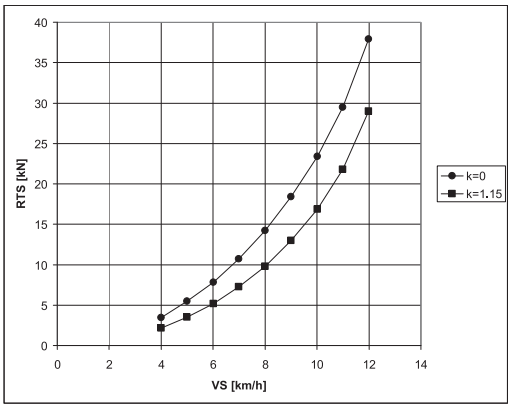

Fig.5. Predicted ship resistance of the motor cargo vessel OBM in shallow water (h/T = 1.56)

Relative differences between resistance predicted using methods (1) and (2) is 28% at VS = 10 km/h through 24% at VS = 12 km/h.

CONCLUSIONS

Three methods were applied to determine the form factor for inland waterway cargo vessel:

- the common method proposed by Prohaska [3] and recommended by ITTC [2],
- fitting the approximation function to test data,
- calculation of form factor using results of CFD computations of ship flow.

The determined values of form factor are similar, and are relatively high. At water depth of 2.50 m (h/T = 1.56) the form factor amounts around 1.15 (1+k ≈ 2.15). In opinion of the present authors, such high value is, on one hand, due to wide-beam hulls of B/T = 5.2, with bow form of wide V-shaped cross sections (form factor determined for the same vessel in deep water amounts 0.33). On the other hand it is the effect of shallow water.

The comparison of resistance predicted without form factor and with form factor reveals that relative difference in predictions may amount up to 28% at ship speed of 10 km/h (speed limit usually imposed by waterway authorities for navigation in canals) and up to 24% at ship speed of 12 km/h (at $Fr_h = 0.67$, i.e. around the hydrodynamically economic speed limit).

REFERENCES

4. ITTC-Recommended Procedures and Guidelines, Resistance Test, 7.5-02-02-01, Rev.03, Effective Date 2011

5. ITTC-Recommended Procedures and Guidelines, 1978 ITTC Performance Prediction Method, 7.5-02-03-01.4, Rev.03, Effective Date 2014

6. Prohaska C.W.: A simple method for evaluation of form factor and the low speed wave resistance, Proc. 11th ITTC, 1966, pp.65-66

7. Sprawozdanie z prób modelowych oporowo-napędowych odrzańskiej barki motorowej (Report from resistance and propulsion model tests of the Oder motor barge), RB-N-M20/B430-13, Ośrodek Hydromechaniki Okrętu, Centrum Techniki Okrętowej, Gdańsk, 1975

8. ITTC-Recommended Procedures and Guidelines, Practical Guidelines for Ship Resistance CFD, 7.5-03-02-04, Revision 00, Effective Date 2014

9. Heuser H., Müller E.: Verdrängungsschiffe auf flachem Wasser - Neuere Ergebnisse hydrodynamischer Forschung und ihre Anwendung beim Entwurf, Schiffstechnik, Band 33, Heft 1, April 1986

MOST WIEDZY Downloaded from mostwiedzy.pl

CONTACT WITH THE AUTHORS

Maciej Zawiślak
e-mail: maciej.zawislak@pwr.wroc.pl

Wrocław University of Technology
5 Łukasiewicza st.
50-371 Wrocław
Poland

MOST WIEDZY Downloaded from mostwiedzy.pl

POLISH MARITIME RESEARCH Special Issue 2018 S1 (97) 2018 Vol. 25; pp. 85-93
10.2478/pomr-2018-0028

NUMERICAL SIMULATION OF CUSHIONING PROBLEM FOR BLUNT BODIES USING BOUNDARY ELEMENT METHOD

Mojtaba Barjasteh
Hamid Zeraatgar
Amirkabir University of Technology, Tehran, Iran

ABSTRACT

Induced air pressure and resulting free surface profile due to air cushioning layer is studied. The study is mainly focused on 2D blunt circular bodies with constant downward speed. The problem is first solved for the air flow between the body and the free surface of the water. Then the results are employed to solve the problem for the water problem, numerically. Both air and water problem are assumed to be governed by Laplace potential equation. Depending on the induced pressure and velocity of the escaping air flow from cushioning layer, compressibility of the air is also included in the modeling. Gravitational acceleration is also included in the model. An iterative boundary element method is used for numerical solution of both air and water problems. Instantaneous pressure distribution and free surface profile are evaluated for different bodies. The results of calculation for large blunt bodies show that inviscid potential method can fairly approximate the problem for large blunt bodies. Additionally, the behavior of the air pressure for the very blunt body is impulsive and the magnitude of the peak pressure is in order of impact pressure of water entry. The obtained results are compared with analytical method. The comparison shows that as the bluntness of a body increases, the better agreement is concluded.

Keywords: Air cushion, compressible potential flow, water entry, slamming

INTRODUCTION

Hydrodynamic evaluation of several typesof marine vehicles are based onsolution of water entry problem. It is common to study a 3D geometry of a vessel by 2D sections along ship length. A 2D section of a ship is a classical water entry problem. The water entry problem may be solved analytically, numerically as well as by experiment. The water entry problem is correlated to some other phenomena which complicates the evaluation of the problem. One of these phenomena is the cushioning layer right before impact. As a body drops and get close to free surface of the water, air between body and the water surface may not scape and compressed as body closes to the surface. An air layer is formed between the body and free surface of the water. Based on the mass continuity, the velocity of escaping air flow from the layer exponentially increases as the body closes the surface. Since the gap layer is usually very narrow and the body momentum is generally high, the induced air pressure along the cushioning layeris very high. Physically, for the force balancein vertical direction, the free surface is deformed to balance the induced air pressure at the air-water interface. This deformation causes a multipoint impact rather than asingle point impact as it is assumed in most of water entry theories. Depending on the shape of impacting body and deformed free surface profile, some volume of air may be entrapped during entry. The cushioning layer reduces the impact speed as well as the hydrodynamic impact pressure

MOST WIEDZY Downloaded from mostwiedzy.pl

due to air drag and compression of entrapped air, respectively. Thus accurate prediction of maximum impact pressure requires considering the cushioning layer particularly for high speed impact of blunt bodies.

There are several researches on the topic mainly focused on the evaluation of impact pressure and free surface deformation in bubble dynamics and droplet impacts. The survey was started by Verhagen[1] who modeled the air layer using a channel flow problem with constant geometry of moving walls. He concluded that the lubrication equation[2] may properly simulate the channel flow instead of traditional equations. The proposed model was just a case study and cannot be further developed for different geometries. The next significant try was made by Asryan[3]. He recommended two different formulation including inviscid incompressible and viscous compressible. Both models are available for initial stage of the body motion when the surface deformation isnegligible. Thus, the free surface deformation was not investigated. The obtained results overestimate the pressure and underestimate the air speed particularly at throat of the air gap layer. Wilson [4] suggested a non-dimensional asymptotic model to simulate the problem based on two dimensional Navier-Stokes equation. The model is initially stable but as the body gets closer to the free surface the results are unstable. This instability also occurred for blunter bodies. Hicks and Purvis [5] conducted a great series of experiments and analytical research on the problem. They studied the problem in all details primarily for a bubble impact onto liquid or solids and its resulting deformation due to presence of cushioning layer. Different parameters such as viscosity dissipation, compressibility, topography and the validity of the proposed models are fully discussed in their works. They employed different forms of lubrication equation for the air problem and potential flow for the bubble deformation. They validated the obtained results with some experimental research [8] and with different available theories.

All studies show that the dimensional analysis generally controls the problem and its corresponding governing equation. Different research were also made on this analysis to provide some better understanding of the problem such as those carried out by Mandre and Brenner [9] and Smith et. all[10]. They introduced different time and length scales based on the different configuration of the problem. On that basis, they concluded which governing equations such as lubrication equation, incompressible potential flow and compressible flow are applicable. Some experimental studies also investigated different applications of cushioning problem. Two distinctive experimental researches are those carried out by Marston et. all[11] and Tran et. all[12]. Both studies were concentrated on cushioning layer and the resulting air entrapment for small bodies. Some unique visualization and precise measurement were reported. One of the interesting tests results is to determine a scaling law for non-dimensional volume of air entrapment. This scaling simply implies that the volume of air entrapment depends to the Stokes number of the flow. This relation is changed for different regimes of the flows. There are also several research to investigate the problem such as those conducted by Lewison and Maclean [13], Thoroddsen et. all[14] and Bouwhuis et. all[15] which have different contribution to the problem consideration.

This study, as a relatively simple approach, represents a fully potential flow for both air and water problem and disregards the lubrication equation for very narrow air layer. Therefore the validity of the formulation is limited to high speed impact of blunt bodies. A fast and practical boundary element method is employed to evaluate all desired parameters of the problem. The proposed method can be efficiently used for developing a commercial software in full prediction of water impact including air cushioning effects.

FORMULATION

The present model investigates the cushioning problem in water entry of blunt body such as depicted in Figure 1. A blunt body with downward speed of v_0 moves toward to the water free surface which is initially at the rest. The downward speed is assumed to be constant and vertical, for the sake of simplicity. Since the body is essentially blunt and its speed is assumed to be high enough, the dominant phenomenonforfree surface deformation is normal pressure balance. Therefore the viscosity is neglected for both air and water problem. Two length scales are defined here to check the model validity as depicted in Figure 1. The first one in horizontal direction and shows the maximum length of disturbed free surface which is called *L*. The second length scale indicates the maximum depth of free surface, *H,* due to air pressure. The present formulation is not valid when *H<<L*. It may be shown that when *H<<L,* the viscous terms cannot be neglected anymore.

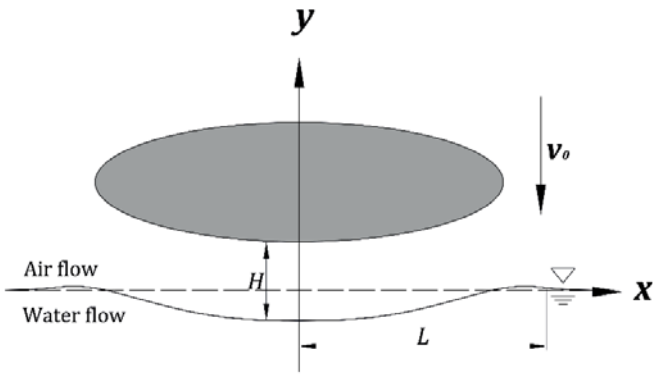

Fig. 1. Problem definition, the free surface profile is schematic and exaggerated

According to the problem configuration, both flows are assumed to be potential. The water flow remains always incompressible. Thus the governing equation in the water flow is the Laplace equation.

$$\frac{\partial^2 \phi}{\partial x^2} + \frac{\partial^2 \phi}{\partial y^2} = 0 \qquad (1)$$

MOST WIEDZY Downloaded from mostwiedzy.pl

The governing equation for the air flow is also the Laplace equation, since it is incompressible. However, as the body is very close to the free surface, high pressure may be induced to the air layer and the escaping speed of air flow considerably increases as a result. At this condition, the air compressibility should be taken into account. From Euler equation in term of differentials, the pressure and momentum correlated to each other.

$$dP = -\rho V dV \tag{2}$$

Where V is the total velocity. This equation is independent to the flow directions for the problem under consideration. Thus, the velocity components can be evaluated from potential equations.

$$dP = -\frac{\rho}{2}\left[\left(\frac{\partial^2\phi}{\partial x^2}\right)^2 + \left(\frac{\partial^2\phi}{\partial y^2}\right)^2\right] \tag{3}$$

The flow is assumed to be isentropic and the air fluid is an ideal gas. So, the pressure gradient is a function of density gradient.

$$\left(\frac{dP}{d\rho}\right)_s = c^2 \tag{4}$$

where c is the local speed of the sound in the air flow. Substituting the pressure gradient with density gradient results in:

$$d\rho = -\frac{\rho}{2c^2} d\left[\left(\frac{\partial^2\phi}{\partial x^2}\right)^2 + \left(\frac{\partial^2\phi}{\partial y^2}\right)^2\right] \tag{5}$$

Continuity equation is also always valid for both compressible and incompressible flow. Substituting the velocity potential in continuity equation yields:

$$\rho\left(\frac{\partial^2\phi}{\partial x^2} + \frac{\partial^2\phi}{\partial y^2}\right) + \frac{\partial\phi}{\partial x}\frac{\partial\rho}{\partial x} + \frac{\partial\phi}{\partial y}\frac{\partial\rho}{\partial y} = 0 \tag{6}$$

Removing density differential from Euler and continuity equation results in the final governing equation of compressible potential flow:

$$\left[1 - \frac{1}{c^2}\left(\frac{\partial\phi}{\partial x}\right)^2\right]\frac{\partial^2\phi}{\partial x^2} + \left[1 - \frac{1}{c^2}\left(\frac{\partial\phi}{\partial y}\right)^2\right]\frac{\partial^2\phi}{\partial y^2} - \frac{2}{c^2}\left(\frac{\partial\phi}{\partial x}\right)\left(\frac{\partial\phi}{\partial y}\right)\frac{\partial^2\phi}{\partial x\partial y} = 0 \tag{7}$$

and

$$c^2 = c_0^2 - \frac{k-1}{2}\left[\left(\frac{\partial\phi}{\partial x}\right)^2 + \left(\frac{\partial\phi}{\partial y}\right)^2\right] \tag{8}$$

where c_0 and k are stagnation local speed of sound and ratio of air specific heat, respectively. The derived governing equation is nonlinear partial differential equation with only one unknown parameter in term of flow potential. This equation can be solved numerically. However, due to moving free surface profile, the solution is not easy. To overcome this drawback, the nonlinear PDE is linearized. One can employ a perturbation analysis for linearization of the problem. The perturbation velocity potential can be defined as $\hat{\phi} = \phi_t - \phi_u$ where ϕ_t and ϕ_u are total and uniform velocity potential. Perturbation velocity components can also be evaluated similarly as $u = u_\infty + \hat{u}$ and $v = v_\infty + \hat{v}$. For vertical downward speed of the body the uniform velocity is the body velocity. To substitute the perturbation parameters in the governing equation, local speed of sound should be stated as a function of perturbation velocity components. Such a task is carried out employing stagnation form of energy equation:

$$\frac{c_\infty^2}{k-1} + \frac{v_0^2}{2} = \frac{c^2}{k-1} + \frac{(\hat{u})^2 + (v_0 + \hat{v})^2}{2} \tag{9}$$

Mach number of uniform flow is very small in comparison with the perturbation velocity components. Substituting the local speed of sound from energy equation into the governing equation yields.

$$\frac{\partial^2\hat{\phi}}{\partial x^2} + (1 - M_\infty^2)\frac{\partial^2\hat{\phi}}{\partial y^2} = 0 \tag{10}$$

The derived equation is a linear partial differential equation but in terms of perturbation potentials. This equation can be transformed from physical domain to a computational domain byintroducing new variables.

$$\begin{aligned} \psi &= x \\ \xi &= (1 - M_\infty^2)^{-\frac{1}{2}} y \end{aligned} \tag{11}$$

This transformation just changes the horizontal coordinate system and does not change the behavior of the equation. Using chain rule of differentiation, one can find new differentials:

$$\begin{aligned} \frac{\partial^2\hat{\phi}}{\partial x^2} &= \frac{\partial^2\hat{\phi}}{\partial\psi^2} \\ \frac{\partial^2\hat{\phi}}{\partial y^2} &= \frac{1}{1 - M_\infty^2}\frac{\partial^2\phi}{\partial\xi^2} \end{aligned} \tag{12}$$

Recalling the new parameters into the governing equation yields:

$$\frac{\partial^2\hat{\phi}}{\partial\psi^2} + \frac{\partial^2\hat{\phi}}{\partial\xi^2} = 0 \tag{13}$$

This is a new form of Laplace equation for transformed perturbation velocity. Now, the air flow problem is always governed by Laplace equation for incompressible potential

MOST WIEDZY Downloaded from mostwiedzy.pl

flow, Equation 1, and another one for compressible potential flow in transformed computational domain, Equation 13. This boundary value problem can be solved if boundary condition at all boundaries are known. Since the geometry of the problem is symmetric, the solution of the problem is carried out for a half space. The boundary condition on the body is no flux boundary condition.

$$\frac{\partial \phi}{\partial n} = V.n \tag{14}$$

where n is the normal vector pointing outward the body surface. On the free surface, both kinetic and kinematic free surface boundary condition should be satisfied.

$$v = \frac{D\eta}{Dt} = \left[\frac{\partial \eta}{\partial t} + u\frac{\partial \eta}{\partial x}\right] \tag{15}$$

$$\frac{\partial \phi}{\partial t} + \frac{1}{2}|\nabla \phi|^2 = g\eta - \frac{\sigma}{\rho_w}\left[\frac{|\partial^2 \eta/\partial x^2|}{(1+(\partial \eta/\partial x)^2)^{3/2}}\right] - \frac{P_a}{\rho_w} \tag{16}$$

here σ, η, P_a and ρ_w are air-water surface tension, free surface profile, air pressure on the interface and water density, respectively. The potential vanishes for far field condition.

$$\phi(\infty, 0) = 0 \tag{17}$$

The free surface profile is assumed to be at rest as an initial condition or $\eta(x, 0) = 0$. Similar boundary conditions can be also derived for the water problem and a transformed form of compressible potential flow. The boundary condition on the water bed can be a wall or a far field condition. It can be shown for a deep water problem,both boundary conditions result in the same potentials. Although the water is deep enough, the problem can be also solved for a shallow water by adjusting the height of symmetry line. At this condition the water bed boundary condition can only be wall boundary condition not a far-field one.

NUMERICAL IMPLEMENTATION:

Depending on the problem configuration and the computational regions, the problem is governed by three different governing equation including an incompressible potential equation for air flow, an incompressible potential equation for water problem and finally a compressible potential flow for high speed escaping air flow. All of the governing equations are in general form of Laplace equation. The most common and practical method of solving such an equation is to employ boundary element method. The numerical solution is started by incompressible potential air flow. First the boundaries of the problem are discretized into linear elements. The important boundaries are Γ1, Γ2 and Γ3 indicating the body, the symmetry line and the free surface. There is also a fourth boundary that closes the problem domain to the farfield boundary condition.

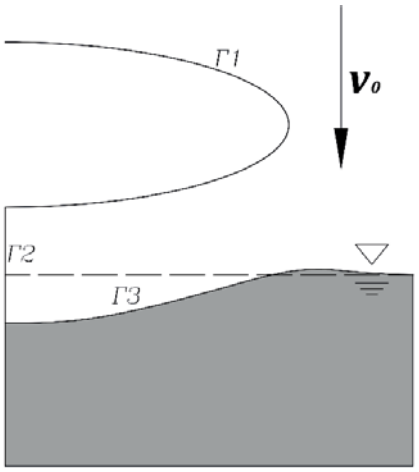

Fig. 2. Computational domain and the main boundaries

The elements are constant and linear. So there is one integration point on the middle of each element called the point q. It can be readily shown that for any in-domain arbitrary point such as P, the potential can be related to distributed sources on each element using second identity of Green'sTheoremin form of an integral equation.

$$\phi(P) = -\int_\Gamma \left[\lambda(F,q)\frac{\partial \phi(q)}{\partial n_q} - \phi(q)\frac{\partial \lambda(F,q)}{\partial n_q}\right] ds_q \tag{18}$$

where λ is the fundamental solution of Laplace equation for two-dimensional problem.

$$\lambda = \frac{1}{2\pi}\ln r\,(F,q)$$
$$\frac{\partial \lambda}{\partial n_q} = \frac{1}{2\pi}\frac{\cos\left(\angle(r,n)\right)}{r} \tag{19}$$

and $r = |q - F|$ is the distance vector. The integral equation can be represented in summation of influence coefficients $\hat{H}$ and $\hat{G}$ assuming constant distribution of potential on each element [16].

$$-\frac{1}{2}\phi^i + \sum_{j=1}^{N}\hat{H}_{ij}\phi^j = \sum_{j=1}^{N}\hat{G}_{ij}\frac{\partial \phi^j}{\partial n} \tag{20}$$

where N is the total number of elements. The influence coefficients are only functions of the problem geometry and they are known. The problem is a mixed Dirichlet-Neumann boundary condition. The number of known and unknown parameters are the same and the problem changes to a system of algebraic equations. So, a linear system of algebraic equations can be rearranged to find unknowns. The numerical solution starts similar to all linear constant boundary element

MOST WIEDZY Downloaded from mostwiedzy.pl

method. At the first time step the initial position of the body and its downward velocity are known. Additionally, the initial free surface profile is at the rest. The solution of the problem at the first time step results in a potential fields in the air flow. Furthermore, the potentials on the free surface are also evaluated. For updating the free surface profile, it is needed to have the data of the next time step. At the first time step the free surface is assumed to be a wall boundary condition, for the sake of simplicity. This assumption is only valid for the first time step. The problem is similarly solved for the second time step with updated position of the body. Once the new values of the potentials are found, the time derivatives of the potential can be easily estimated for reasonably small time increments.

$$\frac{\partial \phi}{\partial t} = \frac{D\phi}{Dt} - |\nabla\phi|^2 \approx \frac{\Delta\phi}{\Delta t} - |\nabla\phi|^2 \tag{21}$$

If the time derivatives of the flow potentials are estimated, the induced air pressure in the air layer and particularly on the free surface is calculated by using unsteady Bernoulli equation.

$$P = -\rho\left[\frac{\partial\phi}{\partial t} + \frac{1}{2}|\nabla\phi|^2 + g\eta\right] \tag{22}$$

The potential gradients which evaluate the velocity components can be estimated using finite difference method. However, these components can be directly evaluated using following equations to remove all disadvantages of finite difference method.

$$\frac{\partial\phi}{\partial x} = -\int_\Gamma \left[\frac{\partial\lambda}{\partial x}\frac{\partial\phi}{\partial n} - \phi\frac{\partial}{\partial x}\left(\frac{\partial\lambda}{\partial n}\right)\right] ds \tag{23}$$

$$\frac{\partial\phi}{\partial y} = -\int_\Gamma \left[\frac{\partial\lambda}{\partial y}\frac{\partial\phi}{\partial n} - \phi\frac{\partial}{\partial y}\left(\frac{\partial\lambda}{\partial n}\right)\right] ds \tag{24}$$

Figure 3illustrates typical non-dimensional velocity components using Equations 23 and 24.

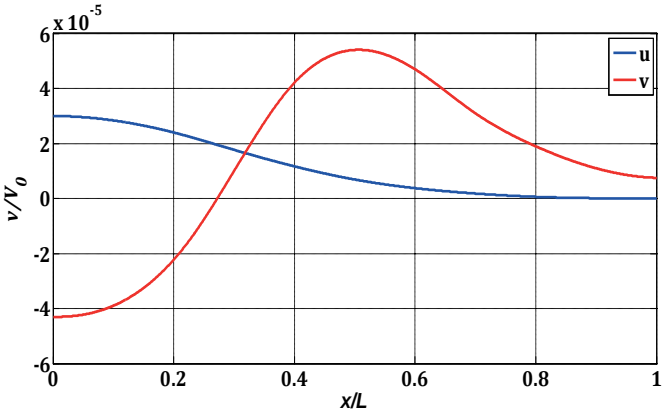

Fig. 3. Typical velocity components on the free surface interface

After the second time step, the induced air pressure on the free surface is known and the numerical solution of the water problem can be started. The primary boundary conditions of the water problem is the symmetry line and the free surface. There is also another boundary condition which closes the domain with far-field boundary condition. This domain is not included in the solution because the BEM is independent of far-field boundary condition in the present problem. From kinetic boundary condition, the induced air pressure in each time step is main source of disturbance in the water problem. Again, the number of known and unknown parameters for the water problem is the same and the system of linear algebraic equations can be solved using different method such as Gauss–Seidel method. The water problem is solved at the current time step of the air problem. Once the water problem is also solve, the free surface profile is updated using velocity component of water problem that estimated from solution of water flow. At the first and second time step, the boundary condition on the free surface is set to free slip condition. In other words, tangential derivatives of the air and water potentials, ϕ_s, are not necessarily the same on the free surface. Therefore, the following kinematic free surface boundary condition readily concluded which must be satisfied on the free surface at each time step.

$$\phi_{na} = \phi_{nw} \tag{25}$$

here the subscripts a and *w*depict the air and water flows, respectively. Moreover, kinetic boundary condition simply relates the air and water pressure at the interface considering the surface tension at two firs time steps.

$$P_w = P_a - \sigma\frac{\partial^2\eta}{\partial x^2} \tag{26}$$

After updating the free surface profile and the body position, the numerical solution of the problem at the third time step is started and continues. The proposed numerical solution in the present model may called a weakly coupled method between air and water flows. At each time step the pressure on the free surface is evaluated from air problem whereas the free surface profile updated from the water problem. After updating the free surface profile the estimated pressure from the air flow is corrected using parameters water potentials. This corrected pressure field on the interface is used as a boundary condition for the air problem at the next time step.It is worth noting that the all of time derivatives are evaluated using a backward time differencing scheme. So, the time marching is not dependent on the next time step. Therefore, the updated value of potentials can be computed as following.

$$\frac{\partial\phi_w}{\partial t} = -\left(\frac{P_a}{\rho_w} + \frac{1}{2}|\nabla\phi_w|^2\right) \tag{27}$$

MOST WIEDZY Downloaded from mostwiedzy.pl

$$\phi_w^{n+1} = \Delta t \left(\frac{\partial \phi_w}{\partial t} + |\nabla \phi_w|^2 \right) + \phi_w^n \quad (28)$$

where the superscript n indicates the current time step. The value of time increments for the air problem and the water problem must be the same but not necessarily uniform.

The numerical solution of the problem for the incompressible air flow as well as water problem using boundary element method is fully discussed. The only remaining governing equation is the compressible perturbation Laplace equation. Generally, the numerical procedure is the same. However, special cares should be taken for appropriate transformation of all parameters. Although, the coordinates are transformed into a different computational domain, the discretization and numerical implementation is the same. The solver always check the maximum Mach number of air flow especially at the throat of the gap layer. Once it exceeds 0.3, the solver change the governing equation from an incompressible potential regime to compressible potential flow. To avoid any discontinuity on the obtained results, there is an asymptotic criteria to check the results when the governing equation of the air flow is changed. According to this criteria the time derivative of the pressure on the any arbitrary line such as the interface should be the same at one time step before and after changing of governing equation. Using Taylor expansion these pressure can be stated as follows.

$$P(x, t_s + \Delta t^-)_{y=\eta} = P(x, t_s) + \Delta t^- \frac{\partial P}{\partial t} + O((\Delta t^-)^2) \quad (29)$$

$$P(x, t_s + \Delta t^+)_{y=\eta} = P(x, t_s) + \Delta t^+ \frac{\partial P}{\partial t} + O((\Delta t^+)^2) \quad (30)$$

where Δt^- and Δt^+ are just one time step before and after the time that the governing equation is changed. The time stepwhere numerical method switches from incompressible potential regime to compressible potential regime is indicated by t_s.In other word, the time derivatives of the pressure shoul be the same when $\Delta t \to 0$. If these time derivatives evaluated using backward time differncing the criterai yields:

$$\left[\frac{P(x, t_s) - P(x, t_s + \Delta t^-)}{\Delta t^-} - \frac{P(x, t_s + \Delta t^+) - P(x, t_s)}{\Delta t^+} \right] < \epsilon \quad (31)$$

where ε is a minimum acceptable deviation which is dependent on the problem configuration. If the solver cannot find the solution for satisfying the criteria, it changes the governing equation as the Mach number exceeds 0.3.

The boundary element method is very sensitive to the element size especially when the main source of the disturbance is close to boundaries. At this condition, the element size should be reasonably small enough to resultastable solution. Similar problem also occurs for choosing the proper values of time step. The time increments are determined based on the Courant-Friedrichs-Lowery (CFL) criterion. If the time increment is not selected carefully, the numerical solution suddenly diverges for transformed compressible potential flow.

RESULTS AND DISCUSSIONS:

The present model is developed for large blunt bodies. The main interest is on the common ship sections. Investigation of the air cushioning problem for large ship sections especially during slamming is the main motivation of this study. The common ship sections start from a nearly circular bulbous bow section at the bow to the approximately flat sections at the fore part of the ship. All of these sections are known as blunt sections. To consider all shapes and checking the model response to the body curvature, the geometry of impacting body is first a circle which gradually converts to a flat ellipse as shown in Figure 4. The bluntness of the body is defined as $\zeta = a/b$ and starts from unity for the circle and continues to 10 for a flat ellipse. There are 10 cases corresponding to each integer value of ζ.

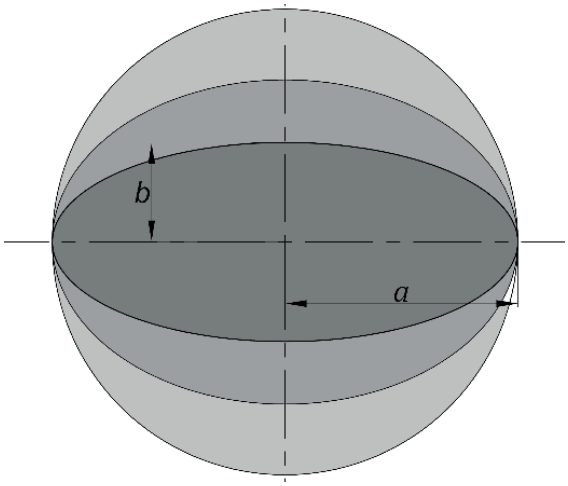

Fig. 4. General representation of the impacting blunt bodies

The numerical simulation starts with a circle and ends with the final flat ellipse. However, only two sets of the results are presented here, for the sake of brevity. The primarily results include the pressure distribution and free surface deformation. Figure 5 depicts pressure distribution for an ellipse with $\zeta = 3$ and and $v_0 = 1$ m/s. The breadth of all sections in the present models is assumed to be the same, $2a = 1$. Additionally, the horizontal direction is presented in non-dimensional form by dividing on the horizontal length scale. Corresponding free surface deformation is also illustrated in Figure 6.

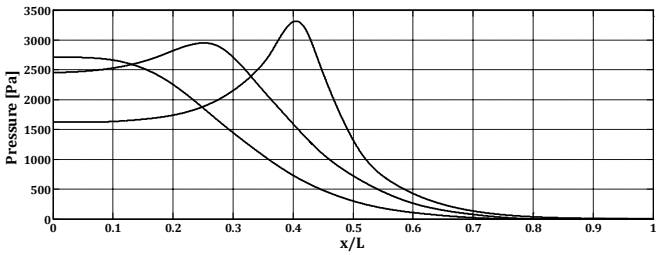

Fig. 5. Pressure distribution for an ellipse with $\zeta = 3$ and $v_0 = 1$ m/s at three consecutive time steps with $\Delta t = 0.008$ ms.

MOST WIEDZY Downloaded from mostwiedzy.pl

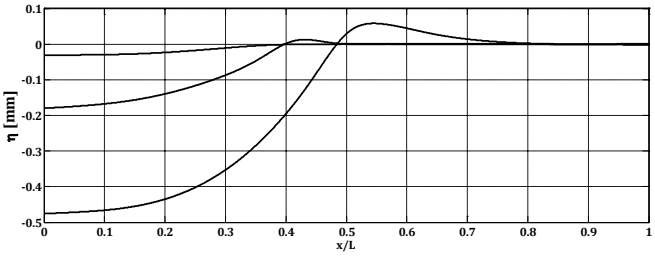

Fig. 6. Free surface deformation for an ellipse with ζ = 3 and v_0=1 m/s at three consecutive time steps with Δt = 0.008 ms.

The maximum pressure at the first time step occurs at origin and exactly beneath the symmetry line of the body. However, the location of the maximum pressure moves toward the throat of the gap layer at the next time step and the keel line pressure reduces. The air pressure rapidly drops after the throat of the layer. As the body gets closer to the free surface, the free surface is more deformed. Since the free surface is deformed, the body will touch the free surface at least on two points. If one can continue the numerical simulation while the body touches the free surface, some amount of air is entrapped between the body and free surface. Similar simulation can be also carried out for a blunter body. Figure 7 illustrates the maximum pressure distribution for an ellipse with ζ = 7 and v_0 = 1. The main difference between this new evaluated pressure and the previous one for ζ = 3, is the behavior of the air pressure. The solver predicts an impulsive response for the induced pressure. The maximum peak pressure also dramatically increases due to contribution of longer part of the body in comparison with the previous body. Although the predicted pressure corresponds with the air flow, its magnitude is in the same order of hydrodynamic impact pressure.

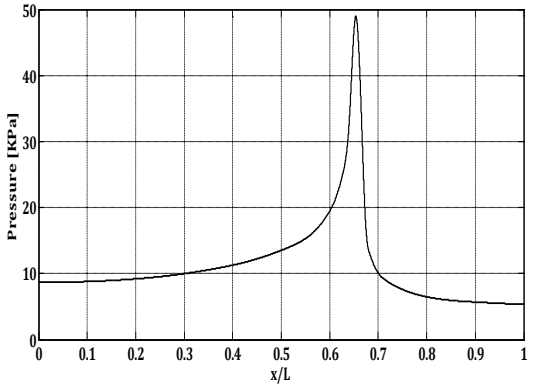

Fig. 7. Pressure distribution for an ellipse with ζ = 7 and v_0 = 1 m/s.

The evaluated pressure distribution for the blunter body shows a keel pressure three times more that the peak pressure of the previous body. In fact, the air layer can effectively tolerate a high pressure. This can significantly reduce the impact speed. One may further develop the present model to consider a rigid body dynamic equation to estimate the speed reduction. Theinduced high pressure compresses the air flow. Consequently, the governing equation should be changed to a compressible flow. To investigate this case, maximum air velocity for both bodies are evaluated and shown in Figure 8.

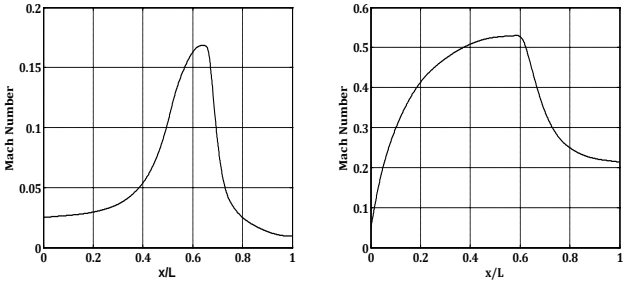

(a) *(b)*

*Fig. 8. Maximum air velocity for (**a**) An ellipse with ζ = 3 and (**b**) An ellipse with ζ = 7.*

For both bodies the maximum velocity occurs at the throat of the air gap layer. However, the behavior is completely different. It is clearly shown that the bluntness of the body can change the induced air speed. The maximum speed in the blunter body exceeds 0.3 and the flow is certainly compressible. The evaluated velocity speed shows that from x/L = 0.1, the Mach number is about 0.3.Additionally, the velocity of air flow after the throat is still considerably high. This can be also interpreted from the impulsive pressure reported in Figure 7. This suggests that another air cushioning layer may form after the throat but with much smaller length scales.

The accuracy of all numerical methods is dependent on the element size. Therefore, a mesh independency analysis should be always carried out to assess the whole performance of the numerical method. Boundary element method is also very sensitive to the element size especially close to the sources of disturbances. Figure 9 indicates mesh dependency analysis which typically figured out for an ellipse with ζ = 4. The error is defined based on the maximum pressure. Similar analysis is also conducted for all other cases.

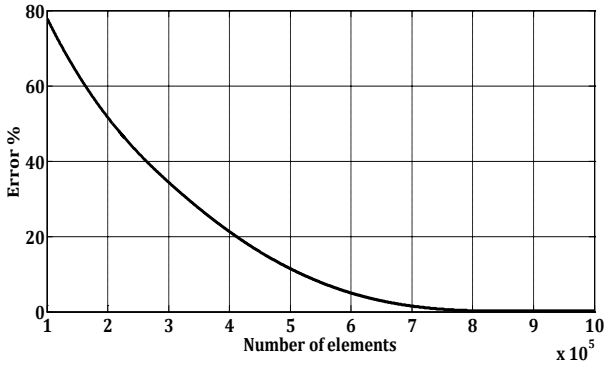

Fig. 9. Mesh dependency analysis

The cushioning problem is a complicated problem and all published researches focus on the special aspects of the problem with different assumption and limitation. This makes it difficult to find a general problem which can be used as a bench mark for long range of applications. Unfortunately,

MOST WIEDZY Downloaded from mostwiedzy.pl

the most of study considers the cushioning problem for small scale impacting bodies such as droplet impacts. However, there are studies which may be considered for validation such as those carried out by Hicks and Purvis [5, 6 and 7] and Hicks et al. [8]. The assumptions and the geometries are not the same as those considered in the present model but their model is effectively available for large sections. The Hicks and Purvis method has been used and a computer code developed to calculate cushioning problem for large blunt bodies. Figure 10 shows the comparison of the results of the present method with Hicks and Purvis method for two ellipses with $\zeta = 3$ and $\zeta = 7$.

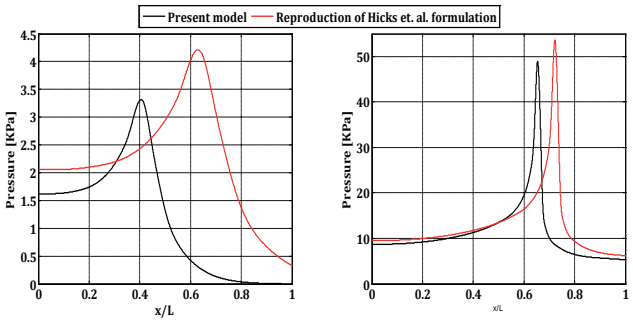

*Fig. 10. Evaluation of the present method and Hicks and Purvis method. **(a)** for a 2D ellipse with and **(b)** for a 2D ellipse with $\zeta = 7$. The Hicks and Purvis results are reproduced by the Authors for the corresponding geometries.*

The comparison depicts that the tendency of the both methods are the same. The blunter body shows a better agreement between both methods. The main source of deviation is neglecting lubrication region in the present method. It can be shown that considering such a region may result in a higher cushioning pressure. However, Mandre and Brenner [9] showed that the high pressure may not happen in real practice where the cushioning layer collapses before experience very high pressure. Anyhow, motivation of this method is to use a simple method by disregarding lubrication layer effect. The method is applicable for the very blunt and large bodies.

CONCLUSIONS

Numerical simulation of the air cushioning problem is investigated in this study. The proposed method based on two different governing equations for modeling the air flow including the incompressible and compressible flow which both are potential. The governing equations are in the forms of Laplace equation. The equation is solved using an iterative boundary element method. Pressure distribution and free surface profile are estimated for different blunt bodies. Typical results corresponding to two ellipses with $\zeta = 3$ and $\zeta = 7$ are presented. It is shown that as the bluntness of the body increases the induced pressure increases and the resulting water surface profile rises. Comparison of the present method with analytical method of Hicks and Purvis shows that the inviscid potential method can fairly approximate the problem for very blunt bodies. Additionally, the behavior of the air pressure for the blunter body is impulsive and the magnitude of the peak pressure is in order of impact pressure of water entry. This suggests that the cushioning problem cannot be neglected for very blunt bodies in water entry problem.

LIST OF SYMBOLS

Below is the list of symbols which are employed in the present text.

ρ_a	Air density
ρ_w	Water density
σ	Air-Water surface tension
P	Pressure
ϕ	Velocity potential
λ	Fundamental solution of Laplace equation
η	Free surface profile
κ	Curvature
$\hat{n}$	Norma vector
H_{ij}, G_{ij}	Influence coefficients
g	Gravitational acceleration
ds	Length differential
Γ	Boundary identity
a, b	Dimensions of an ellipse
ζ	Ellipse dimensional ratio

REFERENCES

1. J.H.G., Verhagen, 1967,"The impact of a flat plate on a water surface.", J. Ship research 11, 211-233.
2. O. Reynolds, 1886, "On the theory of lubrication and its application to Mr. Beauchamp tower's experiments, including an experimental determination of viscosity of olive oil." Philos. Trans. R. Soc. London Ser. A 177, 157-234.
3. N.G., Asryan, 1972, "Solid plate impact on surface of incompressible fluid in the presence of a gas layer between them.", SSR Mek25, 32{49.
4. S.K., Wilson, 1991, "A mathematical model for the initial stages of fluid impact in the presence of a cushioning fluid layer.", J. Engineering mathematics 25, 265-285.
5. P. Hicks and R. Purvis, 2010, "Air cushioning and bubble entrapment in three-dimensional droplet impacts." J. Fluid Mechanics 649, 135-163.
6. P. Hicks and R. Purvis, 2011, "Air cushioning in droplet impacts with liquid layers and other droplets." Physics of fluids 23.
7. P.D. Hicks and R. Purvis, 2013, "Liquid solid impacts with compressible gas cushioning." Journal of Fluid Mechanics 735, 120-149.

MOST WIEDZY Downloaded from mostwiedzy.pl

8. P.D. Hicks, E.V. Ermanyuk, N.V. Gavrilov, and R. Purvis, 2012, "Air trapping at impact of a rigid sphere onto a liquid." J. Fluid Mechanics 695, 310-320.

9. S. Mandre and M.P. Brenner, 2012, "The mechanism of a splash on a dry solid surface." Journal of Fluid Mechanics 690, 148-172.

10. F.T. Smith, L.Li and G.X. Wu, 2003,"Air cushioning with a lubrication/inviscid balance." Journal of Fluid Mechanics 482, 291-318

11. J.O. Marston, I.U. Vakarelski, and S.T. Thoroddsen, 2011, "Bubble entrapment during sphere impact onto quiescent liquid surfaces." J. Fluid Mechanics 680, 660-670

12. T. Tran, H. de Maleprade, C. Sun, and D. Lohse, 2013, "Air entrainment during impact of droplets on liquid surfaces." J. Fluid Mechanics 726.

13. G.R.G. Lewison, and W.M. Maclean, 1968, "On the cushioning of water impact by entrapped air." J. Ship research 12, 116-130

14. S.T. Thoroddsen, T.G. Etoh, K. Takehara, N. Ootsuka and Y. Hatsuki, 2005 "The air bubble entrapped under a drop impacting on a solid surface." J. Fluid Mechanics 545, 203-212.

15. W. Bouwhuis, M.H.W. Hendrix, M.H.W., D. van der Meer, and J.H. Snoeijer, 2015, "Initial surface deformations during impact on a liquid pool." J. Fluid Mechanics 771, 503-519.

16. J.T. Katsikadelis, "BOUNDARY ELEMENTS: Theory and Applications", Elsevier, 2002

CONTACT WITH THE AUTHORS

MojtabaBarjasteh

Hamid Zeraatgar
e-mail: hamidz@aut.ac.ir

Amirkabir Laboratory of Hydrodynamics (ALH)
Faculty of Maritime Engineering
Amirkabir University of Technology
Tehran
Iran

MOST WIEDZY Downloaded from mostwiedzy.pl

POLISH MARITIME RESEARCH Special Issue 2018 S1 (97) 2018 Vol. 25; pp. 94-103
10.2478/pomr-2018-0029

PARAMETRIC COMPARISON OF RECTANGULAR AND CIRCULAR PONTOONS PERFORMANCE AS FLOATING BREAKWATER NUMERICALLY

Seyyed Mohammad Reza Tabatabaei
Hamid Zeraatgar
Amirkabir University of Technology, Tehran, Iran

ABSTRACT

Rectangular and circular pontoons are one of the most widely cross-sections used as floating breakwaters (FB). Although, there are several articles on comparison of behavior of rectangular and circular floating breakwaters however, the Authors try to show some details of difference between these two types where they have not been addressed before. To do so, transmission coefficient (Ct), as a measure of merit, of similar rectangular and circular sections is numerically compared. A computer code is developed for two-dimensional hydrodynamic analysis of floating breakwater based on diffraction theory in frequency domain in regular waves with any configuration of mooring line. The numerical method is the finite element method and validated by comparing with experimental and numerical results. Three types of rectangular sections are defined equivalent to circular section and a numerical comparison is made between 100 similar sections. The Ct versus wave frequency has been considered in detail and three new points called LMinF, LMaxF and LMaxCt are introduced. It has been shown that LMinF and LMaxF of circular section are greater and LMaxCt is much smaller than equivalent rectangular section. The LMaxCt of both sections are very dependent to new non-dimensional parameter B/D (Breadth/Draft). Although, rectangular sections are more common for floating breakwater, however the results of this study show that possibility of using circular sections must be also considered.

Keywords: Floating Breakwater, transmission coefficient, circular section, rectangular section,

INTRODUCTION

For many years, fixed breakwaters have been used to create a calm environment for different purposes such as loading, unloading, fishing, military and even recreational use. They were designed and implemented vertically or sloped. Rubble mound breakwaters are the most common type of sloped fixed breakwaters that is built with stone pouring from the sea floor to above water level. For various reasons, such as high cost especially in deep water, extreme sedimentation, poor sea bed and large changes in water level because of tide, floating breakwater (FB) was introduced.

Sea wave energy is mainly distributed on water surface. Therefore it is not necessary to extend breakwaters up to sea bed, especially in deep water condition. The FB is a floating structure on water surface and its movements are limited by mooring lines. As a system of sea wave hits a FB, it responses by motion in six degrees of freedom, that is surge, sway, heave, roll, pitch and yaw. A FB response depends on its specifications such as, geometry, mass and its distribution and incident wave parameters such as period and height. Additionally, the FB motions in wave are function of mooring characteristics such as material, weight, length, angle and its type. All six motions may have a natural frequency and they can be determined by breakwater geometrical characteristics and mooring line specifications.

Normally, the extreme motions of a FB may happen when direction of wave propagation is perpendicular to

MOST WIEDZY Downloaded from mostwiedzy.pl

the longitudinal axis of the FB. In this case, the motion is limited to the sway, heave and roll and they are coupled to each other. Since, in areas near beach, waves usually propagate perpendicular to the breakwater, thus two-dimensional analysis of FB is realized.

In the past few decades, numerous analytical, experimental and numerical studies have been done, mainly to increase performance and reduce costs of FB. (McCartney, 1985; Mani, 1991) categorized types of FB based on their specifications and expressed the advantages and disadvantages of each type. On that basis, FB types are pontoon, mat and tethered.

The most common type of FB is rectangular section, Ji (2015), due to the ease of production and transportation as well as the flat deck. The other common pontoon sections are circular and trapezoidal, Sawaragi (1995). So far, plenty of researches have been directed to the rectangular pontoon but there is still a lack of enough information on circular sections, Ozeren (2011).

Bloomberg (1998) compared Ct of seven types of rectangular sections and concluded that the catamaran type has the best performance. The types that he considered include single, double, triple, double with 1, 2, 4 meter intermediate skirt and catamaran.

Dimer et al. (1992) analytically investigated 2-D pontoon type of FB in regular wave. They have shown that at intermediate water depth, the pontoon type FB has well performance against wave with wave lengths several times of width of the structures.

Sannasiraj et al. (1998) made a two-dimensional experiment as well as numerical calculation on a rectangular pontoon having three mooring configurations. They measured and calculated motion responses such as sway, heave, roll, Ct and mooring forces. Results showed that numerical code written by finite element method is pretty reliable to predict FB behavior. They concluded that changing type of mooring configuration does not make a significant difference on FB performances.

Behzad et al. (2007) experimentally investigated response and efficiency of five types of pontoon with different drafts in random waves. It was shown that by increasing the wave period the Ct increases, while increase of the mass reduces the Ct.

Mays (1998) summarized works done on the circular cylinder in his PhD thesis. He examined submerged circular cylinder encountering sea waves in oblique and perpendicular directions by a three-dimensional numerical boundary element method. It was shown that circular section is efficient for a wide range of wave directions.

Ozeren et al. (2011) studied single and multiple circular sections with three types of mooring line namely bottom-moored, arm-restrained and pile-restrained in deep and transitional water depth. It was shown that in pile-restrained type, wave reflection was much more than two other types. Additionally, for the pile-restrained type, performance depends on section draft to height ratio. Moreover, for the two other types of mooring line, dissipation had the greatest influence on Ct. Besides, in order to improve performance of FB, the horizontal restraint is more important than the vertical one.

Isaacson et al. (1995) studied circular sections with chain and nylon mooring line in regular waves, experimentally. It was stated that for Ct, the breadth ratio i.e. diameter of cylinder to wavelength will be more effective than wave steepness. The Authors must indicate that this is the only study in which rectangular and circular sections are compared, experimentally. They concluded that the circular and rectangular sections have similar responses where Ct of rectangular section is slightly less than circular section. Moreover, they stated that the concrete circular pontoons have less cost, torsion and tension in corners compared with rectangular one due to wave impact.

Shankar (1998) in his PhD thesis, numerically studied two similar pontoons connected to each other where one had rectangular section and the other had circular section. As far as Ct is concerned, it was shown that the size of pontoon and pontoon's breadth are the most important parameters. They also stated that circular section behaves like rectangular section very much.

Although, there are several articles on comparison of behavior of rectangular and circular FB however, the Authors try to show some details of difference between these two types where they have not been addressed before. To do so, the Ct of 100 similar rectangular and circular sections is numerically compared. A computer code is developed for two-dimensional hydrodynamic analysis of FB based on diffraction theory in frequency domain in regular waves with any configuration of mooring line. The numerical method is the finite element method and validated by comparing with experimental and numerical researches. A parametric study for comparison of these two sections is carried out. It has been shown that generally circular section has better transmission coefficient.

THEORY AND BASIC EQUATIONS

Fig.1 shows a FB with mooring line. A coordinate system is defined where its origin is located on symmetry line of the FB and waterline. The x and y are on water surface and z is perpendicular to the water surface.

The fluid is assumed to be ideal, incompressible and irrotational, and therefore the governing equation is the Laplace equation.

$$\nabla.\nabla\varphi = 0 \rightarrow \nabla^2\varphi = 0 \rightarrow \frac{\partial^2\varphi}{\partial x^2} + \frac{\partial^2\varphi}{\partial y^2} + \frac{\partial^2\varphi}{\partial z^2} = 0 \qquad (1)$$

Where φ is the velocity potential, x, y and z are spatial variables. Wave height and motion assumed to be small. The FB dimensions in respect to wavelength are large where use of diffraction theory is justified.

As shown in Fig .1 the dynamic of the FB is defined as a two-dimensional problem where four different configurations of symmetrical catenaries mooring lines are considered.

MOST WIEDZY Downloaded from mostwiedzy.pl

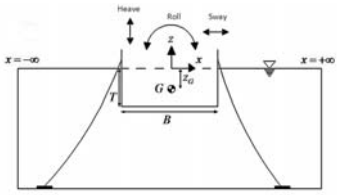

Fig. 1. FB, motions, degrees of freedom and position of coordinate axes

In order to solve the equation (1) the boundary conditions are to be defined according to physical conditions of the problem. Boundary condition on the surface of the rigid body is defined as follows:

$$\nabla\varphi.\hat{n} = \frac{\partial\varphi}{\partial n} = V_B.\hat{n} = V_{Bn} \tag{2}$$

Where $\hat{n}$ is the unit vector normal to the body surface, V_B is velocity of the body at the desired point and V_{Bn} is the component of velocity normal to the surface.

Impermeable boundary of sea bed will be as follows:

$$\left.\frac{\partial\varphi}{\partial z}\right|_{z=-h} = 0 \tag{3)}$$

Linear boundary condition of free surface is defined as follows:

$$\frac{\partial^2\varphi}{\partial t^2} + g\frac{\partial\varphi}{\partial z} = 0 \tag{4}$$

Far field boundary condition is:

$$\frac{\partial\varphi_s}{\partial r} + \frac{1}{c}\frac{\partial\varphi_s}{\partial t} = 0 \tag{5}$$

Where φ_s is velocity potential for scattered wave due to floating body, and c is the wave celerity and r is the radial distance from the desired point on the surface of the body.

The linear diffraction is applicable when wave height and response of the body are small. The total velocity potential can be written in terms of its components as follow:

$$\varphi(x,z,t) = \varphi_I(x,z,t) + \varphi_D(x,z,t) + \varphi_R(x,z,t) \tag{6}$$

Where:

$\varphi_I(x,z,t)$ Is velocity potential of incident wave

$\varphi_D(x,z,t)$ Is velocity potential of diffraction due to floating body

$\varphi_R(x,z,t)$ Is velocity potential of radiated energy due to motions of floating body

Having assumed a sinusoidal regular wave as incident wave, there is an analytical solution for incident wave velocity potential. The diffraction and radiation velocity potentials are obtained by solving boundary value problems, numerically. Having used Bernoulli equation, one may calculate the pressure on the FB. In order to calculate the forces acting on the FB, it is necessary to integrate the pressure exerted on the wetted surface. By implementing Newton's second law, motion of FB could be extracted from the equation of motion.

The equation of motion, boundary condition, boundary value problems and quasi-static analysis of mooring line based on basic catenary equations is fully described by Sannasiraj et all. (1998)

COMPUTER CODE AND VALIDATION

COMPUTER CODE

To analyze the motions of FB in waves, a computer code based on FEM model is developed in MATLAB. Input data are water depth, breadth or diameter of FB, draft, wave frequency range and frequency increment. For each wave frequency, zone of the problem is defined, mesh is generated and velocity potential for each node is calculated. The zone of the problem is set as twice the wavelength plus breakwater breadth. After calculation of pressure, motion amplitude of three degrees of freedom, response amplitude operator and Ct is calculated. The code is able to analyze any geometry of FB. Fig.2 shows flowchart of the computer code.

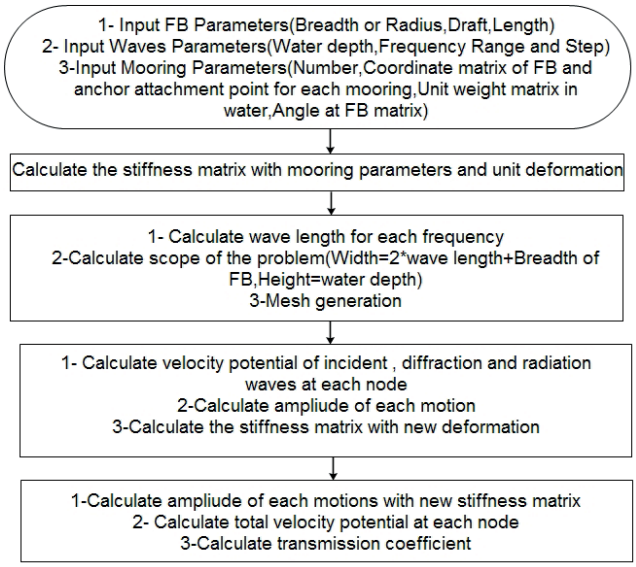

Fig. 2. Flowchart of the computer code

VALIDATION

In order to validate the computer code, two cross sections, rectangular and circular, for which experimental results have been published, are considered.

MOST WIEDZY Downloaded from mostwiedzy.pl

Rectangular pontoon

As mentioned previously, Sannasiraj et al. (1998) studied rectangular pontoons, experimentally and numerically. The experiment performed in constant water depth of 2.35 m, catenary chain mooring with fixed length of 4.7 m and weight of 1.25 N/m, wave with 0.05 mm height and 0.3 to 1.5 Hz frequency range propagating perpendicular to the longitudinal axis of the breakwater. The Sannasiraj et al. model experiment has been widely used for validation of numerical models due to publishing many details of test parameters. The Sannasiraj et al. rectangular pontoon parameters and three symmetrical mooring line configurations called C1, C2 and C3 are shown in Table 1 and Fig. 3.

Tab1. Sannasiraj et al. (1998), rectangular pontoon specifications

Particulars	Symbol	Unit	Value
Length	L	M	3.78
Breadth	B	M	0.40
Draft	T	M	0.10
Mass	M	Kg	150.5
Mass center	(X_g, Z_g)	M	(0.0,0.026)
Transverse Metacentric height	GM_T	M	0.057
Mass MI about transverse axis	I_{xx}	kg m^2	188.0
Mass MI about longitudinal axis	I_{yy}	kg m^2	5.33
Mass MI about vertical axis	I_{zz}	kg m^2	189.8
Roll natural frequency	f_r	Hz	0.592
Heave natural frequency	f_z	Hz	1.012

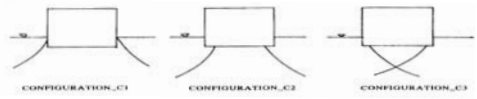

Fig. 3. Sannasiraj et al. (1998), rectangular pontoon and three mooring line configurations

In the case of C1 mooring configuration, the RAO of sway, heave and roll motions and Ct of Sannasiraj et al. experiment as well as numerical model and present study are shown in Figs.4 to 7, respectively. Generally, the present study follows the trend of experiment for three motions as well as for transmission coefficient. However, there is some considerable difference between the present method and experiment for some frequencies. More or less this difference is repeated in Sannasiraj et al. numerical method, too. At natural frequency of roll motion that is 0.592 Hz or 0.2712 in non-dimensional form, the present method has shown better compliance with experiment both for motions and Ct in comparison with the Sannasiraj et al. numerical method. One may aware of uncertainty of experiment in particular at natural frequency as two Ct for a single frequency are reported.

Fig.7 also shows that, at the roll natural frequency, waves generated by FB has significantly decreased the Ct.

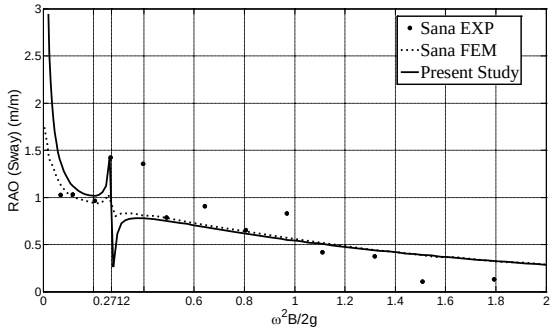

Fig. 4. Comparison RAO of sway motion, C1 mooring configuration

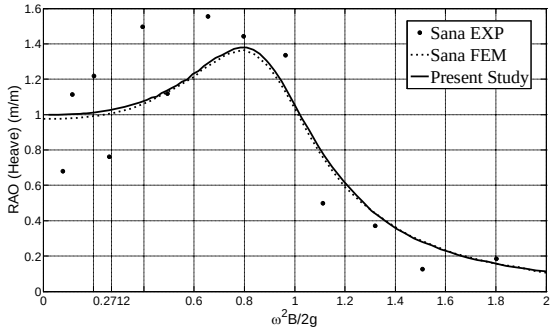

Fig. 5. Comparison of RAO of heave motion, C1 mooring configuration

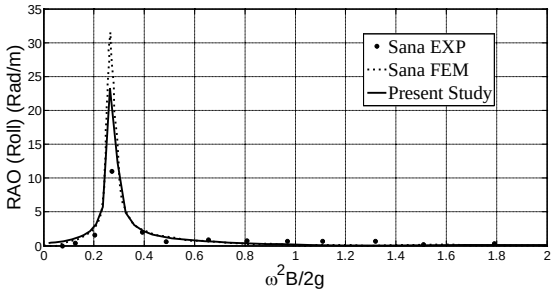

Fig. 6. Comparison of RAO of roll motion, C1 mooring configuration

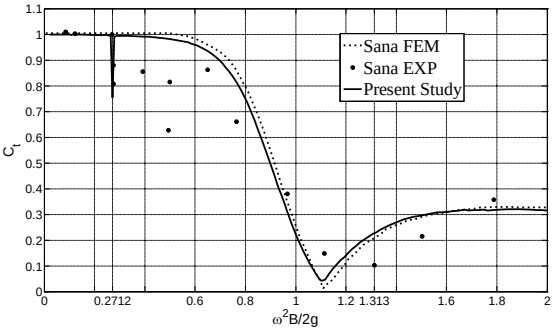

Fig. 7. Ct comparison for C1 mooring configuration

In the case of C2 mooring configuration, the RAO of sway, heave and roll motions of Sannasiraj et al. (1998) experiment and numerical model, Lee and Cho (2003) numerical element-free Galerkin model and Loukogeorgaki et al. (2005 a, b) 3-D panel method are compared with the present study as shown

MOST WIEDZY Downloaded from mostwiedzy.pl

in Figures 8 to 10. It is worth to mention that Loukogeorgaki et al. used Green›s theorem, panel method and static and dynamic analysis of mooring with iteration method. Basically, the present study follows the trend of experiment for three motions. However, there is some difference between present method and experiment for some frequencies. More or less this difference is repeated in other numerical methods, too.

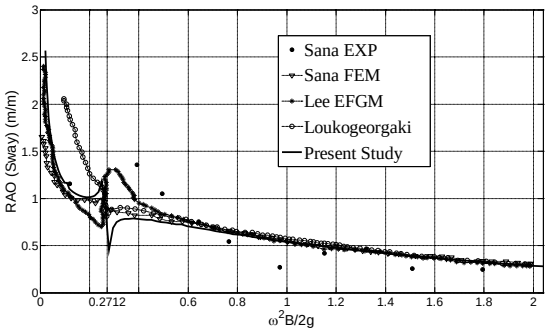

Fig. 8. Comparison of RAO of sway motion, C2 mooring configuration

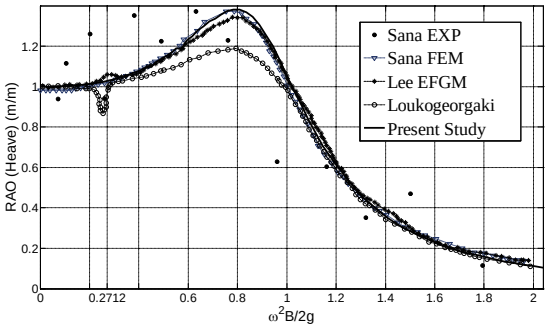

Fig. 9. Comparison of RAO of heave motion, C2 mooring configuration

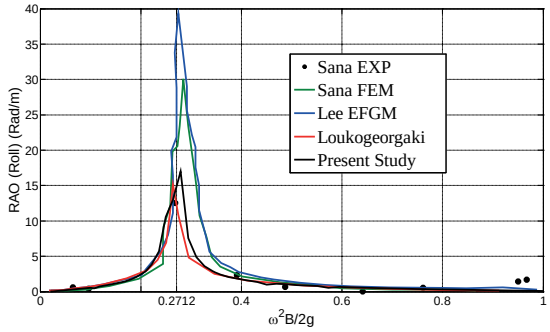

Fig. 10 Comparison of RAO of roll motion, C2 mooring configuration

Fig. 8 shows that for sway motion, all numerical studies follow the same trend as experimental results.

Fig. 9 shows that Loukogeorgaki et al., in some frequency in particular at natural frequency of rolling, better predicts the heave amplitude, but in other frequencies is worse.

As Fig. 10 shows, results of present study at the roll natural frequency are quite better than others in comparison with experiment.

Circular pontoon

Isaacson et al. (1995) provided 2D and 3D experiments and 2D numerical calculation for circular pontoon with different mooring configurations. As depicted in Fig.11, the moorings are chain and nylon types and connected to the pontoon in three configurations called bottom, crossed and uncrossed.

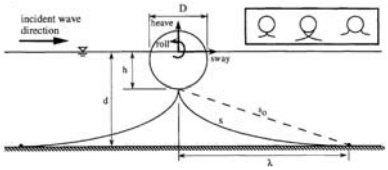

Fig. 11. Circular pontoon cross-section and three mooring configurations, Isaacson et al. (1995)

In 2D experimental study of Isaacson that is called Wave Flume Test, the flume parameters are 0.62 m width, 40 m length and 0.6 m water depth. A PVC model of 321 mm diameter, 0.62 m length, slightly smaller than the width of the flume, manufactured and for several h/D and draught to diameter had been tested. In the case of bottom chain mooring configuration with S/S0=1.060, 140 N/m submerged weight and h/D=0.579, the Ct and the RAO of sway, heave and roll are calculated by present method and compared with Isaacson as shown in Figs. 12 to 15, respectively.

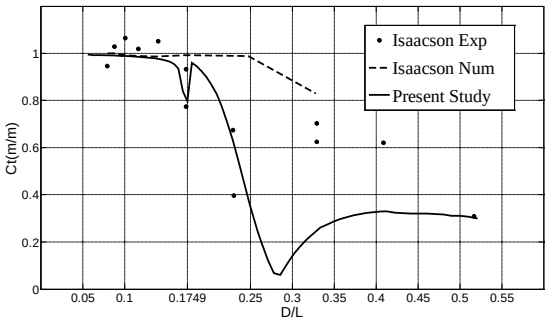

Fig. 12. Ct comparison of circular pontoon, chain moored at bottom of pontoon

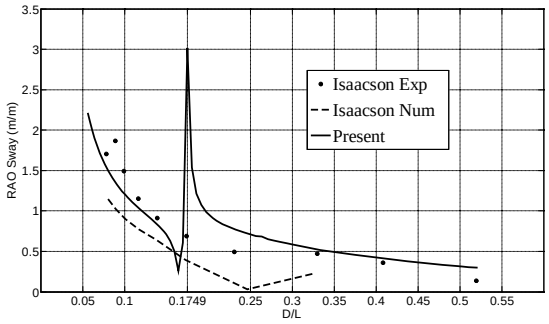

Fig. 13. Comparison of RAO of sway motion of circular pontoon, chain moored at bottom of pontoon

MOST WIEDZY Downloaded from mostwiedzy.pl

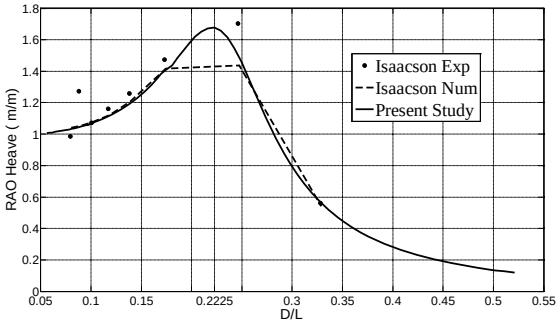

Fig. 14. Comparison of RAO of heave motion of circular pontoon, chain moored at bottom of pontoon

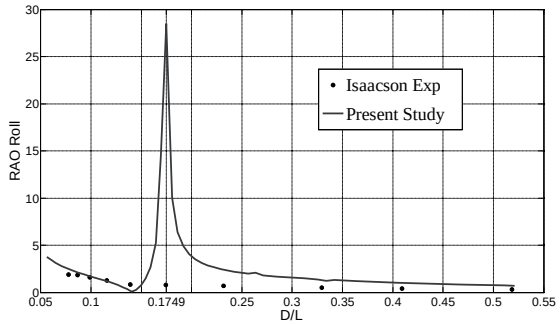

Fig. 15. Comparison of RAO of roll motion of circular pontoon, chain moored at bottom

Fig.12 shows that, in general, the present study follows the Ct trend as in experiment. However, there is significant underestimation for the D/L ranging of 0.30 to 0.40. Furthermore, the Ct trend changes sharply around D/L = 0.3. Besides, a very good compliance with the experiment at resonance frequency is quite promising. One may conclude that the present study is complying with the experiment better than the Isaacson numerical method.

Fig.13 shows that, for sway motion, the present numerical method follows the same trend of experiment except at resonance frequency. As far as roll motion is concerned, the present method depicts the same tendency as shown in Figure 15. Since, the sway and roll motions are strongly coupled, the deviance from experiment at roll resonance frequency for both motions are more pronounced. It may arise from viscous damping which is not included in the present method.

The heave motion is uncoupled to the roll and sway motions. That is why, according to Figure 14, a pretty good prediction of heave motion for all range of D/L in respect to experiment achieved. General speaking, the present method seems to predict the experiment better than the Isaacson numerical method.

Having considered the above validation studies, one may conclude that the present method is an accepted tool to be used for analysis of moored FB with different sections.

A PARAMETRIC STUDY ON COMPARISON OF RECTANGULAR AND CIRCULAR FB

There are several studies comparing effectiveness of circular FB with the rectangular FB such as Isaacson et al. (1995) and Shunkar (1998). However, this study tries to present more comprehensive comparison between these two sections at fair conditions.

Certainly, the rectangular section in comparison with circular section is easy to be manufactured and also better for operation as it provides flat deck. If these two sections are to be compared on the basis of their hydrodynamic performance, the transmission coefficient is the best measure of merit.

DEFINITION OF SIMILAR CIRCULAR AND RECTANGULAR SECTIONS

In order to compare the performance of circular and rectangular sections, the size of them is to be similar to ensure a fair comparison .The similar size of two sections may be defined by three ways:

Type I: rectangular section with the same breadth and draft of circular section, but different buoyancy

$$2 * R_C = Breadth_R = Breadth_c$$

$$R_C = draft_R = Draft_c$$

$$A_C = (\pi {R_C}^2)/2$$

$$A_R = Breadth_R * Draft_R = 2 * R_C^2 > A_C$$

Type II: rectangular section with the same breadth and buoyancy of circular section, but different draft

$$A_C = A_R = (\pi {R_c}^2)/2 = Breadh_R * Draft_R$$

$$Breadth_R = 2 * R_C$$

$$draft_R = \frac{\pi}{4} R_C$$

Type III: rectangular section with the same draft and buoyancy of circular section, but different breadth

$$A_C = A_R = (\pi {R_c}^2)/2 = Breadh_R * Draft_R$$

$$draft_R = 2 * R_C$$

$$breadth_R = \frac{\pi}{4} R_C$$

As shown in Fig.16 R_c, A_c, $Draft_c$ and are radius, section area (wet section area), draft and breadth of circular pontoon, respectively. $Draft_R$, $Breadth_R$, and A_R are draft, breadth and section area of rectangular pontoon, respectively.

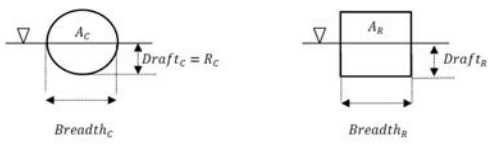

Fig.16 similar rectangular and circular sections parameters

MOST WIEDZY Downloaded from mostwiedzy.pl

CALCULATION OF TRANSMISSION COEFFICIENTS FOR A SET OF CIRCULAR AND RECTANGULAR SECTIONS

For the sake of simplicity, it is assumed that all sections are homogeneous, mass uniformly distributed and center of gravity coincide with center of buoyancy. Among three configuration of mooring line shown in Figure 3, the configuration C1 is chosen for calculation. For the stiffness matrix of mooring line, coordinate of connection point to breakwater has been modified based on geometry change. The present numerical model has been implemented for 25 circular sections and 75 equivalent similar rectangular sections to obtain transmission coefficient. The specifications of these 100 sections are shown in Table2.

A typical Ct versus ω is shown in Figure17. This type of Ct behavior is applicable for circular, rectangular and any other sections. It starts with Ct=1 for low frequency, as low as about 2 radian per second, and then starts to decrease. Suddenly, it sharply decreases and reaches to zero for complete reflection condition theatrically. But in fact, a local minimum Ct <0.1 takes at frequency that called LMinF (Fig.17) which is around 3 to 7 radians per second usually . After that, it rises and reaches a local maximum Ct that called LMaxCt at a frequency that called LMaxF (Fig.17).

Tab. 2 .Specification of 100 similar circular and rectangular sections

	Circular	**Rectangular Pontoons Type I**		**Rectangular Pontoons Type II**		**Rectangular Pontoons Type III**	
		$\begin{cases} Breadth_R = Breadth_C \\ Draft_R = Draft_C \end{cases}$		$\begin{cases} Breadth_R = Breadth_C \\ Buoyancy_R = Buoyancy_C \end{cases}$		$\begin{cases} Draft_R = Draft_C \\ Buoyancy_R = Buoyancy_C \end{cases}$	
No.	**Radius(m)**	**Breadth(m)**	**Draft(m)**	**Breadth(m)**	**Draft(m)**	**Breadth(m)**	**Draft(m)**
1	0.1	0.2	0.1	0.2	0.0785	0.1571	0.1
2	0.125	0.25	0.125	0.25	0.0982	0.1963	0.125
3	0.15	0.3	0.15	0.3	0.1178	0.2356	0.15
4	0.175	0.35	0.175	0.35	0.1374	0.2749	0.175
5	0.2	0.4	0.2	0.4	0.1571	0.3142	0.2
6	0.225	0.45	0.225	0.45	0.1767	0.3534	0.225
7	0.25	0.5	0.25	0.5	0.1963	0.3927	0.25
8	0.275	0.55	0.275	0.55	0.216	0.432	0.275
9	0.3	0.6	0.3	0.6	0.2356	0.4712	0.3
10	0.325	0.65	0.325	0.65	0.2553	0.5105	0.325
11	0.35	0.7	0.35	0.7	0.2749	0.5498	0.35
12	0.375	0.75	0.375	0.75	0.2945	0.589	0.375
13	0.4	0.8	0.4	0.8	0.3142	0.6283	0.4
14	0.425	0.85	0.425	0.85	0.3338	0.6676	0.425
15	0.45	0.9	0.45	0.9	0.3534	0.7069	0.45
16	0.475	0.95	0.475	0.95	0.3731	0.7461	0.475
17	0.5	1	0.5	1	0.3927	0.7854	0.5
18	0.525	1.05	0.525	1.05	0.4123	0.8247	0.525
19	0.55	1.1	0.55	1.1	0.432	0.8639	0.55
20	0.575	1.15	0.575	1.15	0.4516	0.9032	0.575
21	0.6	1.2	0.6	1.2	0.4712	0.9425	0.6
22	0.625	1.25	0.625	1.25	0.4909	0.9817	0.625
23	0.65	1.3	0.65	1.3	0.5105	1.021	0.65
24	0.675	1.35	0.675	1.35	0.5301	1.0603	0.675
25	0.7	1.4	0.7	1.4	0.5498	1.0996	0.7

MOST WIEDZY Downloaded from mostwiedzy.pl

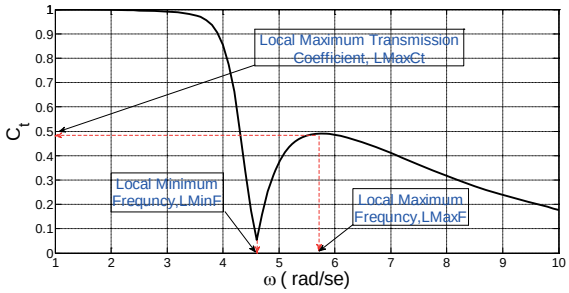

Fig.17. Typical Ct versus ω and definition of LMinF, LMaxF and LMaxCt

If one could so design a FB for which the working condition is set in the range of LMinF and over, then this kind of FB design has the best transmission condition for the whole operation condition. Certainly, among them, the best FB is one which has the lowest LMaxCt.

The transmission coefficient of circular section and three similar rectangular sections as categorized by types I, II and III (Table 2) versus wave angular frequency, ω, are shown in Figs. 18 to 21.

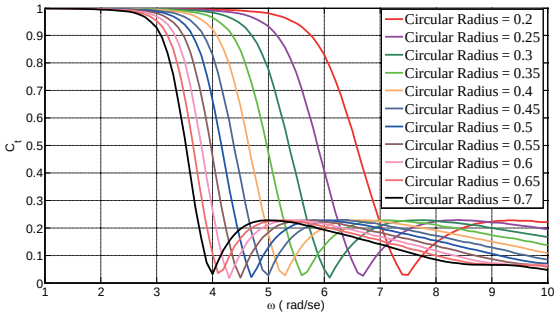

Fig. 18. Ct of circular sections with different radius

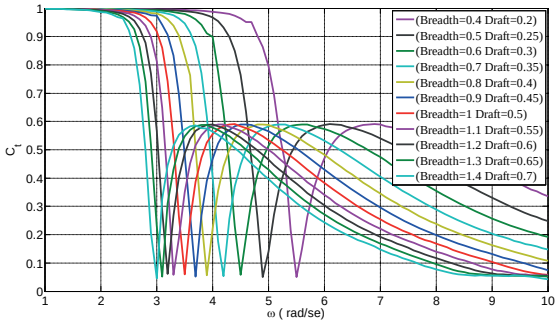

Fig. 19. Ct of rectangular pontoon section, type I

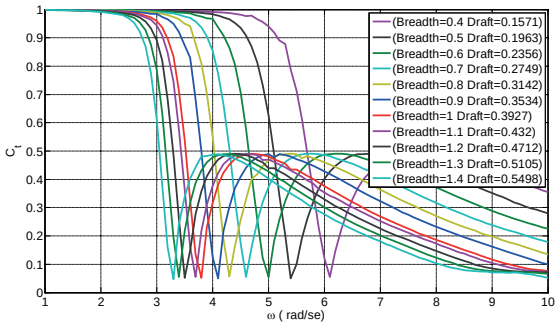

Fig. 20. Ct of rectangular pontoon section, type II

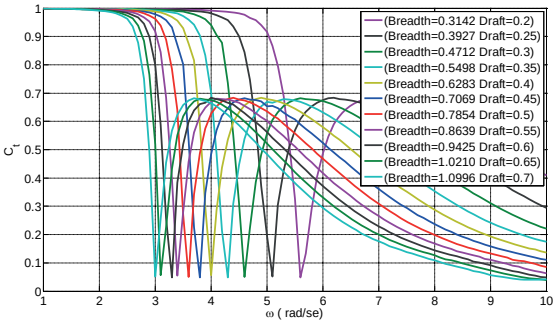

Fig. 21. Ct of rectangular pontoon section, type III

Figure18 depicts transmission coefficient of circular section having radius ranging from 0.2 to 0.7 meter. For all ranges it follows the typical behavior as shown in Figure 17. The LMinF is about 4 to 7.5 radians per second for whole range of circular section radius. However, as circular sections radius increases the LMinF and LMaxF decreases. The LmaxCt is almost constant, 0.22, for whole range of radius.

The typical behavior of Figure 17 is repeated for the rectangular sections. Having seen in circular section, as the size of rectangular section increases the LMinF and LMaxF are shifting to the lower frequencies. However, LMaxCt is 0.59, 0.49 and 0.68 for Type I, II and III, respectively.

As an example of comparison, Figure 22 presents Ct comparison of circular section (radius=0.3 m) and three similar rectangular sections. Although, LMaxCt of circular section is smaller than three equivalent rectangular sections however, the LMinF and LMaxF of three rectangular types are smaller than circular section.

An important conclusion of this comparison is that the rectangular section of Type II is more comparable to the circular section than others. The reason of this kind of similarity returns back to the ratio of B/D. It seems that B/D plays an important role which will be discussed in next section. The same behaviors may be seen for other circular section in comparison with similar rectangular sections.

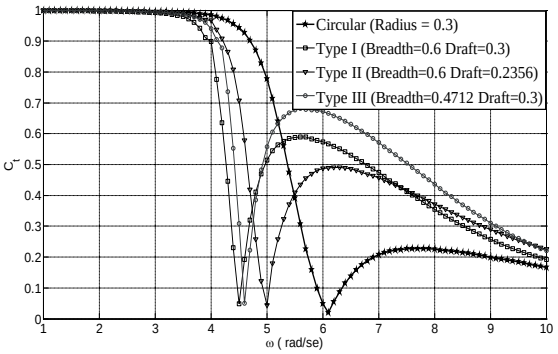

Fig. 22 Ct comparison of circular section (radius=0.3 m) and three similar rectangular sections

MOST WIEDZY Downloaded from mostwiedzy.pl

DISCUSSIONS AND ANALYSIS

TYPICAL FB PARAMETRIC STUDY

Parametric study of FB is classically concerns the Ct versus relative breadth, *B/L* (breadth to wavelength), relative draft, *D/L* (draft to wavelength) and normalized frequency, $\omega^2 B/2g$.

Figures 23 to 25 show Ct against *B/L*, *D/L*, $\omega^2 B/2g$ for 100 sections (circular and three types of similar rectangular), respectively. The domination of wave length on Ct as shown in previous Figures, such as Figures 18 to 21 is repeated here.

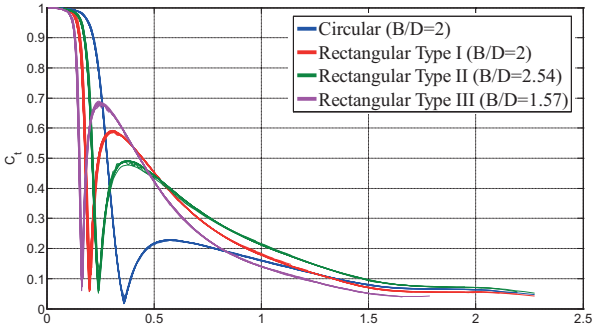

Fig. 23. Ct comparison of circular section and three similar rectangular sections versus relative breadth

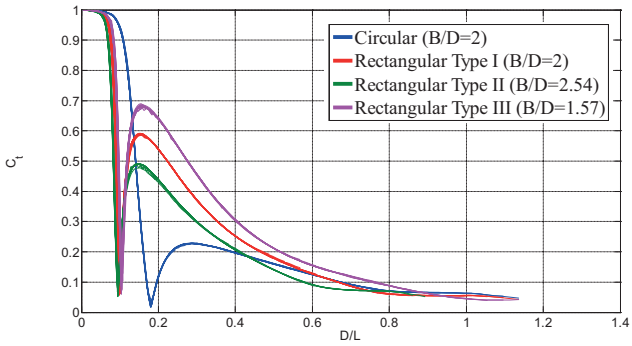

Fig. 24. Ct comparison of circular section and three similar rectangular sections versus relative draft

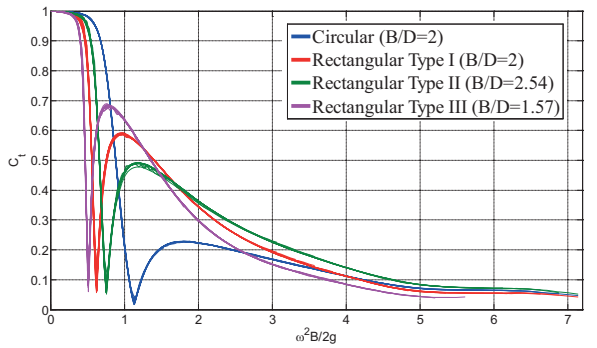

Fig.25. Ct comparison of circular section and three similar rectangular sections versus normalized frequency

CT VERSUS NEW PARAMETER, B/D

Having considered the LMaxCt for different kind and type of sections, the *B/D* may be introduced as a new non-dimensional parameter. For rectangular sections, *B/D* is 2, 2.54 and 1.57 for Type I, II and III, respectively. Furthermore, for circular section the *B/D* is 2 for all cases as per Table 2. Additional calculation for LMaxCt of rectangular sections and circular section are performed and depicted in Figure 26. It can be seen that as B/D increases, the LMaxCt sharply decreases for rectangular sections. Anyway, LMaxCt of circular section is unique as B/D is unique and smaller than all rectangular sizes.

Actually, a FB is working in a range of wave frequencies mostly between LMinF and LMaxF as well as beyond. So, it is important to have low Ct for a range of wave frequencies. In Table 3 the average of LmaxCt is shown for all FB as per Table 2. LMaxCt of rectangular are at least twice than circular and it is simply concluded that the circular section has better performance than all equivalent types of rectangular sections.

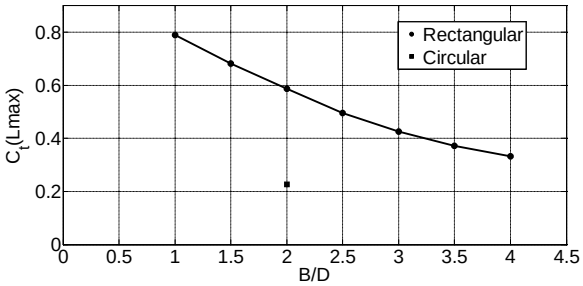

Fig. 26. LMaxCt of rectangular and circular section versus B/D

Tab. 3. LMaxCt comparison of circular and rectangular sections

FB Section	Mean LMaxCt
Circular	0.2274
Rectangular Type I	0.5865
Rectangular Type II	0.4883
Rectangular Type III	0.6778

CONCLUSIONS

The aim of this study is to compare the performance of circular section and rectangular sections as a breakwater in detail. For this purpose a 2-D computer code based on finite element method has been developed. The code results are validated in comparison with experimental methods where good compliance has been achieved.

A set of 100 breakwater sections, 25 circular sections and 75 equivalent rectangular sections, has been defined and their transmission coefficients are calculated. A comparison is made between the circular section and rectangular sections transmission coefficients.

MOST WIEDZY Downloaded from mostwiedzy.pl

Three new points LMinF, LMaxF and LmaxCt defined on Ct versus ω and a new non-dimensional parameter, B/D, has been introduced. It has been shown that the LMaxCt of all sections are very dependent to this parameter.

There are some advantages for rectangular and some for circular sections.

LMinF and LMaxF of similar rectangular sections are smaller than circular sections.

LMaxCt of similar rectangular sections are at least twice of circular sections. It means Ct of circular section does not sharply change between LMinF and LMaxF in comparison with rectangular sections.

Generally, the circular sections have shown better performance than the rectangular section in whole range of wave frequencies.

Actually, the decision regarding type of section for FB not only depends on Ct performance, but also the cost of production is to be considered. However, the application of circular section as FB is not easy to be discarded. Although, rectangular sections are more common for FB, but the results of this study show that possibility of using circular sections must be considered.

REFERENCES

1. Behzad, M. and Akbari, M., 2007.Experimental investigation on response and efficiency of moored pontoon type floating breakwaters, Iranian Journal of Science & Technology, Transaction B, Engineering., 31: 95-99

2. Blumberg, G. P. and Cox, R. J., 1998.Floating breakwater physical model testing for marina applications, Bulletin of the Permanent International Association of Navigation Congresses., 63: 5-13

3. Dimer, N., Agnon, Y., and Stiassnie M., 1992.A simplified analytical model for a floating breakwater in water of finite depth, Applied Ocean Research., 14: 33-41.

4. Isaacson, M., Whiteside, N., Gardiner, R. and Hay, D., 1995.Modeling of a circular-section floating breakwater, Canadian Journal of Civil Engineering., 22:714-722

5. Ji, C. Y., Chen, X., Cui, J., Yuan, Z. M. and Incecik, A., 2015. Experimental study of a new type of floating breakwater., Waterway, Port, Coastal, Ocean Eng., 105: 295-303

6. Lee, J. and Cho, W., 2003.Hydrodynamic analysis of wave interactions with a moored floating breakwater using the element-free Galerkin method, Canadian Journal of Civil Engineering., 30(4):720–33.

7. Loukogeorgaki, E. and Angelides, D., 2005.Performance of Moored Floating Breakwaters, International Journal Of Offshore and Polar Engineering., 15: 264–273

8. Loukogeorgaki, E. and Angelides, D., 2005.Stiffness of mooring lines and performance of floating breakwater in three dimensions, Applied Ocean Research., 27: 187–208.

9. Mani, J. S., 1991.Design of Y-frame floating breakwater. Waterway, Port, Coastal, Ocean Eng., 117(2):105–118.

10. Mays, T. W., Plaut, R. H. and Liapis, S., 1998.Three-dimensional analysis of submerged moored cylinders used as breakwaters, Waterway, Port, Coastal, Ocean Eng 1998., 26(12):1311-1333

11. McCartney, B. L., 1985.Floating breakwater design. Waterway, Port, Coastal, Ocean Eng., 111(2):304–318.

12. Ozeren, Y., Wren, D. G., Altinakar, M. and Work, P. A., 2011.Experimental Investigation of Cylindrical Floating Breakwater Performance with Various Mooring Configurations, Waterway, Port, Coastal, Ocean Eng., 137(6): 300–399.

13. Sannasiraj, S. A., Sundar, V., and Sundaravadivelu R., 1998. Mooring forces and motion responses of pontoon-type floating breakwaters, Waterway, Port, Coastal, Ocean Eng., 25(1): 27–48.

14. Sawaragi, T., 1995.Coastal Engineering Waves Beaches, Wave-Structure Interactions, Amsterdam: Elsevier

15. Shankar, S., 1998.Performance of twin-pontoon floating breakwaters, University of British Columbia

CONTACT WITH THE AUTHORS

Seyyed Mohammad Reza Tabatabaei
e-mail: tabatabai58@aut.ac.ir

Hamid Zeraatgar
e-mail: hamidz@aut.ac.ir

Amirkabir University of Technology
Tehran
Iran

MOST WIEDZY Downloaded from mostwiedzy.pl

POLISH MARITIME RESEARCH Special Issue 2018 S1 (97) 2018 Vol. 25; pp. 104-110
10.2478/pomr-2018-0030

INFLUENCE OF NATURAL CONDITIONS ON THE IMAGING OF THE BOTTOM OF THE GDAŃSK BAY BY MEANS OF THE SIDE SCAN SONAR

Dominika Witos-Okrasińska[1]
Grażyna Grelowska[1]
Eugeniusz Kozaczka[1,2]
[1] Gdańsk University of Technology, Poland
[2] Polish Naval Academy, Gdynia, Poland

ABSTRACT

The interest in underwater resources is the reason for the development of modern hydroacoustic systems, including side sonars, which find numerous applications such as: research of seabed morphology and sediment characteristics, preparation of sea sediment maps, and even in special cases of biocenoses such as sea grass meadows, detection of specific targets at the bottom such as shipwrecks, mines, identification of suitable sites for maritime infrastructure. Such applications require precise information about the position of the objects to be observed. Errors affecting the depiction of the bottom using hydroacoustic systems can be divided into errors associated with improper operation of measuring and support devices, systematic errors and random errors. Systematic errors result from the changing conditions prevailing in the analyzed environment affecting the measurement system. The errors affecting the correct operation of hydroacoustic systems can include: changing angle of inclination of the beam caused by the vessel's movement on the wave or refraction connected to changes in the sound speed as the depth function.

Keywords: side scan sonar imaging, Gdańsk Bay seabed, refraction of sound ray in sea, influence of ship's movement on the wave on underwater imaging

INTRODUCTION

The basic task of hydroacoustic devices are used to observe the underwater environment [1, 2, 8, 9, 14, 15]. Their basic task is to search, locate and identify objects at the bottom of the sea or in water space. In active systems, the information carrier is an acoustic wave, which is sent towards the bottom, after encountering an obstacle, which may be an object, or the seabed returns to the device as an echo signal. Knowledge of the sound speed propagation of in a water and the measurement of the time from the moment of sending the probe pulse to the moment of receiving the echo impulse makes it possible to determine the depth.

The Baltic Sea is characterized by variable hydrological conditions during the year affecting hydroacoustic conditions of the basin [3, 6, 7, 10, 12, 13, 19]. Surface water sound speed ranges from 1420 to 1490 m / s during the year. (Fig.1) presents the sound speed distribution for selected months of 2009 for the Gdańsk Deep region. Based on the measurement of salinity, temperature and depth using the Del-Grosso empirical formula [5], the sound speed distribution was determined. The largest differences are observed in the surface layer, because the sound speed is most dependent on the temperature of the water, which changes according to the seasons. Throughout the year, the minimum value of the sound speed occurs in the intermediate layer - an unusual feature of shallow water, then it grows towards the bottom, where it reaches the value of 1450-1460 m / s.

MOST WIEDZY Downloaded from mostwiedzy.pl

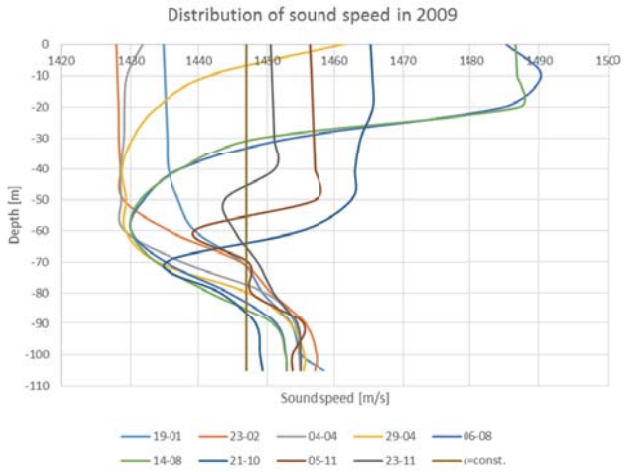

Fig. 1 Statistics of sound speed distribution at the Gdańsk Deep

Nowadays during underwater observation there is a tendency to use a wide beam in order to cover the largest possible bottom surface (multi-beam echo sounder, side scan sonar). Consequently, the beam, or its part, is directed to water at a high angle. Side scan sonars allows to obtain a high distinguishability of objects thanks to a suitably shaped beam, which is very narrow in the horizontal plane (from 0.5˚ to 2˚), and wide in the vertical plane (30˚ - 75˚) (Fig. 2).

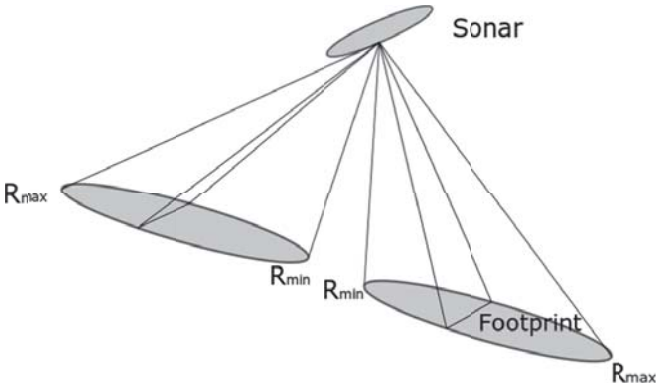

Fig. 2. Side scan sonar beams

The width of the beam depends, among others on the operating frequency of the device. It is connected with on the type of sonar, the resolution that increases with the depth is from about 1 cm to several centimeters (transverse resolution) and from several to several tens of centimeters (longitudinal resolution) [17]. Resolution is not the only parameter determining the accuracy and quality of the mapping. An important role is played by environmental factors such as the spatial distribution of temperature, salinity, water density, which determines the spatial distribution of the sound speed, and consequently the refraction of the acoustic beam. Also the course and speed, as well as the movement caused by the waving of the sea surface of the sonar antenna in relation to the bottom and antenna, distance from the bottom are the factors influencing the quality of sonar data.

The image in the side scan sonar is created by receiving successively sent impulses and connecting them together in the imaging device [16]. The short pulse length allows for high discrimination (Fig. 3). Thanks to combing the bottom with a narrow impulse, we obtain a high resolution. If in this case we applied a long pulse, we would not be able to distinguish objects on the bottom - only a strong reflection would be visible.

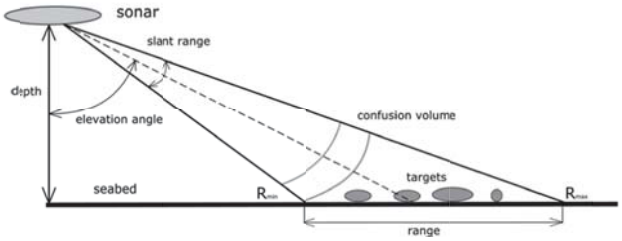

Fig. 3. Creation of seabed image by means of side scan sonar

The quality of the signal is influenced by the shape of the bottom surface and the type and coverage of the sediment. Gas bubbles contained in sediments and the presence of benthos, change the elastic properties of the bottom [18]. Soft acoustic floor - covered with silt disperses less energy, due to lower acoustic impedance. Hard bottom with high acoustic impedance disperses more backward energy. This affects the diversity of the acoustic image for different geological structures (Fig. 4). A brighter image means the occurrence of objects with good acoustic properties, e.g. rock or gravel.

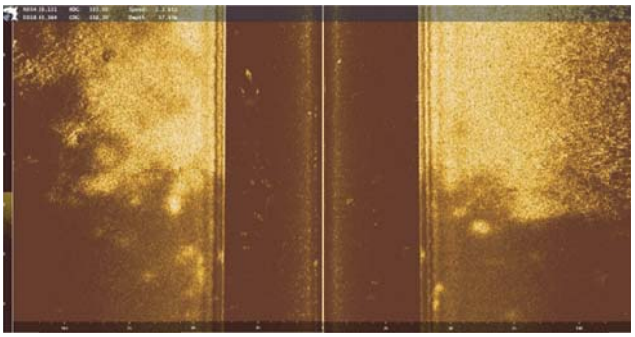

Fig. 4. Change of seabed kind in the vicinity of Hel Peninsula

REFRACTION OF SOUND BEAM IN REAL SEA CONDITION

Two factors influencing the obtained results will be considered in the article. The first is related to the non-uniform distribution of the sound speed as a function of depth, the second relates to the movements of the measuring ship on the undulated surface of the sea.

Changing the sound speed as a function of depth makes the phenomenon of refraction important in the case of devices using acoustic waves as an information carrier. Refraction affects the accuracy of determining the position of objects when the acoustic wave is radiated to the water at a certain

MOST WIEDZY Downloaded from mostwiedzy.pl

angle. Snell's laws [11] were used to determine the effect of refraction:

$$\frac{sin\theta_1}{c_1} = \frac{sin\theta_2}{c_2} = \frac{sin\theta_n}{c_n} = const. \quad (1)$$

where: c_1, c_2 are the values of sound speed in subsequent layers, θ_1 is the angle of incidence of the beam on the boundary of layers, and the angle θ_2 is the angle of refraction into the second layer, n is the number of layers. The water column has been divided into layers characterized by a different value of the sound speed, the number of layers depends on the sound speed distribution. Currently used computational equipment allows the division into any number of layers, which ensures high accuracy.

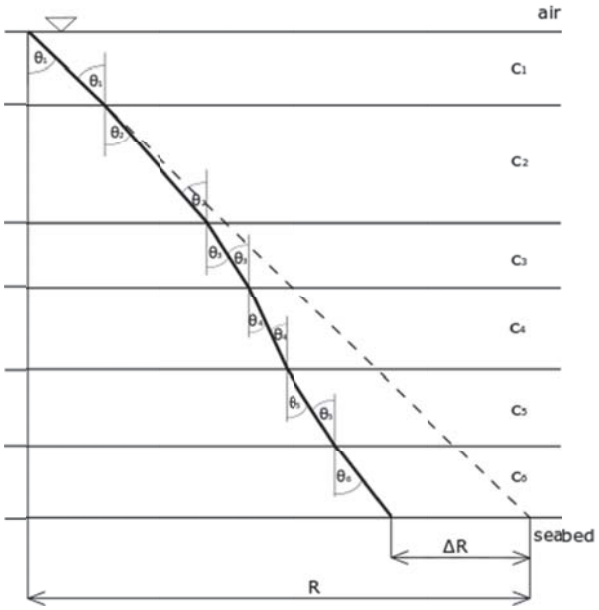

Fig. 5 Refraction of acoustic ray when crossing the boundary of layers with different sound speed

If c_1 is greater than c_2, the direction of the acoustic wave propagation is altered and the refraction angle will be smaller than the angle of incidence (negative refraction). In contrast, if c_1 is smaller than c_2, the direction of the acoustic wave propagation is changed and the angle of refraction will be greater than the angle of incident (positive refraction).

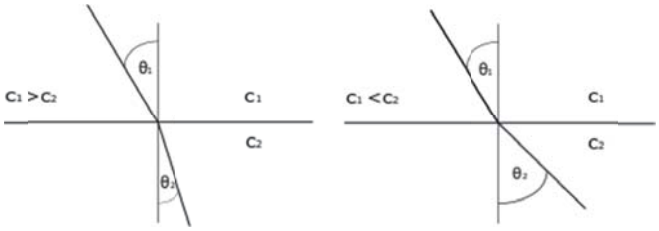

Fig. 6 Refraction principle

The most common assumption in hydroacoustic devices is the uniform distribution of the sound speed. The fact of changing the speed as a function of depth is not taken into account. The graph in (Fig. 7) shows the change in range for internal and external rays of side scan sonar caused by the phenomenon of refraction, assuming that the beam is directed at the angle of 52.5 degree.

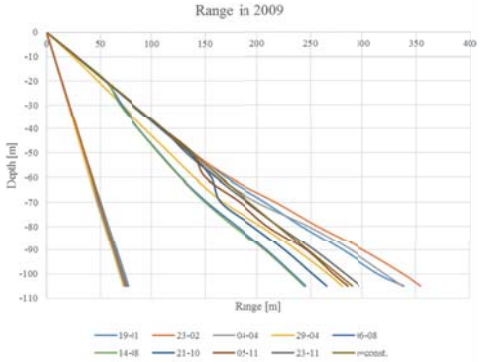

Fig. 7. Side scan sonar range for the speed distribution given at the Fig. 1 $(\alpha_{min} = 35°, \alpha_{max} = 70°)$

For the internal radius changes are small, at the bottom of more than 2 meters depending on the regardless of the season (Fig. 8).

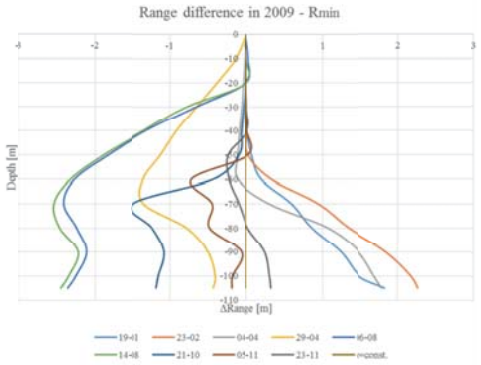

Fig. 8. Range difference for the inner radius of side scan sonar $(\alpha_{min} = 35°)$

We observe much greater range differences for the external radius (Fig. 9). The sonar range varies to over 100 meters in a year.

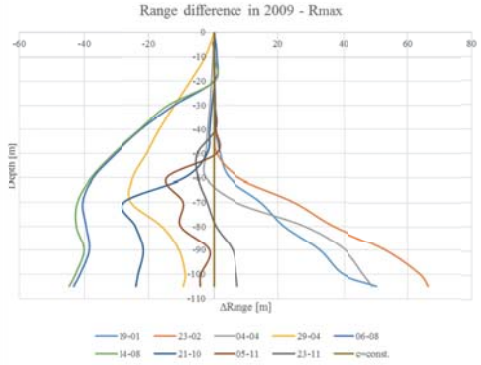

Fig. 9. Range difference for external radius of side scan sonar $(\alpha_{max} = 70°)$

MOST WIEDZY Downloaded from mostwiedzy.pl

A ship moving on a wavy sea has 6 degrees of freedom [4] - three related to a linear shift along the x, y, z axis and three related to the rotation around these axes (Fig. 10).

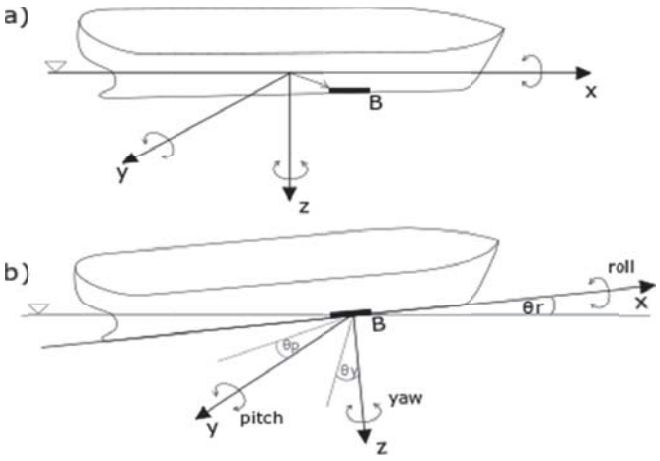

Fig. 10. Ship motions caused by sea surface waving

Movements of the measuring ship cause movement of the sonar transducer mounted to the hull. This affects the intensity and shape of the reflected signals. Transverse and longitudinal swaying of the ship's hull causes changes in the angle of incidence of the acoustic beam, and hence changes in the field of exposure to the seabed. The instantaneous position of the transducer is determined in accordance to the formula [18]:

$$B' = R_r^{-1} R_p^{-1} R_y^{-1} B \tag{2}$$

where: R_r - rotation matrix around the x axis (3); R_p - rotation matrix around the y axis (4); R_y - rotation matrix around the z axis (5), B - initial position of the transducer (Fig. 10).

$$R_r = \begin{vmatrix} 1 & 0 & 0 \\ 0 & cos\theta_r & sin\theta_r \\ 0 & -sin\theta_r & cos\theta_r \end{vmatrix} \tag{3}$$

$$R_p = \begin{vmatrix} cos\theta_p & 0 & -sin\theta_p \\ 0 & 1 & 0 \\ sin\theta_p & 0 & cos\theta_p \end{vmatrix} \tag{4}$$

$$R_y = \begin{vmatrix} cos\theta_y & sin\theta_y & 0 \\ -sin\theta_y & cos\theta_y & 0 \\ 0 & 0 & 1 \end{vmatrix} \tag{5}$$

The relationships described in the formulas (3), (4), (5) have been used to assess the change in radiation surface of the acoustic wave and the change in the range of hydroacoustic devices.

EFFECT OF REFRACTION

Effect of refraction is shown below basing on the results of investigation in June 2017. During the research, images of the bottom's fragments of Gdańsk Bay and information on the conditions of propagation of acoustic waves during measurements were obtained. The registration of bottom images was carried out in a continuous mode. Conditions for the propagation of the acoustic wave in June 2017 in the vicinity of the Hel Peninsula are presented in the (Fig. 11).

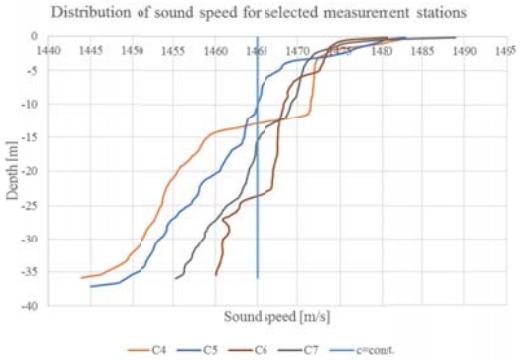

Fig. 11. Sound speed distribution at different statins in the Gdansk Bay in vicinity of the Hel Peninsula in June 2017

Fig. 12. Measuring stations on the Puck Bay

The sound speed at the surface layer varies from 1480 to almost 1490 m/s. For station C4 (Fig. 12), at a depth of about 12 meters, there is a thermocline characterized by a sharp drop in the water temperature by 4 degrees Celsius visible in the distribution of the sound speed. The sound speed at the bottom reaches the value from 1445 to 1460 m/s.

Anomalies in the distribution of the sound speed cause negative refraction. The curves in the (Fig.13) show the range of the side sonar beam under natural conditions and the one determined when assuming a constant sound speed.

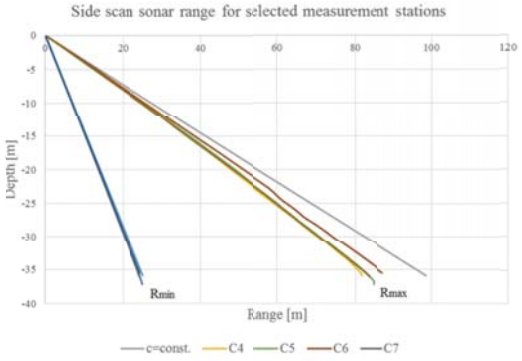

Fig. 13. Side scan sonar range for the speed distribution of given in the (Fig. 10)

MOST WIEDZY Downloaded from mostwiedzy.pl

The largest changes in range are observed at the bottom. The distance difference for the inner radius does not exceed 70 cm.

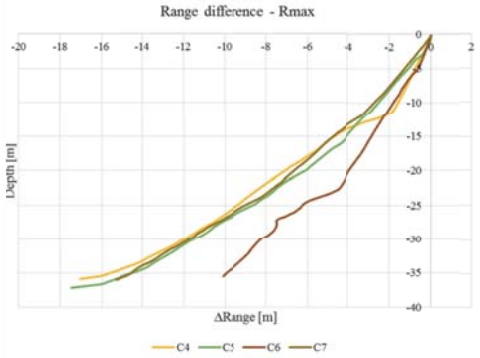

Fig. 14. Range difference for external radius of side scan sonar $(\alpha_{max} = 70°)$

The phenomenon of refraction, even at a small depth, significantly changes the range of the side scan sonar compared to the case where the distribution of sound velocity is homogeneous, but also for different distributions measured on the same day at points slightly distant from each other (Fig. 14). The measurement stations were located close to each other, but the difference in range reaches almost 18 meters compared to the case with uniform distribution, and about 8 meters for different measuring stations. Changing the range affects the footprint area.

Tab. 1. Footprint for measuring stations

	C4	C5	C6	C7
Footprint [m²]	187,46	194,69	206,06	193,47
Δ Footprint [m²]	52,59	45,36	33,99	46,59

Negative refraction caused a reduction of the footprint area by more than 52 m² in relation to the footprint at the assumed constant value of the sound speed (Tab.1).

INFLUENCE OF WAVING

The transverse and longitudinal swaying of a ship's hull and at the same a hydroacoustic transducer attached to it rigidly causes the change of the angle of incidence of the acoustic beam to the bottom and thus the change of the surface of the footprint.

Movements of the measuring ship change the surface of the footprint. Roll increases the beam area on one side of the transmitter, reducing it on the other side (Fig.15). As the roll angle increases, the footprint difference between the actual surface and the surface in the ideal center increases (Tab. 2).

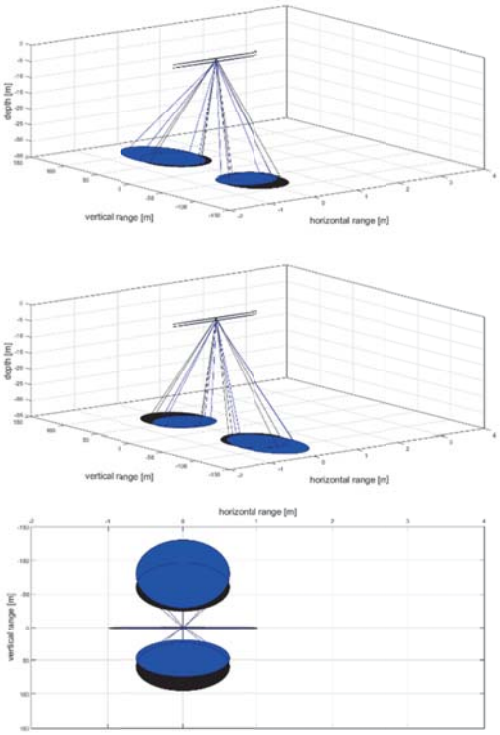

Fig. 15. Difference in footprint of the side scan sonar caused by roll $\theta_r = 5°, \theta_p = 0°$
a),b) roll to starboard, portboard; c) vertical projection
black figures – the ideal footprints; blue figures – instantaneous footprints

Tab.2. Footprint for different roll angles

Depth [m]		35
Footprint [m²]	θ=0°	137,53
	θ=2°	139,38
	θ=5°	149,80
	θ=10°	199,41

Depth [m]		35
Δ Footprint [m²]	θ=2°	1,85
	θ=5°	12,27
	θ=10°	61,88

Pitch does not change the surface of the footprint. Changing the angle of pitch causes the footprint to move along the axis associated with the movement of the measuring vessel (Fig. 16). The larger the pitch angle, the larger the displacement.

MOST WIEDZY Downloaded from mostwiedzy.pl

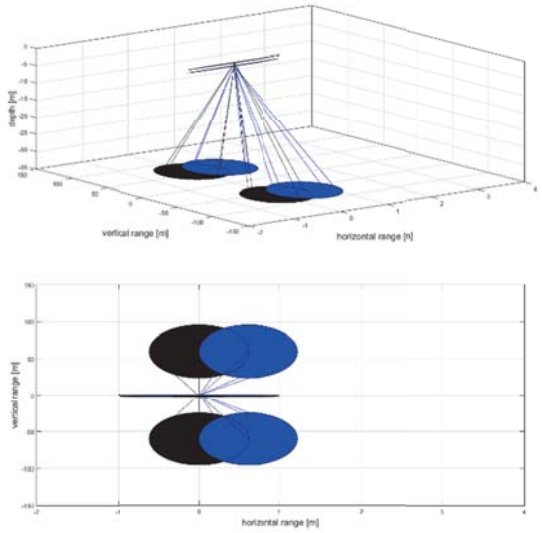

Fig. 16. Changes in the footprint of the side scan sonar caused by pitch $\theta_r = 0°, \theta_p = 1°$

In real conditions we are dealing simultaneously with roll and pitch, which in effect causes a change of area and shift of the footprint (Fig. 17).

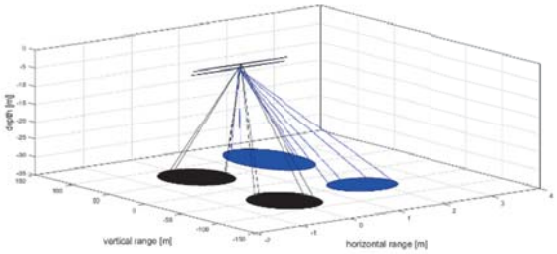

Fig. 17. Footprint of the side scan sonar $\theta_r = 5°, \theta_p = 3°$

The height of the wave also affects the size of the footprint. the higher the wave height, the larger the footprint changes.

When the ship is at the top of the wave, the footprint is the largest (the distance between the transducer and the bottom increases), if in the valley of the wave the footprint is the smallest (the depth is reduced by a value equal to the wavelength). (Tab. 3) presents examples of footprint changes for different roll angles, with a main depth of 35 meters for a wavelength of 1 m

Tab. 3 Footprint for different roll angles and heave

Depth [m]		35 $\lambda = 1\ m$
Footprint [m²]	θ=0°	129,77
	θ=2°	133,77
	θ=5°	141,37
	θ=10°	188,18

Depth [m]		35 $\lambda = 1\ m$
Δ Footprint [m²]	θ=0°	7,76
	θ=2°	5,61
	θ=5°	8,43
	θ=10°	11,23

The lateral inclinations of the measuring vessel cause erroneous assessment of the dimension of the object located on the seabed (Fig. 18).

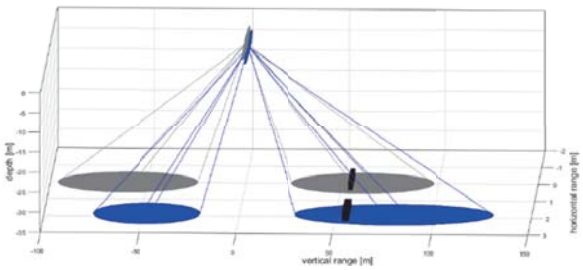

Fig. 18. Change the shape of the object

For example, there is a rectangular element with dimensions of 2m x 0.5m x 2m on the bottom. When roll equal 5° to the right side, its horizontal dimension will be 62% larger – (Fig. 18).

(Fig. 19) and (Fig. 20) show the effect of movement of the ship on the wave on the depiction of the bottom of the Gulf of Gdansk. A small roll distorts sonar images (Fig. 18).

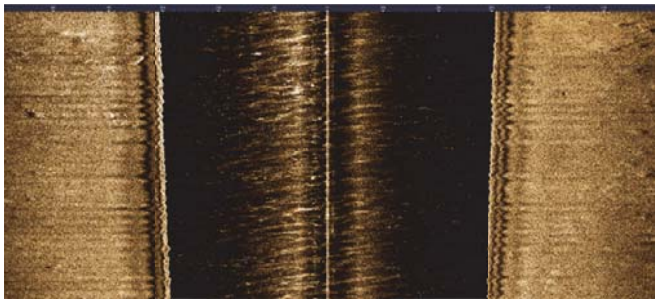

Fig. 19. Bottom image while rolling the ship

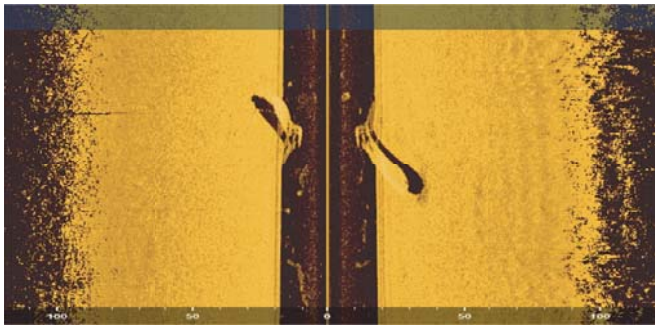

Fig. 20. Image of the bottom from the Puck Bay

MOST WIEDZY Downloaded from mostwiedzy.pl

CONCLUSIONS

Natural conditions have a large impact on underwater images obtained using hydroacoustic devices. The spatial distribution of the sound speed field in the Baltic Sea is a consequence of seasonal changes in hydrological conditions into the basin. The water temperature is the factor having the greatest impact on changes in the sound speed. The non-uniform and changing in the annual cycle the distribution of the sound speed causes the refraction of the acoustic beam, which affects the accuracy of the imaging with the use of hydroacoustic devices. The waving is the second factor that influences underwater data imaging. It is a difficult issue, because the specificity of the ship's motion, and hence the measuring device, is not exactly known. It changes the range of the device and the way of displaying objects. The use of a motion sensor improves the situation to some extent. The presented results of our investigation in the Gdansk Bay show how natural conditions influence the range and the area of observation even at small depth of water.

BIBLIOGRAPHY

1. Belderson R.B., Kenyon N.H., Stride A.H., Stubbs A.R.: Sonographs of the Sea Floor a Picture Atlas. Elsevier, Amsterdam, London, New York, 1972
2. Blondel P.: The Handbook of Side-scan Sonar. Springer Verlag, 2009
3. Dolecki A., Grelowska G., Oceanographic database – a component of naval operations oceanographic support, Polish Journal of Environmental Studies, Vol. 19, 4A, 9-14, 2010
4. Dudziak J., Teoria okrętu, Wydaw. Morskie, Gdańsk, 1988
5. Fofonoff N.P. and Millard Jr. R.C., Algorithms for computation of fundamental properties of seawater (1983), UNESCO technical papers in marine science. No. 44, Division of Marine Sciences. UNESCO, Place de Fontenoy, 75700 Paris
6. Grelowska G., Study of seasonal acoustic properties of sea water in selected waters of the southern Baltic, Polish Maritime Research, V. 23, 1, 25-30, 2016
7. Grelowska G., Kozaczka E., The study of acoustic climate of the Southern Baltic, Proc. Mtgs. Acoust. 28, 005001, 2016; doi: 10.1121/2.0000342
8. Grelowska G., Kozaczka E., Underwater acoustic imaging of the sea, Archives of Acoustics, Vol. 39, 4, 439-452, 2014
9. Grelowska G., Kozaczka E., Kozaczka S., Szymczak W., Gdansk Bay seabed sounding and classification of its results, Polish Maritime Research No 3 (79) Vol 20, s. 45-50, 2013
10. Grelowska G., Witos D., Acoustic climate of the Gulf of Gdansk in years 2000-2010, Hydroacoustics vol. 19, 129-138, 2016
11. Jenkins F.A., White H.E., Fundamental of Optics. McGraw-Hill Book Company, 1957
12. Jones E.J.W., Marine Geophysics. Wiley, 1999
13. Kozaczka E., Grelowska G., Szymczak W., Kozaczka S., The examination of the upper layer of the seabed by means of the acoustic methods, Acta Physica Polonica A, Vol. 119, 6A, 1091-1094, 2011
14. Kozaczka E., Grelowska G., Kozaczka S., Images of the seabed of the Gulf of Gdansk obtain by means of the parametric sonar, Acta Physica Polonica A, Vol. 118, No 1, 91-94, 2010
15. Kozaczka E., Grelowska G., Kozaczka S., Szymczak W., Detection of objects buried in the sea bottom with the use of parametric echosounder, Archives on Acoustics, 38, 1, 99-104, 2013.
16. Lurton X., An Introduction to Underwater Acoustics - Principles and Applications, 2nd Edition, Spinger Verlag, Berlin, 2003
17. Savini A.: Side-Scan Sonar as a Tool for Seafloor Imagery: Examples from the Mediterranean Continental Margin, Sonar Systems, InTech, Available from: http://www.intechopen.com/books/sonar-systems/side scan-sonar-as-a-tool-for-seafloor-imageryexamples-from-the-mediterranean-continental-margin, 2011
18. Tęgowski J., Akustyczna klasyfikacja osadów dennych, Rozprawy i Monografie, 19/2006, PAN Instytut Oceanologii, Sopot 2006
19. The BACC Author Team, Second assessment of climate change for the Baltic Sea basin, Springer, 2015

CONTACT WITH THE AUTHORS

Dominika Witos-Okrasińska
e-mail: dominika.witos@pg.gda.pl

Gdańsk University of Technology
11/12 Narutowicza St.
80 - 233 Gdańsk
Poland

MOST WIEDZY Downloaded from mostwiedzy.pl

POLISH MARITIME RESEARCH Special Issue 2018 S1 (97) 2018 Vol. 25; pp. 111-118
10.2478/pomr-2018-0031

THE IMAGING OF GDANSK BAY SEABED BY USING SIDE SONAR

Grażyna Grelowska[1]
Eugeniusz Kozaczka[1,2]
Dominika Witos-Okrasińska[1]
Wojciech Szymczak[2]
[1] Gdańsk University of Technology, Poland
[2] Polish Naval Academy, Gdynia, Poland

ABSTRACT

This paper is mainly aimed at presentation of an impact of environmental conditions on imaging accuracy by using hydro-acoustic systems in waters of a high non-uniformity of spatial distribution of hydrological parameters. Impact of refraction on erroneous estimation of range, in case of wave radiation into water under a large angle, like in side sonars or multi-beam echo-sounders, is especially important. In this paper seasonal changes in sound speed and its impact on acoustic beam refraction is discussed. And, examples which illustrate errors in determination of side sonar range occurred during last investigations carried out in Gdansk Bay waters are presented.

Keywords:

MOST WIEDZY Downloaded from mostwiedzy.pl

INTRODUCTION

Side sonar is a device which makes imaging a relatively large area of seabed with high resolution, possible. A solution proposed by Prof. H. Edgerton[1] in 1960 to be used in side sonar has served initially to search for submarines and other objects on seabed. Further investigations led to development of this technology into direction of sea geophysics and geology [2,3,4,5]. Contemporary hydro-acoustic systems including also side sonars are implemented in systems for seabed exploration and find many other applications such as e.g.:

– investigations on seabed morphology and sediment characteristics (e.g. occurrence of reliefs, depressions, sediment structures etc)[6,7,8],
– working out maps of distributions of seabed sediments and – in special cases – even bio-ceonosis, e.g. sea grass meadows [9],
– detection of special targets on seabed such as ship wrecks, mines, drown objects[10],
– identification of suitable locations for offshore infrastructures (drilling platforms, pipelines, cables etc)[11],
–seabed monitoring for environment management purposes.

In view of frequencies of acoustic waves radiated to water, sonars are divided into two kinds: of low-frequency (up to 100 kHz) and high-frequency (over 100 kHz up to 1 MHz)[12]. Imaging accuracy increases along with frequency increasing. Observation range of sonars depends on their frequency and for high-frequency sonars it amounts to about 100 m in view

of damping rise proportionally to the square of frequency. At larger depth of water area an often used solution is to tow an immersed sonar behind a floating unit that makes it possible to achieve a distance required between sonar's antenna and seabed.

Side sonar's resolution may be understood in two ways:
- as system's resolution defined by a form of acoustic beam and pulse length [3], or
- as image resolution defined by number of pixels.

The system's resolution depends on spatial distribution of acoustic power which decides on dimensions of the so called footprint. Transverse resolution and range resolution of sonar was described by Jones[3]. It may be meant as a resolution across-track footprint and resolution along-track footprint[5]. The system's resolution depends on a form and kind of transmitting converter. The transverse resolution is also affected by motion speed of sonar's converter in relation to seabed. Horizontal beam breadth amounts to less than 1° for 1 000 kHz frequency and about 1-2 ° for frequencies ranging from 100 to 200 kHz. Vertical beam breadth – for different types of side sonars – ranges from 30 to 75°. Therefore, depending on a type of sonar, the resolution growing with water depth, is equal to about 1 cm (in case of transverse one) up to a few cm (of range one).

The resolution is not the only parameter which decides on accuracy and quality of mapping. Environmental factors such as spatial distributions of water temperature, salinity and density which decide on spatial distribution of sound speed and consequently on acoustic beam refraction, play here an important role. Also course and speed of sonar's antenna relative to seabed, antenna's heel, distance over the bottom and operation range settings are the elements on which quality of sonar's data depends. The factors may significantly influence the mapping.

Considerations presented in this paper deal with an impact of environmental conditions, especially sound speed distribution on mapping accuracy of underwater images, which is exemplified by results of measurements conducted in the area of Gdansk Deeps.

CHANGES IN HYDROLOGICAL CONDITIONS OF GDANSK BAY

The Baltic Sea is characteristic of yearly changeable hydrological conditions which influence hydro-acoustic conditions of the water area [13,14,15,16,17]. A characteristic feature of Baltic Sea waters is their stratification. Three water layers: upper layer, deep layer and intermediate layer are distinguished – Fig. 1. In vertical distribution of salinity the intermediate layer – halocline is characteristic of a sudden change in salinity and occurs, depending on a Baltic Sea region, beginning from the depth of 40 up to 60 m or 60 up to 80 m. In vertical distribution of seasonal temperature a water layer characteristic of a sudden change in temperature – thermo-cline appears in spring and summer months. Surface waters are of a low salinity and their temperature depends on a season of the year. Also a strong influence of wind (the so called wind mixing) on changes in distribution of hydrological parameters is observed. Deep waters have much greater salinity and small temperature variation, and, in contrast to typical shallow seas, in the Baltic Sea deep water temperature increases towards bottom. This results from the fact that irregular episodes of the pouring-in of salt water from the North Sea affect water temperature and salinity of that part of the Baltic Sea.

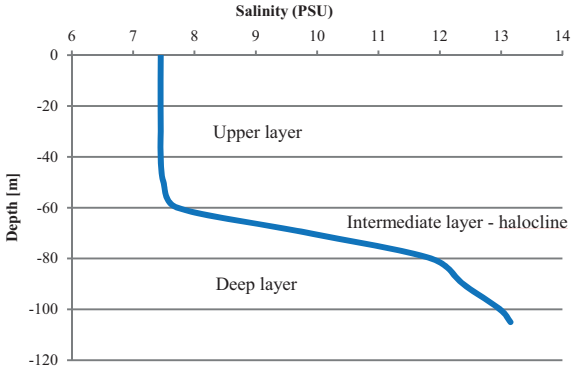

Fig. 1. Stratification of Baltic Sea water

Characteristic features of South Baltic Sea's waters are illustrated in Fig. 2 and 3. They present average values of temperature and salinity in particular month of the year, based on the data collected in the years 2000-2010 for the Gdansk Deep region.

The largest temperature changes are observed in the upper layer – Fig. 2. It is associated with heat exchange through water-atmosphere boundary. The highest temperature is reached in summer months (August, September), the lowest – in winter months (February, March).

In hydrological conditions typical for the South Baltic Sea sound speed changes are most affected by temperature changes. The highest value of sound speed is reached close to water surface in summer month. A characteristic feature of Baltic Sea water is that minimum value of sound speed occurs in the intermediate layer, then it increases towards seabed. The distribution is analogous to that of temperature. As a matter of fact in the Baltic Sea no seasonal changes in salinity are observed. Its lowest value is reached in the upper layer, the highest – in the deep layer. Vertical distribution of salinity in the Baltic Sea changes along with growing distance from Danish Straits. The greater the distance the smaller the salinity. Changes observed in distributions of instantaneous hydrologic and hydro-acoustic parameters result from local phenomena such as vortices, wind mixing, water inflow from big rivers or upwelling*.

* Lifting deep cold water onto surface.

MOST WIEDZY Downloaded from mostwiedzy.pl

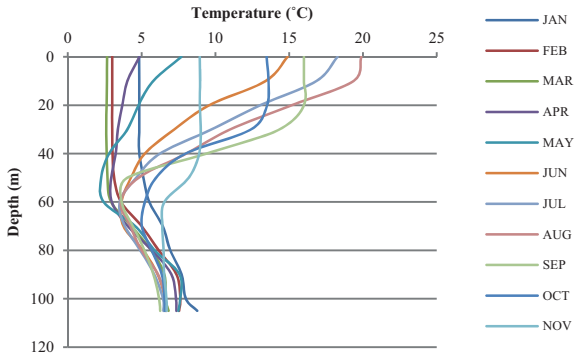

Fig. 2. Vertical distribution of temperature

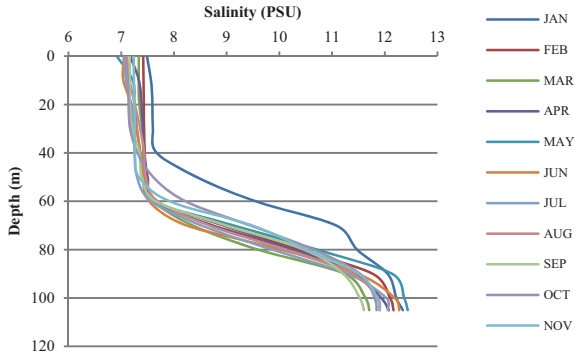

Fig. 3. Vertical distribution of salinity

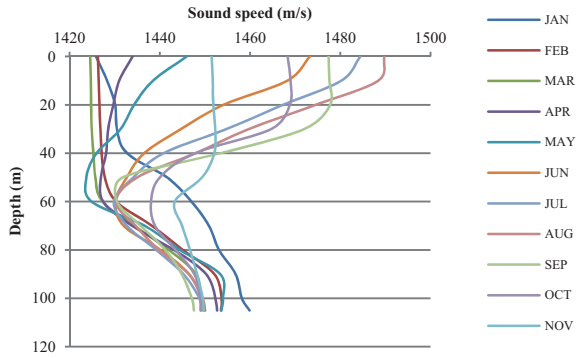

Fig. 4. Vertical distribution of sound speed

The change of sound speed in function of depth results in that refraction phenomenon is of a great importance in case of devices which use acoustic waves for information transmitting. Refraction affects accuracy in location of objects when acoustic wave is radiated into water under an angle. In hydro-acoustic devices sound speed value is most often assumed constant in function of depth. The fact of changeable sound speed in function of depth is not taken at all into account. In subsequent diagrams a difference in path of acoustic wave beam radiated into water under 60° angle in different seasons of the year, is presented. For the calculations the real instantaneous distributions recorded in February, August and November were selected (Fig. 5). The results were then compared with the range determined under the condition of no vertical sound speed gradient: dc/dh=0.

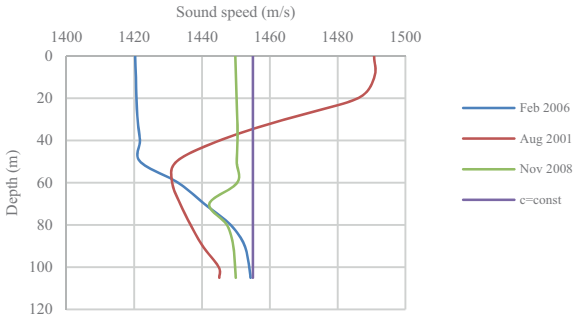

Fig. 5. Example sound speed distributions recorded in Gdansk Deep region in February, August and November and the constant distribution assumed for calculations.

Use was made of a refraction theory adapted from optics, i.e. change in wave propagation during passing into a medium of another sound speed. Water column was divided into horizontal layers to each of them constant sound speed values were assigned. In accordance with Snell law[18] wave diffraction on the boundary of layers with different sound speeds is described by the following relation:

$$\frac{sin\beta_1}{c_1} = \frac{sin\beta_2}{c_2} = const.$$

where: c_1, c_2 – stand for sound speed in subsequent layers, β_1 – beam angle of incidence on the boundary of layers, and β_2 – beam angle of penetration into second layer. The same procedure is used for boundaries of all layers in water column (Fig. 6).

In carrying out the calculations, information about vertical sound speed distribution achieved from a given measurement point is used. In propagating the wave directed under an angle the point of passing the beam through the boundary of subsequent layers is shifted in horizontal plane against the point in which the measurement has been made. As results from the calculations, differences in ranges are not greater than 20 m. In the present stage of this reserch it was assumed that the values of vertical sound speed distribution measured in the point represent spatial sound speed distribution in water column of such radius. A detail assessment of refraction influence on error in estimation of hydro-acoustic device range would require an information about spatial distribution of sound speed. However, to execute such tests in sea conditions is a very difficult task.

MOST WIEDZY Downloaded from mostwiedzy.pl

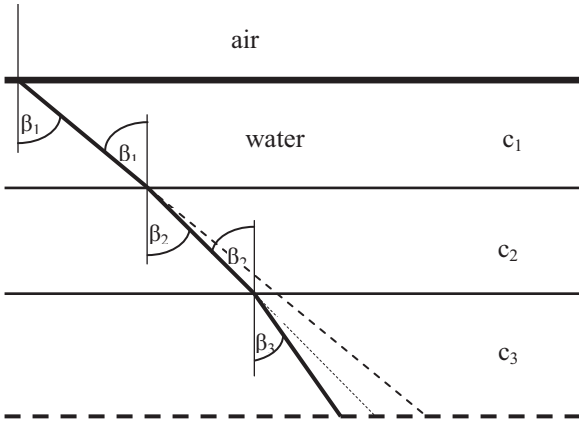

Fig. 6. Odd refraction of acoustic beam during its passing through boundary of layers of different sound speed: $c_1>c_2>c_3$, $\beta_3<\beta_2<\beta_1$

Acoustic wave which propagates into a medium with the sound speed c_1 falls onto boundary of media under the angle β_1 counted against normal to the boundary. After passing into a medium of another sound speed the beam penetration angle changes to β_2. This causes beam deflection and non-linear trajectory forming, that consequently results in an error in determination of position of objects detected by hydro-location devices.

Subsequent diagrams show range differences determined for the sound speed distributions given in Fig. 5 under assumption that acoustic beam is directed to water under 60° angle.

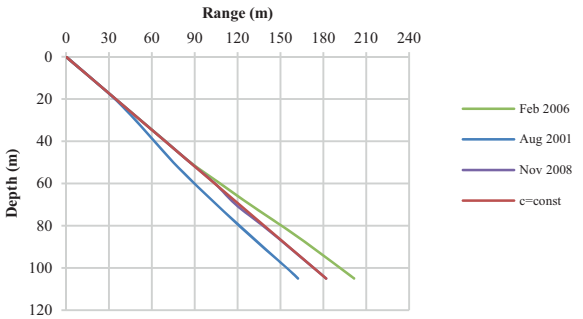

Fig. 7. Trajectory of acoustic beam directed to water given for different months under assumption that sound speed distribution is uniform.

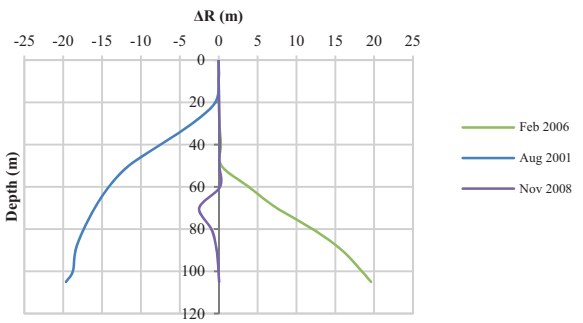

Fig. 8. Error in range determination for the sound speed distributions given in Fig. 5

Depending on a sound speed distribution, differences between real range and its value in a homogenous medium are achieved. If a distribution is close to linear the differences are rather small. It may be illustrated by the distribution taken in November 2008. In this case the range coincides practically with that calculated for homogenous medium. Comparing the errors in range determination conducted in summer and winter months one can observe that the difference between the points of reaching the bottom in the depth of abt. 100 m by acoustic beam comes even to 40 m, Fig. 8.

MEASURING SYSTEM

The measuring system was installed on s/y Freija, a 12 m research boat, Fig. 9. The boat is equipped a.o. with a module of Simrad Structure Scan side sonar cooperating with Simarad NSS9-evo2 plotter – a sending-receiving module. The system, apart from recording sonar images, makes automation of measurements along given cross-sections possible for its operator by using an autopilot integrated with the system. The positioning of research boat on navigation charts is ensured by 12-channel GPS receiver equipped with Garmin GPS 17x location sensor – this way the system's accuracy is ensured to be 3 m. Safety of conducting the investigations is provided by gaining information from AIS system and radar. The side sonar converter was fastened on boat's bottom by means of a special holder. Place of installation of the converter was selected at 3,5 m distance from the stern in order to eliminate influence of disturbances generated by screw propeller and aerated water flowing around the keel. Additionally, the selected place is characteristic of small rolling and pitching motions, otherwise it could affect quality of obtained acoustic images. The maximum range of the system reaches 183 m, maximum sounding depth – 92 m. Acoustic wave radiation frequency is equal to 455 kHz.

Fig. 9. The research boat – s/y Freija

The measurements were performed in Gdansk Bay region in August and September 2016 and June 2017. During recording

MOST WIEDZY Downloaded from mostwiedzy.pl

seabed images the boat was moving with 2 knot speed. Several series of measurements were made in different points and different depths. The recording is carried out continuously and the data are imaged live on the sounder plotter (Fig. 10) installed inside the boat. The data are additionally recorded on an external storage medium.

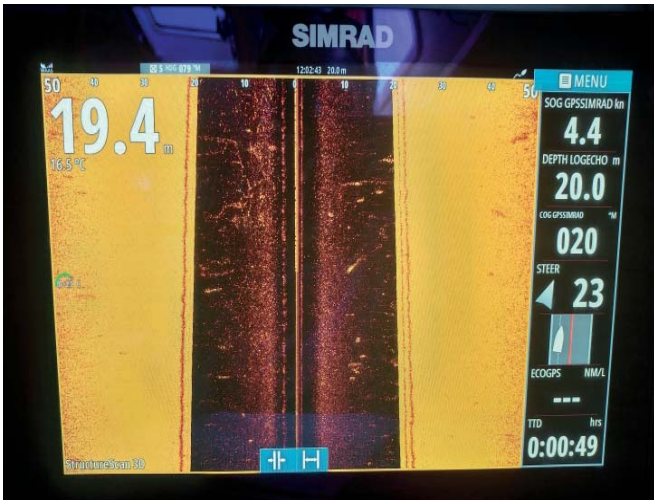

Fig. 10. Plotter

Sound speed measurements were conducted by means of a CastAway CTD compact sounder which allows for fast measuring sound speed. Both the side sonar and CTD sounder are integrated with the GPS receiver, that facilitates to make catalogues of gained profiles by assigning them automatically to particular fragments of an investigated water area.

In comparison with the commonly used measuring modules, transmission of the data recorded in internal memory of the device is possible through an internal Bluetooth module (Fig. 11), i.e. without necessity of connecting any external cables. The sounder allows to take profiles in the depth up to 100 m. Based on the water depth measurements, sound speed value is determined with the use of Chen-Millero empirical formula[19]. The established measuring accuracy is as follows: for salinity – 0,01 PSU, for depth – 0,01 m, for temperature – 0,05 °C, for sampling frequency – 5 Hz.

The device is fitted with a 6-core conductometric sensor connected to a fast-reacting thermistor whose response amounts to less than 200 ms, that allows to reach a high measuring accuracy at high resolution. The sounder is lowered onto seabed due to its own weight; its resolution varies within the range from 0,15 to 0,53 m, depending on lowering speed.

Fig. 11. Sonic sounder for measuring sound speed

RESULTS OF THE MEASUREMENTS

During the performed investigations, images of fragments of Gdansk Bay seabed were achieved together with information on conditions of acoustic wave propagation prevailing in the time of the tests. Recording the images was carried out continuously. Points where sound speed was measured are shown on the chart (Fig. 12).

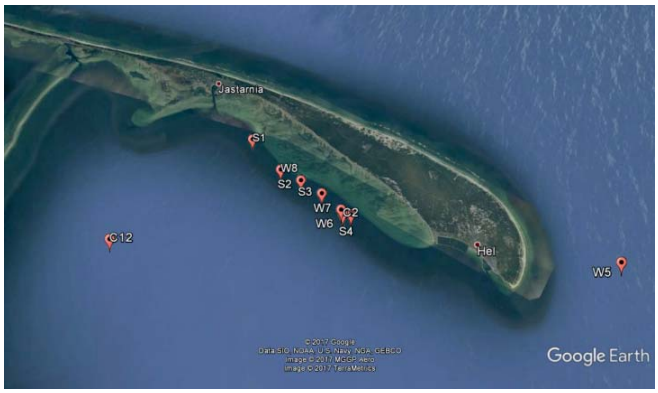

Fig. 12. The chart with marked points where sound speed was measured

Fig. 13 presents a fragment of a signal recorded by the side sonar. 1400 samples per each boat's side were recorded in each sounding operation irrespective of a selected observation range. For instance at the selected range of 80 m the sampling interval is equivalent to the distance of about 5.7×10^{-2} m.

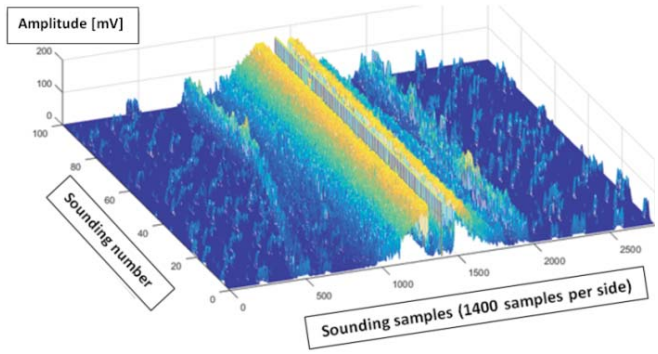

Fig. 13. A signal recorded by side sonar

The signal is transformed into the form of images visible on the plotter. Fig.14 shows the seabed image recorded close to the point W7 in September 2016.

MOST WIEDZY Downloaded from mostwiedzy.pl

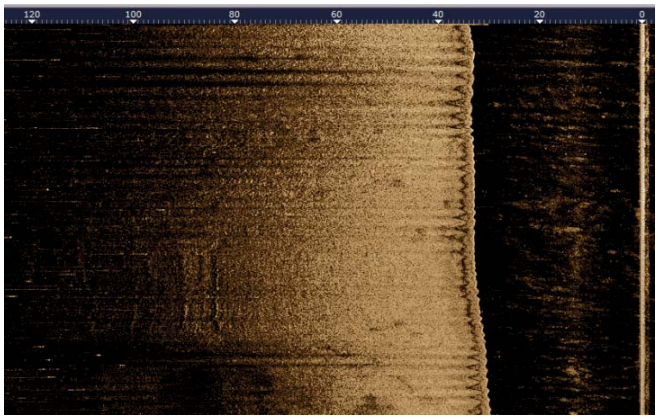

Fig. 14. Seabed image recorded close to the point W7

The wave propagation conditions in September in the investigated region are described by the acoustic wave speed distributions shown in Fig. 15.

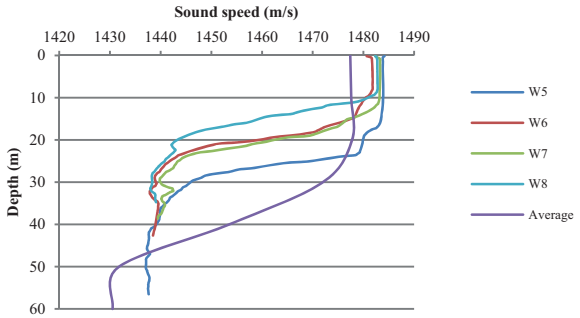

Fig. 15. Vertical sound speed distributions taken in the selected stations in September 2016.

Comparing these distributions with the curve which illustrates a distribution typical for September, determined on the basis of results from the years 2000-2010, it is possible to observe higher sound speed values in the upper layer and a more sudden drop of the speed at the relatively small depth of 23,59 m. It results from occurrence of a higher temperature (17,5°C) in the subsurface stirred-water layer of about 23 m in thickness (Fig. 16). Under the warm water layer a cold water mass was present. In the depth of 30 m the water had temperature of 7,21°C whereas such temperature was usually observed about 15 m deeper. The sharply marked thermocline resulted in a sudden change in sound speed.

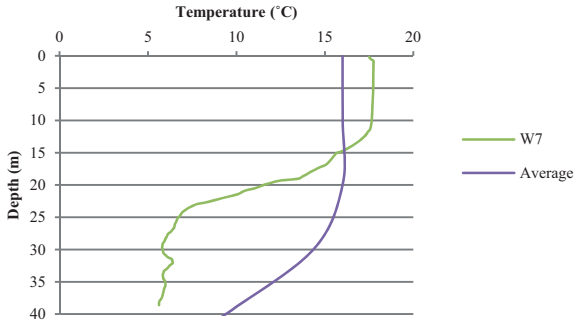

Fig. 16. Water temperature changes in the station W5 in September 2016 and averaged respective data form the years 2000-2010

This anomaly in temperature distribution caused a significant odd refraction. The curves in Fig. 17 show an area covered by side sonar beam in natural conditions compared with the area determined under assumption that sound speed is distributed uniformly within the whole water column. At 38 m depth the beam refraction causes that points on the echo-sounder screen are depicted in the distance of over 100 m from the boat's path whereas they are really located in the distance only a little greater than 80 m.

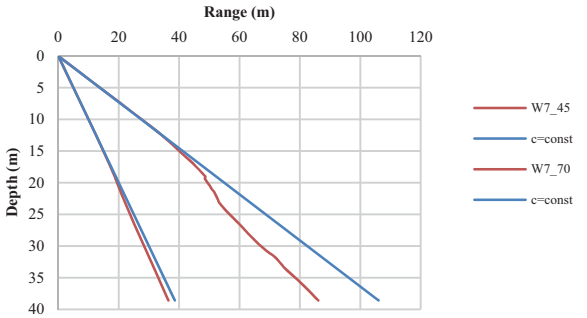

Fig. 17. Side sonar theoretical range versus real one in the station W7

The next figure presents an error in range determination resulting from refraction. At the bottom it amounted to 2,14 m for side sonar internal beam and 19,92 m for its external beam.

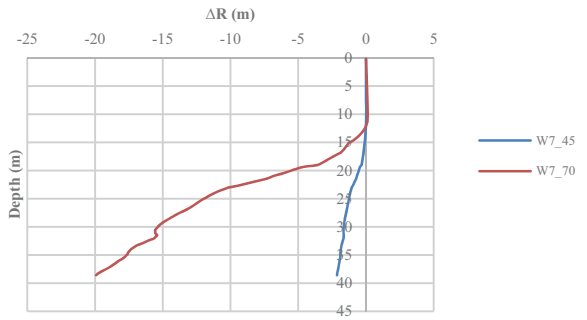

Fig. 18. Range determination error in the station W7 for the acoustic beams directed under the angles of 45° and 70°

Seabed investigations are often aimed at searching objects lying on seabed. Fig. 19 shows the wreck of the ship „Delfin" drown in the middle of Puck Bay (Point C12).

Fig. 19. The wreck of the ship „Delfin" – the image from the point C12

MOST WIEDZY Downloaded from mostwiedzy.pl

Fig. 20 shows the sound speed distribution taken in the point C12 in June 2017.

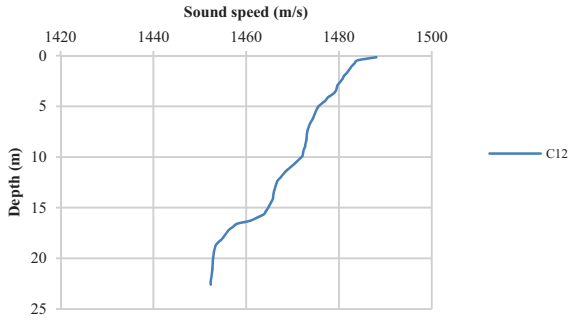

Fig. 20. The sound speed distribution taken in the point C12 in June 2017

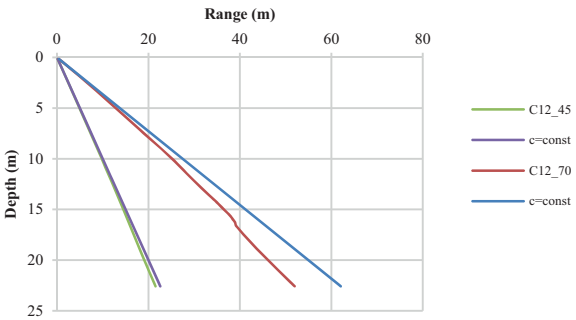

Fig. 21. Side sonar theoretical range versus real one in the station C12

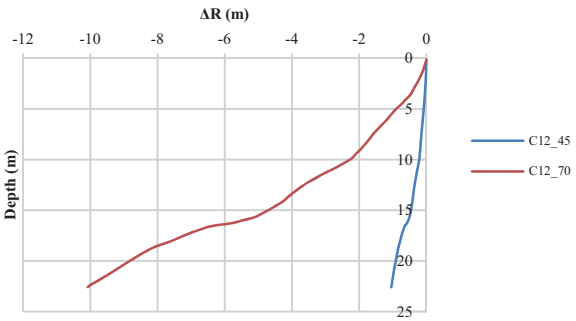

Fig. 22. Range determination error in the station C12 for the acoustic beams directed under the angles of 45° and 70°

Also in this case the odd refraction causes error in range determination in conditions of large beam penetration angles.

SUMMARY

Environmental conditions in shallow sea, especially changeable seasonal temperature distribution which directly affects spatial distribution of sound speed field, are of a great importance for accuracy in seabed imaging by means of side sonar. Based on the research results presented in this paper it can be stated that error in estimating range of sound wave beam penetrating under a large angle is significant even in case of a not very large depth.

For instance, for external acoustic beam of the sonar used in the presented measurements, penetrating water under 70° angle – the error in the tests carried out on the station C12 of 21 m depth in June 2017 amounted to 10 m, and on the station W7 of 38 m depth in September 2016 – 20 m. The GPS system used for the research boat positioning determined its position with the error of 3 m.

Range estimation errors or imaging accuracy in testing with the use of hydro-acoustic devices depend on many instrumental and environmental factors or those associated with ship motion. The presented results indicate that errors associated with refraction should be taken into account during interpretation of test results.

ACKNOWLEDGEMENTS

This research project has been partially financed by the Ministry of Science and Higher Education in the frames of funds intended for statutory activity of Gdansk University of Technology and Polish Naval Academy.

BIBLIOGRAPHY

1. J. P. Fish, H. A. Carr: Sound underwater images-A guide to the generation and interpretation of side scan sonar data. Orleans, MA: Lower Cape Publishing, 1990

2. R.B. Belderson, N.H. Kenyon, A.H. Stride, A.R. Stubbs: Sonographs of the Sea Floor a Picture Atlas. Elsevier, Amsterdam, London, New York, 1972

3. E.J.W. Jones: Marine Geophysics. Wiley, 1999

4. J. Tęgowski: Acoustic classification of sediments (in Polish), Rozprawy i Monografie, 19/2006, PAN Instytut Oceanologii, Sopot, 2006

5. P. Blondel: The Handbook of Side-scan Sonar. Springer Verlag, 2009

6. E. Kozaczka, G. Grelowska, W. Szymczak, S. Kozaczka: The examination of the upper layer of the seabed by means of the acoustic methods, Acta Physica Polonica A, Vol. 119, 6A,, 2011, pp.1091-1094

7. G. Grelowska, E. Kozaczka: Underwater acoustic imaging of the sea, Archives of Acoustics, Vol. 39, 4,, 2014, pp.439-452

8. E. Kozaczka, G. Grelowska, S. Kozaczka: Images of the seabed of the Gulf of Gdansk obtained by means of the parametric sonar, Acta Physica Polonica A, Vol. 118, No 1,, 2010, pp.91-94

9. G. Grelowska, E. Kozaczka, S. Kozaczka, W. Szymczak: Gdansk Bay seabed sounding and classification of its results, Polish Maritime Research No 3 (79) Vol 20,, 2013, pp. 45-50

MOST WIEDZY Downloaded from mostwiedzy.pl

10. E. Kozaczka, G. Grelowska, S. Kozaczka, W. Szymczak: Detection of objects buried in the sea bottom with the use of parametric echosounder, Archives on Acoustics, 38, 1,, 2013, pp. 99-104

11. P. Dymarski, E. Ciba, T. Marcinkowski: Effective method for determining environmental loads on supporting structures for offshore wind turbines. Polish Maritime Research 1(89) Vol. 23, 2016, pp. 52-60

12. A. Savini: Side-Scan Sonar as a Tool for Seafloor Imagery: Examples from the Mediterranean Continental Margin, Sonar Systems, InTech, Available from: http://www.intechopen.com/books/sonar-systems/side scan-sonar-as-a-tool-for-seafloor-imageryexamples-from-the-mediterranean-continental-margin, 2011

13. The BACC Author Team: Second assessment of climate change for the Baltic Sea basin, Springer, 2015

14. G. Grelowska, D. Witos: Acoustic climate of the Gulf of Gdansk in years 2000-2010, Hydroacoustics vol. 19, 2016, pp. 129-138

15. G. Grelowska: Study of seasonal acoustic properties of sea water in selected waters of the Southern Baltic, Polish Maritime Research, V. 23, 1, 2016, pp. 25-30

16. A. Dolecki, G. Grelowska: Oceanographic database – a component of naval operations oceanographic support, Polish Journal of Environmental Studies, Vol. 19, 4A,, 2010, pp. 9-14

17. G. Grelowska, E. Kozaczka: The study of acoustic climate of the Southern Baltic, Proc. Mtgs. Acoust. 28, 005001, 2016; doi: 10.1121/2.0000342

18. X. Lurton: An Introduction to Underwater Acoustics – Principles and Applications, 2nd Edition, Spinger Verlag, Berlin, 2003

19. N.P. Fofonoff and R.C. Millard Jr: Algorithms for computation of fundamental properties of seawater (1983), UNESCO technical papers in marine science. No. 44, Division of Marine Sciences. UNESCO, Place de Fontenoy, 75700 Paris

CONTACT WITH THE AUTHORS

Grażyna Grelowska

Eugeniusz Kozaczka

Dominika Witos-Okrasińska
e-mail: dominika.witos@pg.gda.pl

Gdańsk University of Technology
Faculty of Ocean Engineering and Ship Technology
11/12 Narutowicza St.
80 - 233 Gdańsk
Poland

Wojciech Szymczak
e-mail: w.szymczak@amw.gdynia.p

Polish Naval Academy
69 Śmidowicza St.
81-127 Gdynia
Poland

MOST WIEDZY Downloaded from mostwiedzy.pl

POLISH MARITIME RESEARCH Special Issue 2018 S1 (97) 2018 Vol. 25; pp. 119-123
10.2478/pomr-2018-0032

APPLICATION OF RAPID PROTOTYPING TECHNOLOGY IN THE MANUFACTURING OF TURBINE BLADE WITH SMALL DIAMETER HOLES

Mariusz Deja[1]
Michał Dobrzyński[1]
Paweł Flaszyński[2]
Jacek Haras[1]
Dawid Zieliński[2]
[1] Gdańsk University of Technology, Poland
[2] Institute of Fluid Flow Machinery, Polish Academy of Sciences, Poland

ABSTRACT

The article presents the possibilities++ of using Rapid Prototyping (RP) technology in the manufacturing of turbine blades with small diameter holes. The object under investigation was gas turbine blade with small diameter cooling holes and holes for generating longitudinal vortices. A turbine blade model was produced by means of Direct Metal Laser Sintering (DMLS) technology and subsequently validated in terms of detection and accuracy of the obtained holes. The application of the computer tomography and digital radiography technique resulted in obtaining a series of cross-sections of the turbine blade model with a series of holes. Particular attention was pointed out at the investigation of the locations of micro-holes with a diameter of 0.3 mm. It turned out that it was impossible to make such small holes by the RP method. In the following part the results of the study on the possibilities of making the micro-holes using electrical discharge method have been presented. In addition, proposition of further works such as the development of the considerations and issues discussed in this article, has been offered.

Keywords: turbine blade, small diameter holes, Rapid Prototyping/Rapid Manufacturing, Direct Metal Laser Sintering (DMLS) technology

MOST WIEDZY Downloaded from mostwiedzy.pl

INTRODUCTION

The Rapid Prototyping/Rapid Manufacturing technologies consisted of sets of methods and additive techniques making product manufacturing and prototyping possible, are ones of the most dynamically developing methods for parts forming and manufacturing. Unlike the conventional deductive machining methods, the rapid prototyping and manufacturing technologies allow to obtain an element on the basis of its spatial numerical model worked out by means of a CAD system. The conventional deductive machining technologies have limitations especially in the machining of higher-order surfaces and small-diameter holes, in particular of different angular positions.

Superimposing subsequent material layers on each other during rapid prototyping process result in reaching complete product whose shape and form follow its 3D geometry designed by a CAD system. One of the main merits of application of the Rapid Prototyping/Rapid Manufacturing methods is the forming of prototypes and physical models of products and their use in every stage of product developing process – beginning from concept up to repair. Such approach makes it possible not only to limit costs resulting from incorrectly manufactured product

series but also just in the first stage of product development, i.e. its design stage, to conduct crucial investigations and tests, that allows to elaborate an optimum designed product.

Application of additive techniques allows to produce a very broad spectrum of parts connected e.g. with overhaul or failure of devices installed on ships or offshore steel structures. An advantage of application of the technology is possibility of producing metal elements of complex forms at limited working space required for a device used in rapid prototyping. Devices used in rapid prototyping do not require any special instrumentation but is able to replace several machine tools used in deductive technologies. Rapid Prototyping/Rapid Manufacturing method is of special importance in manufacturing complex geometry products, especially those having higher-order surfaces characteristic a.o. for blades of high-pressure stages of gas turbines intended for ship propulsion or Tesla turbines [1,3,4,7]. Apart from the complex geometry they have holes and ducts for cooling medium flow, whose manufacturing with the use of deductive methods is often impossible.

There are today many methods for rapid prototyping and manufacturing.

The techniques vary both in respect of form and type of processed material, way of building physical model as well as source of energy generated for additive process [8,9]. One of the most dynamically developing additive methods is the direct metal powder laser sintering technology DMLS (Direct Metal Laser Sintering) which was patented by EOS (Electro Optical Systems), a German firm. The method consists in the local melting of material powder and next joining superimposed subsequent layers of material on each other into a uniform solid due to solidifying process. The main advantage of application of the method is the possible manufacturing of products and moulds of complex shapes which, due to their geometrical complexity, are difficult or impossible to be produced by means of traditional deductive or casting methods [2,12]. Another of them is EBM (Electron Beam Melting) method which resembles the DMLS process but, instead of laser sintering, electron beam is used in it for metal powder bonding. The EBM technology is utilized for manufacturing the industrial rotors of complex geometry and thin walls. [6]. The SLM technology (Selective Laser Melting) makes it possible to produce precise parts at maintaining uniform internal structure of material, its density and strength [10,11].

OBJECT AND METHODS OF INVESTIGATIONS

The object of investigations was a turbine blade model designed in Institute of Fluid Flow Machinery, Polish Academy of Sciences (IMP PAN), Gdańsk, which was then manufactured by Intelligent Technologies Unit (ZTI), the Institute of Fundamental Technical Problems, Polish Academy of Sciences (IPPT PAN), Warsaw. Blades of high pressure stages of gas turbines used in ship and aircraft drives as well as power systems operate in high temperature conditions. One of the essential structural elements of the this way loaded blades are properly designed holes ensuring cooling medium flow and effective blade material separation from hot gases. In grid of blades working medium flow is accelerated up to supersonic velocities that results in generating shock wave on blade suction side, whose interaction with boundary layer may initiate formation of separation zones and flow recirculation in boundary layer area. The interaction between shock wave and boundary layer in presence of cooling film and strong pressure gradients forces to search for flow control methods in order to improve flow system's life and rise its efficiency. Such target of investigations was formulated in IMP PAN where a design of gas turbine blade fitted with cooling holes and holes intended for generating longitudinal vortices, was prepared [1]. In view of geometrical complexity an attempt was made to manufacture the profile with cooling medium holes and ducts by applying the DMLS technique.

The turbine blade model was produced by means of DMLS technique with the use of EOS Maraging Steel MS1 in the form of powder, i.e. a hardenable martensitic tool steel of content complying with EU standard 1.2709 [13]. Production of the turbine blade model was executed by using EOSINT M280 machine for which the following process parameters were selected:

- thickness of single layer of laid material – 40 μm,
- total number of model material layers – 3834,
- type and power of used laser – a fibrous ytterbium laser of 400 W effective power,
- length of laser beam – 1060–1100 nm.

Additional tests were conducted to check if it is possible to made a series of micro-holes of 0.3 mm in diameter by using a material deductive method – spark drilling because it turned out that production of the designed holes by applying RP/RM technology was unsuccessful. To this end, a high-speed HGH EDM Drill 528 DZ spark drilling machine which ensures high manufacturing accuracy for small-diameter holes, was used. The drilling process was carried out with the following parameters:

- wire diameter – 0.3 mm,
- extreme electric current value – 5 A,
- condenser capacity (single pulse power) – 4 C,
- spark pause (pause between subsequent pulses) – 3 s.

Fig. 1 presents an image of the designed turbine blade model with indicated arrangement of holes being the object of the investigations in question. The analyzed geometry took into account holes of 3 mm, 2.5 mm, 2 mm, 1.35 mm, 1 mm in diameter and micro-holes of 0.3 mm in diameter. Worth paying attention to their different angular positions which resulted from constructional purposes, i.e. in order to take into account operational factors of turbine blades. The manufacturing of a series of micro-holes of 0.3 mm diameter was especially important for possible application of DMLS technology in the production field.

MOST WIEDZY Downloaded from mostwiedzy.pl

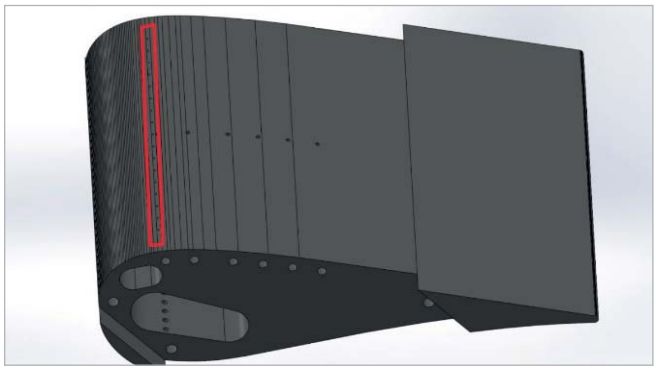

Fig. 1. 3D image of turbine blade

RESULTS OF INVESTIGATIONS

The application of computer tomography as well as digital radiography made it possible to perform series of measurements for turbine blade model. The achieved results allowed to make analysis of geometry of the research turbine blade model and detection of holes and micro-holes manufactured by DMLS method.

The computer tomography imaging was carried out by means of Nikon XT H 450 tomograph in Smart Solutions firm [5]. An example image of longitudinal cross-section of the turbine blade model is presented in Fig. 2.

The conducted tests allowed to carry out measurements of two rows of holes of 1.35 mm diameter. Additionally, based on the achieved image, distances between neighbouring holes were also determined. In order to determine possibility of manufacturing the micro-holes by means of DMLS method the computer tomography tests were also performed in transverse direction. The obtained results are shown in Fig. 3. The presented image shows the holes produced in one of the turbine blade walls. On the basis of the carried out measurements it may be stated that at the assumed parameters of sintering process the micro-holes of the assumed diameter equal to 0.3 mm and angular position were not gained.

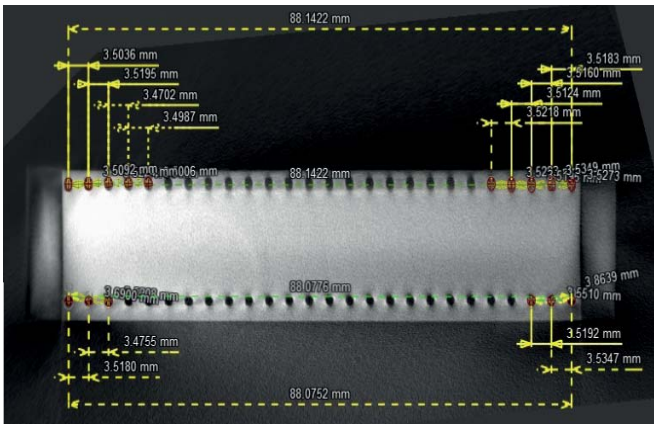

Fig. 2. Measurement results for holes of 1,35 mm diameter. Image of turbine blade cross-section in longitudinal direction

Measurements with the use of digital radiography were performed to make detail analysis of manufacturing holes and micro-holes. The test was carried out with the use of Andreks 300 kW radiograph in the Bonding Engineering Unit laboratory, Mechanical Faculty, Gdańsk University of Technology.

Fig. 4 shows a radiogram where the holes obtained in the turbine blade made by using additive method may be observed.

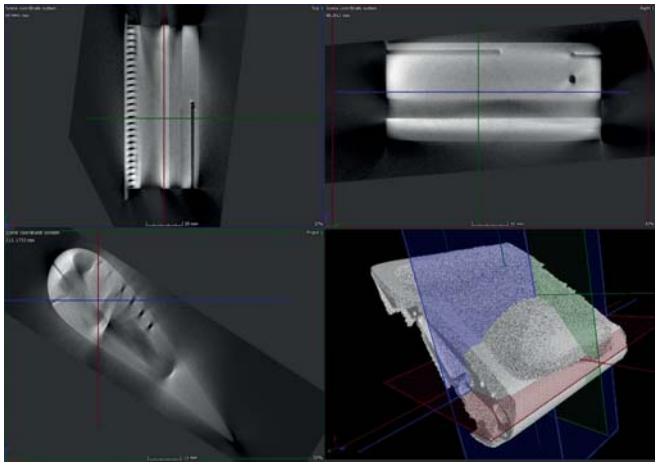

Fig. 3. Exemplary images of cross-section of turbine blade model

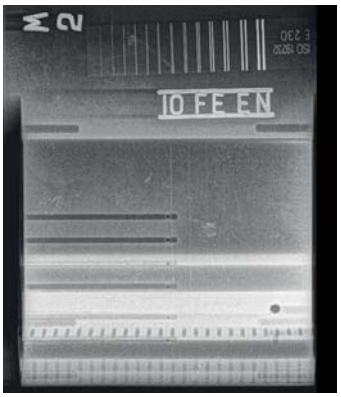

Fig. 4. Radiogram with visible holes obtained in turbine blade made by using additive method

The conducted digital radiography tests made it possible to detect and measure the holes in the diameter range from 1 mm to 3 mm. Tab. 1 contains a set of measurement results for the holes with taking into account their number and diameters.

Tab. 1. Set of measurement results obtained by means of digital radiography

No.	Number of holes	Hole diameter [mm]
1	2	2.5
2	6	2
3	4	2.5
4	6	1
5	1	3
6	26	1.35
7	26	1.35

MOST WIEDZY Downloaded from mostwiedzy.pl

The results obtained from the conducted digital radiography tests confirm the results achieved from computer tomography. In the turbine blade cross-sections no micro-holes of 0.3 mm diameter were found. To examine spots of their forming more precisely a micro-magnifying glass of 1×30 magnification was used. Exemplary spots of forming micro-holes on blade surface are presented in Fig. 5 a) and 5 b).

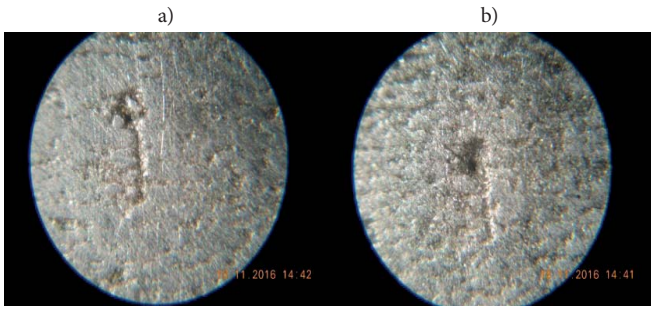

Fig. 5. Spots of forming the micro-holes of 0.3 mm diameter on blade surface: a) a nucleus of micro-hole, b) a tear –off on material surface

Analyzing the obtained measurement results one can observe only nuclei of micro-holes, that indicates a lack in complete metal powder melting. Additionally, material continuity faults in the form of tear-offs are also observed. On the basis of the performed investigations it was stated that the application of DMLS technology at the set values of additive process parameters did not result in producing micro-holes of 0.3 mm diameter.

In the subsequent stage of the investigations micro-holes of 0.3 mm diameter were produced by means of spark drilling (electric discharge) technique whose possible application and precision in manufacturing micro-holes was next validated.

The results of measurements with the use of digital radiography indicate that the formed micro-holes are of 0.4 mm diameter, i.e. somewhat greater than that assumed. Therefore the use of spark drilling technology did admittedly allow to obtain micro-holes but the dimensional accuracy requirement was not fulfilled.

The achieved image of turbine blade cross-section with marked series of micro-holes produced by spark drilling technique is presented in Fig. 6.

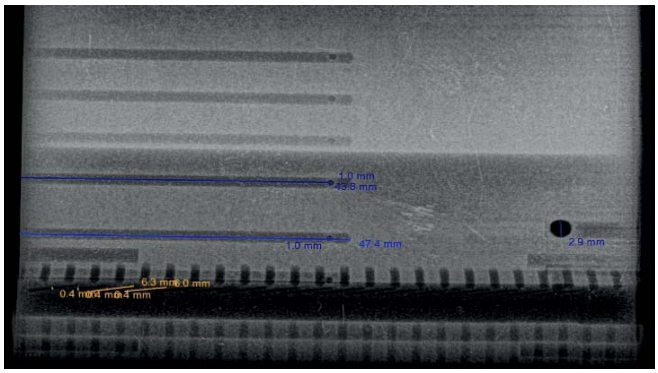

Fig. 6. Micro-holes of 0.3 mm diameter produced by means of spark drilling technique

CONCLUSIONS

Rapid Prototyping/Rapid Manufacturing technologies constitute, in view of their dynamic development, a very important area of today-used methods for products forming and manufacturing. The techniques in question make it possible to work out prototypes and physical models of objects of any shape on the basis of their 3D geometry. These technologies constitute an important element in product development cycle as they allow to do a reliable assessment in every stage of its development.

The application of the selective laser melting method (DMLS) made it possible to produce a real model of gas turbine blade with cooling holes and holes for longitudinal vortices generating. The DMLS technology allowed to produce a series of holes of 3 mm, 2.5 mm, 2 mm, 1.35 mm and 1 mm in diameter under different angles directly during additive process. A lack in complete metal melting did not allow to produce a series of micro-holes of 0.3 mm diameter, revealing this way limitations in application of the selective laser melting technology to making holes of a diameter smaller than 1 mm. The additionally performed spark drilling operation did not allow to produce micro-holes just of 0.3 mm diameter but only of 0.4 mm diameter. Application of an electrode of smaller diameter would allow probably to reach holes of the required dimensional accuracy. The searching for a relation between electrode diameter and dimensional and shape accuracy of produced holes will be a subject of further investigations.

The carrying out of analysis of turbine blade model geometry is a basis for decision making on further investigations dealing with utilization of rapid prototyping methods and deductive methods in the area of micro-holes manufacturing.

The next step is to prepare a test specimen especially designed for this purpose.

An appropriate analysis of the test model geometry will allow to determine possibilities and limitations for application of Rapid Prototyping/Rapid Manufacturing technologies to direct manufacturing micro-holes of a diameter less than 1 mm.

BIBLIOGRAPHY

1. Flaszynski P., Doerffer P., Piotrowicz M.: Effect of Jet Vortex Generators on Shock Wave Induced Separation on Gas Turbine Profile. Proceedings of the 13th International Symposium on Experimental Computational Aerothermodynamics of Internal Flows, 7-11 May 2017, Okinawa, Japan.

2. Gebhard J.: Generative Fertigungsverfahren, Additive Manufacturing und 3D Drucken für Prototyping-Tooling-Produktion; Prototyping-Tooling-Produktion, Carl Hanser Verlag, München 2013.

3. Iftikhar A., Khan M., Alam K., Imran Jaffery S. H., Ali L., Ayaz Y. and Khan A.: Turbine blade manufacturing through rapid tooling (RT) process and its quality inspection.

MOST WIEDZY Downloaded from mostwiedzy.pl

Materials and Manufacturing Processes, Vol. 28, Issue 5, (2013), pp. 534-538.

4. Lampart P., Kosowski K., Piwowarski M. and Jędrzejewski Ł.: Design analysis of Tesla micro-turbine operating on a low-boiling medium. Polish Maritime Research, Special issue 2009/S1; pp. 28-33.

5. Nikon XT H series, X-ray technology and CT for industrial applications, Nikon Metrology/ Vision Beyond Precision, 2017.

6. Tan X., Kok Y., Tor S. B. and Chua, C. K.: Application of Electron Beam Melting (EBM) in Additive Manufacturing of an Impeller. Proceedings of the 1st International Conference on Progress in Additive Manufacturing (Pro-AM 2014), 2014, pp. 327-332.

7. Vaezi M., Safaeian D. and Chua C.K.: Gas turbine blade manufacturing by use of epoxy resin tooling and silicone rubber moulding techniques. Rapid Prototyping Journal, Vol. 17 Issue: 2, 2011, pp.107-115.

8. Vayre B., Vignat F. and Villeneuve F.: Designing for Additive Manufacturing. 45th CIRP Conference on Manufacturing Systems, Procedia CIRP 3, 2012, pp. 632–637.

9. VDI 3405:2014-12: Additive manufacturing processes, rapid manufacturing - Basics, definitions, processes.

10. Yadroitsev I. and Yadroitsava I.: Evaluation of residual stress in stainless steel 316L and Ti6Al4V samples produced by selective laser melting. Virtual and Physical Prototyping. Vol. 10, No. 2, 2015, pp. 67–76.

11. Yakout M., Elbestawi M.A. and Veldhuis S.C.: On the characterization of stainless steel 316L parts produced by selective laser melting. The International Journal of Advanced Manufacturing Technology,2017, pp 1-22.

12. https://drukarki3d.pl/technologie/dmls/

13. https://drukarki3d.pl/materialy/dmls/eos-maragingsteel-ms1/

CONTACT WITH THE AUTHORS

Mariusz Deja
Michał Dobrzyński
Jacek Haras
Dawid Zieliński

Gdańsk University of Technology
Faculty of Mechanical Engineering
Department of Manufacturing and Production Engineering

11/12 Narutowicza St.
80-233 Gdańsk
Poland

Paweł Flaszyński

Institute of Fluid Flow Machinery
Polish Academy of Sciences

14 Fiszera St.
80-231 Gdańsk
Poland

MOST WIEDZY Downloaded from mostwiedzy.pl

POLISH MARITIME RESEARCH Special Issue 2018 S1 (97) 2018 Vol. 25; pp. 124-133
10.2478/pomr-2018-0033

REVIEW OF ASSEMBLY SEQUENCE PLANNING METHODS IN TERMS OF THEIR APPLICABILITY IN SHIPBUILDING PROCESSES

Michał Taraska
Remigiusz Iwańkowicz
Tomasz Urbański
Tadeusz Graczyk
West Pomeranian University of Technology in Szczecin, Poland

ABSTRACT

The article characterises the sea-going vessel hull assembly processes and then reviews the existing assembly methods of mechanisms and welded ship structures. Classification of these methods is done with respect to selected criteria of their applicability to hull assembly. Selected methods are used for calculations performed on a model structure and exemplary database. The analysed aspects include the performance of calculation algorithms and the quality of the obtained solutions. Particular attention is paid to the need for reduction of experts' participation in the planning process due to strong search space explosion effect. The performed analyses have enabled the authors to formulate assumptions for models which would be applicable in real assembly planning in shipyards, as well as to indicate areas of further research which would make it possible to better consider the specificity of production of large-size welded structures.

Keywords: assembly sequence planning, ship hull, welded structure, method review, shipyard

MOST WIEDZY Downloaded from mostwiedzy.pl

INTRODUCTION

An important role of assembly sequence planning (ASP) automatization methods in the shipbuilding industry is frequently stressed in contemporary literature [1] [2] [3]. The need for ship hull assembly sequence planning methods was initially noticed as early as in 1979 [4]. Then, numerous authors have indicated the assembly as most important moment in the ship hull building cycle [5] [6] [7]. Adapting ASP methods used for assembly of mechanisms to the shipbuilding industry is not always possible due to its specificity and the size of the built structures. The biggest obstacle is the number of parts composing the ship hull, and the resultant size of the space of possible assembly sequences. This size can be assessed using the Robinson formula to calculate the number of different directed acyclic graphs (DAG) [8] [9]:

$$G(n)=\sum_{k=1}^{n}(-1)^{k-1}\cdot\binom{n}{k}\cdot 2^{k\cdot(n-k)}\cdot G(n-k),\quad G(0)=1 \tag{1}$$

where n is the number of graph nodes.

The numerical amount of the search space expressed in the above way increases in a very dynamic way. Formula (1) says that for 10 nodes, more than $4\cdot10^{18}$ different graphs can be generated.

For hulls of typical merchant ships, the number of liaisons can exceed hundreds of thousands, and consequently, complete search of the space of acceptable assembly sequence solutions is impossible. This is well illustrated by an attempt

to use the method proposed in [10] for a simple ship structure. The algorithm proposed in that article develops and simplifies the method which is considered classical in the field of assembly of mechanisms [11]. An exemplary solution for a ship structure which bases on that method is shown in Chapter 3.2.

Basic division of ASP methods refers to the purpose of their use. Here, a distinction is made between methods which search for an acceptable solution and those which search for optimum. In the former group, complete search of the space of solutions is frequently applied to extract the acceptable solution based on selected criteria. This is an important methodology for sequence planning of mechanism assembly, therefore it has been developed from very beginning of the appearance of this problem. Attempts to expand the problem by adding new issues most often lead to the optimisation model. Here, a possible direction of development can be taking into account criteria which minimise the number of adjustment operations or the number of changes of the equipment used in the process.

Hull assembly is less sensitive to geometric constraints than typical mechanisms analysed in the literature. The hull is a so-called sparse structure, which means that its parts are distributed in the space in a more dispersed way that elements of mechanisms. The integrity of hull structure is ensured by permanent joints – welds.

The next important aspect of each individual method is the level of experts' involvement in the calculation process. Their assistance cannot be totally eliminated, as they are needed for, among other tasks, assuming weights of optimisation criteria, selecting data introduced to the code at the beginning of the calculation process, and assessing the obtained results. However, a number of methods can be named which base on wider interaction with experts, who are expected to answer a series of questions, or perform cluster analysis of the database.

The aim of this article is to analyse the group of existing methods, concerning both mechanism assembly planning and those clearly dedicated to shipbuilding, with respect to their applicability to ship hull assembly planning. These methods have been classified with respect to their basic and repeating features, and their applicability to hull assembly has been assessed. Selected methods were used in calculations performed on a model structure.

LITERATURE REVIEW

With his Ph.D. thesis in 1984, Bourjault [11] initiated the development of ASP methods for mechanisms. These methods based on complete search of the set of acceptable solutions and consisted in checking whether the execution of certain liaison leads to the state from which the final structure can be obtained. This approach generated trees of all possible assembly plans for a given structure [10] [11]. In [12], the author proposes the use of "And/Or" graphs for backward analysis of mechanism assembly sequences. The next publication of the same authors [13] illustrates the flexibility of "And/Or" graphs and their potential for easy modifications to obtain new functionalities. However, both works reveal dynamic increase of the number of possible solutions as a result of the increased complexity of the analysed task. Consequently, a possibility of their adaptation to ship hull assembly planning problems seems to be marginal.

The complete search-based methods lose dramatically their efficiency when the complexity of the structure increases. In [14], the authors have remarked that taking into consideration geometric constraints of structure assembly is necessary but insufficient for correct assessment of solution acceptability. Four criteria were proposed for assessing the generated sequence.

In the case of ship structures, standard geometric constraints are to be complemented with welding positions. This was taken into account in [5], which proposed the ship hull welding planning assistance system. The presented method was not fully compatible with ASP solutions, it was merely an idea to be used as an assembly planning assistance module. The problem of welding operation sequence planning is frequently considered as a separate issue, solved using intelligent methods, such as genetic algorithms or annealing, or the finite element method [15].

In [16], the authors have remarked that the 3D modelling and simulation-based planning process reveals good performance in terms of work strategy planning. The authors propose the ACIM (advanced computer integrated manufacturing system) type algorithm, but describe its essence in a sketchy way, which makes assessing its efficiency and reconstruction of the computation process impossible.

In [17], the authors were the first to suggest the use of genetic algorithms (GA) as a tool for finding optimal and semi-optimal assembly plans. However, the efficiency of the described algorithm is difficult to assess, as the final result is strongly affected by the initial population of proposed structures, prepared by an expert. The idea to use GA in assembly planning processes was developed in [18], the author of which proposes an adaptive genetic algorithm. This algorithm is characterised by varying weights of appearance of genetic operators (mutation and crossing), which in classical GA are constant for all populations. The author makes distinction between two types of structure constraints: physical and geometric. Meeting all geometric constraints by the proposed assembly plan was identified as the necessary condition for considering it an acceptable solution. Physical constraints concerning such aspects as available equipment, or assembly difficulties and cost, were used as optimisation criteria for the proposed algorithm. The method described in the paper was tested on selected mechanical structures.

In recent years, great interest of shipbuilding industry has been focused on CBR (case-based reasoning) methods as a possible ASP assistance tool. In [19], the authors propose the CBR-CAPP (CBR-computer aided process planning) algorithm for automatic assembly planning of small ship blocks. However, the solution proposed by the authors is difficult to implement in other cases that that discussed in

MOST WIEDZY Downloaded from mostwiedzy.pl

the article, as its correct operation requires a huge database of similar structures, worked out by experts, which is a typical drawback of CBR methods. As a result, for structures which require special assembly principles the method is of little or no use. Using CBR methods reduces participation of experts in the assembly planning process, but their active participation is still required when preparing the database. A positive aspect here is that consecutive solutions obtained using this method are introduced to the database and increase it, which leads to the decrease of general participation of experts in the assembly planning and tool preparation processes.

In [20], the author proposes combining CBR with GA to obtain a tool which enables generating assembly plans for marine structures. The proposed GA makes use of geometric constraints as one of optimisation criteria, and the criterion which minimises changes of component classes during serial assembly as the other criterion. A weak point of the method is the need for extensive database of similar structures, like in all problems making use of CBR methods. For untypical or new assembly units, the genetic algorithms alone may turn our insufficient for generating a satisfying assembly plan. Moreover, an important role in the proposed assembly planning methodology based on the database of similar cases is played be an expert, as this methodology requires unambiguous classification of all components of the analysed structure, which in the case of sea-going hulls is not always evident. All this makes that the reduction of experts' participation in the assembly process, which is typical for intelligent algorithms, is hardly perceivable in the above case.

ANALYSING PROPOSED METHODS WITH RESPECT TO THEIR APPLICABILITY TO HULL ASSEMBLY.

DESCRIPTION OF EXEMPLARY STRUCTURE

To perform the analysis of selected methods in terms of their applicability to practical hull assembly planning, a simplified exemplary structure was defined which consisted of five parts and six liaisons between them. This structure is given the number 0 and name S0, while its parts get consecutive numbers with hyphen: 0-1 – plate, 0-2 – web of T-frame, 0-3 – flange of T-frame, and 0-4, 0-5 – ribs.

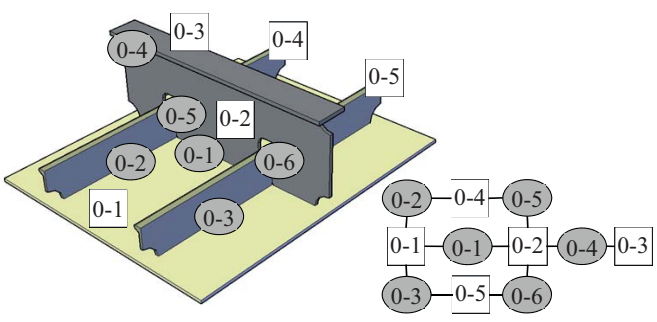

Fig. 1. Exemplary assembly unit S0

All liaisons between parts are made as fillet welds. Fig. 1 shows numbers of parts (in squares) and the so-called liaison graph with number of liaisons (in circles).

The structure can be assembled in a number of different ways. Each sequence includes intermediate stages of structure state (subassemblies) which consist of two, three, or four parts. Fig. 6 shows all possible variants, including those which are irrational from the point of view of traditional assembly planning methods used in shipyards.

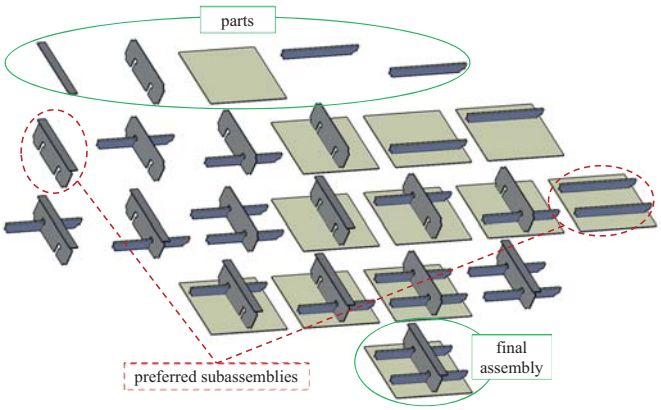

Fig. 2. Possible variants of intermediate stages during assembly process of unit S0

The required assembly sequence for the unit S0 is initial subassembly of the T-frame and welding the ribs to the plate. These two operations can be done simultaneously. The next operation should be connecting the obtained subassemblies together. It should be kept in mind, however, that the correctly prepared process should define not only the order of connecting structure parts, but also the order of making consecutive welded joints. In the analysed case, the T-frame can be connected with the stiffened plate either by making liaisons between the frame and the ribs and then between the frame and the plate, or in the reverse order. Both variants are completely invisible in the plan oriented only on structure parts.

In its further part, the article analyses abilities of different ASP methods to generate assembly sequences which, in authors' opinion, can be of practical applicability or reveal potential for development.

DETERMINING CRITERIA FOR BEST METHOD SELECTION

To assess which method described in the literature review is most useful for ship hull assembly planning, first the desired features of the method are to be determined. Then, these features will be used as criteria for selection of best solutions. For this purpose, the prepared exemplary structure was analysed with the aid of the classical method developed by Bourjault [11] and improved by De Fazio and Whitney [10]. That method bases on numbering liaisons in the structure and formulating a series of questions concerning relations between these liaisons. Further in the paper, this method is

MOST WIEDZY Downloaded from mostwiedzy.pl

referred to as the Q&A (questions & answers) method. The above analysis will make it possible to identify basic problems resulting from the specificity of hull structures and thus determine which features of searched methods will allow us to avoid or minimise these problems.

In the analysed Q&A method, answers to the questions are always given by an expert – process engineer, who has knowledge on the course of assembly processes and on features of the assembled structure. The Q&A method in version given by De Fazio and Whitney [10] consists in two questions concerning each i-th liaison:

– Which liaison must be done prior to doing liaison *i*?
– Which liaisons must be left to be done after doing liaison *i*?

The answers to these questions make the basis for defining precedence relations between liaisons. Experts' answers can take into account arbitrary factors, which in the simplest version can refer to the geometry of elements and physical possibilities of placing them in a right place during the assembly. The expert can answer these simple questions fast, therefore the procedure consisting of tens or even hundreds of questions can be easily applied in practice.

Let us consider a simplified exemplary structure (Fig. 1). If we take into account only geometric constraints, then for each liaison identical answers: "none of the remaining liaisons" are to be given to both questions. This results from the fact that the parts do not create geometrical conflicts and can be added to the structure in an arbitrary order. The same refers to the order of doing liaisons. For instance, after adding T-bar to the plate earlier connected with bulb stiffeners, liaisons between the T-bar and the plate, and between the T-bar and the stiffeners are to be done. Theoretically, these three liaisons can be done in an arbitrary order and in this situation the Q&A method based on geometric constraints fails, as it does not reduce the set of acceptable assembly sequences.

Indeed, along with geometric constrains, the Q&A method can take into account also other aspects. The expert providing the answers can consider typical hull related problems, such as welding deformations, assembly positions, and/or ergonomics and safety of welders' work.

For instance, let us assume that we want to do welding of the greatest possible number of liaisons:

1) in unforced positions,
2) steadily along the entire length.

Let us perform the analyse with the procedure given by De Fazio and Whitney [10]. For consecutive liaisons numbered as i=1,...,6 two questions are to be answered:

Q1 – What Liaisons Must be Done Prior to Doing Liaison 0-*i*?

Answers:

i=1,2,3,4: none of the liaisons must be done prior to doing these liaisons,

i=5,6: doing these liaisons in unforced position requires placing the bulb profile on its side. This operation will not require special technological supports, provided that T-bar and stiffener liaisons with the plate are done prior to them:

$$\{0\text{-}1,0\text{-}2\} \rightarrow 0\text{-}5 \quad (2)$$

$$\{0\text{-}1,0\text{-}3\} \rightarrow 0\text{-}6 \quad (3)$$

Q2 – What Liaisons Must be Left to be Done After Doing Liaison 0-*i*?

Answers:

i=1: none of the liaisons must be done after connecting the web of the T-bar with the plate,

i=2,3: if liaisons 0-2 and 0-3 are to be welded steadily along the entire length, then liaisons 0-1, 0-5 and 0-6 must be done later:

$$0\text{-}2 \rightarrow \{0\text{-}1,0\text{-}5,0\text{-}6\} \quad (4)$$

$$0\text{-}3 \rightarrow \{0\text{-}1,0\text{-}5,0\text{-}6\} \quad (5)$$

i=4: if liaison 0-4 is to be welded in unforced position, then liaisons 0-1, 0-5 and 0-6 must be done later:

$$0\text{-}4 \rightarrow \{0\text{-}1,0\text{-}5,0\text{-}6\} \quad (6)$$

i=5,6: none of the liaisons must be done after doing liaisons 0-5 and 0-6.

After completing all answers, a graph of sequences can be created (Fig. 3-a). Nodes in this graph represent liaisons, while arcs correspond to precedence relations. This is a directed acyclic graph.

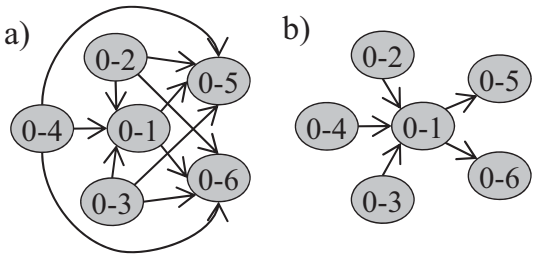

Fig. 3. Solution obtained by the Q&A method

It is noteworthy that the sequence obtained using the Q&A method incudes surplus precedence relations, which can be removed. For instance, the precedence of action 0-4 over action 0-5 is a transitive closure of the precedence chain 0-4→0-1→0-5. After removing all surplus precedence relations, we obtain a so-called minimal sequence graph (Fig. 3-b).

In the case of extensive technological analysis of each question in the Q&A method, the time needed to give the answers becomes a problem. Moreover, methods which base on experts' assessment and are dedicated to mechanisms are difficult to adapt to the shipbuilding environment, due to wide variety of structures. Each structural type reacts to exothermic processes in a different way, as well as has different ergonomics and problematics of work. Adapting those methods leads to large experts' labour intensity and requires involving FEM type calculations, or even experimental methods on physical objects. Hence the conclusion that the searched methods should:

– be dedicated to ship hulls and marine structures,

MOST WIEDZY Downloaded from mostwiedzy.pl

– take into account additional assembly constraints, along with the geometry,
– minimise experts' participation in the assessment and analysis process by applying intelligent and self-learning methods,
– be applicable and replicable for diversified structures.

The above features were recognised as criteria for selecting best methods from the set discussed in the literature review.

SELECTING BEST METHOD FROM ANALYSED SET BASED ON SELECTED CRITERIA

The methods discussed in the literature review were analysed with respect to the required features of the ship hull assembly planning method presented in Chapter 3.2. Table 1 collates results of this analysis. Consecutive columns are to be interpreted in the following way:

1. This column contains the information about the authors of the method, numbers in square brackets refer to the bibliography number of the article in which the method is described.
2. (I) Does the method description allow its calculation procedure to be reproduced?
3. (II) Is the method dedicated to ship hull assembly planning?
4. (III) Does the method take into consideration geometric constraints of assembly?
5. (IV) Does the method take into consideration other, additional assembly constraints?
6. (V) Does the method allow experts' participation to be reduced in the assembly planning process?

Tab 1. Results of applicability analysis of assembly planning methods

1	2	3	4	5	6
Method	**I**	**II**	**III**	**IV**	**V**
Bourjault (1984) [11]	Yes	No	No	No	No
De Fazio i Whitney (1987) [10]	Yes	No	No	No	No
de Mello i Sanderson (1986) [12]	Yes	No	Yes	No	No
de Mello i Sanderson (1988) [13]	Yes	No	Yes	No	No
Eng et al. (1999) [14]	Yes	No	Yes	Yes	Yes
Cho et al. (1999) [5]	No	Yes	No	Yes	-
Sasaki et al. (2003) [16]	No	Yes	Yes	No	Yes
Bonneville et al. (1995) [17]	Yes	No	No	Yes	No
Chen i Liu (2001) [18]	Yes	No	Yes	Yes	-
Seo et al. (2007) [19]	Yes	Yes	Yes	Yes	Yes
Qu et al. (2013) [20]	Yes	Yes	Yes	Yes	No
Zhong et al. (2013) [21]	Yes	Yes	Yes	Yes	No

For two methods, their effect on reducing experts' participation in the assembly planning process could not be assessed. In the case of the solution proposed in [5], this results from insufficient data in the article and the resultant impossibility to reproduce the calculation process needed to assess the scale of the required experts' participation. The article [18], in turn, is not dedicated to ship solutions and its adaptation to this area could dramatically worsen the scale of reduction of experts' work obtained for mechanism assembly planning. That is why a decision was made to assign no values to these two methods in this field.

From among analysed methods, four methods have outstanding results which are, consecutively, methods: [14], [19], [20] and [21]. However, the work [14] is not dedicated to hull assembly, consequently its implementation in this area would be very time and effort consuming. Therefore, a decision was made to omit this method in further considerations. For the remaining methods, numerical calculations were performed on the exemplary structure presented in Chapter 3.1 to identify strengths and weaknesses of each individual method.

APPLYING SELECTED METHODS IN HULL STRUCTURE ASSEMBLY PLANNING

ACTIVITIES-ORIENTED ASSEMBLY PLANNING ON THE BASE OF CASES

The method proposed by Seo, et al. [19] makes use of the database of similar structures and the CBR procedure which comprises typical stages:
– database search for cases similar to the new structure,
– determining a new sequence based on similar cases,
– verification of the solution,
– database updating.

The structures stored in the database are referred to as cases, while the structure for which the assembly sequence is to be created bears the name of a problem. Each structure is characterised by:
– set of parts and assigned classes: plate, rib, girder),
– set of liaisons and assigned classes: fillet, butt, through),
– set of constraints: precedence relations between liaisons, assignment of liaisons to common group, alternativity of liaisons,
– set of assembly sequences – determined only for cases – each sequence is serial in nature, i.e. is a permutation of structure liaison numbers.

A new sequence generated for structure-problem is serial in nature. This is a serious limitation of the method. For instance, a result of serial sequencing can be blockage ofpossible subassembly of all T-frames before their connecting with the rest of the structure. This problem can appear when the structure comprises more than one girder. For the first girder, a good solution could be placing its flange at the beginning of the sequence and its web in the second place.

The authors have introduced graphical way of representation of parts and liaisons in the liaison graph. This approach seems questionable in the case of larger structures, with greater structural diversity. In this case both readability of the graph, and the process of part classification itself, to be done by an expert, can be a problem.

To illustrate the essence of the method, two structure-cases are considered (Fig. 4), similar to the structure-problem

MOST WIEDZY Downloaded from mostwiedzy.pl

(Fig. 1) for which a new sequence is to be created. In these exemplary considerations we neglect the problem of search for similar cases to simplify the analysis. The inference will be performed based on each case separately, and then an attempt will be made to include the information about these two cases from the database.

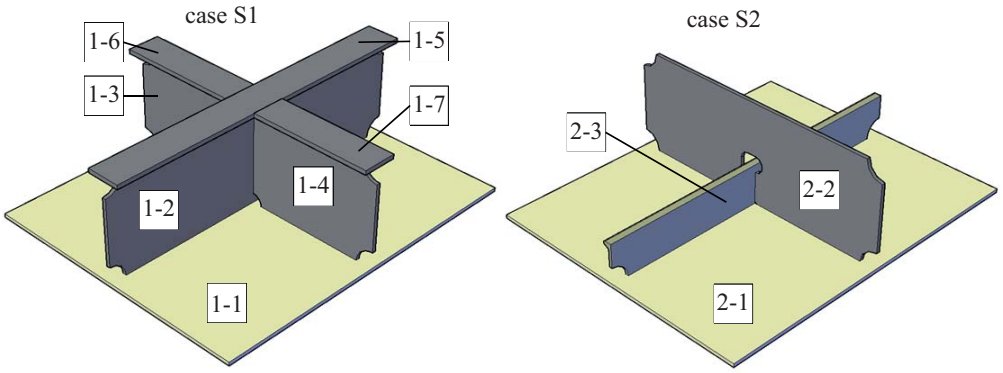

Fig. 4. Assembly units – 'cases' stored in exemplary database

Seo et al. proposed 3 classes of liaisons: fillet, butt, and through, and 3 classes of parts: plate, rib, and girder. Since the analysed structures comprise also other parts, additional classes of parts are assumed, which are: web and flange of T-frame.

The assembly sequences stored in the database according to the model by Seo et al., are the following:

- case S1: fillet(1-2,1-5), fillet(1-3,1-6), fillet(1-4,1-7), fillet(1-5 1-2, 1-1), fillet(1-7 1-4, 1-1 1-2 1-5), fillet(1-7 1-4, 1-2 1-5 1-1), butt(1-4 1-7, 1-5 1-2 1-1), fillet (1-6 1-3, 1-1 1-2 1-5 1-4 1-7), fillet (1-6 1-3, 1-2 1-5 1-1 1-4 1-7), butt (1-3 1-6, 1-5 1-2 1-1 1-4 1-7),
- case S2: fillet(2-1, 2-3), through(2-1 2-3, 2-2), fillet(2-2, 2-1 2-3).

The method of sequence recording proposed in [19] enables parallel assembly planning. This is possible due to planning oriented on activities, i.e. liaison welding operations. It should be kept in mind, however, that parallel doing of liaisons in the discussed model is only possible to a limited extent.

After introducing the classification of parts, we obtain a set of rules to be used when defining the assembly sequence for the new structure, numbered 0. Here, a typical problem for CBR methods can be observed, which is strong dependence of the obtained solution on the quality of the database and the adopted way of case description. Based on case S1, we obtain the rule in which T-frames are prefabricated before welding to the plate. This is insufficient for planning the assembly sequence for the entire structure 0. On the other hand, the rule resulting from case S2 says that ribs should be welded to the plate before their connecting with the girder. Applying this rule to the structure S0 does not provide a comprehensive solution to the structure assembly planning either.

PARTS-ORIENTED ASSEMBLY PLANNING ON THE BASE OF CASES

The method proposed by Qu et al. [20] enables to generate assembly sequences for a new structure based on cases stored in the database. Many similarities can be found between this method and that proposed by Seo et al. [19], the basic of which are the use of CBR procedure and serial nature of sequences.

What is characteristic, the method focuses on setting the order in which parts are to be connected. The planned sequence does not provide opportunities for planning the welding sequence. The parts-oriented approach has been developed for mechanism assembly, but its application to hull structures seems unjustified.

An exemplary analysis is performed based on the same case base (Fig. 4) and the same structure-problem, labelled as S0 (Fig. 1). For the case S1, the sequence of part liaisons is: (1-5, 1-2, 1-1, 1-3, 1-4, 1-6, 1-7), while for the case S2 this sequence is: (2-1, 2-3, 2-2). Drawbacks of the proposed approach to sequence description are clearly visible. For instance, parts 1-3 and 1-6 should be connected together before their connecting with the rest of the structure, but serial description of the sequence makes this solution impossible.

The method bases on assigning each case part in the database and each part of the structure S0 to one of predefined classes. The classification process is conducted by an expert. It is a key, and at the same time most problematic, part of the method. We should remember that hull parts are difficult to classify unequivocally. Geometrically similar parts play frequently different roles in the structure and require different treatment in the assembly sequence.

In [20], Qu et al. propose 14 classes of parts, but they do not define them precisely. To analyse the method, we can assume a smaller number of classes due to significant simplification of the analysed structures. The adopted classification of parts is shown in Tab. 1.

Tab. 1. Classification of parts of analysed structures

Class of parts	Parts of S1	Parts of S2	Parts of S0
A	1-1	2-1	0-1
B	1-2	2-2	0-2
C	1-3, 1-4	-	-
D	1-5	-	0-3
E	1-6, 1-7	-	-
F	-	2-3	0-4, 0-5

According to [20], the structure-case assembly sequences and classification of their parts make the basis for obtaining general rules to be used when creating structure-problem sequences. The case S1 gives the following sequence of classes: D→B→A→C→E, while the case S2 gives: A→F→B.

MOST WIEDZY Downloaded from mostwiedzy.pl

The inference on the new sequence is performed by determining precedence relations between parts belonging to certain classes. The structure-problem assembly sequence resulting from case S1 is the following: 0-3→0-2→0-1, while that resulting from case S2 is: 0-1→0-4→0-5→0-2 or equivalent: 0-1→0-5→0-4→0-2. The following problems can be noticed in the obtained results:

- none of the obtained sequences covers entirely the structure-problem,
- precedence relations obtained based on different structures partially contradict each other (B→A and A→B).

In [20], the authors suggest complementing the missing information in the obtained sequence with the aid of genetic algorithm. In this process, geometric constraints between parts and the criterion of minimisation of component class changes during serial assembly are taken into consideration. As a result, a sequence is obtained which is realisable in geometric terms and groups homogeneous parts in such a way that they are assembled directly after each other. The sequences obtained for the analysed structure S0 are shown in Fig. 5.

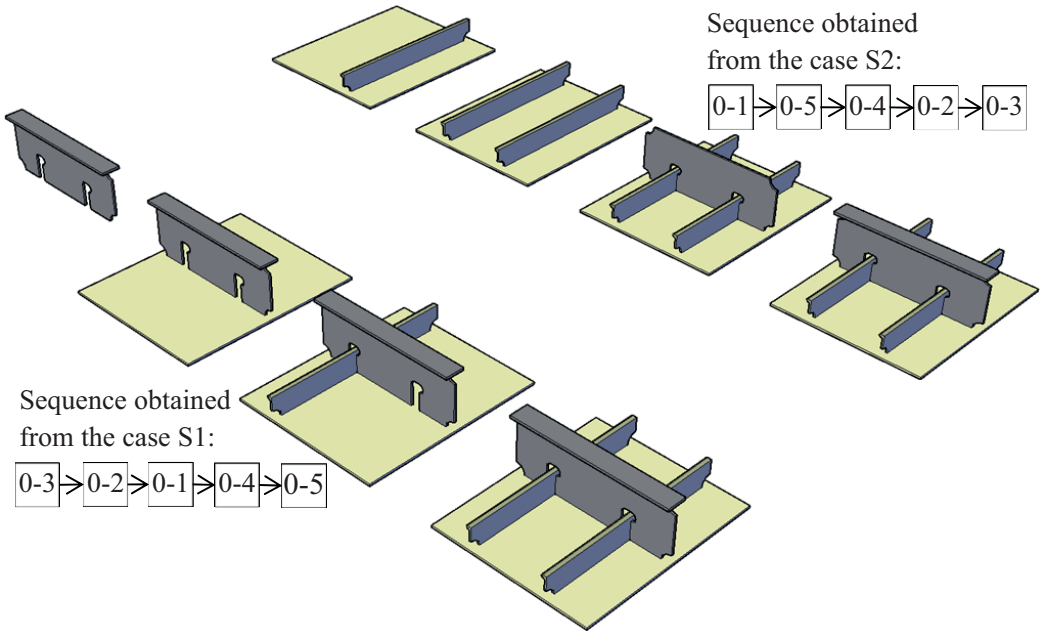

Fig. 5. Two assembly sequences of problem S0 obtained from cases S1 and S2

It is noteworthy that these sequences differ greatly, and none of them is free of disadvantages. The sequence obtained based on case S1 assumes welding the girders with the plate before welding the ribs. As a result, the ribs can be steadily welded on the entire length. On the other hand, the sequence obtained based on case S2 assumes welding the girder flange to the web being already welded to the plate. This solution is completely irrational in terms of the access to the weld and welding position.

HIERARCHICAL CLUSTERING OF ASSEMBLY UNIT PARTS

The method described in [21] consists of two parts:

- Hierarchical clustering of assembly unit parts. It makes use of the so-called rule-based expert system and can be used for dividing the structure into subassemblies, with further creation of assembly sequence,
- Optimisation of clustering diversification degree. It makes use of the analytic hierarchy process (AHP) algorithm, but the solution assessment is done solely by an expert and does not contribute much to the problem of assembly sequencing needs.

The proposed method of hierarchical clustering requires defining the fuzzy similarity relationship $u_{i,j} \in [0,1]$ for each pair (i,j) of structure parts. The rules to assess the quantities $u_{i,j}$ are defined in [21]. They are determined by an expert and their use is somewhat problematic, as the expert is expected to plan partially the assembly before assigning the value of $u_{i,j}$. Prior assembly planning refers to positions in which welded joints are to be made. Different values of $u_{i,j}$ are assigned to fillet welds made in bottom, vertical and top direction of connection. However, these positions are determined after determining the order in which some liaisons are done. Thus, this method, on the one hand, makes it possible to divide the structure into subassemblies, but on the other hand, it requires from the expert to define a priori this division.

The authors of [21] also propose common consideration of identical parts which are to be assembled simultaneously or directly after each other. This refers, for instance, to parallel ribs. In the considered case, parts 0-4 and 0-5 can be grouped, which to a certain extent will simplify the analysis as they will be collectively treated as part 0-4.

The adopted values of fuzzy similarity relationships for the analysed structure S0 (Fig. 1) are given in Tab. 2.

Tab. 2. Fuzzy similarity relationships for S0 structure

		part			
		0-1	0-2	0-3	0-4
part	0-1	1	0.7	0	0.8
	0-2	0.7	1	0.8	0.5
	0-3	0	0.8	1	0
	0-4	0.8	0.5	0	1

MOST WIEDZY Downloaded from mostwiedzy.pl

It was assumed that the plate-rib and plate-T-frame liaisons will be done in bottom position. According to the analysed method, it can be assumed at this stage that the T-frame will also be prefabricated in bottom position, i.e. before welding to the plate and ribs. Prefabricating the T-frame is treated as rib-plate liaison, therefore $u_{2,3} = u_{3,2} = 0.8$.

Finally, hierarchical division of parts into groups is obtained, which can be interpreted as subassembly partition of the assembly unit (Fig. 6). The parameter $\lambda \in [0,1]$ represents granularity of the partition: $\lambda=1$ means partition into individual parts, while $\lambda=0$ means the assembly unit as a whole.

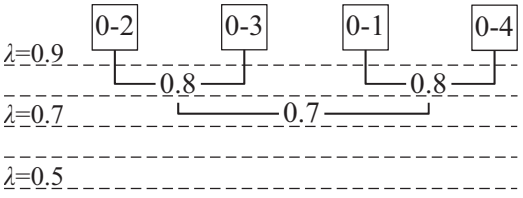

Fig. 6. Clustering tree of assembly unit partition

Partition of the analysed unit at the level of 0.8 enables making distinction between two subassemblies: T-frame, and plate with ribs. This is consistent with the expected assembly sequence, but at a very general level. This way, a lot of relevant information concerning the order of doing liaisons is omitted.

CONCLUSIONS

The article presents a literature review of assembly planning methods. The review takes into consideration both issues focused on assembly of mechanisms and those dedicated to ship hulls, in an attempt to find common features of these methods and development trends in this branch of science. In the world literature, works on assembly of mechanisms significantly dominate over those dedicated to hulls and marine structures. However, these solutions cannot be easily adapted to hull assembly problems. Therefore, the area od search for the best method was narrowed to methods dedicated to the shipbuilding industry. The analysis omits earlier works by the authors of the present article [8] [22] [23] [24] to avoid possible objections on bias in selections made in Chapter 3.3.

The analysis of ASP methods dedicated to hull structures was performed based on three simplified exemplary structures, two of which constitute "cases" stored in the database while one is the "problem", for which the assembly sequence is to be created. Use was made of three methods described in the literature which are dedicated to different ship hull structures. It is noteworthy that all methods:

- require significant participation of an expert in: describing the assembly unit, classifying parts and/or liaisons, and final supplement of the sequence with missing pieces of information,
- were tested by the authors on cases of small assembly units, for which expert's participation was a problem,
- make use of computational intelligence algorithms, which perform well in discrete problems with large search spaces.

Two of the analysed methods are similar to each other, as they make use of the database and the CBR algorithm for generating assembly sequences. A basic difference between them is the method of sequence recording. The performed analysis has revealed that the activities-oriented serial sequence provides opportunities for better mapping of serial-parallel assembly. This type of assembly is widely used in contemporary shipbuilding industry.

The third method was not developed to generate the assembly sequence, it was rather dedicated to plan assembly partition of the structure. This function is very close to sequencing, but the final result of hierarchical partition has only the form of a sketch of sequence, as it is oriented on parts.

Based on the performed observations, some assumptions can be formulated with regard to required features and development directions of hull assembly sequence planning methods:

1. The sequence model should be oriented on activities, i.e. doing liaisons, which constitute the main component of hull assembly labour consumption and cost generation.
2. Possibility of serial-parallel planning – it is especially important in the cases of plans for assembly units composed of hundreds of thousands of parts. Serial plans, in general, do not reflect the essence of parallel production of many hull sections and blocks.
3. Limited experts' involvement in the current calculation process, along with computational complexity of algorithms resistant to the effect of search space explosion – these conditions are necessary for the methods to find practical application for larger structures, such as hull sections and blocks.
4. Use of technological knowledge stored in the database of similar structures – the problem of similarity assessment for efficient assembly sequence generation still remains open. Literature examples and the performed analysis name a number of unsolved problems here.
5. Use of hierarchical grouping methods for hierarchical partition of the assembly unit – this approach seems promising as preliminary stage of assembly planning, as it significantly reduces the sequence search space.
6. Use of evolutionary algorithms in the sequence optimisation process, which are very productive in large search spaces with numerous constraints, due to the penalty function.

During hull assembly, a number of additional problems can occur which have not been taken into consideration yet in ASP methods:

- welding deformations and assembly usefulness ofsubassemblies,
- stability of subassemblies during welding processes and their potential for rotation and transport,
- safety of work at height and in narrow spaces,
- ergonomics of work in forced welding positions,
- accessibility of liaisons for welding robots,

MOST WIEDZY Downloaded from mostwiedzy.pl

– different welding speeds and parameters of welds made in different welding positions,
– synchronisation with hull equipping operations,
– effect of assembly plan on work organization at part machining departments and material management.

The above issues are to be taken into consideration when improving ASP methods dedicated to hulls. This is a serious challenge at both conceptual and efficiency level. It is noteworthy that such a complex problem concerns the assembly unit with gigantic dimensions, not to be found elsewhere.

Wider and wider use of computational intelligence methods, including image processing methods, provides opportunities for automation of processes concerning database development and description of new structures. It is essential for the development of ASP methods to take into consideration aspects of cooperation with CAD/CAM systems which are already in use in design offices. These systems are used for creating full descriptions of parts and liaisons of the entire structure. Moreover, 3D modelling provides opportunities for automatic analysis of geometric conflicts occurring during the assembly. The use of the above information would allow us to reduce significantly experts' participation in ASP processes of ship hulls.

BIBLIOGRAPHY

1. Yun D. H., Choi S. I., Kim S. H., Ko K. H.: Registration of multi-view point clouds for application to ship fabrication, Graphical Models, Vol.90, pp. 1-12, 2017.

2. Back M. –G., Lee D. –K., Shin J. –G., Woo J. –H.: A study for production simulation model generation system based on data model at a shipyard, International Journal of Naval Architecture and Ocean Engineering, Vol.8(5), pp. 496-510, 2016.

3. Zhao-Hui W., Ji-Wang D., Ming-hua Z., Xiu-min F.: Survey on Flexible Shipbuilding Technologies for Curved Ship-Blocks, Procedia Engineering, Vol. 174, pp.800-807, 2017.

4. Banerjee S. K.: Shipyard production systems design: a statistical approach, *International journal of Production Research*, Vol. **6**, pp. 541-555, 1979.

5. Cho K.-K., Sun J.-G., Oh J.-S.: An automated welding operation planning system for block assembly in shipbuilding, International Journal of Production Economics, 60-61, pp. 203–209, 1999.

6. Chi Z., Jun S.: Intelligentized work-preparation for ship hull construction with Optimized Assembly Planning System, Proceedings of the IEEE International Conference on Systems, Man and Cybernetics, Istanbul, Turkey, 10-13, pp. 2740–2744, 2010.

7. Ghandi S., Masehian E.: Assembly sequence planning of rigid and flexible parts, Journal of Manufacturing Systems, Vol. 36, pp. 128-146, 2015.

8. Iwańkowicz R.: Methods of sea-going ship hull assembly sequencing and scheduling, Collegiate Publication of the West Pomeranian University of Technology Szczecin, ISBN 978-83-7663-216-2, 2016.

9. Robinson R.W.: Counting labeled acyclic digraphs, in: New directions in the theory of graphs, Ed. F. Harary, [b.m.], Academic Press, 239–273, ISBN-13 978-0123242556, ISBN-10 012324255X, 1973.

10. De Fazio T., Whitney D.: Simplified generation of all mechanical assembly sequences, *IEEE Journal of Robotics and Automation*, Vol. **3**(6), pp. 640–658, 1987.

11. Bourjault A.: Contribution a uneapprochemkthodologique de l'assemblage automatis: Elaboration automatique des sequences operatiores, Thèse de doctorat, Université de Franche-Comte, 1984.

12. Homem de Mello, L. S., and Sanderson, A. C.: AND/OR graph representation of assembly plans, IEEE Transactions on Robotics and Automation, Vol. 6, no. 2, pp. 188-199, 1986.

13. Homem de Mello, L. S., and Sanderson, A. C.: Planning repair sequences using the And/Or graph representation of assembly plans, Proceedings of the 1988 IEEE International Conference on Robotics and Automation, Philadelphia, USA, pp. 1861-1862, 1988.

14. Eng T.-H., Ling Z.-K., Olson W., McLean C.: Feature-based assembly modeling and sequence generation, Comput. Ind. Eng., Vol. 36, pp. 17-33, 1999.

15. Voutchkov I., Keane A., Bhaskar A., Olsen T.M.: Weld sequence optimization: the use of surrogate models for solving sequential combinatorial problems, Computer Methods in Applied Mechanics and Engineering, vol. 194, pp. 3535–3551, 2005.

16. Sasaki Y., Sonda M., Ito K.: Development of a computer-aided process planning system based on a knowledge base, Journal of Marine Science and Technology, Vol. 7, pp. 175-179, 2010.

17. Bonneville F., Perrard C., Henrioud J.M.: A genetic algorithm to generate and evaluate assembly plans, IEEE Symposium on Emerging Technology and Factory Automation, Vol. 2, pp. 231–239, 1995.

18. Chen & Liu Chen S.F., Liu Y.J.: An adaptive genetic assembly-sequence planner, Int J Comput Integr Manuf, Vol. 14(5), pp. 489–500, 2001.

MOST WIEDZY Downloaded from mostwiedzy.pl

19. Seo Y., Sheen D., Kim T.: Block assembly planning in shipbuilding using case-based reasoning. Expert Systems with Applications, Vol. 32, pp. 245–253, 2007.

20. Qu S., Jiang Z., Tao N.: An integrated method for block assembly sequence planning in shipbuilding, The International Journal of Advanced Manufacturing Technology, Vol. 69 (5-8), pp. 1123–1135, 2013.

21. Zhong Y., Xue K., Shi D.: Assembly unit partitioning for hull structure in shipbuilding, Computer- Aided Design, Vol. 45(12), pp. 1630–1638, 2013.

22. Iwańkowicz R.: An efficient evolutionary method of assembly sequence planning for shipbuilding industry, Assembly Automation, Vol. 36(1), pp. 60-71, 2016.

23. Iwańkowicz R.: Optimization of assembly plan for large offshore structures, Advances in Science and Technology – Research Journal, Vol. 6(16), pp. 31-36, 2012.

24. Iwańkowicz R., Taraska M.: Self-classification of assembly database using evolutionary method, Assembly Automation, Vol. 38(1), 2017.

CONTACT WITH THE AUTHORS

Iwańkowicz Remigiusz
Urbański Tomasz
Graczyk Tadeusz

Taraska Michał
e-mail: michal.taraska@zut.edu.pl

West Pomeranian University of Technology in Szczecin
Faculty of Maritime Technology and Transport
Al. Piastów 41
70-065 Szczecin
Poland

MOST WIEDZY Downloaded from mostwiedzy.pl

POLISH MARITIME RESEARCH Special Issue 2018 S1 (97) 2018 Vol. 25; pp. 134-144
10.2478/pomr-2018-0034

ASSESSMENT OF TECHNOLOGICAL USEFULNESS OF PANEL PRODUCTION LINE IN SHIPBUILDING PROCESS

Tomasz Urbański[1]
Tadeusz Graczyk[1]
Michał Taraska[1]
Remigiusz Iwańkowicz[2]
[1] West Pomeranian University of Technology in Szczecin, Poland
[2] Maritime University of Szczecin, Faculty of Transport Engineering and Economics, Poland

ABSTRACT

This paper presents assessment of technological usefulness of panel production line in prefabrication process of large ship hull sections, in which special attention is paid to producibility of welding operations. Basing on the assessment these authors worked out hierarchy of analyzed sequences of welding technological processes as well as production line stands used for the processes. The assessment was performed on the basis of analysis of a concept of panel production line based on real production lines functioning in shipbuilding industry, as well as technical documentation of typical hull sections of a multi-purpose ferry. The presented analysis took into account impact of technological - constructional parameters onto producibility of welding process of prefabricated sections. Among these parameters the following were numbered: mass of the sections and number of their elements, total length of welds, labour consumption, material consumption as well as linear heat input in welding operations. On the basis of the achieved results, places which worsen effectiveness of production line operation were identified, as a result it was possible to formulate proposals for modernization of flow prefabrication line for hull sections.

Keywords: panel production line, welding technology, SAW, SAW-tandem, GMAW-tandem, FCAW, ship hull

MOST WIEDZY Downloaded from mostwiedzy.pl

INTRODUCTION

Contemporary hulls of sea-going ships are large spatial bodies assembled with several dozen and often more than a hundred (sometimes even several thousand) structural sections of different types. Despite of geometrical diversity between particular structural modules resulting mainly from a given type of ship and region of structure, the main component of every large-size ship hull section is a flat stiffened panel. Therefore prefabrication of stiffened panels conducted usually on a special production line being a part of flow production system constitutes very important element of production process in every shipyard.

The production line used for prefabrication of thin-walled flat sections (PPL - panel production line) is a compact technological line composed of assembly stands and welding stands.

The panel production line makes it possible to produce complete stiffened panels which are the basis for structural modular sections as well as blocks to be used in subsequent stages of ship hull prefabrication process.

Worth remembering that joining the prefabricated technological subassemblies (during flow production of stiffened panels) as well as sections and blocks can be performed efficiently only in the case of obeying an appropriate assembly plan [1], [2].

Ships in production of which the panel production lines suit ideally are those of hulls with many flat surfaces, for instance: ferries (passenger and passenger-car ones), Ro-Ro ships, Con-Ro multi-purpose ships (Fig. 1 shows an exemplary assembly plan of such ship). Hulls of the above mentioned very special types of ships are produced with regime of narrowed tolerances, on account of, a. o., large number of additional outfitting elements. Hence for their building, technological

usefulness of panel production line becomes especially important as it directly impacts subsequent technological processes.

Technological usefulness of the production line is directly associated with the notion of producibility of welded structures, which, through rational selection of factors influencing production process, has to provide structure with required quality at possibly lowest expense of production resources and time [3], [4]. This is especially important for prefabrication of a large number of flat sections which, in case of the ship shown in Fig. 1, amounts to several hundred.

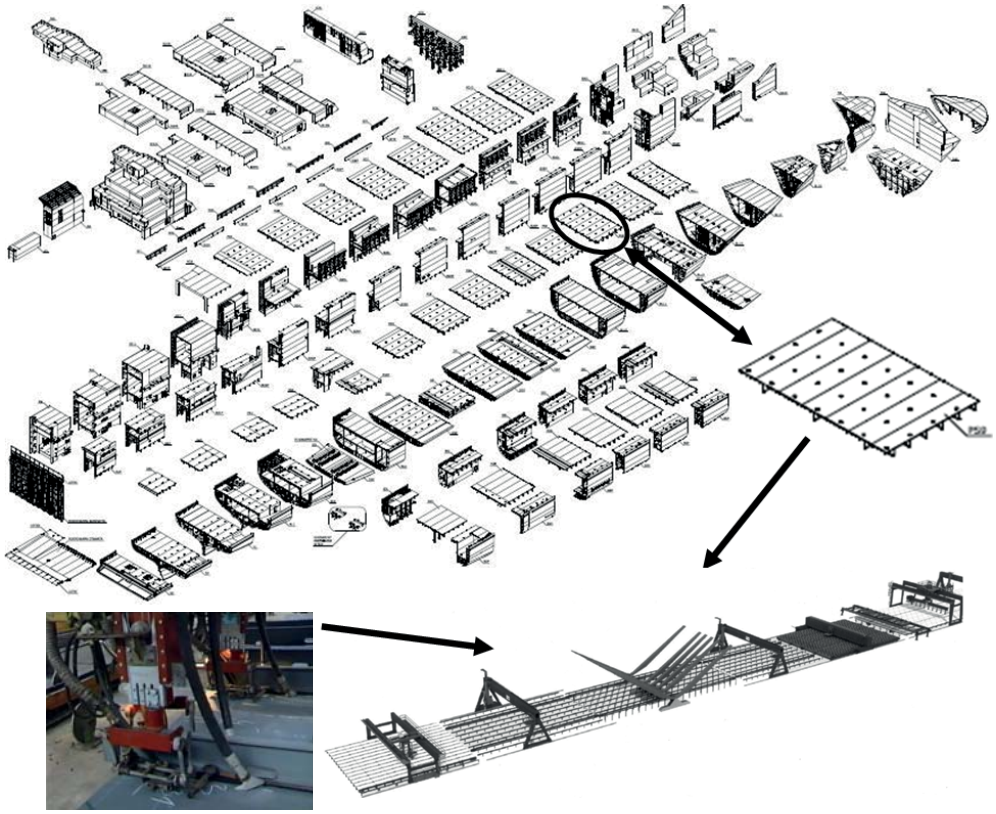

Fig. 1. Expanded isometric drawing of hull structure of a Con-Ro multi-purpose ship and a model of flow production line of flat sections (panels)

Therefore, welding operations are crucial from the point of view of PPL effectiveness as they decide on capacity of the whole prefabrication line. For this reason the presented paper is focused on analyzing four sequences of systems of welding technological processes as well as, consequently, on identifying neuralgic areas of the PPL (i.e. those impairing its capacity). Worth remembering that the assessment of all aspects associated with PPL functioning is a complex and difficult issue as it requires to look at the issue form many points of view, not only from that of welding processes (but also assembling and correcting processes – mainly straightening operations, as well as economic aspects associated with all the above mentioned processes) in order to increase objectivity of such assessment as much as possible. Hence an attempt to do such a complex look requires separate analyses. As it seems to be rather wide issue this paper has been limited to presentation of an analysis dealing with welding technologies only.

For the analysis a flow production line based on the concept of real panel production lines today functioning in shipbuilding industry on which typical ship-hull two-stiffener sections can be prefabricated, was selected.

The below described configuration of the panel production line as well as welding technologies used on it were selected on the basis of available subject-matter literature dealing with production of welded joints, e.g. [5] ÷ [10] (including issue of mechanized welding stands), analysis of welding technology procedures, e.g. [11], [12], supported by expert knowledge and industrial experience.

The proposed configuration consists of seven main stands (see Fig. 2a), namely:
1 – stand for assembling plate sheets,
2 – stand for welding butt joints in plates,
3 - stands for assembling 1st order stiffeners fitted with the use of turntable,
4 – stand for welding 1st order stiffeners,
5 – stand for assembling 2nd order stiffeners,
6 - stand for welding 2nd order stiffeners,
7 – stands for finishing (i.e. assembling and welding of remaining elements of panel) as well as appropriate acceptance procedures.

The used nomenclature dealing with degree of the order of panel stiffeners results from technological procedure where assembling sequence of stiffeners during prefabrication of panels decides on a rank of stiffener order. Hence, flat bars,usually bulb-flats, are considered 1st order stiffeners, and web plates and frame flanges – 2nd order stiffeners.

Worth remembering that number of stands of panel production line may be either lowered or increased depending on scale of production, types of sections as well as degree of process mechanization, e.g. by adding two additional stands, namely:

- A panel turn-over stand – applied in case when one-side welding technology is not sufficient for the designed shell plates. The stand should be fitted with e.g. turn-over scaffolding for plate sections (called also panel turntable) or a gantry crane fitted with special equipment;
- A stand for panel preparation to assembling stiffeners. Such stand should be equipped with a multi-purpose automatic gantry for: shot- peening, lofting as well as panel's outline cutting.

MOST WIEDZY Downloaded from mostwiedzy.pl

The following technologies for producing welded joints were selected:

- SAW or SAW -tandem system – for plate butt welding (SAW - Submerged arc welding with wire electrode, [14]),
- SAW or GMAW (both in tandem system) – for welding 1st order stiffeners (GMAW - Gas-shielded Metal Arc Welding, [14]). In the analyzed case MAG technology (MAG - Metal-arc active gas welding, [14]) was used.
- FCAW – for welding 2nd order stiffeners as well as stiffening-up elements (FCAW - Flux-cored wire metal-arc welding with active gas shield, [14]),

which constitute components of sequences of analyzed welding technology systems used in panel production line (see Fig. 2b), as presented in Tab. 1.

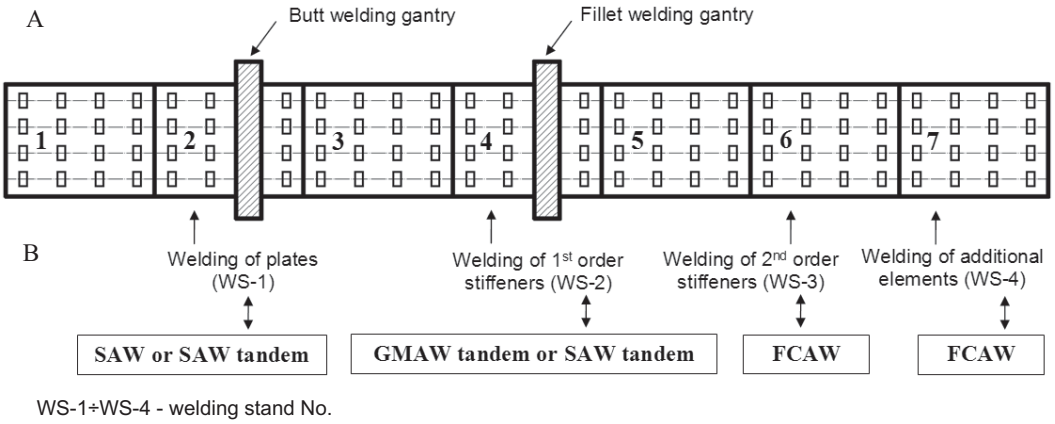

Fig. 2. Main stands - components of panel production line (A) acc. [13] with marked welding stands and technologies (B) subjected to analysis.

Tab. 1. Sequences of analyzed welding technology systems used in panel production line

Sequence No.	Welding stand No. (see Fig. 2B)				
	WS-1	WS-2	WS-3	WS-4	
1	SAW	GMAW tandem	FCAW	FCAW	Welding technology
2	SAW	SAW tandem	FCAW	FCAW	
3	SAW tandem	GMAW tandem	FCAW	FCAW	
4	SAW tandem	SAW tandem	FCAW	FCAW	

ANALYSIS OF WELDING TECHNOLOGIES USED IN PANEL PRODUCTION LINE

The analysis is aimed at presentation of possible utilization of technological – constructional parameters of flat sections as well as parameters of welding processes for assessing the technological usefulness of panel production line and hence possible interference into flow production system of stiffened panels.

The analysis was worked out on the basis of simulations carried-out with making use of the assumed sequences of welding technology systems (see Tab. 1), and the above mentioned crucial parameters among which the following were numbered:

- technological-constructional parameters of sections: their masses, number of elements, number and length of welds, as illustrated in Fig. 3,
- technological parameters of welding processes: welding parameters together with technical details of preparation of welds, as exemplified for selected welding technologies in Fig. 4 and Tab. 2.

The above specified parameters of welding processes are in compliance with the requirements of rules of ship classification institutions technological procedures approved by the institutions and being in force in the shipyard, i.e., for instance: [11], [12], as well as technological standards concerning the use of additional materials (being in line with a. o. [15]).

20 typical two-row stiffened panels (having also additional elements such as stiffening-up brackets, flat bars etc) of the multi-purpose ferry were selected for the analysis. The sections were so selected as to get their geometrical variety as large as possible, e.g.: the minimum dimensions (i.e. length x breadth) of welded sheets amounted to 4500x5000 mm, and maximum ones to 12600x11900mm. The analyzed sections (see Fig.3 A) were hierarchically ordered, regarding their masses, beginning from the smallest up to the greatest value. The hierarchy is kept in all subsequent drawings of this paper (i.e. Section No.1 is that of the smallest mass, whereas Section No. 20 – of the greatest mass). Basic quantitative absolute and percentage relations for the analyzed sections are given in Fig. 3. They were worked out on the basis of technical documentation of typical sections of a multi-purpose ferry, which were made available by one of Polish shipyards. Length of welds shown in Fig. 3E and 3F is the total length from the technological point of view, i.e. that which takes into account number of welding seams.

MOST WIEDZY Downloaded from mostwiedzy.pl

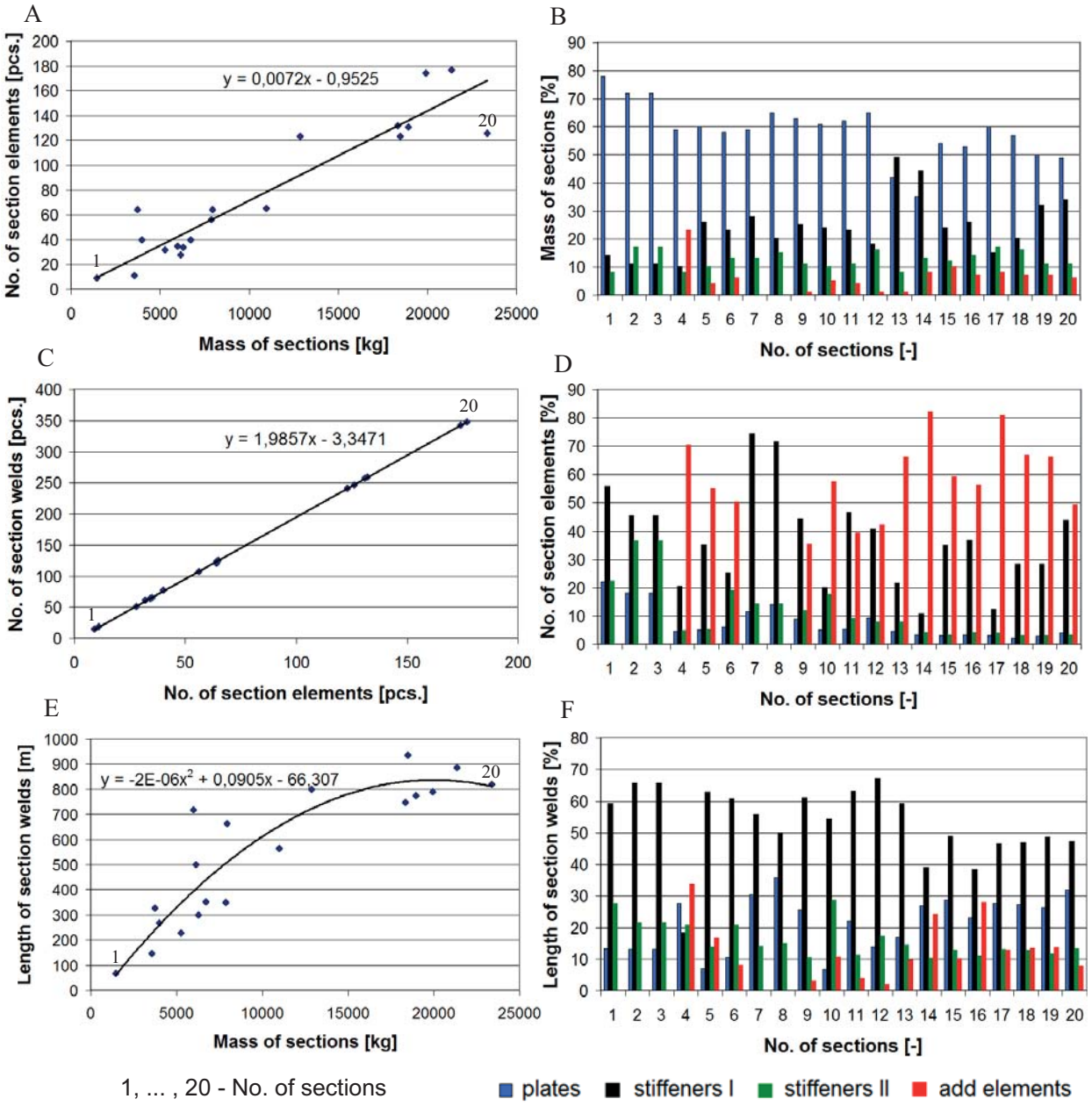

Fig. 3. Basic quantitative absolute and percentage relations for the analyzed sections:
A – mass of sections versus number of their elements,
B – mass of particular groups of welded elements related to mass of sections,
C – number of section elements versus number of welds,
D – number of particular groups of welded elements related to number of section elements,
E – mass of section versus length of welds,
F – length of welds in particular groups of elements related to total length of section welds

MOST WIEDZY Downloaded from mostwiedzy.pl

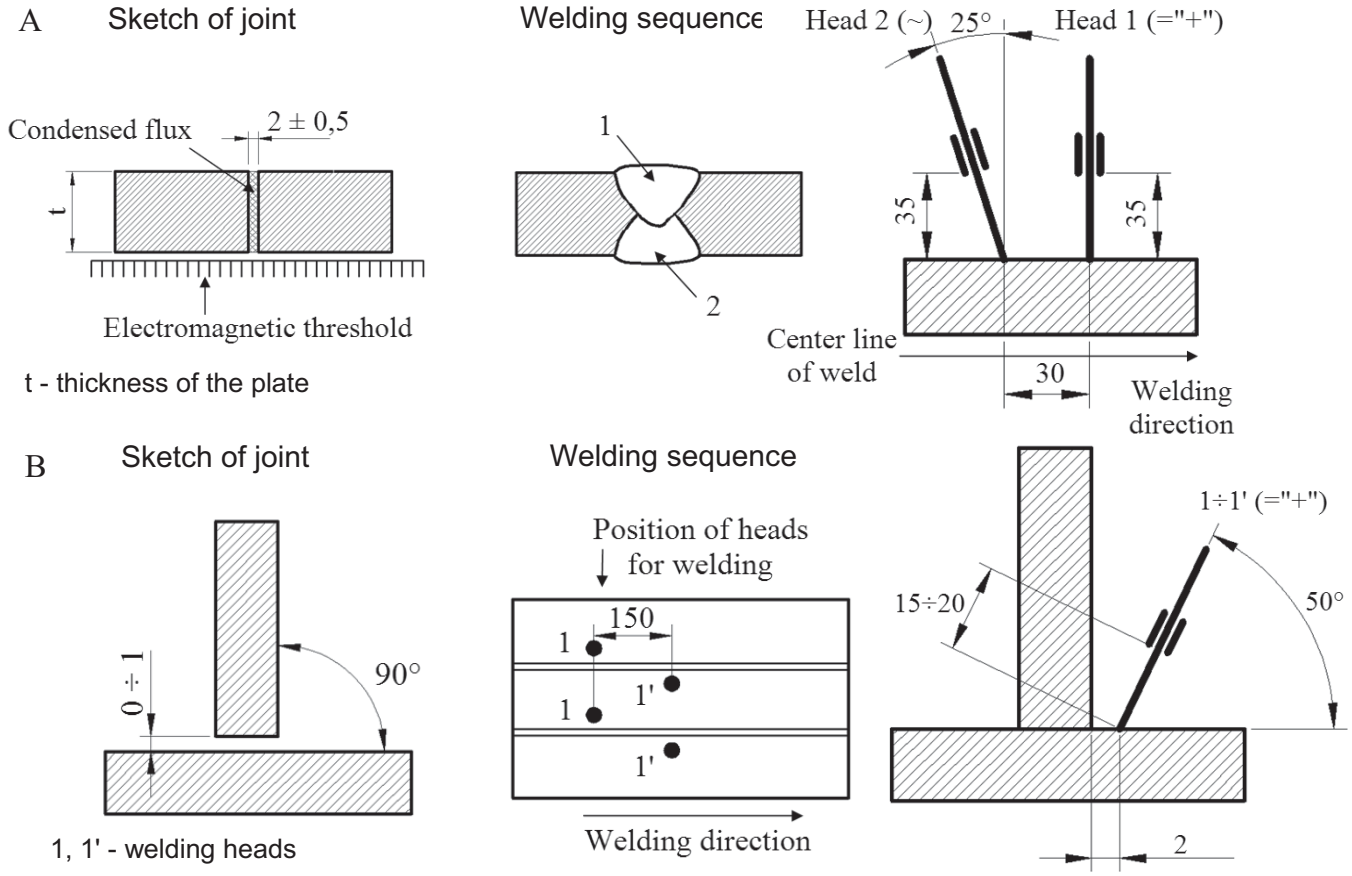

Fig. 4. Details of preparation of elements to welding with the use of SAW-tandem technology:
A – butt joint with butt weld,
B – T–joint with fillet weld (acc. [12])

Tab. 2. Examples of technological parameters for analyzed welding technologies (acc. [11], [12])

Run No.*	Thickness [mm]	Dimension of filler material [mm]	Current [A]	Voltage [V]	Welding speed [cm/min]	Remarks
SAW (butt weld)						
1	8 (*1)	4,0	420 ÷ 450	33 ÷ 35	58 ÷ 65	–
2			530 ÷ 550	33 ÷ 35	60 ÷ 70	
SAW-tandem (butt weld)						
1	10 (*1)	5,0	650 ÷ 670	31 ÷ 32	95 ÷ 110	welding head 1 (*3)
			580 ÷ 600	40 ÷ 41	95 ÷ 110	welding head 2 (*3)
2			600 ÷ 620	31 ÷ 32	90 ÷ 100	welding head 1 (*3)
			550 ÷ 570	40 ÷ 41	90 ÷ 100	welding head 2 (*3)
SAW-tandem (fillet weld)						
1	5 (*2)	2,0	380 ÷ 400	32 ÷ 33	40 ÷ 50	welding head (*3)
1'			400 ÷ 420	33 ÷ 34	40 ÷ 50	welding head (*3)
GMAW-tandem (fillet weld)						
1	5 (*2)	1,6	250 ÷ 270	34 ÷ 36	80 ÷ 120	–
1'			250 ÷ 270	34 ÷ 36	80 ÷ 120	–
FCAW (fillet weld)						
1	4 (*2)	1,2	255 ÷ 260	27 ÷ 28	18 ÷ 24	–

Symbols:
* – Run No. complying with Fig. 4; *1 – Thickness of the plate; *2 – Thickness of the fillet weld; *3 – complying with Fig. 4

MOST WIEDZY Downloaded from mostwiedzy.pl

Comparing the relations presented in Fig. 3 one can state that:

- the greatest percent share in mass of the sections was attributed to shell plating - it amounted on average to abt.. 58%, and the lowest share – to additional elements: abt. 5% on average (see Fig. 3B).
- there is a linear relation between number of section elements and number of welds (see Fig. 3C). The largest percentage of number of elements was found for 1st order stiffeners (see Fig. 3D): (abt. 37%on average) and additional elements (abt. 44%on average), the smallest percentage - to shell plates (abt. 8%on average). Section No. 19 had the largest number of elements (Fig. 3A), namely 177 pcs. Section No. 1 had the smallest number of them, only 9 pcs.
- the largest percentage of weld length (Fig. 3F) was found for 1st order stiffeners (abt. 53% on average), the smallest (abt. 10% on average) – for additional elements. Section No. 16 (Fig. 3E) had the largest length of welds equal to 935 m. The smallest weld length of 68 m was found for Section No. 1.

ASSESSMENT OF TECHNOLOGICAL USEFULNESS

The assessment of technological usefulness of panel production line was performed on the basis of results of analysis of welding technologies by taking into consideration the so called significant parameters obtained with the help of input parameters to this analysis. Among the significant parameters used for the technological usefulness assessment the following were numbered: labour consumption for welding the sections, welding wire consumption as well as linear heat input of welding process.

All the significant parameters greatly influence operational performance of flow production line of ship hull flat sections and are associated with the notion of producibility of welded structures (see: [3], [4]), i.e.:

- labour consumption for welding the sections is directly depending on duration time of welding the sections and on their masses [6],
- welding wire consumption which was selected as one of the factors of material consumption index [6] and is present in all welding operations of every sequence, directly impacts outlays onto production means.
- welding process linear heat input which, out of the all above mentioned assessment parameters, is most connected (however not directly) with influence on required quality of structure. The heat input is one of the crucial factors of welding process which impacts magnitude of deformations of welded structures, [16] ÷ [18], that makes application of corrective treatments (mainly strengthening operations) necessary. The treatments significantly rise labour expenditure for manufacturing the structures. As estimated, various repair operations done on the section assembly line consume about 30% of all labour amount expended for ship hull structure building [19] (i.e. that comparable with percentage of labour time consumed for hull structure welding in relation to total ship building time [20]).

Results of the performed assessment, grouped into absolute value sets (for all sequences of welding technologies) as well as percentage value sets (split according to particular stands of the production line and used welding technologies) are given in Fig. 5 ÷ 9.

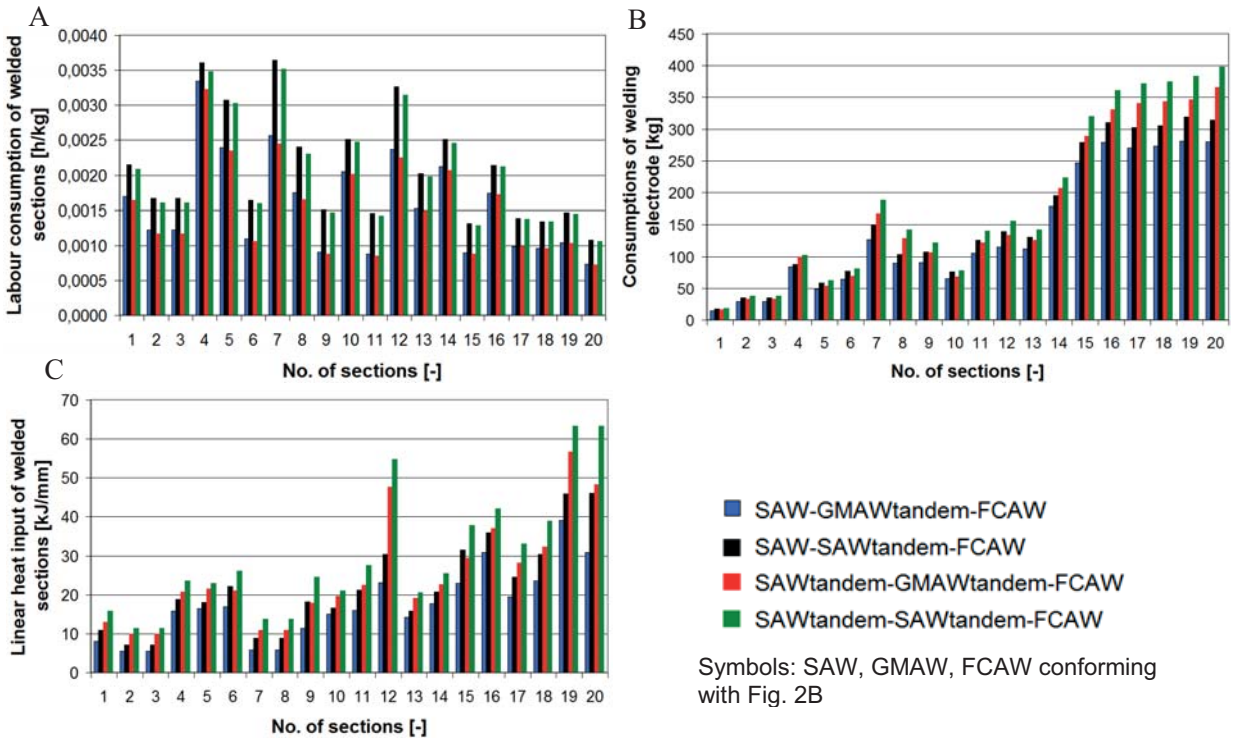

Fig. 5. Sets of absolute values of the selected performance parameters of panel production line, i.e.: A – welding labour consumption, B – welding wire consumption, C – linear heat input, for the assessed welding technologies used on the panel production line

MOST WIEDZY Downloaded from mostwiedzy.pl

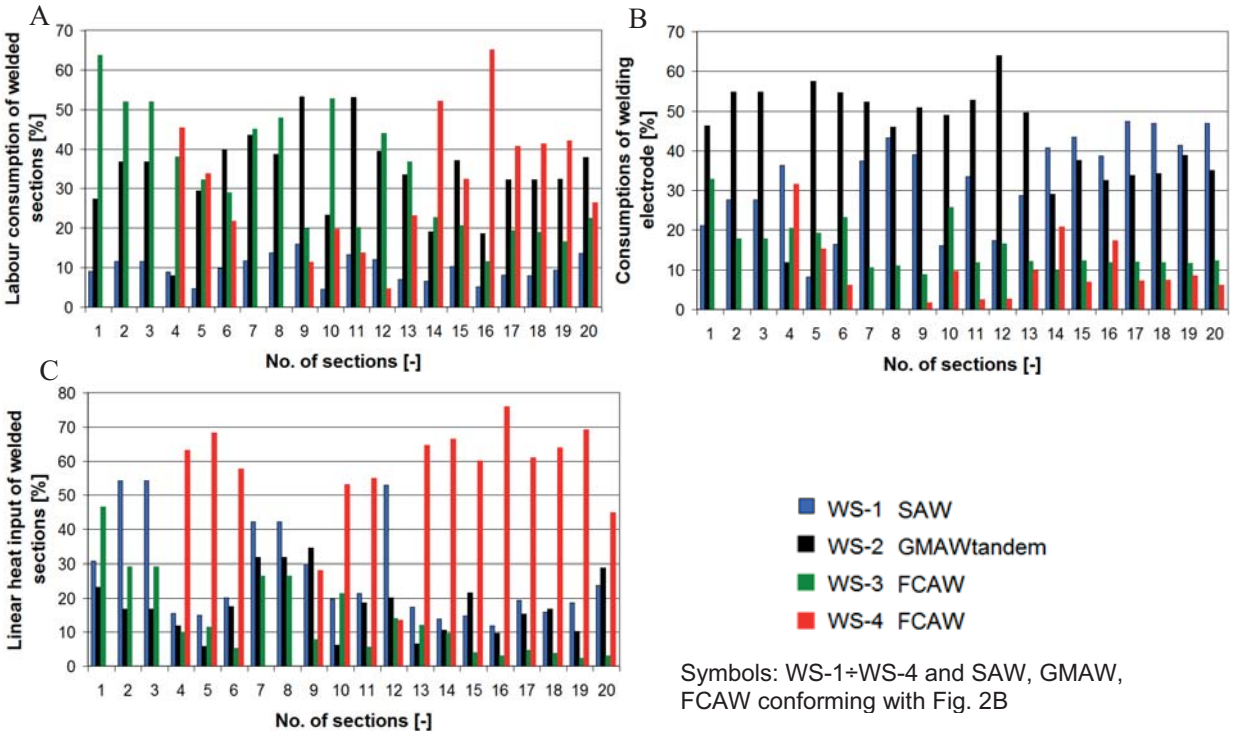

Fig. 6. Sets of percentage values of the selected performance parameters of panel production line, i.e.: A – welding labour consumption, B – welding wire consumption, C – linear heat input, for the particular welding stands of the production line in the sequence: SAW-GMAWtandem-FCAW.

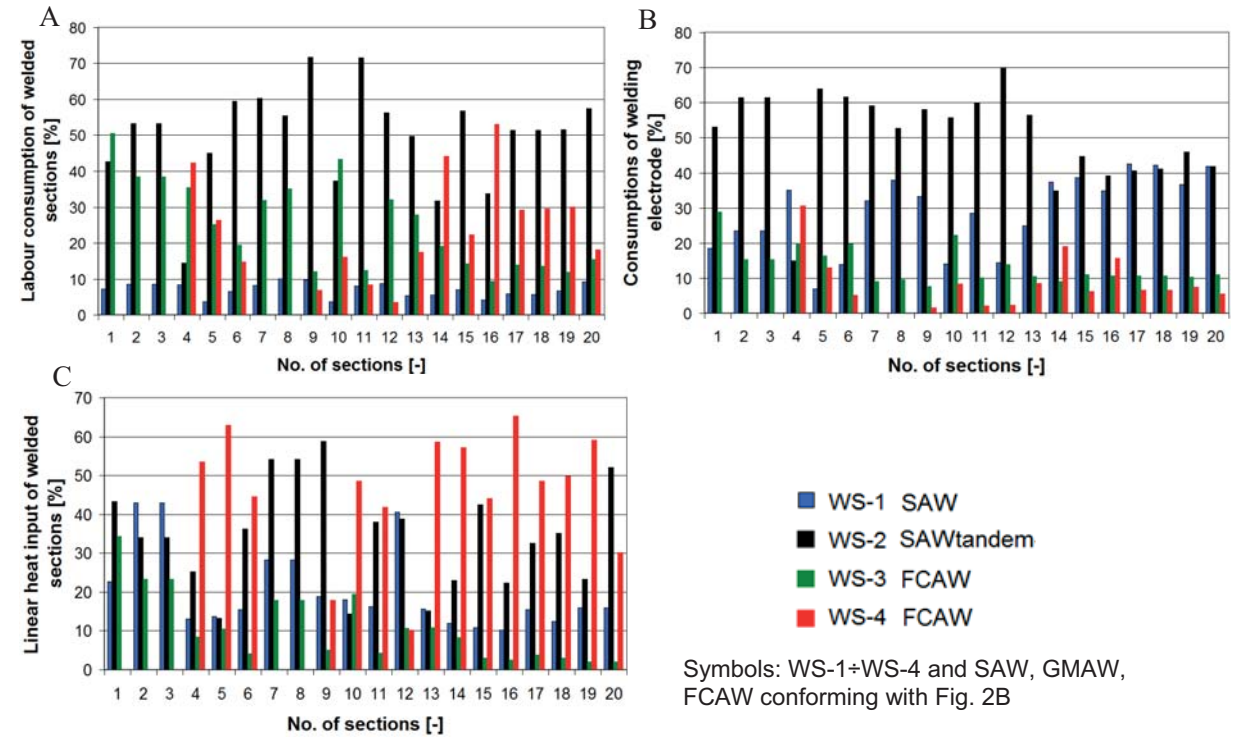

Fig. 7. Sets of percentage values of the selected performance parameters of panel production line, i.e.: A – welding labour consumption, B – welding wire consumption, C – linear heat input, for the particular welding stands of the production line in the sequence: SAW-SAWtandem-FCAW

MOST WIEDZY Downloaded from mostwiedzy.pl

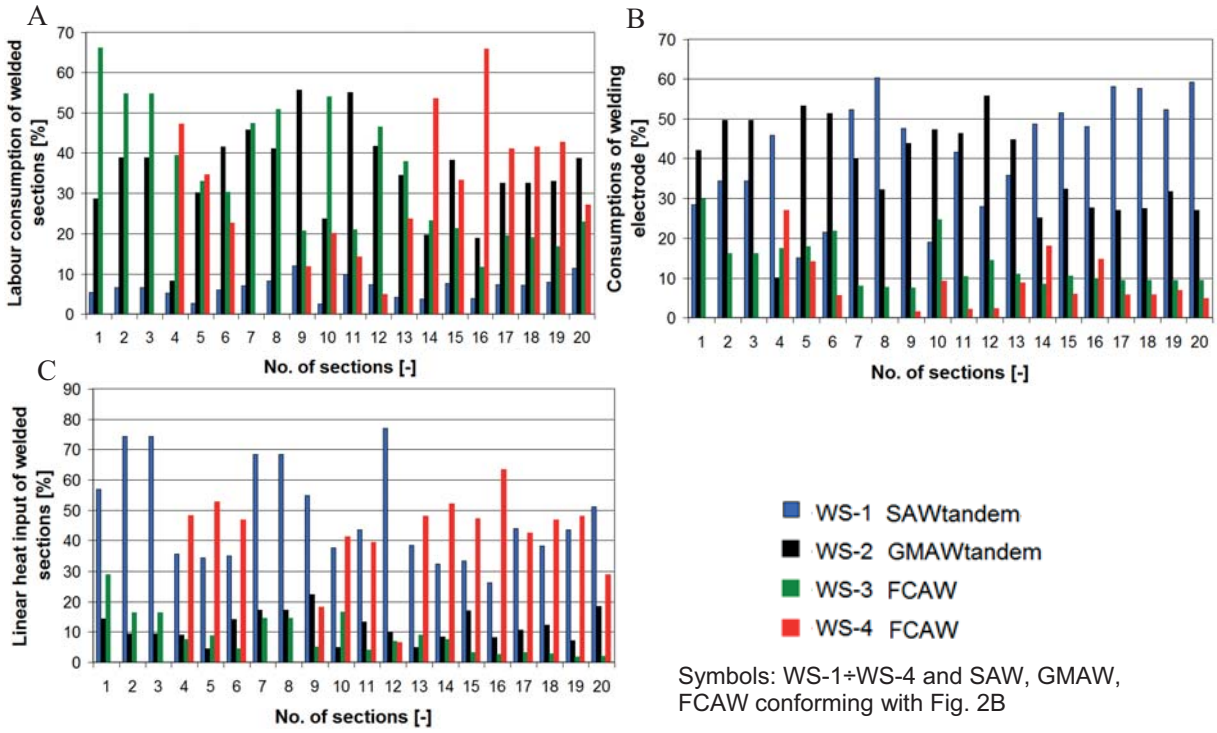

Fig. 8. Sets of percentage values of the selected performance parameters of panel production line, i.e.: A – welding labour consumption, B – welding wire consumption, C – linear heat input, for the particular welding stands of the production line in the sequence: SAWtandem-GMAWtandem-FCAW.

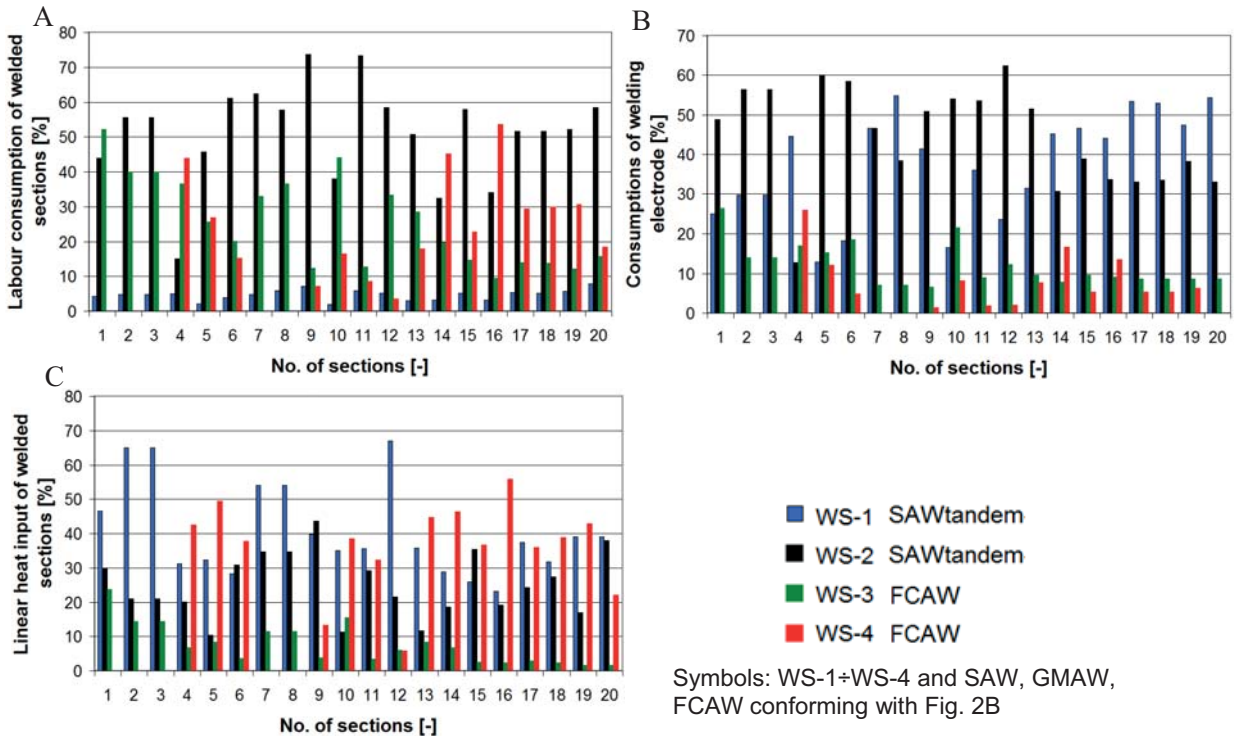

Fig. 9. Sets of percentage values of the selected performance parameters of panel production line, i.e.: A – welding labour consumption, B – welding wire consumption, C – linear heat input, for the particular welding stands of the production line in the sequence: SAWtandem-SAWtandem-FCAW.

MOST WIEDZY Downloaded from mostwiedzy.pl

Comparing quantitative results of the assessment collected for the assumed sequences of welding technologies, shown in Fig. 5, one can observe that:

- growing tendency of labour consumption values is not dependent on increase of mass of sections (Fig. 5A), whereas growing tendencies of: welding wire consumption (Fig. 5B) and linear heat input (Fig. 5C) do depend on it;
- among labour consumption values (Fig. 5A) two distinct group of sequences can be observed: the first in which only tiny differences between particular systems, i.e. the group with the largest labour consumption values – represented by: SAWSAWtandem-FCAW and SAWtandemSAWtandem-FCAW, and the second group of the smallest values - represented by SAWGMAWtandem-FCAW as well as SAWtandemGMAWtandem-FCAW. In both the groups the average difference between labour consumption values equal to 0,0001 [h/kg], which, in the case of the section of the maximum mass (i.e. 23361 [kg]), would be equivalent to 2,3 [h] of its production time, whereas for the section of the minimum mass (i.e. 1444 [kg]) would be as low as 0,14 [h] of its production time. Therefore it was accepted that in a given group every sequence may be considered equivalent;
- the largest labour consumption values were reached for the technologies sequence: SAWSAWtandem-FCAW, and the smallest – for: SAWtandem-GMAWtandem-FCAW (Fig. 5A). The differences in labour consumption values between the sequences were the following: maximum one of 0,0012 [h/kg] for Section No. 7 and minimum one of 0,0004 [h/kg] for Section No. 4 and 14÷20, which in the case of Section No. 7 (having mass of 6000 [kg] and weld length of 717,3 m) is equivalent to 7,2 [h] difference in the section's production time. The generally largest value of labour consumption was noticed in the case of Section No. 7 (i.e. 0,0036 [h/kg]), the smallest – for Section No. 20 (i.e. 0,0007 [h/kg]);
- the largest values of welding wire consumption as well as linear heat input were found for the technologies sequence: SAWtandemSAWtandem-FCAW, whereas the smallest ones for: SAW-GMAWtandem-FCAW (see Fig. 5B and 5C);
- the differences between the above mentioned sequences of technologies in welding wire consumption increase most distinctly in the case of the sections with the largest mass values (see Fig. 5B). The differences amount to: 3,5 [kg] at the minimum (for Section No.1), 118 [kg] at the maximum (for Section No. 20), the average difference amounts to abt. 47 [kg],
- like in the above discussed case, the differences in linear heat input values are as follows (see Fig. 5C): 5,77 [kJ/mm] at the minimum (for Section No. 2), 32,5 [kJ/mm] at the maximum (for Section No. 20), the average difference was equal to abt. 12 [kJ/mm].

Moreover, comparing the percentage values resulting from the assessment which were split into particular welding stands of the production line, shown in Fig. 6 ÷ 9, one is able to observe that:

- the largest labour consumption values were achieved on WS-2 stand for the sequences using SAW-tandem technology (see Fig. 7A and 9A); the values amounted on average to abt. 50% of the total welding labour consumption. However for the same sequences the average total labour consumption on WS-3 and WS-4 stand amounted to abt. 40% only;
- the situation is different in the case of the sequences using GMAW-tandem technology on WS-2 stand (see Fig. 6A and 8A), for which the average labour consumption values are the same as for WS-3 stand and equal to over 30%. Whereas the average total labour consumption on WS-3 and WS-4 stands amounts to abt. 60% for the cases in question;
- the smallest labour consumption values were obtained on WS-1 stand for all the technologies sequences (see Fig. 6 ÷ 9), which amounted on average to abt. 10% of the total labour consumption;
- the percentage values of welding wire consumption are obviously largest for automatic technologies, i.e. those used on WS-1 and WS-2 stands (see Fig. 6 ÷ 9), where they amounted on average to abt. 80% (of total value);
- values which are crucial from the point of view of impact of linear heat input on to post-welding deformations were obtained for the stands on which long continuous welds are made, i.e. WS-1 and WS-2 stands (see Fig. 6 ÷ 9). Hence, on the stands, especially on WS-2 one, one can expect largest deformations which directly impair quality of structures. Admittedly, in some cases (see: Fig. 6C and 7C), the average linear heat input values (on the level of 40% of their total values) were obtained on WS-4 stand, however it should be remembered that on this stand welds really in large number, but short ones, is produced. Moreover, in this final stage of prefabrication the sections reveal rather high stiffness and much lower tendency to deformations than in the initial stages of the process.

On the basis of the presented results (see Fig. 5) as well as conclusions drawn from them it was stated that the most favourable sequence of welding technologies was the following: SAW-GMAWtandem-FCAW (see Tab. 1). The remaining sequences take positions in the order shown in Tab. 1, forming this way a hierarchy of welding technologies sequences from the point of view of their impact onto producibility of welded structures.

Similarly, on the basis of an analysis of the results presented in Fig. 6 ÷ 9, a hierarchy of welding stands was made from the point of view of their impact onto the production line performance (effectiveness).

One of the crucial conclusions resulting from the analysis was that the largest drop in capacity of the production line was caused by semi-automatic welding processes carried out on the stands: WS-3 and WS-4 (see Fig. 2A and Tab. 1). This is most clearly seen when the total labour consumption values obtained for the stands are taken into account; the values may be equal to over 60% of the total labour consumption for welding the sections. Therefore the above mentioned stands are the least efficient areas in the entire production line, whereas WS-1 stand is the most efficient.

MOST WIEDZY Downloaded from mostwiedzy.pl

For that reason the following proposals dealing with improvement of the performance (effectiveness) of the flow production line, have been offered:

- a conventional solution consisting in an increase in number of the stands for semi-automatic welding (i.e. those for welding 2nd order stiffeners and stiffening-up elements),
- an innovative solution consisting in installation of a gantry fitted with highly efficient devices (e.g. articulated robots) for supporting the welding operations on the stand intended for the welding of 2nd order stiffeners.

Following the performed analysis one may assume that e.g. the doubling of semi-automatic welding stands in number will shorten duration time of welding operations by a half at least. However worth remembering that final result of improvement of producibility of the production line will depend in large measure not only on capacity of used facilities, e.g. robots, but first of all on the obeying of an assumed comprehensive technological regime of welding. Analysis of all the above mentioned aspects will constitute an object of future research projects to be conducted by these authors.

CONCLUSIONS

This paper showed that on the basis of technological – constructional parameters of prefabricated sections and technological parameters of welding processes it is possible to make an assessment of flow production line. As the performed analyses indicated, by appropriate selection of significant parameters it is possible to show their impact onto selected aspects of producibility of welded structures.

The presented approach to this issue, based on analysis of significant parameters, may be applied to any conceptual variant of production line for flat sections of ship hull. Moreover, it was indicated which of the assumed sequences of welding technologies and which of the prefabrication line stands are whether the most or least effective. However it should be remembered that, to make full assessment of technological usefulness of a production line, also analyses connected with assembling and corrective operations as well as with economics of processes should be taken into account so as to increase assessment objectivity as much as possible.

BIBLIOGRAPHY

1. Iwańkowicz R. R.: An efficient evolutionary method of assembly sequence planning for shipbuilding industry, Assembly Automation, Vol. 36 (1),, 2016, pp. 60-71

2. Ozkok M.: The effects of matrix module structure on shipyard panel line's throughput, Polish Maritime Research, Vol. 19, No. 3 (75), 2012.

3. Jenney C. L., O'Brien A., ed.: Welding Science and Technology of Welding Handbook. 9th ed., American Welding Society, Miami 2001.

4. Yang Y. P., Brust F. W., Cao Z., Kennedy J. C., Chen X. L., Yang Z., and Chen N.: Weld modeling technology for shipbuilding applications. 6th International Trends in Welding Research Conference Proceedings. Pine Mountain, Ga., 2002, pp. 855–860

5. Gourd L. M.: Principles of Welding Technology. The Welding Institute, London, 1995.

6. Weman K.: Welding processes handbook, Woodhead Publishing Ltd., Cambridge, England 2003.

7. Manz A. F., Hornberger E. G.: Welding processes and practices, John Wiley and Sons. New York 1998.

8. Michaleris P., DeBiccari A.: Predictive Technique for Buckling Analysis of Thin Section Panels due to Welding, Journal of Ship Production,, November 1996, pp. 269-275

9. Yang Y. P., Castner H., Dull R., Dydo J., Fanguy D.: Uniform-panel weld shrinkage data model for neat construction ship design engineering, Journal of Ship Production and Design, Vol. 29(1), February 2013, pp.1-16

10. Yang Y.P., Castner H., Dull R., Dydo J., Huang T.D., Fanguy D., Dlugokecki V., Hepinstall L.: Complex-panel weld shrinkage data model for neat construction ship design engineering. Journal of Ship Production and Design, Vol. 30(1), February 2014, pp.15-38

11. Company standard: T081-02, Gas-shielded arc welding, Part II, Technological instructions for WPS welding (in Polish), Stocznia Szczecińska S.A. 2001.

12. Company standard: T081-03, Automatic shielded arc welding, Part II, Technological instructions for WPS welding (in Polish), Stocznia Szczecińska S.A. 2001.

13. Storch R. L., Hammon C. P., Bunch H. M., Moore R. C.: Ship production, Cornell Maritime Press, Centerville, Maryland USA, 1988.

14. ISO 4063:1990: Welding, brazing, soldering and braze welding of metals - Nomenclature of processes and reference numbers for symbolic representation on drawings.

15. Target project No. 9 T12C 060 97 C/3480 titled: Functional model of designing and building ships in regime of narrowed tolerances (in Polish), Politechnika Szczecińska and Stocznia Szczecińska S.A., 1998-1999.

16. Masubuchi K., Analysis of welded structures: residual stresses, distortion, and their consequences, Pergamon Press, Oxford/New York 1980.

17. Radaj D.: Heat Effects of Welding. 1st ed. Springer Berlin Heidelberg. Berlin 1992.

MOST WIEDZY Downloaded from mostwiedzy.pl

18. Verhaeghe G.: Predictive formula for weld distortion – a critical review, Woodhead Publishing, Abington 1999.

19. Metschkow B., Graczyk T.: Laser welded joints in shipbuilding, Second International Conference on Marine Technology – ODRA 1997, Szczecin 1315 May 1997, ed. Computational Mechanics Publications - Southampton & Boston 1997.

20. Misra S. C: Design Principles of Ships and Marine Structures, Taylor & Francis Group. New York 2016.

CONTACT WITH THE AUTHORS

Tomasz Urbański
e-mail: tomasz.urbanski@zut.edu.pl

West Pomeranian University of Technology in Szczecin
Faculty of Maritime Technology and Transport
Al. Piastów 41
70-065 Szczecin
Poland

Remigiusz Iwańkowicz

Maritime University of Szczecin
Faculty of Transport Engineering and Economics
1-2 Wały Chrobrego St.
70-500 Szczecin
Poland

MOST WIEDZY Downloaded from mostwiedzy.pl

POLISH MARITIME RESEARCH Special Issue 2018 S1 (97) 2018 Vol. 25; pp. 145-150
10.2478/pomr-2018-0035

LABORATORY TEST RIG FOR EXAMINING AGGREGATE MINING FROM SEABED USING THE AIRLIFT METHOD

Czesław Dymarski
Tomasz Pająk
Gdańsk University of Technology, Poland

ABSTRACT

The use of the Airlift method for transporting the mined aggregate from the seabed to the deck of the mining ship is an alternative for presently used solutions, such as suction pumps or scoop transport for instance. Building the laboratory test rig was preceded by tests in natural conditions. The rig was designed in such a way as to model these conditions as close as possible, and to have potential for further development.

Keywords: Airlift method, Airlift test rig, deep-level mining

MOST WIEDZY Downloaded from mostwiedzy.pl

INTRODUCTION

The Airlift method makes use of gas as the carrier of energy converted to the work of water and aggregate transport. In previous tests, performed in natural conditions, pure oxygen was used for this purpose but it will be replaced with air in model tests.

For the purpose of solid substance transport, the flows in vertical pipelines can be divided, based on the criterion of the number of flowing phases, into two- or three-phase gas-water-aggregate mixtures. Initially, the two-phase mixture was examined to determine the flow velocity of the liquid medium. This parameter value was needed for defining initial operating conditions of the examined device in the mathematical model. An attempt was made to assess the effect of gas fraction change in the liquid phase volume, and to determine minimal gas amounts needed to start aggregate mining at a given level. Then, tests were performed with the three-phase mixture to determine the effect of water flow velocity and gas pressure on the mining rate of the aggregate of known granulation and shape from a given depth.

Fig. 1 presents examples of different flows in the water-air mixture. They differ by the course of gas phase extension, the task of which is to create the mixture velocity which will be able to generate sufficiently large resistance on aggregate grains to elevate them up. This task is best reached in the first type of flow, i.e. the bubble flow, for which the contributions of gas fraction and liquid fraction are close to each other along the entire length of the vertical pipeline segment. Other flow types: annular flow, slug flow, and churn flow can be a source of differences between results recorded for the same operating parameters. These types of flow are unfavourable for effective elevation of the mined aggregate. One of the planned research tasks will be determining conditions which ensure obtaining the most favourable flow.

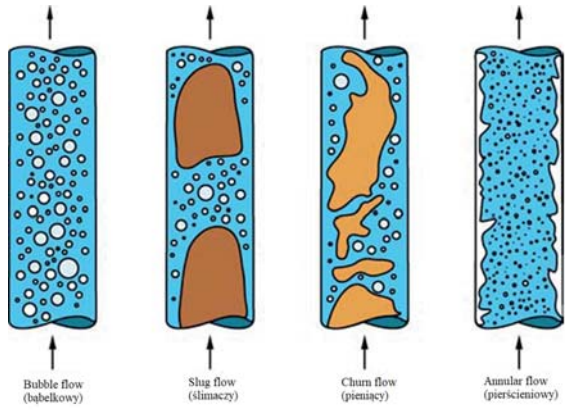

Fig. 1. Types of flows in vertical pipelines [1]

In the case of three-phase flows, the flow of gas and liquid looks similar. Three- measurement series are planned to measure the output of the elevated aggregate for operating conditions differing by various parameters, including:

- air flow rate,
- granulation of the elevated gravel,
- elevation height,
- distance of the mining head from the aggregate,
- distance of the air delivery point to the mining head.

As a result, operating efficiency characteristics will be worked out as functions of the above parameters. The results of these tests will make it possible to verify the developed mathematical models and the associated computer codes.

BUILDING THE LABORATORY TEST RIG

The test rig consists of three units. The first unit comprises a lower tank having the form of vertical cylinder presented in Figs. 2 and 3.

In this unit, the following elements can be named:

1 – base, made of stainless steel,
2 – pipe of ø400mm in diameter, made of PMMA (polymethylmethacrylate),
3 – cover, made of stainless steel,
4 – extension with flange, made of stainless steel,
5 – mining pipe of ø50mm, made of PMMA,
6 – return pipe of ø100mm, made of PMMA,
7 – O-ring type seals,
8 – M6 bolts made of zinc covered material,
9 – M10 pins made of stainless steel.

The cover and the base are screwed together with 8xM10 pins and relevant nuts with washers. Moreover, to ensure tightness between the stainless base and cover on the one hand, and the pipe made of PMMA on the other hand, use was made of polyurethane adhesive sealing mass APP – PU 50.

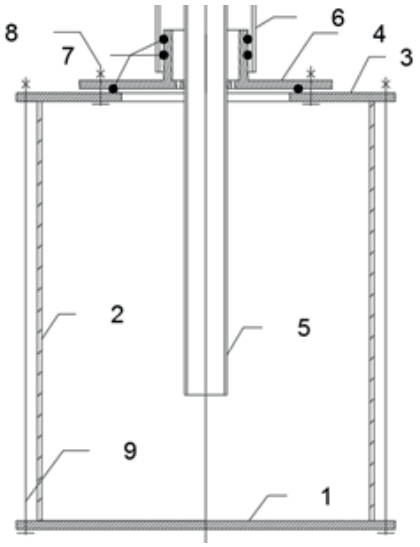

Fig. 2. Lower tank cross section

Fig. 3. View of lower tank

Ball valves mounted in the base and in the cover can be easily connected via a quick-release coupling to the water supply pipe or to the drain pipe to deliver water to or remove it from the lower tank and the entire system.

The system consisting of cover 3 and extension 4 with flange is intended to provide opportunities for rig development. A hole of ø250mm in diameter is made in the cover 2 to allow testing of mining pipes of up to ø200mm. The space between these pipes should allow water to return to the lower tank. Tightness was obtained by the O-ring seal and pressing of the extension flange to the cover 3 with 6xM6 bolts.

MOST WIEDZY Downloaded from mostwiedzy.pl

Fig. 3 shows the excess part of the hose delivering the air from the internal compressed air system to the mining pipe. The connection point of this hose is situated above the extension 4, at the place where the mining pipe made of PCW is connected with the pipe made of PMMA (5).

In the upper part of the system, a tank made of PMMA is situated, see Fig. 4. Aggregate and water are transported to this tank. It comprises the following elements:
1 – container made of PMMA,
2 – crown cap with holes, made of PCW,
3 – mining pipe made of PCW.

Tight connection between the container 1 and the crown cap 2 is ensured by acrylic silicone, which at the expected pressures is sufficient to prevent against water losses. Moreover, the return pipe was also sealed with silicone. The container was made of PMMA plates, which were glued together using the acrylic adhesive ACRIFIX. Silicone was also used at each corner of plate connection places.

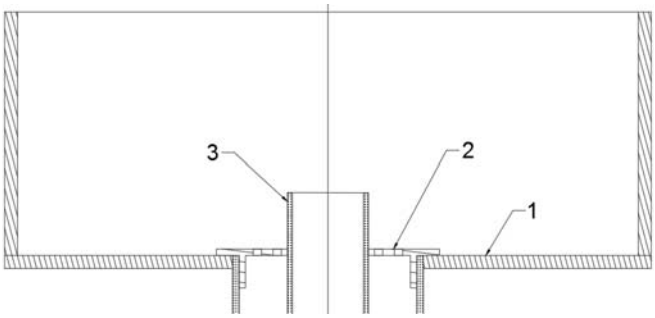

Fig. 4. Upper tank cross section

Both tanks are connected together via two pipelines, i.e. mining and return pipeline made of PCW. A hose which delivers air to the mining head is introduced between these two pipelines. Tightness of all pressed connections is additionally ensured by the use of acrylic silicone.

The measurements are performed using a container with scale, to which the mining pipeline delivers the mixture of water and air with gravel. This way the amounts of the mined gravel and water can be compared at different pressures. It also enables to assess the proportion of gravel in the transported water or, alternatively, the mining time for a given volume and different pressures to define optimal operating conditions.

The laboratory test rig was built based on the experience gained in real tests. Fig. 5 shows the mining output from a pipeline in which we can observe turbulent water 1 and gravel grains 2 of different granulation, while Fig. 6 shows the results of the test performed from the catamaran, at depth of 10m. These tests differed by the mining method. At the platform the gravel was scattered over the bottom, while during mining from the catamaran, a gravel container suspended on strips 3 as used. Water with gravel was transported via the mining pipeline 4 to the container 5.

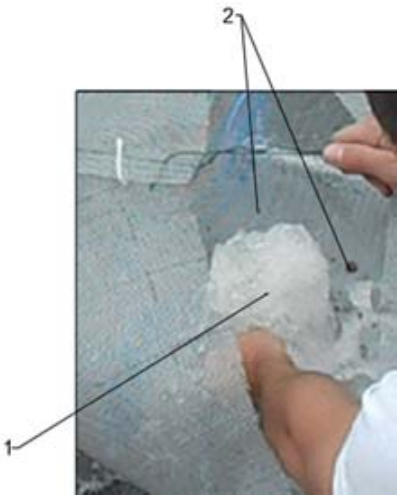

Fig. 5. Photo of mining output from platform

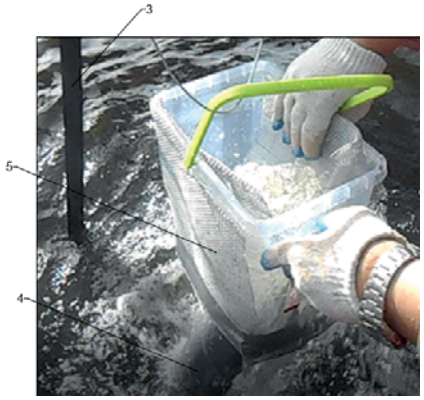

Fig. 6. Photo of mining output from catamaran

Fig. 7 shows the lowered pipe which sucks gravel from the prepared basket and sand from the water region bed. The tests were performed from a boat, on the water region of 8m in depth.

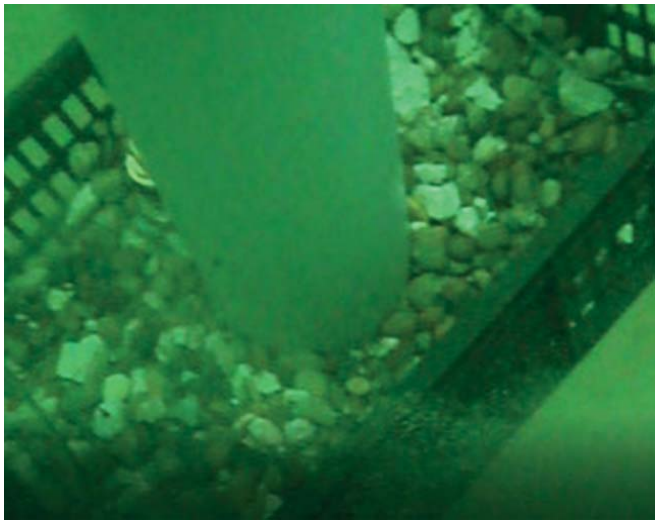

MOST WIEDZY Downloaded from mostwiedzy.pl

Fig. 7. Photos taken by diver

OPERATING CONDITIONS AVAILABLE ON THE RIG

Model test were performed in the laboratory owned by the Faculty of Ocean Engineering and Ship Technology, Gdansk University of Technology. The maximal available height for these tests is approximately equal to 8 m. The maximal pressure available in the laboratory compressed air installation is 800 kPa, which is fully sufficient for model tests. There is also a possibility to analyse the effect of the quality of liquid medium, i.e. salt or fresh water, as well as to perform tests with a pipeline inclined at an angle, to analyse its effect on operating conditions and mining output.

The tests have made it possible to assess the effect of aggregate grain type and size. Gravel granulation and quality of grain edges can affect the results of tests. There is a possibility to use different types of aggregate and grain sizes.

The distance of the gas phase connection point can be controlled, and this point can be situated beyond the lower tank. Moreover, the pressure hose can be inserted inside the lower tank to supply the mining pipe with air from there.

ISSUES

When designing the test rig, a number of issues were recognised which were to be solved to ensure correct rig operation.

The first interesting issue was water delivery and reception. Initially, a method was proposed to deliver water by flooding the upper tank and letting it flow gravitationally to the lower tank via a system of mining pipelines. After a brief analysis, a valve was added in the lower tank upper cover, through which the lower tank can be the filled in such a way that the aggregate layer to be mined is not deformed by the water flowing from the upper tank. The water was drained from the system using a tap mounted additionally in the lower cover. This tap was connected to a garden hose which led the water to a drain sump in the floor. This, however, required moving the entire structure slightly up and placing the lower tank on two supports, the height of which provided access to the tap and allowed connecting it to the drain hose.

The next issue recognised when designing the rig was ensuring tightness of the lower tank, while simultaneously preserving its potential for development and mobility of the entire rig. Initially, elastic rubber which was impermeable for water was used for this purpose. However, taking into consideration the material used for covers, a decision was made that sufficient tightness will be ensured by adhesive sealing mass which can be easily removed after rig disassembly, using a small sharp knife for instance and abrasive paper to remove its remnants. The lower part of the tank was also glued and sealed on both sides using the same mass. Fig. 8 shows sealing of the lower tank structure, between the base and the cylindrical part of the tank.

Fig. 8. Sealing of lower tank

A substantial issue which required deeper analysis to solve was the measuring procedure which should ensure satisfactorily high accuracy. In the case of three-phase mixture, performing a continuous measurement is rather problematic. Taking this into consideration, a decision was made to perform first the measurement of water elevation velocity for the two-phase flow, without the aggregate. For this purpose, a measuring container with scale was used, which was filled with elevated water in a given time interval at different air pressures. The results obtained in this measurement will be compared with those recorded during the three-phase flow measurement, with the aggregate.

The next parameter affecting the efficiency of aggregate mining is the distance of the mining head from the gravel layer. To study this effect, the amounts of water and aggregate will be changed during the complete mining cycle executed for constant air pressure. The measured values of this distance will make the basis for working out aggregate mining characteristics as functions of this parameter, and thus determining its optimal values.

In the described laboratory test rig the distance of the mining head from the aggregate layer can be measured using a scale mounted at the end of the mining pipeline. The measured height difference will give an opportunity to check how this distance changes with the inlet pressure level

MOST WIEDZY Downloaded from mostwiedzy.pl

change, thus providing basic pieces of information concerning operating conditions and their optimisation, including selection of the range of values assumed for optimal mining.

To get a wider insight into the mining phenomenon and its operating conditions, an opportunity of rig development for different diameters of mining pipelines was provided. Decreasing the pipeline diameter does not bring substantial structure changes, while its increasing is limited to ø200mm, which still gives a wide analysing potential, taking into account the mining elevation height obtainable in laboratory conditions.

RESULTS OF TESTS

Within the framework of the tests, time was measured from the appearance of the first mined grain to complete mining of all grains. Additionally, one test included mass measurement of the gravel mined for different pressures.

The model tests were performed for constant pressures and for increasing pressures, which means that mining was executed at the pressure increasing from 0 Pa to the current measurement value (Fig.9)

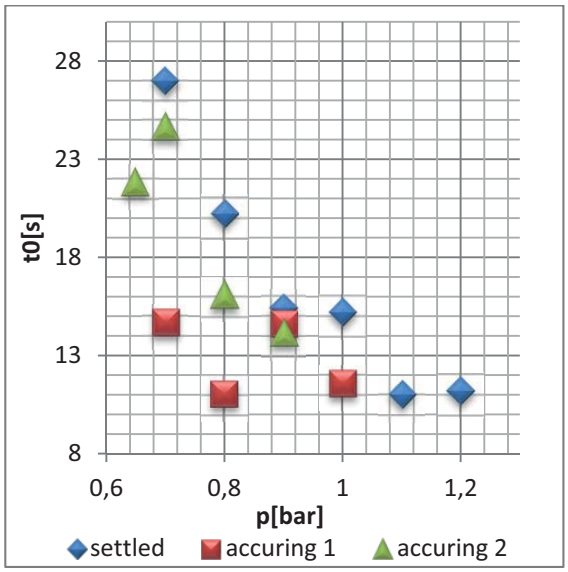

Fig. 9. Time (t0) of appearance of first aggregate grain vs. applied working pressure (p) for different operating conditions

During the examination with the aid of a stop-watch and video recording, the time t0 needed by the gravel grain to cover, in the mining pipeline, the distance from the lower tank to the control container was measured for different pressures. Three measurements were performed: two for increasing pressure and one for constant pressure, which has resulted in modernisation of the rig.

Fig. 10 shows the time tc needed for complete mining of all gravel grains as function of the pressure p used for mining. The time was measured from the beginning of mining to the end of gravel elevation, at unchanged position of the mining pipeline.

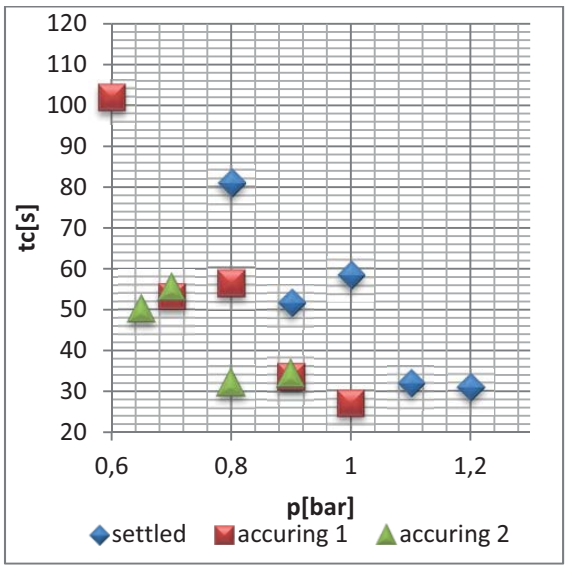

Fig. 10. Time (tc) of complete mining vs. applied working pressure (p) for different operating conditions

Fig. 11 shows the amount of mined gravel as a function of pressure changes, for steady-state operation.

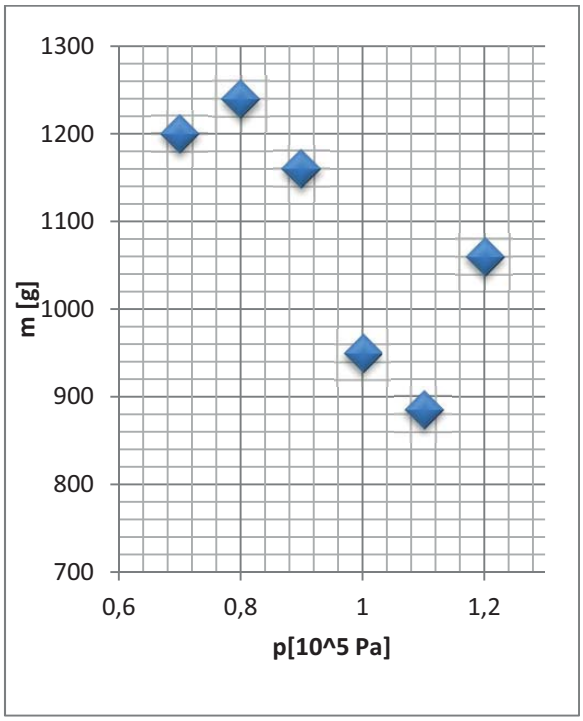

Fig. 11. Mass(m) of mined gravel vs. applied working pressure (p)

CONCLUSIONS

The performed model study aimed at: obtaining results close to those recorded in real conditions, taking into consideration the size effect on the mining output, determining the effect of pressure level and type of water on the flow and resultant mining output, and checking the effect

MOST WIEDZY Downloaded from mostwiedzy.pl

of the above initial conditions on the distance between the suction pipe and the mined material in the lower tank. This latter aspect was an important motivation for building the test rig. Additionally, an attempt was made to assess the expansion coefficient of the gas phase for changing inlet pressures.

The Airlift method is an alternative for other well-known and commonly used methods of aggregate mining from the bed of a water region, for instance methods making use of suction pumps or scoops. The only limiting factor in the Airlift method is expansion of gas phase. Once proper operating conditions are established, the method provides opportunities to mine aggregates from much larger depths than those available in traditional methods.

As can be seen in the diagrams, pressure increase leads to the decrease of time needed for gravel grain mining, with respect to both the appearance of the first grain, and the total time of mining at a given place. Further tests will be performed for identical pressure ranges but they will include presentation of maximal pressures and comparison of time changes.

The diagram illustrating mass changes of the mined gravel reveals irregularity for different pressures, which indicates that the pressure strongly affects the output. The interpretation of these results is difficult as it should take additionally into consideration gravel granulation, the shape of the hopper created during mining, as well as the distance of the suction pipe and its shape. The presented preliminary measurements have revealed that the pressure increase leads to the change of system operation efficiency, which is believed to result from the influence of the pressure level on the type of the generated flow of liquid and the resultant transport of aggregate. Further research, to be performed for a larger number of measurement variants with the aid of more accurate measuring equipment, is expected to determine more precisely relations between pressure and other parameters of aggregate mining.

BIBLIOGRAPHY

1. Mudde, R.F., Gravity-driven bubbly flows. Annu. Rev. Fluid Mech., 2005. 37: p. 393 – 423.

2. J Sobota, S Boczarski, L Petryka, M Zych, Measurement of velocity and concentration of nodules in vertical hydrotransport., 2005.

3. P Vlasak, Z Chara, B Kysela, J Sobota Flow behaviour of coarse-grained slurries in pipes., 2011.

4. DOB Jones, S Kaiser, AK Sweetman, CR Smith; Biological responses to disturbance from simulated deep-sea polymetallic nodule mining; 2017

5. C Starke, PR Bérubé; Reuse of Air for Return Activated Sludge Pumping in Submerged Membrane Bioreactors; 2016

6. A Oueslati, A Hannachi, M Elmaaoui; Effect of Air Humidification on the Pumping Efficiency of Water in a Packed Column Humidifier; 2015

7. A Oueslati, A Hannachi, M Elmaaoui; Effect of Air Humidification on the Pumping Efficiency of Water in a Packed Column Humidifier; 2015

CONTACT WITH THE AUTHORS

Czesław Dymarski
e-mail: cpdymars@pg.gda.pl

Tomasz Pająk
e-mail: tompajak@pg.gda.pl

Gdansk University of Technology
Faculty of Ocean Engineering and Ship Technology
Department of Marine Mechatronics
11/12 Narutowicza St.
80 - 233 Gdańsk
Poland

MOST WIEDZY Downloaded from mostwiedzy.pl

POLISH MARITIME RESEARCH Special Issue 2018 S1 (97) 2018 Vol. 25; pp. 151-158
10.2478/pomr-2018-0036

TESTING CONTRACTION AND THERMAL EXPANSION COEFFICIENT OF CONSTRUCTION AND MOULDING POLYMER COMPOSITES

Łukasz Pyrzowski
Gdańsk University of Technology, Poland

ABSTRACT

The paper presents results of systematic tests of contraction and thermal expansion coefficients of materials based on polymer composites. The information on the above material properties is essential both at the design stage and during the use of finished products. Components for the samples were selected in such a way as to represent typical materials used for production of construction and moulding elements. The performed tests made it possible to monitor the analysed parameters at different stages of the technological process.

Keywords: polymer composites, contraction, thermal expansion

MOST WIEDZY Downloaded from mostwiedzy.pl

INTRODUCTION

Fibre reinforced polymer composite is the material with a relatively short history, as compared to traditional construction materials (wood, metals, concrete). Its development began at the turn of 1930s and 1940s [1]. This material is characterised by small volume density, relatively high mechanical strength and stiffness, high resistance to weather conditions and chemical agents, and high flexibility for geometry shaping. These properties make the composites very applicable in the shipbuilding industry [2,3]. They are used for production of various components and entire watercraft units, such as, for instance, the ferry Vision of The Fjords shown in Fig. 1.

Polymer composites are also appreciated and used in production of cars, airplanes, sports equipment, electrotechnical elements, etc. This material is also being more and more frequently used in civil engineering, in the form of construction profiles, reinforcement elements, and sandwich structures [4-7].

The structure of composites comprises the matrix, most frequently made of polyester, vinyl or epoxy resins, and reinforcement, where glass and carbon fabrics are most popular materials. As a result of resin/reinforcement combination, so-called laminate is created. This laminate can be additionally used as a component of sandwich structure, with polyurethane foam (PU), polyethylene terephthalate foam (PET), or another material, honeycomb for instance, used as core filler.

Samples of selected composites were tested within the framework of the project which aimed at creating a footbridge with sandwich structure (Fig. 2) using the vacuum infusion technology, which is typical for production of yacht hulls, among other applications [8-10]. The implemented project

[11-13] included a series of experimental, numerical and technological tests [14,15], which made it possible to monitor the entire process, from a preliminary concept to building a full-scale object. The finished footbridge was subjected to a series of static and dynamic tests [15,18] and technical monitoring [25] based on earlier gained experience [19-24].

Fig. 1. Passenger ferry Vision of The Fjords

Fig. 2. Footbridge built on the Gdansk University of Technology campus territory within the framework of the project FOBRIDGE

An essential aspect in designing and use of composite structures is analysing the effect of contraction and temperature on the finished product. Thermosetting resins used for production of composites experience chemical contraction during hardening and heat soaking processes. Methods to determine this parameter are divided into two groups: volumetric and non-volumetric. Representative measurement techniques for both groups are discussed in [26]. Numerous publications can be found in the literature which present results for the same resin [27-29]. On the other hand, determining contraction in finished composite elements is much more rarely analysed. The process itself is very complex, as it depends on percentage and direction of reinforcement. This phenomenon was analysed in [30], among other publications. The problem of contraction appearance at the production stage can affect both the dimensions and shape of the finished product, and the residual stresses activated during the hardening and heat soaking processes [31,32]. A similar situation is when assessing the linear thermal expansion coefficient for laminates and sandwich structures, as this parameter also depends of percentage and direction of reinforcement. Its variability can be illustrated by the range of values 1,62 ÷ 2,7 m/m/°C given in the ASME (American Society of Mechanical Engineers) standard B31.3.

This paper analyses the assessment of contraction parameters and thermal expansion coefficients for selected resins, reinforcements, and cores used in sandwich structures. The tests were performed for construction materials, in versions of pure laminate and sandwich structure, and for moulding materials.

MATERIALS, PREPARING SAMPLES

The tests were performed with materials which can be used for production of construction components of finished products, and production of moulds needed in the vacuum infusion technology. The following components were used for preparing samples:

a) glass reinforcements: glass fabrics E, bi-directional, stitched – BAT 800 [0/90], GBX 800 [45/-45], and glass mats E – CSM 300, CSM 450,
b) sandwich materials: construction foam PU of 50 mm in thickness, and Lantor Coremat mat of 3 mm in thickness (used in production of moulds),
c) construction resins: vinyl ester resin BÜFA – Firestop S 440, and vinyl ester resin POLIMAL – VE-2 MM,
d) moulding resins: vinyl ester resin POLYLITE – 410-900, and polyester resin Norester – RM 2000.

Using the above materials, five plates of dimensions of 200×200 mm were prepared. All samples were made using manual laminating technology (Fig. 3). Detailed specifications of plates are collated in Table 1.

Fig. 3. Making test samples

Tab. 1. Specifications of samples

Sample label	Resin	Sequence of layers
P1	BÜFA - Firestop S 440 construction resin	1 × CSM 300 1 × BAT 800 2 × GBX 800 1 × BAT 800 **PU foam** 1 × BAT 800 2 × GBX 800 1 × BAT 800 1 × CSM 450
P2	BÜFA - Firestop S 440 construction resin	1 × CSM 300 1 × BAT 800 2 × GBX 800 1 × BAT 800

MOST WIEDZY Downloaded from mostwiedzy.pl

Sample label	Resin	Sequence of layers
P3	POLIMAL - VE-2 MM construction resin	1 × CSM 300 1 × BAT 800 2 × GBX 800 1 × BAT 800
P4	POLYLITE - 410-900 moulding resin	1 × CSM 300 3 × CSM 450 **Coremat** 3 × CSM 450
P5	Norester - RM 2000 moulding resin	1 × CSM 300 3 × CSM 450 **Coremat** 3 × CSM 450

MEASUREMENT TECHNIQUE

To enable measurements of contraction and thermal expansion coefficient, four benchmarks were placed on each sample, thus creating two deformation measurement bases of 100 mm in length and perpendicular to each other. The benchmarks were embedded into the plate before resin gelation (Fig. 4).

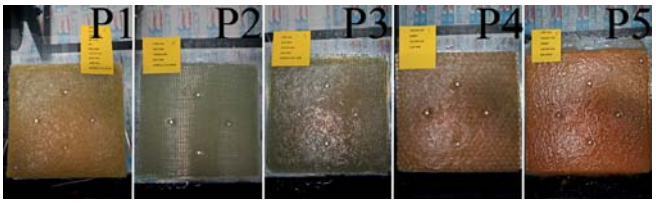

Fig. 4. Benchmarks placed on samples

The length changes were measured using an electronic extensometer Mitutoyo with resolution of up to 0,001 mm (Fig. 5). Additionally, a pyrometer (surface infrared thermometer) TQC model TE1005 was used in tests which aimed at determining the linear thermal expansion coefficient. The measurement range of this pyrometer was –50°C ÷ 750°C and the resolution was 0,1°C.

Fig. 5. Extensometer used for length change measurement

CONTRACTION MEASUREMENT AFTER SAMPLE PREPARATION

Firstly, the sample contraction was measured which appeared as a result of resin gelation. During the tests, the samples remained in the room temperature. The deformation was measured once a day during first four days after plate preparation. During this time interval the contraction stabilised. To check whether the samples do not undergo further contraction in a longer time interval, the contraction was additionally measured after two weeks and after one month. The results are shown in Fig. 6. For each plate, permanent deformation directly after preparation, $\varepsilon_{perm,0}$, was determined. The final value was calculated as the arithmetic mean from two measurements. The results are collated in Table 2.

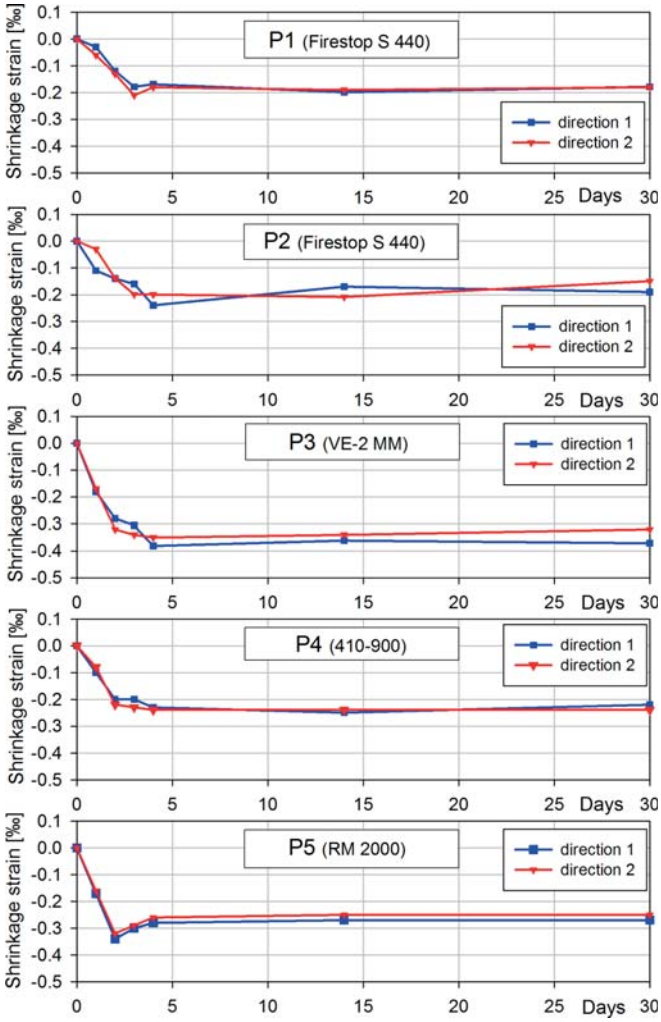

Fig. 6. Measurement of contraction deformations after preparation of samples P1-P5

MOST WIEDZY Downloaded from mostwiedzy.pl

Tab. 2. Permanent contraction deformations directly after sample preparation

Sample label	Resin	$\varepsilon_{perm,0}$ [‰]
P1	Firestop S 440	-0,18
P2	Firestop S 440	-0,18
P3	POLIMAL - VE-2 MM	-0,35
P4	POLYLITE - 410-900	-0,24
P5	Norester - RM 2000	-0,26

Contraction and linear thermal expansion coefficient measurements during heat soaking

The next test step was measuring the contraction and linear thermal expansion coefficient of the samples during and after their heat soaking. The procedure of 10-hour heat soaking in the temperature of 90°C was divided into three phases. The initial sample cooling was done as early as after 30 minutes of soaking, the second – after basic soaking, i.e. after 9,5 hours, and the third – after process completion, i.e. after 10 hours.

MEASUREMENT AFTER FIRST HEAT SOAKING PHASE

The samples were placed inside the thermal chamber for 30 min. Then, after removing them from the chamber, the deformation and surface temperature of the samples were simultaneously measured during sample cooling. The results are shown in Fig. 7. For each plate, permanent deformation after first heating, $\varepsilon_{perm,1}$, was determined. Its final value was calculated as the arithmetic mean from two measurements. Another parameter determined for each plate at this stage was the linear thermal expansion coefficient after first heating, α_1. Here, the final value was also calculated as the arithmetic mean from two measurements, for which the least squares regression line was also determined. The results are collated in Table 3.

Tab. 3. Permanent contraction deformations and linear thermal expansion coefficients after first heat soaking phase

Sample label	Resin	$\varepsilon_{perm,1}$ [‰]	a_1 [m/m/°C]
P1	Firestop S 440	-0,80	2,38e-5
P2	Firestop S 440	-0,81	1,92e-5
P3	POLIMAL - VE-2 MM	-1,19	2,62e-5
P4	POLYLITE - 410-900	-0,78	2,58e-5
P5	Norester - RM 2000	-0,22	1,33e-5

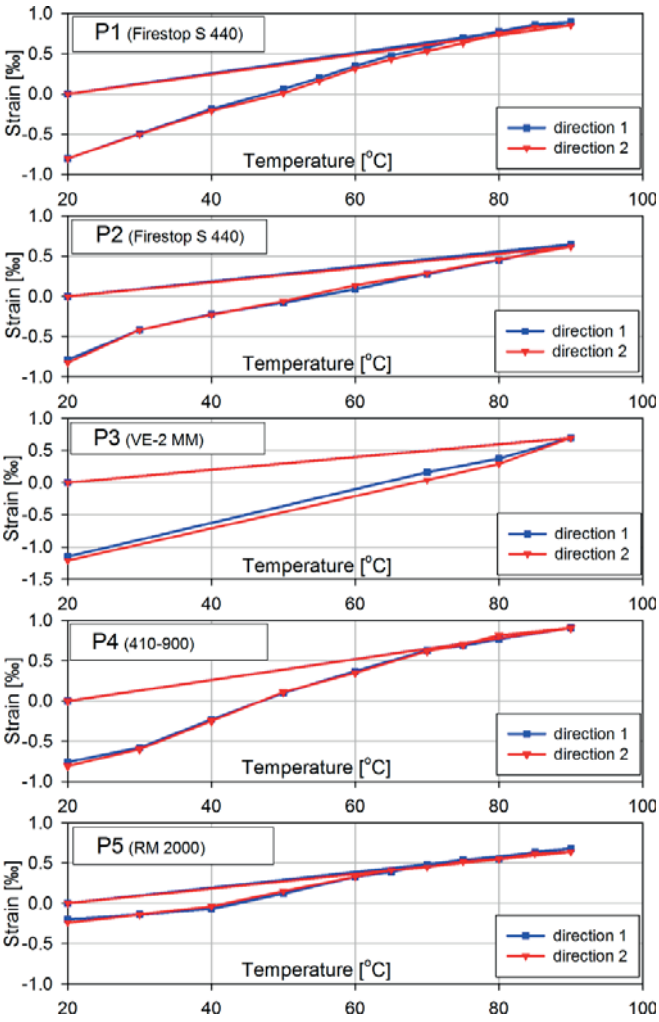

Fig. 7. Results of deformation measurements during cooling of samples P1-P5 after first heat soaking phase

MEASUREMENT AFTER SECOND HEAT SOAKING PHASE

In the second heat soaking phase, the samples underwent basic soaking which lasted 9 hours. After removing them from the thermal chamber, the deformation and surface temperature of the samples were simultaneously measured during sample cooling. For each plate, permanent deformation after basic 9-hour heating, $\varepsilon_{perm,2}$ and the linear thermal expansion coefficient α_2 were determined. The final values were calculated in the identical way as in the previous measurement. The results are shown in Fig. 8 and Table 4.

MOST WIEDZY Downloaded from mostwiedzy.pl

Tab. 4. Permanent contraction deformations and linear thermal expansion coefficients after second heat soaking phase

Sample label	Resin	$e_{perm,2}$ [‰]	a_2 [m/m/°C]
P1	Firestop S 440	-0,01	2,42e-5
P2	Firestop S 440	-0,09	1,81e-5
P3	POLIMAL - VE-2 MM	-0,07	2,50e-5
P4	POLYLITE - 410-900	-0,06	2,79e-5
P5	Norester - RM 2000	-0,25	1,64e-5

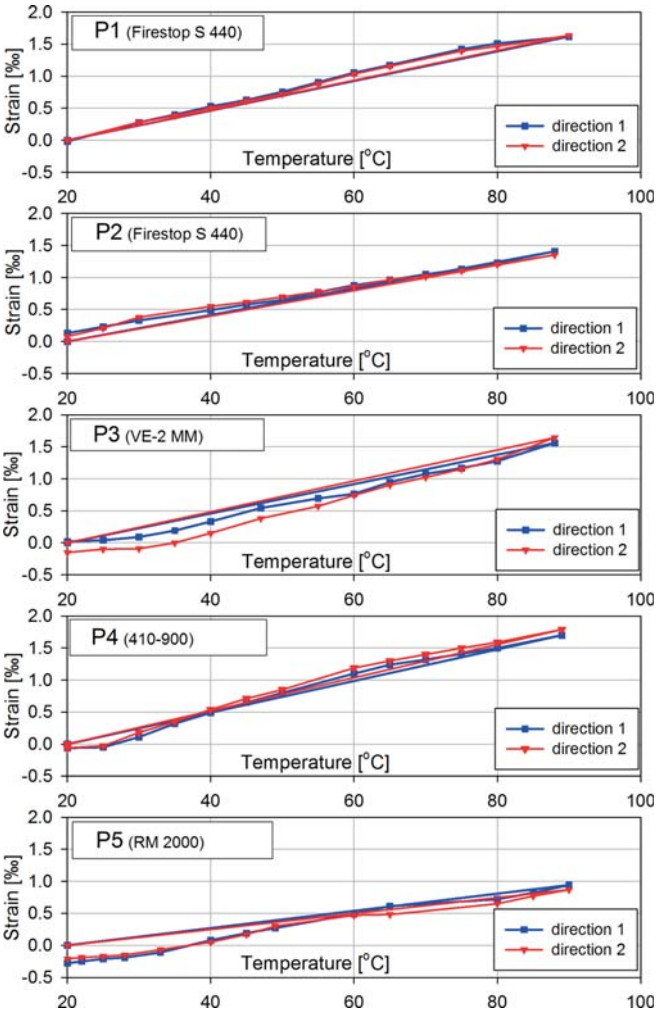

Fig. 8. Results of deformation measurements during cooling of samples P1-P5 after second heat soaking phase

MEASUREMENT AFTER THIRD HEAT SOAKING PHASE

The final test step was measuring sample contraction during cooling after completion of the heat soaking process. For each plate, permanent deformation formed during the last 30-minute soaking stage, $\varepsilon_{perm,3}$, and the linear thermal expansion coefficient α_3 were determined. The final values were calculated in the identical way as in the previous measurements. The results are shown in Fig. 9 and Table 5.

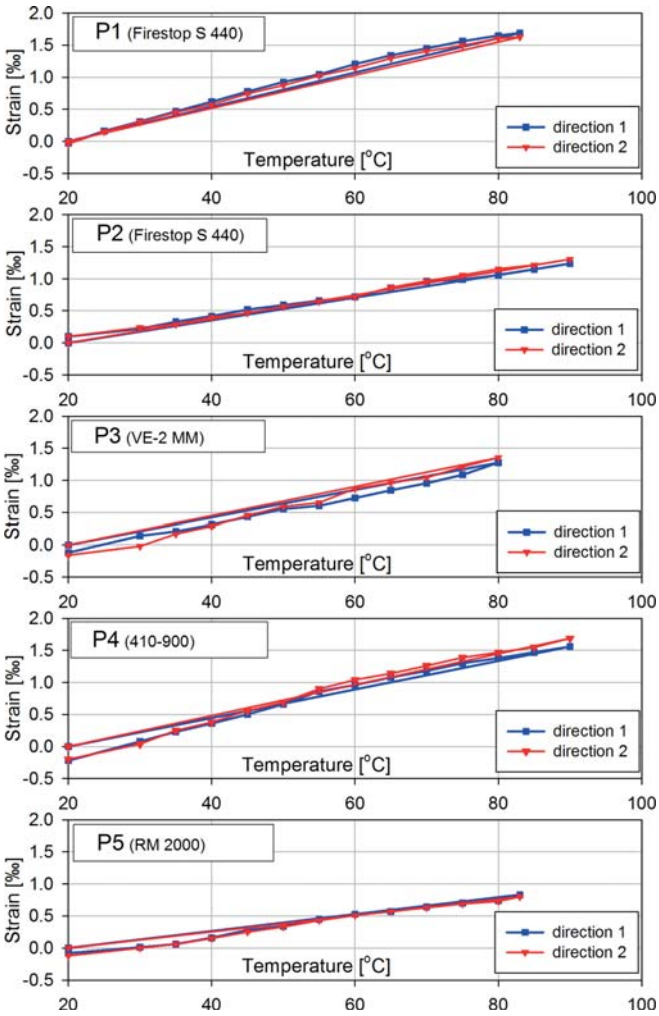

Fig. 9. Results of deformation measurements during cooling of samples P1-P5 after third heat soaking phase

Tab. 5. Permanent contraction deformations and linear thermal expansion coefficients after third heat soaking phase

Sample label	Resin	$\varepsilon_{perm,3}$ [‰]	α_3 [m/m/°C]
P1	Firestop S 440	-0,03	2,60e-5
P2	Firestop S 440	0,03	1,75e-5
P3	POLIMAL - VE-2 MM	-0,14	2,43e-5
P4	POLYLITE - 410-900	-0,21	2,69e-5
P5	Norester - RM 2000	-0,10	1,50e-5

CONCLUSIONS

The values of total permanent contraction deformation ε_{perm} created during the hardening and heat soaking processes are collated in Table 6. It can be noticed that in the case of construction resins (samples P1, P2, P3) the largest total contraction deformation was recorded for sample P3 (Resin POLIMAL - VE-2 MM), while for moulding resins (samples P4, P5) – for sample P4 (Resin POLYLITE - 410-900). After

MOST WIEDZY Downloaded from mostwiedzy.pl

analysing Tables 3-5, a conclusion can be made that the largest increase of contraction deformation takes place as early as after the first, preliminary heat soaking phase. This tendency was observed for all tested materials. Comparing results for samples P1 and P2 leads to the conclusion that, in both the independent form and as sandwich structure component, the laminate has very similar contraction deformation level at each analysis stage.

Tab. 6. Permanent contraction deformations directly after sample preparation

Sample label	Resin	ε_{perm} [‰]
P1	Firestop S 440	-1,02
P2	Firestop S 440	-1,05
P3	POLIMAL - VE-2 MM	-1,75
P4	POLYLITE - 410-900	-1,29
P5	Norester - RM 2000	-0,83

The mean values of linear thermal expansion coefficient α from the results obtained at different test stages are shown in Table 7. Like for the contraction measurement, higher values (i.e. less favourable from the point of view of construction/mould performance) were recorded for samples P3 (Resin POLIMAL - VE-2 MM) and P4 (Resin POLYLITE - 410-900). When analysing the results obtained for samples P1 and P2 we can conclude that incorporating the laminate into the sandwich structure increases the linear thermal expansion coefficient of the entire structure.

Tab. 7. Mean values of linear thermal expansion coefficients

Sample label	Resin	α [m/m/°C]
P1	Firestop S 440	2,47E-05
P2	Firestop S 440	1,83E-05
P3	POLIMAL - VE-2 MM	2,52E-05
P4	POLYLITE - 410-900	2,69E-05
P5	Norester - RM 2000	1,49E-05

What is also noteworthy is highest values of linear thermal expansion coefficients for all tested composites, as compared to traditional materials, such as metals, for instance. The above characteristic and the contraction phenomenon taking place in the composite material production process should be taken into account at the design and technological test stages. In cases of such large-scale elements as yacht hulls or building structures, the compatibility of real dimensions with design assumptions can be verified using, for instance, advanced photogrammetry techniques [33].

ACKNOWLEDGEMENTS

The research was done under the grant entitled "Developing composite footbridge arches for application over GP roads" (Agreement PBS1/B2/6/2013, implementation in years 2013-2015) co-financed by the National Centre for Research and Development.

BIBLIOGRAPHY

1. Marsh G.: *50 years of reinforced plastic boats*. Reinforced Plastics, 50(9), 2006, pp. 16-19. doi: 10.1016/S0034-3617(06)71125-0.
2. Neser G.: *Polymer based composites in marine use: history and future trends.* Procedia Engineering, 194, 2017, pp. 19-24. doi: 10.1016/j.proeng.2017.08.111.
3. Mouritz A.P., Gellert E., Burchill P., Challis K.: *Review of advanced composite structures for naval ships and submarines*. Composite Structures 53(1), 2001, pp. 21-41. doi: 10.1016/s0263-8223(00)00175-6.
4. Bakis C.E., Bank L.C., Brown V.L., Cosenza E., Davalos J.F., Lesko J.J., Machida A., Rizkalla S.H. Triantafillou T.C.: *Fiber-reinforced polymer composites for construction-state-of-the-art review*, Journal of Composites for Construction, 6(2), 2002, pp. 73-87. doi: 10.1061/(asce)1090-0268(2002)6:2(73).
5. Manalo A., Aravinthan T., Fam A., Benmokrane B.: *State-of-the-art review on FRP sandwich systems for lightweight civil infrastructure*, Journal of Composites for Construction, 21(1), 2016, pp. 1-43. doi: 10.1061/(asce)cc.1943-5614.0000729.
6. Mazurkiewicz Ł., Małachowski J., Tomaszewski M., Baranowski P., Yukhymets, P.: *Performance of steel pipe reinforced with composite sleeve*, Composite Structures, 183, 2018, pp. 199-211. doi: 10.1016/j.compstruct.2017.02.032.
7. Gołaś J., Podhorecki A., Jarząb M.: *Vibrations of composite fibre-reinforced beam induced by inertialess moving load*, Shell Structures: Theory and Applications. - Vol. 2/ ed. W. Pietraszkiewicz, I. Kreja, London: CRC Press/Balkema, 2010, pp. 167-170. doi: 10.1201/9780203859766.ch35.
8. Reuterlöv S.: *Cost effective infusion of sandwich composites for marine applications*, Reinforced Plastics, 46(12), 2002, pp. 30-32. doi: 10.1016/s0034-3617(02)80224-7.
9. Summerscales J., Searle T.J.: *Low-pressure (vacuum infusion) techniques for moulding large composite structures*, Proceedings of the Institution of Mechanical Engineers Part L Journal of Materials Design and Applications, 219(1), 2005, pp. 45-58. doi: 10.1243/146442005x10238.
10. Choi H.K., Nam K.W., Ahn S.H.: *Strength characteristics of FRP composite materials for ship structure*, Journal of Ocean Engineering and Technology, 27(4), 2013, pp. 45-54. doi: 10.5574/ksoe.2013.27.4.045.
11. Chróścielewski J., Miśkiewicz M., Pyrzowski Ł., Wilde K.: *Composite GFRP U-shaped footbridge*, Polish Maritime Research, 24(s1), 2017, pp. 25-31. doi: 10.1515/pomr-2017-0017.

MOST WIEDZY Downloaded from mostwiedzy.pl

12. Miśkiewicz M., Okraszewska R., Pyrzowski Ł.: *Composite footbridge – synergy effect in cooperation between universities and industry*. ICERI2014: 7th International Conference of Education, Research and Innovation, ICERI Proceedings, 2014, pp. 2897-2903.

13. Pyrzowski Ł., Miśkiewicz M.: *Application of foam made of post-consumer pet materials for the construction of footbridges*, 17th International Multidisciplinary Scientific GeoConference SGEM 2017, Vol. 17, Issue 62, pp. 9-16. doi: 10.5593/sgem2017/62/s26.002.

14. Pyrzowski Ł., Sobczyk B., Witkowski W., Chróścielewski J.: *Three-point bending test of sandwich beams supporting the GFRP footbridge design process validation*. 3rd Polish Congress of Mechanics (PCM) / 21st International Conference on Computer Methods in Mechanics (CMM), 2016, Taylor & Francis Group, London, pp. 489-492. doi: 10.1201/b20057-104.

15. Miśkiewicz M., Daszkiewicz K., Ferenc T., Witkowski W., Chróścielewski J.: *Experimental tests and numerical simulations of full scale composite sandwich segment of a foot-and-cycle bridge*. Advances in Mechanics: Theoretical, Computational and Interdisciplinary Issues – Kleiber et al. (Eds), Taylor & Francis Group, London, 2016, pp. 401-404. doi: 10.1201/b20057-86.

16. Chróścielewski J., Miśkiewicz M., Pyrzowski Ł., Sobczyk B., Wilde K.: *A novel sandwich footbridge - Practical application of laminated composites in bridge design and in situ measurements of static response*. Composites Part B: Engineering, 126, 2017, pp. 153-161. doi: 10.1016/j.compositesb.2017.06.009.

17. Pyrzowski Ł., Sobczyk B., Rucka M., Miśkiewicz M., Chróścielewski J.: *Composite sandwich footbridge - measured dynamic response vs. FEA*. Shell Structures: Theory and Applications. - Vol. 4/ ed. W. Pietraszkiewicz, W. Witkowski, Leiden: CRC Press/Balkema, 2018, pp. 457-460.

18. Pyrzowski Ł., Miśkiewicz M., Chróścielewski J.: *Load testing of GFRP composite U-shape footbridge*, IOP Conference Series: Materials Science and Engineering, 245, 2017. doi: 10.1088/1757-899X/245/3/032050.

19. Wilde K., Miśkiewicz M., Chróścielewski J.: *SHM System of the Roof Structure of Sports Arena „Olivia"*, Structural Health Monitoring 2013, Vol. II, pp. 1745-1752.

20. Kaminski W., Makowska K., Miśkiewicz M., Szulwic J., Wilde K.: *System of monitoring of the Forest Opera in Sopot structure and roofing*, 15th International Multidisciplinary Scientific GeoConference SGEM 2015, Book 2 Vol. 2, pp. 471-482. doi: 10.5593/SGEM2015/B22/S9.059.

21. Mariak A., Miśkiewicz M, Meronk B., Pyrzowski Ł., Wilde K.: *Reference FEM model for SHM system of cable-stayed bridge in Rzeszów*, Advances in Mechanics: Theoretical, Computational and Interdisciplinary Issues, 2016, pp. 383-387. doi:10.1201/b20057-82.

22. Miśkiewicz M., Pyrzowski Ł., Wilde K., Mitrosz O.: *Technical monitoring system for a new part of Gdańsk Deepwater Container Terminal*, Polish Maritime Research, 24(s1), 2017, pp. 149-155. doi: 10.1515/pomr-2017-0033.

23. Miśkiewicz M., Mitrosz O., Brzozowski T.: *Preliminary field tests and long-term monitoring as a method of design risk mitigation: a case study of Gdańsk Deepwater Container Terminal*. Polish Maritime Research, 24(3), 2017, pp. 106-114, doi: 10.1515/pomr-2017-0095.

24. Miśkiewicz M., Meronk B., Brzozowski T., Wilde K.: *Monitoring system of the road embankment*, Baltic Journal of Roads and Bridge Engineering, 12(4), 2017, pp. 218-224. doi: 10.3846/bjrbe.2017.27.

25. Miśkiewicz M., Pyrzowski Ł., Chróścielewski J., Wilde K.: *Structural Health Monitoring of Composite Shell Footbridge for Its Design Validation*, Proceedings 2016 Baltic Geodetic Congress (Geomatics)/ ed. Juan E. Guerrero Los Alamitos: IEEE Computer Society Order Number E5972, 2016, pp. 228-233. doi: 10.1109/bgc.geomatics.2016.48.

26. Nawab Y., Shahid S., Boyard N., Jacquemin F.: *Chemical shrinkage characterization techniques for thermoset resins and associated composites*. Journal of Materials Science, 48(16), 2013, pp. 5387-5409. doi: 10.1007/s10853-013-7333-6.

27. Schoch K.F., Panackal P.A., Frank P.P.: *Real-time measurement of resin shrinkage during cure*. Thermochimica Acta, 417, 2004, pp. 115-118. doi: 10.1016/j.tca.2003.12.027.

28. Shah D.U., Schubel P.J.: *Evaluation of cure shrinkage measurement techniques for thermosetting resins*. Polymer Testing, 29, 2010, pp. 629-663. doi: 10.1016/j.polymertesting.2010.05.001.

29. Huang Y.J., Liang C.M.: *Volume shrinkage characteristics in the cure of low-shrink unsaturated polyester resins*. Polymer, 37(3), 1996, pp. 401-412. doi: 10.1016/0032-3861(96)82909-0.

30. Nawab Y., Jacquemin F., Casari P., Boyard N., Sobotka V.: *Evolution of chemical and thermal curvatures in thermoset-laminated composite plates during the fabrication process*. Journal of Composite Materials, 47(3), 2010, pp. 327-339. doi: 10.1177/0021998312440130.

31. Casari P., Gornet L.: *Characterization of residual stresses in a composite curved sandwich beam*, Composites: Part A, 37(4), 2006, pp. 672-678. doi: 10.1016/j.compositesa.2005.05.020.

MOST WIEDZY Downloaded from mostwiedzy.pl

32. White S.R., Hahn H.T.: *Process modeling of composite materials: residual stress development during cure. Part II. Experimental validation*. Journal of Composite Materials, 26(16), 1992, pp. 2423-2453. doi: 10.1177/002199839202601605.

33. Janowski A., Nagrodzka-Godycka K., Szulwic J., Ziółkowski P.: *Remote sensing and photogrammetry techniques in diagnostics of concrete structures*. Computers and Concrete, 18(3), 2016, pp. 405-420. doi: 10.12989/cac.2016.18.3.405.

CONTACT WITH THE AUTHOR

Łukasz Pyrzowski

Gdańsk University of Technology
Faculty of Civil and Environmental Engineering
11/12 Narutowicza St.
80 - 233 Gdańsk
Poland

MOST WIEDZY Downloaded from mostwiedzy.pl

POLISH MARITIME RESEARCH Special Issue 2018 S1 (97) 2018 Vol. 25; pp. 159-165
10.2478/pomr-2018-0037

MOBILE LASER SCANNING CALIBRATION ON A MARINE PLATFORM

Jakub Szulwic
Paweł Tysiąc
Gdańsk University of Technology, Poland

ABSTRACT

The article describes the method of calibration of the Riegl VMZ-400 mobile scanning system on a floating platform and an experiment aimed at conducting measurements from a previously calibrated instrument. The issue of factors affecting the quality of measurements was discussed.
Mobile laser scanning is an increasingly popular measurement solution, but it is still innovative on a European scale. The use of a floating platform is unique on a national scale. The presented solution is the result of the work of the Gdańsk University of Technology team on the development of the measurement procedure for scanning land from the sea and the river.

Keywords: mobile laser scanning, marine laser scanning, scanning of a boat, calibration of laser scanning, sea measurements, MarLS

MOST WIEDZY Downloaded from mostwiedzy.pl

INTRODUCTION

Mobile laser scanning is a modern, more and more widely used measuring solution. Scanning from a floating platform, including scanning from the sea, is still an innovative solution on a European scale. The principle of the system operation can be reduced to impulse measurement of the time of the laser beam passing to the object and back. The latest measurement solutions are able to collect up to one million points per second with three-dimensional coordinates while taking digital photos of the area. A fact on a national scale is the use the system on a watercraft and carrying out a measurement mission from such a calibrated instrument [1-2]. Such solutions have already appeared in Europe [3], but due to the location of the measurement mission on the southern coast of the Baltic Sea and obtaining results with accuracy better than 10 cm is an innovation on a European scale.

The authors took part in earlier studies aimed at scanning from the sea (2014). In relation to previous measurement results, the presented study introduced new solutions. Qualitative verification has been performed and limitations of the measurement method were indicated. The authors took into account the vessel selection factor and meteorological factors affecting the measurement to clearly state under which conditions the marine mobile scanning gives the possibility of achieving accuracy of 10 cm, based on the current worldwide knowledge of increasing the accuracy of these data [4].

The continuous development of measurement solutions gives the opportunity for faster, more accurate data acquisition, thus achieving the possibility of using this type of solution, for example for:

- cliff edge monitoring [5] (including cliff stability analysis [6-7]) to obtain measurement results comparable with stationary laser scanning [8-10],
- assessment of the condition of port and quay infrastructure on the basis of analysis of data collected in close proximity to waterways and ports [11],

- creating an inventory of bridges, plate wharves, on piles or with a supporting grid from the water side,
- obtaining data for inventory and promotional purposes of objects that are within the range of the scanner's work during the measurement experiment.

In the measurement experiment described in the article, the Riegl VMZ-400 mobile scanner was used during the implementation of the voucher for innovations "Implementation of the 3D laser scanning measurement procedure from a floating platform" whose main purpose was to obtain a mobile scanning procedure, where the platform is located on the vessel. The project was carried out in cooperation of the Gdańsk University of Technology with the company ZUI Apeks Sp. z o.o. Figures 1 and 2 show a fully operational system during a measurement mission using laser scanning from the sea.

Fig. 1 A mobile platform on a vessel during a measurement mission.

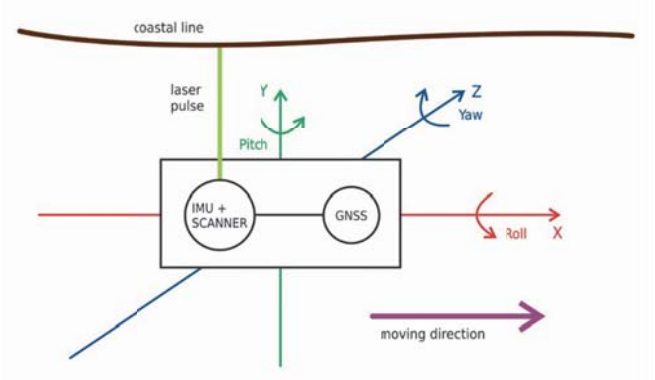

Fig. 2 Diagram of the system during laser scanning from the sea

PLANNING OF THE MEASUREMENT MISSION

When planning a measurement mission - apart from the type of scanning system, the quality of the IMU (Inertial Measurement Unit) and the GNSS receiver (Global Navigation Satellite System) - the following are of particular importance for the measurement results:

1. selection of a vessel,
2. meteorological conditions,
3. geometrical conditions of GNSS signal availability.

In the case of selecting a vessel, special attention should be paid to:

- relatively low immersion depth (up to approx. 1.5 m),
- optimization of the relationship between maneuverability and directional stability,
- the possibility of taking a 2 person measuring team on board (except for the crew of the vessel),
- the possibility of mounting a mobile platform on board.

In the case of immersion depth, the main determining factor is the depth of water at which the platform will move. The range of the scanner is about 400 meters, so it is the maximum distance from this type of scanner to the scanned object. Due to the variability of bottom depth in the coastal zone of the sea, it is difficult to scan the edge with a unit with a large immersion. Therefore, for projects related to scanning from the sea, it is recommended to select a unit with a low immersion depth. At the same time, one should pay attention to its stability, which is associated with the safety of use. Optimization of the relationship between maneuverability and directional stability is important due to the dynamic initialization of the system on the vessel and maintaining the appropriate accuracy of the determined angles of rotation by the IMU. Typically, units do not achieve the speed of movement, such as cars used in standard terrestrial mobile scanning, they cannot accelerate and slow down as rapidly, and therefore optimization is extremely important to achieve the intended purpose, i.e. to properly initiate the system and maintain the appropriate angular values determined by IMU.

The quality of data is influenced by factors related to GNSS positioning and meteorological conditions [13-15]. For meteorological factors, it should be noted that they determine safety, which is related to the stability of the platform, and which can only move under certain weather conditions [9]. It is recommended to scan from the sea in the period from April to November, because during this period there are smaller storm surges, the day is relatively longer, and the sun appears over 20 degrees above the horizon for most of the day (this property favors taking photos, which supplement information on the coordinates of points registered by the scanner). Additionally, when planning the measurement, make sure that there is no slurry or objects preventing the vessel from moving (e.g. an iceberg) and that the wind does not exceed 2-3 degrees on the Beaufort scale, when the unit flows against the wave and 6 degrees, when the unit scans flowing with a wave. At this stage, it should be mentioned that waving occurs not only under the influence of wind, therefore the final decision regarding the measurement must be made by the equipment operator. In addition, the measurement should be carried out in favorable weather such as no precipitation. Cloud cover is important when the purpose of measurements is additionally taking photos from

MOST WIEDZY Downloaded from mostwiedzy.pl

the platform. The temperature range in which this particular measuring set can work is from -10 ° C to + 50 ° C.

In the case of GNSS satellites availability, before the measurements are made, attention should be paid to the signal quality forecast. Due to the fact that the quality of the trajectory is decisive in the final product, it must have sufficient conditions to obtain the appropriate accuracy. An unquestionable advantage of using a measuring solution with a scanning platform on a vessel over a traditional mobile solution is the possibility of full monitoring of coast changes in hard-to-reach places and building spatial models for the reconstruction of the Baltic coast, in particular seaports.

CALIBRATION OF THE MEASUREMENT SYSTEM

The mobile system Riegl VMZ-400 mounted on the watercraft is formed of components corresponding to the numbers in Figure 3 which are:

Fig. 3 Components of the Riegl VMZ-400 system on a vessel 1. Riegl VZ-400 laser scanner. 2. IMU. Connection cables between the scanner, 4. IMU, power source and laptop.5. GNSS antenna.6. Aluminum frame on which individual components are mounted.7. Aluminum clamps securing the platform to the elements of the vessel.8. Straps that fasten the platform to better stabilize the entire platform

Platform calibration refers to calculating the distance from the IMU center to the center of individual components, determining the rotation of the platform relative to the direction of travel and connecting the system to the laptop using the TCP/IP protocol. The view of the operating laptop system is shown in Figure 4.

Fig. 4 View of the laptop that operates the system.

INITIALIZATION OF THE SYSTEM AND TAKING MEASUREMENTS

In order to ensure proper quality, precision and accuracy of data, a measuring network should be designed in order to establish the final product to the global coordinate system. The most suitable solution is to measure planes in order to establish XY and Z scans. The software used to establish the point cloud has been made available by ZUI Apeks Sp. z o.o. In the software, the planes are created in the following scheme, shown below, in which the format specifying the coordinate system and the points P1 - P7, which show the individual coordinates, are marked accordingly.

The plane creation scheme:

TYPE=PlaneObj<CR><LF>
NAME=Plane001<CR><LF>
FORMAT=ECEF_CARTESIAN<CR><LF>
COUNT=7<CR><LF>
P1=0.000 0.000 0.000<CR><LF>
P2=1.000 0.000 0.000<CR><LF>
P3=1.000 0.500 0.000<CR><LF>
P4=2.000 0.000 0.000<CR><LF>
P5=3.000 0.000 0.000<CR><LF>
P6=3.000 1.000 0.000<CR><LF>
P7=0.000 1.000 0.000<CR><LF>

The device initialization itself consists of static and dynamic initialization. Static initialization consists of a 5-minute collection of data on the position of the device based on GNSS measurements. Dynamic initialization is used to stabilize the angles roll, pitch and yaw, recorded by the IMU. The second stage on the vessel is very difficult to implement due to the limited possibility of accelerating and slowing down the device, which is why the maneuverability parameter plays a key role here. Sudden turning of the platform in motion can provide sufficient accuracy of the measured rotation angles of the platform to obtain a suitably accurate spatial model.

MOST WIEDZY Downloaded from mostwiedzy.pl

The corresponding values measured by the IMU unit are shown in Figure 5.

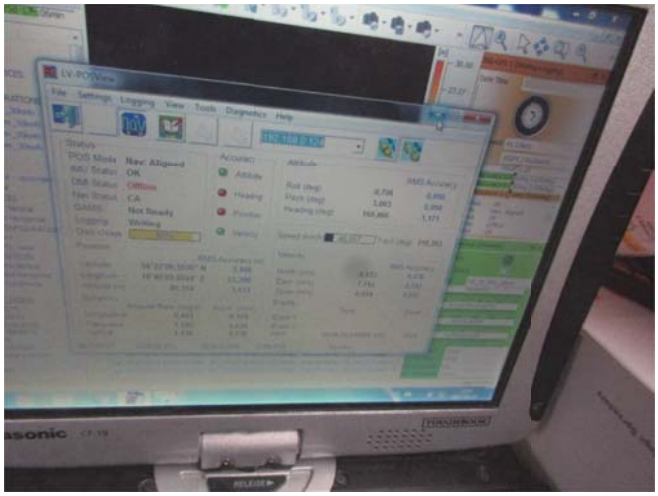

Fig. 5 Display of values measured by the IMU in real time.

IMPLEMENTATION OF THE MISSION AND THE ACQUIRED DATA ALIGNMENT ACCURACY

The measurement mission was carried out in the Władysławowo Sea Port and the sea shore in the section from this port to the vicinity of the North Star located in Jastrzębia Góra. The place of measurement is shown in Figure 6 inside the red polygon.

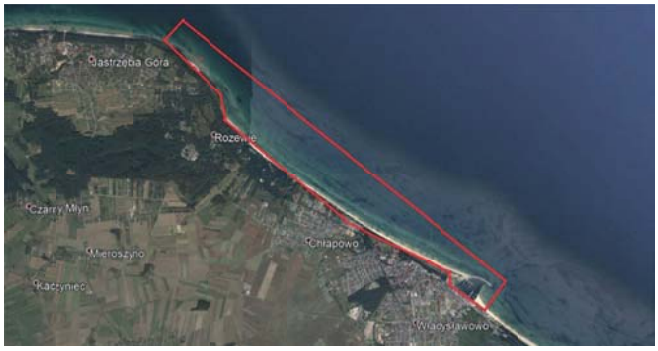

Fig. 6 Location of measurements on the seacoast inside the red polygon [source: Google Earth TM]

The trajectory alignment results are shown in Figures 7-9 showing the mean square error on each axis.

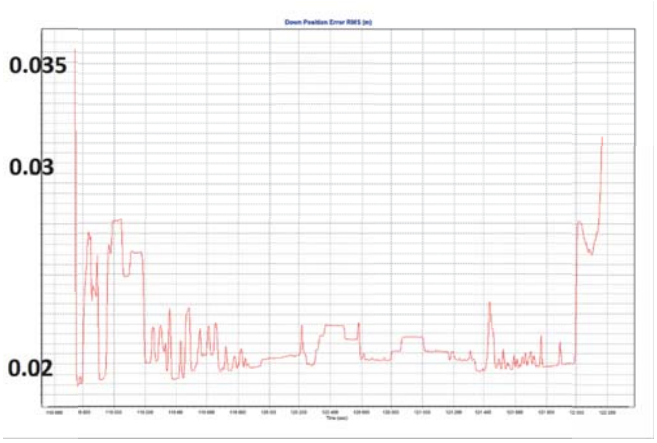

Fig. 7 Trajectory to height alignment mean square error.

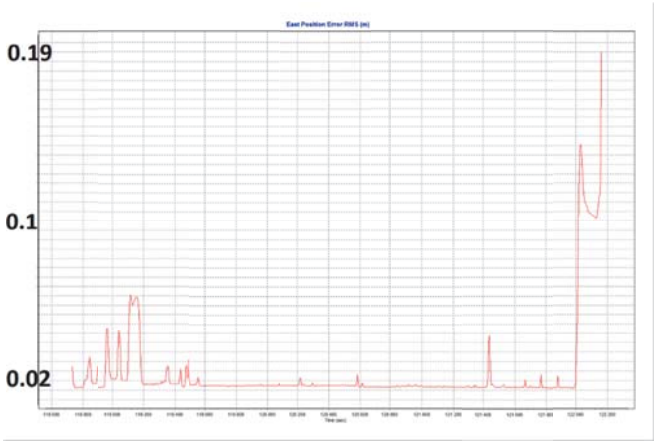

Fig. 8 Trajectory alignment of the Y-axis mean square error

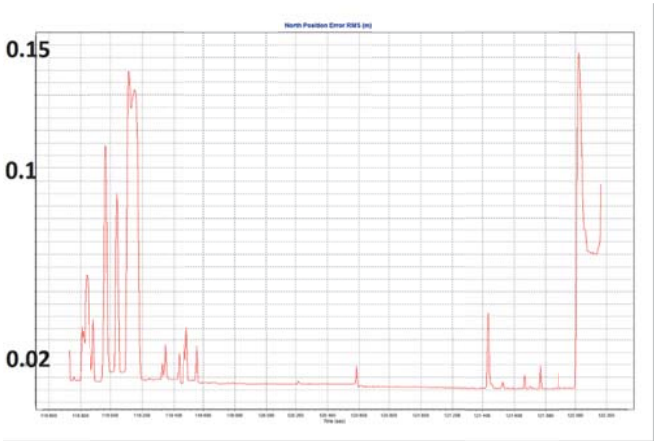

Fig. 9 Trajectory alignment of the Y-axis mean square error

The analysis of diagrams (Fig. 7-9) allows to indicate the moment of commencement of the measurement mission (the place where the error on the X and Y axes did not exceed 2

MOST WIEDZY Downloaded from mostwiedzy.pl

cm). At the same time, it can be stated that the accuracy of the data obtained has the greatest error at height, while the average error on each axis does not exceed 5 cm, so there is a real chance to obtain data with accuracy not worse than 10 cm. The result of establishing data on control points is shown in Figures 10 and 11 in the form of a report for all records and a histogram of residues from the planes used.

Calculation results

Number of free parameters: 24

Number of observations: 782

Error (Std. deviation) [m]: 0.0620

Fig. 10 Standard deviation of the alignment of individual records.

Formula for standard deviation:

$$\sigma = \sqrt{\frac{\sum_{i=1}^{n}(X - \bar{X})^2}{N}}$$

In order to transform the database, the 7- parameter transformation of Helmert is used.

$$\begin{bmatrix} X \\ Y \\ Z \end{bmatrix} \text{Target} = \begin{bmatrix} X \\ Y \\ Z \end{bmatrix} Source + \begin{bmatrix} T_x \\ T_y \\ T_z \end{bmatrix} + \begin{bmatrix} D & -R_z & R_y \\ R_z & D & -R_x \\ -R_y & R_x & D \end{bmatrix} \begin{bmatrix} X \\ Y \\ Z \end{bmatrix}$$

XYZ source- XYZ coordinates of the source data
XYZ target – XYZ coordinates of the target data
Tx, Ty, Tz – translation factors
Rx, Ry, Rz- rotation factors
D – scale factor.

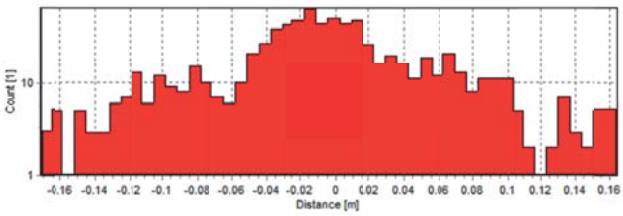

Fig. 11 Histogram of Residues of used planes

The last step in checking the accuracy of the data was to determine the coordinate differences between the control points measured with traditional methods, not used in the alignment and the point corresponding to this point on the scan (3D model). The results are presented in Table 1. The obtained result in the form of a point cloud is shown in Figure 12.

Table 1 Difference of distance in 3D space from points measured by classical methods to scanned details.

Object number	Difference in the distance between the detail and the scan
149	0.071 m
141	0.092 m
135	0.106 m
119	0.082 m
146	0.063 m

In reference to Table 1, an average result of 8.28 cm was obtained, and the numerical analysis showed an accuracy better than 10 cm.

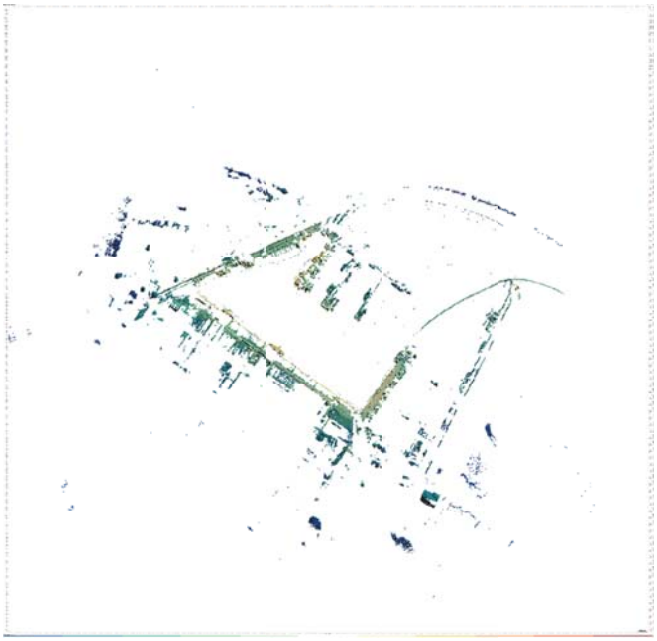

Fig. 12 Cloud of points showing the Port of Władysławowo, originating from scanning from the sea.

CONCLUSIONS

As a new measurement solution, mobile scanning using a watercraft may have a wide range of applications such as: sea coast monitoring, assessment of durability of seaports or obtaining data for inventory of buildings in close proximity to the scanner's range or above the water level. On the market, stationary laser scanners are used more and more often. However, through continuous development of data acquisition methods, methods employing their use are slowly becoming time-consuming and ineffective compared to mobile scanning of longer sections exceeding several hundred meters. This opens up new possibilities, constituting competition with traditional solutions and as a supplement for other types of laser scanning, increasing the possibilities of data analysis on real estate markets and creating hazard maps for infrastructure objects and people

MOST WIEDZY Downloaded from mostwiedzy.pl

in the near degradation impact zone [16-18]. In addition, solutions used by the authors may be used in other areas not related to the marine environment, e.g. to monitor and assess the condition of the structure [19-28], also in combination with imaging methods and photogrammetry using UAV [29-31]. The use of proprietary algorithms in the field of laser scanning [32-34] allows to increase the accuracy and analysis of the geometry of objects based on MarLS (marine laser scanning) and MLS (mobile laser scanning) made from inland and port waterways.

ACKNOWLEDGMENTS AND FINANCING

The article was created as part of the operation from the Intelligent Development Operational Program for 2014-2020 Measure 2.3 "Pro-innovative services for enterprises", Sub-measure 2.3.2 of SG OP "Bonus for innovations for SMEs." Co-financing was obtained by ZUI Apeks Sp. z o.o., represented by the director Dorota Kminikowska and the proxy Krzysztof Matysik

ZUI Apeks Sp. z o.o. was the client and the applicant. The team from the Gdańsk University of Technology has developed a task titled "Implementation of the measurement procedure for a 3D laser scanning service from a floating platform", led by Jakub Szulwic, and the main performer was Paweł Tysiąc [35].

The authors thank all persons and entities involved in the preparation and implementation of the project.

LITERATURE

1. Burdziakowski P., et al. (2015) Maritime laser scanning as the source for spatial data. Polish Maritime Research. Vol. 22, Iss. 4(88) (2015), pp.9-14, DOI: 10.1515/pomr-2015-0064

2. Kholodkov A., et al. (2014) Morski skaning laserowy infrastruktury portowej na przykładzie portu we Władysławowie (in Polish). Logistyka, Vol. 6, pp. 14317-14328

3. Mobile Laser Scanning on Board Hydrographic Survey Vessels - Applications and Accuracy Investigations - Volker Böder, Thomas P. Kersten, Thomas Thies, Arne Sauer, Germany

4. Chen C., et al. (2013) High accuracy calibration for vehicle-based laser scanning and urban panoramic imaging and surveying system. MIPPR 2013: Multispectral Image Acquisition, Processing, and Analysis, SPIE 8917, 89170Y, DOI: 10.1117/12.2031466

5. Dudzinska-Nowak J., Wezyk P. (2014) Volumetric changes of a soft cliff coast 2008-2012 based on DTM from airborne laser scanning (Wolin Island, southern Baltic Sea). Journal of Coastal Research, Vol. 70, pp. 59-64, DOI: 10.2112/SI70-011.1

6. Ossowski R. (2017) Environmental aspects of coastal earth structures made of soil-ash composites. Polish Maritime Research, Vol. 24,Iss. S1(93), pp.166-173, DOI: 10.1515/pomr-2017-0035

7. Ossowski R., Gwizdała K. (2017) Mechanical Properties of a Dike Formed from a Soil-ash Composite. Procedia Engineering, Vol. 172, pp. 816-822, DOI: 10.1016/j.proeng.2017.02.129

8. Szulwic J., et al. (2016) Coastal cliffs monitoring and prediction of displacements using terrestial laser scanning. 2016 Baltic Geodetic Congress (BGC Geomatics), 2016, IEEE Computer Society, DOI: DOI: 10.1109/BGC.Geomatics.2016.20

9. Furmańczyk K. (2013) Coastal Erosion and Protection in Europe, pp. 81-95, ISBN 978-1-84971-339-9

10. Abellan A., et al. (2009) Detection of millimetric deformation using a terrestrial laser scanner: experiment and application to a rockfall event. Nat. Hazards Earth Syst. Sci., 9, 365–372, 2009

11. Bobkowska K., et al. (2017) Implementation of spatial information for monitoring and analysis of the area around the port using laser scanning techniques. Polish Maritime Research, Vol. 24, Iss. S1(93), pp.10-15, DOI: 10.1515/pomr-2017-0015

12. Wolski T. (2017) Czasowa i przestrzenna charakterystyka ekstremalnych poziomów wód Morza Bałtyckiego (in Polish). Szczecin 2017, ISBN 978-83-7972-091-0

13. Szafranek K., at al. (2014) Configuration of the reference stations as the element of national reference frame reliability. Acta Geodynamica et Geomaterialia, Vol. 11, Iss. 1, pp. 5-15, 2014

14. Nykiel G., et al. (2017) Atmospheric opacity estimation based on IWV derived from GNSS observations for VLBI applications. GPS Solutions, Vol. 22, Iss. 1, Art. UNSP 9

15. Nowak A. (2017) Dynamic GNSS mission planning using DTM for precise navigation of autonomous vehicles. Journal of Navigation, Vol. 70, Iss. 3, pp. 483-504, DOI: 10.1017/S0373463316000679

16. Renigier-Biłozor M., et al. (2017) Rating engineering of real estate markets as the condition of urban areas assessment. Land Use Policy, Vol. 61, pp. 511-525, DOI: 10.1016/j.landusepol.2016.11.040

17. Renigier-Biłozor M., et al. (2014) Rating methodology for real estate markets – Poland case study. International Journal of Strategic Property Management, 18, 198-212, DOI: 10.3846/1648715X.2014.927401

MOST WIEDZY Downloaded from mostwiedzy.pl

18. Apollo M., et al. (2017) Application of BN in risk diagnostics arising from the degree of urban regeneration area degradation. 2017 Baltic Geodetic Congress (BGC Geomatics), Gdansk Univ Technol, Poland, JUN 22-25, 2017, pp. 83-88, DOI: 10.1109/BGC.Geomatics.2017.47

19. Miśkiewicz M. et al. (2017) Technical monitoring system for a new part of Gdansk Deepwater Container Terminal. Polish Maritime Research, Iss. S1 (93), vol. 24, pp. 149-155, DOI: 10.1515/pomr-2017-0033

20. Chróścielewski J., et al. (2017) A novel sandwich footbridge – Practical application of laminated composites in bridge design and in situ measurements of static response. Composites Part B-Engineering. Vol. 126, pp. 153-161. DOI: 10.1016/j.compositesb.2017.06.00

21. Mitrosz O., et al. (2017) Preliminary field tests and long-term monitoring as a method of design risk mitigation: a case study of Gdansk Deepwater Container Terminal. Polish Maritime Research No 3(95), vol. 24, pp. 106-114, DOI: 10.1515/pomr-2017-0095.

22. Bobkowska K., et al. (2017) DMI measurements impact on a position estimation with lack of GNSS signals during Mobile Mapping. Journal of Physics: Conference Series, Vol. 870, DOI: 10.1088/1742-6596/870/1/012010

23. Paszotta Z., et al. (2017) Internet Photogrammetry for Inspection of Seaports. Polish Maritime Research, 24 (s1), pp. 174-181. DOI: 10.1515/pomr-2017-0036

24. Miśkiewicz M., Pyrzowski L. (2017) Load Tests of the Movable Footbridge Over the Port Canal in Ustka. 2017 Baltic Geodetic Congress (BGC Geomatics), pp. 242-246. DOI: 10.1109/BGC.Geomatics.2017.7

25. Miśkiewicz M., Makowska K. (2017) Displacement measurements during load testing of railway arch bridge. 17th International Multidisciplinary Scientific GeoConference SGEM 2017, Vol. 17, Iss. 22, 257-264 pp, DOI: 10.5593/sgem2017/22/S09.032.

26. Kamiński W., et al. (2015). System of monitoring of the Forest Opera in Sopot structure and roofing, 15th International Multidisciplinary Scientific GeoConference SGEM 2015, Book 2 Vol. 2, pp. 471-482, DOI: 10.5593/SGEM2015/B22/S9.059.

27. Chróścielewski J., et al. (2014). Assessment of tensile forces in Sopot Forest Opera membrane by in situ measurements and iterative numerical strategy for inverse problem, Shell Structures: Theory and Applications. Vol. 3, 2014, CRC Press/Balkema, pp. 499-502, DOI: 10.1201/b15684-125

28. Pyrzowski Ł., et al. (2016) Structural Health Monitoring of Composite Shell Footbridge for Its Design Validation. Proceedings 2016 Baltic Geodetic Congress (Geomatics), IEEE Computer Society, pp. 228-233, DOI: 10.1109/BGC.Geomatics.2016.48

29. Przyborski M., et al. (2015) Photogrammetric development of the threshold water at the dam on the Vistula river in Wloclawek from unmanned aerial vehicles (UAV). In SGEM2015 Conference Proceedings (pp. 18-24), DOI: 10.5593/SGEM2015/B31/S12.063

30. Kedzierski M., Delis P. (2016) Fast orientation of video images of buildings acquired from a UAV without stabilization. Sensors, Vol. 16, Iss. 7, Article Number: 951, DOI: 10.3390/s16070951

31. Glowienka E., et al. (2017) Use of LIDAR Data in the 3D/4D Analyses of the Krakow Fortress Objects. IOP Conference Series-Materials Science and Engineering, Vol. 245, Article Number: UNSP 042080, WMCAUS, Prague, Czech Republic, DOI: 10.1088/1757-899X/245/4/042080

32. Janowski A. (2018) The circle object detection with the use of Msplit estimation. E3S Web Conf. Vol. 26, 2018 Seminary on Geomatics, Civil and Environmental Engineering, Gdańsk, Poland, 2017, DOI: 10.1051/e3sconf/20182600014

33. Bobkowska K., et al. (2018) 3D modelling of cylindrical shaped objects from LIDAR data – an assessment based on theoretical modelling and experimental data. Metrology and Measurement Systems, Vol. 25, Iss. 1/2018, DOI: 10.24425/118156

34. Janowski A., et al. (2016) Remote sensing and photogrammetry techniques in diagnostics of concrete structures. Computers and Concrete, Vol. 18, Iss. 3, pp. 405-420

35. Bobkowska K., et al. (2017) Procedura pomiarowa usługi skanowania laserowego 3D z platformy pływającej (in Polish). Gdańsk, FCEE GUT, ISBN 978-83-60261-05-7, pp. 1-98.

CONTACT WITH THE AUTHORS

Jakub Szulwic
e-mail: szulwic@pg.edu.pl

Paweł Tysiąc
e-mail: pawel.tysiac@pg.edu.pl

Gdańsk University of Technology
Faculty of Civil and Environmental Engineering
11/12 Narutowicza St.
80 - 233 Gdańsk
Poland

MOST WIEDZY Downloaded from mostwiedzy.pl

POLISH MARITIME RESEARCH Special Issue 2018 S1 (97) 2018 Vol. 25; pp. 166-171
10.2478/pomr-2018-0038

MODELING OF THE TWO-DIMENSIONAL FLOW CAUSED BY SEA CONDITIONS AND WIND STRESSES ON THE EXAMPLE OF DEAD VISTULA

Piotr Zima
Gdańsk University of Technology, Poland

ABSTRACT

The article presents the results of two-dimensional modeling of flows caused by the sea conditions and wind stresses on the example of Dead Vistula. Based on the available bathymetric data, a numerical model of the river section was created, which was supplemented with data on the position of the water table depending on hydrometeorological conditions. To describe the flow field in steady conditions, a simplified model of two-dimensional flow in the form of the bi-harmonic Helmholtz equation for the current function has been adopted, taking into account additional impacts caused by wind stresses on the water surface. Then the current function was converted into the velocity vector components. This equation, supplemented with appropriate boundary conditions, has been solved numerically using the finite difference method. On the basis of the available literature, 4 variants of hydrometeorological conditions were adopted, depending on the direction and strength of wind and sea conditions. The obtained results were compared with the results of published measurements taken on the studied section of the river. These calculations were the basis for the implementation of a two-dimensional model of the spread of pollutants in the studied section of the Dead Vistula.

Keywords: two-dimensional modeling of flows, bi-harmonic Helmholtz equation, hydrodynamics of water flow

INTRODUCTION

Flow modeling in rivers is an important tool to support design work in the field of hydrotechnical construction. It is also the first stage in the work on the analysis of the spread of pollutants and their impact on the receiver's waters and the surrounding environment (Wielgat and Zima, 2016). In such a situation there is a need to reconstruct the hydrodynamics of water flow on the analyzed section of the river. In practice, different models are used, and their choice depends on the characteristics of the object and the needs for which the analysis is performed (Szymkiewicz, 2010). For long sections of rivers, one-dimensional models are used, importing the tested section into a linear object, averaging all parameters across the entire cross-section. In the case of wide rivers, two-dimensional models are used, averaged vertically (along the depth). This applies to cases when the analysis requires evaluation of variable conditions along the river's width - for example, any reproduction of flow in the vicinity of the hydro-technical building and in the case of inflow of water from the shore or discharge of additional contaminated water. Three-dimensional models are used very rarely, mainly in scientific works and relate to research on specific objects (Jasińska, 2002).

In the cases of modeling two-dimensional flows, the often used mathematical model are the so-called shallow water equations (SWE), or the Saint-Venant equations for a two-dimensional area (Tan 1992, Szydłowski et al., 2013). They are a proven tool, but from a formal point of view

MOST WIEDZY Downloaded from mostwiedzy.pl

they constitute an initial-boundary problem and require to define the boundary conditions, i.e. the initial condition and boundary conditions. In the case of a flow simulation in the so-called characteristic flow conditions, hydrological calculations give information on flows and characteristic states. In the case of many analyzes (including analysis regarding the spread of pollutants - Wielgat and Zima, 2016, Winter 20017, and Winter 2018), this information is insufficient. It is then necessary to determine the distribution of the speed field throughout the analyzed section of the river. The SWE solution first requires a solution in accordance with the adopted conditions regarding the position of the water table for a given flow. In many cases, this involves calculations that allow the identification of resistance to movement until the position of a water table similar to the characteristic states is obtained. The SWE solution also requires time integration, which in the case of fixed (permanent) motion requires simulation until the flow conditions are established, which is not always unambiguous. Therefore, in the case of calculations for characteristic conditions (for flow and condition), the natural way will be to look for simplified models. In computational hydraulics, such models are often used. This article presents one such model that allows to obtain velocity distribution in two-dimensional area with variable depth solving the modified Helmholtz equation (Anderson, 1995). Additionally, due to the nature of external interactions resulting from the location of the analyzed section of the river, the influence of wind stresses was taken into account in the equation. The calculations were made for the section of Dead Vistula, whose hydrodynamics are caused by sea conditions in the Gulf of Gdańsk and wind accumulation. Obtained results of calculations carried out in specific weather conditions were compared with the results of carried out measurements presented in this work (Jasińska, 2002).

MATHEMATICAL MODEL

To describe the river water flow field, a model was adopted in this work in which, along with the fulfillment of the mass behavior equation, the variability of rotation of the fluid element is also assumed (Anderson, 1995). In the case of a two-dimensional speed vector: u=[u_x,u_y] this condition can be written as follows:

$$\mathrm{rot}\,\mathbf{u} = \Omega(x, y) \tag{1}$$

where: $\Omega(x, y)$ is the assumed function of the vorticity distribution. If the Stokes assumption (neglecting the forces of inertia) is applied for fixed flow conditions and constant water temperature and relation (1) is taken into account, the result is:

$$\Delta\Omega = 0 \tag{2}$$

This is the equation for the harmonic of the Ω function, called the Helmholtz equation. If the current function $\psi(x, y)$ for vertically averaged plane motion is defined in the following way:

$$\frac{\partial \psi}{\partial y} = h \cdot u_x, \quad -\frac{\partial \psi}{\partial x} = h \cdot u_y \tag{3}$$

(where h is the depth), finally, equation (2) (the biharmonic equation) can be written in the following form:

$$\Delta\Omega = \Delta\Delta\psi = \Delta\left(\frac{1}{h}\Delta\psi - \frac{1}{h^2}\nabla\psi\nabla h\right) = 0 \tag{4}$$

Equation (4) can be obtained by transforming the equation of momentum conservation in stationary motion conditions, taking into account the Stokes assumption. In this equation, speed rotation is a harmonic function described by the Laplace equation. Taking into account additional forces affecting the water movement caused by stress on the surface from the wind, causes equation (4) to take the following form:

$$\Delta\left(\frac{1}{h}\Delta\psi - \frac{1}{h^2}\nabla\psi\nabla h\right) = -\frac{1}{\kappa} rot_z \frac{\mathbf{T}}{h} \tag{5}$$

where: κ coefficient of turbulent viscosity, **T** stress vector of tangential wind in tow-dimensional space (x,y) T=[T_x,T_y]. The coordinates of the wind stress vector are defined as follows (Tan, 1992):

$$T_x = \frac{\rho_\alpha}{\rho} \cdot \alpha \sqrt{w_x^2 + w_y^2} \cdot w_x \tag{6}$$

$$T_y = \frac{\rho_\alpha}{\rho} \cdot \alpha \sqrt{w_x^2 + w_y^2} \cdot w_y \tag{7}$$

where: α coefficient of wind stresses, $\alpha = 2.5 \times 10^{-3}$, ρ and ρ_α density of water and air, w_x, w_y components of the wind velocity vector.

In general, the Dirichlet problem should be solved for the biharmonic operator. A 4th order equation is obtained, which requires to solve simultaneously the determination of two conditions at the edge of the Γ area: the Dirichlet $\psi|_\Gamma = const$ type condition and the Neumann $\left.\frac{\partial \psi}{\partial n}\right|_\Gamma = 0$ type. The solution to this problem in the two-dimensional space *(x, y)* is the current function. Using the relation (3), you can calculate the components of the velocity vector in the whole area. To solve the equation (5) the finite difference method (FDM) was used (Anderson 1995, Potter 1980), covering the solution area with a square mesh of $\Delta x=\Delta y$. The adoption of a square mesh with fixed dimensions has its advantages and disadvantages. The advantage is that such an approach significantly simplifies the final formula of the model (especially considering additional forces at the level of the basic equation). However, the disadvantage is the inability to differentiate it in some parts of the computing area. This requires, unfortunately, the adoption of a suitable dense grid in the entire computational area. This approach also improves the stability of the solution.

The use of differential diagrams leads to the final solution of algebraic linear equations. This system is characterized

MOST WIEDZY Downloaded from mostwiedzy.pl

by the lack of dominant elements on the main diagonal matrix of ratios, which unfortunately negatively affects the accuracy of the solution for most known numerical methods (Szymkiewicz, 2010). In this work, the simple iteration method (Jacobi's method) was used. The properties of the created system of equations cause that the iterative process is slowly convergent and there is a danger of the solution being under-iterated. Therefore, during the solution of each task, the iteration termination test was individually selected, analyzing its impact on the final solution.

CHARACTERISTICS OF THE STUDIED AREA

The Dead Vistula is part of the hydrographic complex delta that has developed over the last centuries. This area is characterized by the interaction of land and sea waters, it has changed in a natural way and as a result of human activity. The current hydrographic state of the Vistula delta cutoff was significantly influenced by the dug-thru at the end of the 19th century, draining the Vistula waters directly to the sea and the sluice in Przegalin. This changed significantly the hydrodynamic conditions on the section of the Vistula delta, creating a dead branch – Dead Vistula. The Vistula river ceases to be powered by the waters of the Vistula, it is connected with the sea by two arms: the port channel in Nowy Port and the Vistula Śmiała river. Only small amounts of Vistula waters get to the Dead Vistula thru the ship sluices in Przegalina. This fact has a significant impact on the hydrodynamic conditions prevailing in the Dead Vistula, in which the water movement is determined primarily by sea conditions and blowing winds. Works on modeling hydrodynamics of this section of the Vistula River were carried out at the IBW PAS in Gdańsk. Modeling results are presented in the paper (Jasińska, 2002). As part of this study, in the assumed hydrodynamic model, the results included in this work were assumed as boundary conditions (adopted speed distributions in cross-sections limiting the assumed mathematical model - near the Siennicki Bridge, in the estuary cross-section of the Vistula Śmiała and cross-section at Sobieszewo height).

Fig.1. Dead Vistula with available cross-sections (red lines) and the adopted computational area (area shaded in read) (source: ortofotomap from http://mapy.geoportal.gov.pl)

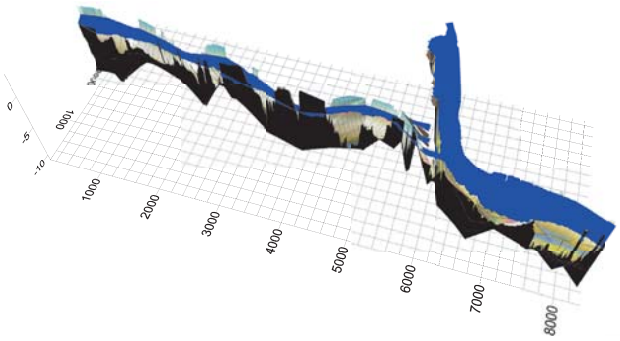

Fig.2. Numerical model of the bottom with the location of the water table

In the latter part of the work, a numerical model of the Dead Vistula section was made from the cross-section at the height of the Siennicki Bridge to the cross-section at Sobieszewo (about 8.5 km), including the 2.5-kilometer section of the Vistula Śmiała, to its mouth at the Gulf of Gdańsk. Using the available data on the measured computational cross-sections, a numerical model of the bottom of the Dead Vistula section was generated. The bathymetry between the measured cross-sections was generated by linear interpolation (Fig. 2).

Due to the assumed hydrodynamic model, the water table was also required to be assumed. Information on the location of the water table was adopted adequately to the conditions for which calculations of the velocity field distribution were made (Jasińska, 2002).

NUMERICAL SIMULATIONS

The hydrodynamic calculations were made in four variants presented in the study (Jasińska, 2002): for the eastern wind of 5 m/s, for the western wind of 5 m/s and for extreme conditions, i.e. for the western wind of 15 m/s and 25 m/s. When determining boundary conditions in the calculations performed, averaged vertical velocity values were assumed (despite the often occurring diversity of flows in the near bottom and near surface layers), assuming in the majority of values presented in the work (Jasińska, 2002) obtained in the near surface layer.

Regardless of the computational variant adopted, the velocity field distribution on the section of the Dead Vistula concerned was calculated using equation (5). The calculations were made using a square grid with sides $\Delta x=\Delta y$=5,0m. The size of the grid was based on the dimensions of the calculation area in the Isthmus region. The obtained results are shown in Figures 3 to 6. Due to the density of the calculation grid, it was presented by every 65th vector of speed (Fig. b) and by every 10th vector (Fig. c).

Fig. 3 presents the results of the distribution of the current line and the corresponding velocity distribution for the variant of weak eastern wind with the strength E 5 m/s. This wind causes the inflow from the Gulf of Gdańsk section of the Vistula Śmiała, inflow from the Przegalin side, and flow in the branch of the Dead Vistula towards the west and outflow to

MOST WIEDZY Downloaded from mostwiedzy.pl

the Gulf of Gdańsk near Nowy Port. The calculations assume: an influx of the Vistula Śmiała River due to the average sea state with an average speed of 0.05 m/s, inflow in the section from Świbno with the speed of 0.02 m/s and outflow through the section near the Siennicki Bridge at the speed of 0,04 m/s. As a result of the calculations carried out, speed distribution was achieved that reproduced the basic flow directions.

The maximum values of the velocity vector module occurred at the level of the Isthmus and were at the level of 0.25 m/s, which is consistent with the results presented in the work (Jasińska, 2002).

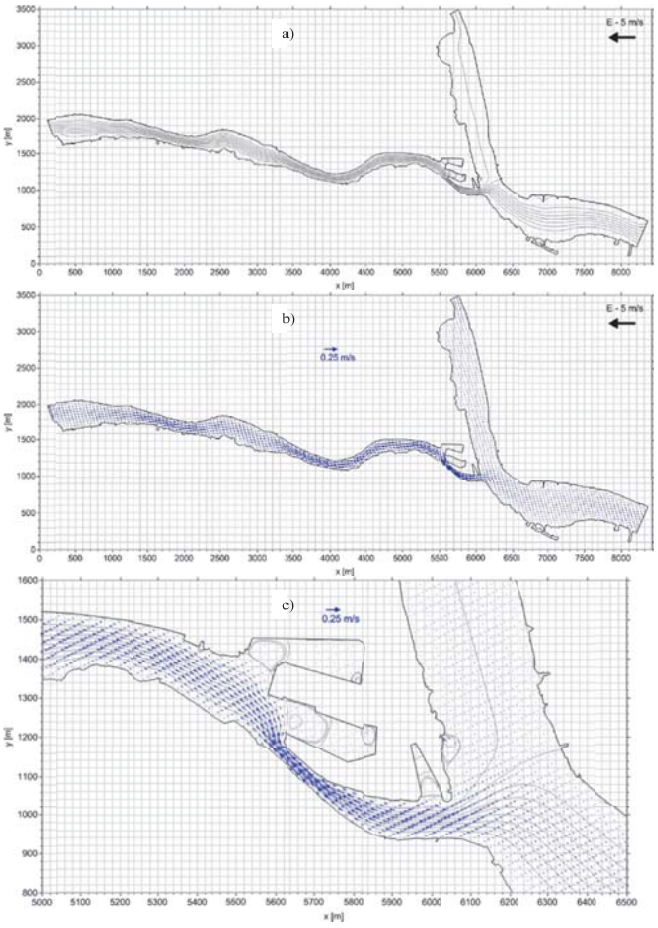

Fig.3. Results of hydrodynamic calculations: a) distribution of current lines, b) their corresponding speed field, and c) detailed results near Isthmus, in eastern wind conditions E - 5 m/s

Weak wind from the west (W) with a force of 5 m/s, causes an almost completely different current circulation in Dead Vistula. The outflow in section at the mouth of the Vistula Śmiała towards the Gulf of Gdańsk with a speed of about 0.05 m/s is registered. In the Sobieszewo region, the water flow is consistent with the wind direction at a speed of about 0.03 m/s. From the direction of Siennicki Bridge, the water inflow is visible with the speed of about 0.06 m/s. As a result, a directed flow in the branch of the Dead Vistula towards the east can be observed, assuming the maximum values of the velocity vector module in the vicinity of the Isthmus at the level of 0.28 m/s. The results obtained are shown in Fig. 4.

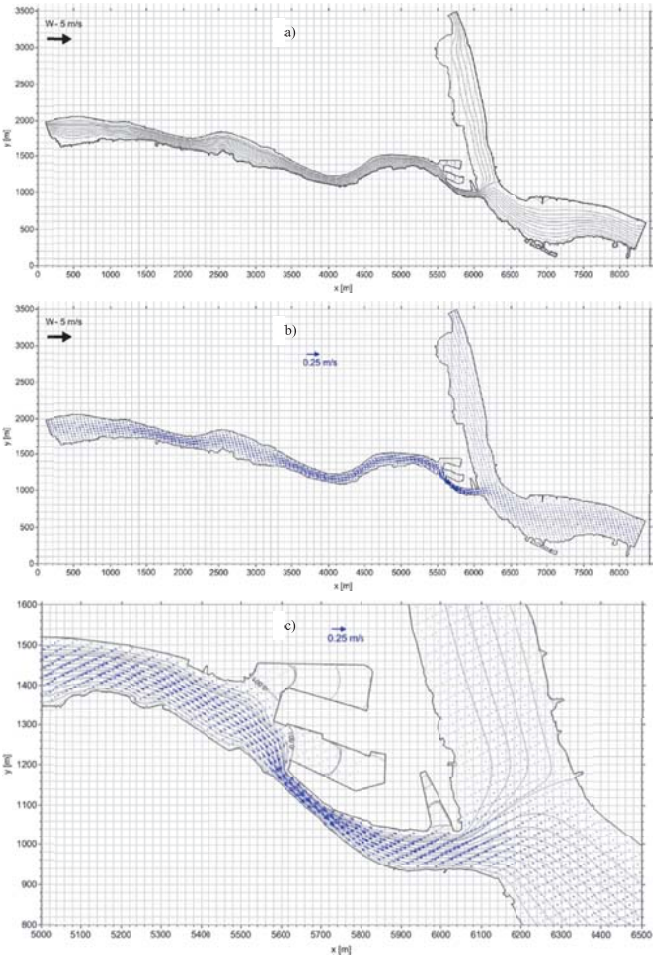

Fig.4. Results of hydrodynamic calculations: a) distribution of current lines, b) their corresponding speed field, and c) detailed results near Isthmus, in western wind conditions W - 5 m/s

The next two variants of calculations were made for extreme hydrometeorological conditions occurring in the Dead Vistula region. In the first place (variant no. 3), simulations were carried out for the case of the western wind (W) with a force of 15 m/s, assuming an increase in the sea state by approx. 0.7 m from the average state (up to 570 cm). In the area of the mouth of the Vistula Śmiała, there is an outflow to the Gulf of Gdańsk with a speed of 0.6 m/s. At the west arm of the Dead Vistula in the area of the Siennicki Bridge there is a flow towards the east (inflow) with the speed at the level of 0.3 - 0.4 m/s. At the eastern arm of the Dead Vistula (in the Sobieszewo region), a stronger flow towards the east (outflow) is visible with speeds of 0.3 m/s. As a result, a clear flow is visible in the branch of the Dead Vistula towards the east, with maximum values in the vicinity of the Isthmus at 1.5 m/s, which is in line with the results presented in the work (Jasińska, 2002). Obtained results in this calculation variant are shown in Fig. 5.

MOST WIEDZY Downloaded from mostwiedzy.pl

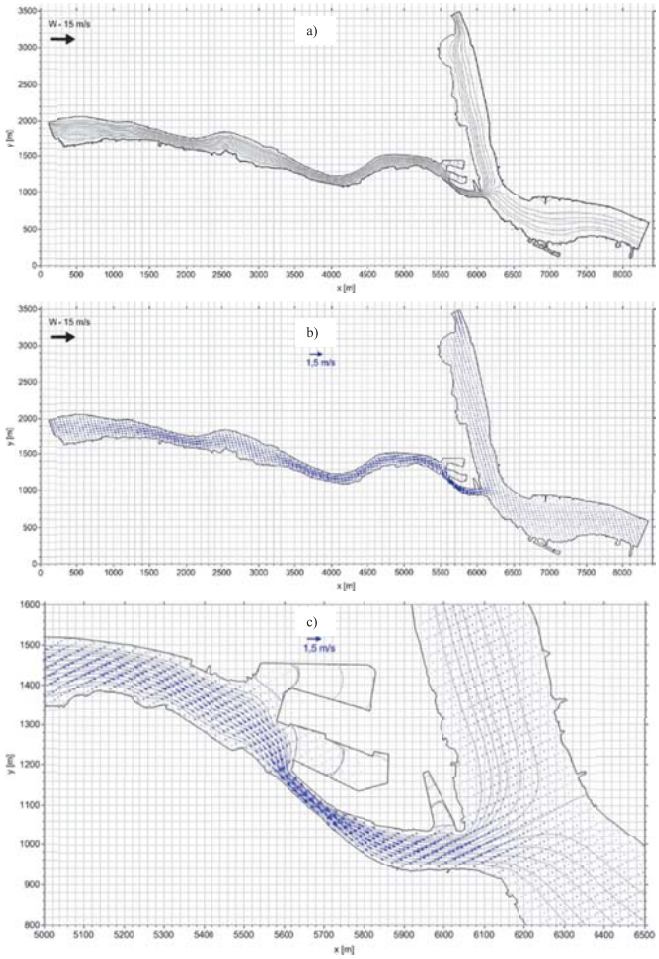

Fig.5. Results of hydrodynamic calculations: a) distribution of current lines, b) their corresponding speed field, and c) detailed results near Isthmus, in western wind conditions W - 15 m/s

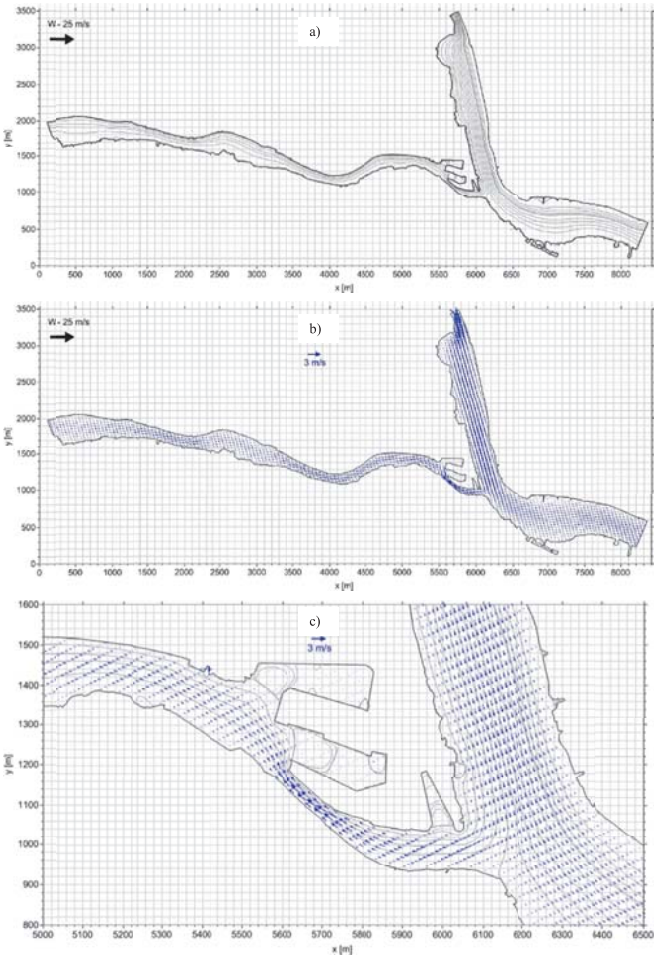

Fig.6. Results of hydrodynamic calculations: a) distribution of current lines, b) their corresponding speed field, and c) detailed results near Isthmus, in western wind conditions W - 25 m/s

The last variant concerned the case of the western wind (W) with a force of 25 m/s, assuming the sea rise from a high level of 570 cm to a level of 625 cm. In such extreme conditions of very high sea state and very strong western wind, the conditions of the flow in the estuary change. In the area of the estuary of the Wisła Śmiała, an inflow in the entire section from the Gulf of Gdańsk occurs at very high speeds of 3.0 m/s. On the west branch of the Dead Vistula in the area of the Siennicki Bridge there is a flow towards the west (outflow) at a speed of 0.5 - 0.6 m/s. At the eastern branch of the Dead Vistula (in the Sobieszewo region) a stronger flow towards the east (outflow) is visible with speeds of 0.5 m/s. As a result, a clear flow is visible in the branch of the Dead Vistula towards the west, with maximum velocities around the Isthmus at the level of over 1.0 m/s. Obtained results in this calculation variant are presented in Fig. 6.

DISCUSSION OF THE RESULTS OBTAINED AND CONCLUSIONS

The conducted computer calculations made it possible to plot the field of current function and calculate the values of the components and velocity field in the section of Dead Vistula from Sobieszewo to Siennicki Bridge (about 18.5 km) together with the section of Vistula Śmiała that flows into the Gulf of Gdańsk (about 2.5 km). On the basis of available cartographic materials, the boundary of the shoreline was marked out, and on the basis of the data on cross-sections a numerical model of the bottom was created of the considered section of the river. The model was supplemented with data on the position of the water table depending on hydrometeorological conditions. On the basis of the available literature, 4 variants of these conditions were adopted, depending on the wind direction and strength and sea conditions (for the eastern wind with a force of 5 m/s, for the western wind with a force of 5 m/s and for extreme conditions, i.e. for the western wind o strength 15 m/s and 25 m/s). Then, calculations of the velocity distribution in the traffic conditions set for each of the adopted variants were made. The obtained results of computer simulations

MOST WIEDZY Downloaded from mostwiedzy.pl

were consistent with the averaged results of velocity distribution measurements in characteristic cross-sections of Dead Visutla presented in the work (Jasińska, 2002). This comparison was the final criterion confirming that the use of a two-dimensional model to describe hydrodynamics in the studied section of the Dead Vistula gave correct results. These calculations were the basis for the implementation of a two-dimensional model of pollution spread on the analyzed section of the Dead Vistula, which requires a solution to the transport equation in a two-dimensional case (Sawicki and Zima, 1997).

BIBLIOGRAPHY

1. Anderson J. D.: Computational Fluid Dynamics. The Basics with Applications, McGraw-Hill Inc., New York (1995), pp. 1–547
2. Jasińska E.: Hydrology and hydrodynamics of the Martwa Vistula and Vistula Przekop, (in Polish), Wydawnictwo Instytutu Budownictwa Wodnego Polskiej Akademii Nauk, Gdańsk (2002), pp. 1-133
3. Potter D. E.: Computational Physics, John Wiley & Sons Ltd., Chichester (1980), pp.1-304
4. Sawicki J.M., Zima P.: The Influence of Mixed Derivatives on The Mathematical Simulation of Pollutants Transfer. 4th International Conference on Water Pollution, Slovenia (1997), pp. 627-635
5. Szydłowski M., Szpakowski W., Zima P.: Numerical simulation of catastrophic flood: the case study of hypothetical failure of the Bielkowo hydro-power plant reservoir, Acta Geophysica (2013), pp. 1229-1245
6. Szymkiewicz R.: Numerical Modeling in Open Channel Hydraulics, Book Series: Water Science and Technology Library, vol. 83 (2010), pp. 1-419
7. Tan W.Y.: Shallow Water Hydrodynamics, Mathematical Theory and Numerical Solution for a Two-dimensional System of Shallow Water Equations, Elsevier Oceanography Series, vol. 55 (1992), pp. 1-434
8. Wielgat P, Zima P.: Analysis of the impact of the planned sewage discharge from the 'North' Power Plant on the Vistula water quality, 16th International Multidisciplinary Scientific GeoConference SGEM 2016, Vienna, Book 3 Vol. 3 (2016), pp. 19-26
9. Zima P.: Investigations on water circulation in animal sea-water basins – on the example of seals' breeding pools, Polish Maritime Research, Vol. 24 (2017), No S1(93), pp. 224-229
10. Zima P.: Mathematical Modeling of the Impact Range of Sewage Discharge on the Vistula Water Quality in the Region of Włocławek. Chapter in book: Free Surface Flows and Transport Processes. Verlag: Springer Int. Publishing (2018), pp. 489-502

CONTACT WITH THE AUTHOR

Piotr Zima

Gdańsk University of Technology
Faculty of Civil and Environmental Engineering
11/12 Narutowicza St.
80 - 233 Gdańsk
Poland

MOST WIEDZY Downloaded from mostwiedzy.pl

POLISH MARITIME RESEARCH Special Issue 2018 S1 (97) 2018 Vol. 25; pp. 172-177
10.2478/pomr-2018-0039

INFLUENCE OF LUBRICATING OIL IMPROVERS ON PERFORMANCE OF CRANKSHAFT SEALS

Piotr Bzura
Gdańsk University of Technology, Poland

ABSTRACT

This paper presents an original method for checking influence of lubricating oil improvers on performance of crankshaft seals of combustion piston engine. Crankshaft seals were tested with the use of a modified friction node of T-02 four-ball apparatus in laboratory conditions. The tests were conducted according to a worked-out algorithm. Their results confirmed usefulness of the method for determining „harmful" performance of sealing systems, which makes it possible to assess operational usability of lubricating oil improvers. On the basis of an analysis of the results a scientific hypothesis saying that lubricating oil quality affects correctness of performance of crankshaft seals of combustion piston engine, was formulated. The hypothesis was verified by means of induction inference and statistical method with taking into account Fisher statistics.

Keywords: performance, scientific hypothesis, sealing systems

INTRODUCTION

During operation of combustion piston engine a part of thermal energy generated by fuel combustion in working space is transformed into mechanical energy. Such form of transformation is called work. Energy transformation efficiency influences mode of operation of a. o. crankshaft bearings . Such operation of an arbitrary slide bearing can be interpreted to be energy transfer over a given time, which makes to-and-fro motion of piston and simultaneously crankshaft rotation possible in given conditions and time t. Wear of all elements of the bearing (i.e. journal, sleeves and lubricating oil – a separating medium) is the main factor affecting slide bearing operation .

Physical and chemical properties of lubricating oil which determine its quality condition operational durability and failure-free operation of crankshaft bearings. In the subject-matter literature a lack of oil in engine is usually called "oil consumption". However in opinion of this author it is important to distinguish a shortage or loss of oil from real oil consumption. The latter should be meant to be a quantity of oil which goes to combustion chamber and is burned there, whereas a shortage i.e. loss of oil occurs when oil gets off the engine system as a result of leakage.

The shortage (oil loss) depends on operational correctness of crankshaft seals which is affected by quality of improvers. Therefore it is important to investigate the influence.

To perform analysis of influence of improvers on performance of crankshaft seals the friction node of T-02 four-ball apparatus was modified [1]. As a result, it was possible to compare lubricating properties (lubricity) of SAE30 lubricating oil free of improvers with the properties of two samples of the same oil but containing various improvers which make it possible to improve regeneration of boundary layer and consequently to assure boundary lubrication conditions. The so rebuilt boundary layer is characterized by a. o. lowered friction factor, higher durability and resistance to breaking [2].

The presented analysis of results of the tests on the sealing system made it possible to formulate and verify the following scientific hypothesis.

MOST WIEDZY Downloaded from mostwiedzy.pl

A sudden break of boundary layer occurs as a result of sudden increase of average value of "harmful" performance of the seal.

Consequences of the hypothesis are the following :

1. An increase of temperature of the unit associated with greater friction,
2. An increase of vibration of the unit associated with direct contact between its elements.

The formulated consequences $K_i(i = 1, 2)$ reveal probabilistic law of wear in the tested crankshaft seal. They are not mutually inconsistent and their logical truth does not involve any doubt. Therefore the condition for consistency of the consequences is satisfied, hence they may be used for empirical testing truthfulness of the presented hypothesis (H), i.e. its verification aimed at either its acceptance or falsification (of course in logical and empirical sense). The verification was done by experimental testing the seal performance and checking truthfulness of the consequences $K_i(i = 1, 2)$. The test confirmed that the consequences really (in fact) occurred. The verification of the hypothesis H was conducted with taking into account truthfulness of the following syntactic implication [3, 4]:

$$\boldsymbol{H} \Rightarrow \boldsymbol{K}_i(i=1,2) \tag{1}$$

This made it possible to do non-deductive (inductive) inference in accordance with the following scheme [3]:

$$[\boldsymbol{K}_i(i = 1, 2), \boldsymbol{H} \Rightarrow \boldsymbol{K}_i(i = 1, 2] \vdash H \tag{2}$$

Logical interpretation of the inference scheme is as follows : If the empirical test of the consequences $K_i(i = 1, 2)$ confirmed their truthfulness then, if the implication (1) is also correct, the hypothesis H is also correct and can be accepted. The inductive inference conducted according to the scheme (2) is called reductive inference. Such inference – like any else belonging to this group of inference – does not lead to certain conclusions but only to probable ones [5]. The tests performed with taking into account the relations (1) and (2) confirmed truthfulness of the formulated hypothesis.

The correctness of the hypothesis – as it was considered probable – was additionally verified by means of Fisher statistics [6].

Results of the verification are given in Sec. 5 of this paper.

The tests in question were carried out on the engine crankshaft standard sealing system whose schematic diagram is presented in Fig. 1.

CRANKSHAFT SEALING SYSTEM

The sealing system (seal) of crankshaft was consisted of elements which prevent or limit lubricating oil escaping from working space of the seal into the environment.

The aim of sealing technique is to form structural features of the seal itself or the entire sealing unit in such way as to cause it working with a given tightness degree in given operational conditions.

Today, among the seals in rotational motion the most commonly applied design is the so called „simmering" (Fig.1). It is consisted of the metal casing (5) in which a dynamic sealing edge is placed in the form of the lip (3) made usually of an elastomer and pressed towards surface of the shaft (2) by means of the tension spring (4).

The seal operates on lubricating oil boundary layer of abt. 1 μm in thickness, that is assured owing to balance between the radial forces (P_r) exerted by the tension spring (3), as well as rubber elastomer (2) and the elastohydrodynamic force (P_h) resulting from rotational motion of the shaft against the elastomer rubber lip separated from the shaft surface by the oil film (1) [7].

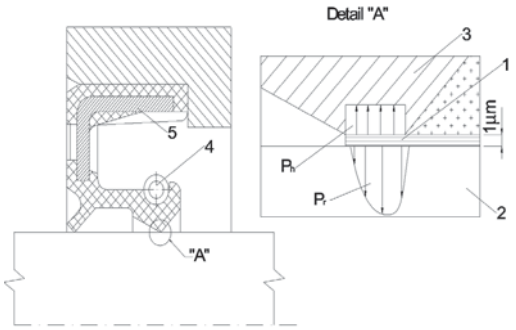

Fig.1. Schematic diagram of the rotating shaft sealing system: 1 – oil film, 2 – crankshaft, 3 – rubber lip, 4 – tension spring, 5 – metal casing, P_h – elastohydrodynamic force, P_r – radial force

Dynamic seal cannot be always perfectly tight. Permanent tightness may be assured only when a determined amount of oil is able to escape outside and lubricate this way the seal and prevent it against wear and possible failure.

Perfect tightness (in physical sense) is not possible to occur, therefore a technical tightness which takes place when "leakage" is reduced to a level which does not cause any negative consequences for both the environment and device itself, is defined.

Possible assurance of required tightness may be defined as a "harmful" work of the seal, i.e. that which causes a minimum (but necessary) energy dissipation. Such operation of the sealing system intensifies along with increasing wear of one of the crucial elements of crankshaft seal and it may be presented in the following form as the "harmful" performance [3,4,8]:

$$D_S = L_S \cdot \tau \tag{3}$$

where:

D_S – "harmful" performance of sealing system,

τ – period of one crankshaft rotation,

L_S – "harmful" work done during one crankshaft rotation, i.e:

$$L_S = 2 \cdot \pi \cdot P_r \cdot r \cdot \mu \tag{4}$$

where:

P_r – radial load [N];

μ – friction factor [-];

r – shaft radius [m].

MOST WIEDZY Downloaded from mostwiedzy.pl

For purposes of assessment of tightness degree ("harmful" performance) of sealing system the following states are distinguished :

I. Full serviceability state – technical tightness (full),
II. Partial serviceability state – „sweating seal " or oil leaking through seal,
III. Unserviceability state -leakage.

In determining whether a given sealing system is in the serviceability state (technical tightness) or in the unserviceability state (leakage) a permissible degree of " harmful" performance ($D_{S(dop)}$) should be selected as that which causes the highest necessary energy dissipation which does not yet disturb regeneration of the boundary layer formed on friction surfaces of the sealing system. If quantity of the "harmful" performance $D_S \leq D_{S(dop)}$ then the system in question is in the state of full serviceability (technically tight), and, when quantity of the "harmful" performance $D_S > D_{S(dop)}$ then the system in question goes either to the state of partial serviceability or unserviceability.

Preliminary tests of the so defined performance of the sealing system were conducted on the test stand shown in Fig. 2 and 3.

LABORATORY STAND FOR TESTING "HARMFUL" PERFORMANCE OF SEAL

The main element of the test stand (Fig.2) was a friction unit formed of four balls of 12,7 mm in diameter immersed in the tested lubricating medium. The three balls (4) are placed in a lower holder (a sump made of a bearing steel of 62,7 HRC hardness) and considered to represent a crankshaft. Into the sump the tested lubricating medium (a volume of 8 ± 2 cm^3) is poured. The fourth ball (3) fixed in the upper holder (a modification of friction unit) is made of rubber of hardness in the range of 15–80°sh, and considered to represent physical model of the crankshaft seal ring. The balls located in the sump (5) are pressed with the force P produced by the weight (8) against the ball fixed in the upper holder. The rubber ball in the holder (2) is loaded by the reaction force R equal to the force P exerted onto the steel balls.

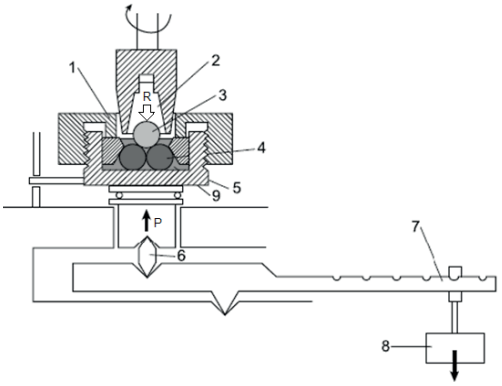

Fig. 2. Kinematic scheme of the four- ball apparatus : 1 – casing to fix lower balls, 2 –upper ball holder, 3 – upper rubber ball (rotating), 4 – lower balls (motionless), 5 – sump with tested oil, 6 – prism, 7 – lever, 8 – weights, 9 – tested oil, P – force applied to steel balls placed in sump, R – reaction force [1].

As results from the distribution of forces over the contact of friction pairs according to the standard [9] Fig. 3, shaft radius may be taken equal to that of the circle built by contact points of the balls (3) in friction node, and the acting forces may be determined as follows: $P \equiv 3 \cdot P_r$.

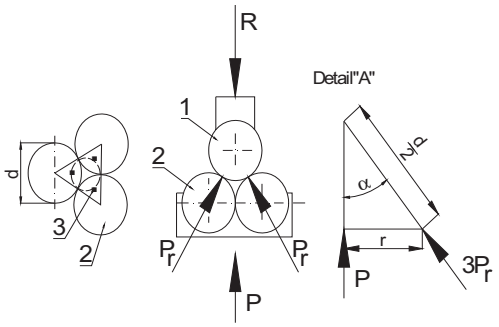

Fig. 3. Distribution of forces in friction node of four-ball apparatus : 1- upper rubber ball, 2 – lower steel balls, 3 – contact points, d – ball diameter equal to 12,7 mm, r – radius of the circle formed by contact points, a = 35,2644° – angle which determines contact points between the upper (rubber) ball and the lower (steel) balls; P – load applied to steel balls placed in the sump, R – eaction force, P_r – radial load.

Based on the detail "A" in Fig. 3, the radius $r = \frac{d}{2} \cdot \sin\alpha$ and the radial load $P_r = \frac{P}{3 \cdot \cos\alpha}$ was calculated.

During the tests the measuring system of the apparatus makes it possible to determine friction factor of the tribological system presented in Fig. 2 and 3. The so determined radius r, force P_r and friction factor μ were necessary for calculation of the work L_S (4), that made it possible to determine performance of the crankshaft sealing system in compliance with the formula (3).

DETERMINATION OF PERFORMANCE OF CRANKSHAFT SEALING SYSTEM

Crucial impact onto performance of crankshaft sealing system results from : crankshaft rotational speed, friction node temperature, friction in seal-shaft pair (depending on the oil viscosity η[mPa·s]), power losses (depending on drag torque and shaft rotational speed), oil pressure, materials of which crankshaft and seal is made, principal dimensions of sealing system etc.

For the testing of sealing action with the use of the modified friction node of T-02 four-ball apparatus the constant oil temperature of 20°C and constant load of 150 N was assumed and variable rotational speed of the upper ball holder was selected as the control parameter of influence of lubricating oil improvers on the action.

The three following clean lubricating oils whose dynamic viscosity at 20°C was determined by means of DV-1P apparatus produced by Anton Paar GmbH, were tested:

1. SAE30 lubricating oil (η = 240 mPas) – marked A.
2. SAE30 lubricating oil containing improving liquid (η = 350 mPas) – marked B.
3. SAE30 lubricating oil containing improving powder (η = 375 mPas) – marked C.

MOST WIEDZY Downloaded from mostwiedzy.pl

Series of measurements were done on the test stand in accordance of the algorithm shown in Fig. 4. The start-up instant when a sudden rise of " harmful" work occurs giving evidence for breaking the lubricating oil boundary layer, was assumed the permissible degree of the" harmful" performance ($D_{S(dop)}$).

The tests of each model were repeated four times. Average values of the test results are contained in Tab. 1, 2 and 3 and illustrated in Fig. 5, 6 and 7.

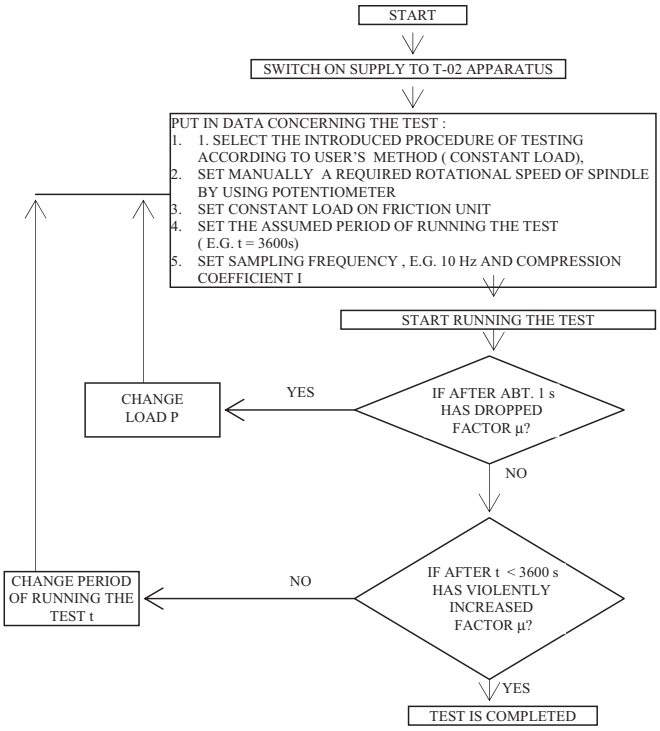

Fig.4. Algorithm of the tests carried out on the measurement stand

Results of the tests according to the worked – out algorithm (Fig. 4) are presented for the rotational speed n = 312 rpm in Tab. 1 which contains values of the "harmful" performance determined in compliance with the formula (3) for given measurement duration times. And, the performance in function of measurement duration time is illustrated in Fig. 5.

Tab. 1. "Harmful" performance of the seal ring for the rotational speed of 312 rpm

Measurement duration time [s]	Harmful" performance [mJ·s]		
	Mark A	Mark B	Mark C
0,19	82,54	65,85	77,90
10,00	40,81	38,02	38,02
20,00	35,24	36,17	41,73
50,00	28,75	38,95	37,10
80,00	38,95	38,95	40,81

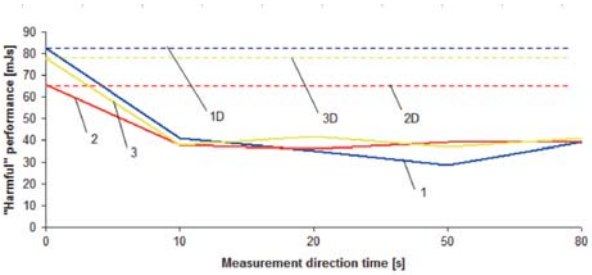

Fig.5 Comparison of seal ring performance for various lubricating oils at the rotational speed of 312 rpm under the load of 61,2 N: 1 – mark A, 1D – permissible performance – mark A; 2 – mark B; 2D – permissible performance – mark B; 3 – mark C; 3D – permissible performance – mark C

At the set load and rotational speed of 312 rpm the permissible level of "harmful" performance $D_{S(dop)}$ was not exceeded in any case – it means that the lubricating oil boundary layer was regenerated in all the cases.

Similar tests were conducted for the rotational speed of 500 rpm. Their results are contained in Tab. 2 and illustrated in functional form in Fig. 6.

Tab. 2. "Harmful" performance of the seal ring for the rotational speed of 500 rpm

Measurement duration time [s]	"Harmful" performance [mJ·s]		
	Mark A	Mark B	Mark C
0,12	45,10	40,42	48,03
10,00	22,26	22,84	26,36
20,00	20,50	22,84	25,19
50,00	21,09	22,84	25,77
100,00	22,84	22,26	25,19
120,00	55,06	23,43	26,36
150,00		24,60	28,11
200,00		19,33	28,70
201,00		20,50	28,11
209,00		21,09	50,24
280,00		17,57	

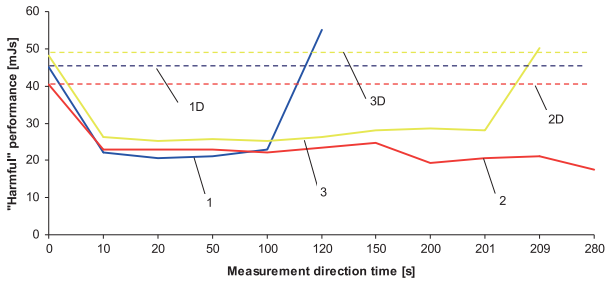

Fig.6. Comparison of seal ring performance for various lubricating oils at the rotational speed of 500 rpm under the load of 61,2 N: 1 – mark A, 1D – permissible performance – mark A; 2 – mark B; 2D – permissible performance – mark B; 3 – mark C; 3D – permissible performance – mark C

At the set load and the rotational speed of 500 rpm only SAE 30 oil with improving liquid prevented against exceeding

MOST WIEDZY Downloaded from mostwiedzy.pl

the permissible level of 'harmful" performance $D_{S(dop)}$ and the boundary layer was regenerated.

And, the tests carried out at the rotational speed n=1450 rpm made it possible to achieve the results presented in Tab. 3. Fig. 7 shows the "harmful" performance in function of measurement duration time ($D_S = f(\tau)$).

Tab. 3. "Harmful" performance of the seal ring for the rotational speed of 1450 rpm

Measurement duration time [s]	"Harmful" performance [mJ·s]		
	Mark A	Mark B	Mark C
0,04	14,06	15,03	12,50
10,00	17,38	3,71	5,66
20,00		4,49	6,64
50,00		5,86	4,10
60,00		22,26	4,30
70,00			6,05

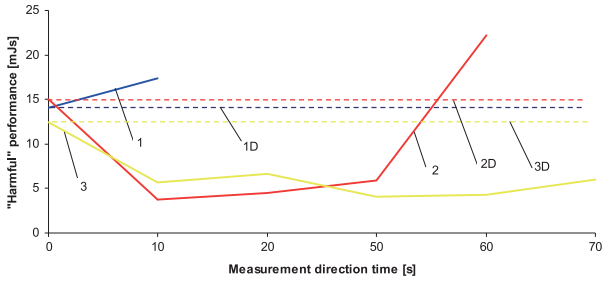

Fig.7. Comparison of seal ring performance for various lubricating oils at the rotational speed of 1450 rpm under the load of 61,2 N: 1 – mark A, 1D – permissible performance – mark A; 2 – mark B; 2D – permissible performance – mark B; 3 – mark C; 3D – permissible performance – mark C

In the third series of the tests at the set load and the rotational speed n = 1450 rpm only SAE 30 lubricating oil with improving powder prevented against the exceeding of the permissible level of "harmful" performance $D_{S(dop)}$.

The tests confirmed that the consequences K_i (i = 1,2) do occur during operation of the seal. Therefore on the basis of the inference rule (2) it may be stated that the hypothesis is correct. However its truthfulness is not certain but only probable. For this reason the statistical method (statistical inference) was used for its further verification.

VERIFICATION OF THE TEST HYPOTHESIS

The statistical testing of the scientific hypothesis which states that: *sudden break of boundary layer occurred because a sudden rise in average "harmful" performance of seal was revealed*, was carried out in the three stages [6]:

1. It was demonstrated that the "harmful" performance of seal is a quantity which may be considered a random variable. The hypothesis that quality of lubricating oil improvers does not affect the "harmful" performance of sealing system was assumed to serve as the zero hypothesis (H_O). The hypothesis that quality of lubricating oil improvers affects the "harmful" performance of sealing system was assumed to serve as the alternative hypothesis (H_a).
2. From the Kolmogorov-Smirnov goodness-of-fit test for tests of the sample size n < 100 and the confidence interval b = 95% it results that normal distribution is the function which describes mode of assigning probabilities to particular values of random variable.
3. After verification of the hypotheses H_O and H_a by means of Fisher statistics for the significance level a = 0,05 the hypothesis (H_O) was rejected and the alternative hypothesis (H_a) was approved.

FINAL REMARKS AND CONCLUSIONS

The physical model of seal ring should be considered preliminary but that which makes it possible to work out a more adequate physical model of the tested seal ring because it allowed to confirm truthfulness of the hypothesis formulated in the tests. Obviously, the final confirmation of truthfulness of the hypothesis should result from the testing of an original crankshaft sealing system, which is planned in the near future.

From the presented results of the tests arises that:

1. The upper rubber ball of the friction unit may be considered a sealing lip;
2. The three balls inside the cuplike sump were assumed to represent crankshaft;
3. After start-up and the first rotation of the shaft, the permissible level of "harmful" performance was calculated ; its exceeding had to demonstrate that the seal passed to the state of partial serviceability or complete unserviceability;
4. In the instant of losing capability of regenerating boundary layer between the edge of the upper rubber ball (sealing lip) and the edges of the balls inside the oil sump (crankshaft) a violent rise of friction factor (increase in temperature of the set of balls) occurs and consequently results in a failure of the upper ball (a rise in vibration level of the set of balls and separation of a rubber part off the upper ball);.
5. Improvers added to SAE30 lubricating oil increased its lubricity (capability of regenerating its boundary layer) which is not strictly equivalent to dynamic viscosity . The sample marked B of a lower dynamic viscosity than that of the sample marked C demonstrated a higher lubricity for n = 500 rpm.

As results from the tests, the interpretation (proposed by this author) of operation of the sealing system tested in T-02 four-ball apparatus may be used for the determining of usability of improvers added to lubricating oils in service of the systems. The achieved results of the tests allow to state that the test method, proposed by this author, for the testing of influence of lubricating oil improvers on crankshaft operation will be also useful for carrying out similar tests on other sealing systems.

MOST WIEDZY Downloaded from mostwiedzy.pl

BIBLIOGRAPHY

1. Michalczewski R., Szczerek M., Tuszyński W., Wulczyński J.: *A four-ball machine for testing anti-wear, extreme-pressure properties, and surface fatigue life with a possibility to increase the lubricant temperature*. Tribologia 1/2009, pp.113-127

2. Laber A.: *Modifying the operating conditions of friction pairs with solid lubricant based additives.* Tribologia 5/2011, pp.137-145

3. Girtler J.: *A method for evaluating the performance of a marine piston internal combustion engine used as the main engine on a ship during its voyage in different sailing conditions*. Polish Maritime Research, No. 4/2010, vol.17

4. Girtler J.: *Method of evaluation of lubricating ability of lube oils, diesel oils and heavy fuel oils in energetistic formulation*. Journal of POLISH CIMEEAC, Vol. 3, No. 1, 2008

5. Girtler J.: *Physical aspect of application and usefulness of semi-Markovian processes for modeling the processes occurring in operational phase of technical objects*. Polish Maritime Research, No. 3/2004, vol. 11, pp. 25-30.

6. Bzura P., Dziedzic A.: *Analysis of influence of lubricating oil quantity and quality on operational correctness of crankshaft slide bearings* (in Polish. Publishing House of Maritime Academy of Szczecin, Szczecin 2016, pp.30-36.

7. Beek A. V.: *Machine lifetime performance and reliability*, TU Delft, Delft, 2004.

8. Rudnicki J.: *Evaluation of compression realization in diesel engine based on performance indicator changes.* Journal of Polish CIMEEAC, Vol. 7, No. 1, Gdańsk 2012

9. Designation: ASTM D5183 – 05(2016) *Standard Test Method for Determination of the Coefficient of Friction of Lubricants Using the Four-Ball Wear Test Machine*

CONTACT WITH THE AUTHOR

Piotr Bzura

Gdańsk University of Technology
11/12 Narutowicza St.
80 - 233 Gdańsk
Poland

MOST WIEDZY Downloaded from mostwiedzy.pl

POLISH MARITIME RESEARCH Special Issue 2018 S1 (97) 2018 Vol. 25; pp. 178-188
10.2478/pomr-2018-0040

THE INFLUENCE OF WATER AND MINERAL OIL ON MECHANICAL LOSSES IN THE DISPLACEMENT PUMP FOR OFFSHORE AND MARINE APPLICATIONS

Paweł Śliwiński
Gdańsk University of Technology, Poland

ABSTRACT

In this paper mechanical losses in a positive displacement pump supplied with water and mineral oil (two liquids having significantly different viscosity and lubricating properties) are described and compared. The experimental tests were conducted by using a prototype satellite pump of a special design. The design of the satellite pump is presented in the article. The pump features and a non-circular tooth working mechanism was developed to work with both water and mineral oil. The sources of mechanical losses in such pump are also characterized in this paper. On this basis, a mathematical model of the losses has been developed and presented. The results of the calculation of mechanical losses according to the model are compared with the results of the experiment. The experimental studies have shown that the mechanical losses in the water pump are even 2.8 times greater than those in the oil pump. It has been demonstrated that the mathematical model well describes the mechanical losses both in the water pump and the oil pump. It has been found that the results from the loaded pump simulation (at Δp=25MPa) differ from the results of the experiment by no more than 5% both for oil and water.

Keywords: mechanical losses, satellite pump, water, oil

MOST WIEDZY Downloaded from mostwiedzy.pl

INTRODUCTION

The pump is the most important element in a hydraulic system [3-7,13,14]. Its purpose is to convert mechanical energy into hydraulic one. The energy carrier in hydraulic systems is liquid. The type of liquid is determined by the requirements for the system. The liquid commonly used in hydraulic systems is mineral oil. However, in some industrial sectors, the requirement is to apply a non-flammable (mining, steel mills, etc.) or non-toxic (food industry) liquid. In such case, non-flammable synthetic liquids, water or water -based liquids (i.e. HFA-E emulsion) are used instead of mineral oil [18,27]. Water is a liquid which is non-flammable, non-toxic and certainly suitable for energy transfer in hydraulic systems. In comparison to mineral oil, water has a very low viscosity and low lubricating properties [10]. These parameters have a significant impact on the size of mechanical, volumetric and pressure losses in hydraulic machines [20]. The losses have an impact on the energy conversion efficiency in the machines and on the noise emission [11,15,16,18,24-26,28]. Furthermore, the design parameters of hydraulic components have an influence on energy conversion efficiency [8,9,17,21,22,27].

Generally, each hydraulic device is dedicated to a specific type of working liquid. For example, a positive displacement pump dedicated to oil systems should not be used in systems where the working medium is water.

There is a worldwide growing trend towards research and development of components and hydraulic systems supplied with water [2,3,8,9,18,27].

Studies on hydraulic systems where water is the working medium are especially important in marine technology. In offshore technology and marine applications, hydraulic power circuits are used frequently and water is generally available as a working liquid [2]. Thus, in order to eliminate the pollution of the environment, it seems reasonable and justified to eliminate oil systems and replace them with water systems. To this end, it is necessary to develop and test innovative components for hydraulic water systems [17-22]. Thus, it was reasonable to develop a new positive displacement water pump called the satellite pump and mark it with the PSM symbol. The pump contains an innovative operating mechanism consisting of non-circular gears [17,20-23]. The construction of this pump is described in the next section.

The development of the PSM pump enabled an investigation of the influence of the working liquid type (that is water and oil) on the energy losses which occur in this pump. This article is limited to the description of mechanical losses only.

The impact of the type of liquid on mechanical losses in positive displacement pumps has not yet been analyzed by other researchers. Of course, in the literature, mechanical losses have been described only for one liquid: mineral oil. Furthermore, mechanical losses have been described in general, without specifying the sources of losses [1,15,16]. Nonetheless, there is rich literature on the lubricating properties of liquids and tribological research. However, the literature concerns the basic issues only, such as the tribology of gear wheels, flat friction nodes, etc. [8-10,19]. Therefore, the influence of the type of liquid on mechanical losses in a positive displacement pump is a new issue, it is cognitive and represents an important scientific problem. Consequently, the following objectives have been defined for this article:

a) indicate and describe sources of mechanical losses in the satellite pump;
b) describe a mathematical model of mechanical losses;
c) compare mechanical losses in the oil pump to those in the water pump;
d) compare the results of experimental research with a mathematical model.

SATELLITE PUMP

The experimental research on the influence of the type of liquid on volumetric losses was carried out by using a prototype of a positive displacement pump developed by this author. For experimental tests, a prototype of a satellite pump was selected and marked with the symbol PSM-0,75/15 (Fig. 1). The design of this pump is presented in Fig. 2. The working mechanism of the satellite pump is a specific gear mechanism in which the rotor rotates around the shaft axis and the revolving motion is done by satellites which are in gear with the stator and the rotor (Fig. 3).

Fig. 1. General view of PSM-0,75 pump

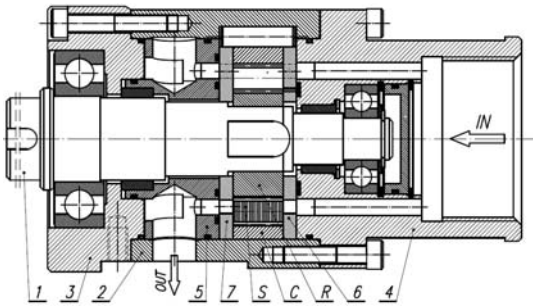

Fig. 2. Axial cross section of the novel PSM-0,75 pump: C – curvature, S – satellite, R – rotor, 1 – shaft, 2 – casing, 3 – front casing, 4– rear casing (suction manifold), 5 – pressure manifold, 6 and 7 – compensation (commutation) plates

The toothed unit shown in Fig. 3, is the satellite working mechanism of the pump. It consists of a toothed rotor R (4 humps), toothed curvature C (6 humps) and ten wheels S(satellite).

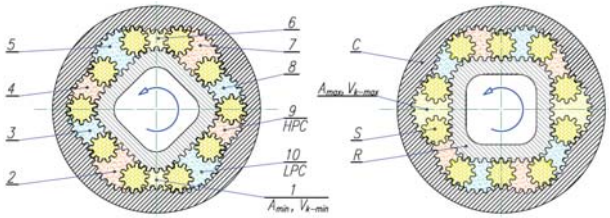

Fig.3. The working mechanism of a satellite pump: C – curvature, R – rotor, S – satellite, 1÷10 – working chambers, LPC – low pressure working chamber, HPC – high pressure working chamber, $V_{k\text{-}min}$ – working chamber with the minimum area A_{min} (dead chamber), $V_{k\text{-}max}$ – working chamber with the maximum area A_{max} [17,19-23]

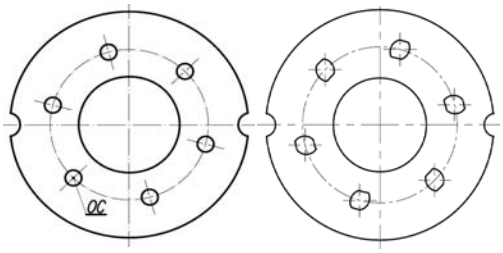

Fig. 4. High pressure commutation plate (left) and suction commutation plate (right) [17,20,22]

The principle of operation of the satellite mechanism is that when the rotor rotates, the volume of the space

MOST WIEDZY Downloaded from mostwiedzy.pl

between the satellites changes. This space forms the working chamber. When its volume increases, the filling cycle takes place. Conversely, when its volume decreases, the emptying cycle occurs. Twenty-four cycles correspond to one shaft revolution. The chambers in the satellite mechanism are closed by commutation plates (Fig. 2 – elements 6 and 7, Fig. 4), which also play the role of compensation plates. Thus, the satellite pump has the ability to compensate axial clearances of the rotor and the satellites [17,19-23].

Experimental studies of the PSM-0,75/15 pump were carried out by using the following liquids:
- the Total Azolla 46 oil (ν=40cSt, ρ=873kg/m^3, μ =35mPas);
- tap water (ν=0,853cSt, ρ=996kg/m^3).

The tested pump was characterized by the following parameters:
- theoretical displacement q_t=18,63 cm^3/rev.;
- teeth module m=0,75mm;
- height of working mechanism H=15mm.

TEST STAND

The PSM pump was tested on the test stand with power recuperation. The diagram of the measurement system of the test stand is shown in Fig. 5.

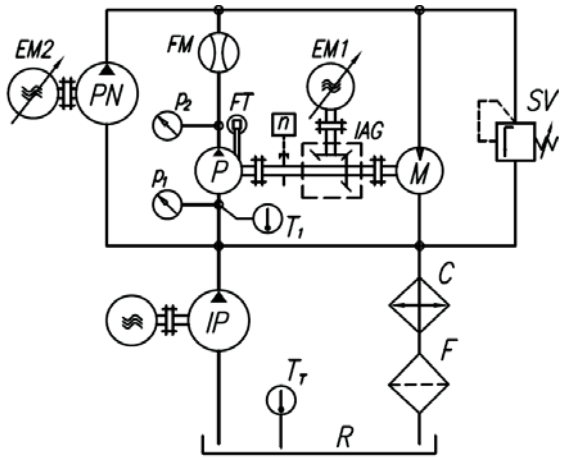

Fig. 4. The diagram of the measurement system of the test stand: P – tested pump, M – hydraulic motor, PN – pump for filling the leaks in P and M, IP – impeller pump (pre-supply pomp), SV – safety valve, C – cooler, F – filter, R – reservoir, IAG – intersecting axis gear, EM1 and EM2 – electric motors with frequency converters, other designations – see description in the text below

During the test of the pump the following parameters were measured:
- pressure p_1 in suction port (strain gauge pressure transducer, range: –1÷+3 bar, class 0,3);
- the pressure p_2 in pumping port (strain gauge pressure transducers, range: 0÷25 bars and 0÷250 bars, class 0,3);
- the pump delivery Q (mass flow meter FM, range: 0÷33 l/min, class 0,1);
- the torque M (strain gauge force transducer FT mounted on the arm of 0,5m (arm attached to the pump body), range: 0÷100N, class 0,1);
- the rotational speed of shaft n [rpm] (inductive sensor, measurement accuracy: ±1rpm);
- the temperature T_1 of liquid in the suction port of the pump (RTD temperature sensor, class A, max. measurement error: 0,5°C).

PRESSURE DROP IN INTERNAL CHANNELS

The pressure losses in the pump are a combination of the pressure drop in the internal channels and the pressure drop in the commutation unit.

The volumetric losses depend on the pressure increase in the working chambers of the pump. This pressure is difficult to measure. On the other hand, it is easy to measure the pressure increase Δp in the pump ports. The relationship between Δp and Δp_i is as follows:

$$\Delta p_i = \Delta p - \Delta p_{ich} \tag{1}$$

where Δp_{ich} is the pressure drop in internal channels of the pump. The methodology of measuring Δp_{ich} is described in [21].

The internal channels have a complicated geometry. The non-fully developed turbulent flow takes place in the channels. Therefore, to describe Δp_{ich}, it is proposed to adopt the following simplified relationship [21]:

$$\Delta p_{ich} = C_t \cdot \rho \cdot Q^2 + C_l \cdot \mu \cdot Q \tag{2}$$

where C_l and C_t are coefficients mainly dependent on the geometrical dimensions of the internal channel. The values of the coefficients (for Δp in [MPa], Q in [l/min], μ in [mPas] and ρ in [kg/m^3]), calculated on the basis of the experimental results, are as follows:

a) for oil: $C_t = 0{,}282 \cdot 10^{-7}$ and $C_t = 0{,}583 \cdot 10^{-5}$.
b) for water: $C_t = 0{,}146 \cdot 10^{-7}$ and $C_t = 0{,}343 \cdot 10^{-3}$.

The characteristics of Δp_{ich}=f(Q) in a pump pumping oil and water, calculated according to formula (3), are shown in Fig. 6.

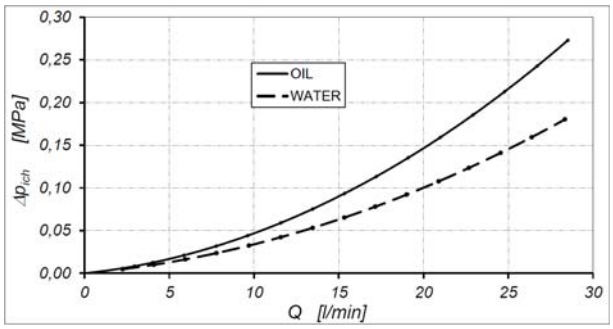

Fig. 6. Characteristics of Δp_{ich}=f(Q) for oil and water – result of calculation acc. Eq. (2)

MOST WIEDZY Downloaded from mostwiedzy.pl

SOURCES OF MECHANICAL LOSSES

Mechanical losses in a satellite pump result from:

a) rolling and sliding friction between the gear mechanism elements;
b) compression of liquid in the death volumes $V_{k\text{-}min}$ of the satellite working mechanism (Fig. 3);
c) compression of liquid in the space between the teeth of the working mechanism elements (Fig. 7);
d) the inertia of the working mechanism elements and the inertia of liquid in working chambers;
e) friction in the bearings and seals;
f) viscous friction in the gaps between all moving parts of the pump.

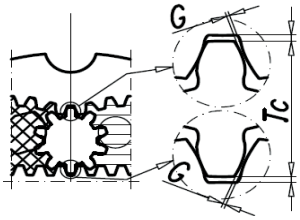

Fig. 7. Tip clearance Tc and backlash G [19,21]

TORQUE OF LOSSES IN UNLOADED PUMP

RESULTS OF EXPERIMENT

There are two experimental methods of measuring the torque of losses $M_{l\,(\Delta p=0)}$ in an unloaded pump ($\Delta p=0$):

1) by measuring the torque on the shaft of the pump. It is then necessary to eliminate the torque corresponding to the pressure drop in the suction pipe and the outflow pipe;
2) by measuring the pressure drop in the pump working as a motor (the pump is supplied with liquid and the shaft is uncoupled) [21].

In the tested pump $M_{l\,(\Delta p=0)}$ was determined according to the second method. Hence, it can be assumed that $M_{l\,(\Delta p=0)} = M_{l\,(M=0)}$. $M_{l\,(M=0)}$ was calculated from the relationship:

$$M_{l\,(M=0)} = \frac{q \cdot \Delta p_i}{2 \cdot \pi} \quad (3)$$

The experimentally determined characteristics of mechanical losses $M_{l\,(M=0)}$ in an unloaded pump are shown in Fig. 8 and in Fig. 9.

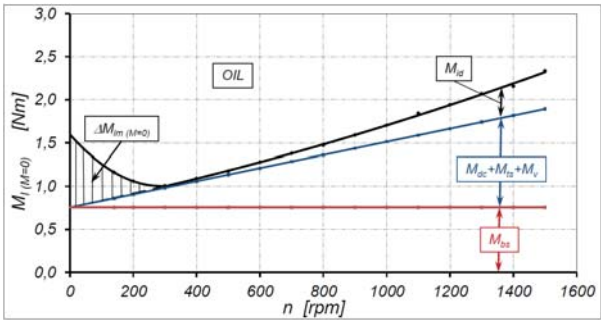

Fig. 8. Characteristics of Ml (M=0) = f(n) in unloaded pump. Working medium: oil

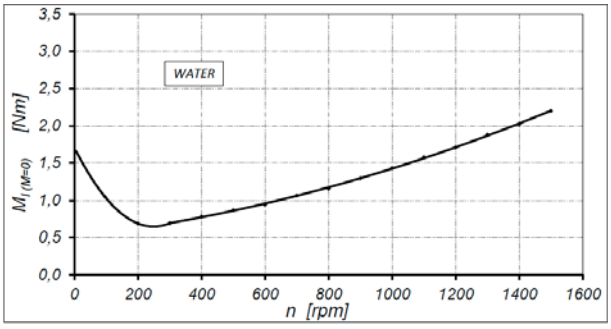

Fig. 9. Characteristics of $M_{l\,(M=0)} = f(n)$ in unloaded pump. Working medium: water

COMPONENTS OF MECHANICAL LOSSES IN AN UNLOADED PUMP

An analysis of experimental results indicates a non-linear relationship $M_{l(M=0)} = f(n)$ (Fig. 8 and Fig. 9). Mechanical losses $M_{l(M=0)}$ in an unloaded pump can be expressed as the sum of components:

$$M_{l\,(M=0)} = M_{bs} + M_{id} + M_{dc} + M_{ts} + M_v + \Delta M_{lm\,(M=0)} \quad (4)$$

where:

- M_{bs} – the torque of losses in the bearings and seals;
- M_{id} – the torque of losses dependent on the inertia of the working mechanism elements and the inertia of liquid in the working chambers;
- M_{dc} – the torque of losses caused by compression of liquid in death volumes;
- M_{ts} – the torque of losses caused by compression of liquid in the spaces between the teeth;
- M_v – the torque of losses caused by viscous friction in the clearances of the working mechanism;
- $M_{lm\,(M=0)}$ – the torque of losses at low speed. This loss component reaches its maximum value for a speed close to zero.

TORQUE OF LOSSES IN BEARINGS AND SEALS

The results of experimental studies on seals used in hydraulic machines show that the torque of friction in seal to the greatest extent depends on the pressure of the liquid contained in the seal chamber. The rotational speed of the shaft has a much smaller effect on M_s. In addition, M_s depends on the working fluid (lubricating properties) [19,21]. In a satellite pump, the rubbing speed of seals relative to the shaft neck exceeds 2 m/s. Additionally, the fluid pressure in the seal chamber is strictly dependent on the pressure in the suction port (leaks from the working mechanism are discharged into the chamber of the shaft to the suction port). During the pump tests, the pressure in the suction port was p_1=<0,1MPa.

The results of the seal tests have shown that the torque of friction in the seals (at the shaft speed of 1500 rpm) does not exceed M_b=0,8 Nm in the oil pump and M_b=0,9 Nm in the water pump.

MOST WIEDZY Downloaded from mostwiedzy.pl

However, for simplicity, the model assumes that the torque of friction in the seals is a function of the pressure in the seal chamber and does not depend on the rotational speed.

Bearings in satellite machines have no contact with the working liquid. Hence, the torque of losses in bearings M_b does not depend on the liquid lubricant type. Furthermore, for simplicity, it is assumed that the friction in the bearings is independent from the shaft speed. The pump working mechanism is hydrostatically balanced. Therefore, the load Δp of the pump has no influence on the torque of losses in the bearings.

Thus, the torque of losses in the bearings and seals of the satellite pump can be described by the equation:

$$M_{bs} = M_b + M_s = M_b + C_s \cdot p_2 \cong C_{bs} \cdot p_2 \quad (5)$$

in which C_s $[\frac{Nm}{MPa}]$ and C_{bs} $[\frac{Nm}{MPa}]$ are constants. The value of the constant C_{bs} is shown in Tab. 1.

TORQUE OF LOSSES DEPENDENT ON INERTIA OF SATELLITES AND INERTIA OF LIQUID IN WORKING CHAMBERS

During the operation of a satellite mechanism, the satellites are moving with a variable plane motion – there is a cyclic variation in the speed of each satellite. Mechanical energy is supplied to the satellite during acceleration. Later, during deceleration, the energy is returned. The difference between the delivered and returned energy is the energy consumed in the process of friction. Similarly, during the operation of a satellite mechanism, there is acceleration and deceleration of the liquid in the working chambers. Thus, the energy lost depends on the inertia of the liquid and the satellites. During the commutation change (e.g. at the time of the opening of the inflow channel and cutting off the outflow channel by a satellite), inertial forces resist changes in the position of the satellite teeth in the space between the rotor teeth and the curvature. The inertia force of the satellite depends on its mass and hence the module m of the teeth, the height H of the satellites and the density of the material from which these components are made. Similarly, the inertia of the liquid depends on its density and the working chamber volume.

The torque of losses M_{id} dependent on the inertia of satellites and inertia of liquid in working chambers can be described with the equation:

$$M_{id} = C_{id} \cdot m^4 \cdot H \cdot n^2 \quad (6)$$

where C_{id} $[\frac{Nm}{rpm^2 mm^5}]$ is a constant depending on the type of the satellite material and the type of liquid.

At the current stage, no experimental studies have been carried out to determine the influence of:
a) the inertia of satellites;
b) liquid parameters (density and viscosity);
c) backlash of satellites in working mechanism
on the value of the constant C_{di}.

It can be assumed that for oil the value of C_{di} will be smaller than for water because the density of oil is smaller than the density of water.

TORQUE OF LOSSES CAUSED BY VISCOUS FRICTION IN GAPS AND BY COMPRESSION OF THE LIQUID IN DEATH VOLUMES AND SPACES BETWEEN TEETH

The process of compressing the liquid in the death volumes of the working mechanism occurs when the mechanism rotates and there is no flow from the death volume to both the outflow channel and the inflow channel.

During the motor shaft rotation, the walls of gaps of the working mechanism move relative to each other. This causes the drift of the liquid layers in the gaps. Viscous friction in the liquid in the gaps can be expressed as the torque of losses M_v. The torque is proportional to the relative speed of the gap walls and the viscosity of liquid [1]. Thus:

$$M_v = C_v \cdot \mu \cdot n \quad (7)$$

where C_v $[\frac{\mathrm{Nm}}{\mathrm{mPas \cdot rpm}}]$ is the constant.

The M_v component reaches very small values, it is very difficult to determine and hence very often neglected (M_v=0) [1]. Furthermore, the M_{dc} and M_{ts} components are impossible to determine. Therefore it is proposed to introduce a replacement component M_{dsv} of the torque of losses, which is expressed by the empirical formula:

$$M_{dsv} = M_{dc} + M_{ts} + M_v = C_{dsv} \cdot \mathrm{m}^4 \cdot H^2 \cdot n \quad (8)$$

where C_{dsv} $[\frac{Nm}{mm^6 \cdot rpm}]$ is the constant.

TORQUE OF LOSSES AT LOW SPEED

Pumps do not work at low speeds. Hence, the component of torque of losses $M_{lm\,(M=0)}$ occurring at low speeds, i.e. speed in the range from a value close to 0 ($n=0^+$) to a certain limit speed n' can be eliminated from consideration.

TORQUE OF LOSSES IN UNLOADED PUMP

After inserting (5), (6) and (8) to (4), the following equation is obtained:

$$M_{l\,(M=0)} = C_{id} \cdot m^4 \cdot H \cdot n^2 + C_{dsv} \cdot \mathrm{m}^4 \cdot H^2 \cdot n + C_{bs} \cdot p_2 \quad (9)$$

Hence, the equation describing the torque of losses in the unloaded pump is a square equation. The values of coefficients C_{id} and C_{dsv} can be calculated from the equation of the trend line (Fig. 8 and Fig. 9). The values C_{id} and C_{dsv} are shown in Tab. 1.

MOST WIEDZY Downloaded from mostwiedzy.pl

TORQUE OF LOSSES IN LOADED PUMP

RESULTS OF EXPERIMENT

The mechanical losses M_l in a loaded pump was calculated according to the formula:

$$M_l = \frac{q \cdot \Delta p_i}{2 \cdot \pi} - M \tag{10}$$

The experimentally determined characteristics of the mechanical losses M_l in function of Δp_i, and the rotational speed n of the pump shaft are shown in Fig. 10÷13.

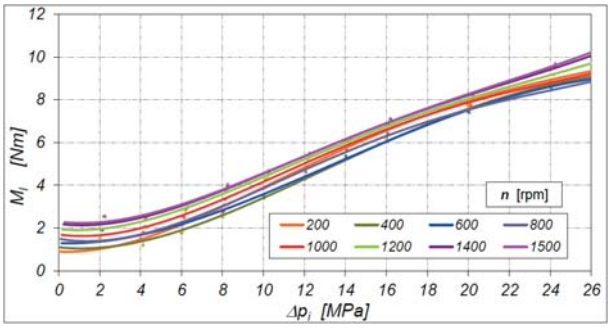

Fig. 10. Characteristics of M_l=f(Δp_i). Working medium: oil

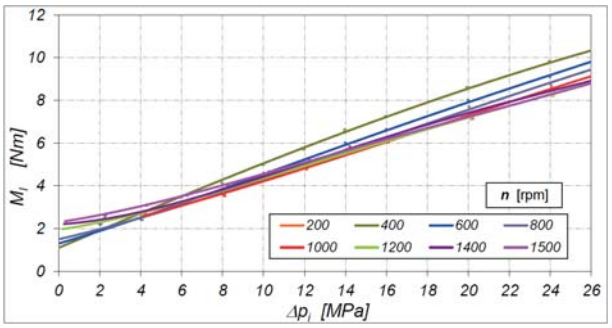

Fig. 11. Characteristics of M_l=f(Δp_i). Working medium: water

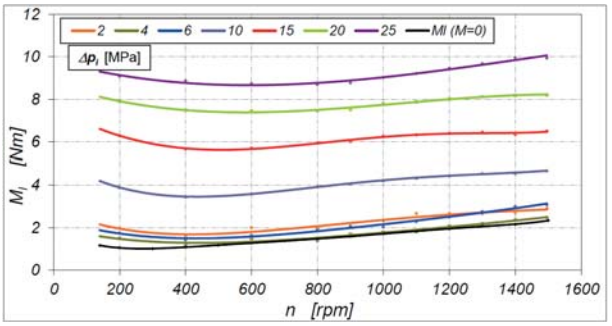

Fig. 12. Characteristics of M_l=f(n). Working medium: oil

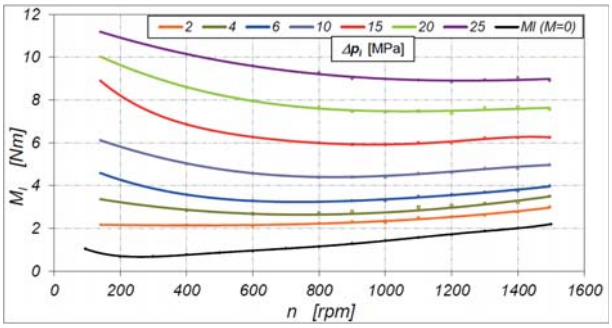

Fig. 13. Characteristics of M_l=f(n). Working medium: water

COMPONENTS OF MECHANICAL LOSSES IN A LOADED PUMP

The torque of mechanical losses M_l in a loaded pump is the following sum:

$$M_l = \underbrace{M_{bs} + M_{id} + M_{dsv} + \Delta M_{lm\,(M=0)}}_{M_{l\,(M=0)}} + \underbrace{\Delta M_{lm} + M_{lm}}_{M_{mf}} \tag{11}$$

where:

– M_{lm} – the torque of losses caused by mixed friction (depending on the increase in pressure Δp_i in the working chambers of the pump). The torque M_{lm} is calculated on the basis of experimental data as:

$$M_{lm} = M_l - M_{l\,(M=0)} \tag{12}$$

assuming that $\Delta M_{lm} = 0$;

– ΔM_{lm} – the torque of losses in a loaded pump occurring at low speeds and reaching the maximum value for a speed close to 0. Due to the fact that the pumps never operate at low speeds, this component can be skipped in the consideration, that is ΔM_{lm}=0.

TORQUE OF LOSSES M_{mf}

The experimentally determined characteristics of M_{mf}=f(Δp_i)$_{n=const}$ and M_{mf}=f(n)$_{\Delta pi=const}$, for M_{lm}=0, are shown in Fig. 14÷16.

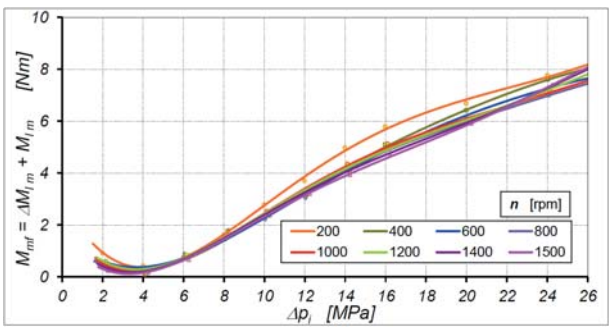

Fig. 14. Characteristics of M_{lm}=f(Δp_i). Working medium: oil

MOST WIEDZY Downloaded from mostwiedzy.pl

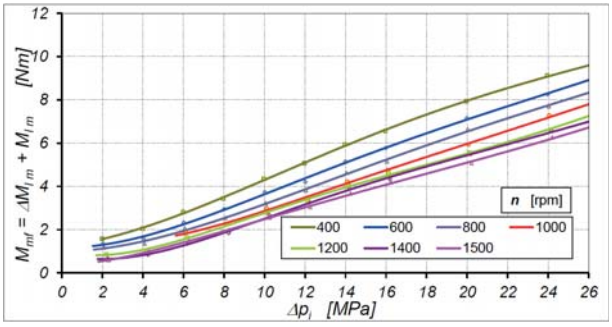

Fig. 15. Characteristics of $M_{lm}=f(\Delta p_i)$. Working medium: water

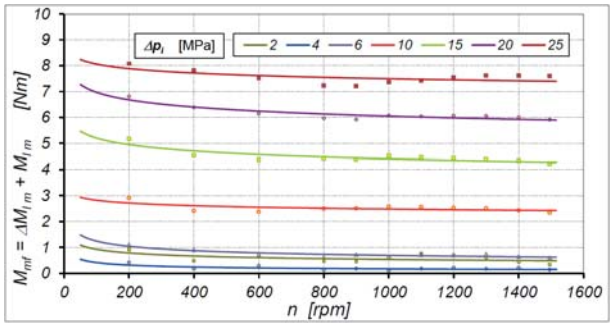

Fig. 16. Characteristics of $M_{lm}=f(n)$. Working medium: oil

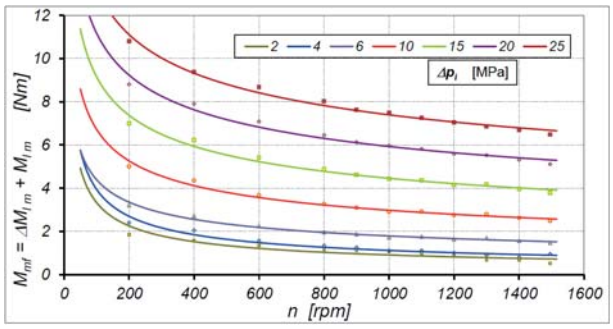

Fig. 17. Characteristics of $M_{lm}=f(n)$. Working medium: water

According to the characteristics (Fig. 17÷17) M_{mf} varies throughout the range of speed n and increases nonlinearly (disproportionately) with increasing the load Δp_i.

According to Niemann [12], the mean friction coefficient in the gear teeth can be described by the equation:

$$f = 0{,}048\left(\frac{F}{b\cdot v\cdot\rho}\right)^{0,2}\mu^{-0,05}R_a{}^{0,25}\left(\frac{F}{b}\right)^{-0,065} \quad (13)$$

where:
- F [N] – the circumferential force on the rolling circle;
- b [mm] – the width of the gear wheel;
- μ [mPas] – the dynamic viscosity of the liquid;
- v [m/s] – the summary speed of the cooperating wheels;
- ρ [mm] – the replacement radius of the tooth profile at the pitch point;
  R_a [μm] – the mean surface roughness of the side gear of interacting teeth.

In the above equation, there is no compatibility between the units of measurement. Thus, it is supposed that the above equation is purely hypothetical (or empirical).

In satellite machines:
- the radius ρ of the curvature of the teeth is dependent upon the module m of the teeth;
- the width b of the teeth is tantamount to the height H of the satellite mechanism;
- the pitch diameter D_p is a function of the teeth module m;
- the summary speed v of the cooperating wheels depends on the rotor (or shaft) rotational speed and the size of the mechanism (and the size of the teeth module m).

Taking into account the above-mentioned dependence, it is proposed to describe the torque of losses M_{mf} in the satellite mechanism by the empirical relationship:

$$M_{mf} \approx M_{lm} = C_{lm}R_a{}^{\gamma}(\mu H m^3)^{-\gamma}M^{\alpha}n^{-\beta} \quad (14)$$

where C_{lm} is the coefficient.

The load of the pump is a parameter independent of the pump. Hence, M_{lm} should be written as a function of Δp_i. Then:

$$M_{mf} = C_{lm}R_a{}^{\gamma}(\mu H m^3)^{-\gamma}\left(\frac{q\cdot\Delta p_i}{2\cdot\pi}\right)^{\alpha}n^{-\beta} \quad (15)$$

The coefficient α was read directly from the equation of the trend line of the characteristics shown in Fig. 14 and in Fig. 15. There was no correlation between the value of the coefficient α and the speed n of the pump. Therefore, it was assumed that coefficient α does not depend on n. Thus, the value of this coefficient is calculated as the arithmetic average of the obtained results. The values of α are shown in Tab.1.

The coefficient β can be read from the equation of the trend line of the characteristics shown in Fig. 16 and in Fig. 17. The value of this coefficient varies nonlinearly in function of the pressure increase Δp_i in the pump working chambers (Fig. 18).

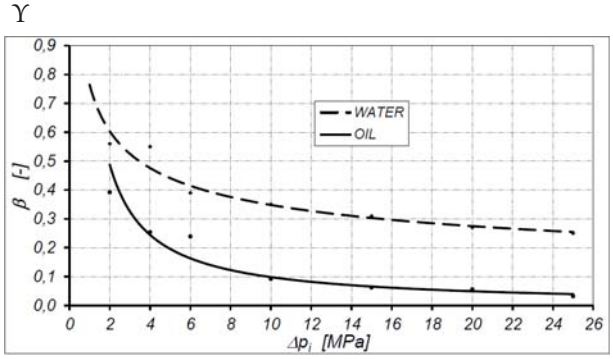

Fig. 18. Characteristics of $\beta = f(\Delta p_i)$. Working medium: oil and water

MOST WIEDZY Downloaded from mostwiedzy.pl

The factor β can be described as an empirical formula:

$$\beta = a \cdot \Delta p_i^{-b} \quad (16)$$

where a and b are coefficients. The values of a and b are shown in Tab. 1.

The coefficients Υ and C_{lm} were so selected as to obtain the best fit of a curve to the results of the experiment. It should be added that R_a=0,1μm in the satellite mechanism. The values of Υ and C_{lm} are shown in Tab. 1.

Tab. 1. Values of the coefficients in model of mechanical losses

	C_{bs}	C_{id}	C_{dsv}	C_{lm}
	$\left[\frac{Nm}{MPa}\right]$	$\left[\frac{Nm}{mm^5 rpm^2}\right]$	$\left[\frac{Nm}{mm^6 rpm}\right]$	[-]
Oil	8,0	$40{,}1 \cdot 10^{-9}$	$10{,}6 \cdot 10^{-6}$	0,21
Water	9,0	$49{,}6 \cdot 10^{-9}$	$16{,}6 \cdot 10^{-6}$	1,23
	•	•	a	b
	[-]	[-]	[-]	[-]
Oil	1,35	0,2	0,955	1
Water	1,32	0,2	0,765	0,342

The characteristics of M_{mf}=f(Δp_i) and M_{mf}=f(n) plotted according to the formula (15) and Tab.1 are shown in Fig. 19÷22.

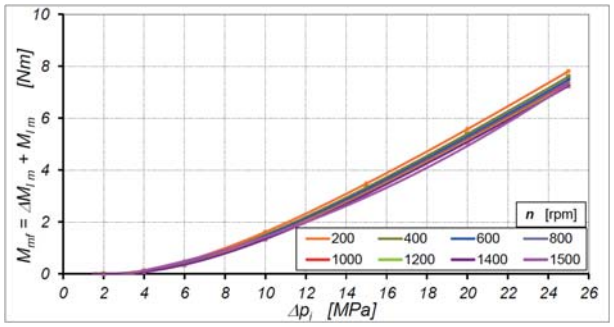

Fig. 19. Characteristics of M_{mf}=f(Δp_i) – result of calculation acc. Eq. (15). Working medium: oil

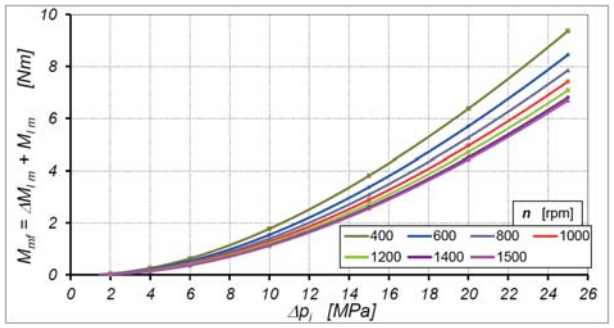

Fig. 20. Characteristics of M_{mf}=f(Δp_i) – result of calculation acc. Eq.(15). Working medium: water

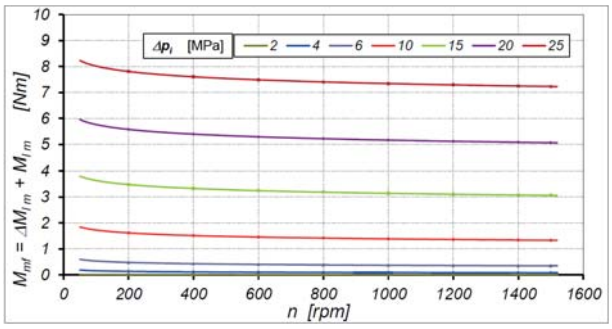

Fig. 21. Characteristics of M_{lm}=f(n) – result of calculation acc. Eq. (15). Working medium: oil

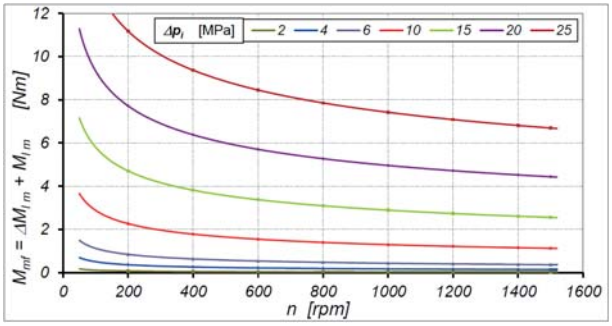

Fig. 22. Characteristics of M_{lm}=f(n) – result of calculation acc. Eq.(15). Working medium: water

TORQUE OF LOSSES IN LOADED PUMP

The torque of losses M_l in a pump, expressed by formula (11), when written in the expanded form, looks as follows:

$$M_l = C_{id} m^4 H n^2 + C_{dsv} m^4 H^2 n + C_{lm} (\mu H m^3 n)^{-\beta} \left(\frac{q \cdot \Delta p_i}{2 \cdot \pi}\right)^{\alpha} + C_{bs} p_2 \quad (17)$$

The characteristics of M_l=f(Δpi) and M_l=f(n), plotted according to the formula (17), are shown in Fig. 23÷26.

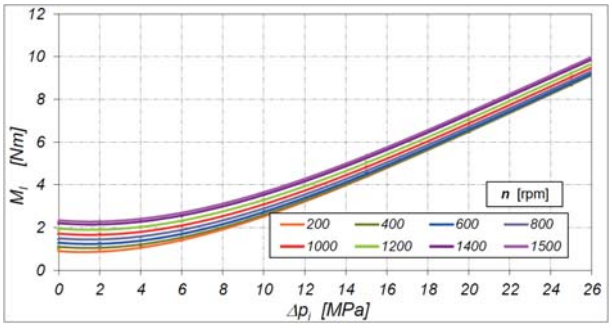

Fig. 23. Characteristics M_l=f(Δp_i) – result of calculation acc. Eq.(17). Working medium: oil

MOST WIEDZY Downloaded from mostwiedzy.pl

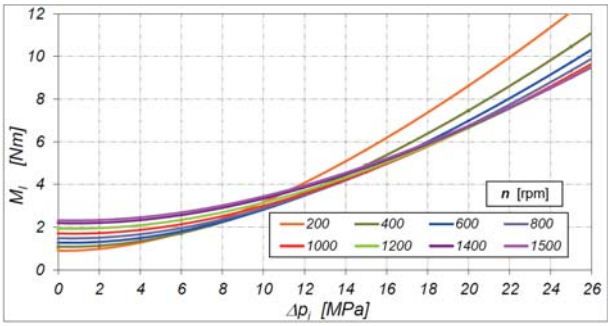

Fig. 24. Characteristics $M_l=f(\Delta p_l)$ – result of calculation acc. Eq. (17). Working medium: water

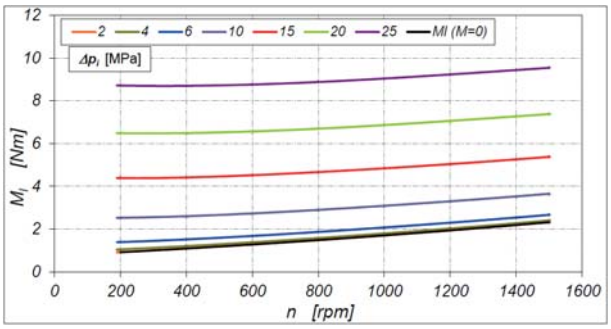

Fig. 25. Characteristics $M_l=f(n)$ – result of calculation acc. Eq.(17). Working medium: oil

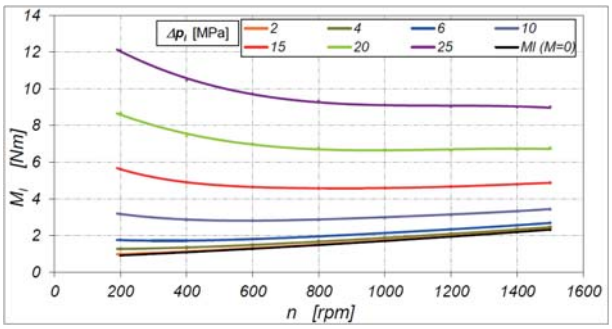

Fig. 26. Characteristics $Ml=f(n)$ – result of calculation acc. Eq.(17). Working medium: water

MECHANICAL LOSSES RATIO

The research results prove that the mechanical losses in the water pump are greater than those in the oil pump. The biggest difference is observed in the pump working at a low speed and low load. Furthermore, the ratio of the losses decreases with increasing Δp (Fig. 27).

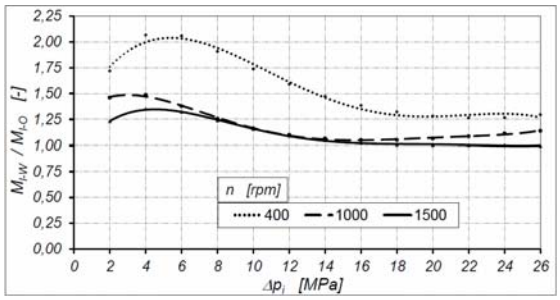

Fig. 27. Characteristics of the mechanical losses ratio $M_{l\text{-}W}/M_{l\text{-}O}=f(\Delta p)$

ERROR IN MECHANICAL LOSSES CALCULATION

The values of mechanical losses M_l in the oil pump and in the water pump, calculated according to (17), are different from the values determined experimentally.

The differences are defined as follows:

$$\delta M_l = \frac{M_l - M_{l-sym}}{M_l} \cdot 100\% \quad (18)$$

The characteristics of $\delta M_l=f(\Delta p_l)$ are shown in Fig. 28 and 29.

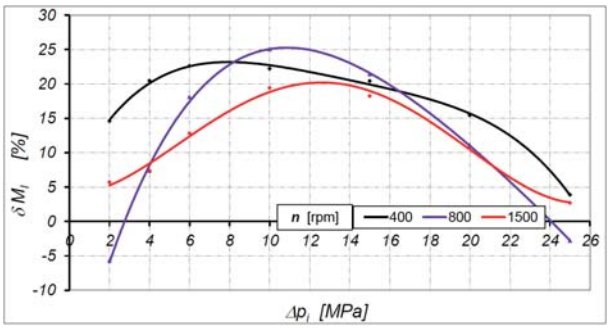

Fig. 28. Characteristics of $\delta M_l=f(\Delta p_l)$. Working medium: oil

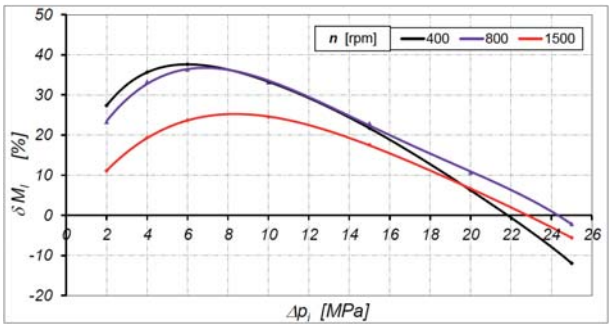

Fig. 29. Characteristics of $\delta M_l=f(\Delta p_l)$. Working medium: water

From the above presented characteristics it can be concluded that the proposed mathematical model describes quite accurately the torque of losses in the pump supplied with both mineral oil and water. Therefore, mechanical losses in the pump working with various liquids can be assessed by comparing the model coefficients.

SUMMARY

The article presents the results of experimental research on mechanical losses in the novel satellite pump, for which the working medium was water and mineral oil. The experimental studies have shown that the type of liquid has an impact on the values of losses. The mechanical losses are bigger in a water pump than in an oil pump – especially at low values of the load Δp and speed n.

Experimental studies have shown that the greatest source of mechanical losses in the pump is friction in the working

MOST WIEDZY Downloaded from mostwiedzy.pl

mechanism. Much smaller mechanical losses occur in the bearings and seals, and the type of liquid has the least impact on the mechanical losses in these elements. The smallest component of the mechanical losses is that depending on the liquid viscosity, i.e. the mechanical losses caused by viscous friction in gaps.

The mathematical model of the torque of mechanical losses described in the article has been developed based on an analysis of the sources of the losses. The coefficients in the mathematical model were calculated on the basis of the experimental data and plotted characteristics of losses in the oil pump and water pump. The described mathematical model will provide a more accurate simulation of the characteristics of mechanical losses in a satellite pump.

BIBLIOGRAPHY

1. Balawender A.: Physical and mathematical model of losses in hydraulic motors. Developments in mechanical engineering, Gdansk University of Technology Publishers. Gdansk 2005

2. Dymarski C., Dymarski P.: Developing Methodology for Model Tests of Floating Platforms in Low-Depth Towing Tank. Archives of Civil and Mechanical Engineering, No. 1/2016, DOI: dx.doi.org/10.1016/j.acme.2015.07.003

3. Guzowski A., Sobczyk A.: Reconstruction of hydrostatic drive and control system dedicated for small mobile platform. American Society of Mechanical Engineers, 2014. DOI: dx.doi.org/10.1115/FPNI2014-7862.

4. Jasinski R.: Influence of design of hydraulic components on their operation in low ambient temperatures. Key Engineering Materials, Vol. 490, 2012. DOI:10.4028/www.scientific.net/KEM.490.106.

5. Jasiński R.: Influence of type of material on performance of hydraulic components in thermal shock conditions. Solid State Phenomena, Vol. 183, 2012. DOI: 10.4028/www.scientific.net/SSP.183.95.

6. Jasinski R.: Problems of the starting and operating of hydraulic components and systems in low ambient temperature (Part IV). Modelling the heating process and determining the serviceability of hydraulic components during the starting-up in low ambient temperature. Polish Maritime Research, No 3 (95) 2017. DOI: 10.1515/pomr-2017-0089

7. Kollek W., Osinski P., Warzynska U.: The influence of gear micro-pump body asymmetry on stress distribution. Polish Maritime Research, No 1/2017. DOI: https://doi.org/10.1515/pomr-2017-0007

8. Litwin W., Dymarski C.: Experimental research on water lubricated marine stern tube bearings in conditions of improper lubrication and cooling causing rapid bush wear. Tribology International Vol. 95 (2016). DOI: 10.1016/j.triboint.2015.12.005

9. Litwin W., Olszewski A.: Water-Lubricated Sintered Bronze. Journal Bearings - Theoretical and Experimental Research. Tribology Transactions, vol. 57, No. 1/2014. DOI: 10.1080/10402004.2013.856980

10. Lubinski J., Sliwinski P.: Multi parameter sliding test result evaluation for the selection of material pair for wear resistant components of a hydraulic motor dedicated for use with environmentally friendly working fluids. Solid State Phenomena, No 225/2015.

11. Maczyszyn A.: Investigation method and mathematical model of pressure losses in hydraulic rotary motor. Polish Maritime Research, No. 97/2018 Vol. 25. DOI: 10.2478/pomr-2018-0011

12. Niemann G., Winter H.. Maschinenelemente – Band 2 (in German) , Springer-Verlag. Berlin, 2003.

13. Osinski P., Chruscielski G.: Strength calculations of an element compensating circumferential backlash in the external gear pump. Journal of Theoretical and Applied Mechanics. Vol. 54, No. 1/2016. DOI: 10.15632/jtam-pl.54.1.251

14. Osinski P., Deptula A., Partyka M.: Discrete optimization of a gear pump after tooth root undercutting by means of multi-valued logic trees. Archives of Civil and Mechanical Engineering, No. 4/2013, DOI: 10.1016/j.acme.2013.05.001.

15. Paszota Z.: Energy losses in hydrostatic drive. LABERT Academic Publishing, 2016.

16. Paszota Z.: Theoretical models of the torque of mechanical losses in the pump used in a hydrostatic drive. Polish Maritime Research, No. 4/2011.

17. Patrosz P.: Deformation in the axial clearance compensation node in the satellite pump unit. Hydraulika i Pneumatyka 1/2014

18. Pobedza J., Sobczyk A.: Properties of high pressure water hydraulic components with modern coatings. Advanced Materials Research. Trans Tech Publications Ltd, 849/2014. DOI: 10.4028/www.scientific.net/AMR.849.100.

19. Sliwinski P.: High pressure rotational seals for shaft of hydraulic displacement machines. Hydraulics and Pneumatics, 3/2014, Poland.

20. Sliwinski P.: New satellite pumps. Key Engineering Materials, No 490/2012.

MOST WIEDZY Downloaded from mostwiedzy.pl

21. Sliwinski P.: Pressure losses and power balance in the unloaded satellite pump. Hydraulika a Pneumatika, No 1-2/2013, Slovakia

22. Sliwinski P.: Satellite pumps. Hydraulika i Pneumatyka, No. 5/2012, Poland

23. Sliwinski P.: The flow of liquid in flat gaps of satellite motors working mechanism. Polish Maritime Research, No 2/2014. DOI: 10.2478/pomr-2014-0019

24. Stosiak M.: The impact of hydraulic systems on the human being and the environment. Journal of Theoretical and Applied Mechanics, Vol. 53 No 2/2015. DOI: 10.15632/jtam-pl.53.2.409

25. Stosiak M.: The modeling of hydraulic distributor slide–sleeve interaction. Archives of Civil and Mechanical Engineering, No 2/2012. DOI: 10.1016/j.acme.2012.04.002

26. Stosiak M., Kollek W., Osiński P., Cichon P., Wilczynski A.: Problems relating to high-pressure gear micro-pumps. Archives of Civil and Mechanical Engineering, No 1/2014. DOI: 10.1016/j.acme.2013.03.005

27. Walczak P., Sobczyk A.: Simulation of water hydraulic control system of Francis turbine. American Society of Mechanical Engineers, 2014. DOI: dx.doi.org/10.1115/FPNI2014-7814

28. Zloto T., Nagorka A.: An efficient FEM for pressure analysis of oil film in a piston pump. Applied Mathematics and Mechanics, vol.30, No 1/2009. DOI: 10.1007/s10483-009-0106-z.

CONTACT WITH THE AUTHORS

Paweł Śliwiński
e-mail:pawel.sliwinski@pg.edu.pl

Gdańsk University of Technology
Faculty of Mechanical Engineering
11/12 Narutowicza St.
80 - 233 Gdańsk
Poland

MOST WIEDZY Downloaded from mostwiedzy.pl

POLISH MARITIME RESEARCH Special Issue 2018 S1 (97) 2018 Vol. 25; pp. 189-197
10.2478/pomr-2018-0041

INCREASING POWER SUPPLY SAFETY IN THE ASPECT OF SUPPORTING THE RENEWABLE ENERGY SOURCES BY CONVENTIONAL AND VIRTUAL POWER STORES

Damian Jakowski
Marek Dzida
Gdańsk University of Technology, Poland

ABSTRACT

This paper presents characteristics and purposefulness of supporting the renewable energy sources (OZE) by means of energy stores. The main emphasis was placed on analysis of virtual energy stores available for implementation in Polish economy conditions. A role which management of Demand Side Response (DSR) may play in balancing Polish electric power system, is discussed. Implementation of such solutions together with conventional energy stores may significantly influence power supply safety by assuring continuity of electric power supply at an acceptable price. Involvement of electric power consumers (DSR) should be one of the basic solutions for power markets in Poland and Europe.

Keywords: OZE, power market, energy stores, DSR, power supply safety, electric power system, mangement of electric power demand

MAJOR ACRONYMS USED IN THE TEXT

OZE – Renewable Energy Sources
CAES – Compressed Air Energy Storage
DSR – Demand Side Response
EOM – Energy Only Market
KSE – Polish Electric Power Network
LAES – Liquefied Air Energy Storage
MD – Point of Delivery
MC – Missing Capacity
NN/WN – Low Voltage/High Voltage
OSD – Supply Network Operator
OSP – Transmission Network Operator
PCM – Phase Change Material
PMC – Energy Phase Transition
POB – Body Responsible for Commercial Balance
SEE – Electric Power Network
SN – Intermediate Voltage
SZU – Official Energy Seller
TES – Thermal Energy Storage
TTES – Tank Thermal Energy Storage
UTES – Underground Thermal Energy Storage

INTRODUCTION

Assurance for supplying sufficient amount of energy constitutes one of the basic challenges which economies of various countries, especially those highly developed, must cope with. Risk of occurrence of breaks in electric power supply has triggered debate on effectiveness of the functioning of uniform power market. The conducted analyses show that yearly increase in electric power demand is close to 1% and in Polish conditions it amounts to 2% in recent years. In the light of EOM (Energy Only Market), the one-good power market which does not allow to return investment capital engaged by producers caused that investment decisions partly or entirely stopped. Consequently, it leads to a decrease in production capacity (Missing Capacity).

In Poland, in case of lack of appropriate economic signals, about 10 GW production capacity will be withdrawn till 2025 [21].

There is necessity of continuous development of production sources, modernization of existing high-power blocks, support for dissipated power industry as well as investment into conventional and virtual energy stores and renewable energy sources (OZE).

MOST WIEDZY Downloaded from mostwiedzy.pl

Profitability of investment into new production capacity is closely associated with development of OZE. Support systems, subsidies in the area of capital costs, low changeable costs of power production from OZE all that results in shortening the lifetime of conventional production units. It generates the problem of Missing Money – shortage of financial resources for covering operational and investment costs [2].

Energy from alternative power sources, though inexhaustible and commonly available, is characterized by a high changeability of occurrence and is not correlated with power demand from the system [3]. Costs of wind and solar power plants are dropping but do not guarantee supply stability without changing the functioning paradigm and way of thinking about the whole electric power system.

Development of energy storage and its capacity is one of the crucial research issues in recent years. It is necessary to assure a stable mode of operation of electric power system [4]. Storage of huge amounts of power is rather questionable due to technological limitations therefore a great emphasis is recently placed on development and application of virtual power stores based on including the demand side into balancing the power demand system (incentive programs for electric power consumers) [15].

CHANGES WHICH OCCUR IN ELECTRIC POWER SYSTEM

In recent years very dynamic changes have been observed in Polish electric power system : increasing demand for electric power, increasing share of OZE, transborder exchange, new fuels, certification systems, power effectiveness, electric driven cars, intelligent measuring systems. These are only some factors which cause greater and greater problems in balancing the system and safety assuring. Fig. 1 presents the statement of amounts of produced and consumed electric power in particular years. The year 2014 was a breakthrough with respect to electric power consumption in Poland – more power was consumed than that produced by the system (indicated by red arrows in Fig. 1).

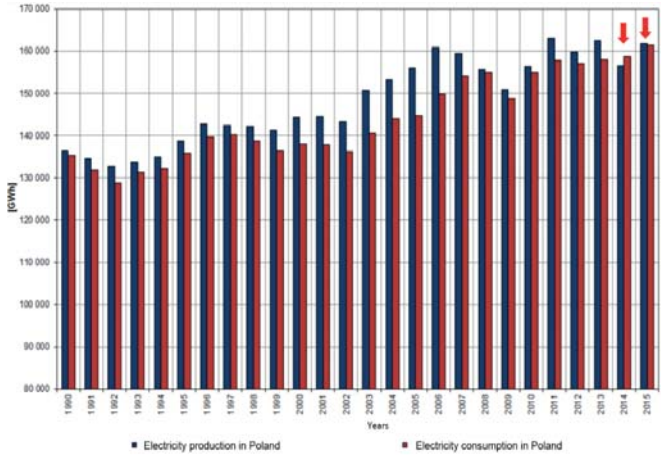

Fig. 1. Electric power production and consumption in the last years, [5]

However on 9th January 2017 the power demand in Poland exceeded 26,2 GW (this way the record of 2012 was broken). Despite 40 GW power capacity installed in the system, the events in which the available power reaches the level of only 26 GW, occur (such situation is illustrated in Fig. 2) [5]. This results due to non-availability of OZE (RES), heat and power stations, industrial electric power plants, breakdowns or repair down times.

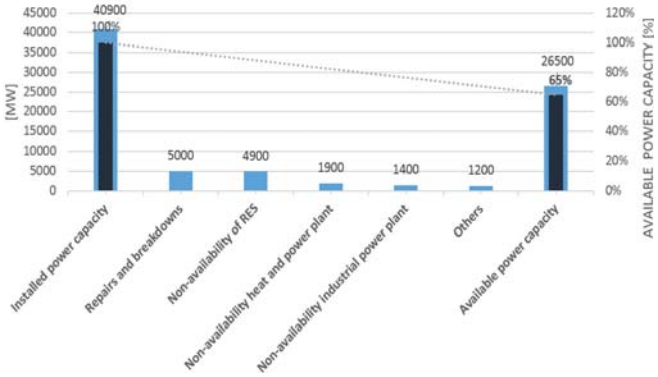

Fig. 2. Average power capacity available at the summit in September 2016. Own study based on data from [5]

A more and more serious problem for the electric power system results from the increase of the installed wind-generated power (from 1 200 MW power installed until the end of 2010 up to 4254 MW power installed until the end 2015, and up to 5 800 MW until the end of March 2017 – Fig. 3.)

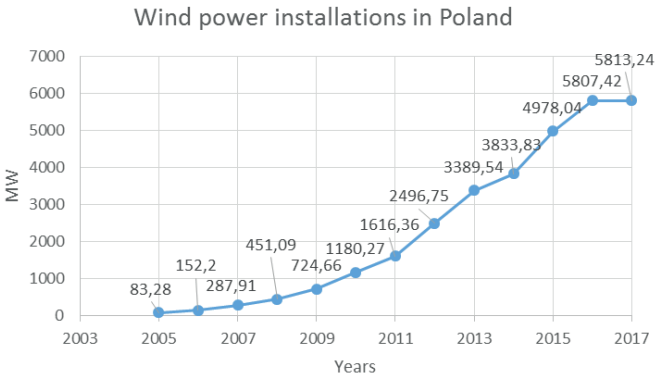

Fig. 3. Wind- generated power installed in Poland in particular years. Own study based on data from [5]

Nominal power of wind turbines is taken into account in balance of Polish electric power system however its availability depends on hard predictable atmospheric conditions (see an example given in Fig. 4.). The below given figures (Fig. 4, Fig 5) present discrepances between planned and actual amount of wind- generated electric power.

MOST WIEDZY Downloaded from mostwiedzy.pl

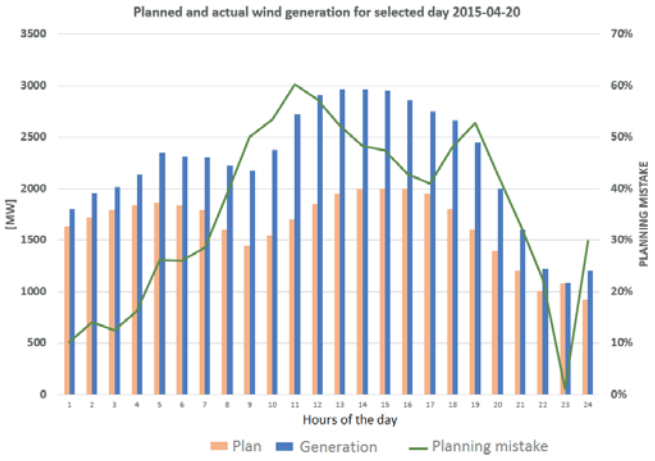

Fig. 4. Planned and actual amount of wind- generated electric power on the selected day : 2015-04-20. Own study based on data from [5]

The discrepances in daily prediction of power production from wind power sources may reach the level of over 60%, which is equivalent to the not planned emount of wind-generated power reaching more than 1000 MW in particular hours of the day.

According to Fig. 5, the difference between maximum and minimum amount of wind -generated power during about a month may exceeds 3500÷4000 MW.

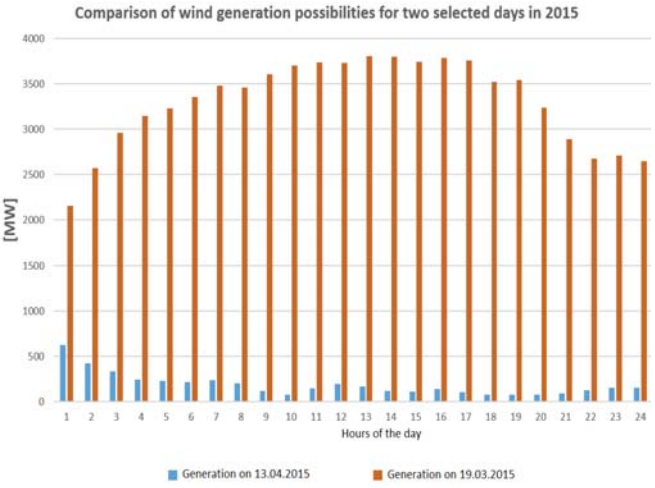

Fig. 5. Comparison of wind generation possibilities for two selected days : 19.03.2015 and 13.04.2015 . Own study based on data from [5]

In the subsequent stage of analysis of the data, a coefficient of impact or share in electric power production, which shows consequences for stability and characteristics of the electric power system, may be determined. The wind turbine impact coefficient is time-variable. On the ordered characteristics of yearly power loading it can be observed that the largest percentage of share of wind-generated power is achieved in the situations of the lowest demand for power from side of the system (Fig. 6.)

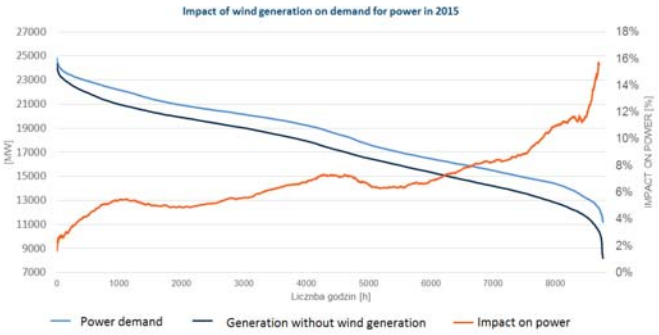

Fig. 6. Impact of wind generation on power demand in 2015. Own study based on data from [5]

The situation presented in Fig.6 results in an increase and variation of prices on the electric power market.

According to various analyses, even 4,4 GW production power capacity may be cut off in subsequent years [5, 21].

To counteract consequences of lack of peak power capacity in the system the Supply Network Operator has a few solutions at his disposal. First, he can make use of the so called Operational Power Reserve (of yearly cost of about 400 mln PLN). Secondly, he can activate the so called Intervention Cold Reserve (of yearly cost of about 170 mln PLN) which artificially supports extension of lifetime of unprofitable and non-ecological production units [5]. Thirdly, he can increase power import. Fourthly, he can optimize timetable of repair of production units being at central disposal. In spite of that the two last solutions are rationally justified their results do not yet solve any cause of shortage of peak power. It should be remembered that the highest load intervals occur in the system during 100÷150 h per year only.

The assuring of appropriate power production capacity and power reserves, hence power supply safety, requires to introduce stable and long-lasting stimulation mechanisms for investing into new production sources and energy stores. The power market which limits risk associated with long-term investment into power industry constitutes such mechanism . It also supports realization of climatic policy.

For building the power market it is necessary to develop DSR services despite future energy decisions . Examples from USA, France or Great Britain show that demand-side resources may be less expensive than building new production units [20]. In case of providing appropriate conditions as well as possible participation and equal functioning conditions on the market for DSR services they are also stable and achieve high effectiveness.

POWER MARKET

Power supply safety is conditioned by availability of fuels, an appropriate network's infrastructure which is developed by control mechanisms as well as an appropriate production capacity developed by competition mechanisms. In long-term horizon it will be possible to assure power supply safety

MOST WIEDZY Downloaded from mostwiedzy.pl

by working out power mechanisms, i.e. implementation of a power market.

Power rewarding mechanism which functions aside power market and balancing one can be considered as an additional, transient power rewarding mechanism only after undertaking actions aimed at elimination of imperfections of the power market . It is usually introduced in the situation when evaluation of adequacy of resources, carried out in compliance with European standards, demonstrates that in the near future the relevant resources would be not fully invested which may endanger power supply safety [2].

Power resurces which make profit from support or/and public help systems (operational assistance for OZE and CHP – combined heat and power, difference contracts etc) cannot take part in the power market.

The power market is technologically neutral and forms therefore uniform competition conditions for all production technologies as well as DSR with taking into account parameters of how much particular technologies contribute in the assuring of electric power supply safety [2]. In various analyses of power markets and mechanisms a taxonomy based on their operational modes is usually implemented. The aspects of which entities determine quantity of production capacities, which are to be bought and in how big amount, are taken into account (Tab. 1). Such solutions are already under operation in France, Belgium, Great Britain, Spain and Ireland [2].

Tab. 1. Typology of power capacity markets [2, 6]

Based on quantity	**Based on price**
Auction organized by a control body (in Poland e.g. by Polish Electric Power Networks[1]) assures an appropriate level of power. Alternatively, the control body requires from retail sellers to have power certificates covering the peak demand.	Payment for power is determined by a control body and it constitutes an additional income for power producers (supplier is paid for a unit of delivered energy as well as for assurance of power delivery to the system).
Centralized	**Decentralized**
Overall domestic auction is organized to cover lacking power. The control body transfers its cost onto final consumers.	The control body requires from retail sellers to cover peak power demand appropriately. The sellers are made resposible for realization of the task.
Dedicated	**General**
Only a part of producers make profit from the mechanism, e.g. planned installations, or a part of those which fulfill criteria.	All consumers make profit from the mechanism irrespective of a used technology.

In compliance with a proposal offered in [6], on identification of all problems as well as because of lack of possibility to balance demand for power,it is planned in Polish electric power system to introduce a centralized auction for production capacities accompanied by a reform of power capacity market and system's services.

[1] The operational body of Polish Electric Power Networks is to render services of electric power transmission under condition of fulfilling required criteria for operational safety of Polish Electric Power System (KSE) [5].

In Poland a crucial aim for changes in power market should be to assure an appropriate quantity of available power in the electric power system. A standard level for power supply safety can be determined both deterministically and stochastically. In case of designing a new mechanism the two methods should be initially used, making this way it possible to verify results of stochastic approach by means of the deterministic method which is better known in Poland.

In the proposed project of power market volumes of power in MW units will be contracted in the form of the so called Dutch auction, i.e. the "dropping price" auction . In the power market DSR services will be able to participate.

European experience, especially the implementation of power market in Great Britain, Has revealed trends and specifity of functioning a two-good market.

In Great Britain in auction for the winter season 2020/2021 stores based on batteries (e.g. Li-Io ones) won about 1% of contracted power capacity (about 500 MW). However investments into new big electric power stations could not count on any support. Only small gas power plants reached contracts (3412 MW power capacity in total for 129 units which gives 25 MW per unit) [22].

Among eight winning investments into support and stabilization services of electric power system operation, five were devoted to storage systems, two to DSR (detail analysis of the solutions is given in Chapter 5 and 6 of this paper) and one to a gas power plant.

CONVENTIONAL ENERGY STORES

According to the definition of energy stores being in force in Poland, which was approved including the last amendment of the act of OZE, energy store is defined as "a separate facility or a set of facilities which serve to store energy in an arbitrary form and in the way which makes it possible to win at least some amount of it back, as well as does not cause any emission burdensome for environment".

The today applied technologies which allow to store electric energy can be divided into those for intermediate electric energy storage (with the use of converting electric energy into other kind of energy, e.g. kinetic or chemical) and those for direct storage of it (in electric or magnetic field) [19].

Undertakings aimed at application of energy storage technology make it possible [14]:
- to moderate variability in power generation from wind sources, introduced into electric power network in shorter time intervals,
- to limit the using of conventional peak sources in situations of changes in generation from wind sources,
- to shift electric power production from non-summit load hours to summit load ones.

A good enegy storage system should be characterized by [7]:
- high energy density,
- easiness of loading and unloading and a high number of their cycles,

MOST WIEDZY Downloaded from mostwiedzy.pl

– high energy output of the cycles,
– possibly simple conversion of energy into its other forms,
– it should reach a required economical effectiveness and do not cause any danger to the environment,
– an assumed duration time of energy storage and time of delivery it to consumers .

Tab. 2 presents the basic operational parameters for different modes of energy storage recommended by American Electric Power Research Institute, aimed at support for integration of wind electric generation plants with electric power system.

Tab. 2. Basic operational parameters of selected types of energy storage technology [1]

Lp.	Technology	Cycle efficiency %	Nominal power [MW]	Discharge time [h]
1.	Pumped-storage Hydroelectricity	80	100-1000	> 1 hour
2.	Compressed Air Energy Storage	60-75	0,1 – 1000	few hours
3.	Flywheel Energy Storage	90	0,1 – 10	0,1
4.	Conventional Batteries	60-80	0,1 – 10	0,1 … > 1
5.	Rechargeable electrochemical	70	0,1 – 20	> 1
6.	Fuel cell	50	0,1 – 1	> 1

COMPRESSED- AIR ENERGY STORAGE (CAES)

Pumped-storage power stations are commonly used for energy storage. This is a large-scale technology when taking into account that such amount of available power can be of importance from point of view of the entire electric power system. Alternative storing facilities of comparable capacity, but more profitable, are compressed air installlations [17].

The example technical solution of interaction of gas turbines and compressed air tanks is given below (Fig. 7.) There are a few systems for energy storage in compressed air. Fig. 7 presents a system which reaches the highest efficiency of over 70%. It contains in its turbine part both a combustion chamber and recuperator. Beyond the last compressor stage there is no cooler as the produced heat is stored in a tank for waste heat which can be used for heating the compressed air directed either to turbine stages (in the systems without combustion chamber) or to combustion chamber (Fig. 7.).

Such solutions are designed and tested in the countries where wind power industry is developed the most. The German project ADELE (Adiabatic Compressed-Air Energy Storage for Electricity Supply) may serve as an example of such solution. The main aim of carried out investigations is to develop air tanks as well as heat exchangers and stores recovering waste heat from compression [1, 3].

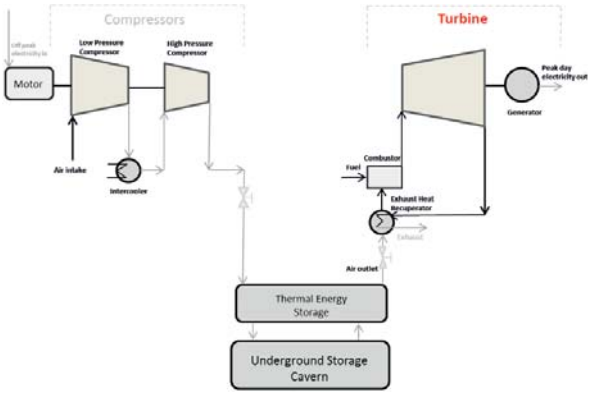

Fig. 7. A CAES system with exhaust [waste] heat storage, combustion chamber and recuperator [3]

HEAT STORAGE

Accummulation (storage) of heat takes place in the devices called Thermal Energy Storages (TES). They are split into three groups depending on a temperature range of storing medium: low-temperature (up to 120°C), intermediate-temperature (120-500°C) and high-temperature ones (over 500°C).

The following three basic heat storage systems may be distinguished:
– by using specific heat,
– by using energy phase transition (PMC),
– by using chemical heat transition.

Tab. 3 presents comparison of the three storage systems.

Tab. 3. Typical parameters of Thermal Energy Storage Systems [8, 9]

TES System	Capacity (kWh/t)	Power (MW)	Efficiency (%)	Storage period (h, d, m)	Cost (€/kWh)
Sensible (hot water)	10-50	0.001-10	50-90	d/m	0.1-10
PCM	50-150	0.001-1	75-90	h/m	10-50
Chemical reactions	120-250	0.01-1	75-100	h/d	8-100

Heat accumulators, the so called UTES (Underground Thermal Energy Storage), are able to use ground, water or gravel as a storing medium. These also may be water reservoirs, i.e. TTES (Tank Thermal Energy Storage).

LIQUEFIED –AIR ENERGY STORAGE

One of the most effective methods of surplus energy storage is storing in liquefied air (LAES method – Liquefied Air Energy Storage) [18]. Such process consists in compression of air and next cooling it until the instant of its transition from gaseous state to liquid state of matter. Consequently, the liquefied air is stored. In the periods of increased demand for energy the pressure of liquefied air is increased by pumping and as a result it starts to vapourize. The air in gaseous state (under pressure) is heated and used for production of electric

MOST WIEDZY Downloaded from mostwiedzy.pl

power in electric power stations equipped with compressed-air turbines or gas turbines [10, 11].

VIRTUAL ENERGY STORES

One of the verified and efficient means for assuring efficiency, stability and competitiveness of dispersed energy production sources is to implement technology of virtual energy stores (called also virtual electric power plants – Virtual Power Plants). Solutions based on virtual energy stores constitute a closed controllable entity (unit) which is capable of satisfying energy needs of a single installation or it may be integrated with electric power network increasing this way its energy effectiveness.

The concepts of virtual energy stores find greater and greater industrial/commercial application in EU countries.

The notion of virtual energy storage (Virtual Energy Storage) should be meant an aggregated and accessible – on request by means of teleinformatical solutions, i.e. virtually-structure which covers controllable units (manufacturing, consuming and storing). Such structures may render system's services supporting this way operation of SEE on the level of the entire system (i.e. in aid of transmission network's operator – OSP) or locally (in aid of delivery network's operator – OSD) to optimize power purchase costs with simultaneous limiting network's losses and investments associated with short-lasting occurrence of power demand peaks.

Virtual energy stores may be also used as economic tools for POBs (Bodies Responsible for Commercial Balance) to balance elements of commercial contracts. Activity of virtual energy stores results in improvement of SEE balance conditions.

Execution of services rendered by virtual energy stores may be carried out in two ways :

- by power supply management (delivery of energy generated by managing-subjected, small disperse sources – electric generating sets, industrial/ private units) or
- by power demand management (management of power absorption – most often by shifting load towards other time of the day).

A very important aspect necessary for functioning such services are informatic and measuring tools used for verification of correct run of supporting activity directed to the electric power system.

In the worldwide existing solutions there are demand aggregators which are responsible for aggregation of energy in virtual energy stores [2]. These are bodies which are able to sell and deliver – both in quantitive and qualitative sense – energy (power) to SEE or to limit demand

(to activate the so called „ negawatts" on the market).

As services rendering bodies, i.e. those which offer power generation on call or its reduction (shifting electric power demand in time) may serve e.g. large industrial enterprises (foundries, mines, water supply networks, metalurgical works, food processing plants, manufacturing plants, collocation centres, trade centres equipped with BMS systems (Building Management Systems).

DSR SOLUTIONS

An act of electromobility has to introduce, into Polish legal order, issues associated with management of electric power demand, i.e. the so called DSR [16].

The notion of " demand management" has to be applied to "final consumer's installation whose devices make it possible to change profile of electric power absorption on call from the side of power supply system's operator, power transmission system's operator or operator a joint system which may be consisted in particular of an energy store, production installation which does not coopoerate directly with the network, or loading point".

The below given analysis presents ways of making use of DSR services (demand side management – virtual energy store management) for the puropses of participants of Polish energy market.

DSR FOR OSP

The intervention reserve is used in situation of critical load in the system. Earlier, OSP contracts power demand reduction by means of a tender/auction. Till now, OSP have announced seven tenders for rendering demand reduction services. They allowed not to contract abt. 200 MW for winter season (October-March) and 185 MW for summer season (April-September). In May 2017, PSE announced next auction to enlarge the quantities, that was a consequence of concern resulting from increasing load during summer. Appropriate contracts were signed with three big consumers and one aggregator [13].

The contracts are described by detail regulations in which requirements for the attendance, execution and accounting of services are defined. Till now, OSP has made use of the services in 4h reduction periods . Fig. 8 presents an example of such services.

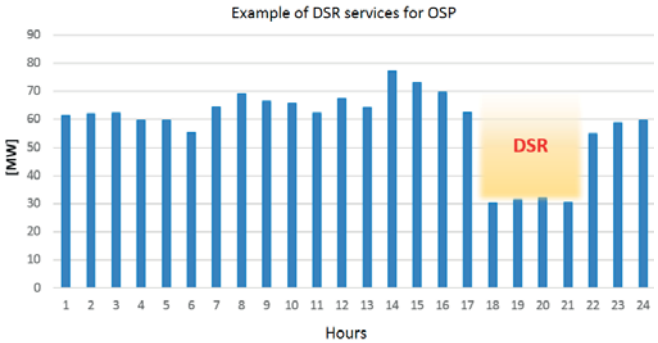

Fig. 8. Example of DSR services for OSP

According to the new conditions (available from OSP web page) OSP is going to put into operation two following programs:

- guarranteed one – services provider is to response on OSP call – the so called stand-by fee,
- current one – services provider may response on OSP call – payment for rendered services.

MOST WIEDZY Downloaded from mostwiedzy.pl

DSR FOR POB

Issues which are present in activity of bodies responsible for trade balancing (POB) always result from the situation which occurs on electric power markets where prices are varying within the range from 70 PLN/MWh to 1400 PLN/MWh. The variations result from three main commercial-technical factors :

- a level of electric power produced by wind turbines,
- a level of power available from centrally administered production units, and
- a service time of coal power plants put in operation only in power shortage periods.

In Poland consequences of varying prices most afflict POBs which do not have capital connections with conventional production sources but simultaneously face a high level of wind generation in the region where they operate in the role of an official seller (SZU). POBs are obliged to buy back electric energy at a price announced by the Office for Energy Control . Such price is usually higher than that contracted with final clients.

The used trade model (following-up) assuming to buy electric energy on long-term markets contributes to the bad situation.

Implementation of DSR services in regions under demand control may be greatly useful in levelling unfavourable market trends for POBs being in the above described situation. Their commercial application in reduction region (activation of demand reduction in an appropriate moment, in aid of POB) consists finally in limiting number and value of deficit transactions on the Next Day Market (optionally on the Current Day Market) as well as on the Balancing Market, indirectly. The transactions are considered to be obligatory energy purchase at a higher price than that of selling to final client with taking into account necessary price mark-ups.

Analogous situation of commecial application of DSR in generation regions consists in activation on demand clients' power generation sources (which are not centrally administered units) in hours of high electric power prices on spot markets. However in case of occurrence of low electric power prices on spot[2] markets (e.g. in the night) such application consists in limitation on demand a more expensive generation from clients' sources, this way making it possible to increase volume of cheap energy purchase from the market. In case of a lack of access to client's generation, the increasing of electric energy demand in response to low electric power prices on spot markets is a natural consequence of activation of DSR services.

DSR FOR OSD

Problems which appear for operators of supply systems (OSD) consist first of all in the over-dimensioning of network infrastructure to cope with short-lasting rises of demand for electric power. It leads to higher investment costs and is directly associated with maintainance and operation costs of electric power supply produced by means of an infrastructure not adjusted to needs.

The earlier discussed problems of OZE and the increasing share of dispersed generation affect character of network operation. It generates additional losses and forces not only decision on new infrastructural investments but also a change in view on rendering supply services. Present business model does not consider to apply an active demand – supply management on the OSD level but it is only focused on maintaining distribution capability of the network. The situation results from a stiff structure of tariff building process which does not take into account changes in market situation.

Today, OSDs assure power level in OSP's network. In case of OSP, payment operations are made on the basis of an average value taken from maximum amounts of total power absorbed by OSDs. In order to assure power level in the assumed account model, amount of contracted power is over-dimensioned against usual needs. This is associated with generation of additional costs which are entirely transferred onto electric energy consumers.

Commercial application of DSR services on the level of OSD may be made in analogous regions as in the case of POB. When dynamics and characteristics of power demand in the Polish electric power system is analyzed the demand peaks which occur in very short-lasting periods can be observed.

Potential profits for OSD which may arise from implementation of system services rendered by producers wired into intermediate voltage (SN) network, are analyzed in Tab. 4,[4].

Tab. 4. Profits from implementation of system services rendered for OSD

Action	Profit	Alternative
Active power control	Frequency control (fast control), overload mitigation (slow control), substitutivity of network investments or possible shifting system's extension investments in time, possible voltage control, lowering tariff payments for contracted power in NN/WN (the highest voltage / high voltage) stations	System generators, absorption control, energy dispensers, investments
Passive power control	Voltage control, optimization of losses, lack of necessity of passive power transmission over large distances, limitation of use of already installed passive power (Q) sources as well as transformers	Passive power sources,, WN/SN (intermediate/ low voltage) transformers, control of sources connected to 110 kV switching stations
Island operation (+blackstart)	Lowering breaks in power supply (lowering SAIDI and SAIFI coefficients), lowering danger of occurrence of system failures, lowering probability of loss of a part of generation, resulting from disturbances	Multi-side supply, electric generating set

Services for OSD may be also rendered by sources incapable of regular increasing generation in peak demand periods

[2] Cash market – in this case the Next Day Market.

MOST WIEDZY Downloaded from mostwiedzy.pl

but able to increase power during a dozen or so hours per year (i.e. heat and power stations, over-dimensioned power sources).

To render services it is necessary for a producer to have a permanent margin of power to be produced over that delivered to network. The increasing of generation is executed on OSD's demand immediately Just after stating a risk of exceeding an assumed level of hourly average power absorption in a given MD. Determination of power amonut contracted by OSP consists in averaging five (out of seven) highest hourly average measurements taken at NN/WN station. Duration of time during which the increased level of generation has to be maintained should be determined on the basis of statistical data about flow of maximum power amounts into particular power delivery points (MD).

CONCLUSIONS

The analysis presented in this paper illustrates a number of changes which occur in the field of electric energy . New solutions and mechanisms are compulsory in this area. It is essential to abandon the one-good model of electric energy market in aid of a two-good market. In the new model, a power market, i.e. mechanism of rewarding production capacities which store electric energy indispensable for assuring power supply safety for the country should function in parallel to the electric energy market.

The power market is a mechanism in which resources of both supply side and demand side (i.e. production sources and consumers of electric energy) may take part. Virtual stores which make use of DSR (demand side management) can effectively lower cost of maintaining stable electric energy supply to consumers making this way possible to balance KSE . Integration of technological systems making use of OZE with traditional electric energy system imposes necessity of searching for more useful forms of energy which may be consumed in any time.

This became a motivation for searching for and developing new forms of energy storage. Flywheels, fuel cells, CAES, LAES, supercondensers, electrochemical cells represent only some of conventional technological solutions of energy stores, which are under permanent development and improvement.

BIBLIOGRAPHY

1. Jakowski D., Dzida M.: *Energy storage in compressed air – solution supporting renewable energy sources*, Journal of Polish CIMAC. Vol. 9., No. 1 (2014), pp. 35-45

2. Polski Komitet Energii Elektrycznej: *Power market - in other words how to avoid blackout* (in Polish), August 2016

3. Jakowski D., Dzida M.: *Gas turbines – technological development and potential use in CAES systems, Combustion Engines.* 2016, 165(2), pp. 46-53

4. Badyda K. Milewski J., *CAES electric power plants – possible accumulation of energy and cooperation with renewable sources* (in Polish), Monthly : Instal –Teoria i praktyka w instalacjach – Warszawa 2010 pp. 58-65

5. Polskie Sieci Elektroenergetyczne www.pse.pl, http://www.pse.pl/index.php?dzid=115&did=581 (visit on 15.05.2017)

6. Ministerstwo Energii, Polskie Sieci Elektroenergetyczne: *Power market – proposal of functional solutions* (in Polish). Meeting to open consulting process on 4 July 2016, Warszawa http://www.pse.pl/uploads/pliki/2016-07-04_Rynek_Mocy_-projekt_rozwi%25B1zan_funkcjonalnych.pdf

7. Herlender K. : *Storage of electric energy in SEE* (in Polish), ENERGETAB 2013, Bielsko-Biała, September 2013 pp. 61-66

8. IEA-ETSAP and IRENA Technology Brief E17 – January 2013, www.etsap.orgy, www.irena.org (odsłona z dnia 19.05.2017)

9. Hauer, A. : *Storage Technology Issues and Opportunities*. Committee on Energy Research and Technology (International Energy Agency), International Low-Carbon Energy Technology Platform, Strategic and Cross-Cutting Workshop "Energy Storage – Issues and Opportunities", 15 February 2011, Paris, France

10. Mirek P.: *Energy storage technique in liquified air* (in Polish). Polityka Energetyczna – Energy Policy Journal 2016, Vol. 19, Issue 1 pp. 73-86

11. Wojciechowski H.: *Energy storage technologies*. Part II, Instal 3/2017 pp. 16-27

12. Ke Meng, Member, Zhao Yang Dong, Zhao Xu, Yu Zheng, David J. Hill: *Coordinated Dispatch of Virtual Energy Storage Systems in Smart Distribution Networks for Loading Management*. IEEE transactions on systems, man, and cybernetics: Systems, 14.04.2017

13. pse.pl: *Specification of crucial conditions to order (SIWZ) Intervention Operation service : Demand reduction on command of OSP* (in Polish), (visit on 18.05.2017)

14. Majchrzak H. Tomasik G., Kwiatkowski M.: *Using energy storage technology for integration of wind power industry with electric power system* (in Polish). Energetyka, October 2012

15. Pakulski T, Czarnecki B.: *Strategies of using energy stores and resulting* profits (in Polish). Instytut Energetyki Gdańsk, cire.pl (visit on 20.05.2017)

MOST WIEDZY Downloaded from mostwiedzy.pl

16. Polskie Sieci Elektroenergetyczne: *Mechanism of DSR (OP-DSR) intervention programs* (in Polish). Konstancin Jeziorna, 30.11.2016, ttp://www.pse.pl/index.php?dzid=14&did=3215

17. Jannelli E., Minutillo M., Lubrano Lavadera A., Falcucci G.: *A small-scale CAES (compressed air energy storage) system for stand alone renewable energy power plant for a radio base station: A sizing-design methodology*, Energy 78 (2014) pp. 313-322

18. Sciacovelli A., Vecchi A., Ding Y.: *Liquid air energy storage (LAES) with packed bed cold thermal storage – From component to system level performance through dynamic modeling,* Applied Energy 190 (2017) pp. 84-98

19. Kousksou T., Bruel P., Jamil A., Rhafiki T., Zeraouli Y.: *Energy Storage: Applications and challenges*. Solar Energy Materials & Sollar Cells 120 (2014) pp. 59-80

20. Forum Energii: *How to develop DSR potential in Poland and lower cost of electric power system* (in Polish), www.forum-energii.eu, March 2017 (visit on 05.06.2017)

21. Polskie Sieci Elektroenergetyczne: *Prediction of covering power peak demand in the years 2016 – 2035* (in Polish), Konstancin-Jeziorna, 20 May 2016.

22. Forum Analiz Energetycznych: *Power market in Great Britain – an experience important for Poland* (in Polish), April 2015.

CONTACT WITH THE AUTHOR

Damian Jakowski

e-mail: damian.jakowski@pg.edu.pl

Gdańsk University of Technology
11/12 Narutowicza St.
80-950 Gdańsk
Poland

Marek Dzida

e-mail: dzida@pg.edu.pl

Gdańsk University of Technology
11/12 Narutowicza St.
80-950 Gdańsk
Poland

MOST WIEDZY Downloaded from mostwiedzy.pl

POLISH MARITIME RESEARCH Special Issue 2018 S1 (97) 2018 Vol. 25; pp. 198-203
10.2478/pomr-2018-0042

SELECTED COMBINED POWER SYSTEMS CONSISTED OF SELF-IGNITION ENGINE AND STEAM TURBINE

Wojciech Olszewski
Marek Dzida
Gdańsk University of Technology, Poland

ABSTRACT

This paper presents optimization of selected combined diesel engine-steam turbine systems. Two systems: the system combined with waste heat one-pressure boiler only and its version containing additionally low-pressure boiler proper feeding degasifier and the system of two-pressure cycle, were taken into considerations. Their surplus values of power output and efficiency associated with utilization of waste heat contained in piston engine exhaust gas were compared to each other. For the considerations two high-power low-speed engines were taken into account. The main engines of comparable power of about 54 MW produced by Wartsila and MAN Diesel & Turbo firms, were selected.

Keywords: self-ignition engine , combined systems, steam turbine

INTRODUCTION

For many years in Polish economy the striving to improve efficiency of land and marine power plants has been observed. It results from economic conditions associated with varying level of fuel prices as well as ecological reasons (the lower fuel consumption the lower emission of harmful substances to the atmosphere). Therefore new solutions are searched for in order to increase efficiency of driving systems by means of combining self-ignition engines with other thermal engines such as steam and gas turbines.

Heat contained in exhaust gas from self-ignition engine may be utilized for production of superheated steam feeding steam turbine. Such solution makes it possible to increase efficiency of the combined system without any additional fuel dose.

The most suitable engine for such systems is a low-speed, piston combustion engine fed with heavy fuel oil. Efficiency of such engines is contained within the range of 40–50%. [10, 14].

At such high unit power outputs, in exhaust gases leaving the engine huge amounts of heat which may be utilized for production of steam used in steam turbine cycle, are contained. The heat is used for production of steam utilized in steam turbine cycle.

IDENTIFICATION OF THE INVESTIGATION OBJECT

In marine drives, combined diesel engine – steam turbine power systems are designed to increase thermodynamic cycle efficiency. In such system the steam turbine cycle is driven by water vapour produced in waste heat boiler fed with exhaust gas from diesel engine. The solution may be applied to ship propulsion as well as to a floating marine electric power station for production electric power in regions of a higher demand for electricity. Fig. 1 through 3 present concepts of combined diesel engine – steam turbine power systems.

MOST WIEDZY Downloaded from mostwiedzy.pl

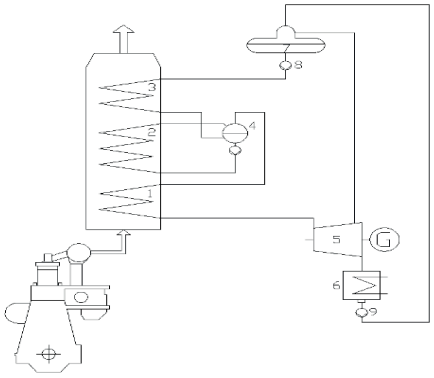

Fig. 1. Variant of a power system with one-pressure cycle
Designations: 1. Steam superheater, 2. Boiler proper, 3.Economizer, 4. Boiler drum, 5. Steam turbine, 6. Condenser, 7. Degasifier, 8. Main feed-water pump, 9. Condenser pump.

Fig. 1 presents the simplest solution of the combined system, i.e. a steam cycle with waste heat one-pressure boiler. It comprises the waste heat boiler, steam condensing turbine, condenser, feed-water heater, as well as degasifier fed from steam turbine extraction. The boiler produces steam of one pressure value, in the turbine only one regeneration tap point for water heating is provided in the mixture heater – degasifier. The waste heat boiler is composed of the three parts:

- feed-water heater (economizer);
- boiler proper;
- steam superheater.

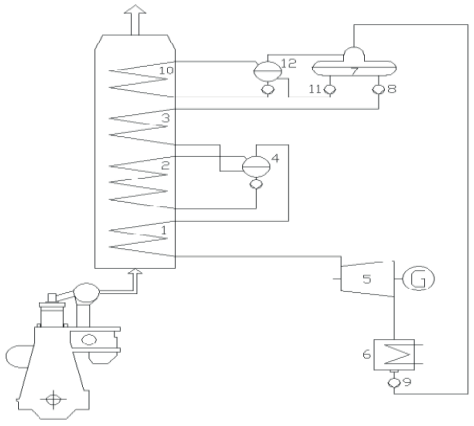

Fig. 2 Variant of a power system with one-pressure cycle containing additionally a low-pressure boiler proper to feed degasifier
Designations: 1. Steam superheater, 2. Boiler proper, 3.Economizer, 4. Boiler drum, 5. Steam turbine, 6. Condenser, 7. Degasifier, 8. Main high-pressure feed-water pump, 9. Condenser pump. 10. Low – pressure loop heater (of boiler proper), 11.Low-pressure pump, 12. Low-pressure boiler drum .

Fig. 2 presents a version of the cycle in which saturated vapour from the low-pressure boiler proper feeds degasifier of the steam system. As a result, amount of the power necessary to drive feed-water pump is low and constitutes only about 10% of power of the main feed-water pump.

Because it is two-phase flow, it is necessary to assure (during designing the piping) the flowing of water/ steam mixture into the boiler proper.

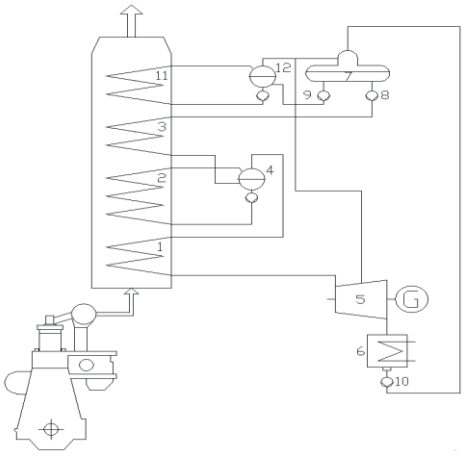

Fig. 3 A combine cycle composed of diesel engine and two-pressure waste heat boiler to feed steam turbine
Designations: 1. High-pressure superheater, 2. High-pressure boiler proper, 3. High-pressure economizer, 4. High-pressure boiler drum, 5. Steam turbine, 6. Condenser, 7. Degasifier, 8. High-pressure feed-water pump, 9. Low-pressure feed-water pump, 10. Condenser pump, 11. Low-pressure boiler proper, 12.Low-pressure boiler drum.

Fig. 3 presents the cycle fitted with two feed-water heaters. Such solution assures not only a better utilization of waste heat but also causes that use of low pressure improves thermodynamic properties of the cycle. Compared with one-pressure cycle, an additional steam flux from low-pressure cycle feeds steam turbine.

To improve cycle thermodynamic properties it is advised to apply fuels of a low sulphur content. Such solution makes it possible to reach a low level of saturation point . It allows to utilize exhaust gas for heating feed water at a low temperature in feed-water heater. Optimum temperature and pressure parameters in the boiler proper allow to decrease amount of produced steam.

Combined systems comprising steam cycle should best utilize heat contained in exhaust gas from diesel engine. Therefore its optimization means determination of such values of steam cycle parameters for which steam turbine reaches maximum power. It is necessary to limit area of searching for optimum parameters to that for which the constraints imposed on the system in question are satisfied. Calculations of the combined system based on diesel engine were conducted for both one-pressure and two-pressure systems. Steam turbine cycles in combined systems were calculated for the same assumptions and parameters as in the case of constraints.

THERMAL CALCULATIONS

The proposed concept of the combined power system for ships as well as floating marine electric power station requires to perform energy balance evaluation for the analyzed cycle. The power output of the combined cycle of electric power plant was determined by summing particular power values of the system's elements (i.e. diesel engine and steam turbine):

MOST WIEDZY Downloaded from mostwiedzy.pl

$$N_{combi} = N_D + N_{TP} = \\ = N_D(1+\frac{N_{TP}}{N_D}) \quad (1)$$

On this basis, efficiency of the combined system was determined:

$$\eta_{combi} = \frac{N_{combi}}{m_{fD} \cdot Wu} = \eta_D \cdot \left(1 + \frac{N_{TP}}{N_D}\right) \quad (2)$$

where:

$$\eta_D = \frac{N_D}{m_{fD} \cdot Wu} \quad (3)$$

as well as specific fuel consumption:

$$b_{e\,combi} = b_{e\,D} \cdot \frac{1}{(1+\frac{N_{TP}}{N_D})} [g/kWh]$$

Designations: m_{fD} – fuel mass flux; Wu – fuel calorific value.

According to the formula (2) the addition of a steam cycle to the diesel engine cycle makes it possible to increase power output of the combined cycle and consequently its efficiency.

In combined steam turbine systems of a low live steam power and temperature one-pressure systems are used [2, 5, 8], Fig. 1. The application of one-pressure system does not guarantees to reach optimum utilization of energy contained in exhaust gas in case when its temperature is high. In such steam turbine systems a solution with another low-pressure boiler proper is most often applied [2,5], Fig. 2. It leads not only to increased utilization of waste heat contained in exhaust gas but also to better thermodynamic usage of low-pressure steam.

Numerical calculations of combined diesel engine-steam turbine systems were conducted for the two following low-speed piston engines: Wartsila 9RTA96C diesel engine and MAN Diesel & Turbo 9K98MC-C7.1-TII diesel engine, (Tab. 1).

ASSUMPTIONS

During analyzing any cycle a very important stage is consideration of its limitations which result both from strength, technical and lifetime conditions of particular elements of the system as well as from design and economic constraints.

Value of difference between exhaust gas temperature and live steam temperature for shipboard waste heat boilers was assumed equal to ·t = 10 °C in accordance with the subject – matter literature [8,9]. Feed-water temperature in gasifier was assumed equal to todg = twz – 2 °C. The limit degree of steam dryness behind the steam turbine was assumed in the range of x_{limit}=0,86-0,88. For shipboard seawater – cooled condensers the MAN Diesel & Turbo firm [5] recommends to assume the pressure in condenser, p_k=0,065 bar. Temperature of water feeding the boiler is of importance for lifetime of feed-water heater in the boiler. The MAN firm [9] recommends to assure feed-water temperature not lower than 120 °C, at its sulphur content not greater than 2%. The limit temperature of exhaust gas from waste heat boiler tspal> 137 °C (because of sulphur content in fuel) [7]. In the calculations the fuel calorific value was assumed constant and equal to Wu = 42700 kJ/kg, and the mechanical efficiency ηm = 0,98.

The calculations of the combined system with diesel engines were conducted for one-pressure and two-pressure solutions in compliance with the assumed parameters of the engines in question.

Tab 1. Principal parameters of the selected diesel engines [11,14]

Parameter	Unit	9RTA96C WARTSILA	9K98MC-C7.1-TII MAN DIESEL & TURBO
ND	kW	46332	48762
m_{sD}	kg/s	104,504	134,25
m_{fD}	kg/s	2,146	2,369
t_{wyl}	oC	271	232,8
b_{eD}	g/kWh	166,8	174,9

COMPARISON OF THE COMBINED SYSTEMS COMPRISING DIESEL ENGINE AND ONE OF THE SELECTED VARIANTS OF STEAM CYCLES

For calculations of the combined diesel engine – steam turbine systems the two ship low-speed engines: Warstsila diesel engine [14] and MAN Diesel & Turbo 9K98MC diesel engine [10] of similar power output were selected. The considerations were conducted for the combined system with steam turbine cycle comprising either one-pressure boiler acc. Fig. 1 or two-pressure boiler acc. Fig. 3. The calculations were done in accordance with producer's data for the reference point acc. ISO Conditions: Ambient air temperature of 25 °C and Barometric pressure of 1 bar, Tab.1.

Results of the calculations for the presented combined diesel engine – steam turbine systems can be found in the publication [7] where algorithm of the calculations was also described in detail.

Results of the performed numerical calculations are presented in a graphical form showing the statement of: steam turbine power output in function of live steam pressure, efficiency of the combined cycles in function of live steam pressure as well as temperature of exhaust gas from waste heat boiler in function of live steam pressure as well as temperature in degasifier.

The combined systems are marked as follows:
Ob_I – comprising one-pressure waste heat boiler;
Ob_II – comprising one-pressure waste heat boiler and additional low-pressure boiler proper feeding degasifier;

MOST WIEDZY Downloaded from mostwiedzy.pl

Ob_III_1- with two-pressure cycle (pI = 1,05*p_{odg});
Ob_III_2 – with two-pressure cycle (pI = 1,5*p_{odg}).

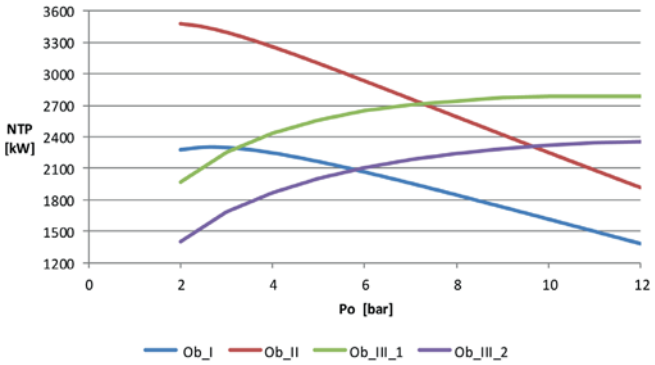

Fig. 4 Steam turbine power output in function of live steam pressure as well as the feed-water temperature in degasifier todg=150 °C, for 9K98MC engine

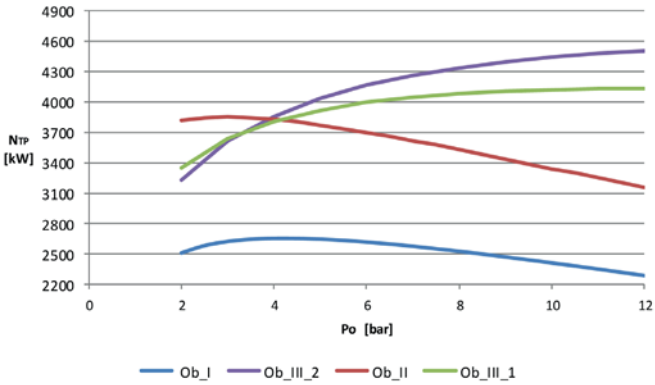

Fig. 5 Steam turbine power output in function of live steam pressure as well as the feed-water temperature in degasifier, todg=150 °C, for 9RTA96C engine

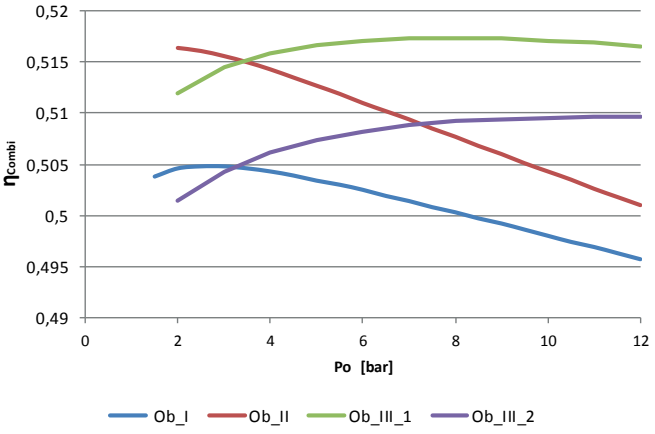

Fig. 6 Efficiency of the combined systems in function of live steam temperature as well as feed-water temperature in degasifier, todg=150 °C, for 9K98MC engine

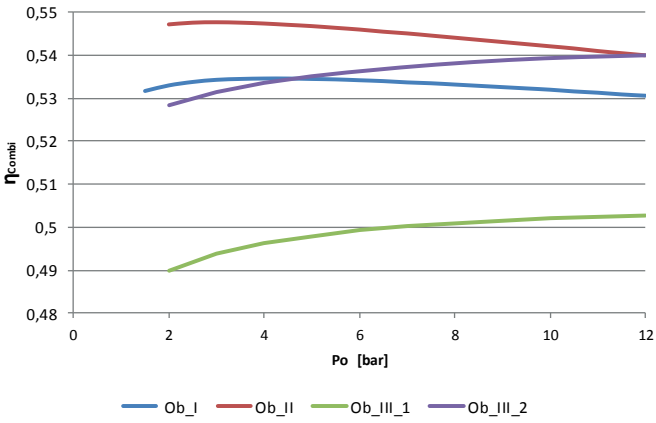

Fig. 7 Efficiency of the combined systems in function of live steam temperature as well as feed-water temperature in degasifier, todg=150 °C, for 9RTA96C engine

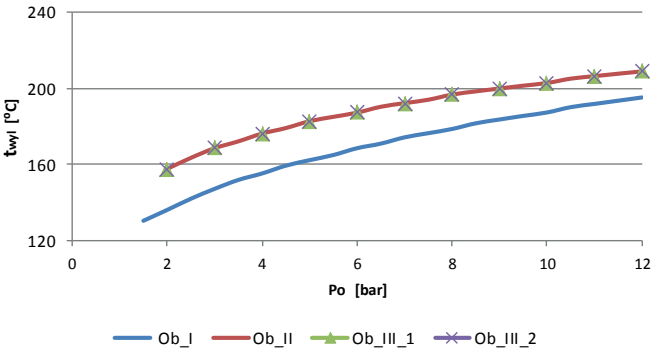

Fig. 8 Temperature of exhaust gas from waste heat boiler in function of live steam pressure as well as the feed-water temperature in degasifier, todg=150 °C, for 9K98MC engine

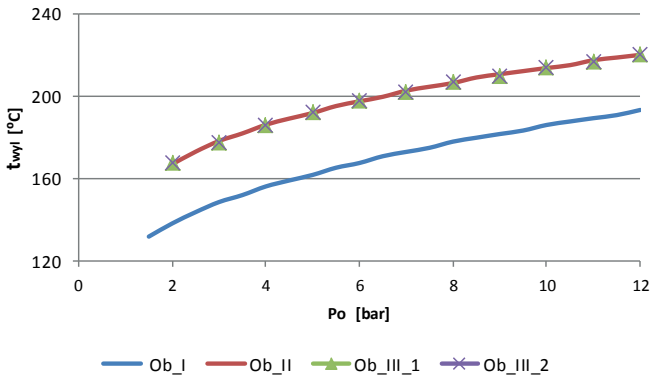

Fig. 9 Temperature of exhaust gas from waste heat boiler in function of live steam pressure as well as the feed-water temperature in degasifier, todg=150 °C, for 9RTA96C engine

Tab. 2 shows calculation results for the analyzed combined cycles compared with those for two low-speed piston engines: 9RTA96C and 9K98MC-C7.1-TII alone.

MOST WIEDZY Downloaded from mostwiedzy.pl

Tab. 2 Parameters of the combined diesel engine – steam turbine systems

Parameter	Unit	9RTA96C				9K98MC-C7.1-TII			
ND	kW	46332				48762			
η_D	%	50,56				48,2			
t_4	°C	271				232,8			
t_{wz}	°C	151,8				152			
t0	°C	261				222,8			
		Ob_I	**Ob_II**	**Ob_III_1**	**Ob_III_2**	**Ob_I**	**Ob_II**	**Ob_III_1**	**Ob_III_2**
NTP	kW	2656	3855	4588	3157	2301	3479	2786	2349
Po	bar	4	3	12	12	2,5	2	11	12
x2		0,9223	0,9005	0,8149	0,8157	0,9258	0,9052	0,8033	0,7948
t_{wyl}	°C	156,3	178,4	220,6	220,3	142	160,9	206,6	209
NTP / ND	%	5,73	8,32	9,9	6,81	4,73	7,18	5,71	4,82
η_{Combi}	%	53,46	54,77	50,26	54,01	50,48	51,64	50,96	50,53

The performed calculations was aimed at determination of optimum parameters of the analyzed combined cycles comprising diesel engine and steam turbine in case of application of two types of diesel engines.

From the analysis of steam cycle calculations of the considered combined systems of ship power plant results that maximum power developed by the steam turbine reaches, depending on a diesel engine, percentage value of 9,9 % and 7,18 % in relation to power of piston engine alone. The higher value of combined system efficiency is achieved in case of the system with 9RTA96C engine compared with that comprising 9K98MC-C7.1-TII engine.

The performed numerical calculations of the analyzed combined diesel engine – steam turbine cycle allow to formulate the following conclusions:

- Without any additional fuel dose it is possible to increase the power output from the combined system comprising 9RTA96C diesel engine by 9,9% and 7,18 % for that with 9K98MC-C7.1-TII diesel engine in relation to the conventional power plant;
- Owing to application of a combined power plant it is possible to increase energy efficiency of power plant for optimum parameters of 9RTA96C diesel engine – up to 54,77 %, and up to 51,64 % for optimum parameters of 9K98MC-C7.1-TII diesel engine.

FINAL CONCLUSIONS

It is possible to apply a combined system composed of diesel engine and steam turbine cycle which utilizes waste heat contained in exhaust gas. Such systems reach higher thermodynamic efficiency due to utilization of waste heat contained in exhaust gas without any need of supplying additional fuel dose.

The performed numerical calculations of the analyzed combined diesel engine – steam turbine system made it possible to state:

- an increase in energy efficiency of power plant at optimum parameters due to application of a combined power plant;
- an increase in power output of combined power plant in relation to conventional one without application of any additional fuel dose;
- possible application of diesel engine of a lower output in view of possibility to increase it by applying a combined system with steam turbine.

In this work only thermodynamic analysis of ship power plants was performed without necessary additional technical – economical analysis which could fully justify application of such system to ship power plants.

BIBLIOGRAPHY

1. ABB ALSTOM POWER Ltd. Gas Turbine and Combined-Cycle Power Plants, Switzerland, CH-50 5401, Baden

2. Dzida M: Possible Efficiency Increasing of Ship Propulsion and Marine Power Plant with the System Combined of Marine Diesel Engine, Gas Turbine and Steam Turbine. A chapter in the book on Advances in Gas Turbine Technology edited by Dr Ernesto Benini. (ISBN 978-953-307-611-9.) INTECH, 2011

3. Altosole, M.; Benvenuto, G.; Campora, U.; Laviola, M.; Trucco, A.: Waste Heat Recovery from Marine Gas Turbines and Diesel Engines. Energies 2017, 10, 718

4. Chmielniak T.: Thermodynamic cycles of thermal turbines (in Polish). PAN, Gdańsk 1988

MOST WIEDZY Downloaded from mostwiedzy.pl

5. Dzida M.: On the possible increasing of efficiency of ship power plant with the system combined of marine diesel engine, gas turbine and steam turbine at the main engine – steam turbine mode of cooperation. Polish Maritime Research, Vol. 16, No.1(59), (2009), pp. 47-52, ISSN 1233-2585

6. Dzida, M., Dzida, S., Girtler, J.: On the possible increasing of efficiency of ship power plant with the system combined of marine Diesel engine, gas turbine and steam turbine in case of main engine cooperation with the gas turbine fed in series and the steam turbine, Polish Maritime Research, No. 3 (61), Vol. 16, pp. 26-31, 2009

7. Dzida, M., Olszewski, W.: Comparing combined gas turbine/steam turbine and marine low speed piston engine/steam turbine systems in naval applications, Polish Maritime Research, Vol. 18, No. 4(71), pp. 43-48, 2011

8. Kehlhofer R.:Combined-Cycle Gas & Steam Turbine Power Plants, The Fairmont Press, INC., ISBN 0-88173-076-9, USA, 1991

9. MAN B&M:The MC Engine. Exhaust Gas Date. Waste Heat Recovery System. Total Economy, MAN B&W Publication S.A., Denmark, 1985

10. MAN Diesel & Turbo & Turbo: Stationary Engine. Programme, 4th edition. Branch of MAN Diesel & Turbo & Turbo SE, Germany, Available from www.mandieselturbo.com, 2010

11. Olszewski, W.: Possible use of combined diesel engine/steam turbine in ship power plant, Zeszyty Naukowe, Szczecin Maritime University, Vol. 28(100), No. 1, pp. 88-94, 2011

12. Olszewski W., Dzida M.: Issues of economic analysis of electric energy generation in a floating power plant. Journal of Polish CIMAC, Vol. 9, No. 1 (2014), pp.103-110

13. Perycz S.: Steam and gas turbines (in Polish). Publishing House of Gdańsk University of Technology, Gdańsk 1988

14. Sulzer RTA 96C: Engine Selection and Project Manual, Wartsila, June 2001

15. Wajand J.A.: Self-ignition engines (Diesel engines) (in Polish). WN-T, Warszawa 1980.

CONTACT WITH THE AUTHORS

Wojciech Olszewski
Marek Dzida

Faculty of Ocean Engineering and Ship Technology
Gdańsk University of Technology
11/12 Narutowicza St.
80-950 Gdańsk
Poland

MOST WIEDZY Downloaded from mostwiedzy.pl

POLISH MARITIME RESEARCH Special Issue 2018 S1 (97) 2018 Vol. 25; pp. 204-210
10.2478/pomr-2018-0043

COMPARISON ANALYSIS OF SELECTED NUCLEAR POWER PLANTS SUPPLIED WITH HELIUM FROM HIGH-TEMPERATURE GAS-COOLED REACTOR

Natalia Szewczuk-Krypa[1]
Marta Drosińska-Komor[1]
Jerzy Głuch[1]
Łukasz Breńkacz[2]
[1] Gdansk University of Technology, Poland
[2] Institute of Fluid Flow Machinery, Polish Academy of Sciences, Poland

ABSTRACT

The article presents results of efficiency calculations for two 560 MW nuclear cycles with high-temperature gas-cooled reactor (HTGR). An assumption was made that systems of this type can be used in so-called marine nuclear power plants. The first analysed system is the nuclear steam power plant. For the steam cycle, the efficiency calculations were performed with the code DIAGAR, which is dedicated for analysing this type of systems. The other system is the power plant with gas turbine, in which the combustion chamber has been replaced with the HTGR. For this system, a number of calculations were also performed to assess its efficiency. Moreover, the article names factors in favour of floating nuclear power plants with HTGRs, which, due to passive safety systems, are exposed to much smaller risk of breakdown than other types of reactors which were in common use in the past. Along with safety aspects, it is also economic and social aspect which make the use of this type of systems advisable.

Keywords: HTGR, nuclear power plants, floating marine plants, nuclear power

MOST WIEDZY Downloaded from mostwiedzy.pl

INTRODUCTION

In March, 2011, an earthquake with magnitude of 9 M_w occurred in the north eastern part of Japan. Then the tsunami, formed as a result of most intensive tectonic movements in this area in recent 140 years, destroyed the east coast of Japan, killing nearly 20 000 people and demolishing nearly 350 000 homesteads. Among other objects, it was the Fukushima Daiichi nuclear power plant which was badly hit by the tsunami. Its damage resulted in loss of control over one of power plant blocks in operation, which further led to the leakage of radioactive substances to the environment [12, 6]. The nuclear disaster caused by forces of nature in the Fukushima Daiichi power plant has launched a public discussion over the risk of use of nuclear energy. Despite safety concerns, the energy extracted from the atom, due to its advantages, is commonly believed to be difficult to replace by other well-known fossil energy resources. These advantages undoubtedly include infinitesimal emission of carbon dioxide during the entire lifetime of nuclear power plant. Moreover, the nuclear fuel is relatively cheap, compared to other available energy resources [8]. That is why, instead of resigning from the use of nuclear energy, it is advisable to improve the operational safety of installations supplied with nuclear fuels. A solution which will reduce the risk of damage of a nuclear power plant due to, for instance, earthquake, tsunami, or another natural disaster, consists in moving such a system from land far into the ocean [9].

Although initial concepts to make use of nuclear energy concerned its marine applications, it is inland production units which are dominating in its use now. Until the beginning of the 21st century, marine nuclear energy was mainly used for military purposes [2]. Only a small number of civilian ships with nuclear drive were built, including NS Savannah, Otto Hahn, Mutsu, and Russian icebreakers, the Yamal for instance [5]. Although nuclear systems are not very popular as off-shore solutions, attempts are made to build marine nuclear

power plants. Here, the Americans and Russians are believed to be precursors of this type of solutions. The first floating power plant supplied with nuclear fuel was built in the USA. The electric power of this plant was 10 MW(e). It was used in the US military base situated in the Panama Canal [4]. The Russians, on the other hand, are the authors of the first nuclear power plant built for civilian purposes. Since nearly 50% of Russian territory is situated in the far north, this country faces the problem of electric power delivery to places where natural conditions are extremely severe, which makes building inland infrastructure and production units extremely difficult [13]. Hence, attempts are made to develop alternative energy sources. In this context, marine nuclear power plants can operate well in difficult circumpolar conditions, as these systems do not require elaborate infrastructure. Moreover, they can be operated for long time without reactor re-fuelling, which seems to be very favourable in far north conditions, in both economic and logistic terms [14, 10]. The next country which follows the USA and Russia is China. Due to smog problems, the government of China has made a decision to create as many sources of alternative energy as possible. This list includes nuclear power plants situated far from inhabited territories, which well corresponds with the idea of floating production units. Hence, there are plans to build in the nearest future a fleet of more than 20 units of this type. These systems are expected to ensure stable delivery of energy for projects carried out on the South China Sea (for instance, power supply for drilling platforms).

There are also other favourable aspects concerning the use of marine systems for electric energy production which are worth analysing. In the time of overpopulation and large worldwide need for food production, all areas which can be developed are of great value. This leads to the dilemma whether it is worthwhile to use next valuable territories for building power objects on them. This problem becomes particularly important on islands, where the growth of population enforces the use of each free patch of land for development of residential and agricultural areas. When analysing nuclear solutions, the landscape aspect is also of some importance. Power islands can be successfully used in tourist regions, in which the elaborate structure used for energy production would distort the landscape and discourage potential visitors.

A popular type of reactor which could be successfully used in nuclear power plants situated on sea is the high-temperature gas-cooled reactor (HTGR). First reactors of this type were built in the 1970s but were not introduced to common use for economic reasons. At present, they attract strong interest and many research activities are in progress to improve the efficiency and safety of the newly designed high-temperature reactors. The HTGRs make use of gravel deposit. The reactor itself has the shape of a cylinder filled with triple coated isotropic fuel (TRISO). This fuel has the form of small graphite balls filled with fissile material of 0,5 mm in diameter, which usually is low-enriched uranium oxide [1,7]. The greatest advantage of HTGRs is their high safety of operation.

After the failure, the fuel can only be emptied from the reactor with the aid of passive systems making use of natural force of gravity. What is noteworthy, this action can be undertaken even when there is no power supply to the nuclear power block. Moreover, if helium is used as cooling agent in the system, its leakage will not lead to environment contamination, since helium as noble gas is chemically inert and is not radioactively activated, while all radioactive products of nuclear reaction remain tightly locked in fuel balls. HTGRs are characteristic for very high level of fuel burnup [7], which is great economic advantage. Moreover, the amount of generated radioactive waste is small. This aspect is of high importance for off-shore power plants. High fuel burnout allows the fuel to be used longer, and consequently, fuel deliveries to keep the plant operate can be less frequent. Smaller amounts of radioactive waste are desirable due to space limits.

AIM OF WORK

The article presents two nuclear power plants which can be used for energy production on so-called power islands and compares their efficiency. Both systems cooperate with the HTGR. A substantial part of the article is presentation of numerical calculations. For one of these systems, the calculations were made with the code DIAGAR, which is a helpful tool in calculations concerning systems with steam turbine.

DESCRIBING OBJECT OF EXAMINATION

The first analysed system is the steam turbine cycle supplied with the energy obtained in the high-temperature helium-cooled reactor (Fig.1).

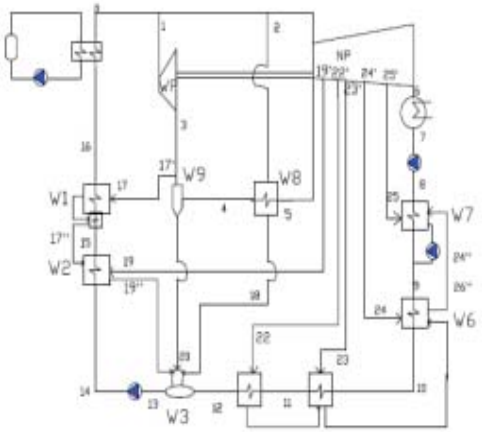

Fig.1. Scheme of steam cycle supplied from HTGR

The cycle has been designed for power of 560 MW. The assumed temperature of live steam is 600°C. This value results from the amount of heat which can pass from the cooling medium to water in the steam cycle. The initial pressure of live

MOST WIEDZY Downloaded from mostwiedzy.pl

steam is 285 bars. In the analysed cycle, seven regenerative heat exchangers are used, the task of which is to increase the temperature of working medium at steam generator inlet. This procedure significantly improves the system efficiency. The regenerative heat exchangers are supplied with the steam taken from regenerative extraction points in the turbine bodies. One of these exchangers which are used in the system is deaerator. Moreover, an interstage steam superheater and a moisture separator are also used. These two solutions increase the dryness degree in last stages of the low-pressure (LP) turbine, which results in the improvement of operating safety and better efficiency of the turbine being part of the cycle.

The other analysed object is the gas turbine cycle with recuperation (Fig.2.). In this case the combustion chamber has been replaced with the HTGR. The applied recuperation makes it possible to use the waste heat of the medium at gas turbine exit for heating the medium at reactor inlet. This procedure improves the efficiency of the system. The cooling medium is helium (He), due to its favourable physical characteristics. Helium reveals 5-6 times as high thermal conductivity as other gases: air, nitrogen, or carbon dioxide. Consequently, the smallest dimensions of heat exchangers and the reactor itself can be obtained, compared to other cooling media commonly used in reactors.

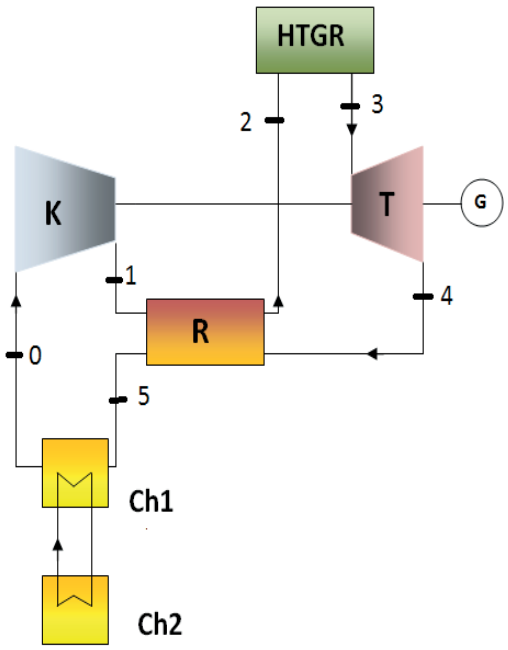

Fig.2. Scheme of gas cycle with HTGR and recuperation. K – compressor, R – recuperator, HTGR – high-temperature gas-cooled reactor, T – gas turbine, G – generator, Ch1, Ch2 – coolers.

METHODOLOGY OF CALCULATIONS

For calculating purposes, a scheme of the analysed steam cycle supplied from HTGR is created in the software Projdiag, dedicated for creating numerical schemes of thermal cycles. In this case the structure of the analysed cycle (Fig.3.) consists of individual elements and connections between them. Each element corresponds to one apparatus composing the steam cycle. In the next step, the scheme is introduced to the code DIAGAR used for steam cycle calculations. For this purpose, the code makes use of graph theory to relate thermodynamic and flow parameters of the cycle with characteristics of apparatuses and their geometry.

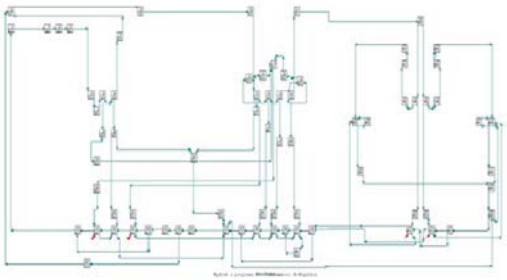

Fig.3. Numerical scheme of cycle created in numerical software Projdiag

The input data for DIAGAR are numerical schemes and geometric data of apparatuses, as well as independent parameters (Fig.4.), understood as autonomous quantities which are not affected by changes of other system parameters. In the analysed case, the list of independent parameters includes: power, live steam pressure, superheated steam temperature, flow rate, inlet temperature, and exit pressure. This way of assignment of the above parameters makes it possible to use the Stodola-Flugel equation in the code. The list of dependent parameters in the code includes: pressure, temperature, mass, specific enthalpy, specific entropy, and volume – numerically calculated based on independent variables [3]. The results of DIAGAR calculations can be used as simulators for physical processes and for obtaining diagnostic thermal-flow relations. In that case, the result of code operation is elementary heat consumption, cycle efficiency, and efficiency of electric energy generation.

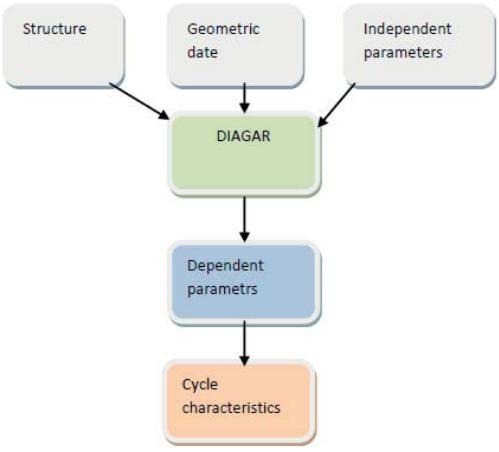

Fig.4. DIAGAR operation scheme

MOST WIEDZY Downloaded from mostwiedzy.pl

A series of simulations were performed for the steam cycle cooperating with high-temperature helium-cooled reactor. These simulations based on numerical results obtained from DIAGAR and their task was to optimise the condenser pressure in such a way as to reach the value corresponding to maximum cycle efficiency. The condenser pressure was changed from 0.03 to 0.,1 bar, with step equal to 0,01 bar. As already mentioned, the assumed power of the cycle was 560 MW. The mass flow rate corresponding to this power was assumed to be equal to 370 kg/s. As a result of the simulation, the values of net and gross efficiency were obtained. The gross efficiency value was related to elementary heat consumption (1), while the net efficiency, taking into account own demands of the steam turbine power plant, was approximately smaller by 9% than the gross efficiency (2).

$$\eta_{brutto} = \frac{3600}{\text{Unit Heat Consumption}} * 100 \quad (1)$$

$$\eta_{netto} = 91\% * \eta_{brutto} \quad (2)$$

The parameters of the gas cycle with HTGR (Tab.1.) were determined taking mainly into account the requirements of the reactor. The helium pressure at reactor inlet was assumed at the level of 70 bar. This pressure p_2 is required for correct operation of HTGR and takes into account limitations concerning the cooling medium volume. When this volume is excessively large, it results in oversizing the heat exchangers and the reactor itself, with further negative effect on the economic efficiency of the system. To ensure correct medium pressure at reactor inlet, an assumption was made, taking into account the lower temperature t_1 and pressure p_1 of the medium in the cycle, that the compression π_K of the compressor is at the level of 2,27 [-]. In the preliminary calculations it was assumed that HTGR heats helium to the upper temperature t_3 = 1223 K, while in further calculations the cycle efficiency was optimised with respect to this temperature. For optimisation purposes, the temperature t_3 was allowed to vary from about 1073 K to 1273 K [15]. It was also assumed that medium expansion in the turbine reaches a slightly higher pressure than that recorded at compressor inlet. This assumption took into account the fact that helium, after leaving the gas turbine, flows through a recuperator and a cooler, which contributes to small medium pressure losses. To meet the above assumptions, the turbine compression π_K was assumed to be equal to 2,5 [-]. For helium as cooling medium, the specific heat cp was assumed to keep a constant value equal to 5,19 kJ/kgK, regardless of medium temperature, while the adiabatic exponent was assumed equal to 1,66 [-].

The numerical calculations were performed based on the assumed values of compression and cooling medium temperature behind the HTGR. The calculations made use of the adiabatic equations to determine isentropic parameters for the compressor and turbine in the system. Real work of these devices was calculated based on theoretical efficiency values. The compressor efficiency η_K was assumed at the level of 85%, while the gas turbine efficiency η_T at the level of 90%. The working medium temperatures behind and in front of the recuperator were calculated based on the theoretical value of recuperator efficiency η_R equal to 85%. For the assumed values, thermodynamic parameters were calculated at characteristic points, along with the efficiency of the entire cycle. The cycle efficiency was optimised with respect to different values of cooling medium temperature T_2 behind the reactor. For calculation purposes, the characteristics of helium (He) as cooling medium were assumed not to depend on temperatures and pressures recorded in individual system elements. Both the specific heat cp, and the adiabatic exponent were assumed constant. This assumption was made based on the analysis of changes of medium parameters in relation to changing conditions of the environment in which the medium worked.

Tab.1. Thermodynamic parameters calculated at characteristic points of the cycle for assumed values of compression and cooling medium temperature behind HTGR

Parameters of gas cycle with HTGR			
Gas turbine power	Ne	560	MW
Medium pressure at compressor inlet	p0	2,8	MPa
Medium temperature at compressor inlet	T0	299,15	K
Medium enthalpy at compressor inlet	i0	1552,59	kJ/kg
Medium pressure at compressor exit	p1	70	bar
Medium temperature at compressor exit	T1	453,83	K
Medium enthalpy at compressor exit	i1	2355,4	kJ/kg
Medium pressure at HTGR inlet	p2	70	bar
Medium temperature at HTGR inlet	T2	837,94	K
Medium enthalpy at HTGR inlet	i2	4348,9	kJ/kg
Medium pressure behind HTGR	p3	68	bar
Medium temperature behind HTGR	T3	1223	K
Medium enthalpy behind HTGR	i3	6348,15	kJ/kg
Medium temperature at gas turbine exit	T4	917	K
Medium pressure at gas turbine exit	p4	30	Bar
Medium enthalpy at gas turbine exit	i4	4759	kJ/kg

The performed calculations aimed at assessing the efficiency of the gas cycle with high-temperature helium-cooled HTGR reactor. The efficiency was optimised with respect to cooling medium temperature behind HTGR.

The cycle efficiency was calculated from equation 3:

$$\eta = \frac{N_{eTG}}{Q_{dHTGR}} = \frac{N_{TG} - N_K}{Q_{dHTGR}} \quad (3)$$

where:
η – efficiency of gas cycle with HTGR
N_{eTG} – power output of the system
Q_{dHTGR} – heat taken by cooling medium from HTGR
N_{TG} – gas turbine power
N_K – compressor power

MOST WIEDZY Downloaded from mostwiedzy.pl

RESULTS

The results of numerical calculations performed for the steam cycle made a basis for determining the relation between the condenser pressure pk and gross efficiency of the cycle. (Fig.5.)

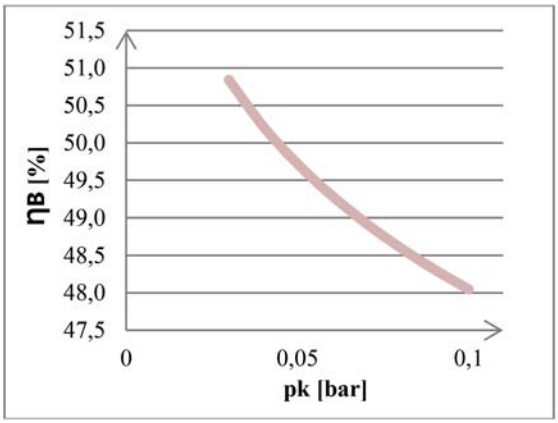

Fig.5. Gross efficiency η_B vs. condenser pressure pk

Based on formula (2) and gross efficiency values, the net efficiency of the steam cycle supplied from HTGR was determined. The calculated net values were used for creating the relation shown in (Fig.6.)

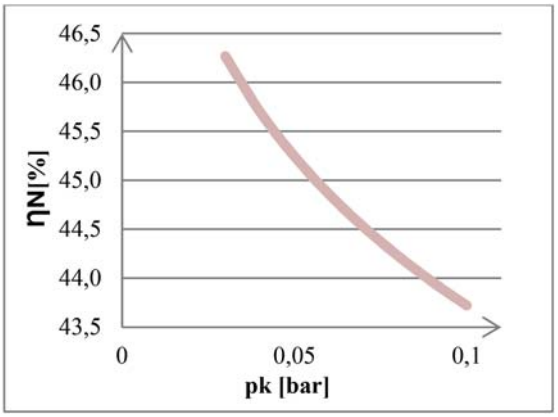

Fig.6. Net efficiency η_B vs. condenser pressure pk

These characteristics reveal that the increase of condenser pressure leads to the decrease of system efficiency. The optimal condenser pressure value equals 0,03 bar. The difference between the highest and lowest pressure values, which is equal to 0,7, causes the decrease of net efficiency by 2,545 %, and gross efficiency by 2,797%. These efficiency losses increase the operating costs due to higher fuel consumption. In the case of nuclear power plants, of high importance is the cost of spent nuclear fuel storage. That is why greater amount of consumed nuclear fuel is unprofitable in economic terms.

Based on numerical calculations, the relation between the efficiency of the analysed gas cycle and the cooling medium temperature behind HTGR was determined. This temperature was assumed within the range of temperatures available in the HTGR type reactor. The highest efficiency was obtained for the working medium temperature equal to 1000 [°C]. The created characteristic (Fig.7.) is consistent with expectations based on the knowledge about gas turbine cycles. These expectations say that the increase of medium temperature behind the combustion chamber, or another source of heat, should lead to the increase of system efficiency.

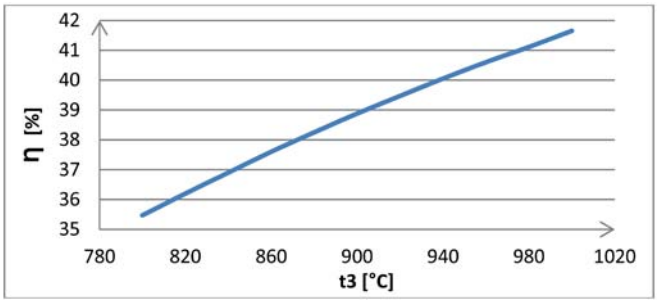

Fig.7. Efficiency of gas cycle with HTGR vs. working medium temperature at reactor exit

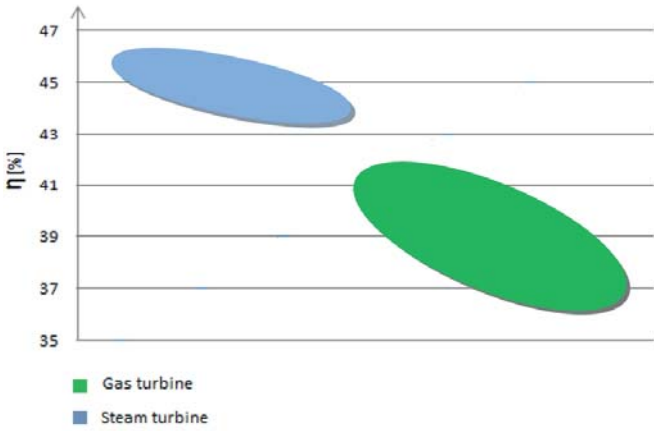

Fig.8. Efficiency ranges of compared systems

CONCLUSIONS

When analysing the results of numerical calculations for two selected variants of nuclear systems with high-temperature gas-cooled reactor (HTGR), the following conclusions can be drawn:

- Comparing the nuclear steam cycle and the nuclear gas cycle, both of the same power of 560MW (Fig.8.), we can easily notice that the system with steam turbine has much higher efficiency than the gas system. The net efficiency of the steam power plant varies from 43,7% to 46,3%, while for the gas power plant it is within 35,5% to 41,7%.
- The increase of condenser pressure provokes the efficiency decrease of the nuclear steam cycle. The highest efficiency of the analysed cycle was obtained for the condenser pressure equal to 0,03 bar. In this case the gross efficiency was equal to 50,84 %. Increasing the condenser pressure to 0,1 bar resulted in the efficiency loss approximately amounting to 2,8%, which in the case of high-power

MOST WIEDZY Downloaded from mostwiedzy.pl

steam systems is equivalent to significant worsening of economic indices of system operation, due to much higher expenditures on fuel for the reactor.

- The observed high efficiency values of steam cycle could be mainly obtained due to the use of interstage superheater and regenerative heat exchangers. These two measures significantly improve the efficiency of steam systems.
- In the case of the gas system with HTGR, the system efficiency increase was obtained by increasing the working medium temperature at reactor exit. For optimisation purpose, this temperature was allowed to vary from 1073K to 1273K, depending on possibilities of HTGR. Within this temperature range, the cycle efficiency took values from about 35,5 % to about 41,7%.
- The efficiency of the gas system is highly affected by the use of the recuperator, thanks to which the heat of the exhaust gas can be additionally used for heating the working medium at reactor inlet. Consequently, less fuel is needed to obtain the required medium parameters at turbine inlet, which is reflected in measurable increase of system efficiency.
- In fact, decision making about selection of technology to be used in given conditions is a complex process, which is affected by numerous aspects concerning economy, safety (of utmost importance), as well as political and social issues. Indeed, the efficiency of the analysed systems is also the aspect which is taken seriously into account when making such a complex decision.

Due to their advantages, high-temperature gas-cooled reactors can be successfully used in marine nuclear power plants, either as steam or gas variants. Marine production units can become an ideal solution for areas with severe natural conditions, which make developing transporting infrastructure very difficult. Such areas may include, for instance, islands, or densely populated areas with poor water resources (insufficient for cooling purposes). Offshore nuclear systems can also be advantageous in safety terms. Unlike inland power plants, marine production units will be much less exposed to damage or destruction caused by such natural disasters as earthquake, tsunami or flood.

BIBLIOGRAPHY

1. Baek J-K., Mistarihi Q., Yeo S., et al.: *A Preliminary Study for Diffusion Experiments of Metallic Fission Products in Graphite for HTGR*. Transaction of the Korean Nuclear Society Autumn Meeting Gyeongiu, Korea, October 29-30, 2015

2. Carlton J S., Smarta R., Jenkins V.: *The nuclear propulsion of merchant ships: Aspects of engineering, science and technology*. Journal of Marine Engineering & Technology 2011, pp. 47-59

3. *Gardzilewicz A., Głuch J., Bogulicz M. (1994): DIAGAR manual for turbine set No. 3 at Kozienice Power Plant (in Polish). Maszyny Przepływowe, Sp. z o.o., Report no. 19/9*

4. Gorlinski Yu.E., Kut'kov V.A, Lystsov V.N., et al.: *Securing the radiological safety of people and the environment at all stages of the life cycle of floating nuclear heat-and-power plants*. Atomic Energy Vol. 107, No. 2, 2009, pp. 122-129

5. Hirdaris, S.E.; Cheng, Y.F.; Shallcross, P.; Bonafoux, et al.: *Considerations on the potential use of Nuclear Small Modular Reactor (SMR) technology for merchant marine propulsion*. Ocean Engineering Vol. 79, 2014, pp. 101–130.

6. Hirose, K.: *2011 Fukushima Dai-ichi nuclear power plant accident: Summary of regional radioactive deposition monitoring results*. Journal of Environmental Radioactivity, 2012, pp. 13–17.

7. Kowalczyk T., Głuch J., Ziółkowski P.: *Analysis of possible application of high-temperature nuclear reactors to contemporary large-output steam power plants on ships*. Polish Maritime Research, 2016 Vol. 23, No. 2 (90), pp. 32-41

8. Lee K., Lee K-H., Lee J., et al.*: A new design concept for offshore nuclear power plants with enhanced safety features*. Nuclear Engineering and Design 254 2013, pp. 129-141

9. Lee K-H., Kim M-G., Lee J-I., Lee

10. P-S.: *Recent Advances in Ocean Nuclear Power Plant*, Energies, 2015, Vol 8 pp. 11470-11492

11. Lepekhin A., Andreeva-Andrievskaya L., Kuznetsov V.: *Status of Russian small and medium sized reactor activities. In Proceedings of the Meeting of the International Framework for Nuclear Energy Cooperation, Rome*, Italy, 6 December 2010

12. McDonald C.F.: *A nuclear gas turbine perspective: The indirect cycle (IDC) offers a practical solution,* Proceedings of the 31. intersociety energy conversion engineering conference. Volume 2: Conversion technologies, electro-chemical technologies, Stirling engines, thermal management

13. Nagatani K., Kiribayashi S., Okada Y. et al.: *Emergency response to the nuclear accident at the Fukushima Daiichi Nuclear Power Plants using mobile rescue robots*. Journal of FIELD ROBOTICS Vol. 30, Issue 1 2013, pp. 44-63

14. Sarkisov A. A., Vysotskii V. L., Bilashenko V.P., at al.: *Expected radiological and radioecological consequences of operating floating nuclear heat and power plants*. Atomic Energy Vol. 104, No. 3, 2008, pp. 237-248

15. Standring W.J.F, Dowdall M., Amundsen I., Strad P.: *Floating nuclear power plants: Potential implications for radioactive pollution of the northern marine environment*. Marine Pollution Bulletin, 58, 2009, pp.174-178

MOST WIEDZY Downloaded from mostwiedzy.pl

16. Takamatsu K., Hu R.: *New reactor cavity cooling system having passive safety features using novel shape for HTGRs and VHTRs*. Annals of Nuclear Energy, 77, 2015, pp. 165-171

CONTACT WITH THE AUTHORS

Marta Drosińska-Komor
e-mail: mardrosi@pg.edu.pl

Natalia Szewczuk-Krypa
e-mail: natszew1@pg.edu.pl

Jerzy Głuch
e-mail: jgluch@pg.edu.pl

Faculty of Ocean Engineering and Ship Technology
Gdańsk University of Technology
11/12 Narutowicza St.
80-233 Gdansk
Poland

Łukasz Breńkacz
e-mail : lbrenkacz@imp.gda.pl

Energy Conversion Department
Institute of Fluid Flow Machinery
Polish Academy of Sciences
14 Fiszera St.
80-231 Gdansk
Poland

MOST WIEDZY Downloaded from mostwiedzy.pl

POLISH MARITIME RESEARCH Special Issue 2018 S1 (97) 2018 Vol. 25; pp. 211-217
10.2478/pomr-2018-0044

ENERGY ANALYSIS OF PROPULSION SHAFT FATIGUE PROCESS IN ROTATING MECHANICAL SYSTEM
PART I
TESTING SIGNIFICANCE OF INFLUENCE OF SHAFT MATERIAL FATIGUE EXCITATION PARAMETERS

Zbigniew Korczewski
Konrad Marszałkowski
Gdańsk University of Technology, Poland

ABSTRACT

The article discusses the problem of mathematical modelling of energy conversion processes in a rotating mechanical system for the purpose of identifying fatigue states of propulsion shafts in this system. A simplified physical model of the analysed system, constructed in an appropriate scale, has made the basis for the experimental research. The research programme took into consideration mechanical fatigue excitation of the model propulsion shaft to find the correlation between the dynamic system load generated by a bending moment and the energy state of a specified shaft segment. A physical model of the analysed process was proposed, for which the plan of static randomised block experiment was worked out. The recorded experimental results were used for statistical analysis of the significance of influence of the quantities exciting the propeller shaft fatigue process and the adequacy of the developed mathematical model describing shaft's durability. The analysis made use of the F-Snedecor test.
The article describes the general concept of the research, the constructed laboratory test rig, and the methodology of statistical inference concerning the significance of influence of input (exciting) parameters of the physical model on the recorded output parameters. The results of the performed statistical tests confirm the absence of the significance of influence of the rotational speed of the propulsion shaft on the selected types of rotating operation of the mechanical system. As a consequence, only one exciting parameter, which is the loading mass, is going to be taken into account in the functional description of fatigue life of the propulsion shaft.

Keywords: rotating mechanical system, modelling of energy processes, propulsion shaft fatigue, testing of statistical hypotheses

INTRODUCTION

A crucial condition for correct quantitative evaluation of energy related consequences of high cycle fatigue of the structural material of the propulsion shaft operating in the rotating mechanical system is developing an adequate mathematical model of unsteady and low-frequency physical processes taking place in the shaft. According to the theory of mathematical modelling and methods of experimental research planning, presented in [1, 7, 11] among other publications, two ways of proceeding are possible, which are:

1. Deductive way: starting from the theoretical background of the modelled processes and adopting certain simplifying assumptions, equations are formulated which define relations between input and output signals (so-called balance equations), based on fundamental laws of physics (energy, momentum, angular momentum, and mass conservation laws, for instance). The mathematical model developed in the above way should undergo verification tests by comparing relevant results of numerical simulations of physical processes performed using this model with the results of experimental examination of a real object after introducing the same excitations. This way the adequacy of the model is assessed.
2. Inductive way: firstly, based on a precisely planned experiment the examination of a real object is performed.

MOST WIEDZY Downloaded from mostwiedzy.pl

The time-histories of output signals are recorded for the assumed variations of input signals. The regression analysis of both types of signals makes the basis for defining mathematical relations between them. These relations are then subject to verification, according to the theory of testing of parametric statistical hypotheses.

Due to high structural complexity of rotating mechanical systems of real objects, the equations which describe their motion are very sophisticated, and a large number of assumptions simplifying the physical model of the analysed energy processes are to be adopted [2, 3]. This makes the verification of correctness of the developed mathematical model very difficult, especially in the situation when the detailed information on the used structural materials (their mechanical and thermal characteristics) is missing. That is why a decision was made to apply the inductive approach to the identification of the propulsion shaft fatigue process in the rotating mechanical system, and to determine a general formula describing the influence of the bending moment load of the system on the energy state (and durability) of the specified shaft segment. However, this approach is not an obstacle in the identification research, as the rule applies in empirical sciences that examining arbitrary physical processes should start with developing their simplest models.

2. CHARACTERISTICS OF OBJECT OF RESEARCH

To model real energy processes taking place during the operation of the rotating mechanical system, a simplified physical model of this system was constructed in relevant scale to model structural and functional characteristics of the real object. For this purpose, the testing machine produced by Schenck was used. It was initially designed for tests oriented on assessing fatigue limits of structural materials subject to reverse bending – Fig. 1.

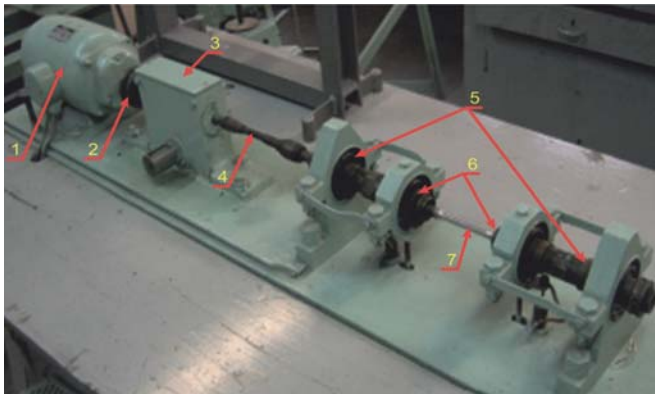

Fig. 1. Standard testing machine produced by Schenck for assessing the fatigue limit at reverse bending: 1 – propulsion motor (DC shunt motor); 2 – flexible disc coupling (with pins and rubber pads); 3 – cycle counter worm gear (transmission ratio 1:100); 4 – flexible spring coupling; 5 – fixed bearing bracket; 6 – mobile bearing bracket; 7 – tested sample

The fatigue cycle is executed on this machine by bending the rotating cylindrical sample of constant cross-section with constant load (loading mass m_{obc}) situated in the same plane. The scheme of the physical model of the rotating mechanical system which executes this fatigue cycle is shown in Fig. 2. Acharacteristic feature of the machine used for these tests is no power take-off at the end of the propulsion line, while the basic advantage is uniform load distribution with the bending-twisting moment along the entire length of the tested material sample. This way of modelling laboratory conditions in the fatigue test which take into account real operating conditions of a rotating mechanical system (ship propulsion unit, for instance), can simulate loss of coaxiality or bending of the shafting, which leads to the increase of pressure forces acting in bearings and the resultant increase of mechanical losses connected with friction in the shafting. Also for this reason, like in the full-scale propulsion system, the modernised Schenck's testing machine provides an option of rotational speed stabilisation by feeding the electric motor via a thyristor controller – Fig. 2.

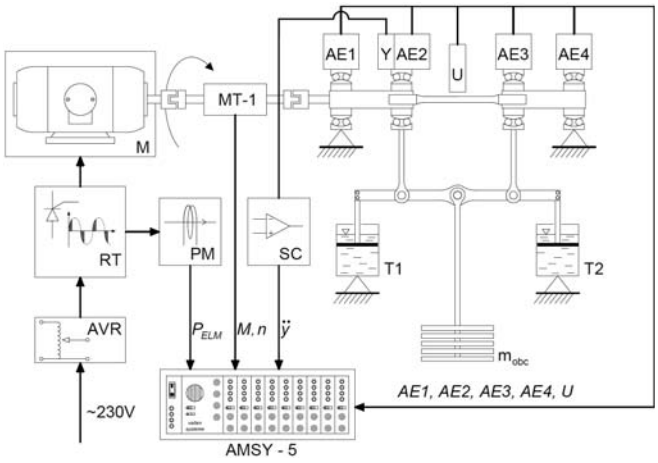

Fig. 2. Scheme of the physical model of the rotating mechanical system, with the distribution of measuring converters: M – electric motor 0,25 kW; MT-1 – torque meter; AE1-AE4 – acoustic emission converters; Y – vibration acceleration converters; U – sample deflection converter; RT – thyristor rotational speed controller; AVR – network voltage stabiliser; PM – measuring converter of electric power; SC – conditioner of vibration acceleration converter signal; T1, T2 – oil dampers; m_{obc} – loading mass. Recorded voltage signals: AE1, AE2, AE3, AE4 – acoustic emission; U – sample deflection; M– torque; n – rotational speed, P_{ELM} – electric power taken by propulsion motor, ÿ – mechanical vibration acceleration

The unsteady mechanical energy balance of the tested system leads to fluctuations of the rotational speed of the propulsion line. Moreover, the consequences of the excited elastic and plastic deformations of the sample are: transverse vibration generated at bearing nodes, acoustic emission of a series of decaying elastic waves, and thermal emission (infrared radiation) of elements of the system accumulating the internal energy. Taking into consideration the above aspects, the already existing standard test rig had to be modified in such a way as to allow simultaneous, multi-symptom, energy related observation of the high-cycle fatigue process of the standard sample. The designed measuring system was expected to allow continuous recording of parameters

MOST WIEDZY Downloaded from mostwiedzy.pl

characterising accumulation and dissipation of different forms of energy during the unsteady low-frequency process accompanying the properly planned fatigue test. For this purpose, the following measuring signals were recorded during the operation of the physical model:
- rotational speed and transmitted torque,
- deflection and temperature of the sample,
- mechanical vibration and acoustic emission (generated by bearing nodes),
- voltage and electric current supplying the electric motor.

A detailed characteristic of the measuring system installed on the test rig was given in earlier publications by the authors [8, 9, 10]. A general view of the rig with the measuring equipment is shown in Fig. 3.

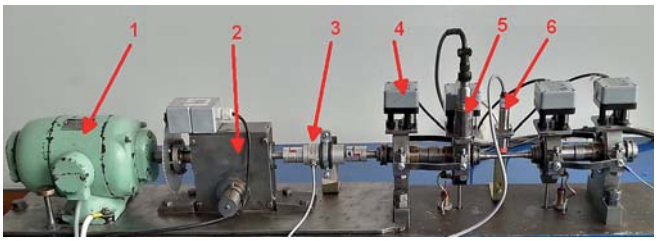

Fig. 3. General view of the test rig: 1 – electric motor; 2 – cycle counter worm gear; 3 – torque meter MT-1; 4 – acoustic emission converter; 5 – vibration acceleration converter; 6 – sample deflection converter

MODELLING OF PROPULSION SHAFT FATIGUE PROCESS

Modelling of the propulsion shaft fatigue process in the rotating mechanical system aims at determining the function which describes its durability. The independent variables in this function are energy parameters describing the action during transmission of mechanical energy and its conversion to work and heat forms [5, 6]. In a descriptive sense, this operation can be interpreted as conversion of energy E at given time τ, which in formal approach can be expressed by the formula:

$$D(\tau)=\int_{\tau_1}^{\tau_2} E(\tau)\,d\tau \tag{1}$$

where:
$D(\tau)$ – action at time τ [J·s],
τ – time [s],
$E(\tau)$ – system energy at time τ [J],
$[\tau_1, \tau_2]$ – time interval of operation.

Each energy parameter, expressed in joule-seconds, characterises the potential of the energy source, the measure of which is a number with unit of measurement [J·s] and the area bounded by: the graph of changes of energy (or its carrier), the time axis, and vertical lines representing the limits of integration $\tau = \tau_1$ and $\tau = \tau_2$ of the definite integral of function $E(\tau)$ given by formula (1). The limits of integration of this function, i.e. τ_1 (lower) and τ_2 (upper) are the time limits of the fatigue process observation – Fig. 4.

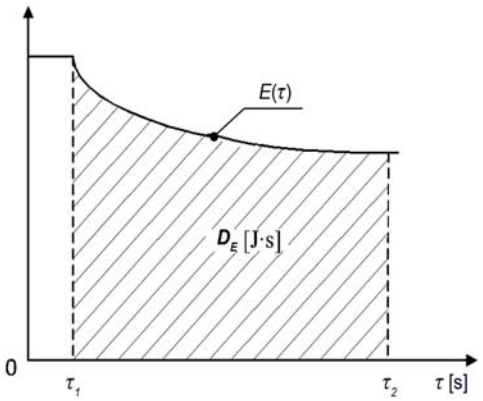

Fig. 4. Geometrical interpretation of the energy parameter characterising the potential of the energy source

Developing the mathematical model of the propulsion shaft (sample) fatigue process in the analysed mechanical system needs defining the physical model, in which the input parameters exciting the fatigue process in the conditions of really introduced deflection of the sample are determined along with the output and disturbance parameters – Fig. 5. It was assumed that the input (set) parameters in the modelled process are:
- mass loading the sample – m_{obc},
- rotational speed of the sample – n,

while the output parameters characterising the accumulating potential of the sample are:
- action related with conversion of mechanical energy to mechanical work form – D_W,
- action related with generation of mechanical vibration – D_V,
- action operation related with generation of elastic acoustic emission waves – D_{EA},
- action operation related with conversion of mechanical energy to heat form – D_U.

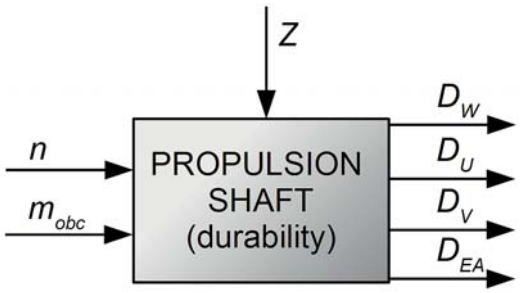

Fig. 5. Physical model of the propulsion shaft (sample) fatigue process in the rotating mechanical system

Basic disturbance parameters (Z) which disturb the course of the modelled process include:
- environmental conditions (location of use of the tested physical model, environment parameters),
- non-homogeneousness and anisotropy of the structural material of the sample representing the propulsion shaft,
- technical condition of bearing nodes.

MOST WIEDZY Downloaded from mostwiedzy.pl

Since the tests were performed in similar ambient conditions (closed and air-conditioned room), the material samples were made from the same drown bar, and the bearing degradation was relatively small, an assumption was made [10] that the effect of disturbances is negligibly small.

STATISTICAL ANALYSIS PROGRAMME

As the first stage of identification of the propulsion shaft fatigue process in the rotating mechanical system, the eliminating statistical analysis was performed to determine the correlation between the adopted input parameters: m_{obc} and n, and output parameters D_W, D_V, D_{EA} and D_U of the physical model. The analysis was performed based on the randomised plan of active experiment, applicable for determining the influence of the progressive process of fatigue wear of propulsion shaft material, along with the execution ofsuccessive cycles of periodically changing stresses resulting from shaft deflection, on the analysed output parameter, which is the fatigue life of the shaft [13]. In the analysed fatigue problem, an assumption was made that this output parameter is defined by energy parameters characterising the operation of the examined mechanical system, while the influence of the set input parameters on it depends on the sequence of realisation of elements of the adopted plan of experiment. That is why the basis for randomisation of the plan of experiment is a random order of successive test executions for the a priori assumed variability levels of input parameters [11].

The values of input parameters m_{obc} and n were assumed at three variability levels which guarantee feasibility of the experiment. In each measuring series, five repeated tests were performed. The plan of experiment is shown in Table 1.

The values of the rotational speed n of the shaft and the loading mass m_{obc} which were adopted in the plan of experiment result from the observations made during preliminary studies. These observations enabled to assess the variability ranges of the parameters intended to excite the fatigue process. For the applied shaft material (structural steel C45), as well as for the given geometrical dimensions and capabilities of the test rig, the system mass load was assumed (provided) at the level of 25 kg. Below this level, the shaft material reveals unlimited fatigue life in the bending-rotating test, which makes recording the fracture process impossible. On the other hand, the maximal excitation value is limited by static bending resistance of the material of the sample. The upper limit of the loading mass m_{obc} is equal to 45 kg.

A similar relation was observed when analysing the variability range of the rotational speed of the shaft. In order to minimise disturbances of the mechanical stability of the test rig, the nominal rotational speed was assumed at the level of n = 1500 rpm. Below n = 1200 rpm and above 800 rpm the run of the fatigue machine is unsteady, which results from insufficient damping of mechanical vibration by oil dampers – Fig. 2.

Tab. 1. Plan of eliminating experiment

No.	Loading mass m_{obc} [kg]	Rotational speed of shaft n [rpm]
1	40	1800
2	35	1800
3	30	1800
4	40	1500
5	35	1500
6	30	1500
7	40	1200
8	35	1200
9	30	1200

Each time before the beginning of the experiment, the fatigue machine worked for about 30 minutes without sample loading to warm up the bearings and the motor. After this warm-up time, no significant changes in electric parameters of the motor and the transmitted torque were recorded. Additionally, at the beginning of data acquisition, the initial 100 s were always recorded as the sample run without loading, after which the loading mass was automatically released and the basic part of the test started. Selected representative results of a single fatigue test are shown in Fig. 6.

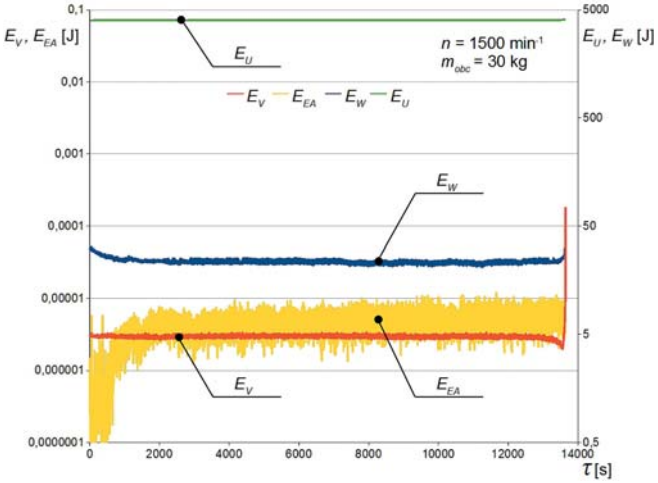

Fig. 6. Results of single fatigue test: E_U – internal energy of the system, E_w – system energy related to mechanical work, E_{EA} – energy of elastic acoustic emission waves, E_V – energy of mechanical vibration, τ – time of the test

5. MATHEMATICAL PROCESSING OF STATISTICAL TEST RESULTS

A characteristic feature of material fatigue studies is high dispersion of results obtained in individual tests, which is mainly caused by material non-homogeneousness of samples and their manufacturing inaccuracy [14]. A similar conclusion can be formulated based on experimental tests performed by the authors. The observed dispersion in fatigue test duration (number of cycles) reached as much as 50%. That is why a method had to be worked out to analyse test results in

MOST WIEDZY Downloaded from mostwiedzy.pl

energy approach which would allow their comparison for different combinations of input parameters and examine their influence on output parameters. The result of each measuring sequence consisting of five repetitions is the arithmetic mean of operation values of the given system. Averaging reduces the number of results which need analysing from z 45 to 9.

The significance of the influence of input parameters on output parameter was verified using the parametric F-Snedecor test [9]. The null hypothesis formulated for this test assumes the absence of significant influence of two selected input parameters on four analysed output parameters. Mathematical processing of results of tests performed in accordance with the randomised static block plan consists in calculating the values of coefficients F_{mobc} and F_n for each input parameter. The results of these calculations are compared with the critical value determined based on statistical tables of critical values of the F-Snedecor test for the assumed confidence level α and the number of degrees of freedom f. For the assumed confidence level $\alpha = 0{,}05$ and the numbers of degrees of freedom $f_1 = 2, f_2 = 4$ the critical value of the F-S distribution is $F_{kr} = 6{,}9443$. The influence of the analysed input parameter on output parameters is considered significant when the calculated test value of the given coefficient, F_{mobc} or F_n, is greater than or equal to the critical value.

According to the adopted plan of experiment and the set of parameters selected for a given physical model, the significance of influence of input parameters on output parameters was verified. The results of statistical tests are given below.

ACTION AS RESULT OF ENERGY CONVERSION TO WORK FORM

The performed experiment allowed to determine the action related with mechanical energy conversion and the resultant mechanical work, D_W. The rotational speed of the shaft was recorded along with the transmitted torque. This allowed to calculate the instantaneous work values in the rotational motion which were related with the fatigue process excitation. The obtained time-history of work, being the form of energy conversion as a function of time, was used for determining the action for each test, via integration performed with the aid of the trapezoidal rule (according to formula 1). The averaged action values related with mechanical energy conversion to mechanical work form are collated in Table 2 for different combinations of input values.

Tab. 2. Action values related with execution of mechanical work, DW [J·s]

m_{obc} [kg]	n [rpm]		
	1200	1500	1800
30	306946,69	260594,36	205767,71
35	152235,22J	109525,1	128929,16
40	98334,2	45447,12	51010,87

The coefficients F_n and F_{mobc} calculated for the input parameters: rotational speed and loading mass, are equal to 5,3081 and 54,5366, respectively. Since the value of coefficient F_n is smaller than the critical value ($F_{kr} = 6{,}9443$) we can assume that there is no significant influence of this input parameter on the action related with execution of mechanical work.

ACTION AS RESULT OF ENERGY CONVERSION TO HEAT FORM

Studying the action related with heat emission D_U consisted in the qualitative and quantitative analysis of thermographic images of the cyclically loaded shaft. The recorded thermograms were used for determining, with 100s intervals, instantaneous internal energy values of the specified shaft segment. Changes of these values resulted from mechanical energy conversion to heat form. Since the highest shaft temperature rise recorded during all tests was equal to $\Delta T = 25$ K, the specific heat value of the structural material of the shaft was assumed constant and equal to $c_p = 470$ J/kg·K during the entire experiment. The mass of the specified shaft segment was $m_p = 0{,}028$ kg. The recorded time-history of changes of internal energy of the shaft during the fatigue test was used to determine, via numerical integration, the action related with mechanical energy conversion to heat form. The averaged action values related with heat emission are given in Table 3.

Tab. 3. Action values related with heat emission, DU [J·s]

m_{obc} [kg]	n [rpm]		
	1200	1500	1800
30	43662499,46	42843494,45	38502003,54
35	25576545,13	24671248,06	21349759,43
40	17481255,6	8266451,78	8019399,83

The coefficients F_n and F_{mobc} calculated for the input parameters: rotational speed and loading mass, are equal to 5,0334 and 118,0695, respectively. Like for the action related with mechanical energy conversion to work form, also in this case no significant influence of the rotational speed of the propulsion shaft on the action related with heat emission was detected.

ACTION MODELLED IN THE VIBRATION PROCESS

The action related with generation of mechanical vibration, D_V was assessed based on the recorded time-histories of deflection (vibration) of the geometrical shaft centre. These time-histories were differentiated numerically to determine the speed of transverse vibration. Then the RMS value of the vibration speed was calculated (square averaging) for every second of the test. The amount of kinetic energy dissipated in the form of mechanical vibration during the rotational motion of the shaft is always a function of the square of vibration speed

MOST WIEDZY Downloaded from mostwiedzy.pl

[8, 9, 10]. Therefore, for each one-second interval, the amount of energy dissipated in the form of mechanical vibration was calculated as the product of mass and the square of RMS value of vibration speed. Like in previous cases of energy conversion, the time-histories of propulsion shaft transverse vibration energy changes, obtained in the above way, were integrated numerically to determine the action related with vibration generation. The averaged values of action D_V for constant values of input parameters are given in Table 4.

Tab. 4. Action values related with generation of mechanical vibration, D_V [J·s]

m_{obc} [kg]	n [rpm]		
	1200	1500	1800
30	0,079332578	0,047725485	0,075701043
35	0,062292588	0,0041851675	0,018446676
40	0,020791802	0,01073448	0,005595129

The coefficients F_n and F_{mobc} calculated for the input parameters: rotational speed and loading mass, are equal to 3,9590 and 11,3140, respectively. Like in previous cases, also in this case no significant influence of the rotational speed of the propulsion shaft on the action related with generation of mechanical vibration was detected.

ACTION MODELLED IN ACOUSTIC EMISSION

The fatigue life of the propulsion shaft can also be characterised by the action related with generation of elastic acoustic emission waves, D_{EA}. The mechanical (kinetic) energy dissipated in the form of elastic acoustic emission waves is expressed in the apparatus AMSY-5 in the form of arbitrary units (so-called eu units) introduced by the apparatus producer [15]. Since the developed model is expected to return not only qualitative but also quantitative results, the real amount of energy dissipated in the form of elastic acoustic emission waves was to be determined. The measuring lines of the acoustic emission sensors were calibrated using the method in which the elastic wave was released in the material by dropping a small steel ball [12]. This method allows to determine this part of energy of the falling ball which is converted to elastic energy of the material on which the ball falls. The energy of elastic deformation is entirely converted to the energy of elastic waves. In an auxiliary experiment, the ball with mass of 0,00105 kg was dropped from three heights: 10, 20 and 30 mm, onto the hardened plate made of NC10 steel. The differences between the dropping height and the rebound height were used to determine the amount of potential energy converted to the elastic wave energy. The relation between the dropping height and the amount of the recorded energy is linear within this range, therefore one correction value equal to: 1eu = 0,00000036916 J was used for calibration. The averaged action values related with generation of elastic acoustic emission waves are given in Table 5.

Tab. 5. Action values related with generation of elastic acoustic mission waves, DEA [J·s]

m_{obc} [kg]	n [min^{-1}]		
	1200	1500	1800
30	0,0107207904	0,0393590177	0,0247581099
35	0,0038553507	0,0147507758	0,0118168544
40	0,0023520564	0,0012492075	0,0035523067

The coefficients F_n and F_{mobc} calculated for the input parameters: rotational speed and loading mass, are equal to 2,2030 and 6,9561, respectively. Also in this case no significant influence of the rotational speed of the propulsion shaft on the action related with generation of elastic acoustic emission waves was detected.

FINAL REMARKS AND CONCLUSIONS

It was assumed when analysing the significance of influence of the parameters exciting the propulsion shaft fatigue in the rotating mechanical system that the fatigue life of the shaft material depends on action. For the purpose of the above analysis, the operation of the mechanical system and the propulsion shaft was interpreted as energy conversion at given time. The operation interpreted in the above way was expressed by a number with the unit of measurement called joule-second [J·s].

Since no significant influence of the input parameter related with the rotational speed of the propulsion shaft on the selected types of action was detected (proved) in the performed analysis, the parameter related with the loading mass will be only taken into account in the developed functional description of the fatigue process. Consequently, a new plan of experiment needs to be worked out which will take into account the influence of only one input parameter. In this new plan, the resolution of loading mass changes is to be refined, this way providing more information on the course of the propulsion shaft fatigue degradation process. This information will be needed when preparing a new physical model of the rotating mechanical system.

As a further step, the theoretical model is to be made closer to the operating conditions of real objects by finding relations between the loading mass and real shaft deflection, and comparing these relations with the results of measurements obtained during diagnostic tests of watercraft shafting [4].

BIBLIOGRAPHY

1. Cannon R.H. (2003). Dynamics of physical systems. New York, Dover Publication.

2. Cempel C., Natke H.G. (2012). Model-aided diagnosis of mechanical systems: Fundamentals, detection, localization, assessment. Springer Science & Business Media.

MOST WIEDZY Downloaded from mostwiedzy.pl

3. Cichy M. (2001). Modelling of energy systems (in Polish). Gdansk, Wydawnictwo Politechniki Gdańskiej.

4. Dragantchev H. (2000). Control and diagnostics of ship shafting. Proceedings of the IMAM 2000, Ischia, 2–6 April, Session L, s. 115–122.

5. Girtler J. (2013). A method to evaluate operation of machines using technical diagnostics. Chapter 4, pp. 101-127, Monograph entitled "Diagnostic examination and inference. Selected issues" (in Polish). Warsaw, Wydawnictwo Wojskowej Akademii Technicznej.

6. Girtler J. (2015). Problems of rational use of diagnostic systems for decision making in power equipment operation phase, taking into account quantum issues. Chapter 5, pp. 91-123, Monograph entitled "Selected issues of diagnostics and use of devices and systems" (in Polish). Warsaw, Wydawnictwo Wojskowej Akademii Technicznej.

7. Gutenbaum J. (1992). Mathematical modelling of systems (in Polish). Warsaw, Instytut Badań Systemowych Polskiej Akademii Nauk.

8. Korczewski Z. (2012). The conception of energetic investigations of the multisymptom fatigue of the simple mechanical systems constructional materials. Journal of Polish CIMAC vol. 7 no 1 Energetic aspects. Gdansk, Wydawnictwo Politechniki Gdańskiej.

9. Korczewski Z. (2017). Operating diagnostics of marine internal combustion piston and turbine engines. Selected issues (in Polish). Gdansk. Wydawnictwo Politechniki Gdańskiej.

10. Korczewski Z., Marszałkowski K. (2016). Physical model of energy-related processes in a rotating mechanical system for the purposes of diagnosis of transmission shafts. Journal of Polish CIMEEAC, Vol. 11, No. 1.

11. Korzyński M. (2006). Methodology of experiment (in Polish). Warsaw, Wydawnictwa Naukowo-Techniczne.

12. Malecki I., Ranachowski J. (1994). Acoustic emission: sources, methods, applications (in Polish). Warsaw, Instytut Podstawowych Problem Techniki PAN.

13. Polański Z (1984).: Planning of experiments in engineering (in Polish). Warsaw PWN.

14. Szala J., Boroński D. (2008). Evaluating material fatigue state in diagnostics of machines and devices (in Polish). Bydgoszcz, Wydawnictwo Instytutu Technologii Eksploatacji – PIB.

15. VALLEN Systeme GmbH (2011). AMSY-5 System Specification.

CONTACT WITH THE AUTHORS

Zbigniew Korczewski
Konrad Marszałkowski

Gdańsk University of Technology,
Faculty of Ocean Engineering and Ship Technology
Department of Marine and Land Power Plants
11/12 Narutowicza St.
80–233 Gdansk
Poland

MOST WIEDZY Downloaded from mostwiedzy.pl

POLISH MARITIME RESEARCH Special Issue 2018 S1 (97) 2018 Vol. 25; pp. 218-224
10.2478/pomr-2018-0045

COMPARATIVE ANALYSIS OF THERMODYNAMIC CYCLES OF SELECTED NUCLEAR SHIP POWER PLANTS WITH HIGH-TEMPERATURE HELIUM- COOLED NUCLEAR REACTOR

Natalia Szewczuk-Krypa
Anna Grzymkowska
Jerzy. Głuch
Gdańsk University of Technology, Poland

ABSTRACT

This paper presents a comparative analysis of thermodynamic cycles of two ship power plant systems with a high-temperature helium- cooled nuclear reactor. The first of them is a gas system with recuperator , in which classical gas chamber is substituted for a HTGR reactor (High Temperature Gas-cooled Reactor) . The second of the considered cycles is a combined gas-steam system where working medium flux from gas turbine outlet is directed into waste heat boiler and its heat is utilized for production of superheated steam to drive steam turbine. Preliminary calculations of the combine cycles showed that it is necessary to expand the system by adding to its steam part an inter-stage overheat for secondary steam, owing to that a required degree of steam dryness at outlet from the turbine can be reached, ensuring its correct operational conditions. The analyzed power systems were compared to each other with regard to efficiency of their thermodynamic cycles. Also, efficiency of particular cycles were subjected to optimization in respect to such parameters as : working gas temperature at outlet from reactor in gas system as well as steam pressure at outlet from waste heat boiler and partition pressure in steam part of combined system. Advantages of nuclear power plants compared with the classical power systems dominating currently in sea transport were also discussed.

Keywords: nuclear ship power plant, nuclear reactor, HTGR, gas turbine, steam turbine, combined cycle

INTRODUCTION

Progressing usage of fossil fuels resources and more and more restrictive requirements concerning mitigation of emission of greenhouse gases lead to an increasing interest to alternative propulsion systems for maritime transport purposes. The commonly applied conventional propulsion systems with self-ignition engines or oil firing boilers are emission sources of large amounts of carbon dioxide, sulphur oxides and nitrogen. Their exhaust gases pollute air both in coastal and offshore areas [4, 5, 6].

Nuclear power plants [14] which are sucessfully used for propulsion of both naval and civilian ships [2] may serve as an alternative for the conventional systems.

One of the types of reactors applicable to nuclear power plants is the high-temperature gas-cooled reactor (HTGR) [9]. It is characteristic of a high temperature at core outlet that makes it possible to use the cooling medium for both driving gas turbine [10] and carrying out various chemical processes such as hydrogen production or crude oil refining. Subsequent advanages of the HTGR reactor is its safety and a high degree of fuel burnup. It is ensured due to a high thermal capacity of graphite which is commonly used as a moderator which maintains structural stability even in high temperature conditions. Moreover, waste heat from nuclear power plant can be used for desalting sea water, heating or producing superheated steam in gas-steam combine power system, namely in the so called waste heat boiler [15].

MOST WIEDZY Downloaded from mostwiedzy.pl

Nuclear power plants allow to generate power in large amounts. They are characteristic of a high reliability and lowered fuel supply frequency that results in increasing operational range of ships and becoming independent of tankers. The advantages caused that, beginning from the 1950s, nuclear power plants found their wide application [6, 8, 12] to propulsion of icebreakers intended for the operating in polar regions where they perform well in extreme operational conditions delivering necessary supply of food, fuel, equipment etc [1, 8, 11, 13]. In present, nuclear propulsion is widely used in the navy and less often in civilian ships [5,6].

ANALYZED CYCLES OF NUCLEAR POWER PLANTS

The performed calculations were aimed at comparison of efficiency of two nuclear - gas cycles with high- temeperature helium-cooled reactor. Owing to its favourable thermal properties, helium performs very well as a cooling medium for the reactor and simultaneously as a working medium in the gas turbine cycle. Thermal conductivity coefficient of helium is five time greater than that of air which commonly serves as a working medium in turbine cycles of combustion engines [3]. Moreover, helium, being a perfect gas, does not undergo ionization, hence it is more friendly to the environment than other cooling media used for nuclear reactors [9].

The first of the considered systems was the gas power system with recuperator (Fig. 1). As opposed to the classical turbine cycle of combustion engine, a high- temperature reactor HTGR was substituted for combustion chamber. And, in view of the high temperature (934 K) of working medium at outlet from gas turbine, a recuperator intended for the heating of working medium before reactor, was applied. As a result, amount of heat wasted in the cycle was lowered and this way the system's effectiveness was improved.

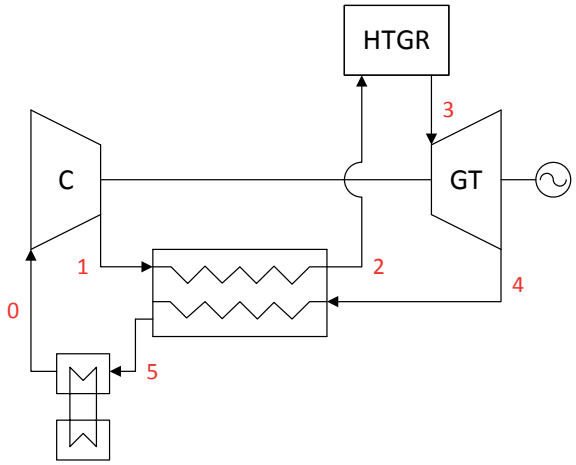

Fig. 1. The gas power system fitted with the high-temperature reactor HTGR and gas recuperator: C – compressor, HTGR – high-temperature reactor, GT – gas turbine

The cycle's parameters were so selected as to suit requirements of the reactor. As assumed, the pressure of helium cooling the reactor, p_2, is equal to 7 MPa. Application of a lower pressure could cause a significant rise in specific volume of working gas, that would detrimentally influence dimensions and weight of the whole installation. The desired level of cooling medium pressure was reached by appropriate selection of the compression ratio π_K of the compressor by assuming values of the temperature T_1 and pressure p_1 of working gas at inlet to the compressor equal to 299 K and 2,8 MPa, respectively. Under the so selected parameters the applied high-temperature reactor heats working medium up to the temperature T_3 of 1273 K [4]. The gas temperature value at outlet from the reactor was determined on the basis of predicted amount of heat transferred to cooling medium as a result of nuclear reaction in the reactor. Under assumption that working medium in gas turbine expands up to the pressure, a little greater than that at inlet to the compressor, as well as by taking into account pressure losses in the recuperator and cooler, the value of the expansion ratio in the turbine was taken equal to 2,5. For simplification it was assumed that the parameters which characterize working medium, such as the specific heat cp or adiabate exponent κ, are constant within the considered range of pressure and temperature changes. For the working medium such as helium the specific heat cp = 5,19 kJ/kgK, and adiabate exponent κ = 1,66 was assumed.

Another analyzed power system was the combine gas-steam cycle shown in Fig. 2 [7]. In such systems working medium from gas turbine outlet is directed to waste heat boiler in which the heat is used to produce superheated steam supplying steam turbine. Such usage of waste heat of the gas cycle makes it possible to gain an additional portion of power on steam turbine shaft, that significantly increases efficiency of the whole system. In relation to the first of the considered cycles, the working medium parameters at inlet to and outlet from the compressor and turbine in the gas part were maintained without any change. In the combined system the waste heat boiler which produces superheated steam to feed steam turbine is substituted for the recuperator. The steam temperature at outlet from the boiler, t_A, was assumed on the basis of the constant value of difference between live steam temperature and helium temperature at inlet to waste heat boiler (δt_2=30°C). Fig. 3 shows a diagram of temperatures in the waste heat boiler. The live steam pressure at outlet from the waste heat boiler was subjected to optimization to make effectiveness of the considered system as good as possible. In selecting its value, a dryness degree of steam at outlet from the steam turbine (which cannot be lower than 0,87 in the final point of expansion) played a similarly significant role as the effectiveness of the cycle. The final pressure in condenser, p_B, was assumed equal to 5 kPa. Also, a minimum temperature difference in the beginning of vaporization process in the waste heat boiler, the so called temperature threshold (Fig. 3), was assumed equal to 8 °C.

MOST WIEDZY Downloaded from mostwiedzy.pl

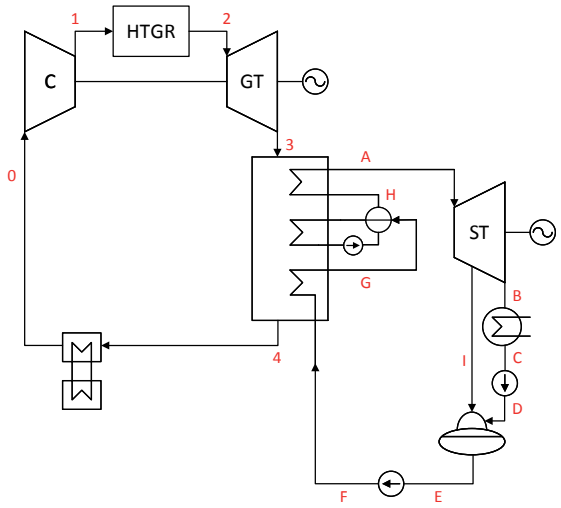

Fig. 2. The combined gas-steam power system fitted with the high-temperature reactor HTGR: C – compressor, HTGR – high-temperature reactor, GT – gas turbine, ST – steam turbine

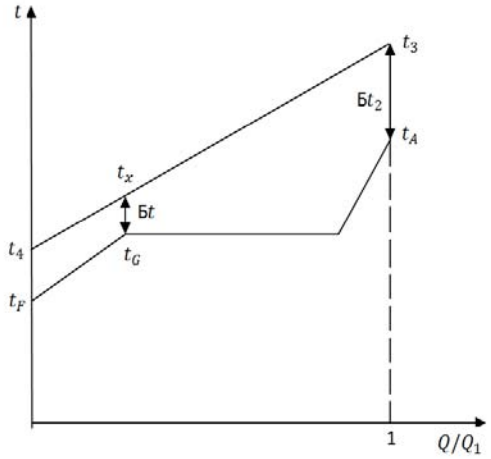

Fig. 3. Diagram of temperatures in waste heat boiler

After performing the preliminary thermodynamic calculations for the combined system its steam part was modified (Fig. 4). In view of a low dryness degree of steam at outlet from the turbine, the system was expanded by adding an inter-stage overheat dividing this way the turbine into two parts: high-pressure (HP) and low-pressure (LP) part. In the so modified system the secondary steam is directed from outlet of HP part into the overheat to be heated there up to a temperature close to that of live steam at outlet from the waste heat boiler. Such operation makes it possible to decrease steam wetness at outlet from LP part and reach consequently a significant improvement in efficiency of the considered combined system.

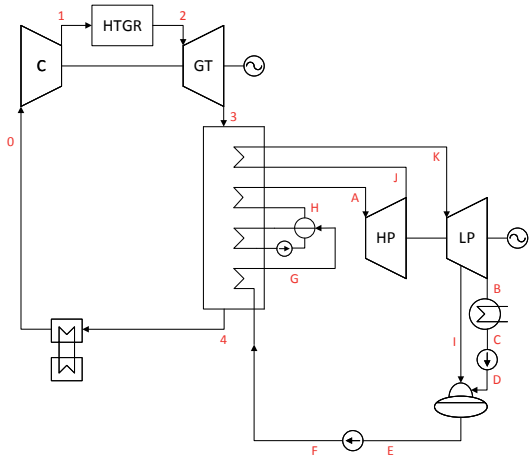

Fig. 4. The combined gas-steam power system fitted with the high-temperature reactor HTGR and inter-stage overheat: C – compressor, HTGR – high-temperature reactor, GT – gas turbine, HP – high-pressure part of steam turbine, LP – low-pressure part of steam turbine

RESULTS OF THE ANALYSIS

Based on the assumed values of the working medium parameters, values of pressures, temperatures and entalphies were determined in characteristic points of the considered cycles. In each case, the gas turbine output power was assumed equal to 50 MW. The calculation results for the particular systems are presented in Tab. 1, 2 and 3.

Tab. 1. Thermodynamic parameters of gas cycle with HTGR reactor and gas recuperator

Parameters of gas cycle with HTGR reactor and gas recuperator			
Gas turbine output power	Ne	50	MW
Working medium pressure at inlet to compressor	p0	2,8	MPa
Working medium temperature at inlet to compressor	T0	299,2	K
Working medium entalphy at inlet to compressor	i0	1552,6	kJ/kg
Working medium pressure at outlet from compressor	p1	7	MPa
Working medium temperature at outlet from compressor	T1	453,8	K
Working medium entalphy at outlet from compressor	i1	2355,4	kJ/kg
Pressure at inlet to HTGR reactor	p2	7	MPa
Working medium temperature at inlet to HTGR reactor	T2	837,9	K
Working medium entalphy at inlet to HTGR reactor	i2	4348,9	kJ/kg
Working medium pressure behind HTGR reactor	p3	6,8	MPa
Working medium temperature behind HTGR reactor	T3	1273	K

MOST WIEDZY Downloaded from mostwiedzy.pl

Parameters of gas cycle with HTGR reactor and gas recuperator			
Working medium entalphy behind HTGR reactor	i3	6607,2	kJ/kg
Working medium temperature at outlet from gas turbine	T4	954	K
Working medium pressure at outlet from gas turbine	p4	3	MPa
Working medium entalphy at outlet from gas turbine	i4	4953,5	kJ/kg

Tab. 2. Thermodynamic parameters of combined gas-steam cycle with HTGR reactor without inter-stage overheat

Parameters of combined gas-steam cycle with HTGR reactor without inter-stage overheat			
Gas turbine output power	Ne	50	MW
Working medium pressure at inlet to compressor	p0	2,8	MPa
Working medium temperature at inlet to compressor	T0	299,2	K
Working medium entalphy at inlet to compressor	i0	1552,6	kJ/kg
Working medium pressure at outlet from compressor	p1	7	MPa
Working medium temperature at outlet from compressor	T1	453,8	K
Working medium entalphy at outlet from compressor	i1	2355,4	kJ/kg
Working medium pressure behind HTGR reactor	p2	6,8	MPa
Working medium temperature behind HTGR reactor	T2	1273	K
Working medium entalphy behind HTGR reactor	i2	3648,2	kJ/kg
Working medium temperature at outlet from gas turbine	T3	954	K
Working medium pressure at outlet from gas turbine	p3	3	MPa
Working medium entalphy at outlet from gas turbine	i3	4953,5	kJ/kg
Working medium temperature behind waste heat boiler	T4	410	K
Working medium pressure behind waste heat boiler	p4	3	MPa
Working medium entalphy behind waste heat boiler	i4	2128,4	kJ/kg
Live steam pressure	pA	22	MPa
Live steam temperature	tA	914,3	K
Live steam entalphy	iA	3636,7	kJ/kg
Final pressure	pB	5	kPa
Steam temperature at outlet from steam turbine	tB	305,9	K
Steam entalphy at outlet from steam turbine	iB	2168	kJ/kg
Water pressure behind degasifier	pE	23	kPa
Water temperature behind degasifier	tE	335,9	K
Water entalphy behind degasifier	iE	263,5	kJ/kg

Tab. 3. Thermodynamic parameters of combined gas-steam cycle with HTGR reactor and inter-stage overheat

Parameters of combined gas-steam cycle with HTGR reactor and inter-stage overheat			
Gas turbine output power	Ne	50	MW
Working medium pressure at inlet to compressor	p0	2,8	MPa
Working medium temperature at inlet to compressor	T0	299,2	K
Working medium entalphy at inlet to compressor	i0	1552,6	kJ/kg
Working medium pressure at outlet from compressor	p1	7	MPa
Working medium temperature at outlet from compressor	T1	453,8	K
Working medium entalphy at outlet from compressor	i1	2355,4	kJ/kg
Working medium pressure behind HTGR reactor	p2	6,8	MPa
Working medium temperature behind HTGR reactor	T2	1273	K
Working medium entalphy behind HTGR reactor	i2	6607,6	kJ/kg
Working medium temperature at outlet from gas turbine	T3	954	K
Working medium pressure at outlet from gas turbine	p3	3	MPa
Working medium entalphy at outlet from gas turbine	i3	4953,5	kJ/kg
Working medium temperature behind waste heat boiler	T4	334,7	K
Working medium pressure behind waste heat boiler	p4	3	MPa
Working medium entalphy behind waste heat boiler	i4	1737,3	kJ/kg
Live steam pressure	pA	22	MPa
Live steam temperature	tA	914,3	K
Live steam entalphy	iA	3636,7	kJ/kg
Steam pressure at outlet from HP part of steam turbine (partition pressure)	pJ	1,76	MPa
Steam entalphy at outlet from HP part of steam turbine	iJ	2964,8	kJ/kg
Steam pressure at inlet to LP part of steam turbine	pK	1,67	MPa
Steam temperature at inlet to LP part of steam turbine	tK	914,3	K

MOST WIEDZY Downloaded from mostwiedzy.pl

Parameters of combined gas-steam cycle with HTGR reactor and inter-stage overheat			
Steam entalphy at inlet to LP part of steam turbine	iK	3786,3	kJ/kg
Final pressure	pB	5	kPa
Steam temperature at outlet from LP part of steam turbine	tB	305,9	K
Steam entalphy at outlet from LP part ofsteam turbine	iB	2330	kJ/kg
Water pressure behind degasifier	pE	23	kPa
Water temperature behind degasifier	tE	335,9	K
Water entalphy behind degasifier	iE	263,5	kJ/kg

Efficiency of the gas cycle with recuperator was determined form the following formula:

$$\eta_{GT} = \frac{N_T - N_C}{Q_d} = \frac{(i_3 - i_4) - (i_1 - i_0)}{i_3 - i_2}$$

where:
N_T – gas turbine output power
N_C – compressor output power
Q_d – heat flux transferred to cooling medium as a result of nuclear reaction.

Optimization of the efficiency was made in respect to the working medium temperature behind the reactor, T_3 (Fig. 5). Taking into account capability of HTGR reactor, value of T_3 temperature was taken within the range from 1073 to 1273 K [4].

The highest efficiency of 41,7% was obtained for the highest temperature at outlet from the reactor. For lower temperatures, the efficiency of the gas cycle with recuperation varies within the range from 35,5% to 41%.

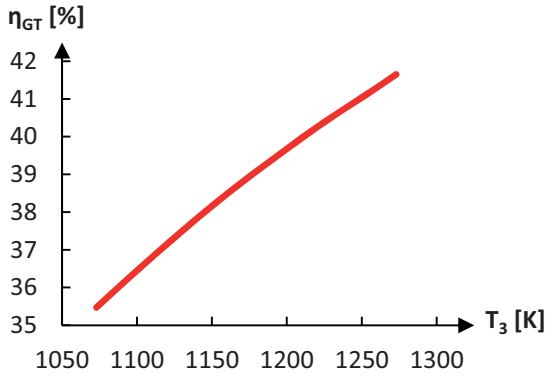

Fig. 5. Diagram of relation between efficiency of the gas cycle with recuperation and working medium temperature at outlet from HTGR reactor

The efficiency of the combined gas-steam cycle without inter-stage overheat was determined from the following formula:

$$\eta_{GS} = \eta_{GT}\left(\frac{N_{ST}}{N_{GT}} + 1\right)$$

$$N_{ST} = m_0(i_A - i_I) + (m_0 - m_{SE})(i_I - i_B)$$

$$\eta_{GT} = \frac{N_{GT} - N_C}{Q_d} = \frac{(i_2 - i_3) - (i_1 - i_0)}{i_2 - i_1}$$

where:
η_{GS} – efficiency of combined gas-steam cycle
η_{GT} – efficiency of gas part of the system
N_{ST} – steam turbine output power
N_{GT} – gas turbine output power
m_0 – live steam mass flux
m_{SE} – mass flux of steam transferred from regenerating extraction to degasifier
N_C – compressor output power
Q_d – heat flux transferred to cooling medium due to nuclear reaction

The combined cycle efficiency was optimized in respect to live steam pressure at outlet from waste heat boiler (Fig. 6).

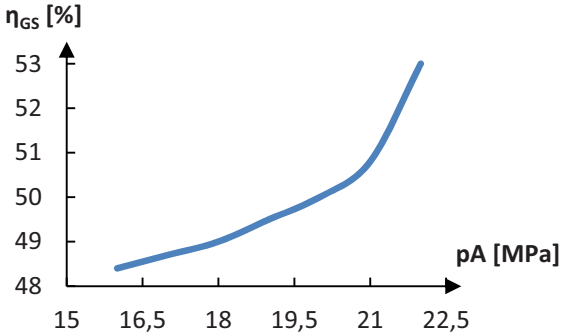

Rys. 6. Relation between the efficiency of combined gas-steam cycle with HTGR reactor and the live steam pressure (pA) at outlet from waste heat boiler

Steam dryness degree at outlet from the turbine was also checked. It was assumed that the steam dryness degree should not be lower than 0,87 in order to maintain correct conditions for turbine operation. Value of that factor depends in large measure on an assumed value of live steam pressure . For the assumed range of steam pressure at outlet from waste heat boiler within limits from 16 to 22 MPa it is clearly visible (Fig. 7) that moisture content in working medium increases along with live steam pressure increasing, that unfavourably affects turbine operational conditions. For the preliminarily assumed cycle parameters, any pressure value within the considered range did not allow to reach the desired value of steam dryness degree.

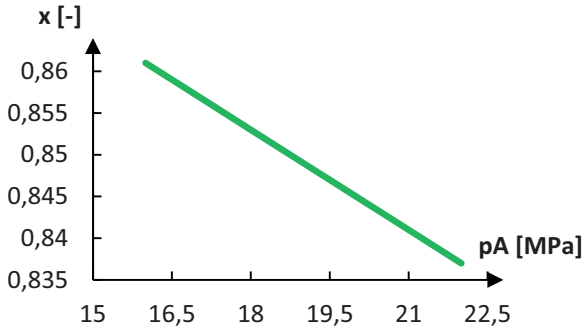

Fig 7. Relation between the steam dryness degree at outlet from turbine and the live steam pressure (pA)

MOST WIEDZY Downloaded from mostwiedzy.pl

The efficiency of the combined system with inter-stage overheat was determined on the basis of the following formulae:

$$\eta_{GS} = \eta_{GT}\left(\frac{N_{ST}}{N_{GT}} + 1\right)$$

$$N_{ST} = m_0(i_A - i_J) + m_0(i_J - i_I) + \\ +(m_0 - m_{SE})(i_I - i_B)$$

$$\eta_{GT} = \frac{N_{GT} - N_C}{Q_d} = \frac{(i_2 - i_3) - (i_1 - i_0)}{i_2 - i_1}$$

The system was optimized in respect to value of the live steam pressure pA at outlet from waste heat boiler as well as the partition pressure pJ (Fig. 8 and 9). As mentioned above, the introduction of inter-stage overheat makes it possible to apply higher live steam pressure values, however, for purposes of the next comparative analysis of the considered systems, the same values of the principle parameters of the considered cycles, including a. o. live steam pressure range, were assumed.

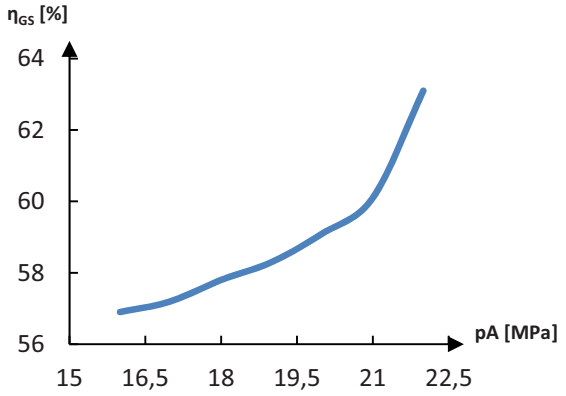

Fig. 8. Relation between the efficiency of combined gas-steam cycle with inter-stage overheat and the live steam pressure (pA)

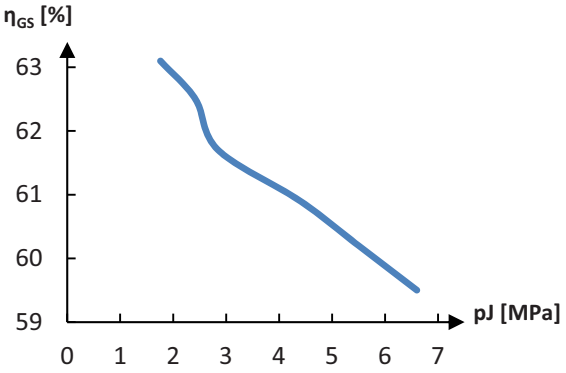

Fig. 9. Relation between the efficiency of combined gas-steam cycle with inter-stage overheat and the partition pressure (pJ)

Like in the case of the combined cycle without inter-stage overheat, the efficiency of the whole system increases along with live steam pressure increasing. For the assumed live steam pressure range the efficiency varies within the limits from 56,9% to 63,1%. The highest efficiency was obtained for the pressure pA = 22 MPa.

The performed optimization of the partition pressure showed that the cycle efficiency decreases along with pressure increasing at outlet from HP part of the turbine. The optimum value of that parameter was assumed equal to 1,76 MPa which is equivalent to 8% value of the steam pressure pA at outlet from waste heat boiler.

SUMMARY

The performed comparative analysis of thermodynamic cycles of the selected ship nuclear power systems with high-temperature helium - cooled nuclear reactor showed that:

- from the point of view of cycle efficiency and amount of generated power, the using of waste heat for production of superheated steam to drive steam turbine is more favourable than the application of gas recuperator ;
- the rise in working medium temperature at outlet from the core affects favourably thermodynamic cycle efficiency, that explains growing interest for VHTR reactors;
- in the case of the combined gas-steam power system a level of live steam pressure and partition pressure is strictly dependent upon steam dryness degree at outlet from the turbine;
- to reach a desired value of steam dryness degree in the combined cycle, it is necessary to apply inter-stage overheat for secondary steam.

Widespread of application of nuclear propulsion systems with high-temperature reactors would allow to reduce emission of noxious gases in coastal and offshore areas and diversify fuels currently used in sea transport . Along with growing popularity of nuclear power plants their unit cost of production would be dropping and they would become, as a result of growing public awareness, strongly competitive for the commonly used classical power plants.

BIBLIOGRAPHY

1. Alekseev P.N., Kukharkin N.E., Udyanskii Yu.N., Shchepetina T.D., Belov I.A., Subbotin S.A., Sedov A.A., Dudnikov A.A., Kashka M.M., Bashaev V.V.: A*dvanced nuclear power systems with micropelleted fuel for nuclear-powered ships*, Atomic Energy 99:1(2005), pp.441-445

2. Carlton J.S., Smart R., Jenkins V.: *The nuclear propulsion of merchant ships: Aspects of engineering, science and technology*, Journal of Marine Engineering & Technology, 10:2(2011), pp. 47-59

3. Crever F.E., Trocki T.: *Nuclear power plants for ship propulsion*, Electrical Engineering 73:4(1954), pp. 331-335

4. Ferreiro Garcia R., Carbia Carril J., DeMiguel Catoira A.: *Efficiency enhancement of GT-MHRs applied on ship*

MOST WIEDZY Downloaded from mostwiedzy.pl

propulsion plants, Nuclear Engineering and Design 250(2012), pp. 326-333

5. Freire L.O., de Andrade D.A.: *Historic survey on nuclear merchant ships*, Nuclear Engineering and Design 293(2015), pp. 176-186

6. Hirdaris S.E., Cheng Y.F., Shallcross P.: *Considerations on the potential use of Nuclear Small Modular Reactor (SMR) technology for merchant marine propulsion*, Ocean Engineering 79(2014), pp. 101-130

7. Jefferson M., Zhou P.L., Hindmarch G.: *Analysis by computer simulation of a combined gas turbine and steam turbine (COGAS) system for marine propulsion*, Journal of Marine Engineering & Technology 2:1(2003), pp. 43-53

8. Khlopkin N.S., Zotov A.P.: *Merchant marine nuclear-powered vessels*, Nuclear Engineering and Design 173:1-3(1997), pp. 201-205

9. Kowalczyk T., Gluch J., Ziolkowski P.: *Analysis of possible application of high-temperature nuclear reactors to contemporary large-output steam power plants on ships*, Polish Maritime Research 23:2(2016), pp. 32-41

10. *McDonald C.F.: A nuclear gas turbine perspective… the indirect cycle (IDC) offers a practical solution*, IECEC 96. Proceedings of the 31st Intersociety Energy Conversion Engineering Conference 2(1996), pp. 1029-1035

11. Mitenkov F.M.: *Prospects for applications of ship-propulsion nuclear-reactors*, Atomic Energy 76:4(1994), pp. 308-3016

12. Papkovskii B.P.: *Ship nuclear power plants (current status and future prospects)*, Atomic Energy 83:5(1997), pp. 779-782

13. Ulasevich V.K.: *Small nuclear-power-plants based on ship-propulsion nuclear-reactors*, Atomic Energy 77:6(1994), pp. 889-895

14. Witzke R.L., Haverstick S.A.: *Nuclear power plants for ship-propulsion application*, Electrical Engineering 74:2(1955), pp. 116-121

15. Zare V., Mahmoudi S.M.S.: *A thermodynamic comparison between organic Rankine and Kalina cycles for waste heat recovery from the Gas Turbine – Modular Helium Reactor*, Energy 79(2015), pp. 398-406

CONTACT WITH THE AUTHORS

Natalia Szewczuk-Krypa
Anna Grzymkowska
Jerzy Głuch

Gdańsk University of Technology
11/12 Narutowicza St.
80 - 233 Gdańsk
Poland

MOST WIEDZY Downloaded from mostwiedzy.pl

POLISH MARITIME RESEARCH Special Issue 2018 S1 (97) 2018 Vol. 25; pp. 225-233
10.2478/pomr-2018-0046

COMPARISON ANALYSIS OF BLADE LIFE CYCLES OF LAND-BASED AND OFFSHORE WIND POWER PLANTS

Andrzej Tomporowski
Izabela Piasecka
Józef Flizikowski
Robert Kasner
Weronika Kruszelnicka
Adam Mroziński
Kazimierz Bieliński
UTP University of Science and Technology, Bydgoszcz, Poland

ABSTRACT

In recent years, the offshore wind power industry has been growing dynamically. A key element which decides upon power output of a wind power plant is blades. They are most frequently produced from polymers – laminates with epoxy resins and fiberglass. In the near future, when the blade life cycles are over, large amounts of waste material of this type will have to be reused. This paper presents a comparison analysis of the impact of particular material existence cycle stages of land-based and offshore wind power plant blades on the environment. Two wind power plant blades, of about 49 m in length each, were examined using the LCA method, the programme SimaPro, and Ekowskaźnik 99 modelling (phase LCIA).

Keywords: life cycle assessment (LCA), wind power plant blades, post-consumer reuse of materials, offshore wind power plants, Ekowskaźnik 99

MOST WIEDZY Downloaded from mostwiedzy.pl

INTRODUCTION

The comparison analysis of blade life cycles of land-based and offshore wind power plants should assess, on the one hand, the amount of potential resources of waste materials of this type and, on the other hand, their systematic growth in time due to, for instance, reaching the assumed durability.

Among the available renewable energy sources, particular attention should be given to wind power plants (Haapala i inni, 2014). Year by year, the power of the installed wind power plants is steadily increasing. According to Global Wind Energy Council (GWEC) and EurObserv'ER, the total installed power capacity of wind turbines reached approximately 500 GW in year 2016 (Fig. 1) and is expected to reach nearly 800 GW in year 2020 (GWEC, 2016).

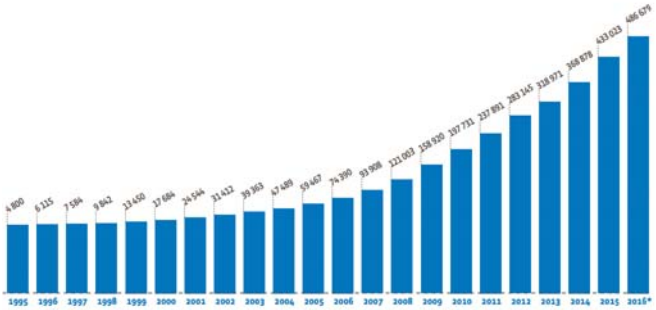

Fig. 1. Total cumulative wind power capacity installed worldwide since 1995 MW (Estimate Source: EurObserv'ER 2017)*

It is expected that, following the technological progress, the offshore wind power plants will be a significant part of

world power industry. A good example of profitable and cost-efficient investments in this area can be offshore wind farms in Europe (Denmark, UK) and North America (Breton et al., 2009).

The wind power industry is widely regarded as environment friendly, as wind energy conversion to electric power is not accompanied by emission of toxic gases nor pollutants. In year 2016, the amount of CO_2 emitted to the atmosphere exceeded 4 Gt. However, there is no technical object which is free from impact on the environment. The wind power plant existence cycle influences the environment mostly at the manufacturing stage, but also in the post-consumer reuse phase (on a landfill site or via recycling). From the point of view of environment friendly designing, an important issue is analysing the impact of the used materials on the environment and forms of their post-consumer reuse for the object to have minimal negative impact on the environment. The construction element manufacturing process itself is characterised by high power consumption. It is therefore justified to analyse the impact of wind turbine existence cycle on the environment (Davidsson et al., 2012).

Rapid development in the number of wind power plants has been a motivation for many scientists to identify environmental profits resulting from the existence of wind power plants. The life cycle analysis is a method which makes it possible to determine the impact of the existence cycle of a selected technical object on the environment. The research studies carried out to date suggest that the energy put into the wind power plant life cycle is returned after ten to twenty months of power plant operation. For offshore wind power plants this assessment is even more satisfying due to higher wind speeds and higher annual power output (Crawford, 2009).

In energy terms, it is offshore wind turbines with large areas swept by blades which are most profitable. In this context, blades can be considered a crucial element which decides upon power output of the wind power plant. Consequently, proper blade modelling and manufacturing is an important issue. A properly designed blade, of relatively small weight, makes it possible to limit requirements concerning the structure of hub and tower, which results in the decrease of wind power plant production and operation costs (Świtoński et al., 2007) (Piasecka et al., 2015).

The article aims at adopting the criteria and analysing the amount, type and potential of used materials, as well as energy consumption, at each existence stage of land-based and offshore wind power plant blades. The analysis will also include environmental profits and expenditures, and harmful actions of dominating life cycle areas/phases of the adopted blade structures.

STRUCTURE OF LAND-BASED AND OFFSHORE WIND POWER PLANT BLADE

Due to the performed function and operating conditions, the blades of an offshore wind power plant should have small weight, high durability, and resistance to changing atmospheric conditions and corrosion. Therefore, of high importance is proper selection of construction materials for blades and their structure, which will then affect the way of post-consumer reuse of elements and materials composing the blade (Shokrieh et al., 2010), (Kong et al., 2005), (Świtoński et al., 2007).

A typical wind power plant blade consists of three components, which are: outer shell, vertical spars, and root joint (Fig. 2) (Shokrieh et al., 2010).

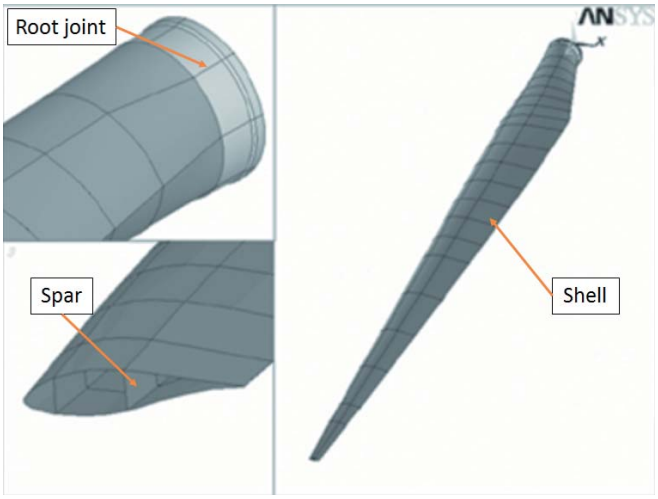

Fig. 2. Basic structural components of wind power plant blade (Shokrieh et al., 2010)

Blades of commercial wind power plants are made of composite materials (laminates), balsa wood, and steel. Each blade component plays different function and is made of different construction materials. The outer shell is produced from composites, plastics and balsa wood, using the lamination method. The core of the laminate is made of balsa or polyvinyl chloride (PVC) and fiberglass, while epoxide, polyester, or vinyl ester resins are used as warp. These materials are relatively light and robust, which provides good opportunity for maximal use of the lift generated on the blades. The blade surface is protected using gelcoats and polyurethanes. Protecting layers for offshore wind turbine blades are thicker than those for land-based turbine blades, due to the nature of marine environment (high humidity, salinity) which contributes to weakening of outer shells. Front blade edges are covered with thermoplastic foils or special paints. Figure 3 shows the blade structure cross section, with marked elements made of composites (Shokrieh et al., 2010), (Xiaohui et al., 2013) (Composite recycling: Characterizing end of life wind turbine blade material, 2014) (Kasner et al., 2015) (Kong et al., 2005).

MOST WIEDZY Downloaded from mostwiedzy.pl

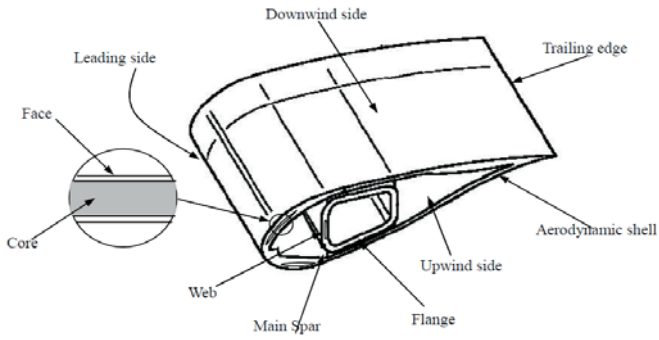

Fig. 3. Wind power plant blade structure (cross section) (Xiaohui, et al., 2013)

The task of the wind turbine suspension tower is to carry forces and stresses coming from different sources, therefore it is constructed from durable laminate composites made of carbon fibre and fiberglass, as well as resins (most frequently epoxy resins) (Composite recycling: Characterizing end of life wind turbine blade material, 2014) (Shokrieh et al., 2010).

The part fixing the blade to the hub, i.e. the root joint, is made of steel. It has holes for fixing screws. This part is covered from inside and outside with laminates to protect it against the action of corrosive agents. In new blade designs, root joints are rarely made of steel. Like other elements, they are made of composites. Fiberglass reinforced polymers constitute about two thirds of the entire mass of the wind turbine (Shokrieh et al., 2010) (Composite recycling: Characterizing end of life wind turbine blade material, 2014) (Xiaohui et al., 2013).

WIND TURBINE BLADE EXISTENCE CYCLE

In the existence cycle of each technical object, including wind power plant blades, five basic stages can be named: expressing the need (NE), designing/constructing (C), manufacturing (M), exploitation (E) and post-consumer reuse/disposal (D). At each stage the object performs different tasks to meet the initially formulated goals (Legutko, 2007) (Thomson et al., 2015). Figure 4 shows a scheme of the wind power plant blade existence cycle.

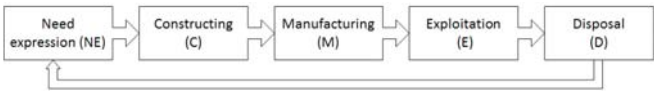

Fig. 4. Phases of wind power plant blade existence cycle (own elaboration)

The first stage of blade existence cycle consists in expressing the need. It should be expressed in such a way that methods of its fulfilling are not suggested a priori. The next stage is blade constructing/designing. At this stage, requirements concerning blade strength, principle of operation and relations between structural elements are defined, and construction materials selected. As early as at this stage, selection of construction materials should take into account future post-consumer reuse of materials and elements. The manufacturing stage, in turn, consists in production of wind power plant rotor blades with required features and the resultant utility potential predicted in the project. This stage includes actions oriented on designing technological processes and organisation of production processes, as well as material production of elements. The next stage, exploitation, is considered most important in the blade existence cycle. In that time, the blades perform functions for which they were designed and manufactured. The blade exploitation time is usually 20-25 years, during which they are subject to many exploitation processes, such as surface maintenance, and service and repairs resulting from harmful action of the environment on construction materials (especially in marine environment). In cases when large cracks are detected on blade surface, the blade is to be replaced by a new one (Composite recycling: Characterizing end of life wind turbine blade material, 2014).

The last, and simultaneously most problematic stage of wind power plant blade existence is disposal/post-consumer reuse. For some time, it was not mentioned as a separate phase in the existence cycle. The problem of post-consumer reuse should be taken into account at the stages of constructing, manufacturing and exploitation. From the point of view of rationalisation of material and energy use, the most appropriate approach is reuse of elements as a whole, or their processing. A number of possible ways of post-consumer reuse of wind turbine blades were worked out, including reuse of compete blades, recovery of materials and components, energy recovery, use of fragmented composite materials as fillers, and landfill storage (Composite recycling: Characterizing end of life wind turbine blade material, 2014). A systematised division of post-consumer reuse methods for materials composing wind power plant blades is given in Fig. 5.

The first form can be reuse of complete wind turbine blades, after their earlier regeneration. Solutions of this type were applied in many European countries with respect to relatively short blades. The regenerated blades were mounted in turbines with powers ranging from 10 kW to 1 MW, which radically decreased their cost.

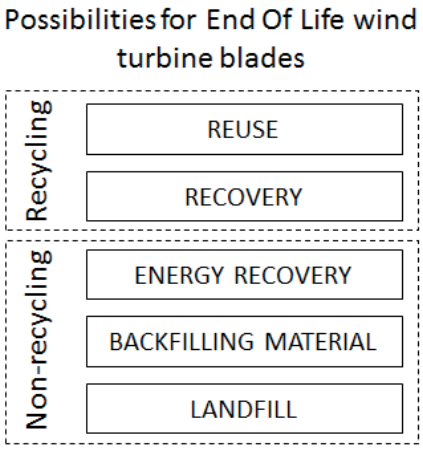

Fig. 5. Ways of post-consumer reuse of wind power plant blades (own elaboration)

MOST WIEDZY Downloaded from mostwiedzy.pl

Turbine regeneration procedures can include: visual and ultrasound diagnosis of blade condition, repainting, repair and balancing. They can also take into account recovery of materials and entire blade elements with their further reuse (without processing) in new blade constructions (Composite recycling: Characterizing end of life wind turbine blade material, 2014).

Another way of post-consumer reuse of materials coming from wind power plant blades can be recovery of energy contained in the structure of polymers. The energy recovery can take a form of combustion or co-combustion of polymers in high temperature, for instance in cement kilns (this solution was introduced by the German company Holcim). In this case, fragmented blades are introduced to the cement kiln and burnt. However, burning fiberglass in this way is difficult. The last method of post-consumer reuse is blade storage in a landfill. From the point of view of rational use of raw materials and post-consumer reuse of materials, this form is least profitable, as it does not make use of material and energy potentials contained in composites (Composite recycling: Characterizing end of life wind turbine blade material, 2014).

METHODOLOGY OF EXAMINATION

The objects of examination were two wind turbine blades, of about 49 m in length each, made of material being a combination of polymers with carbon fibre and fiberglass, and laminated using the pre-preg type production process. The first examined blade had been a component of land-based wind power plant rotor, while the second one – of an offshore wind power plant (producers' data).

The examination was performed using the LCA method and the software SimaPro 7.1. The LCA method makes it possible to assess the impact of the technical object existence cycle on the environment. The analysis covers the entire life cycle, taking into account its consecutive stages. The assessment is based on the information concerning the amounts and types of materials used at each existence cycle stage and the data concerning energy consumption. Environmental impacts and harmful actions have the form of numbers, which makes it possible to identify dominating life cycle areas. This model can be used by a producer for structural modernisation or improvement of the product. It can also be helpful for designers who have to choose an individual construction solution (Piasecka et al., 2015). Figure 6 shows possibilities of use of the LCA methodology to assess the environmental impact of wind power plant blade life cycle.

The LCA method-based assessment was done in accordance with the standard ISO 14000 and consisted of four consecutive basic steps: expressing goal and range, analysing the set of inputs and outputs (LCI), assessing the impact (LCIA), and interpretation.

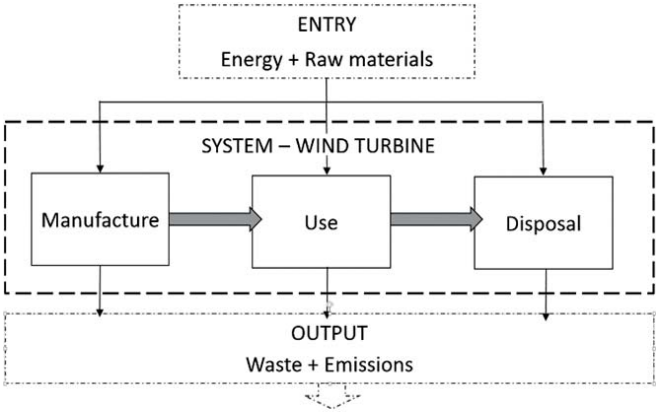

Fig. 6. Scheme of relations with environment, taking into account flow of raw materials and elements composing the wind turbine blade system in LCA method (own elaboration)

The LCIA phase made use of Ekowskaźnik 99 modelling. The analysis was iterative by nature and was characterised by numerous feedbacks. After each analytical step, current interpretation of the obtained pieces of information was performed. In the paper, the comparison analysis of two objects is presented, which were the land-based wind power plant blade and the offshore wind power plant blade. The basic goal of the analysis was describing the existing reality (retrospective LCA), but it also included modelling of future changes and formulating recommendations for working out more pro-environmental solutions (prospective LCA). The applied procedure has the character of classical LCA process examination. The starting point for the analysis was the thesis that blades of land-based wind power plants generate smaller negative impact on the environment that those of offshore wind power plants (which have to be more robust and resistant to the action of aggressive marine environment).

The majority of processes executed within the analysed blade life cycle stages (constructing, manufacturing, exploitation, and post-consumer reuse) take place in Europe. Since the performed LCA analysis in comparative by nature, the systems of analysed products were arranged in a comparable manner with respect to the depth and width of the analysis, as well as the data quality. The basic assumption of the analysis is presenting differences in the scale of impact on the environment, which mainly result from changes in production and materials used for blades. The geographical range and time interval of the data are the same, while the technological ranges are different. The geographical range is European-wide, which results from the fact that companies being data providers have very strong position on the entire European market. Part of data, especially those concerning the place of manufacturing, had specific, local nature related to a given source. On the other hand, taking into account European-wide sales range, the exploitation and post-consumer reuse can be executed on the entire European territory and the data and recommendations concerning these blade life cycle stages are continent-wide. The time interval covers the same 25 years of exploitation. From the

MOST WIEDZY Downloaded from mostwiedzy.pl

spatial point of view, no significant effects are observed, therefore the same place of manufacturing is assumed, but different technologies which lead to manufacturing of blades with different parameters for land-based and offshore applications.

All limitations and exclusions were done simultaneously for all product systems. The analysis neglected stages of blade storage, sales and distribution of both examined blades. As a result, product systems were uniformly loaded with the same simplifications, which introduced a similar level of uncertainty. The exclusion criterion was below 0,01% of participation, both at the level of entire life cycle, and contribution to environmental impact at the level of a given stage of life cycle of both examined blades. The performed analysis can be qualified as *bottom-up* type analysis. The planned analysis advancement level places it among detailed analyses. The term "manufacturing" is understood in the paper as all processes related with blade production, its individual materials and components and, wherever possible, processes reaching the elementary streams (raw material mining and final emission to the environment). The LCI results for stages of manufacturing, exploitation, and post-consumer reuse will be the object of complete LCA assessment, including the assessment of LCIA impact. The data used in the analysis were obtained from blade producers or taken from programme SimaPro 7.1 databases.

RESULTS AND THEIR ANALYSIS

The paper presents solely the results obtained for the grouping and weighting phases. A characteristic feature of the used method Ekowskaźnik 99 is possibility to present the obtained results as environmental points (Pt). A thousand of environmental points corresponds to the impact of one European on the environment during one year. The object of analysis was the range of negative environmental after-effects generated during one life cycle, or during its individual stages, for one land-based wind turbine blade and one offshore wind turbine blade, taking into account three impact areas, eleven impact categories, and three emission areas.

The life cycle of the offshore wind power plant blade has higher level of negative impact on the environment. The total number of environmental points is equal to 3688 Pt for post-consumer reuse in the form of landfill storage, and 1258 Pt for recycling. For both blade types, the life cycle taking into account recycling processes generates a smaller number of negative environmental after-effects (Fig. 7).

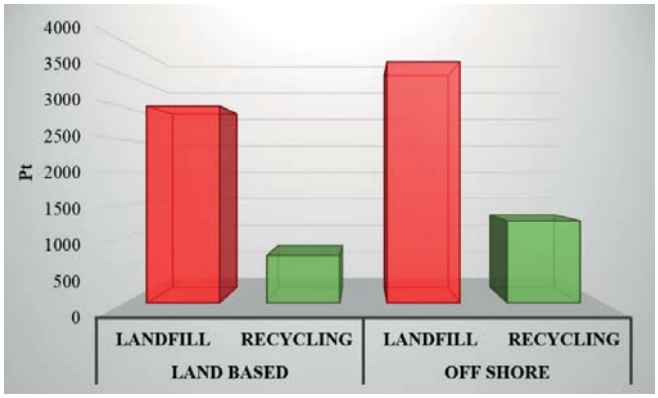

Fig. 7. Results of grouping and weighting of environmental after-effects in one material existence cycle of wind power plant blades, taking into account possibility of their post-consumer reuse [own research]

Larger number of negative environmental after-effects in the existence cycle of offshore wind power plant blade is mainly caused by higher level of harmful substance emissions at the manufacturing stage, which amounted to 2669 Pt. In the remaining existence cycle stages of both blade types, no significant differences in total level of environmental impact were observed (Fig. 8).

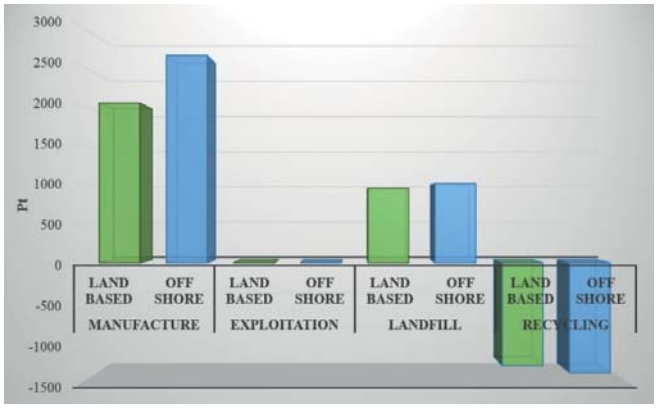

Fig. 8. Results of grouping and weighting of environmental after-effects in consecutive stages of material existence cycle of wind power plant blades, taking into account possibility of their post-consumer reuse [own research]

The list of substances and processes causing the largest number of negative environmental after-effects in consecutive stages of material existence cycle of land-based and offshore wind power plant blades includes emission of cadmium ions, nitrogen oxide, sulphur dioxide, arsenic, dinitrogen oxide, cuprum ions, and particles of up to 10 μm in size (Table 1).

Tab. 1. Results of grouping and weighting of substances and processes causing the largest number of negative environmental after-effects in consecutive stages of material existence cycle of wind power plant blades, taking into account possibility of their post-consumer reuse [own research]

Substance	Compartment	Manufacture		Exploitation		Landfill		Recycling	
		Land-based	Off shore	Land-based	Off shore	Land-based	Off shore	Land-based	Off shore
Cadmium, ion	Water	2,236	2,814	0,000	0,000	869,570	925,761	0,173	0,190

MOST WIEDZY Downloaded from mostwiedzy.pl

Substance	Compartment	Manufacture		Exploitation		Landfill		Recycling	
		Land-based	Off shore	Land-based	Off shore	Land-based	Off shore	Land-based	Off shore
Gas, natural, in ground	Raw	680,518	725,142	0,003	0,003	0,680	0,720	0,000	0,000
Oil, crude, in ground	Raw	474,997	506,145	0,002	0,002	5,480	5,807	0,000	0,000
Nitrogen oxides	Air	128,227	143,172	0,000	0,001	1,592	1,686	-86,649	-92,205
Carbon dioxide, fossil	Air	112,879	120,281	0,000	0,000	0,991	1,052	0,000	0,000
Sulphur dioxide	Air	104,057	105,935	0,000	0,000	0,200	0,211	0,000	0,000
Cadmium	Air	98,680	106,113	0,000	0,000	0,030	0,031	0,236	0,264
Particulates, < 2.5 µm	Air	76,632	81,657	0,000	0,000	1,012	1,071	0,000	0,000
Arsenic	Air	53,632	57,323	0,000	0,000	0,004	0,004	0,000	0,000
Particulates, > 2.5 µm, and < 10µm	Air	50,325	53,625	0,000	0,000	0,135	0,143	0,000	0,000
Dinitrogen monoxide	Air	45,204	48,299	0,000	0,000	0,012	0,012	0,115	0,123
Arsenic, ion	Water	25,649	33,426	0,000	0,000	19,173	20,388	8,782	9,546
Copper, ion	Water	0,648	0,806	0,000	0,000	28,822	30,180	0,127	0,139
Nickel	Air	16,271	32,583	0,000	0,000	0,017	0,018	4,318	4,629
Methane, fossil	Air	8,245	8,785	0,000	0,000	1,791	1,904	0,000	0,000

The majority of negative after-effects generated in the manufacturing stage of both land-based and offshore wind power plant blades leads to deterioration of human health, decrease of environmental quality, and depletion of fossil resources. Storage of blades which cannot be further exploited poses a significant threat to health (land-based blade: 896 Pt, offshore blade: 954 Pt). Post-consumer reuse of plastics, and other materials and elements of blades of both types in the form of recycling would make it possible to reduce significantly negative impacts concerning depletion of fossil resources (land-based blade: -1256 Pt, offshore blade: -1338 Pt) (Fig. 9).

In the cases of compounds leading to deterioration of human health, the highest level of harmful emissions at the manufacturing stage for both blade types is recorded for inorganic substances causing respiratory diseases (land-based blade: 370 Pt, offshore blade: 697 Pt). During landfill storage of blades, in turn, many harmful carcinogens may penetrate to the environment (land-based blade: 889 Pt, offshore blade: 946 Pt) (Fig. 10).

Quality decrease of natural environment is mainly caused by emissions of ecotoxic substances, the largest amounts of which are created at the manufacturing stage (land-based blade: 64 Pt, offshore blade: 91 Pt) and the landfill storage stage (land-based blade: 54 Pt, offshore blade: 57 Pt) (Fig. 11).

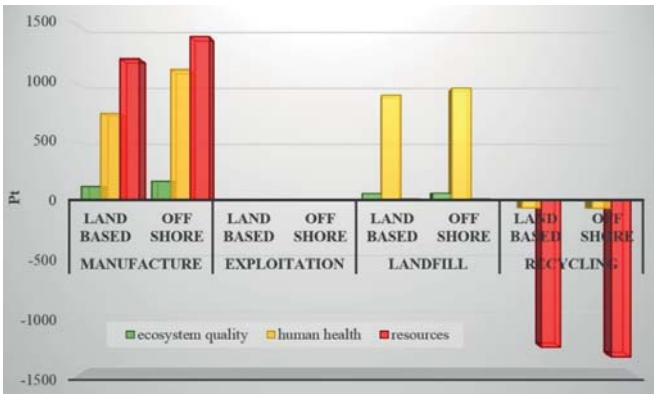

Fig. 9. Results of grouping and weighting of environmental after-effects for three areas of impact, in consecutive stages of material existence cycle of wind power plant blades, taking into account possibility of their post-consumer reuse [own research]

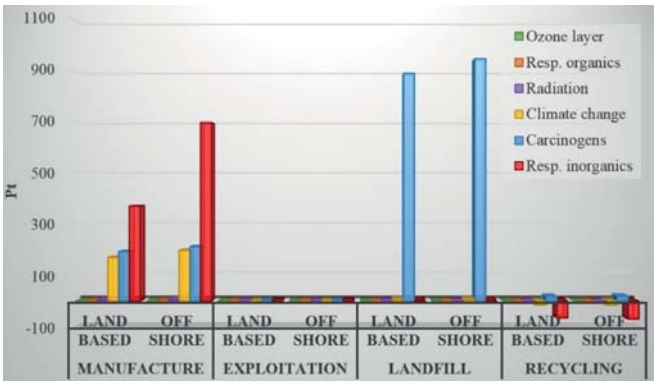

Fig. 10. Results of grouping and weighting of emissions leading to deterioration of human health, in consecutive stages of material existence cycle of wind power plant blades, taking into account possibility of their post-consumer reuse [own research]

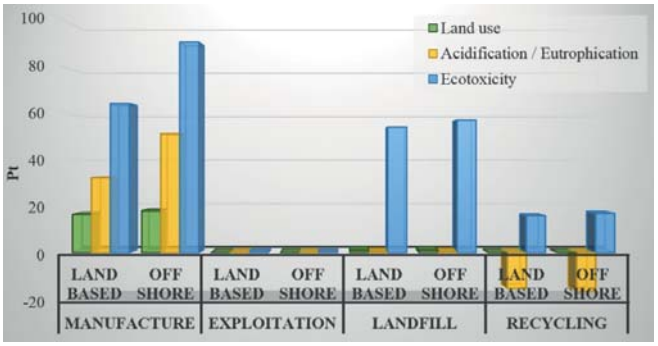

Fig. 11. Results of grouping and weighting of processes and emissions leading to the decrease of environmental quality, in consecutive stages of material existence cycle of wind power plant blades, taking into account possibility of their post-consumer reuse [own research]

As far as processes affecting depletion of fossil resources are concerned, the highest level of negative environmental afters-effects is recorded for the category of processes related with mining of fossil fuels (mainly crude oil), at the manufacturing stage (land-based blade: 1178 Pt, offshore blade: 1321 Pt). The post-consumer reuse in the form of recycling would limit

MOST WIEDZY Downloaded from mostwiedzy.pl

the harmful impact in the analysed range by 1256 Pt for land-based blade and by 1337 Pt for offshore blade (Fig. 12).

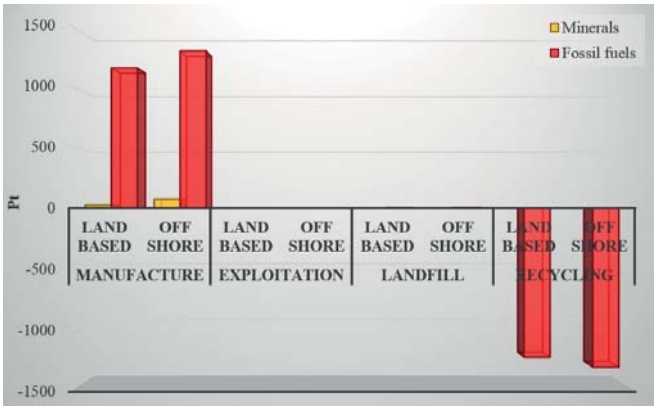

Fig. 12. Results of grouping and weighting of processes leading to depletion of fossil resources, in consecutive stages of material existence cycle of wind power plant blades, taking into account possibility of their post-consumer reuse [own research]

Taking into account three main areas of emissions of compounds having negative environmental effect, the highest level of harmful impacts for the land-based wind power plant blade life cycle was recorded in the case of emission to water environment, while for the offshore blade life cycle – in the case of emission to the atmospheric environment. The post-consumer reuse of plastics, and other materials and elements of both blade types in the form of recycling would limit radically the emission of harmful substances to the water environment (by about 75-80%) (Fig. 13).

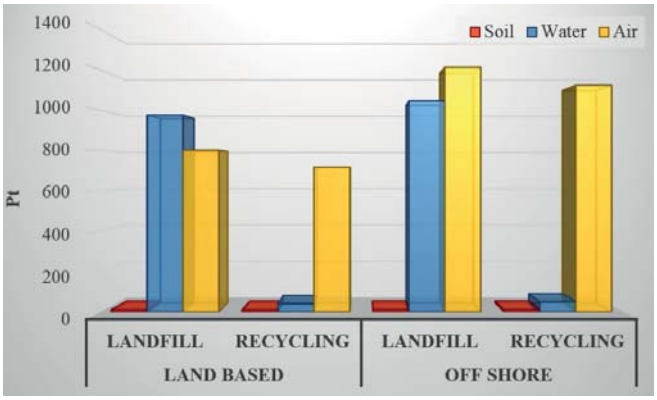

Fig. 13. Results of grouping and weighting for three areas of emission, in material existence cycle of wind power plant blades, taking into account possibility of their post-consumer reuse [own research]

The highest level of emissions of harmful substances to the atmosphere was recorded at the manufacturing stage (land-based blade: 793 Pt, offshore blade: 1204 Pt), while to the water environment – at the landfill storage stage (land-based blade: 943 Pt, offshore blade: 1003 Pt) (Fig. 14).

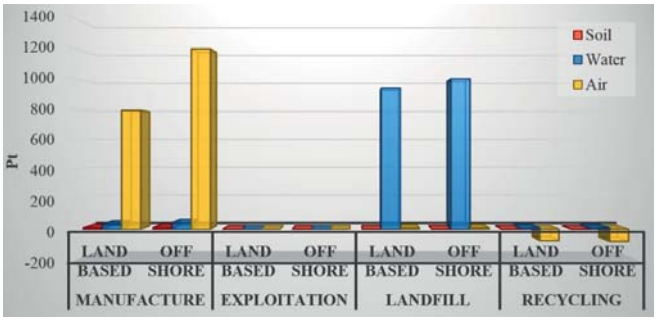

Fig. 14. Results of grouping and weighting for three areas of emission, in consecutive stages of material existence cycle of wind power plant blades, taking into account possibility of their post-consumer reuse [own research]

SUMMARY AND CONCLUSIONS

Year by year, growing interest is being observed in renewable energy sources, including wind energy (of both land-based and offshore type). Each power plant affects somehow the environment, bout not to the same extent. The element of a wind power plant which has a key impact on the plant's power output, but also causes most problems with post-consumer reuse, are rotor blades. In the modern world, growing attention is paid to eco-designing which aims at reducing negative environmental impact of a given object during its entire life cycle – from construction, though exploitation, until post-consumer reuse. A tool for environment friendly designing is *Life Cycle Assessment* (LCA).

The main goal of the paper was achieved through performing a comparison analysis of material existence cycle stages for land-based and offshore wind power plant blades.

Higher level of harmful impacts on the environment was recorded for the life cycle of offshore wind power plant blade. For both blade types, the life cycle taking into account recycling processes had smaller negative environmental impact. The greatest number of negative environmental after-effects in the existence cycles of both blade types was mainly caused by very high level of emissions of harmful substances at the manufacturing stage. The list of substances which have the highest harmful impact on the environment in the wind power plant blade existence cycle includes, among others, cadmium, nitrogen oxide, carbon dioxide, sulphur dioxide, arsenic, dinitrogen oxide, cuprum, and particles of up to 10 μm in size.

The manufacturing stage is a source of the majority of negative impacts in each of the analysed impact areas. In the case of substances leading to the deterioration of human health, the highest level of harmful emissions was recorded for inorganic substances causing respiratory diseases. The decrease of environmental quality, in turn, was mostly affected by emissions of ecotoxic substances. Within the range of processes leading to depletion of fossil resources, the highest level of negative environmental after-effects was

MOST WIEDZY Downloaded from mostwiedzy.pl

recorded for the category of processes related with mining of fossil fuels (mainly crude oil).

For the life cycle of land-based wind power plant blade, the highest level of harmful impact was recorded in the case of emission to the water environment, while for offshore blade – to the atmospheric environment. Most of harmful substances are emitted to the atmosphere at the manufacturing stage, while to the water environment - at the landfill storage stage.

Based on the performed research, it is postulated to:

- reduce the negative environmental impact of the manufacturing process, being the existence cycle stage of highest negative impact to human health, environmental quality, and depletion of fossil resources, through introducing modern technologies with lower energy and material consumption, and lower emission of harmful substances;
- create the best possible pro-environmental algorithm of management for plastics, and other materials and elements of wind power plant blades after the end of their exploitation, taking into account in particular recycling processes;
- work upon more pro-environmental construction materials, which will simultaneously preserve relevant technical, mechanical and quality parameters needed for playing certain roles in wind power plant elements;
- design a structure which would enable simpler segregation of individual materials and their easier identification for post-consumer reuse,
- work out comprehensive, pro-environmental standards concerning methods of post-consumer reuse of plastics, and other materials and elements of wind power plant blades.

BIBLIOGRAPHY

1. Breton, S. P. and Moe, G. 2009.Status, plans and technologies for offshore wind turbines. Renewable Energy. 2009, Tom 34.

2. Composite recycling: Characterizing end of life wind turbine blade material. Beauson, J., Bech, J. I. i Brøndsted, P. 2014. Montréal, Canada : 19th International Conference on Composite Materials, 28.07-02.08.2013, Montréal, Canada, 2014. Proceedings of 19th International Conference on Composite Materials.

3. Crawford, R. H. 2009. Life cycle energy and greenhouse emissions analysis of wind turbines and the effect of size on energy yield. Renewable and Sustainable Energy Reviews. 2009, Tom 13.

4. Davidsson, S., Höök, M. and Wall, G. 2012. A review of life cycle assessments on wind energy systems. Int J Life Cycle Assess. 2012, Tom 17.

5. GWEC. 2016.Global Wind Report. Annual Market Update 2015. Bruksela : Global Wind Energy Council, 2016.

6. Haapala, K. R. and Prempreeda, P. 2014.Comparative life cycle assessment of 2.0 MW wind turbines. Int. J. Sustainable Manufacturing,. 2014, Tom 3, 2.

7. Kasner, R., et al. 2015. Zastosowanie metody CML do oceny wpływu na środowisko wybranych środków transportu łopat elektrowni wiatrowych. Logistyka. 2015, 3.

8. Kong, C., Bang, J. and Sugiyama, Y. 2005. Structural investigation of composite wind turbine blade considering various load cases and fatigue life. Energy. 2005, Tom 30.

9. Martinez, E., et al. 2009. Life cycle assessment of a multi-megawatt wind turbine. Renewable Energy. 2009, Tom 34.

10. Piasecka, I. and Mroziński, A. 2015. Selected aspects of building , operation and environmental impact of offshore wind power electric plants. Polish Maritime Research. 2015, Tom 22, 2.

11. Shokrieh, M. M. and Rafiee, R. 2010. Fatigue life prediction of wind turbine rotor blades manufactured from composites. [aut. książki] Vassilopoulos i P. Anastasios . Fatigue Life Prediction of Composites and Composite Structures. Oxford : Woodhead Publishing, 2010.

12. Świtoński, E., Jureczko, M. and Mężyk, A. 2007. Optymalne projektowanie kompozytowych łopat elektrowni wiatrowej. Acta Mechanica et Automatica. 2007, Tom 1, 1.

13. Thomson, R. C. and Harrison, G. P. 2015.Life Cycle Costs and Carbon Emissions of Offshore Wind Power. brak miejsca : ClimateXChange, 2015.

14. Xiaohui, D., Tiejun, Y. and Ruhong, M. 2013. Corrosion Mechanism on Offshore Wind Turbine Blade in Salt Fog Environment. Applied Mechanics and Materials. Vol. 432, 2013, pp 258-262.

MOST WIEDZY Downloaded from mostwiedzy.pl

CONTACT WITH THE AUTHORS

Andrzej Tomporowski
Izabela Piasecka
Józef Flizikowski
Robert Kasner
Weronika Kruszelnicka
Adam Mroziński

Department of Technical Systems
Institute for Production Techniques
Faculty of Mechanical Engineering
UTP University of Science and Technology
Al. Prof. S. Kaliskiego 7
85-796 Bydgoszcz
Poland

Kazimierz Bieliński

Department of Electrical Power Engineering
Institute for Electrical Engineering
Faculty of Chemical Technology and Engineering
UTP University of Science and Technology
Al. Prof. S. Kaliskiego 7
85-796 Bydgoszcz
Poland

MOST WIEDZY Downloaded from mostwiedzy.pl

POLISH MARITIME RESEARCH Special Issue 2018 S1 (97) 2018 Vol. 25; pp. 234-242
10.2478/pomr-2018-0047

RANKING OF TOXIC COMPOUND CONCENTRATIONS AS DIAGNOSTIC PARAMEETRS OF MARINE INTERNAL COMBUSTION ENGINE

Ryszard Zadrąg
Tomasz Kniaziewicz
Polish Naval Academy, Gdynia, Poland

ABSTRACT

Changing selected engine structure parameters, especially fuel system parameters, affects the emission of harmful compounds in the exhaust gas. Changes in harmful compound emission are frequently ambiguous, as they highly depend on parameters controlling the combustion process. An additional problem is that simple interactions are frequently accompanied with mutual influence of these parameters. Therefore, we can say about different sensitivity of diagnostic parameters to the same excitations coming from the engine structure but executed at different loading states. When the set of diagnostic parameters is numerous and the values of these parameters are similar, there is a real problem with their correct classification, frequently based on subjective assessment by the analyst. In the article, the authors propose a methodology to classify the recorded diagnostic parameters. In earlier works by the authors [4,6,7], the information capacity index method (the Hellwig method) was proposed as the measure of diagnostic parameter sensitivity. Based on this method, a rankling of diagnostic parameters can be created which divides the set of diagnostic variables into stimulators and destimulators. Novel authors' approach to the presented problem consists in including nominants, i.e. variables with the most favourable value for the analysed aspect of the research, in the set of diagnostic variables. This normalisation of the set is believed to be helpful for making a diagnostic decision free from analyst's arbitrariness. The zero unitarization method can also be helpful in creating diagnostic tests.

Keywords: diagnostic model, Diesel engine, exhaust components, ranking of parameters

INTRODUCTION

Transient states are special states in internal combustion engine operation, as they interfere into thermodynamic equilibrium of the cylinder, reached during steady engine load periods. This affects the course of the combustion process by, first of all, transient changes of the flow of fresh charge delivered to the cylinder, but also by changing the rate of the delivered fuel. Thus, the fuel/air ratio changes temporarily, which results in changes in the excess air number and, consequently, increased emission of combustion products created at local oxygen deficit. Further consequence of the appearance of the increased volume of CO and unburned hydrocarbons HC is the decrease of the combustion temperature, which decides upon reduction in emission of nitrogen oxides NO_x.

Thus, the decisive factor for the amounts of toxic compounds emitted in transient states is the scale of excitations provoking these states. However, an additional factor which also should be taken into account is technical condition of the engine. This condition, described by engine structure parameters, is subject to permanent changes during engine operation, and it is wear processes which are responsible for this. The increasing engine wear intensifies changes in the creation of toxic compounds during transient states, as those processes, although short-lasting, are so dynamic in their nature that instantaneous concentrations of toxic compounds exceed the steady-state levels by many times. Consequently, we may

MOST WIEDZY Downloaded from mostwiedzy.pl

expect that the engine with structure parameters changed due to wear will be more sensitive to the action of transient states and thus determining its technical condition will be easier. However, a problem arises how to identify unambiguously the sensitivity of diagnostic parameters, and not only the parameters alone. This problem gains in importance in cases of large amount of research material and/or high variability of transient state courses. The abovementioned sensitivity of the diagnostic parameter can be defined as information capacity, and its value can be used for selecting parameters which best describe the analysed phenomenon [4,6,7].

A basic parameter which decides upon the correctness of the combustion process in Diesel engines is the fuel injection timing. Even small deviations of this parameter result in significant changes of basic engine operation parameters, including exhaust gas emission indicators. In classical engine constructions, self-acting change of fuel injection timing is highly unlikely to occur. However, in modern constructions, in which the majority of control parameters is controlled electronically, a situation can occur which will lead to damage of the control system, with the resultant change of fuel injection timing.

The present work is continuation of the issues analysed by the authors in [6,7]. Here, the authors' attention was focused on defining and analysing the information capacity of the diagnostic parameter, which is, as already mentioned, a set of coefficients and characteristics of exhaust gas component emission.

EXAMINING INFORMATION CAPACITY INDICES OF TOXIC COMPOUND CONCENTRATIONS DURING DYNAMIC PROCESSES

The object of examination was the fuel supply system (the fuel injection timing) of a single-cylinder test engine 1-SB installed at the Laboratory of Power Plan Operation, Polish Naval Academy [5]. The experimental material was collected based on a trivalent complete test plan. According to the test plan, measurements in individual systems (measuring points) were performed using a programmable controller, which made it possible to reach high repeatability of dynamic processes. The dynamic process duration time was assumed equal to the time between the beginning of parameter change in injection system elements and new stabilisation of output parameters. This time was selected experimentally as approximately equal to 106 sec.

To identify the effect of technical condition of the fuel supply system on energy parameters of the engine during dynamic processes, sets of input quantities (asked parameters) and output quantities (observed parameters) were defined.

For the purpose of present work, the set of input quantities X was limited to three elements, which were: x_1 – engine rotation speed n [rpm]; x_2 – engine torque T_{tq} [N·m]; x_3 – fuel injection timing α_{ww} [°OWK]. The analysis was performed in accordance with the adopted complete plan for three rotational speeds equal to: 850, 950 and 1100 [rpm]. For each rotational speed, the torque T_{tq} was increased to the load of 10, 20, 30, 50 and 70 [Nm], thus generating subsequent transient states. For the rotational speed of 850 rpm, the loads of 50 and 70 Nm were abandoned to avoid significant engine overload. The same was done for the rotational speed of 950 rpm and load of 70 Nm. The fuel injection timing was changed by o ±5°OWK, thus obtaining three values, i.e. nominal timing N, advanced timing W, and delayed timing P. This way 36 repeatable transient states were obtained. The functional model of the examined object is schematically shown in Fig. 1.

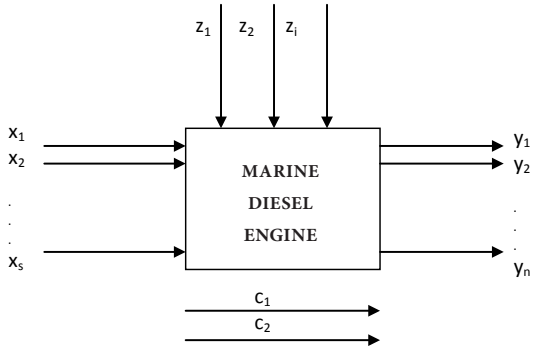

Fig. 1. Quantities characterising the examined object: x – input quantities, y – output quantities, z disturbances, c – constants

A similar procedure was applied to the set of output quantities Y limiting the number of its elements only to basic toxic compounds in the exhaust manifold: y_1 – carbon oxide concentration in the exhaust manifold C_{CO} [ppm]; y_2 – hydrocarbon concentration in the exhaust manifold C_{HC} [ppm]; y_3 – nitrogen oxide concentration in the exhaust manifold C_{NOx} [ppm], y_4 – exhaust gas temperature t_{sp} [°C], y_5 – excess air number λ.

The detailed analysis of dynamic processes was performed using the data measured during an active experiment and the multi-equation model created based on these data [5]. Both the empirical and model data underwent statistical identification. Equation coefficients of particular output variables were estimated using the least-squares method. The estimation aimed at verifying the significance of parameters and resultant rejection of quantities of minor significance. All this has finally led to significant simplification of the models. The Pearson correlation coefficient was assumed the measure of strength and direction of correlation between examined variables (Y, X).

The correlation coefficients between the variable Y and variables X_k compose the correlation coefficient vector $\mathbf{R_0}$, while the correlation coefficients between individual explanatory variables (X_k, Y_s) compose the correlation coefficient matrix $\mathbf{R}$ having the form (1):

$$\boldsymbol{R_0} = \begin{bmatrix} r_{yx_1} \\ r_{yx_2} \\ \vdots \\ r_{yx_K} \end{bmatrix}_{K\times 1}, \boldsymbol{R} = \begin{bmatrix} r_{x_1x_1} & r_{x_1x_2} & \cdots & r_{x_1x_K} \\ r_{x_2x_1} & r_{x_1x_2} & \cdots & r_{x_2x_K} \\ \vdots & \vdots & \ddots & \vdots \\ r_{x_Kx_1} & r_{x_Kx_2} & \cdots & r_{x_Kx_K} \end{bmatrix}_{K\times K} \quad (1)$$

MOST WIEDZY Downloaded from mostwiedzy.pl

The presented analysis of the obtained results reveals a great advantage of multi-equation models, which is a possibility of multi-criteria analysis of output quantities when they are mutually corelated. However, despite their clear advantages, multi-equation models do not provide directly the information on the quality of changes, i.e. in the analysed case: concentration changes of individual toxic compounds resulting from the change of fuel injection timing. Only combining together transient courses which were experimentally recorded or obtained from the model analysis brings some picture of the phenomenon. Individual relations, along with examination of model fitting to the values obtained from the experiment performed on the engine, are described in detail in [3,4,5].

As already mentioned, the concentrations of individual toxic compounds in transient states reveal some regularity and repeatability. However, this does not make the analysis easier, due to high similarity of all transient states, regardless of the values of applied excitations. Therefore, a method was to be found which would be able to describe as precisely and objectively as possible the nature of changes of individual concentrations of toxic compounds. This method is believed to consist in analysing correlations of individual transient states. In this method, the correlation of the examined transient state with that assumed as the reference pattern for the analysed phenomenon is assessed. The correlation function analysis makes it possible to determine the degree and nature of the correlation. After analysing function components, we may conclude about the abovementioned nature of the transient state, i.e. about the presence and intensity of its individual phases.

A method to select explanatory variables for the model (input quantities for the test plan) based on correlation coefficient values is the information capacity index method (the Hellwig method) [6,7]. This method consists in selecting a combination of variables for which the information capacity is the greatest. The information carriers in that case are all possible explanatory variables. The arrangement of the test plan imposes a number of possible combinations. In the analysed case, for the three assumed input quantities, $K = 3$ (x_1 – engine rotation speed n [rpm]; x_2 – engine torque T_{tq} [N·m]; x_3 – fuel injection timing α_{ww} [°OWK]), the number of possible combinations is:

$$L(K) = 2^K - 1 \tag{2}$$

This way, for each dependent (output) value the following combinations exist:

- single-element combinations: $C_1 = \{X_1\}$, $C_2 = \{X_2\}$, $C_3 = \{X_3\}$,
- two-element combinations: $C_4 = \{X_1, X_2\}$, $C_5 = \{X_1, X_3\}$, $C_6 = \{X_2, X_3\}$,
- three-element combinations: $C_7 = \{X_1, X_2, X_3\}$.

For each above defined combination, the individual information capacity index h_{mx_k} is calculated for variable X_k in m-th combination of variables:

$$h_{mx_k} = \frac{r_{yx_k}^2}{1 + \sum_{\substack{k,s \epsilon K_m \\ k \neq s}} |r_{x_k x_s}|} \tag{3}$$

where:

r_{yx_k} – correlation coefficient between dependent variable Y and explanatory variable X_k (correlation coefficient matrix $\mathbf{R}_0$),

$r_{x_k x_s}$ – correlation coefficient between explanatory variables (correlation coefficient matrix $\mathbf{R}$),

m – number of combination,

k – number of explanatory variable X_k for which the individual information capacity index h_{mx_k} is calculated.

The next step in the Hellwig analysis is calculating the integral information capacity index H_m for each combination

$$H_m = \sum_{k \epsilon K} h_{mx_k} \tag{4}$$

The highest value of this index is the criterion for selecting relevant combination of explanatory variables. Indeed, taking into account the goal of analysis, which was sensitivity identification of diagnostic parameters, i.e. concentrations of individual exhaust gas components, to changes of the structure parameter, which was the fuel injection timing, particular attention was focused on those combinations of input parameters which included the structure parameter, i.e. combinations C_3, C_5, C_6 and C_7.

Due to a large amount of collected empirical material and limited form of the article, the analysis of information capacity index changes was limited to one engine rotation speed, n = 1100 [rpm]. The concentrations which were subject to analysis were HC, CO and NO_x concentrations. Moreover, the analysis included changes the excess air number λ.

The highest values of the index H_m were observed for the air excess number λ, then for the concentration of carbon oxide CO and unburned hydrocarbons HC. The lowest values of H_m were recorded for nitrogen oxides NO_x.

What is noteworthy here is that some regularity can be observed, which is characterised by higher values of index H_m recorded for the delayed fuel injection timing (22 °OWK), which undoubtedly has its substantive justification, as the delayed timing affects unfavourably combustion conditions in the engine cylinder. First of all, the excess air number decreases which leads to the creation of incomplete combustion products and, consequently, to the increase of CO and HC concentrations.

Correct model estimation is also testified by negative correlations for both the excess air number and NO_x concentration, as local deficit of oxygen leads to the decrease of concentration of this compound.

The highest values of the index H_m occur, first of all, for the combination C_5, which relates the rotational speed (x_1) and the engine structure parameter, which was the fuel injection timing (x_3), for both delayed and advanced fuel injection. Only slightly lower values of the index H_m occur for the combination C_7 which relates three input quantities of the test plan (Fig. 2–5).

MOST WIEDZY Downloaded from mostwiedzy.pl

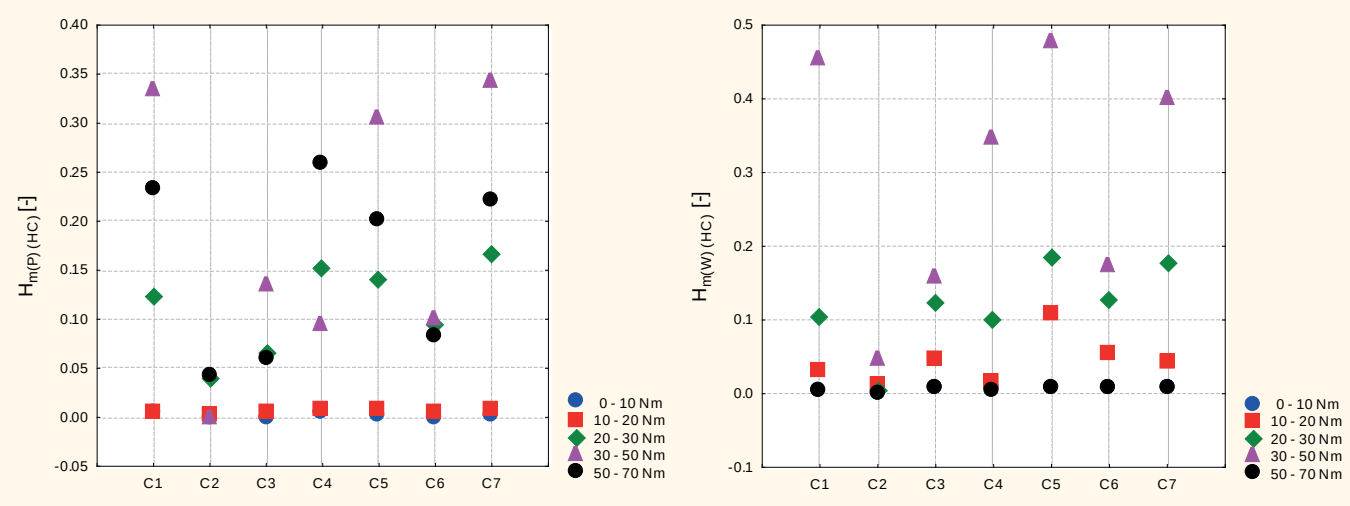

Fig.2. Values of information capacity index Hm for HC and transient state: n = 1100 rpm, load change from T_{tq} = 0 Nm to T_{tq} = 70 Nm. P – delayed fuel injection timing, W – advanced fuel injection timing, C1 – C7 – combinations of explanatory variables

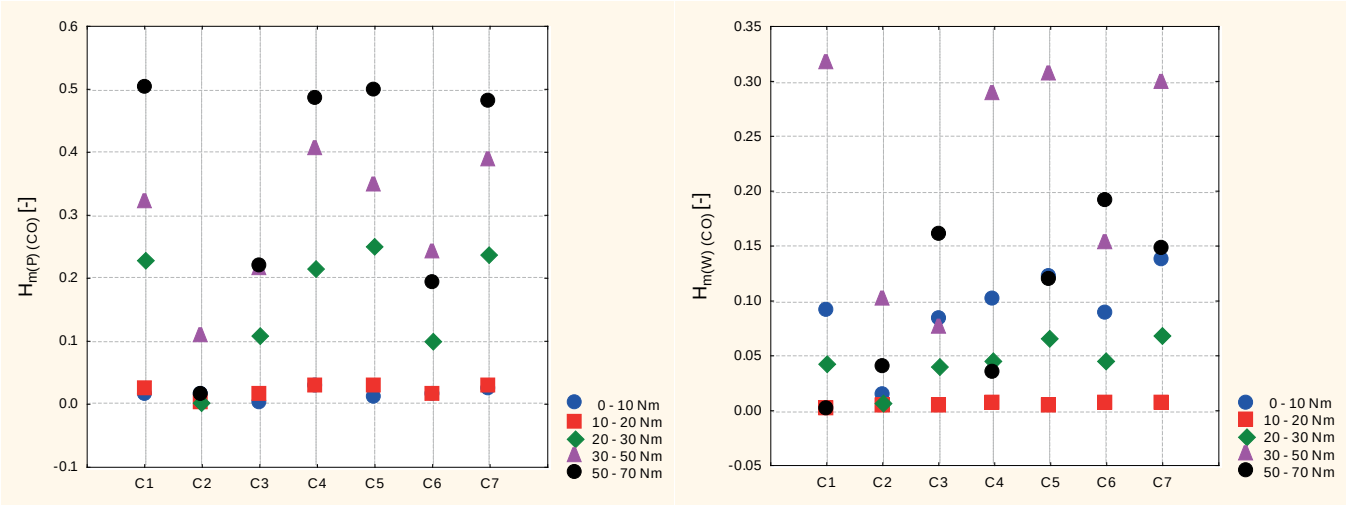

Fig. 3. Values of information capacity index Hm for CO and transient state: n = 1100 rpm, load change from T_{tq} = 0 Nm to T_{tq} = 70 Nm: P – delayed fuel injection timing, W – advanced fuel injection timing, C1 – C7 – combinations of explanatory variables

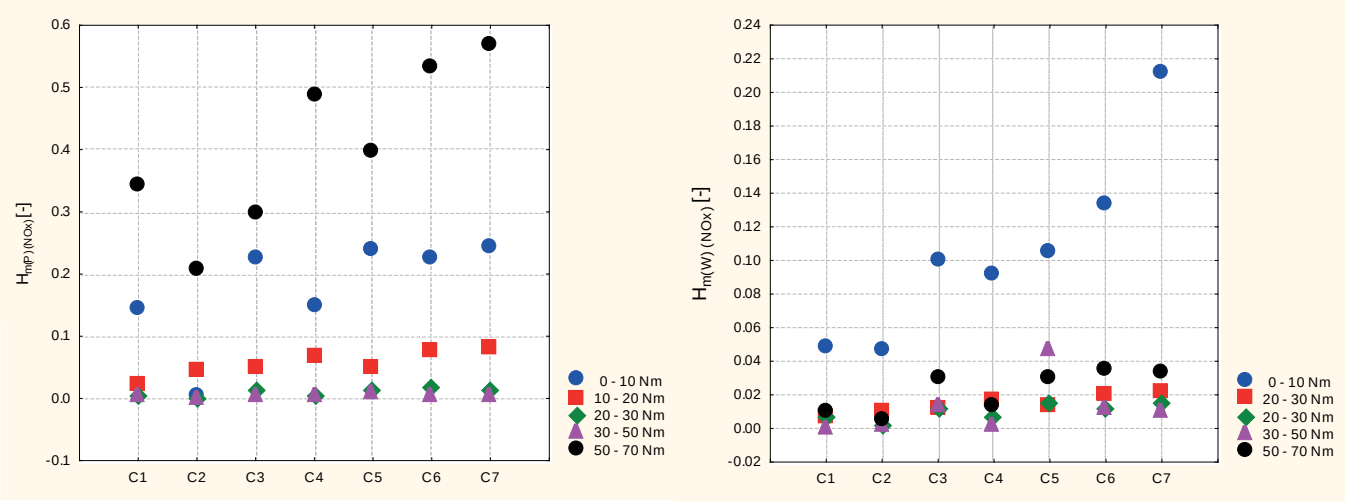

Fig.4. Values of information capacity index Hm for NO_x and transient state: n = 1100 rpm, load change from T_{tq} = 0 Nm to T_{tq} = 70 Nm: P – delayed fuel injection timing, W – advanced fuel injection timing, C1 – C7 – combinations of explanatory variables

MOST WIEDZY Downloaded from mostwiedzy.pl

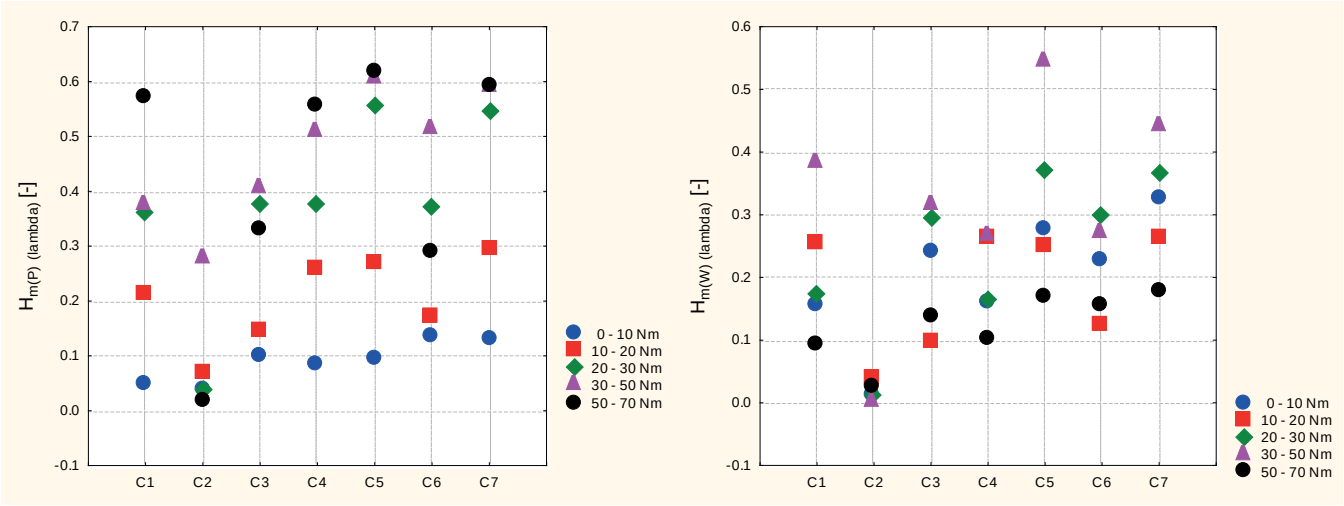

Fig.5. Values of information capacity index Hm for λ and transient state: n = 1100 rpm, load change from T_{tq} = 0 Nm to T_{tq} = 70 Nm: P – delayed fuel injection timing, W – advanced fuel injection timing, C1 – C7 – combinations of explanatory variables

The analysis of the integral information capacity index H_m provides not only the possibility for correct model estimation (for which, in fact, it is intended). Thanks to this analysis, from an extremely large dataset we can, along with specifying important variables, define conditions in which their effect on the examined object is the highest. On the other hand, the H_m values are very close to each other which makes it difficult to assess which arrangement of the test plan brings maximal information value, the more so that these values refer to one parameter only, or one combination of those parameters.

In the above situation, what seems to be of some help is the use of a ranking of parameters, as the ranking taking into account multi-criterial assessments (including all parameters and their combinations) is a basic condition for making correct diagnostic decisions.

RANKING CREATION

Due to a large amount of the recorded research material and the need for objective indication of a most favourable, in sensitivity terms, diagnostic parameter, a ranking was created based on the zero unitarization method. Earlier, each explanatory variable of the test plan was analysed using the information capacity index method (the Hellwig method), therefore at the preliminary stage of ranking creation it was the Hellwig index value which was assumed a diagnostic variable for each explanatory variable. These values for individual test plan arrangements and combinations of input parameters: *HC*, *CO*, NO_x and λ, are shown in Fig. 2–5.

The first step of ranking creation was dividing the set of diagnostic variables into three subsets: *S*, *D* and *N*, i.e.:

$$X = S \cup D \cup N \tag{5}$$

where:
S – subset of diagnostic variables called stimulators,
D – subset of diagnostic variables called destimulators,
N – subset of diagnostic variables called nominants.

The stimulants were transformed to the normalised form using the relation:

$$z_{ij} = \frac{x_{ij} - \min_i x_{ij}}{\max_i x_{ij} - \min_i x_{ij}}, \quad \begin{pmatrix} i = 1,2,\ldots,r \\ j = 1,2,\ldots,s \end{pmatrix}, \; X_i \in S \tag{6}$$

while for the destimulants the normalisation relation had the form:

$$z_{ij} = \frac{\max_i x_{ij} - x_{ij}}{\max_i x_{ij} - \min_i x_{ij}}, \quad \begin{pmatrix} i = 1,2,\ldots,r \\ j = 1,2,\ldots,s \end{pmatrix}, \; X_i \in D \tag{7}$$

Combinations C_1, C_3, C_4, C_5 and C_7 of the dependent variables were assumed the stimulants, i.e. diagnostic variables the increase of which is to be associated with the increase of the complex phenomenon and the decrease – with the decrease. Simultaneously, combinations C_2 and C_6 were assumed the destimulants, i.e. diagnostic variables the increase of which is to be associated with the decrease of the complex phenomenon and the decrease – with the increase.

The next step was normalisation of diagnostic indicators. This step is very important, as it provides opportunities for cumulative multi-criterial assessment of the analysed object. The cumulative assessment is obtained via aggregation, i.e. determining the aggregate (synthetic) variable Q_i.

$$Q_i = \frac{1}{s}\sum_{j=1}^{s} z_{ij} \qquad (i = 1, 2, \ldots, r) \tag{8}$$

The information on individual values of variable *Q* makes it possible to create a ranking with respect to non-increasing Q_i. Indeed, the position in the ranking will depend on the value of the synthetic variable Q_i., the set of which is collated in Tables 1–4.

MOST WIEDZY Downloaded from mostwiedzy.pl

Tab. 1. Values of normalised diagnostic variables and synthetic variable for HC

Plan arrangement	z_{i1}	z_{i2}	z_{i3}	z_{i4}	z_{i5}	z_{i6}	z_{i7}	Q_i
1	2	3	4	5	6	7	8	9
1100P(50-70)	0,5071	0,1178	0,3531	0,7443	0,4104	0,5418	0,5460	3,2205
1100P(30-50)	0,7355	1	0,8560	0,2688	0,6361	0,4326	0,8523	4,7813
1100P(20-30)	0,2676	0,1692	0,4050	0,4372	0,2849	0,4714	0,4043	2,4396
1100P(10-20)	0,0058	0,9571	0	0,0117	0	1	0	1,9746
1100W(50-70)	0	0,9764	0,0250	0	0,0020	0,9761	0,0013	1,9808
1100W(30-50)	1	0	1	1	1	0	1	5,0
1100W(20-30)	0,2284	0,9293	0,7909	0,2785	0,3750	0,2822	0,4350	3,3193
1100W(10-20)	0,0613	0,7302	0,2676	0,0316	0,2154	0,7148	0,0838	2,1047

Tab. 2. Values of normalised diagnostic variables and synthetic variable for CO

Test plan arrangement	z_{i1}	z_{i2}	z_{i3}	z_{i4}	z_{i5}	z_{i6}	z_{i7}	Q_i
1	2	3	4	5	6	7	8	9
1100P(50-70)	1	0,8520	1	1	1	0,1983	1	6,0503
1100P(30-50)	0,6336	0	0,9841	0,8349	0,6928	0	0,3826	3,5280
1100P(20-30)	0,4485	1	0,4974	0,4346	0,4992	0,6036	0,4887	3,9720
1100P(10-20)	0,0498	0,9880	0,0515	0,0458	0,0515	0,9693	0,0497	2,2056
1100W(50-70)	0	0,6488	0,7314	0,0589	0,2304	0,2103	0,2975	2,1773
1100W(30-50)	0,6280	0,0625	0,3388	0,5913	0,6139	0,3797	0,6186	3,2328
1100W(20-30)	0,0820	0,9558	0,1736	0,0791	0,1253	0,8331	0,1309	2,3798
1100W(10-20)	0,0023	0,9687	0	0	0	0	0	0,9710

Tab. 3. Values of normalised diagnostic variables and synthetic variable for NO_x

Test plan arrangement	z_{i1}	z_{i2}	z_{i3}	z_{i4}	z_{i5}	z_{i6}	z_{i7}	Q_i
1	2	3	4	5	6	7	8	9
1100P(50-70)	1	0	1	1	1	0	1	5,0000
1100P(30-50)	0,0123	0,9995	0	0,0065	0	1	0	2,0183
1100P(20-30)	0,0146	1	0,0266	0,0090	0,0225	0,9754	0,0134	2,0615
1100P(10-20)	0,0607	0,2218	0,1419	0,1333	0,1258	0,8656	0,1349	1,6840
1100W(50-70)	0,0293	0,9788	0,0844	0,0236	0,0681	0,9431	0,0466	2,1739
1100W(30-50)	0	0,9937	0,0242	0	0,1185	0,9868	0,0067	2,1299
1100W(20-30)	0,0184	0,9951	0,0181	0,0114	0,0219	0,9859	0,0147	1,0339
1100W(10-20)	0,0191	0,9499	0,0194	0,0297	0,0190	0,9699	0,2819	2,2889

Tab. 4. Values of normalised diagnostic variables and synthetic variable for λ

Test plan arrangement	z_{i1}	z_{i2}	z_{i3}	z_{i4}	z_{i5}	z_{i6}	z_{i7}	Q_i
1	2	3	4	5	6	7	8	9
1100P(50-70)	1	0,2631	0,7524	1	1	0,5723	1	5,5878
1100P(30-50)	0,5914	0	1	0,9000	0,9731	0	0,9922	4,4567
1100P(20-30)	0,5594	0,8784	0,8980	0,6013	0,8556	0,3661	0,8864	5,0452
1100P(10-20)	0,3544	0,9992	0,0061	0,2976	0,0696	0,7786	0,1372	2,6427
1100W(50-70)	0	0,9249	0,1332	0	0	0,9142	0	1,9723
1100W(30-50)	0,6119	1	0,7024	0,3682	0,8409	0,6193	0,6347	4,7774
1100W(20-30)	0,1672	0,9736	0,6345	0,1446	0,4508	0,5486	0,4542	3,3735
1100W(10-20)	0,3356	0,8755	0	0,3539	0,1795	1	0,2037	2,9482

MOST WIEDZY Downloaded from mostwiedzy.pl

When analysing the tables with normalised diagnostic variables we can notice that their highest values refer to arrangements executed at the delayed fuel injection (22 °OWK), for both CO and NO_x concentrations, and the excess air number λ. A characteristic test plan arrangement is the arrangement 1100P(50-70), representing the transient state executed at the rotational speed of 1100 rpm, when the load changes from 50 to 70 Nm, and for the delayed fuel injection angle, equal to 22 °OWK (Table 1–4). The next arrangements in the information capacity ranking which are characteristic for high values of normalised diagnostic variables are those executed for intermediate loads, i.e. in the first place for the load change from 20 to 30 Nm and then, for the change from 30 to 50 Nm. This mainly refers to changes of CO concentration and the excess air number λ. As for NO_x concentration (Table 4), the next arrangements in the ranking are those executed for similar load changes but for the advanced fuel injection angle, (30 °OWK). This has its substantive justification resulting from the physics of creation of individual toxic compounds in the cylinder. For instance, the dominant for the creation of nitrogen oxides is, first of all, high combustion pressure, at high excess air number, and the accompanying high combustion temperature.

Like for NO_x concentrations (apart from arrangement 1), for hydrocarbon concentrations, (Table 1) we can notice that the highest values refer to the test plan arrangement 1100W(30-50), i.e. to the transient state executed at rotational speed of 1100 rpm, when the load changes from 30 to 50 Nm and for the advanced fuel injection angle, equal to 30 °OWK. This may testify to the fact that this arrangement carries the greatest information value. The next arrangement in the information capacity ranking with respect to changes of structural parameters of the fuel supply system is the arrangement 1100P(30-50), with the ranking values only slightly lower than the top values. It is noteworthy that in both cases these arrangements do not represent the highest moment load. In this context a conclusion can be made that when arranging diagnostic tests, an important role in measurements can be played by intermediate load variants.

The above presented approach to ranking creation, which consists in considering all variables only as stimulants and destimulants, can be considered sufficient in the case when those variables are independent from each other, or their values are significantly different. When creating the ranking taking into account interactions between individual elements (which is the case here for the exhaust gas components) and changes in the structure parameter (fuel injection timing), this parameter is to be included in the subset of nominants, i.e. variables which have the most favourable value in the context of the analysed aspect of study. This way the fuel injection timing as the nominant will have a specified nominal value for the state of object serviceability. This nominal value will correspond to nominal concentrations of the earlier analysed CO, HC and NO_x compounds, and the excess air number λ.

A classical version of the zero unitarization method considers two approaches to HC and CO normalisation. The former approach refers to the case when only one nominal value c_{0j} exists, and in that case the normalisation is performed using formula (8). In the latter case, when the nominal values compose an interval $[c_{1j}, c_{2j}]$, the normalisation formula (9) is applied.

$$z_{ij} = \begin{cases} \dfrac{x_{ij} - \min\limits_i x_{ij}}{c_{0j} - \min\limits_i x_{ij}}, & \text{gdy } x_{ij} < c_{0j}, \\ 1, & \text{gdy } x_{ij} = c_{0j},\ X_i \in N, \\ \dfrac{x_{ij} - \max\limits_i x_{ij}}{c_{0j} - \max\limits_i x_{ij}}, & \text{gdy } x_{ij} > c_{0j} \end{cases} \tag{8}$$

$$z_{ij} = \begin{cases} \dfrac{x_{ij} - \min\limits_i x_{ij}}{c_{1j} - \min\limits_i x_{ij}}, & \text{gdy } x_{ij} < c_{1j}, \\ 1, & \text{gdy } c_{1j} \le x_{ij} \le c_{2j},\ X_i \in N, \\ \dfrac{x_{ij} - \max\limits_i x_{ij}}{c_{2j} - \max\limits_i x_{ij}}, & \text{gdy } x_{ij} > c_{2j} \end{cases} \tag{9}$$

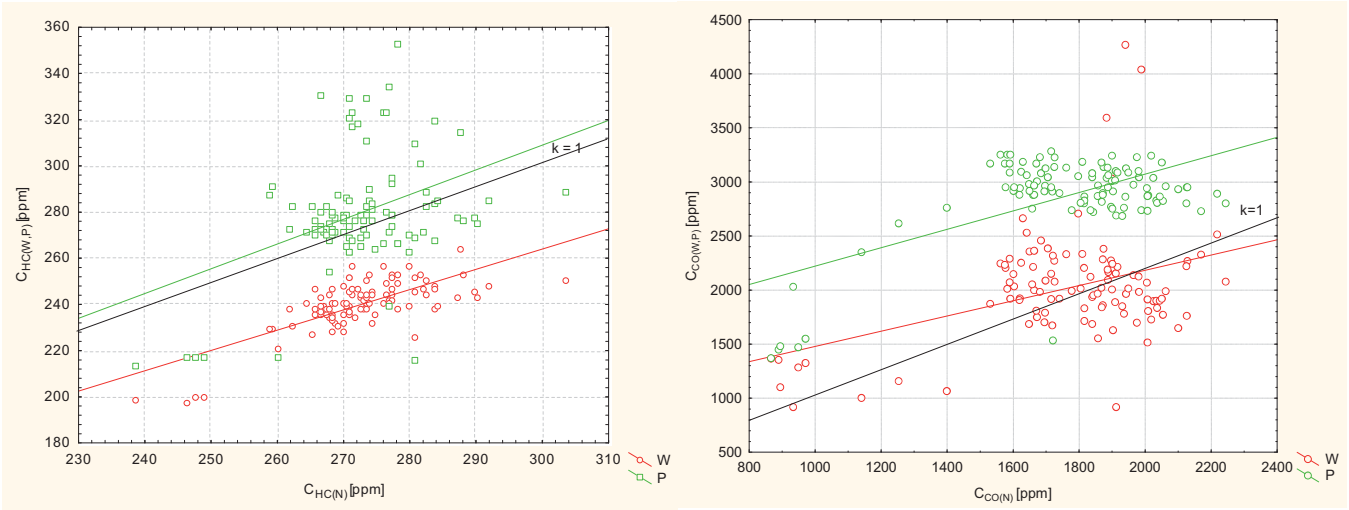

Fig. 6. Values of HC and CO concentration for transient state at n = 1100 rpm and load change from T_{tq} = 0 Nm to T_{tq} = 70 Nm: $C_{HC\,(N,\,W,\,P)}$ – HC concentration, $C_{CO\,(N,\,W,\,P)}$ – CO concentration for nominal (N), advanced (W), and delayed (P) fuel injection timing

MOST WIEDZY Downloaded from mostwiedzy.pl

The above described way of data analysis, in which the information capacity index values are analysed for individual test plan arrangements, will base on an interval of nominal values, which suggests that the formula (9) is to be used.

However, in the analysed case, due to the goal of the performed analysis, the highest information value will be attributed to test plan arrangements with values significantly differing from that determined by the nominal value interval. Graphical illustration of this problem is the dispersion diagram in Fig. 6, which shows the linear correlation function for concentration of unburned hydrocarbons HC and carbon oxide CO, and its position with respect to nominal values (black lines). That is why the normalisation formula (10) was applied in the present analysis.

$$z_{ij} = \begin{cases} \dfrac{1}{1+\dfrac{x_{ij}-\min\limits_i x_{ij}}{c_{1j}-\min\limits_i x_{ij}}}, & \text{gdy } x_{ij} < c_{1j}, \\ 0, & \text{gdy } c_{1j} \le x_{ij} \le c_{2j},\ X_i \in N, \\ \dfrac{1}{1+\dfrac{x_{ij}-\max\limits_i x_{ij}}{c_{2j}-\max\limits_i x_{ij}}}, & \text{gdy } x_{ij} > c_{2j} \end{cases} \quad (10)$$

The values obtained from normalisation of nominants of individual variables were aggregated with corresponding values of stimulants and destimulants (Tab. 1–4). As a result, synthetic variables were obtained which can be considered multi-criterial assessments of the influence of fuel injection timing.

As already mentioned, the position in the ranking will depend on the value of the synthetic variable Q_i. To organize objects (in the analysed case: normalised diagnostic indicators) with respect to non-increasing Q_i values, the entire set of objects can be divided into three parts, being the subgroups of best, average, and worst objects. For this purpose, the constant U can be used in the form:

$$U = \frac{max_i Q_i - min_i Q_i}{3} \quad (11)$$

This way leads to the creation of the subgroup of best objects for $Q_i \in (max_i Q_i - U, max_i Q_i]$, the subgroup of average objects for $Q_i \in (max_i Q_i - 2U, max_i Q_i]$ and the subgroup of worst objects for $Q_i \in (min_i Q_i, max_i Q_i - 2U]$.

The normalisation of synthetic variables performed in the above way is presented in Table 5, in which, for better display of their values, the subgroups of best and average objects are marked green and yellow, respectively.

When analysing the synthetic variable values collated in Table 5, it is noteworthy that compared to values which did not take into account nominants, (Tables 1-4) the test plan arrangements which reveal the highest information value remain basically unchanged, although taking into account the nominal values has led to the increase of differences between the variable values. This is an obvious advantage which makes the ranking easier to analyse. The highest values were observed for the delayed fuel injection angle, for NO_x and CO concentrations in the arrangement executed at load change from 50 Nm to 70 Nm. A slightly lower value of the synthetic variable was observed for the excess ait number in the same test plan arrangement. It is noteworthy that this is the parameter for which the largest population of arrangements with highest information values exist. This undoubtedly has its substantive justification, as even small disturbances of the combustion process result in changes of the excess air number [1,2,4]. Comparing synthetic variable values for NO_x concentration is also very interesting, as the majority of measuring arrangements of the test plan have average information value (most frequently in its upper limit). This can be explained by strong correlation of NO_x concentration with the combustion temperature and the excess air number. Concentration changes are rather small, but always occur when changing one of the abovenamed factors. This suggests a conclusion that the analysis of the relationship between NO_x concentration and the excess air number should be given more attention.

SUMMARY

The values of H_m, coefficient, which are close to each other, do not provide an answer to the question which test plan arrangement brings the maximal information value due to changes in the structure of the object of analysis, the more so that they refer to only one parameter or one combination of parameters. On the other hand, the ranking taking into account multi-criterial assessments (including all parameters and their combinations) is a basic condition for making correct diagnostic decisions. More complicated rankings can

Tab. 5. Values of synthetic variables for HC, CO, NO_x, and λ

Test plan arrangement	$Q_{i\,(HC)}$	$Q_{i\,(CO)}$	$Q_{i\,(NOx)}$	$Q_{i\,(\lambda)}$
1	2	3	4	5
1100P(50-70)	3,2205	11,5616	12,000	10,1481
1100P(30-50)	6,3675	7,7194	7,6813	10,6292
1100P(20-30)	2,4396	3,9720	7,9542	8,9860
1100P(10-20)	1,9746	3,8689	2,3474	2,6427
1100W(50-70)	3,9808	4,2771	6,7428	2,9723
1100W(30-50)	11,0000	4,6686	6,7000	8,2111
1100W(20-30)	3,3193	2,3798	6,6309	5,8062
1100W(10-20)	2,1047	4,9347	7,2735	3,4513

MOST WIEDZY Downloaded from mostwiedzy.pl

be created which take into account, for instance, compilation of explanatory and dependent variables, for the ranking to cover simultaneously all toxic compounds recorded during the experiment along will other parameters essential for the correctness of the combustion process.

Referring directly to the results of the presented ranking, some regularity in their distribution is worth noticing. Namely, except the absolutely highest value, in all remaining cases higher values of synthetic variable Q_i were observed for the delayed fuel injection angle (22 °OWK). This undoubtedly has its substantive justification, as the delayed fuel injection affects unfavourably combustion conditions in the engine cylinder. First of all, the excess air number decreases which leads to the creation of incomplete combustion products and, consequently, to the increase of CO and HC concentrations, which were the main object of this analysis.

BIBLIOGRAPHY

1. Markowski J.: *Emission of harmful exhaust gas compounds from aircraft piston engines (in Polish).* Poznan University of Technology, Thesis no. 517, ISSN: 0551-6528, Poznan 2013.

2. Pielecha J.: *Identifying parameters of particulates from internal combustion engines (in Polish).* Poznan University of Technology, Thesis no. 467, ISSN: 0551-6528, Poznan 2012.

3. Rudnicki J., Zadrąg R.: *Problems of modelling toxic compounds emitted by a marine internal combustion engine in unsteady states.* POLISH MARITIME RESEARCH, Vol. 21, ISSN: 1233-2585, pp. 57-65, Gdansk 2014.

4. Zadrąg R.: *Criteria for the selection of the diagnostic parameter for diagnosis of marine diesel engine*, LOGISTYKA No. 4/2010, ISSN 1231-5478, Poznan 2010.

5. Zadrąg R., Zellma M.: *Modelling of toxic compounds emission in marine diesel engine during transient states at variable pressure of fuel injection.* JOURNAL OF POLISH CIMAC, Vol.8, No 1, ISSN 1231-3998, Gdansk 2014.

6. Zadrąg R., Kniaziewicz T.: *The identification of toxic compound emission sensitivity as a diagnostic parameter during dynamic processes of the marine engine.* JOURNAL OF POLISH CIMEEAC, Vol.10, No 1, ISSN 1231-3998, pp. 161-170, Gdansk 2015.

7. Zadrąg R., Kniaziewicz T.: *Identification of diagnostic parameter sensitivity during dynamic processes of a marine engine*. The 6th INTERNATIONAL CONGRESS ON COMBUSTION ENGINES, PTNSS-2015-3507, Olsztyn 2015.

CONTACT WITH THE AUTHORS

Ryszard Zadrąg
e-mail: r.zadrag@amw.gdynia.pl

Polish Naval Academy
69 Śmidowicza St.
81-127 Gdynia

MOST WIEDZY Downloaded from mostwiedzy.pl

POLISH MARITIME RESEARCH Special Issue 2018 S1 (97) 2018 Vol. 25; pp. 243-247
10.2478/pomr-2018-0048

INDICES FOR ASSESSING POTENTIAL ENVIRONMENTAL HAZARD FROM FUTURE SHIP SCRAPPING PROCESS, DETERMINABLE IN SHIP DESIGN STAGE

Roman Liberacki
Gdańsk University of Technology, Poland

ABSTRACT

This paper shortly presents the issue of utilization of ships after their withdrawal from service. Information on number of floating units liquidated in previous years was presented. Hazards to the environment , health and life of workers employed in the Far East ship scrapping yards operating on the beaches, were indicated. Then, the most important rules which have to make the ship recycling process safe were referred to. This author proposed to supplement the rules by environmental hazard indices which would be determined already in ship design stage. According to the concept the indices should take into account amount of dangerous substances used for building the ship as well as degree of their harmfulness (weighing factors). Two approaches to the issue of determining the weighing factors were proposed: deterministic and fuzzy.

Keywords: ship utilization, safety, environmental protection, safety indices, weighing factors

MOST WIEDZY Downloaded from mostwiedzy.pl

INTRODUCTION

The issue of liquidation of ships is presently a subject of interest of international community, especially in EU countries. According to the NGO Ship-breaking Platform coalition, over 70% ships end their life on the South Asia beaches: in India, Bangladesh and Pakistan [11]. The scrapping is carried out there with the use of cheap labour, often by hands of under-age workers. As a result of bad working conditions lethal accidents happen. In 2016 in Bangladesh only about 20 persons were killed in such accidents [13]. Moreover such practice produces great danger to the environment because the disassembling is performed on the beach tide areas. Dangerous materials and substances contaminate shores and coastal waters. Moreover, they are spread over farther regions due to action of sea currents, consumed by living organisms, including fish caught for consumption.

In 2016 as much as 862 ships were liquidated worldwide, including 305 in India, 222 – Bangladesh, 141 – Pakistan, 92 – Turkey, 74 – China, 22 – EU and 6 in other regions of the world. It is essential that as much as 668 ships out of their total number were broken on the beaches. Their total tonnage amounts to 27,4 m. GT, including 23,8 m. GT tonnage of ships scrapped on the beaches. According to the data published by the NGO [12], on the list of disreputable champions which liquidated their ships on the beaches in 2016 the following EU countries can be found: Germany (with 98 ships scrapped on the beaches, out of 100 altogether), Greece (with 104 ships scrapped on the beaches, out of 113 altogether).

LEGAL REGULATIONS

To assure safe and environmentally friendly process of ship-breaking there were prepared a number of legal regulations which are presented almost in detail in [3] and [14]. The following can be found among them:

- Basel Convention on 22 March 1989, dealing with trans-border movement and liquidation of dangerous waste ;
- International Convention on Safe and Environmentally Friendly Recycling of Ships, 2009;
- Series of ISO 30 000 standards – an integrated guide for ship recycling issues dealing with safety, health and environmental protection;
- IMO Resolutions (MEPC 62, MEPC 63, MEPC 64, MEPC 68) – guidelines containing detail solutions in the area of ship recycling and operation of ship repair yards;
- Directive of EU Parliament and Council No.1257/2013 of 20 November 2013 on the recycling of ships.

The Directive came into force on 30 December 2013. It introduces obligation to keep a register of ship recycling enterprises which fulfil requirements of Hong Kong Convention. The current register can be found in the appendix to the Executive Decision of EU Commission 2016/2323 [15]. It contains 18 ship-recycling enterprises, including one located in Poland (Almex firm of Szczecin).

ENVIRONMENTAL HAZARD INDICES

In order to assure a high level of environmental safety for ship during its scrapping process it is necessary to make appropriate decisions already in design stage. To this end, it should be strived to use as low amount of dangerous materials for building the ship as possible. The materials both hazardous and neutral for the environment should be fit for recycling and using again. Hence they would not fill waste stockpiles (scrap-yards). Therefore it's worth to strive after reaching a high susceptibility to recycling of a ship during its design stage. The next issue is to decide as early as in ship design stage in what way ship disassembling process would be carried out in future. It should be so designed as to obtain a scrapping process characterized by low energy and time consumption, as well as low emission of noxious substances during such operations as paint removal, plate cutting etc.

It is required to provide new designed ships with a list of dangerous materials. It should be worked out already in ship design and building stage. According to the PRS publication on ship recycling [14], such list should cover all dangerous materials used for ship construction and outfit, operational waste as well as reserves. The list [14] specifies forbidden materials as well as those of limited allowable content, such as asbestos, polychlorinated biphenyls (PCB), substances reducing ozone layer (CFC), tin-organic compounds in anti-growth systems, heavy metals (e.g. lead, mercury), radioactive compounds. The list comprises also fuel and lubricating oils and oily bilge water.

Environmental hazard resulting from ship scrapping should be determined in compliance with the standard format of the list of dangerous materials given in the second appendix to the above mentioned publication [14].

Hence it is proposed to introduce indices which estimate potential environmental hazard caused by a ship during process of its scrapping. This would be a useful supplement to the rules worked out in this area.

The index which takes into account dangerous materials used for building a ship would have the following form:

$$I = \sum_{i=1}^{n} W_i \cdot M_i \tag{1}$$

where:

I – environmental hazard index,

W_i – harmfulness weighing factor of *i-th* dangerous material, (taking values in the range between 0 and 1),

M_i – mass of *i-th* dangerous material, expressed in kg.

Of course, the larger value of the index the greater environmental hazard from a ship under scrapping work.

It's worth to introduce one index more in order to take into account that a part of elements which contain dangerous materials may be recycled and used again. The other index would cover possible degree of the materials recycling. Its numerical value would be the smaller the greater amount of the materials could be useful again, i.e. not subjected to storage.

The index would have the form as follows:

$$I_R = \sum_{i=1}^{n} W_i \cdot M_i \cdot (1 - \frac{R_i}{100}) \tag{2}$$

where:

I_R – environmental hazard index which covers possible degree of recycling,

W_i – harmfulness weighing factor of *i-th* dangerous material (taking values in the range between 0 and 1),

M_i – mass of *i-th* dangerous material, expressed in kg.

R_i – recycling degree, i.e. recyclability of elements containing *i-th* dangerous material, (expressed by percentage number in the range between 0 and 100).

The above given values of the indices are of absolute form. They represent real mass of dangerous substances comprised in a ship. As a result, they will be advantageous for small ships but non-advantageous for large ones. In a sense it seems to be correct because under similar conditions scrapping the ships of small tonnage will be less hazardous to the environment than that of the ships of large tonnage.

In order to make it possible to compare potential environmental hazard from ships of different size the above mentioned indices should be related to ship mass. This way they will become relative ones expressed by the dimensionless ratio of mass of dangerous substances and mass of ship itself. Designer should strive to assure possibly low values of the

MOST WIEDZY Downloaded from mostwiedzy.pl

indices. However, on the other hand he/she must take into account economic aspects and proceed in compliance with the ALARP approach (As Low As Reasonably Practicable).

The ALARP approach (principle) was described, a. o., in [6, 9]. It says that impermissible risk is to be lowered regardless of cost. Ship designer would have to deal with such situation if he/she used unpermitted materials or exceeded their allowable contents. In consequence, he/she would be forced to resign from them. ALARP area is another component of the risk. It requires from the designer to perform an analysis of possible reduction of risk and cost associated with this approach.

The risk should be reduced to as low level as rationally justified for economic reasons.

The third area deals with negligible risk when it is as much low that there is not necessary to attempt to its lowering.

In practice, an impermissible risk does not ought to occur as it is associated with violating the rules. In ship scrapping a negligible risk would rather not happen. Therefore it should be taken into account that such process will be in ALARP area, which is connected with necessity to conduct an analysis of possible reduction of the risk and cost associated with this.

WEIGHING FACTORS

The above discussed potential environmental hazard indices require to establish weighing factors. They have to represent harmfulness degree of used dangerous material.

Determination of the weighing factors will require forming the group of experts and conducting the tests of their opinions.

Following the Norwegian method for the environmental indexing of ships [4, 8], one assumed that the experts will assign values in the range from 0 to 10, where zero stands for a non-dangerous material and 10 – for an extremely dangerous material. Then, the values obtained as a result of elaboration of experts' opinions will be standardized, i.e. scaled down to the numerical interval from 0 to 1, where 1 will stand for weighing factor for an extremely dangerous material.

The below presented calculation example follows the document [10] which contains supplements to recommendations of the formal ship safety assessment method (FSA) worked out under auspices of International Maritime Organization (IMO).

In fact, one should expect several dozen dangerous materials for which it will be necessary to determine weighing factors. In the presented example only five materials are assumed to be considered and that only five experts will be at one's disposal. The below presented Tab. 1 shows hypothetical results of experts' activity which consisted in assigning rank values from the interval (0, 10) to the five selected materials.

Tab. 1. Rank values assigned by experts to dangerous materials

	Dangerous material				
	S1	S2	S3	S4	S5
Expert No.1	5	8	7	9	6
Expert No. 2	5	8	6	9	7
Expert No. 3	5	8	7	9	6
Expert No. 4	5	9	7	8	6
Expert No. 5	5	9	6	8	7
Sum of x_{ij} values	**25**	**42**	**33**	**43**	**32**

The next step in determining values of weighing factors is their standardization.

As we have five experts the maximum value of weighing factor possible to be assigned by each of them is 10, hence the maximum value of the sum of weighing factors amounts to 50. Individual standardized values of weighing factors amounts to, respectively:

$W_1 = 25/50 = 0{,}5$
$W_2 = 42/50 = 0{,}84$
$W_3 = 33/50 = 0{,}66$
$W_4 = 43/50 = 0{,}86$
$W_5 = 32/50 = 0{,}64.$

It should be expected that the experts would not be fully unanimous in their opinions. Some divergence in the opinions may be observed in the example data of Tab. 1. In such situation a conformity level of the achieved opinions should be estimated. For differences in weighing factors assigned to given dangerous materials either standard deviation from mean value or range may be used.

For material No.1 the standard deviation from the mean equal to 5 amounts to 0, the range –0, and the relative range –also 0%, because full conformity of experts' opinions was reached in this case.

For material No.2 the standard deviation from the mean equal to 8,4 amounts to 0,48, the range – 1, and the relative range – 10%. It may be said that we have to do with low discrepancy of experts' opinions, i.e. high conformity level.

An experts' conformity coefficient which simultaneously takes into account all estimates made for all considered cases is described in [7, 10]. It is called Kendall – Smith coefficient which can be determined from the following formula:

$$W_{K-S} = \frac{12\sum_{i=1}^{i=I}\left[\sum_{j=1}^{j=J} x_{ij} - \frac{1}{2}J(I+1)\right]^2}{J^2(I^3 - I)} \quad (3)$$

where:
W_{K-S} – conformity coefficient,
I – number of considered dangerous materials,
J – number of experts.

It is assumed that $W_{K-S} > 0{,}7$ stands for a high conformity of experts' opinions. In the considered example $W_{K-S} = 0{,}904$; it means that the conformity level of the opinions given in Tab. 1 is high.

In case when opinion conformity level obtained during analysis seems too low it should be checked whether this concerns weighing factors assigned by experts to all dangerous materials or only to some of them.

MOST WIEDZY Downloaded from mostwiedzy.pl

In case when the discrepancies are large it would be useful to engage additional experts or another group of them. It is advised to strive after achieving a high conformity of experts' opinions as only in such case obtained values of weighing factors can be deemed appropriate.

FUZZY WEIGHING FACTORS

If to achieve a high conformity of opinions of experts asked on numerical values appears impossible even after limitation of scale range down to values between 0 and 3, then it will be at one's disposal to try another approach, namely to apply fuzzy logic. It was developed for investigating uncertain or unclear issues [1].

This author already used it for analyzing reliability and risk of technical systems.

A reference to fuzzy logic can be found in [5].

The idea to use fuzzy numbers for finding values of weighing factors consists in putting questions to experts in another way.

Firstly, amount of numbers possible for selection should be reduced from 10 to 3.

Secondly, instead of the numbers, to use linguistic variables such as:

– extremely dangerous material,
– very dangerous material,
– dangerous material.

To ask experts to assign, by means of brainstorming or voting, particular materials to the sets defined by the above given linguistic variables.

Thirdly, it is necessary to replace the linguistic variables by fuzzy numbers with the use of the so called fuzzy values of Baldwin truth, described in [2].

Membership functions of fuzzy numbers corresponding to linguistic variables, hence also materials harmfulness weighing factors, take the following form:

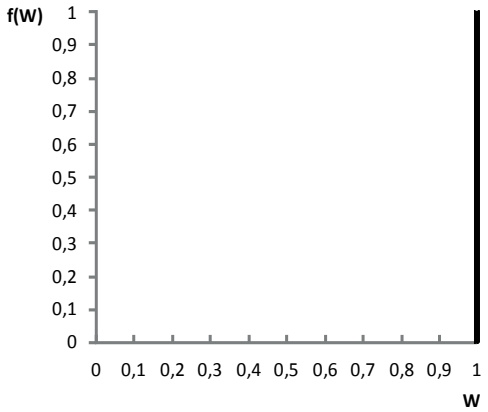

Fig.1. Membership function of fuzzy number for extremely dangerous materials

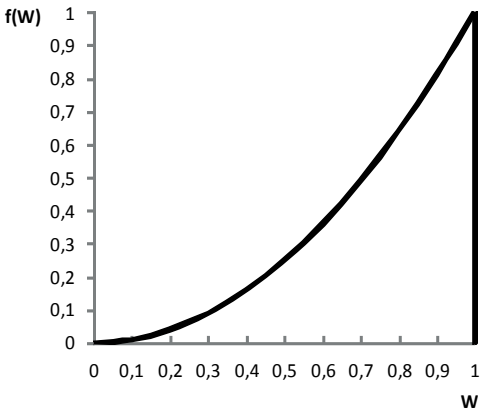

Fig. 2. Membership function of fuzzy number for very dangerous materials

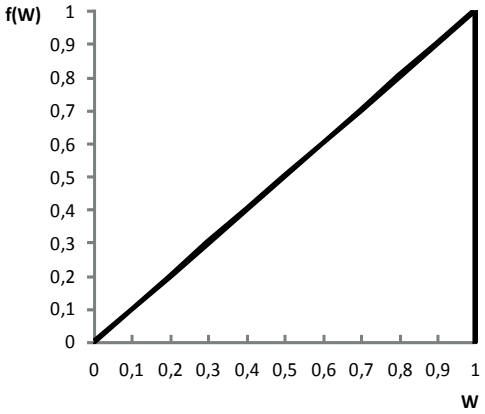

Fig.3. Membership function of fuzzy number for dangerous materials

This way we obtain weighing factors in the form of three fuzzy numbers with membership functions given in Fig. 1,2 and 3, respectively. Having them in this form we can to substitute them into the formulae (1) and (2) as it is allowed to multiply fuzzy number by real numbers. As a result, we obtain the indices in the form of fuzzy numbers. It makes it possible to achieve index values in the form of "about x "instead of the number„x", and the form of membership functions provides us with information on uncertainty level of the performed assessment.

Designers who do not intend to make use of fuzzy numbers, may use values of fuzzified weighing factors "hardened" to the form of real numbers.

By applying the calculation method of abscissa of centre of gravity:

$$W_o = \frac{\int_0^1 W \cdot f(W)dW}{\int_0^1 f(W)dW} \tag{4}$$

where:
Wo – weighing factor;
$f(W)$ – membership function (Fig. 1 through 3),
W – a value on abscissa axis (Fig.1 through 3)

MOST WIEDZY Downloaded from mostwiedzy.pl

the factors in question take the following values: 1 – for extremely dangerous materials, 0,75 – for very dangerous materials and 0,67 – for dangerous materials.

SUMMARY

The issue of scrapping the ship after its withdrawal from service should be taken into account already during ship design stage.

It should be strived after use of possibly small amount of dangerous materials, ensure as large as possible application of materials which would be suitable for recycling, as well as apply modular system to ship power plant, which would facilitate disassembling the ship.

Environmental hazard connected with ship scrapping should be estimated already in ship design stage by using the proposed indices based on the compulsory list of dangerous materials and which constitute a proposal for supplementing the rules.

BIBLIOGRAPHY

1. Januszewski E.: Logic and philosophical issues connected with fuzzy logic (in Polish). Roczniki Filozoficzne. Vol LV, No. 1, 2007.
2. Kacprzyk J.: Fuzzy sets in systems analysis (in Polish). PWN, Warszawa, 1986
3. Koziński M.: Recycling of ships in EU legislation (in Polish). Zeszyty naukowe Akademii Morskiej w Gdyni (Scientific bulletins of Gdynia Maritime University). No. 87. December, 2014.
4. Liberacki R.: A probabilistic model of environmental safety of ship power plant. Polish Maritime Research. Special Issue. Gdańsk, 2004.
5. Liberacki R.: Effect of adopted rules of inference and methods of defuzzification on the final result of the evaluation of reliability made using the fuzzy logic methods. Journal of Polish CIMAC. Gdańsk, 2011.
6. Skjong R.: Criteria for establishing risk acceptance. Proceedings of ESREL Conference. Vol.2. Maastricht. June 2003.
7. Wójcik M.: Assessment methods of conformity of experts' opinions for foresight research purposes (in Polish). Zeszyty Naukowe Uniwersytetu Ekonomicznego w Katowicach. (Scientific bulletins of Katowice Economic University) No. 220, 2015.
8. DNV: Environmental Differentiation of Dues and Fees for Ships. Technical Report No. 97-0212.1997.
9. IMO (MEPC 45/13). Formal Safety Assessment Including Environmental Indexing of Ships. 27 June 2000.
10. IMO (MSC – MEPC 2/Circ.5): Amendments to the guidelines for formal safety assessment (FSA) for use in the IMO rule – making process. 16.10.2006.
11. http://www.shipbreakingplatform.org/shipbrea_wp2011/wp-content/uploads/2016/04/Worldwide-overview_FINAL.pdf (30.05.2017)
12. http://www.shipbreakingplatform.org/shipbrea_wp2011/wp-content/uploads/2017/02/Stats- Graphs_2016-List_FINAL.pdf (30.05.2017)
13. http://www.shipbreakingplatform.org/ngo-platform-annual-report-2015/ (30.05.2017)
14. PRS: Recycling of ships (in Polish). Publikacja informacyjna (Informing publication) No. 33/I,. Gdańsk, 2016.
15. http://eurlex.europa.eu/legalcontent/PL/TXT/?qid=1484129918570&uri=CELEX:32016D2323 (30.05.2017)

CONTACT WITH THE AUTHOR

Roman Liberacki
e-mail: romanl@pg.gda.pl

Gdańsk University of Technology
11/12 Narutowicza St.
80 - 233 Gdańsk
Poland

MOST WIEDZY Downloaded from mostwiedzy.pl